

PGC1 α -driven transcriptional control of the cell secretome in prostate cancer: molecular and biological analysis

Ariane Schaub Clerigué
2022

Directors:
Verónica Torrano Moya & Arkaitz Carracedo Pérez

eman ta zabal zazu



Universidad
del País Vasco

Euskal Herriko
Unibertsitatea

PGC1 α -driven transcriptional control of the cell secretome in prostate cancer: molecular and biological analysis

Doctoral Thesis

Report of the experimental work to apply to the academic degree of Doctor in Biological Sciences, from the Doctorate Program of Molecular Biology and Biomedicine at the University of the Basque Country. The work herein presented has been performed by Ariane Schaub Clerigué at the Center for Cooperative Research in Biosciences (CIC bioGUNE) under the mentorship of Dr. Verónica Torrano Moya and Dr. Arkaitz Carracedo Pérez.

Ariane Schaub Clerigué

2022

Supported by:



*“ Unless you try to do something beyond
what you have already mastered, you will never grow”*

Ralph Waldo Emerson

About the cover

The cover was designed and painted by Nerea Larretxi Gallastegi.
It represents the communication networks established between cells.

-Dox	Non-induced with doxycycline
+Dox	Induced with doxycycline
2D	2 dimensions
ABC	ATP-binding cassette
ADAM10	Disintegrin and metalloproteinase domain-containing protein 10
ADT	Androgen deprivation therapy
AKT	Protein kinase B
ALDOC	Fructose-bisphosphate aldolase C
ALIX	Programmed cell death 6 interacting protein
AMPK	Serine/threonine kinase AMP-activated protein kinase
ANOVA	Analysis of variance
AR	Androgen receptor
AREs	Androgen response elements
ARF6	ADP ribosylation factor 6
ATCC	American Type Culture Collection
ATF2	Activating-transcription factor 2
ATM	Ataxia Telangiectasia Mutated
ATP1B1	Sodium/potassium-transporting ATPase subunit beta-1
B2M	Beta-2-Microglobulin
BAD	BCL2 associated agonist of cell death
BCa	Breast cancer
BMDCs	Bone marrow derived cells
BPH	Benign prostatic hyperplasia
BRCA1	Breast cancer type 1 susceptibility protein
BRCA2	Breast cancer type 2 susceptibility protein
CAFs	Cancer-associated fibroblasts
cAMP	Cyclic adenosine monophosphate
cGAS	cyclic GMP-AMP synthase
CLDN3	Claudin 3
COXIV	Cytochrome c oxidase subunit 4
CPI	Checkpoint inhibitors
CRC	Colorectal cancer
CRISPR	Clustered regularly interspaced short palindromic repeats
CRPC	Castration resistant prostate cancer
CSCs	Cancer stem cells
CTC	Circulating tumor cell
Ctl	Control
CTLA-4	Cytotoxic T-Lymphocyte Antigen 4
DAMPs	Damage-associated molecular patterns
DDR	DNA damage repair
dH2O	Distilled water
DHT	Dihydrotestosterone
DiIC18 (3)	1,1'-DIOCTADECYL-3,3,3'-Tetramethylindocarbocyanine Perchlorate
DKO	Double Knockout
DMEM	Dulbecco's Modified Eagle Medium
DMEM Exo-free	DMEM depleted of FBS-derived EVs
DMSZ	Deutsche Sammlung von Mikroorganismen und Zellkulturen GmbH
DNA	Desoxyribonucleic acid
Dox	Doxycycline
DPBS	Dulbecco's phosphate-buffered saline
DRE	Digital rectal examination

ECM	Extracellular Matrix
ECs	Endothelial cells
EDIL3	EGF-like repeat and discoidin I-like domain-containing protein 3
EGFR	Epidermal growth factor
EGR1	Early growth response protein 1
ELISA	Enzyme-linked Immunosorbent Assay
EM	Electron microscopy
EMT	Epithelial mesenchymal transition
eNOS	Endothelial nitric oxide synthase
ER	Endoplasmic reticulum
ERK	Extracellular-regulated kinase
ERRα	Estrogen related receptor alpha
ESCRT	Endosomal sorting complex required for transport
EVs	Extracellular Vesicles
EVs_sgCtl-Dox	EVs from cells with no PGC1 α expression in the presence of ERR α
EVs_sgCtl+Dox	EVs derived from cells with expression of PGC1 α and presence of ERR α
EVs_sgERRα#2-Dox	EVs from cells with no PGC1 α expression and deletion of ERR α
EVs_sgERRα#2+Dox	EVs from cells with PGC1 α expression and deletion of ERR α
EVs-Dox	EVs from non-PGC1 α -expressing cells
EVs+Dox	EVs from PGC1 α -expressing cells
EZH2	Enhancer of zeste 2 polycomb repressive complex 2 subunit
F11R/JAM1	Junctional adhesion molecule A
FASP	Filter-aided sample preparation
FBS	Fetal Bovine Serum
FDA	Food and Drug Administration
FGFBP1	Fibroblast growth factor binding protein 1
FOXO1	Forkhead Box O
FXR	Farnesol X receptor
GAPDH	Glyceraldehyde-3-Phosphate Dehydrogenase
GCN2	general control nonderepressible 2
GEMMs	Genetically engineered mouse models
GFP	Green fluorescent protein
GNB2	G Protein Subunit Beta 2
GnRH	Gonadotropin releasing hormone
GO	Gene Ontology
GPCRs	G protein-coupled receptors
GRP78	78 KDa glucose-regulated protein
GSEA	Gene set enrichment analysis
H&E	Hematoxylin & Eosin
HAT	Histone acetyltransferase
HCC	Hepatocellular carcinoma
HER2	Human epidermal growth factor receptor 2
HGPIN	High grade prostatic intraepithelial neoplasia
HNF4α	Hepatocyte nuclear factor 4 alpha
HRS	Hepatocyte growth factor-regulated tyrosine kinase substrate
HSP90	Heat shock protein 90
IACR	International Agency for Research in Cancer
IC	Intra-cardiac
ID2	Inhibitor of DNA binding 2
IF	Interstitial fluid

IFN	Interferon
IFN-β	Interferon beta
IFNA1	Interferon alpha 1
IFNB1	Interferon beta 1
ILVs	Intraluminal vesicles
IRFs	IFN regulatory factors
ISEV	International Society of Extracellular Vesicles
ISGs	IFN-stimulated genes
ISREs	IFN-stimulated response elements
ISUP	International Society of Urological Pathology
ITGA2	Integrin alpha-2
ITGB1	Integrin beta-1
Kda	Kilodalton
kg	Kilogram
KO	Knockout
KPNA2/IMA1	Importin subunit alpha-1
LC-MS	Liquid chromatography-mass spectrometry
LH	Luteinizing hormone
LHRH	Luteinizing hormone releasing hormone
luc	Luciferase
LXR	Liver X receptor
MAPK	Mitogen activated protein kinase
MDA5	Melanoma differentiation associated gene 5
MDSCs	Myeloid-derived suppressor cells
MEF2	Myocyte enhancer factor-2
MEFs	Mouse embryonic fibroblasts
MHC	Major histocompatibility complex
min	Minute
miR	micro RNA
MITF	Microphthalmia-associated transcription factor
ml	Mililiter
MLCK	Myosin light chain kinase
mM	Milimolar
MRI	Magnetic resonance imaging
mRNA	Messenger RNA
mtDNA	mitochondrial DNA
mTOR	Mammalian target of rapamycin
MVB	Multivesicular bodies
MVs	Microvesicles
MX1	Interferon-induced GTP-binding protein Mx2
n.s	Not significant
NCOR1	Nuclear Receptor Corepressor 1
ng	Nanogram
NK	Natural killer
NLRC5	NOD-Like Receptor C5
nm	Nanometer
NRF1/2	Nuclear Respiratory Factor 1/2
NRP1	Neuropilin 1
NSCLC	Non-small cell lung carcinoma
NTA	Nanoparticle-tracking analysis

ODC1	Ornithine decarboxylase 1
OXPHOS	Oxidative phosphorylation
PAMPs	Pathogen-associated molecular patterns
PBS	Phosphate Buffer Saline
PCa	Prostate cancer
PCA3	Prostate cancer associated 3
PCR	Polymerase Chain Reaction
PD-1	Programmed cell death 1
PD-L1	Programmed cell death ligand 1
PDAC	Pancreatic ductal adenocarcinoma
PKD1	Phosphoinositide-dependent kinase-1
PGC1α	Peroxisome proliferator-activated receptor gamma coactivator 1-alpha
PGC1α	Peroxisome proliferator activated receptor coactivator 1 α
PHI	Prostate health index
PI(3)K	Phosphatidylinositol-4,5-bisphosphate 3-kinase
PIN	Prostatic intraepithelial neoplasia
PLD2	Phospholipase D2
PPAR	Peroxisome proliferator activated receptor
PRC	PGC1-related coactivator
PRRs	Pathogen recognition receptors
PSA	Prostate-specific antigen
PTEN	Phosphatase and tensin homolog
PTMs	Post-translational modifications
RAC1	Ras-related C3 botulinum toxin substrate 1
RB	Retinoblastoma
RLRs	RIG-like receptors
ROS	Reactive Oxygen Species
RP	Radical prostatectomy
RT	Room Temperature
RT-qPCR	Reverse-Transcriptase quantitative PCR
RTK	Receptor tyrosine kinase
RXR	Retinoid X receptor
S	Secretome
S-Dox	Secretome produced by non-PGC1 α -expressing cells
s.e.m	Standard error of the mean
S+Dox	Secretome produced by PGC1 α -expressing cells
S<10K	Secretome containing molecules smaller than 10 KDa size
S>10K	Secretome containing molecules bigger than 10 KDa size
sEVs	Small Extracellular Vesicles
SFs/SFs	Soluble factors
SFs_sgCtl-Dox	SFs from cells with no PGC1 α expression and presence of ERR α
SFs_sgCtl+Dox	SFs from cells with expression of PGC1 α and presence of ERR α
SFs_sgERRα#1-Dox	SFs from cells with no PGC1 α expression and deletion of ERR α
SFs_sgERRα#1+Dox	SFs from cells with PGC1 α expression and deletion of ERR α
SFs_sgERRα#2-Dox	SFs from cells with no PGC1 α expression and deletion of ERR α
SFs_sgERRα#2+Dox	SFs from cells with PGC1 α expression and deletion of ERR α
sg	Single guide
sgCtl-Dox	Cells with no PGC1 α expression and presence of ERR α
sgCtl+Dox	Cells expressing PGC1 α and presence of ERR α
sgERRα#1-Dox	Cells with no PGC1 α expression and combined with ERR α deletion

sgERRα#1+Dox	Cells expressing PGC1α and combined with ERRα deletion
sgERRα#2-Dox	Cells with no PGC1α expression and combined with ERRα deletion
sgERRα#2+Dox	Cells expressing PGC1α and combined with ERRα deletion
shRNA	Short hairpin RNA
SIRT1	Sirtuin 1
SN	Supernatant
SNAREs	N-ethylmaleimide-sensitive fusion attachment protein (SNAP) receptors
SOD3	Extracellular superoxide dismutase
SP	Signal peptide
SRM	Spermidine synthase
STAT	Signal transducer and activator of transcription
STING	Stimulator of interferon genes
STXBP2	Syntaxin binding protein 2
TCA	Tricarboxylic acid cycle
TCF4	Transcription factor 4
TIL	Tumor interstitial liquid
TLRs	Toll-like receptors
TNBC	Triple negative breast cancer
TNM	Tumor, node, metastasis
TNXB	Tenascin B
TP53	Tumor protein P53
Treg	Regulatory T cell
TRUS	Transrectal ultrasound
VHL	Von Hippel-Lindau
WHA	Wound healing assay
WHO	World Health Organization
x g	Times gravity
YBOX1	Nuclease-sensitive element-binding protein 2
µg	Microgram
µl	Microliter
µM	Micromolar

Summary	39
----------------------	-----------

Introduction

I Cancer	43
II Prostate cancer	46
II.1 Human prostate anatomy	46
II.2 Prostate cancer epidemiology and risk factors	48
II.3 Prostate cancer diagnosis, pathology, and treatment	48
II.3.1 Prostate cancer diagnosis and pathology.....	48
II.3.2 Prostate cancer treatment.....	50
II.4 Prostate cancer progression	52
II.5 Molecular drivers of prostate cancer	53
II.6 PGC1 family of coregulators	56
II.6.1 PGC1 α	57
II.6.2 Role of PGC1 α in other types of cancer.....	60
III Cell communication	63
III.1 Types of intercellular communication	64
III.1.1 Ligands and receptors.....	65
III.2 Extracellular vesicles (EVs)	66
III.2.1 Classification of extracellular vesicles.....	67
III.3 Extracellular vesicles as active players in cancer progression	72
III.4 Extracellular vesicles as non-invasive biomarkers	74
III.5 Soluble factors (SFs)	75
III.6 Transcriptional regulation of the cell secretome	82

Hypothesis and Objectives

Objectives	87
-------------------------	-----------

Materials and Methods

I. Materials	91
I.1 Cell lines and culture conditions	91

I.2	Prostate cancer stable cell lines	91
I.3	Generation of stable cell lines	93
I.3.1	Generation of PC3 TGL cell line	93
I.3.2	Generation of PC3 GFP-luc cell line	94
I.4	Drugs	95
II	Cellular analysis	95
II.1	Production of cell secretome	95
II.1.1	Whole secretome production.....	95
II.1.2	Production and isolation of extracellular vesicles	99
II.1.3	Generation of soluble factors fraction of the secretome	100
II.1.4	<i>In vitro</i> cell biology assays.....	101
III	Molecular Assays	105
III.1	Gene expression analysis	105
III.1.1	RNA extraction and retrotranscription	105
III.1.2	Real time quantitative polymerase chain reaction (RT qPCR)	105
III.1.3	RNA sequencing	107
III.2	Protein expression analysis	108
III.2.1	Enzyme-linked Immunosorbent Assay (ELISA).....	108
III.2.2	Secretome protein precipitation	109
III.2.3	Protein extraction	109
III.2.4	Protein quantification and sample preparation	110
III.2.5	Western blotting (WB).....	110
III.2.6	Proteomics analysis	111
III.3	EVs characterization techniques	114
III.3.1	Nanoparticle-tracking analysis (NTA).....	114
III.3.2	Electron Microscopy (EM).....	115
IV	<i>In vivo</i> analysis	115
IV.1.1	Animal maintenance.....	115
IV.1.2	Genetically engineered mouse models (GEMMs)	116
IV.1.3	Isolation of tumor interstitial liquid from GEMMs	116
IV.1.4	Subcutaneous xenograft experiments in nude mice	116
IV.1.5	<i>In vivo</i> metastasis assay: soluble factors	117
IV.1.6	<i>In vivo</i> metastasis assay: extracellular vesicles.....	118
V	Bioinformatics analysis and statistics	119

Results

I	<i>Evaluation of the biological impact of the cell secretome on prostate cancer aggressiveness</i>	123
I.1	Biological effect of PGC1α-driven secretome in PCa cell lines	126
I.1.1	Effect of the cell secretome in cell proliferation	126
I.1.2	Role of the cell secretome in cell migration	129
I.1.3	The PGC1 α -ERR α transcriptional axis regulates the cell secretome.....	131
II	<i>Study and description of the EVs fraction of the secretome</i>	135
II.1	EVs physical and molecular characterization	136
II.1.1	EVs general characterization by western blot, electron microscopy, nanoparticle tracking analysis and protein content.	136
II.1.2	EVs proteomics analysis.....	142
II.2	Biological impact of the EVs: <i>in vitro</i> and <i>in vivo</i> assays	146
II.2.1	<i>In vitro</i> EVs uptake	146
II.2.2	Role of EVs in 2D cell growth and migration.....	147
II.2.3	Role of EVs in an <i>in vivo</i> metastasis assay.....	148
II.3	EVs as bystanders of prostate cancer aggressiveness	150
III	<i>Study and description of the soluble factors fraction of the cell secretome</i>	156
III.1	Biological impact of the soluble factors fraction of the secretome: <i>in vitro</i> and <i>in vivo</i> assays	156
III.1.1	<i>In vitro</i> study of the soluble factors effect in PCa cell proliferation	156
III.1.2	Role of the soluble factors in an <i>in vivo</i> model of metastasis.....	158
III.2	Proteomics characterization of the secretome and its cell-intrinsic regulation by the producer cells	160
III.2.1	Proteomics characterization of the secretome	160
III.3	Molecular events triggered upon treatment of PCa recipient cells with the differential secretomes	180
III.3.1	RNA sequencing analysis of PCa recipient cell lines	180
IV	<i>To examine the cell-intrinsic molecular events triggered by PGC1α in PCa producer cells that could mediate the effects of the secretome</i>	192
IV.1	Molecular cues activated in PCa producer cells upon expression of PGC1α	192
IV.1.1	<i>In vitro</i> and <i>in vivo</i> validation of RNA sequencing candidates	198
	Type I IFN signaling.....	201

Discussion

I	<i>PGC1α: beyond the cell boundaries</i>	211
I.1	Dissecting the cell secretome	213
I.1.1	Extracellular vesicles	214
I.1.2	Soluble factors	217
I.1.3	Tumor interstitial liquid (TIL)	221
I.2	Extracellular vesicles as a source for biomarker discovery	224
II	<i>Understanding the impact of the cancer secretome in the stromal compartment</i>	226
II.1	Cell secretome: priming the soil for metastatic cells seeding?	226
II.1.1	Extracellular vesicles: on the road to the pre-metastatic niches.....	228
II.1.2	Soluble factors: unexpected role on priming the pre-metastatic niches.....	229
III	<i>Effect of the PGC1α-driven secretome in the tumor compartment: beyond the cell barriers and back to the roots?</i>	231
III.1	Puzzling the pieces	233
III.2	Spatial architecture for the study of cell communication	240
I	<i>Conclusions</i>	247
II	<i>Future perspectives</i>	248

Bibliography and Annex

I	<i>Bibliography</i>	251
II	<i>Annex</i>	299

Figures Introduction

Figure I 1. Total number of cancer cases diagnosed in 2020 worldwide.	43
Figure I 2. Overview of the tumor progression cascade.	44
Figure I 3. Revised hallmarks of cancer proposed by Hanahan and Weinberg.	45
Figure I 4. The metastatic cascade.	46
Figure I 5. Anatomy and histology of the human reproductive systems.	47
Figure I 6. Diagram of the original Gleason Grading system by Dr. Donald Gleason ...	49
Figure I 7. Revised Gleason grading for diagnosis of PCa.	50
Figure I 8. Schematic representation of PCa progression.	52
Figure I 9. Cellular functions activated upon phosphorylation of AKT.	54
Figure I 10. Prostate-specific deletion of Pten and Pgc1 α in the mouse epithelium.	56
Figure I 11. Sequence homology and domains found in PGC1 α , PGC1 β , and PRC members of PGC1 family of coactivators.	57
Figure I 12. Regulation of PGC1 α gene expression, activity and main biological functions triggered upon interaction with different transcription factors.	59
Figure I 14. PGC1 α expression levels vary within the same and different cancer types..	62
Figure I 15. Types of cell-cell communication.	64
Figure I 16. Classification of extracellular vesicles according to biogenesis and size. ...	67
Figure I 17. Biogenesis of exosomes.	68
Figure I 18. ESCRT machinery is composed of ESCRT sub-complexes that mediate membrane scission and cargo sorting.	69
Figure I 19. MVs formation and release through the outward budding of the plasma membrane.	70
Figure I 20. Apoptotic cell disassembly into apoptotic bodies.	71
Figure I 21. Role of EVs along the different stages of cancer and the crosstalk established between different cell populations.	74
Figure I 22. Overview of the three major mechanisms of protein secretion found in cells.	77
Figure I 23. Type I, II and III interferon signaling transduction.	80
Figure I 24. Cell-intrinsic and extrinsic anti-tumor roles of interferons.	81

Figures Objectives

Figure O 1. Transcriptional control of the PCa cell secretome	87
---	----

Figures Materials & Methods

Figure M 1. Overview of the TRIPZ inducible lentiviral vector (Dharmacon).	92
Figure M 2. Culture settings for the generation of cell secretomes.....	96
Figure M 3. Secretomes obtained from PGC1 α -expressing and non-expressing cells are mixed in different proportions and used for treating recipient cells.....	97
Figure M 4. Cell secretome concentration and separation through 10 K Amicon tubes.....	98
Figure M 5. Seeding conditions for the production of EVs.....	99
Figure M 6. Protocol followed for the isolation of EVs.	100
Figure M 7. Protocol followed for obtaining the soluble factors.	101
Figure M 8. Proliferation assay by crystal violet staining to assess the impact of whole secretome, EVs or SFs in recipient cells.....	101
Figure M 9. Boyden chamber migration assay to assess the impact of whole secretome or EVs on the migration ability of recipient cells.....	102
Figure M 10. Wound healing assay to evaluate migration capacity of recipient cells treated with differential secretomes.....	103
Figure M 11. Migration assay in Boyden chambers using co-cultures of producer and recipient cells.....	104
Figure M 12. DiIC ₁₈ (3)-labelled EVs produced by PGC1 α -expressing and non-expressing cells are used for treating recipient cells and assess uptake by flow cytometry.	104
Figure M 13. RNA sequencing experimental settings.....	107
Figure M 14. Measurement of IFN- β in cell secretomes produced by PGC1 α -expressing and non-expressing cells by ELISA.....	109
Figure M 15. Experimental settings followed for LC-MS proteomics analysis.	112
Figure M 16. In vivo metastasis assay.....	117
Figure M 17. In vivo metastasis assay.....	118

Figures Results

Figure R 1. Experimental setting and system to assess the biological role of PCa cells secretome.....	125
Figure R 2. The PGC1 α -driven cell secretome reduces 2D proliferation of a panel of aggressive PCa cell lines.	127
Figure R 3. Proliferation of PC3 recipient cells educated with secretomes produced by doxycycline treated and untreated PC3 producer cells.....	128
Figure R 4. Cell proliferation of recipient cells is recovered when treated with ever-increasing proportions of secretome derived from non-PGC1 α expressing cells.....	129
Figure R 5. Effect of the secretome in cell migration..	130
Figure R 6. PGC1 α cell-extrinsic anti-proliferative effect is dependent on ERR α	132
Figure R 7. The cell extrinsic PGC1 α anti-proliferative effect is observed in the secretome fraction containing molecules bigger than 10 KDa.	133
Figure R 8. Schematic timeline of the optimized experimental conditions set to yield EVs from PCa cells.	136
Figure R 9. Western blot analysis of EVs derived from PCa cells confirms sample purity.	137
Figure R 10. Electron microscopy characterization of EVs from PCa cells..	138
Figure R 11. Electron microscopy characterization of EVs produced by doxycycline-induced and non-induced PC3 TRIPZ cells.	139
Figure R 12. Physical characterization by NTA of EVs produced by PC3 PGC1 α -expressing and non-expressing cells.	139
Figure R 13. NTA characterization of EVs isolated from PC3 PGC1 α -expressing and non-expressing cell lines in combination with ERR α deletion.....	140
Figure R 14. EVs protein content measured by BCA.....	141
Figure R 15. Correlation analysis between number of EVs and EVs protein content..	141
Figure R 16. Gene Ontology analysis of the genes encoding for the proteins found altered in EVs upon expression of PGC1 α in the producer cell lines.....	144
Figure R 17. Gene set enrichment analysis of the genes encoding for the significantly altered proteins associated to EVs.....	145
Figure R 18. EVs uptake by PC3 recipient cells..	146
Figure R 19. Impact of EVs in 2D proliferation.....	147
Figure R 20. Impact of EVs in the migration capacity of recipient cells..	148
Figure R 21. In vivo study of the impact of EVs on the preparation of the pre-metastatic niche.	149
Figure R 22. Ex vivo luciferase signal intensity of PCa cells measured in legs (A), lungs (B), ribs (C) and spinal cord (D) after mice sacrifice, at day 35.	150
Figure R 23. Candidates identified by EVs proteomics analysis are transcriptionally regulated by PGC1 α in PCa producer cells. RT-qPCR of CD44, STXBP2 and ADAM10 genes.	151

Figure R 24. The PGC1 α -ERR α transcriptional axis regulates the genes encoding for the proteins differentially present in PCa EVs.....	152
Figure R 25. Doxycycline treatment exerts no effect on expression levels of candidate genes.....	153
Figure R 26. Correlation analyses between CLDN3, KPNA2, STXBP2 and ATP1B1 against PGC1A mRNA expression in PCa patients.....	154
Figure R 27. PGC1 α -derived SFs reduce 2D growth of aggressive PCa cells.....	157
Figure R 28. Schematic view of the protocol followed for the in vivo metastasis assay using SFs produced by PCa cells with differential expression of PGC1 α	158
Figure R 29. Study of the impact of the SFs on the preparation of the pre-metastatic niche.....	159
Figure R 30. Overview of the experimental time-points set for obtaining pure cell secretomes and performing label-free LC-MS proteomics analysis.	160
Figure R 31. Western blot analysis of the secretome quality produced by PC3 TRIPZ PGC1A cells.	161
Figure R 32. Western blot analysis of proteins found altered in the proteomics analysis of the secretome produced by PGC1 α -expressing and non-expressing PC3 producer cells.....	166
Figure R 33. Gene ontology analysis showing the biological processes related to the genes encoding for the proteins found differentially present in the cell secretomes..	167
Figure R 34. Gene ontology analysis showing the cellular component (A) and molecular functions (B) associated to the genes encoding for the proteins found differentially present in the cell secretomes obtained from PGC1 α -expressing and non-expressing PCa cell lines.....	168
Figure R 35. Molecular functions and transcription factor enrichment analyses of upregulated genes encoding for the proteomics-identified candidates.....	169
Figure R 36. Molecular functions and transcription factor enrichment analyses of downregulated genes encoding for the proteomics-identified candidates.	170
Figure R 37. RT-qPCR analysis reveals that genes coding for altered proteins found in the cell secretome are transcriptionally regulated by PGC1 α in the producer cells..	171
Figure R 38. ERR α mediates transcriptional regulation of most of the genes encoding for the altered proteins identified in the cell secretome.....	172
Figure R 39. Silencing of c-MYC in producer cell lines. m.....	173
Figure R 40. Gene expression levels analysis by RT-qPCR of proteomics candidates in control PC3 producer cell lines reveal no changes in gene expression produced by the treatment with doxycycline.....	173
Figure R 41. Cancertool enrichment analysis of the genes encoding for the proteins differentially present in the proteomics of the TIL of KO and DKO mice.....	176
Figure R 42. Analyses of the genes found correlated to PGC1A in PCa datasets.....	178
Figure R 43. Correlation analysis in PCa datasets shows no relation between PGC1A and SRM.....	179

Figure R 44. Overview of the experimental setting followed for performing RNA sequencing analysis of PC3 recipient cells treated with differential secretomes.....	180
Figure R 45. PCA from the RNA sequencing analysis performed on PC3 recipient cells treated with differential secretomes..	181
Figure R 46. Analysis of the RNA sequencing performed on PC3 cells treated with differential secretomes..	182
Figure R 47. Pathway and GO biological process analyses of the genes found altered in recipient cells reveal an enrichment of functions linked to metabolism, immune system and cell death.....	185
Figure R 48. Transcription factor enrichment analysis of the genes found altered in recipient cells by RNA sequencing analysis.	186
Figure R 49. RT-qPCR analysis of genes found altered by RNA sequencing analysis of recipient cells.....	187
Figure R 50. RT-qPCR analysis of genes found altered by RNA sequencing analysis of recipient cells.....	188
Figure R 51. Gene expression levels of candidates found altered by RNA sequencing analysis of recipient cells assessed at later secretome treatment time-points..	189
Figure R 52. Experimental overview of the steps followed for performing RNA sequencing of PGC1 α -expressing and non-expressing PCa cells.....	193
Figure R 53. PCA and heatmap displaying two clusters of samples and genes identified by RNA sequencing analysis of PGC1 α -expressing and non-expressing PCa cells.....	193
Figure R 54. Venn diagram and volcano plot of the RNA sequencing analysis performed on PGC1 α -expressing and non-expressing PC3 cells.....	194
Figure R 55. Gene ontology analysis displaying biological process and pathway enrichment from the genes found differentially expressed by RNA sequencing of PGC1 α -expressing and non-expressing PCa cells..	195
Figure R 56. Gene Set Enrichment Analysis reveals an increase of type I and type II IFN response in PGC1 α -expressing PC3 cells.....	196
Figure R 57. MAZ and ERR α emerge among the top TFs to mediate transcriptional control of the genes found differentially expressed in PGC1 α -expressing and non-expressing PC3 cells.	196
Figure R 58. Enrichment analyses of the genes found upregulated upon expression of PGC1 α in PC3 cells.....	197
Figure R 59. Enrichment analyses of the genes found downregulated upon expression of PGC1 α in PC3 cells.....	198
Figure R 60. RT-qPCR analysis reveals that IFN-related genes are upregulated in PGC1 α -expressing cells compared to non-expressing ones.....	199
Figure R 61. Doxycycline treatment does not alter expression levels of candidate genes.	199

Figure R 62. RT-qPCR analysis of IFN-related genes in an in vivo xenograft mouse model.....	200
Figure R 63. RT-qPCR analysis in KO and DKO mice of gene candidates identified by RNA sequencing and proteomics analysis of the cell secretome from PGC1 α -expressing and non-expressing cells.....	201
Figure R 64. JAK-STAT signaling pathway is activated upon expression of PGC1 α in vitro.....	202
Figure R 65. Western blot time-course analysis of JAK-STAT signaling pathway reveals STAT1 activation is downstream c-MYC.	203
Figure R 66. Timeline of the experimental flow to produce and collect the secretomes produced by PGC1 α -expressing and non-expressing cells for measuring levels of IFN- β	203
Figure R 67. IFN- β levels are increased in the secretomes produced by PGC1 α -expressing PC3 cells compared to the non-expressing ones..	205

Figures Discussion

Figure D 1. Heterogeneity of signaling networks. 213

Figure D 2. Overview of the normal (A) and tumor intersticium (B).. 222

Figure D 3. EVs as surrogate markers of PCa..... 226

Figure D 4. Preparation of the pre-metastatic niches.. 227

Figure D 5. Autocrine and paracrine effects of the cell secretome. 234

Figure D 6. PGC1 α -driven cell intrinsic and cell-extrinsic phenomena that contribute to the suppression of PCa aggressiveness..... 235

Figure D 7. The PGC1 α -driven anti-tumoral effect might be restored through different strategies..... 240

Figure D 8. Deconstructing tumors for precision medicine. 243

Tables Introduction

Table I 1. Stage-matched therapeutic strategies for PCa	51
---	----

Tables Materials & Methods

Table M 1. Cell lines used in this work including their main characteristics.	91
Table M 2. Viral packaging vectors, TK-GFP-luciferase plasmid and reagents used for the retroviral infection of PC3 cells and generation of luciferin-inducible PC3 TGL cells.	94
Table M 3. Commercial information, dose and usage of doxycycline employed in the present work.	95
Table M 4. Information about primer sequences and correspondent probe number obtained from Universal Probe Library (Roche).....	106
Table M 5. References and preparation of primary and secondary antibodies employed for Western Blotting.....	111

Tables Results

Table R 1. List of proteins differentially present in EVs produced by PGC1 α -expressing and non-expressing PC3 cells.....	143
Table R 2. Panel of proteins found significantly altered by proteomics analysis of the secretome produced by PGC1 α -expressing and non-expressing PCa cell lines.	162
Table R 3. Proteomics analysis identifies a panel of 44 proteins differentially present in TIL obtained from KO and DKO mice..	175
Table R 4. Correlation analysis of proteomics-identified candidates against PGC1A in PCa datasets.....	177
Table R 5. Genes found differentially expressed by RNA sequencing analysis of PC3 recipient cell lines treated with distinct secretomes for 48 hours.....	183
Table R 6. Genes found enriched in the GO biological process analysis.	186

Tables Discussion

Table D 1. Experimental details of experiments involving EVs-injection into mice.....	229
---	-----

Tables Annex

Table 1. Transcriptional analysis of PGC1 α -expressing and non-expressing cells. FC: fold change.....	299
---	-----

Summary

The transcriptional co-regulator peroxisome proliferator-activated receptor gamma co-activator 1 alpha (PGC1 α) was shown to exert a tumor suppressive role in prostate cancer (PCa) by means of regulating the balance between anabolism and catabolism. This anti-tumoral activity happened to be dependent on its partner oestrogen-related receptor alpha (ERR α). Classically, the roles attributed to PGC1 α under physiological and pathological conditions were linked to the regulation of metabolic processes. Yet, in the present work we have deciphered that the transcriptional reprogramming induced by PGC1 α in PCa epithelial cells extends to novel functions. We show that the anti-tumoral effects of PGC1 α seem to be driven by cell-intrinsic and cell-extrinsic phenomena that include the regulation of cell cycle, interferon response and the secretome composition. Indeed, secretome fractionation into extracellular vesicles (EVs) and soluble factors (SFs) revealed a differential protein composition upon expression of PGC1 α . This secretome fractionation also drove us to conclude that despite EVs produced by PGC1 α -expressing and non-expressing cells showed no distinct biological roles, they could be used as non-invasive bystanders of PCa progression. We also show that PGC1 α -driven SFs seem to promote metastasis formation *in vivo*. On the other hand, PGC1 α -ERR α -regulated SFs were shown to suppress proliferation capacity of PCa cells *in vitro*. Overall, data further suggests that PGC1 α -regulated SFs (probably involving IFN- β secretion) activate autocrine and paracrine tumor-suppressive mechanisms in PCa cells.

Hence, due to the tumor suppressive role and stratification potential of PGC1 α , we believe that understanding its contribution on the regulation of the cell secretome could allow us to decipher the cell communication networks established between PCa epithelial cells and the stromal compartment. This could open new avenues for the identification of non-invasive biomarkers of PCa progression as well as the development of novel therapeutic strategies to treat aggressive PCa.

The background features a collection of overlapping, semi-transparent green circles of various sizes, resembling watercolor splatters. Superimposed on this are several blue line graphs with circular nodes at their vertices. Some lines are thick and dark blue, while others are thin and light blue. The overall aesthetic is clean, modern, and data-oriented.

Introduction



I Cancer

The term “cancer” derives from the Greek word “karkinoma”, which means crab and was first used by the Greek physician Hippocrates (460-370 BC) to describe crab-like projections he observed in what happened to be breast tumors. It was later that roman physician Celsus (25-50 BC) translated the Greek word into the Latin term of crab, “cancer”. We now know that cancer is a heterogeneous family of diseases that can be originated from almost any cell type of the body, being a sole tissue able to give rise to several cancer types with unique features. Cancer cells proliferate in an uncontrolled manner to form an abnormal cellular mass known as tumor. To progress, tumors need to go through a series of genetic and epigenetic changes that will grant malignant cells with novel adaptative features (Weinberg R 1996; Hanahan and Weinberg 2011). These traits make cancer study, diagnosis, and treatment all the more challenging.

According to the World Health Organization (WHO, with data obtained from the International Agency for Research in Cancer, IARC on the Globocan 2020), over 19 million new cancer cases were diagnosed in 2020 worldwide (**Fig 1**). Among the most diagnosed types of cancers, breast (11.7%), lung (11.4%), colorectal (10%), prostate (7.3%), stomach (5.6%), liver (4.7%) and cervix (3.1%) were included (gco.iarc.fr).

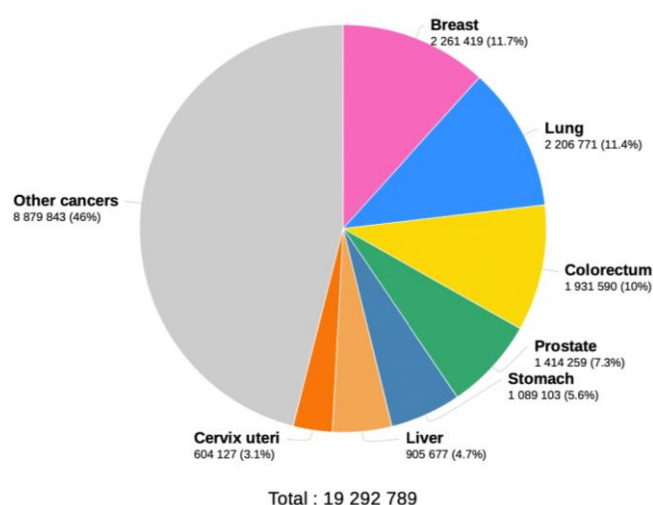


Figure I 1. Total number of cancer cases diagnosed in 2020 worldwide. Both sexes and all ages are included. Data source: Globocan 2020. Graph production: Global Cancer Observatory (<http://gco.iarc.fr>).

Despite some cancers have experienced reduced mortality due to the early diagnosis and availability of more efficient therapies identified through the extensive research (Arnold et al. 2019), it is estimated that by year 2040, cancer deaths worldwide will be close to 30.2 million. A distribution of certain types of cancers can be observed based on the socio-economic development of the countries, thus evidencing the impact of environmental and lifestyle factors on promoting the disease (Bray et al. 2018). Overall, numbers reflect the urge of fostering cancer research and prevention programs to limit cancer increasing morbidity and mortality.

Tumor progression and hallmarks of cancer

Cancer is accompanied by changes in the genome (Vogelstein and Kinzler 2004). In the last decades a great number of genes involved in tumor progression have been identified to be altered in different types of cancer. Tumor formation can take decades and it is usually originated with the retention of genetic alterations that endow cells with proliferation advantages compared to rest of the cells within the tissue (**Fig 2**). After years, these cells may continue to expand due to the accumulation of additional alterations that lead to the formation of pre-malignant lesions such as hyperplasia and dysplasia. Cells may become more abnormal in growth and appearance due to the accumulation of genetic alterations, becoming a tumor mass. If this tumor does not break through the basal membrane and remains in the tissue of origin, it is called *in-situ* cancer. However, some cells within the mass may acquire specific traits that endow them with the capacity of invading adjacent tissues and reaching the blood or lymphatic systems. Among them, some may be even capable of surviving and progressing in distant organs, constituting what is known as metastatic tumors (Weinberg R 1996). It is important to highlight that no sole genetic alteration is responsible for the origin of cancer, but rather the accumulation of various genetic or epigenetic defects, which are usually greater in more advanced or highly metastatic cancers (Yokota Jun 2000). In this regard, three types of genes have been described as relevant in tumorigenesis: oncogenes, tumor-suppressor genes, and genome stability genes. Gain of function of oncogenes and loss of function alterations of tumor suppressor genes are both related to an exacerbated cell growth that drives tumorigenesis. On the other hand, stability genes (also known as caretakers) are responsible for DNA repairing processes within the cells and therefore, when inactivated, mutation rates in other types of genes dramatically increase (Vogelstein and Kinzler 2004).

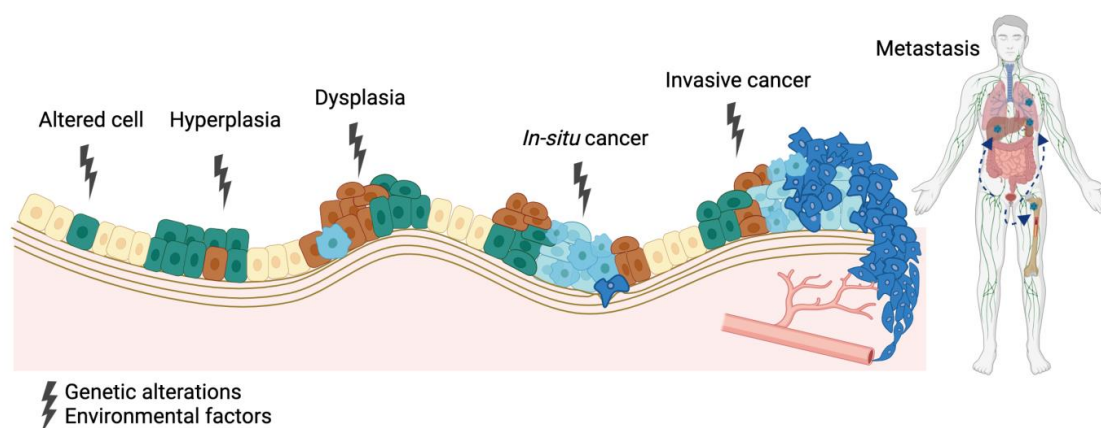


Figure 1 2. Overview of the tumor progression cascade.

With the aim of shaping the complex body of knowledge generated in the field of cancer research, Douglas Hanahan and Robert A. Weinberg proposed key features that cells must gain in order to sustain malignant growth and that were proposed to be shared in most of the existing cancer types: 1) self-sufficiency in growth signals, 2) insensitivity to anti-growth signals, 3) evasion of programmed cell death, 4) limitless replicative potential, 5) sustained angiogenesis, 6) tissue invasion and metastasis 7) evasion of immune destruction and 8) reprogramming of energy



metabolism, 9) unlocking phenotypic metabolism, and 10) senescent cells (Hanahan and Weinberg 2000) (Hanahan and Weinberg 2011; Hanahan 2022) (**Fig 3**). In addition, four enabling features crucial for the acquisition of the hallmark capabilities were identified: genome instability which, concomitantly leads to higher mutation rates, inflammation, nonmutational epigenetic reprogramming and polymorphic microbiomes (Hanahan and Weinberg 2011; Hanahan 2022).

Already in 1863, pathologist Rudolf Virchow described the presence of leukocytes in neoplastic samples, thus establishing a link between inflammation and cancer (Balkwill and Mantovani 2000). Research in the past years has supported the hypothesis of Virchow, and we do know now that tumor-associated inflammatory responses promote cancer through different mechanisms that include the production of pro-survival factors, ECM-modifying enzymes and reactive oxygen species that induced DNA damage in proliferating cells (Hanahan and Weinberg 2011). Inflammation responses can be triggered by cell-extrinsic events, via exposure to environmental factors, pathogens, and diet, (Bald et al. 2014; Ernst and Gold 2000; Zitvogel, Pietrocola, and Kroemer 2017) and by cell-intrinsic factors, such as oncogenic mutations that orchestrate inflammatory programs essential for the tumor progression (Soucek et al. 2007).

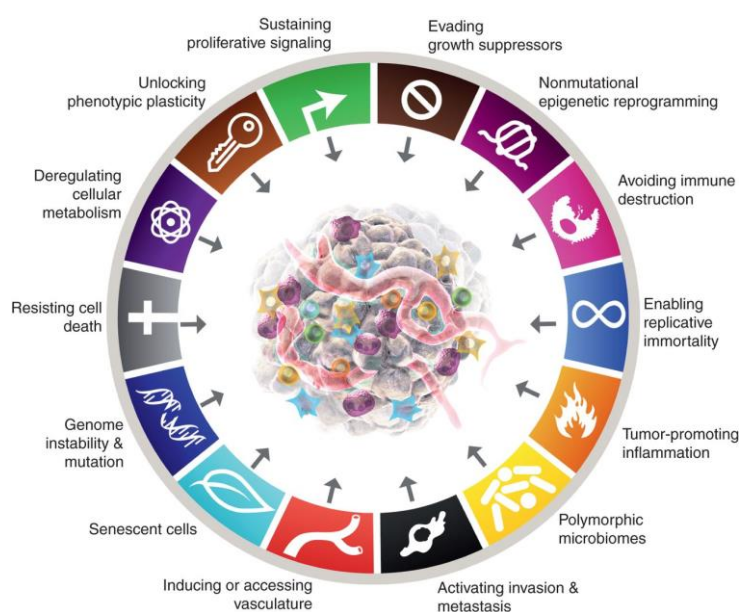


Figure 1.3. Revised hallmarks of cancer proposed by Hanahan and Weinberg. Hanahan D. *Cancer Discovery* (2022).

Yet, beyond the malignant cell itself, interactions established between cancer cells and with their environment evidence that both cell-autonomous and non-cell autonomous signaling circuits govern progression of tumors (Hanahan and Weinberg 2011; Hanahan 2022). The cancer cell secretome is involved in the recruitment of stromal cells, in promoting ECM remodeling and cell growth, among other processes, hence showing to be pivotal during the different stages of tumor progression (Bafico et al. 2005; Cox and Eler 2011; Cerezo-Wallis et al. 2020). These concepts will be further addressed in coming sections of the present thesis work.

Tumor progression to metastasis

Cancer progression towards metastasis is accompanied by a series of steps that malignant cells need to overcome and that culminate with the successful settlement and progression of primary tumor cells in a new organ (Valastyan and Weinberg 2011). These steps include (**Figl 4**): 1) local invasion, by which primary tumor cells penetrate the basal membrane and invade adjacent tissues, 2) intravasation to the blood or lymphatic vessels, 3) survival in circulation, 4) arrest at distant organ sites, 5) extravasation into the recipient tissue, 6) survival and formation of micrometastasis at foreign organs and 7) metastatic colonization.

Each step of the metastatic cascade is inefficient and under the influence of the microenvironment, which may contribute or suppress metastatic progression. In addition, metastatic tumor cells need to acquire traits that allow them to survive and progress in the new environments they enter (Joyce and Pollard 2009).

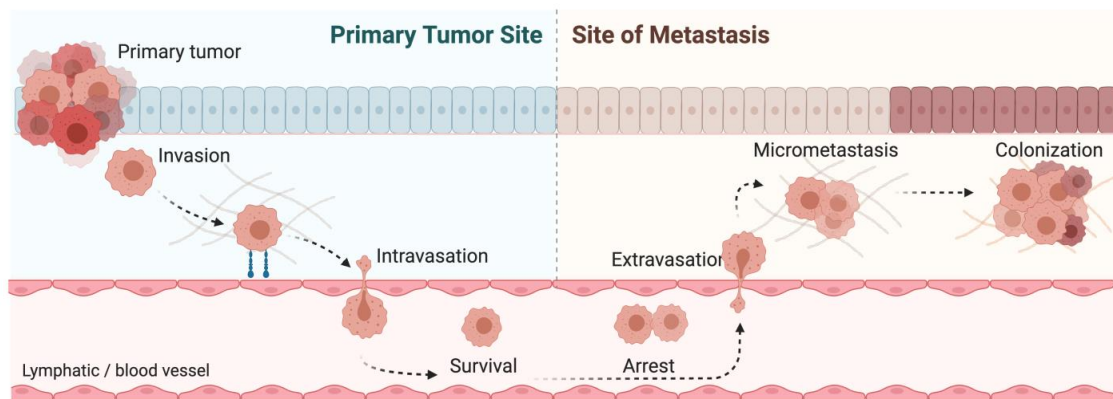


Figure I 4. The metastatic cascade.

II Prostate cancer

II.1 Human prostate anatomy

The prostate gland is part of the male reproductive system, and it is the largest male accessory gland. The normal prostate weights close to 20 grams, is located beneath the bladder and due to its morphology, it has classically been described as "walnut-shaped" (**Figl 5A**). The gland encircles the proximal urethra as it exists from the urinary bladder and it secretes a thin and slightly alkaline fluid that constitutes part of the seminal plasma, which ensures sperm viability through its way from the male urogenital tract into the female reproductive tract (C. H. Lee, Akin-Olugbade, and Kirschenbaum 2011; Bromfield 2014).

Four histological regions can be distinguished in the human prostate gland (**Figl 5B**): the central zone (located in the base of the prostate, and that accounts for the 25% of the glandular tissue), transition zone (composed of two small lobules surrounding the proximal urethra and accounts 5% of the total glandular mass), peripheral zone (that surrounds the distal urethra and



comprises 70% of the glandular tissue) and finally, the fibromuscular stroma, which forms a pseudo-capsule that surrounds the gland (Bhavsar and Verma 2014; Ittmann 2018).

The prostate glandular epithelium is composed of acini (glands) and ducts, where three types of epithelial cells can be distinguished: luminal, basal, and neuroendocrine cells (**Figl 5C**).

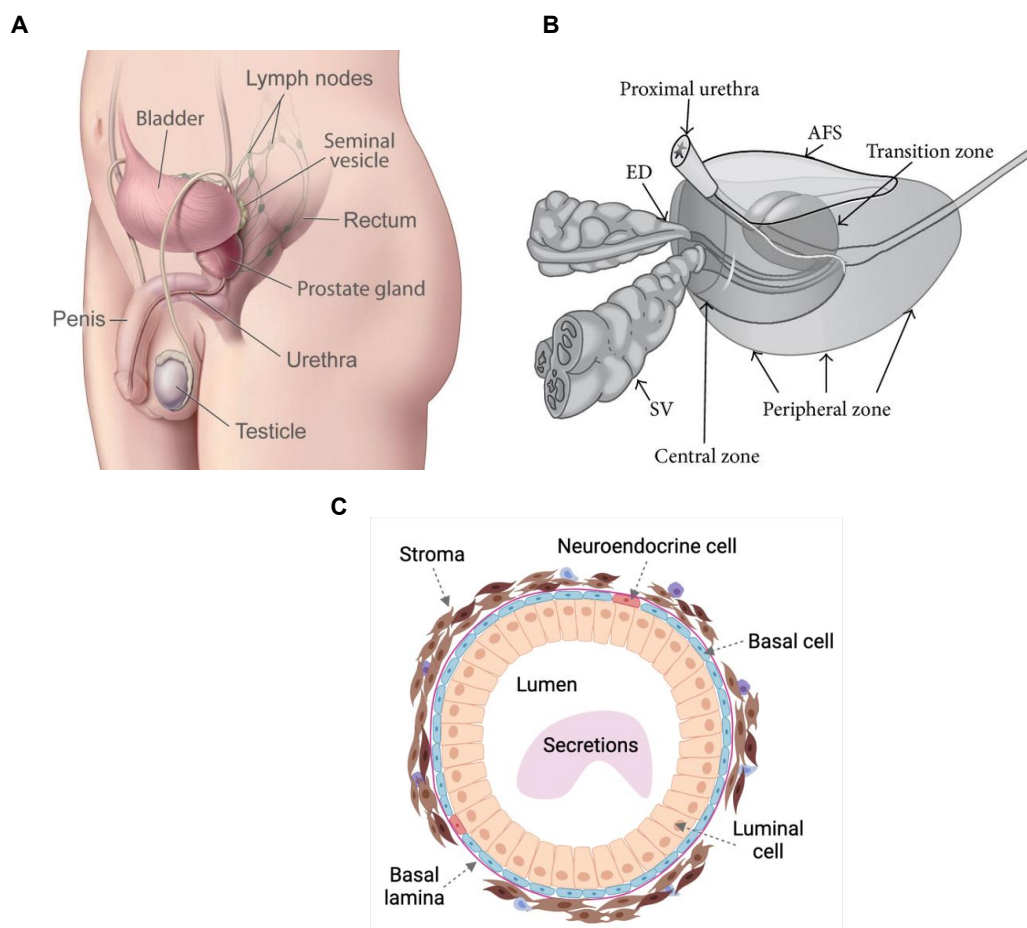


Figure 15. Anatomy and histology of the human reproductive systems. A-B. Localization of the prostate gland (A) and its detailed anatomy (B). **C.** Histological section of the prostate duct and surrounding stroma displaying the different cellular types that compose the gland. AFS: anterior fibromuscular stroma, SV: seminal vesicles, ED: ejaculatory ducts. Images adapted from (in panel order A and B): National Cancer Institute (NIH). Bhavsar, A. & Verma, S. *Biomed Research International* (2014).

Column-shaped luminal cells are in the luminal side of the glands and have secretory functions, contributing to the formation of the seminal fluid. Interestingly, these are the only type of cells in the prostate that express and secrete prostate-specific antigen (PSA). On the other hand, basal cells are located close to the basal membrane and together with the luminal cells, they constitute the major cell types in the prostate epithelium. In a minor proportion (close to 1%), neuroendocrine cells can be found scattered among basal and luminal cells. Finally, the stromal compartment of the prostate is highly fibrous and abundant in smooth muscle cells, fibroblasts, blood vessels and nerves (Ittmann 2018; Y. H. Huang, Zhang, and Huang 2019).



II.2 Prostate cancer epidemiology and risk factors

According to the GLOBOCAN 2020 data, prostate cancer (PCa) is the second most frequent cancer diagnosed in men after lung cancer. In 2020, more than 1.4 million men were diagnosed with PCa worldwide, and it caused 375,304 fatalities, thus making it the fifth leading cause of cancer-related deaths among men.

PCa aetiology is unknown, but incidence is intimately associated with ageing: 1 in 350 men under 50 years are diagnosed with PCa, and it increases to up to 1 in 52 men for ages comprised 50 to 59 years and close to 1 in 2 men for ages over 65. Besides from advanced age, other factors are known to contribute to the disease appearance, including ethnicity, family history, diet, obesity, physical inactivity, inflammation, infections, and exposure to chemicals among others (Rawla 2019). With no doubt, prevention programs such as PSA testing together with the increasing therapy possibilities have reduced the number of PCa fatalities, however, still no cure exists for men suffering from more advanced disease (Catalona 2018).

II.3 Prostate cancer diagnosis, pathology, and treatment

II.3.1 Prostate cancer diagnosis and pathology

PCa is a highly heterogeneous disease in what it comes to symptomatology and progression; it ranges from low-grade asymptomatic patients (that are often diagnosed through PSA screening prevention programs) to highly aggressive metastatic tumors. Diagnosis and staging are fundamental for designing clinical and care strategies for patients, and it has classically been done by digital rectal examination (DRE) and measurement of PSA blood levels. DRE method has its limitations; it often happens that PCa patients have a normal DRE but present elevated PSA levels that lead to the disease suspicion and diagnosis. PSA is a glycoprotein with serine proteinase enzymatic activity that is abundantly secreted by the epithelial compartment of the prostate gland, making it one of the three most abundant secreted proteins that compose the semen (Christersson, Thulin, and Siegbahn 2017). Levels of PSA in serum usually increase with age, due to architectural distortions of the gland that allow PSA release into the bloodstream. Elevated PSA levels can be due to benign conditions such as prostatitis and benign prostatic hyperplasia (BPH), as well as to malignant ones, such as PCa. Therefore, PSA cannot be considered as a PCa-specific marker; indeed, there is still no consensus in the field on where to establish a cut-off threshold that allows distinguishing between benign and malignant prostate conditions. Traditionally, PSA cut-off value has been set in 4.0 ng/ml, although men with lower PSA values seem to have 12-23% probability of being diagnosed with PCa. Men with PSA levels ranging 4.1-10.0 ng/ml are in the "grey zone", and usually a biopsy of the prostate needs to be done for confirming the presence or absence of malignant lesions. Close to 30-35% of these men are diagnosed with PCa, thus evidencing the need of finding specific biomarkers for diagnosis and for avoiding unnecessary biopsies. Finally, close to 67% of the men with PSA values greater

than 10 ng/ml present PCa. Hence, the probability of being diagnosed with PCa increases with increasing PSA serum levels (Pienta 2009; R. Lee et al. 2006; Catalona 2018).

Yet, for a definitive PCa diagnosis a transrectal ultrasound (TRUS) guided biopsy is performed (Descotes 2019). Biopsies are histopathologically evaluated and classified by two methods: Gleason Score and the TNM (tumor, node, metastasis) system (Shen and Abate-Shen 2010). However, according to the International Society of Urological Pathology (ISUP) before performing a biopsy, a multiparametric magnetic resonance imaging (MRI) should be done to locate suspicious lesions that could be of clinical relevance (Rouvière et al. 2019).

Gleason scoring is analyzed by H&E staining of the prostate tissue and based on the histological arrangement pattern of carcinoma cells, a score is given. Five basic grade patterns are used to generate a histologic score that ranges 2-10 and which is calculated by adding the two most common patterns found in the tissue section. If only one grade pattern is found, it is multiplied by two to obtain the score (Gleason and Mellinger 1974; Humphrey 2004). Despite the Gleason grading system was established around the 1970's, it continues to be a powerful diagnosis tool for PCa (**Figl 6**).

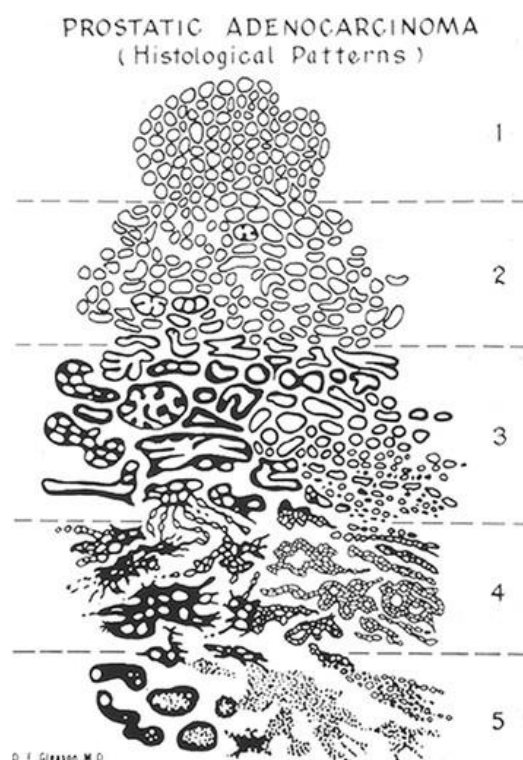


Figure I 6. Diagram of the original Gleason Grading system by Dr. Donald Gleason

In the last years, Gleason Score system has undergone revisions that have made grading simpler. Among these changes, Gleason pattern 1 was removed and high-grade components present in any quantity, should be included as it indicates a high probability of finding high-grade tumor in the prostate. In addition, low-grade patterns that occupy less than 5% of the tumoral mass should not be reported. These points are key for producing Gleason scores from needle

biopsies (N. Chen and Zhou 2016). The updated Gleason Score includes five grade groups that can be found in **Fig 7**.

Most of the PCa diagnosed are acinar adenocarcinomas, although other variants exist, including ductal adenocarcinomas, adenosquamous and squamous carcinoma, mucinous carcinoma signet ring carcinoma, neuroendocrine carcinoma, basaloid and adenoid carcinomas, sarcomatoid carcinoma, lymphoepithelioma-like and urothelial carcinomas (Grignon 2004).

Once PCa has been diagnosed, it is crucial to find out if cancer cells have spread to other organs or if they remain in the gland. For that, TNM system of classification is applied considering the following points: if it is organ-confined (T1-T4), if carcinoma cells have spread to the lymph nodes (N0-N1) and if there is presence of distant metastasis (M0-M1a-c) (Ohori et al., n.d.; Shen and Abate-Shen 2010).

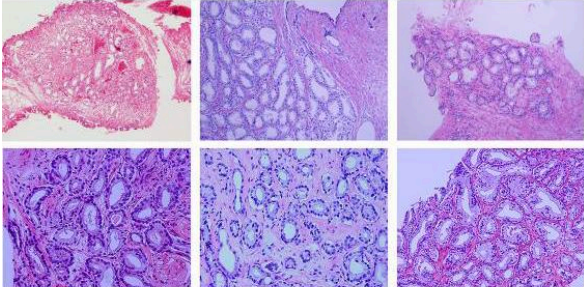
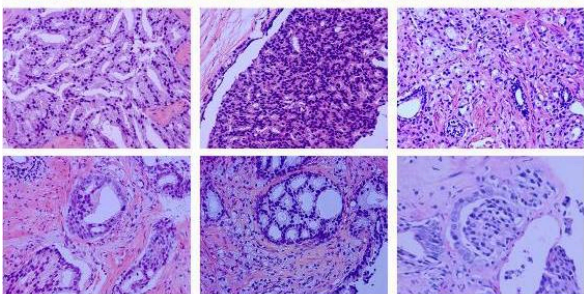
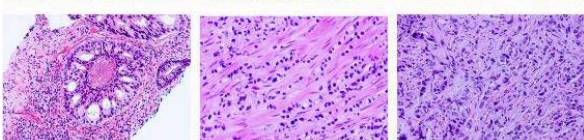
	Gleason patterns 1-3 distinct, discrete, individual glands	Gleason score ≤ 6	Grade group I
	Gleason pattern 4 fused, cribriform, or poorly-formed glands, or glomerular	Gleason score 3+4=7	Grade group II
	Gleason pattern 5 comedo necrosis, cords, sheets, solid nests, single cells	Gleason score 4+4=8 3+5=8 5+3=8	Grade group III
		Gleason score 4+4=8 3+5=8 5+3=8	Grade group IV
		Gleason score 4+5=9 5+4=9 5+5=10	Grade group V

Figure 17. Revised Gleason grading for diagnosis of PCa. Chen and Zhou. *Chinese Journal of Cancer Research* (2016).

II.3.2 Prostate cancer treatment

Based on the TNM system, Gleason score, PSA levels and DRE, tumor stage is determined, and this is fundamental for choosing the most suitable therapeutic option. Due to the prevention programs, PCa diagnosis most often occurs at early stages, when the disease is latent or indolent. Low-grade Gleason carcinomas are considered of low risk and usually do not require treatment; therefore, they can be managed through active surveillance. But a fraction of these cancers does progress, and thus, therapy options ought to be considered based on the tumor stage (**Table 11**).



Table 1. Stage-matched therapeutic strategies for PCa. ²²³Ra, radium-223; M0 CRPC, non-metastatic castration-resistant prostate cancer; RT, radiotherapy. Parker et al. *Annals of Oncology* (2020).

Localised disease	Low risk	Active surveillance Brachytherapy RP Radical RT
	Intermediate risk	RP Radical RT ± neoadjuvant ADT Brachytherapy Active surveillance
	High risk	Long-term ADT + radical RT ± neoadjuvant docetaxel RP + pelvic lymphadenectomy
Locally advanced disease		Neoadjuvant ADT + radical RT + adjuvant ADT ± neoadjuvant docetaxel RP + pelvic lymphadenectomy
M0 CRPC	High risk	ADT + apalutamide ADT + darolutamide ADT + enzalutamide
Metastatic disease	Hormone-naive	ADT + abiraterone ADT + docetaxel ADT + enzalutamide ADT + apalutamide RT for low volume ADT alone for frail patients who cannot tolerate the above treatments Bone health agent
	Castration-resistant (first line)	Abiraterone Docetaxel Enzalutamide ²²³ Ra for patients unfit for above treatments (and bone- only metastases)
	Second line or post-docetaxel	Abiraterone Cabazitaxel Enzalutamide ²²³ Ra

PCa therapy options include radical prostatectomy (RP, surgical removal of the prostate), radiotherapy, brachytherapy (by which, radioactive material is set close to the tumor mass, allowing a higher radiation dose specifically in the tumor zone), chemotherapy and androgen deprivation therapies (ADT) (Shen and Abate-Shen 2010) (C. Parker et al. 2020). ADT is based on the discovery made 80 years ago that showed PCa tumors reliance on androgens (Huggins and Hodges 1941). ADT can be achieved by surgical removal of the testes (orchiectomy) or using luteinizing hormone releasing hormone (LHRH) agonists and antagonists that interfere with the hypothalamus-pituitary-gonadal axis and block the production of androgens.

In addition, inhibition of enzymes involved in the biosynthesis of testosterone or the use of anti-androgen molecules that prevent the binding of androgens to AR are other mechanisms for PCa hormonal treatments (Crawford et al. 2019). PCa tumors are highly dependent on androgens at initial and more advanced stages; therefore, ADT usually leads to tumor regression. Nonetheless, most of these tumors become resistant to ADT and start growing again, developing castration resistant prostate cancer (CRPC) (Imamura and Sadar 2016). Although new drugs have improved the therapeutic landscape for CRPC, still none of them has overcome resistance mechanisms developed by tumors, thus remaining an incurable form of PCa disease (Imamura and Sadar 2016).

Overall, one of the major challenges up to date in the field of PCa is the need of finding novel markers that can identify and stratify patients with low and high-risk of developing a more aggressive type of disease. This is a critical step for achieving a better clinical management of PCa patients.

II.4 Prostate cancer progression

Most of the tumors rising in the prostate are adenocarcinomas, and together with chronic prostatitis and post-inflammatory atrophy, they commonly rise in the peripheral zone of the gland. On the other hand, the transition zone of the prostate is typically enlarged in men with benign prostatic hyperplasia (BPH). Indeed, it is not unusual to find variable degrees of BPH in the prostates removed for the treatment of PCa (Ittmann 2018).

Genetic alterations in prostate epithelial cells drive the origin of PCa, and these accumulations lead to what is known as prostatic intraepithelial neoplasia (PIN). This condition is defined by the neoplastic growth of epithelial cells within the prostatic ducts or acini (Brawer 2005). Due to additional genetic errors, PIN can progress to high-grade prostatic intraepithelial neoplasia (HGPIN), a condition that is of clinical significance as it is accepted to be a precursor of prostate adenocarcinoma (Brawer 2005). Epithelial cells may acquire more aggressive features due to the accumulation of further genetic insults, and thus become able to disrupt the basal membrane and invade the surrounding stroma, establishing a local invasive carcinoma (Nardella et al. 2010). Carcinoma cells may remain confined in the prostate gland or spread to other organs, generating a metastatic tumor (**Fig 8**).

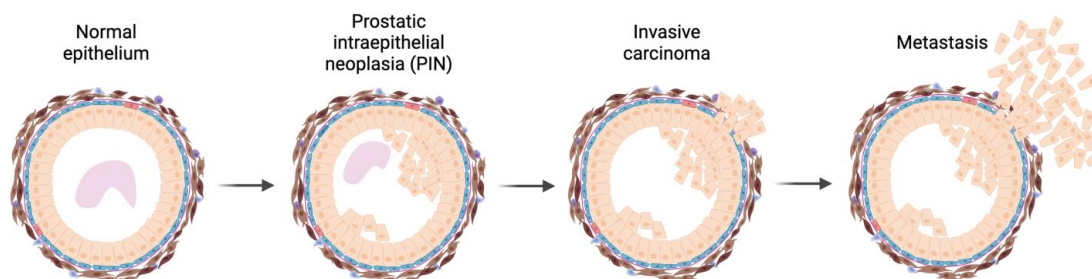


Figure I 8. Schematic representation of PCa progression.



Men suffering from localized PCa have a five-year survival rate close to 100%, however, around 17% of these patients develop advanced metastatic PCa, which dramatically sinks the five-year survival rate to 29.3%. The main sites of metastasis include bones, lymph nodes, lungs, liver, pleura, and adrenal glands, although bone remains the major target (90%) compared to other organs (Cui et al. 2020; Bubendorf et al. 2000; Damodaran, Kyriakopoulos, and Jarrard 2017). Within the bone structure, cancer cells are more prone to metastasize in trabecular bone, which can be found in ribs, pelvis, vertebrae, and the skull. For succeeding in the colonization, metastatic cells need first to arrest in vascular beds and bind to endothelial cells. The vascular structure in the trabecular bones is sinusoidal and with a reduced flow rate, thus enabling the process of cell attachment. Despite the clinical importance of bone metastasis, still not much is known about the molecular mechanisms driving it, although it seems that the bone microenvironment plays a crucial role (Edlund, Sung, and Chung 2004).

II.5 Molecular drivers of prostate cancer

In the last years, different molecular drivers involved in PCa progression have been identified. Androgens like testosterone, which are important for the sustenance of prostate cells are mainly synthesized by Leydig cells in the testes. Their synthesis is under the regulation of luteinizing hormone (LH) that is released by the pituitary gland, and which is regulated by gonadotropin-releasing hormone (GnRH). Circulating testosterone enters the prostate cells and is converted into 5 α -dihydrotestosterone (DHT), which binds to androgen receptor (AR) and are both translocated into the cell nucleus. Once in the nucleus, AR dimers bind to the androgen response elements (AREs) found in the promoter regions of AR-target genes (Tan et al. 2015). AR-target genes are important for the survival and growth of prostate cells under physiological and pathological conditions. Upregulation of AR happens in up to 85% of advanced PCa patients and reactivation of AR signaling pathway occurs through diverse mechanisms including the androgen-independent activation of AR, AR amplification or overexpression, AR posttranslational modifications, AR splicing variants and gain of function mutations in AR ligand-binding domain (Crawford et al. 2019; González del Alba et al. 2021). Finally, the conversion of adrenal androgens into testosterone and DHT can also be an alternative ligand source for sustaining AR signaling in hormone-deprived tumors (Stanbrough et al. 2006).

The epigenetic regulator enhancer of zeste homolog-2 (*EZH2*), a histone lysine methyltransferase catalytic subunit of the polycomb repressive complex 2 is frequently upregulated in PCa and contributes to all PCa phases, including PIN lesions and metastasis (Koh et al. 2010; Varambally et al. 2002). *EZH2* expression was shown to be stimulated by oncogene *MYC* (Koh et al. 2011). Indeed, *MYC* is highly expressed in PCa (close to 90% of primary PCa lesions), and this over-activity, which is mostly due to amplifications, can be evident in PIN lesions (Koh et al. 2010). Disrupted WNT signaling has also been reported in different stages of PCa (Robinson, 2015). Indeed, 22% of CRPC patients harbor genetic alterations in *APC* and *CTNNB1*, involved in the canonical WNT signaling activation (Murillo-Garzón and Kypta 2017).

Tumor suppressor genes retinoblastoma (*RB*) and tumor protein P53 (*TP53*) are altered in 21% and 40-50%, respectively of metastatic PCas (D. Robinson et al. 2015a). Indeed, combined loss of *RB* and *TP53*, is linked with a more aggressive type of neuroendocrine PCa (González del Alba et al. 2021). It is also not unusual to find alterations in DNA damage repair genes *BRCA1*, *BRCA2*, *ATM*, *CDK12* and *PALB2*, which appear mutated in close to 23% of metastatic PCas (González del Alba et al. 2021; Castro et al. 2013).

The tumor suppressor phosphatase and tensin homolog (PTEN) and PI3K signaling axis are one of the most altered pathways in primary PCas (Jamaspishvili et al. 2018). Malignant activation of PI3K-AKT-mTOR signaling pathway enables tumor formation, progression and promotes resistance to therapy, especially in CRPC (Bitting and Armstrong 2013). Indeed, deregulation of this pathway happens in 42% of localized PCa and 100% of advanced PCa (Taylor et al. 2010a). PTEN opposes PI3K-dependent signaling by means of dephosphorylating 3' position of secondary messenger phosphatidylinositol 3, 4, 5 triphosphate (PIP3) (Carracedo, Alimonti, and Pandolfi 2011). PIP2 conversion to PIP3 results in downstream activation of serine-threonine kinase AKT and mammalian target of rapamycin (mTOR) signaling cascades that further drive the activation or inhibition of a series of enzymes and transcription factors involved in the regulation of a large number of biological processes (**Figl 9**) (Shorning et al. 2020; Manning and Cantley 2007).

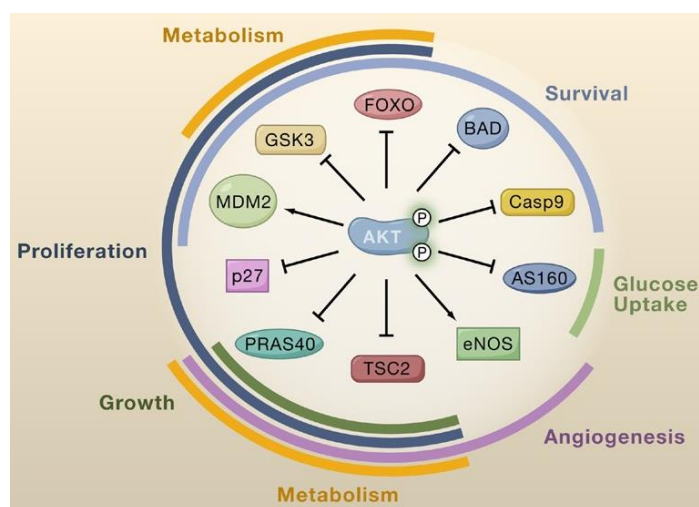


Figure 1 9. Cellular functions activated upon phosphorylation of AKT. FOXO: Forkhead Box O family of transcription factors, BAD: BCL2 associated agonist of cell death, Casp9: caspase 9, AS160: Akt substrate of 160 kDa, eNOS: endothelial nitric oxide synthase, TSC2: tuberous sclerosis complex 2, PRAS40: proline-rich AKT1 substrate 1, MDM2: mouse double minute 2, GSK3: glycogen synthase kinase 3. B. D. Manning, et al., *Cell*, 2007.

AR and PI3K are the most commonly deregulated pathways in PCa, and it seems that interactions between both pathways could be a mechanism contributing to therapy resistance (Crumbaker, Khoja, and Joshua 2017).

Besides its phosphatase activity, PTEN exerts other functions, including the regulation of genomic stability, cell cycle progression, differentiation, and gene expression (Carracedo,



Alimonti, and Pandolfi 2011). *PTEN* inactivation in PCa most frequently occurs due to biallelic deletions, although other mechanisms such as genomic rearrangements and epigenetic modifications have also been described (Jamaspishvili et al. 2018). *PTEN* is gradually lost throughout PCa progression, and it is associated to poor survival of patients. *PTEN* deletions or mutations account for 20% of primary PCa tumors, and 40-50% of CRPCs (Ferraldeschi et al. 2015; Jamaspishvili et al. 2018).

Using a genetically engineered mouse model (GEMM) with specific deletion of *Pten* in the prostate epithelium, it was shown that complete loss of the tumor suppressor leads to PIN lesions at three months of age. These mice develop invasive cancer at six months of age, but never undergo metastasis (Z. Chen et al. 2005). A PCa GEMMs in which *Pten* deletion was combined with *SMAD4* developed distal metastases, although not in the bone. Opposite to that, combined deletion of *Pten* and *p53* showed no metastasis. (Ding et al. 2011). Still, another GEMM in which *Pten* deficiency was combined with deletion of *p53* via surgical delivery of viral transgenes into the prostate, reported metastasis to the lung (Cho et al. 2014). (Ding et al. 2011; Cho et al. 2014). Altogether, these data further suggest that other mechanisms beyond *PTEN* loss might be involved on the progression to metastatic PCa. Based on this idea, and using data mining analyses of PCa datasets, cellular systems and GEMMs, the transcriptional coregulator peroxisome proliferator-activated receptor gamma coactivator 1 alpha (PGC1 α) was identified as a PCa tumor and metastasis suppressor (Torrano, Valcarcel-Jimenez, et al. 2016). In this work, our group generated a GEMM with complete loss of *Pten* and *Pgc1 α* in the prostate epithelium. These mice develop invasive carcinoma at three months of age (data not published), further developing clinical metastasis to the lymph nodes and disseminated cells to the bone at later time points (**Fig 10**). PGC1 α exerts its tumor suppressive activity by means of rewiring the cell metabolism from an anabolic towards a catabolic state. This metabolic rewiring driven by PGC1 α is dependent on its transcriptional partner estrogen-related receptor alpha (ERR α). Importantly, in patients *PGC1A* gene expression levels are progressively decreased from normal towards primary and metastatic tissues, and these levels were shown to correlate with Gleason score. This endows the transcriptional coregulator PGC1 α with prognostic and stratification potential of patients. In addition to this study, the group contributed to further understand the tumor-suppressive role the PGC1 α -ERR α transcriptional axis by means of blunting the acquisition of invasive properties of PCa cells. This was shown to happen through inhibition of c-MYC and subsequent cytoskeletal rearrangements and downregulation of adhesion molecules (Valcarcel-Jimenez et al. 2019). Almost at the same time, another study by Kaminski and colleagues reported a PGC1 α -ERR α -mediated inhibitory role of polyamines metabolism via c-MYC and enzyme ornithine decarboxylase 1 (ODC1) repression, thus demonstrating how PCa cells aggressiveness is sustained by polyamines (Kaminski et al. 2019). In the last years, other studies have contributed to set light on the role of PGC1 α along PCa progression. Shiota and collages reported that in androgen dependent PCa cells, the interaction of PGC1 α with AR enhances the transcriptional activity of AR target genes, promoting PCa cells growth. Opposite to this, silencing of PGC1 α induced cell cycle arrest at G1 phase (Shiota et al. 2010). On the other hand, activation

of AMPK in response to androgens was shown to increase PGC1 α levels, conferring growth advantages to PCa cells through the metabolic rewiring and induction of mitochondrial biogenesis (Tennakoon et al. 2014).

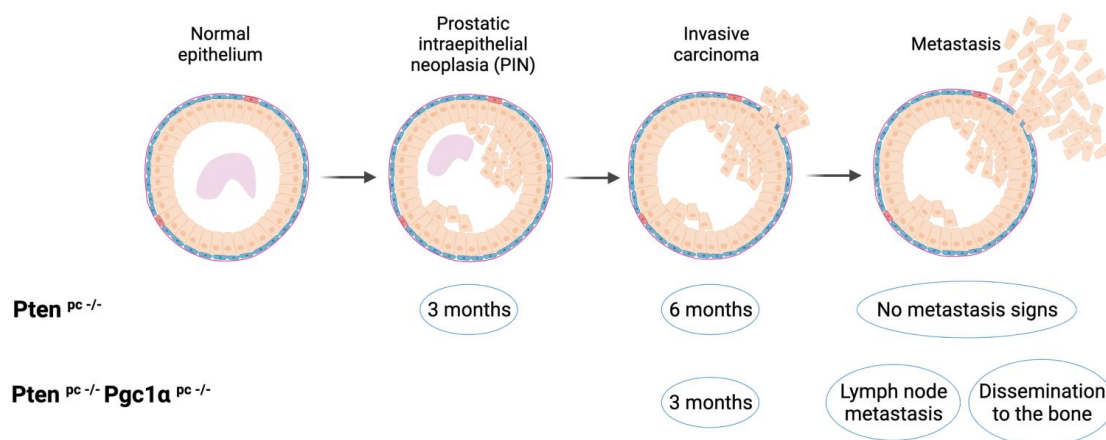


Figure 10. Prostate-specific deletion of *Pten* and *Pgc1 α* in the mouse epithelium. Genotypes according to evolution of PCa disease are represented. *pc*: prostate specific, *-/-*: two copy loss.

Hence, the studies herein presented show how PCa progression can be driven by changes in cell metabolism, which indeed is a cancer hallmark that endows malignant cells with adaptation capacities to sustain their growth (Hanahan and Weinberg 2011; Pavlova and Thompson 2016). Within tumors, metabolic phenotypes are diverse and flexible, and can be triggered by cell-intrinsic events such as mutations in oncogenes as well as epigenetic alterations, and through cell-extrinsic phenomena that is usually conditioned by the tumor microenvironment (Jiyeon Kim and DeBerardinis 2019) (Hanahan 2022).

II.6 PGC1 family of coregulators

PGC1 is a small family of transcriptional coregulators that include three members: PGC1 α , PGC1 β and PGC1-related coactivator (PRC) (Martínez-Redondo, Pettersson, and Ruas 2015b). Transcriptional coregulators modulate (enhance or repress) gene expression based on their interaction with diverse partner transcription factors, which makes them important mediators of different physiological processes. Compared to other transcriptional coregulators, the PGC1 family lacks enzymatic activity, exerting their function as an anchorage platform that allows the assemblance of the transcriptional machinery (Bost and Kaminski 2019). While PRC shows little homology, PGC1 β and PGC1 α share close homology with extensive amino acid sequence identity clustered in an N-terminal activation domain, a central regulatory domain, and a C-terminal RNA binding domain (**Fig 11**) (J. Lin et al. 2005).

PGC1 coactivators have no DNA binding domain; they interact with a wide range of transcription factors and nuclear receptors that drive the activation of diverse biological programs



in disparate tissues. Most of these interactions occur in the central region, between the N-terminal and the C-terminal domains (J. Lin et al. 2005). All three PGC1 members have binding spots at their N-terminal regions, where several histone acetyltransferases (HAT)-containing proteins can bind. These proteins include p300, CBP and SRC1, and drive chromatin structure remodeling processes, allowing the access of transcription factors to induce gene expression. The C-terminal domain has a serine-arginine-rich domain, an RNA binding domain that can couple pre-mRNA splicing with transcription, and a nuclear localization signal that maintains PGC1 in the nucleus. This domain is absent in some PGC1 α variants found in cytosol and mitochondria (J. Lin et al. 2005; de Vitto, Bode, and Dong 2019).

Regarding the different PGC1 family members, PGC1 β is ubiquitously expressed in the body, and it mainly regulates energy expenditure. On the other hand, PRC expression is predominant in endothelial cells and vascular smooth muscle cells (Tyagi et al. 2011). The third member of the family, PGC1 α , was first identified as a PPAR γ interactor in the context of cold-induced thermogenesis in the brown adipose tissue (P Puigserver et al. 1998). The gene encoding for PGC1 α (*PPARGC1A*) is transcribed from two different promoters, and together with alternative splicing events and post-translational modifications (PTMs), it gives rise to co-activator variants with different transcript and protein structure that display distinct regulation and tissue distribution, allowing cellular adaptation to diverse environmental conditions (Martínez-Redondo, Pettersson, and Ruas 2015a; C. F. Cheng, Ku, and Lin 2018).

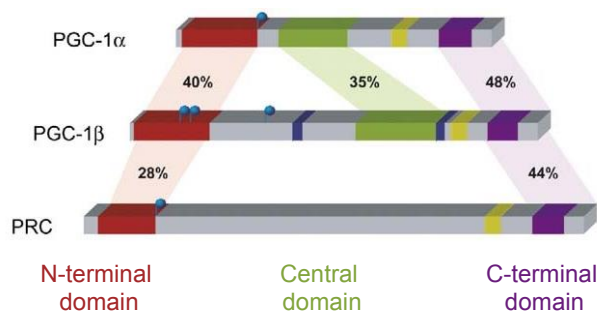


Figure I 11. Sequence homology and domains found in PGC1 α , PGC1 β , and PRC members of PGC1 family of coactivators. Adapted from J. Lin et al., *Cell Metabolism*. (2005).

II.6.1 PGC1 α

PGC1 α is a master regulator of cell metabolism (Liang and Ward 2006). In mammals, PGC1 α is mostly expressed in tissues with high energy demands including the brain, kidneys, liver, cardiac and skeletal muscle, and brown adipose tissue, where the expression of the co-activator is induced through different stimuli that include physical activity, fasting, exposure to cold, and hypoxia (C. F. Cheng, Ku, and Lin 2018; Thom et al. 2014). Therefore, PGC1 α activity needs to be tightly regulated through different mechanisms that, indeed, vary among tissues. In the brown adipose tissue, expression of PGC1 α is triggered through the cAMP signaling pathway and PKA activation. In the muscle, PGC1 α activation is known to happen via direct phosphorylation of two threonine and serine residues by direct binding of AMPK (Jäger et al. 2007). PGC1 α was also shown to be induced after exercise via activation of Ca²⁺/calmodulin-

dependent protein kinase IV and calcineurin. Another activation mechanism in the muscle occurs via p38 mitogen activated protein kinase (p38 MAPK) activation leading to phosphorylation of myocyte enhancer factor-2 (MEF2) and activating-transcription factor 2 (ATF2) transcription factors. In the liver, PGC1 α expression is increased upon secretion of pancreatic hormone glucagon during fasting periods, and it involves further activation of cAMP and transcription factor CREB (Bost and Kaminski 2019). Finally, PGC1 α is also under the control of epigenetic mechanisms (Krämer and Handschin 2019). Methylation levels of PGC1 α promoter are decreased by exercise, thus leading to increase levels of the coactivator (Barrès et al. 2012). In addition, several post-translational modifications including phosphorylation, acetylation, methylation, and ubiquitination modulate the activity of PGC1 α . These modifications affect the capacity of PGC1 α for recruiting chromatin remodeling complexes and determine its interaction with transcription factors (Bost and Kaminski 2019)

Activation of PGC1 α further triggers pathways that are mostly linked to metabolism and are essential for energy supply, including mitochondrial biogenesis, oxidative phosphorylation (OXPHOS), fatty acid oxidation, gluconeogenesis, thermogenesis, detoxification of reactive oxygen species (ROS), cardiac health and angiogenesis (Herzig et al. 2001; Vega, Huss, and Kelly 2000; Wu et al. 1999; Yoon et al. 2001; Lehman et al. 2000; R. Lin and Kerkelä 2020). Importantly, these pleiotropic functions are enabled by the presence of specific leucine-rich motifs (LXXLL) in the N-terminal domain, where different nuclear receptors, transcription factors and other transcriptional co-activators can bind, including NRF1/2, PPARs, ERRs, HNF4 α , FXR, LXR, Sox9, MEF-2, FOXO1 and SRC-1/p300 complex (Kressler et al. 2002; Wu et al. 1999; Yoon et al. 2001; Huss et al. 2004; Kamei et al. 2003; Vega, Huss, and Kelly 2000; Kawakami et al. 2005; Pere Puigserver and Spiegelman 2003; Oberkofler et al. 2003; Wallberg et al. 2003). An overview of the mechanisms of PGC1 α gene expression regulation, activity and interaction with transcription factors and biological roles can be found in **Fig 12**.

Following the previous data we have in the laboratory, regarding how the dysregulation of the PGC1 α -ERR α transcriptional axis impacts on PCa, we will focus on explaining PGC1 α transcriptional control through its interaction with ERR α .

The nuclear receptor ERR α is a member of the ERR family of orphan nuclear receptors composed of three members: ERR α (NR3B1), ERR β (NR3B2) and ERR γ (NR3B3). These three members share sequence homology with estrogen receptor, but do not require hormones for activating their transcriptional activity and can bind to coregulators. Structurally, ERRs have a N-terminal region that contains a DNA binding domain and a ligand-independent transcriptional activation function. The DNA binding domain presents an element responsive sequence (ERRE) that specifically allows binding of other ERRs (Tripathi, Yen, and Singh 2020). On the other hand, the C-terminal region presents a ligand binding domain that is required for the interaction with co-activator and co-repressor proteins, including PGC1 α . Among the three ERRs, ERR α regulates lipid catabolism as well as mitochondrial activity and biogenesis, and like PGC1 α , it is highly expressed in metabolically active tissues that utilize fatty acids as fuel, including brown fat, heart, muscle, and kidney (Tripathi, Yen, and Singh 2020). ERR α interaction with nuclear receptor co-

repressor 1 (NCOR1) and receptor interaction protein 140 (RIP140), reduces its transcriptional activity. Opposite to that, PGC1 α positively regulates ERR α , transforming it in a potent transcription factor. Indeed, binding of PGC1 α -ERR α dimers to ESRR α response elements present in the ERR α gene promoter induces its gene expression in a feedback-loop manner (Tripathi, Yen, and Singh 2020). Interestingly, PGC1 α usually interacts with nuclear receptors through LXXLL motif at amino acid position 142-146. Yet, it seems that the interaction between PGC1 α and ERR α is unique and occurs at leucine-rich motifs positioned at amino acids 209-213 (Huss, Kopp, and Kelly 2002).

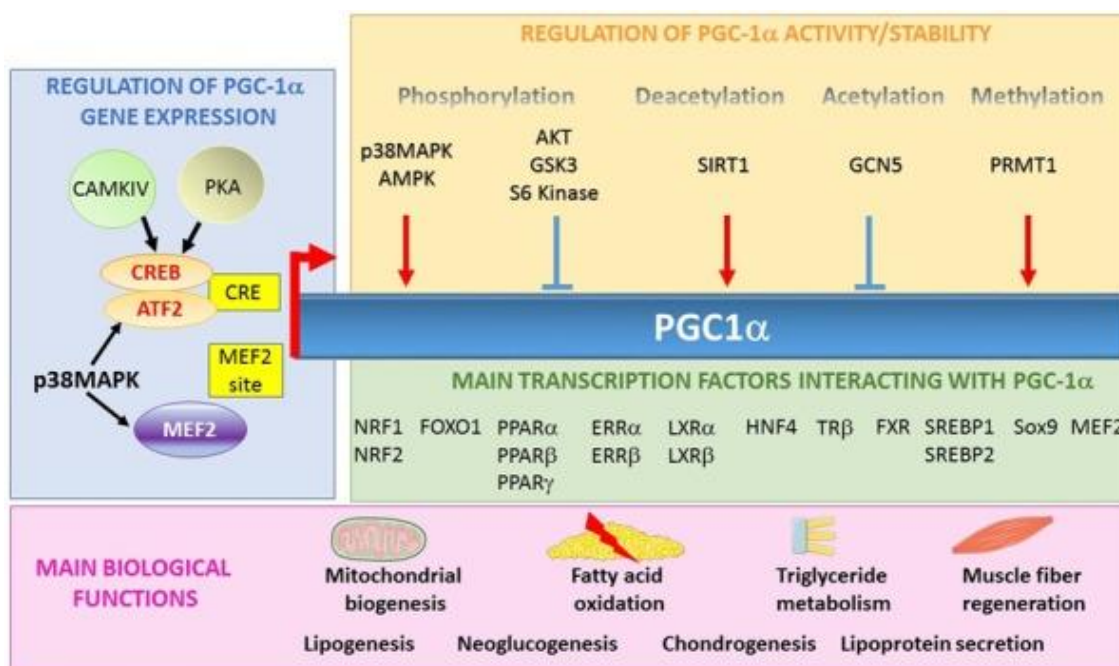


Figure I 12. Regulation of PGC1 α gene expression, activity and main biological functions triggered upon interaction with different transcription factors. Bost & Kaminski, *American Journal of Cancer Research* (2019).

PGC1 α regulates a great number of biological responses in an ERR α -dependent manner. In response to exercise, PGC1 α together with ERR α induce vascular endothelial growth factor (VEGF), promoting angiogenesis (Chinsomboon et al. 2009). Indeed, VEGF expression levels in the muscle are increased in response to hypoxic conditions through a PGC1 α -ERR α -dependent mechanism. This again, leads to the promotion of angiogenesis (Thom et al. 2014). Under physiological conditions, PGC1 α together with ERR α controls the expression of OXPHOS genes and mitochondrial biogenesis (Schreiber et al. 2004). The PGC1 α -ERR α transcriptional axis also regulates cardiac and skeletal muscle lipid metabolism (Huss, Kopp, and Kelly 2002).

Finally, it was proposed that transcriptional regulators could function as direct sensors of the metabolic state of cells, and for it to happen, signals need to be transduced into the cell nucleus (Yujiang Shi and Shi 2004) (Atrice Desvergne, Michalik, and Wahli 2006). The concept of metabolic sensors and transcriptional regulation is predominantly attributed to nuclear receptors, which, are characterized by being activated upon binding to specific ligands followed by their association to response elements located close to the promoter region of the target genes

(Atrice Desvergne, Michalik, and Wahli 2006). Transcriptional control of cell metabolism can be also mediated by transcriptional coregulators, which contribute to the fine-tuned regulation of transcription through different mechanisms that include chromatin remodeling processes through the activity of HATs, and proteins such as TRAP/DRIP/Mediator/ARC complex that are involved on the recruitment of RNA polymerase II. Finally, ATP-dependent chromatin remodeling complexes such as SWI/SNF, IMO80, and ISWI also regulate transcriptional activity (Stallcup and Poulard 2020; Spiegelman and Heinrich 2004). Besides from PGC1 α , hundreds of coregulators have been reported up to date among them, steroid receptor coactivator 1 (SRC-1) and class III histone deacetylase sirtuin 1 (SIRT1), which have shown to be effective metabolic sensors and transcriptional effectors, hence providing metabolic plasticity to the cells (Mouchiroud et al. 2014). A list of the main coregulators involved in the regulation of metabolism can be found in **Figl 13**.

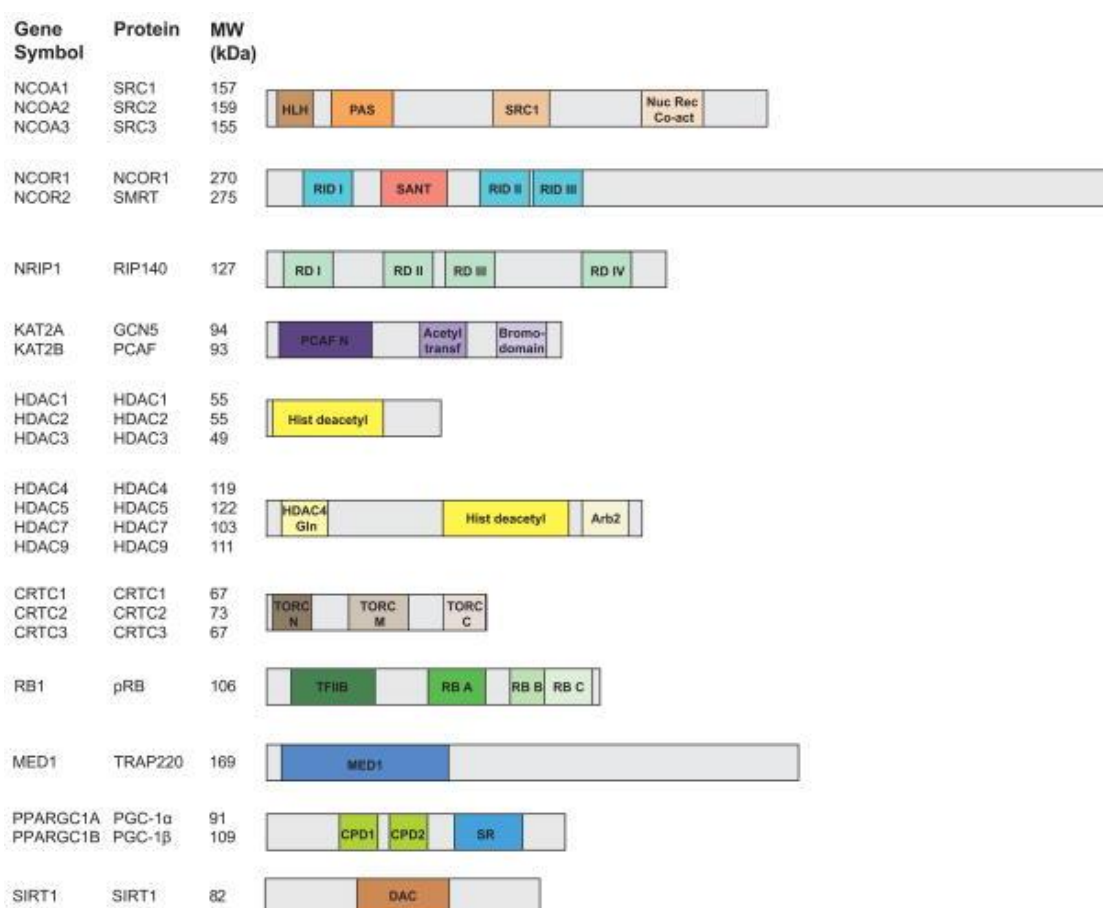


Figure I 13. Families of metabolic coregulators. Mouchiroud et al. *Cell Metabolism* (2014).

II.6.2 Role of PGC1 α in other types of cancer

As mentioned before, the PGC1 family of coregulators is highly reactive to environmental stimuli, including physical activity and changes in temperature and nutritional status. PGC1 coregulators respond to these environmental fluctuations by means of regulating cell metabolism, thus allowing organisms to adapt to their environment. This family of transcriptional coactivators



are involved in the regulation of glucose, lipid, and energy metabolism, and therefore dysregulation of PGC1 proteins is behind the development of different pathologies, including cardiomyopathies, insulin resistance, liver fibrosis and neurodegenerative diseases (J. Lin, Handschin, and Spiegelman 2005; Besse-Patin et al. 2017).

In a cancer context, the expression levels (**Fig 14**) and functions attributed to PGC1 α are ample; both, tumor suppressive and pro-tumorigenic roles have been related to this transcriptional coregulator.

ERBB2+ BCa cells were shown to have advantages in growth due to the activation of genes involved in glutamine metabolism via PGC1 α -ERR α transcriptional axis. In addition, BCa patients harboring high levels of PGC1 α were shown to have reduced survival (McGuirk et al. 2013). Another work demonstrated how BCa invasion and metastasis is sustained through the PGC1 α -mediated increase of mitochondrial biogenesis that endows cells with higher ATP production capacity (Lebleu et al. 2014). This data is in line with another more recent study that also provided evidence on the role of PGC1 α on sustaining BCa metastasis and drug resistance by conferring tumor cells increased bioenergetic capacity (Andrzejewski et al. 2017). Opposite to these works, activation of the PGC1 α -ERR α was shown to suppress folate cycle and purine metabolism in BCa cells, sensitizing malignant cells to anti-folate therapy (Audet-Walsh et al. 2016).

Pancreatic cancer stem cells (CSCs) and non-CSCs metabolism are regulated by the balance of c-MYC- PGC1 α levels. Pancreatic CSCs were shown to express low c-MYC and high PGC1 α levels making them highly dependent on mitochondrial OXPHOS. On the other hand, non-CSCs are highly reliant on glycolysis due to their high c-MYC and low PGC1 α status. Resistance to metformin treatment can be avoided through the suppression of c-MYC and subsequent increase of PGC1 α due to the limited metabolic plasticity of CSC (Sancho et al. 2015).

Melanoma shows heterogeneity regarding PGC1 α expression levels. Microphthalmia-associated transcription factor (MITF) is known to drive the expression of PGC1 α in melanoma cells (Haq et al. 2013; Vazquez et al. 2013), and this further contributes to define two cell subpopulations: ones with high PGC1 α levels and others with low PGC1 α levels. These subpopulations are characterized by displaying disparate metabolic profiles that confer them different survival strategies; PGC1 α -high melanoma cells have increased mitochondrial oxidative metabolism and high ability of ROS detoxification, which makes them resistant to oxidative stress. On the other hand, PGC1 α -low cells are linked to a more glycolytic metabolism and are less resistant to oxidative stress. These data clearly evidence the metabolic plasticity that is defined by PGC1 α , which could also be exploited for therapeutic strategies (Vazquez et al. 2013). In the context of melanoma metastasis, PGC1 α was also shown to play an active role through the regulation of ID2 and TCF4, both involved in the downregulation of invasion and metastasis-related genes (Luo et al. 2016). Overall, melanoma is a heterogeneous type of cancer where changes between proliferative and invasive cell phenotypes are found. High levels of PGC1 α promote cell survival whereas low PGC1 α status plays a key role on metastasis sustenance.

PGC1 α was found to act as a tumor suppressor in the formation and progression of hepatocellular carcinoma (HCC) (R. Liu et al. 2017). In ovarian cancer tissues, PGC1 α was shown to be decreased compared to non-malignant adjacent tissue (Y. Zhang et al. 2007). On the other hand, PGC1 α expression is increased in ovarian cancer cisplatin resistant cells, where it seems to inhibit apoptosis (Yanqing Li et al. 2021).

In colorectal cancer (CRC) PGC1 α displays decreased levels compared to non-malignant tissues (Feilchenfeldt et al. 2004). In agreement with this data, the work performed by D'Errico and colleagues also demonstrated the tumor suppressive role of PGC1 α in CRPC, where it promotes mitochondrial-mediated apoptosis via accumulation of ROS (D'Errico et al. 2011). PGC1 α also exerts a protective role in clear renal cell carcinomas, in the context of VHL loss that leads to HIF1 α stabilization and switch to glycolytic metabolism. PGC1 α restores mitochondrial function leading to decreased tumor growth and increased sensitivity to therapy (LaGory et al. 2015). Following the same trend, a recent *in vivo* study reported that decreased levels of PGC1 α in renal cell carcinoma were linked to disease progression via increased expression of collagens that drive the activation of discoidin domain receptor signaling. This further leads to SNAIL stabilization and promotion of EMT processes (Nam et al. 2020). In lung cancer, p53 wild type cells express higher levels of PGC1 α compared to cells with p53 loss and mutations. High-PGC1 α expressing cells have higher proliferation rates (Taguchi et al. 2014). Of note, another work suggests that p53 induces PGC1 α stability, which further triggers cisplatin resistance in non-small cell lung carcinoma (NSCLC) (Deng et al. 2020). Finally, in contrast to the work by Kaminski (Kaminski et al. 2019) and to the data provided by our group (Torrano, Valcarcel-Jimenez, et al. 2016; Valcarcel-Jimenez et al. 2019), where decreased expression of PGC1 α was linked to a more aggressive PCa, Tennakoon and colleagues reported a subset of PCa patients (5%) where PGC1 α was overexpressed. These patients, that in average were young, had an early onset of the disease. In this study, PGC1 α was shown to promote *in vitro* malignant outgrowth through the metabolic rewiring and induction of mitochondrial biogenesis (Tennakoon et al. 2014).

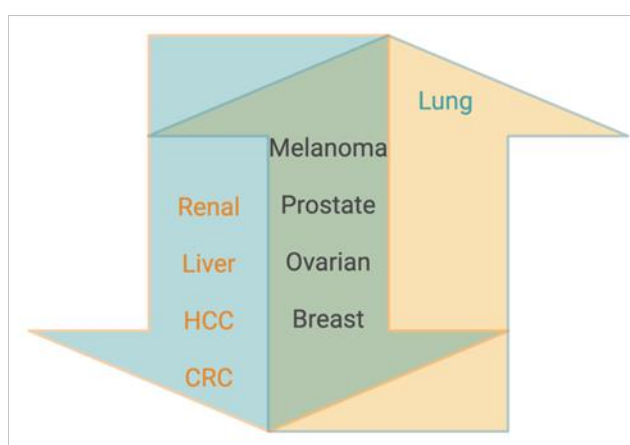


Figure I 14. PGC1 α expression levels vary within the same and different cancer types. The green arrow contains the cancer types where expression of PGC1 α was reported to be low, and the yellow arrow lists cancers where PGC1 α was shown to be expressed at high levels. The area shared by both arrows includes cancers where low and high PGC1 α levels were reported.



III Cell communication

From the simplest to the most complex of the living organisms, life cannot be conceived without communication. Communication between cells probably exists since the first unicellular organisms inhabited Earth (about 3.5 billion years ago) and is an essential feature of evolution. Indeed, it was suggested that evolution can be reduced to communication between 1) unicellular organisms and their environment, 2) the cell communication that constitutes the basis for multicellularity and 3) communication of genetic material from one generation to other (Torday and Rehan 2015).

Communication allows cooperation, which further brings survival advantages (King 2004; Christensen et al. 1997). Millions of years ago, unicellular organisms started cooperating, culminating in phenomena such as biofilm formation and quorum sensing. Perhaps, this event constituted a selective pressure for eukaryotes to start cooperating too, hence developing cell-cell communication mechanisms that, via secreted factors, mediate plenty of biological processes such as homeostasis maintenance, reproduction, or regeneration (Torday and Rehan 2015). The path towards multicellularity also involved the formation of cellular clusters that was accompanied by the loss of autonomy due to cell differentiation (Libby and Ratcliff 2014). Differentiation renders cells more efficient in specific processes whilst making them reliant on other cells for survival. These specialized cells cope to sustain life. Therefore, communication in multicellular organisms seems natural, as indeed specialized cells may become part of an ever-increasing complex environment in which tissues conform organs that are further integrated into a sole system, the multicellular organism body. Cell communication networks are critical for maintaining tissue homeostasis and coordinating immune responses, among the ample functions that take place in an organism. Stimuli need therefore to be sensed and integrated. Compared to intracellular signaling, intercellular communication is not that well understood; mapping the interactions that are established between different types of cells through secreted entities is complex as each cell is being regulated by a complex signaling network which further influences the communication established with surrounding cells, which further affects other cells. Communication is key under physiological and pathological conditions, and in fact, altering the networks established between cells might be a way of changing their fate and, for example, sustain malignant growth. Nowadays studies are focusing on understanding the cells at the simplest of the levels, and for that, great efforts on performing single-cell RNA sequencing are being done. In addition, novel technologies are focusing on analyzing at a single-cell level chromatin, genome, methylation, and cell proteome (Papalexi and Satija 2018). This “cell dissection” is allowing the classification of hundreds of different types of cells which, are determined by the array of regulatory factors (mainly transcription factors and transcriptional coregulators) with which cells are endowed. Nonetheless, although the study of cell-intrinsic regulation is providing great understanding on cellular biology and has allowed the identification of specific gene signatures involved in certain types of disease, it is crucial that this deconstructed information gets integrated within the environment of the cell. Intercellular communication mechanisms can happen through direct cell to cell interactions as

well as via secreted factors, which include a plethora of molecules such as proteins, small peptides, amino acids, fatty acids, nucleotides, gases, and extracellular vesicles (EVs). Regardless of the nature of the signal, the target cell will respond by means of orchestrating a cascade of intracellular signals that end up with the alteration of its behavior. The distances at which signaling molecules act can be short or large, and different secretion strategies and uptake mechanisms can be found within cells.

The term “secretome” remains ample, as different definitions regarding what composes it can be found throughout literature. Most of the publications define “secretome” as secreted proteins (Feizi et al. 2017; Villarreal et al. 2013; Pavlou and Diamandis 2010). Yet, other studies extend the definition of secretome to secreted proteins, lipids, exosomes, and other small molecular messengers (Brady et al. 2016). Other works distinguish different fractions, including secreted soluble factors, secreted proteins and EVs (de Lope et al. 2018) or just the EV and a soluble fraction (Jung et al. 2009). Finally, the secretome was also defined as soluble factors (growth factors, cytokines, chemokines, and ECM components) and different populations of EVs (Villatoro et al. 2019). For the sake of experimental simplicity, along the present thesis work, two major compartments of the cell secretome were distinguished: extracellular vesicles and soluble factors (SFs). Bearing in mind that cells release diverse types of molecules, we have focused our attention on studying the protein content found in the EVs and SFs compartments of the secretome. Proteins are released to the extracellular milieu via different secretion pathways that will be explained in the coming sections.

III.1 Types of intercellular communication

Although different classification systems exist, classically, depending on the distance at which signaling molecules travel to the target cell, four main types of signaling mechanisms are distinguished: 1) autocrine, 2) paracrine, 3) endocrine and 4) direct signaling (Alberts et al. 2002) (Fig 15).

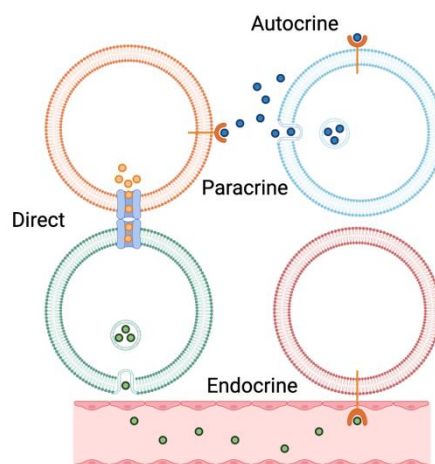


Figure I 15. Types of cell-cell communication.



- 1) Autocrine communication involves a cell secreting a signaling molecule that binds back to its own receptors. This type of signaling is typical during differentiation processes as it creates a "community effect" between groups of cells.
- 2) Paracrine communication occurs between cells that are proximally located and usually occurs through the release of a molecule that is taken up by neighboring cells or immobilized in the ECM. As an example, synapsis in nerve cells ends with the release of neurotransmitters within membrane-bound vesicles to the presynaptic space. These vesicles next bind to the postsynaptic membrane of the recipient nerve cell. Chemokine release by immune cells is another type of paracrine signaling.
- 3) Endocrine communication involves long distance communication, and it is usually mediated by hormones, which are produced by endocrine cells located in the glands and are transported through the blood to the target cells.
- 4) Direct or juxtacrine communication, mediated through gap junctions, are cell-cell bindings that connect the cytoplasm from bounded cells, without secretions to the extracellular space.

It is important to highlight that, as mentioned earlier, one of the hallmark capabilities of malignant cells is the self-sufficiency in growth signals (Hanahan and Weinberg 2000). In this sense, most growth factors released by a cell seem to be directed to stimulate the growth of other surrounding cells (paracrine communication). Yet, it is common that cancer cells acquire the capacity of releasing growth factors to which they are responsive, thus generating a feedback loop (autocrine communication) (Ruan and Lai 2004). Indeed, receptors involved in the signal transduction of growth factors are often deregulated. A clear example is the overexpression of human epidermal growth factor receptor 2 (HER2), which sustains HER2 positive BCa tumors (Moasser 2007).

III.1.1 Ligands and receptors

Signaling molecules (ligands) include a wide range of molecules that depending on their solubility can be grouped in hydrophobic and hydrophilic (Alberts et al. 2002). Hydrophobic ligands can diffuse through the plasma membrane and interact with intracellular receptors. Steroid hormones such as estrogen, progesterone, and androgens as well as other lipid-soluble molecules like retinoic acid, oxysterols and thyroid hormones are hydrophobic ligands. Gases as nitric oxide (NO) are also included into this category of signaling molecules. (Sever and Glass 2013)

On the other hand, hydrophilic ligands include a diverse type of molecules such as peptides, proteins, and amino acids. Due to their nature, these ligands cannot pass through the cell membrane and therefore need to bind to specific receptors found in the target cell surface. In this manner, cell surface receptors act as signal transducers by converting extracellular signals into intracellular signals. Based on the transduction mechanism, three main categories of



receptors can be distinguished: G-protein coupled receptors (GPCRs), ion channels and enzyme-linked receptors (Alberts et al. 2002).

III.2 Extracellular vesicles (EVs)

According to the guidelines established by the International Society of Extracellular Vesicles (ISEV), “extracellular vesicles” stems for “generic term for particles naturally released from the cell that are delimited by a lipid bilayer and cannot replicate” (Théry, Witwer, Aikawa, Alcaraz, et al. 2018). No consensus in marker specificity for EVs subtypes has been endorsed, therefore, unless a life-image of a given EV is taken in the act of release, ISEV 2018 guidelines encourage using the term “EV”. Importantly, a minimum data from the EVs preparations should be provided: 1) quantitative measure of the EVs source (volume of fluid, number of producer cells or tissue mass), 2) determine abundance of EVs (particle number and/or protein/lipid content), 3) check for presence of EV-associated markers (usually CD9, CD63 or CD81) and 4) verify no contamination with other cell membrane compartments such as Golgi, mitochondria, or the endoplasmic reticulum (ER).

The first time “extracellular vesicle” was used as a title for a scientific publication, was in 1971, where electron microscopy images of EVs biogenesis from *Ochromonas danica* algae were shown (Aaronson et al. 1970). Nonetheless, this paper already referred to previous works published during the 1960's describing “membranous structures found extracellularly and within organelles of a large number of organisms” (Aaronson et al. 1970). Since then, EVs have been shown to be nano to micro-sized vesicles that are released by almost any cell type (including prokaryotes and eukaryotes) under physiological and pathological conditions. Due to their ability for transferring biologically active molecules (including lipids, nucleic acids, and proteins), they have emerged as important mediators of cell-cell communication in a wide range of biological processes that include cardio-protective roles, immunity, cancer, and neurodegenerative diseases among others (Ciullo et al. 2019; Mittelbrunn et al. 2011; Kalluri 2016; J. Y. Lee and Kim 2017). Different types of interaction mechanisms of EVs with target cells have been described, and it includes binding to specific receptors, direct membrane fusion, as well as internalization by clathrin-mediated endocytosis and macropinocytosis (Segura et al. 2007; Parolini et al. 2009; T. Tian et al. 2014). Understanding how and under which conditions EVs are internalized by target cells is of special interest as it might explain pathological events, such as organ-specific metastases (Hoshino et al. 2015). In fact, it seems both, proteins present in EVs and in the recipient cells influence uptake (Escrevente et al. 2011). Finally, the proven importance of EVs on mediating diverse biological roles has contributed to the expansion of the field and has led to the generation of specific databases that comprise EV-related data (Kalra et al. 2012; D. K. Kim et al. 2013).

III.2.1 Classification of extracellular vesicles

EVs are classified according to their mechanism of origin and to their size in three major groups that include: exosomes, microvesicles and apoptotic bodies (György et al. 2011). Importantly, new guidelines recommend classifying EVs in small (sEVs) and large (lEVs), where exosomes are considered sEVs and microvesicles and apoptotic bodies are considered lEVs (**Figl 16**) (Witwer and Théry 2019). It is also important to highlight that exosome and microvesicles are part of the unconventional protein secretory pathway that will be explained in **section III.5**. Still, as mentioned above, it is important to bear in mind that both types of EVs can mediate transport of other non-proteic molecules.

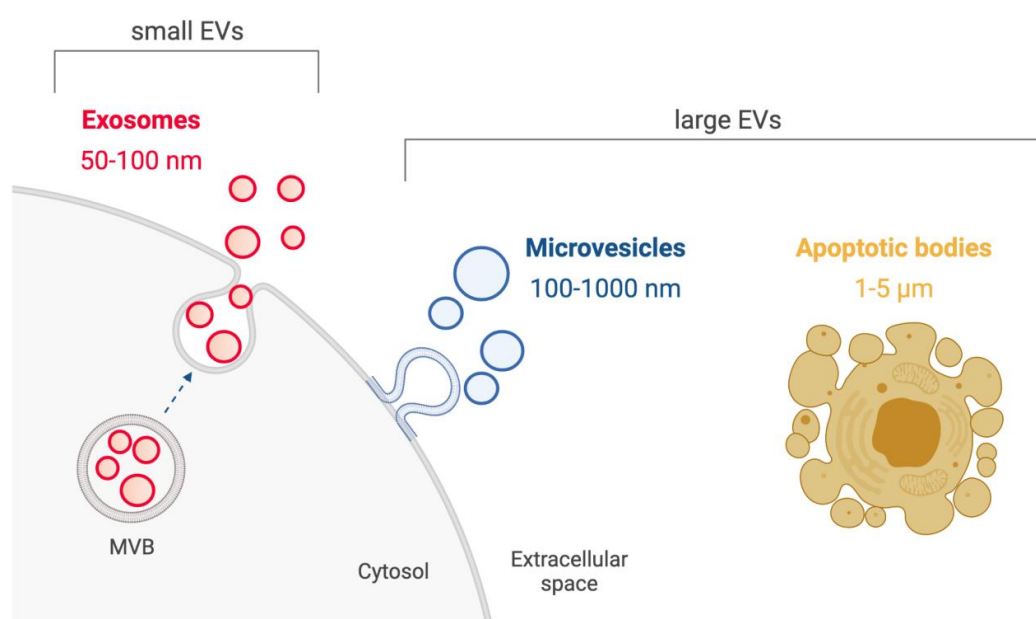


Figure I 16. Classification of extracellular vesicles according to biogenesis and size.

Exosomes

Exosomes were first described in 1981 by Trams and colleagues as exfoliated vesicles with ecto-enzyme activity (Trams et al. 1981). They proposed these vesicles could have physiological functions and suggested to name them “exosomes”. This work was shortly followed by other studies by Harding and Pan in reticulocytes (Pan,1983) (Harding,1983), where they described exosomes were formed in multivesicular bodies (MVBs). For some years exosomes were viewed as cell debris, nonetheless in 1996 Raposo and colleagues showed B lymphocytes secrete MHC class II-containing exosomes, inducing antigen-specific T cell responses. This study therefore demonstrated that exosomes are active mediators in physiology (Raposo et al. 1996).

Exosomes are vesicles surrounded by a phospholipid bilayer with a size comprising 50-100 nm diameter. Biogenesis of exosomes takes place within the endosomal network. First, early endosomes fuse with endocytic vesicles and incorporate their content, which can be further destined for degradation, recycling, or exocytosis. From this point, three steps are distinguished (**Figl 17**) (Hessvik and Llorente 2018; Akers et al. 2013):

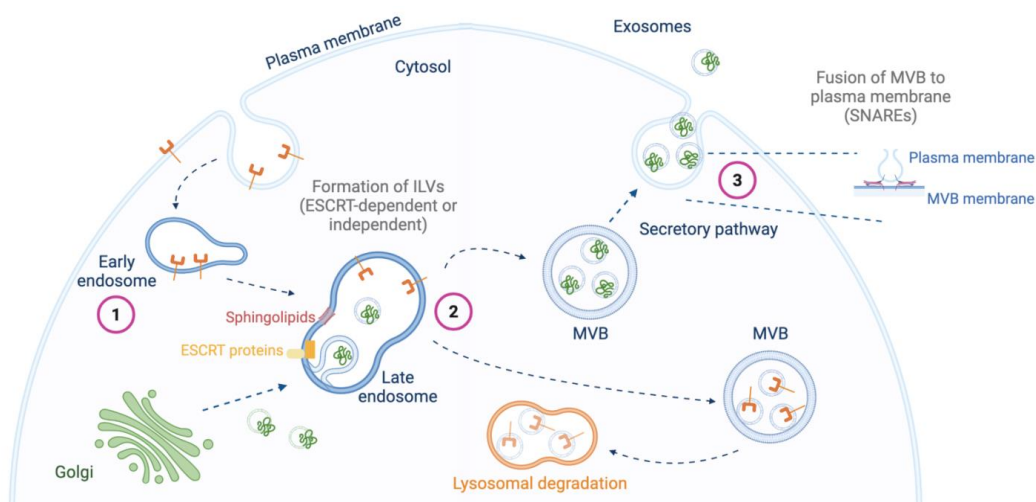


Figure I 17. Biogenesis of exosomes. The process can be divided in three main steps that include ILVs formation, transport of the MVB to the plasma membrane, followed by its fusion and release of exosomes to the extracellular space.

- 1) Early endosomes go through a series of transformations to become late endosomes, where small vesicles known as intraluminal vesicles (ILVs) are formed by inward budding of the late endosome membrane (also known as MVB). This process is mediated by specific protein machinery, the endosomal sorting complex required for transport (ESCRT) that comprises four protein complexes to which additional proteins are associated. Briefly, ESCRT-0 drives cargo clustering through ubiquitin-mediated processes. ESCRT-I and ESCRT-II induce membrane budding and ESCRT III mediates vesicle scission (Kowal, Tkach, and Théry 2014). ESCRT activity is triggered by the binding of ESCRT-0 protein hepatocyte growth factor-regulated tyrosine kinase substrate (HRS), which further activates by sequential protein binding ESCRT-I, ESCRT-II and ESCRT-III complexes (**Figl 18**) (Christ et al. 2017). Tetraspanins (such as CD9, CD81 and CD63) also seem to be involved in the ILVs formation and cargo sorting (Andreu and Yáñez-Mó 2014).
Asides from the ESCRT ILVs formation mechanism, ESCRT-independent mechanisms exist. One involves the formation of endosomal membrane microdomains that contain high concentrations of sphingolipid ceramide, which due to its cone-shaped structure promotes membrane budding (Trajkovic et al. 2008). The second ESCRT-independent mechanism is mediated by the small GTP-binding protein ADP ribosylation factor 6 (ARF6), which activates phospholipase D2 (PLD2) and syntenin. The latter further interacts with protein ALIX to produce ILVs (Ghossoub et al. 2014).
- 2) MVB can either be directed to the lysosomes for degradation or transported to the plasma membrane for exosomes release. The cell cytoskeleton and the RAB family of GTPase proteins control vesicular trafficking (Stenmark 2009).
- 3) The final step of exosomes biogenesis requires the fusion of the MVB membrane with the plasma membrane, process that is enabled by N-ethylmaleimide-sensitive fusion attachment

protein (SNAP) receptors (SNAREs), located in both membranes (Zylbersztejn and Galli 2011).

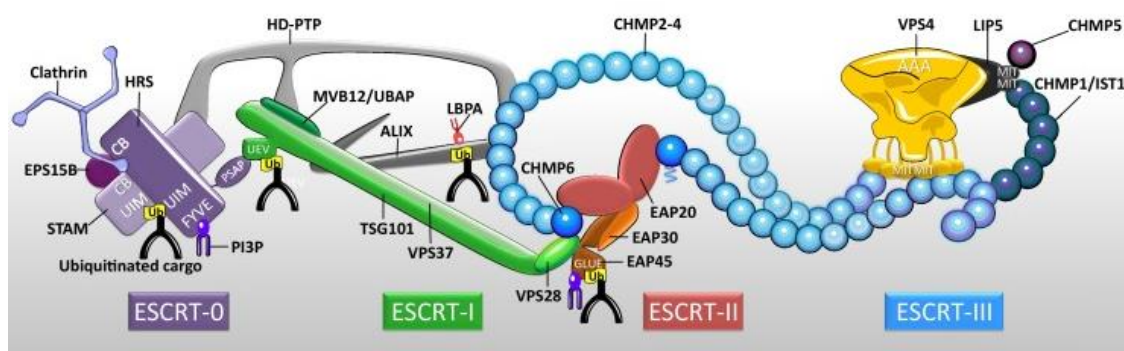


Figure 18. ESCRT machinery is composed of ESCRT sub-complexes that mediate membrane scission and cargo sorting. L. Christ et al. *Trends in Biochemical Sciences* (2016).

Although no consensus in EV-specific markers for distinguishing different populations of EVs has been set, the first exosomes proteomics studies revealed these vesicles were enriched in endosomal, plasma membrane and cytosolic proteins, hence confirming they derive from a specific cell compartment. Among the markers suggested to be enriched in exosomes, tetraspanins CD63, CD8 and CD81, Rab proteins, heat-shock proteins as well as ESCRT complex proteins TSG101 and ALIX are included (Théry et al. 2001; Moreno-Gonzalo, Fernandez-Delgado, and Sanchez-Madrid 2018). It is also interesting to mention that often exosomes are referred as the pellet obtained after 100,000 xg ultracentrifugation step, referring to the methodology of isolation by serial ultracentrifugation steps.

Microvesicles

Microvesicles (MVs) were first described in 1946 by Chargaff and West as a precipitable factor with the potential to generate thrombin (Chargaff and West 1946). MVs are surrounded by a phospholipid bilayer and range 100-1,000 nm size, although the latter can vary significantly depending on the MV-producing cell (György et al. 2011). These vesicles are formed by the outward blebbing and pinching of the plasma membrane, releasing microvesicles to the extracellular space. The process requires reorganization of membrane phospholipids and the use of cytoskeleton contractile machinery. ARF6 activates phospholipase D (PLD), which recruits extracellular-regulated kinase (ERK) to the membrane. ERK further activates myosin light chain kinase (MLCK), triggering the release of the microvesicles (**Fig 19**) (Akers et al. 2013). Of note, cargo selection into the nascent microvesicles is known to be mediated by ARF6 (Tricarico, Clancy, and D'Souza-Schorey 2017)

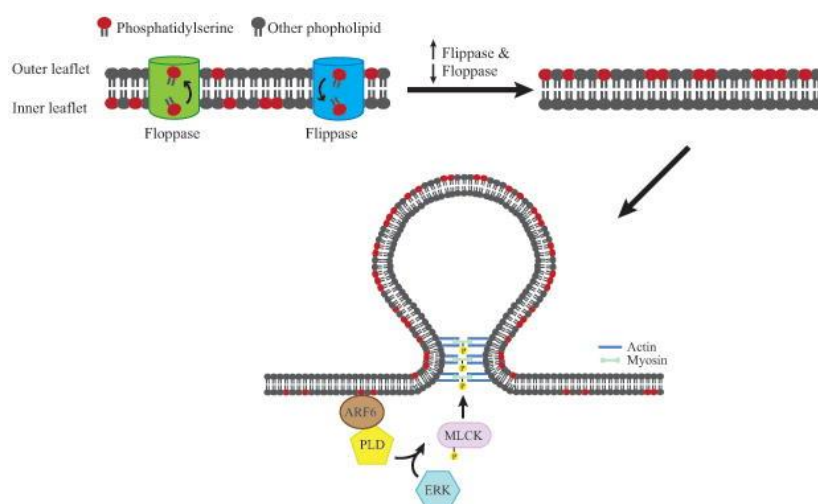


Figure 19. MVs formation and release through the outward budding of the plasma membrane. J. C. Akers et al. *Journal of Neuro-Oncology* (2013).

MVs are mainly produced by platelets, red blood cells, endothelial cells, and leukocytes, and this determines the markers that can be found specifically on each type of MVs. For example, endothelial MVs express E-selectin (CD62E), endoglin (CD105) and endothelial adhesion molecule 1 (PECAM-1) among other markers. On the other hand, platelet-derived MVs usually express glycoprotein Ib and IIb/IIIa, P-selectin and PECAM-1, among other markers (Słomka et al. 2018).

MVs mediate diverse biological functions through the transfer of bioactive molecules (nucleic acids and proteins) that can modify the environment at proximal and distal sites (Tricarico, Clancy, and D'Souza-Schorey 2017). They are involved in the regulation of diverse functions, including feto-maternal communication, prothrombogenic and proinflammatory responses in the vasculature, and oncogenic transformation (Pap et al. 2008) (Leroyer, Tedgui, and Boulanger 2008) (Antonyak et al. 2011).

Apoptotic bodies

Apoptotic bodies are the largest type of EVs, ranging 1-5 μm size and they are released as blebs of cells undergoing apoptosis (György et al. 2011). In the final phase of apoptotic death, some cell types undergo a series of changes in morphology, process that is known as apoptotic cell disassembly and can be divided into three steps (**Figl 20**) (Atkin-Smith and Poon 2017):

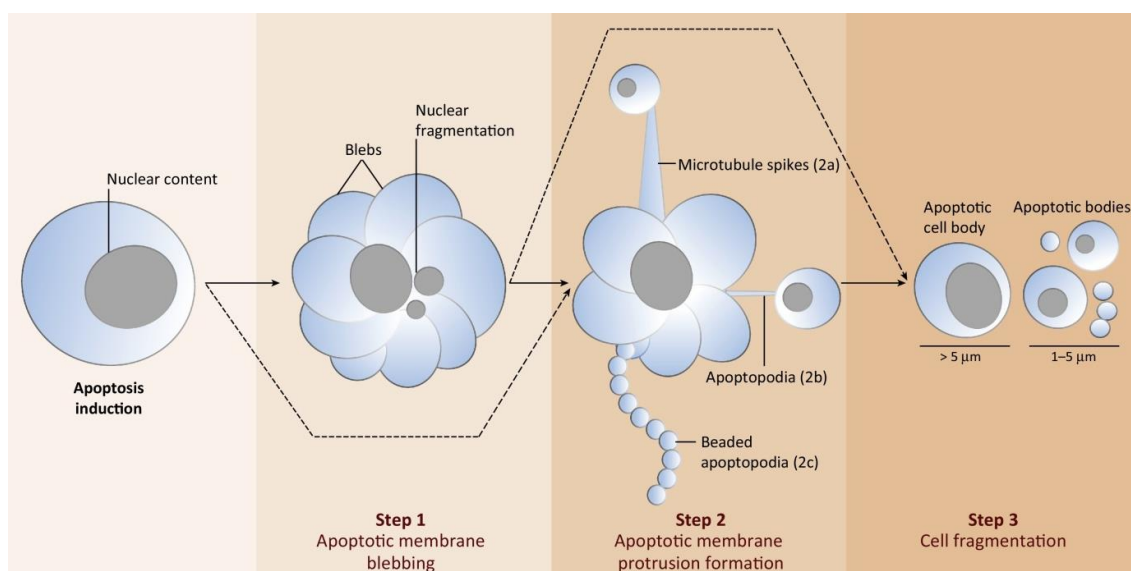


Figure 1 20. Apoptotic cell disassembly into apoptotic bodies. G. K. Atkin-Smith et al. *Trends in Cell Biology* (2016).

- 1) Plasma membrane blebs are formed during the early steps of apoptosis. This involves hydrostatic pressures that enable the movement of fluids into the membrane blebs and cytoskeleton contractions. This last step process is mediated through caspase 3-mediated Rho-associated protein kinase 1 (ROCK1) activation which further phosphorylates myosin light chain (MLC) and promotes actomyosin contraction.
- 2) Only certain cell types require this step, and it involves the formation of membrane protrusions including microtubule spikes (rigid and microtubule-rich protrusions), apoptopodia (string-like protrusions) or beaded apoptopodia.
- 3) Once apoptotic membrane blebs and protrusions have formed, dissociation of the apoptotic bodies from the cell body takes place. The mechanisms by which fragmentation takes place is not well known, but it may involve cell-intrinsic and cell-extrinsic factors, including abscission-like processes and shear forces from the extracellular environment, respectively.

Apoptotic bodies are characterized by having a variety of cellular components such as cytosol portions, nucleic acids, lipids, and functional organelles (L. Jiang and Poon 2019). Once released, apoptotic bodies are phagocytosed by macrophages within phagolysosomes, thus contributing to cell clearance. In fact, during apoptosis cell membrane lipids rearrange and phosphatidylserine (PS) is translocated to the outer leaflet. PS is also present in the membrane of apoptotic bodies, and it seems to help on their recognition by phagocytes (Battistelli and Falcieri 2020). As it happened with other types of EVs, apoptotic bodies were thought to be just “garbage sacs”, but lately it has been demonstrated they are also capable of transferring material, including oncogenes, to intact cells (Zernecke et al. 2009; Bergsmedh et al. 2001).

It is important to highlight that the number of studies focusing on apoptotic bodies is not that high as up to date, more interest has been set on other type of EVs. Nonetheless, it seems clear that apoptotic bodies formation allows both, maintenance of tissue homeostasis through cell clearance and intercellular communication.



Overall, EVs research field has largely expanded in the last years and great advances on defining the different EV populations have been done. Currently EVs classification is based on the biogenesis as well as physical and molecular properties. Nonetheless, increasing evidence suggests that within these three major populations described above, different subpopulations exist. In fact, EVs linked to concrete diseases have been described (Willms et al. 2018). As an example, EVs released from brain tumor cells ranging 100-400 nm size were called “oncosomes” as they were carrying oncogenic form of epidermal growth factor (EGFR), EGFRvIII, which is specific of glioblastoma (Al-Nedawi et al. 2008). Another example of EV subpopulations are tissue-specific EVs, such as prostasomes, which are produced by prostate epithelial cells and released into the prostatic fluid. Ranging 40-500 nm size, these vesicles are localized in large storage vesicles and seem to be originated at Golgi apparatus, fusing directly with the plasma membrane (Sahlén et al. 2010). Prostasomes seem to be involved on the regulation of male reproduction and were shown to play a role in PCa (Aalberts, Stout, and Stoorvogel 2014; Ronquist and Nilsson 2004; Llorente, van Deurs, and Sandvig 2007).

Thus, with no doubt, nowadays, EVs heterogeneity is probably the major challenge in the field, which might be solved with the development of novel and more sensitive devices and techniques that will allow a more precise characterization of the vesicles.

III.3 Extracellular vesicles as active players in cancer progression

EVs are active contributors of cancer progression, through the transfer and maintenance of cancer hallmarks and promoting resistance to therapy (Xavier et al. 2020). Communication between malignant cells as well as with their microenvironment can be established via EVs, and this contributes to the progression of cancer through different mechanisms. The work by El-Sayed and colleagues showed how PCa-derived EVs inhibit AR signaling in less aggressive PCa cells. These recipient cells turned phenotypically more mesenchymal, and enhanced their migratory, invasive and therapy resistance capacities (El-Sayed et al. 2017). In the same line, highly aggressive HCC-derived EVs were shown to promote migration of less malignant HCC cells (Qu et al. 2019). Oncogenic miR-424 transfer via EVs derived from an aggressive PCa context was shown to reprogram low tumorigenic PCa cells and normal prostate epithelial cells towards more aggressive phenotypes. These events were shown to further contribute to PCa recurrence and progression (Albino et al. 2021).

Development of de novo vasculature is essential for tumor growth and metastasis. Indeed, glioma derived EVs containing a specific non-coding RNA were able to promote angiogenesis, inducing endothelial cells (ECs) migration and proliferation capacities and suppressing apoptosis. Mechanistically, it was associated to an upregulation of VEGFA, TGF β and Bcl-2 and downregulation of pro-apoptotic mediators Bax and caspase 3 in EV-recipient ECs (Lang et al. 2017).



PCa-derived EVs were also related to tumor escape by means of inducing an immune-suppressive environment. This was shown to happen through the presence of MICA/B and ULBP2 ligands in the EVs, which downregulate the surface receptor NKG2D in natural killer (NK) and CD8+ T cells (Lundholm et al. 2014). Gastric cancer EVs were also shown to induce an immunosuppressive environment in the lung via regulation of different immune cell populations, although the exact mechanism remains to be elucidated (J. Liu et al. 2020).

Another interesting example of the role that EVs play in cancer progression concerns metastasis to the brain. The elegant work performed by Zhang et al, showed how metastatic cells lose PTEN after colonizing the brain. This loss of PTEN was triggered by astrocyte-derived EVs containing various PTEN-targeting microRNAs. Mechanistically, PTEN loss in the brain triggered the release of chemoattractant CCL2, leading to the recruitment of myeloid cells that further contributed to the increased proliferation and apoptosis inhibition of malignant cells (L. Zhang et al. 2015). In the same line, stromal-derived EVs produced by cancer-associated fibroblasts (CAFs) were shown to boost PCa cells growth. This happened through the transfer of metabolites that replenished central carbon metabolism of PCa cells under nutrient deprivation (Zhao et al. 2016).

Finally, EVs role on preparing the sites of metastasis cannot be obviated. Why primary tumors can progress in certain tissues was long time ago proposed by Paget with his "seed and soil" hypothesis, in which he claimed that metastatic cells had affinities for organs that could provide them with a certain milieu where to grow (Paget 1889). This hypothesis is favored by the concept of "pre-metastatic niche", which suggests that tumor cells at their primary site can modify the sites of metastasis before their arrival. In this sense, the work by Peinado and colleagues demonstrated how melanoma exosomes educate bone marrow derived cells (BMDCs), which further boost metastasis formation in the lungs (Peinado, Alečković, et al. 2012). In addition, EVs produced by hypoxic PCa PC3 cells were shown to be involved on the induction of matrix metalloproteinases at the metastatic sites (Deep et al. 2020). Indeed, tumor organ-tropism seems to be directed by the presence of specific adhesion molecules in the EVs (Hoshino et al. 2015).

Finally, EVs have also been related to therapy resistance. CAFs were shown produce EVs containing whole mitochondrial DNA (mtDNA). Uptake of these EVs by BCa stem cells restored OXPHOS and promoted exit from dormancy. These recipient cells acquired self-renewal traits and resistance to therapy (Sansone et al. 2017). Other studies have shown the contribution of EVs to therapy in different cancer types seemingly through the transfer of lipids, ncRNAs, and proteins among other molecules (Soekmadji and Nelson 2015; D. Sousa et al. 2020).

Overall, the impact of EVs in cancer is evident, contributing along different tumor stages and to the acquisition of cancer hallmarks. EVs mediate crosstalk between distinct cell populations, which added to the myriad of molecules they can transfer, makes the study of EVs role in cancer challenging (**Figl 21**). Still, understanding EVs ample roles in cancer opens new avenues for the development of therapeutic strategies, including the disruption of EVs secretion or EV-based drug delivery systems.

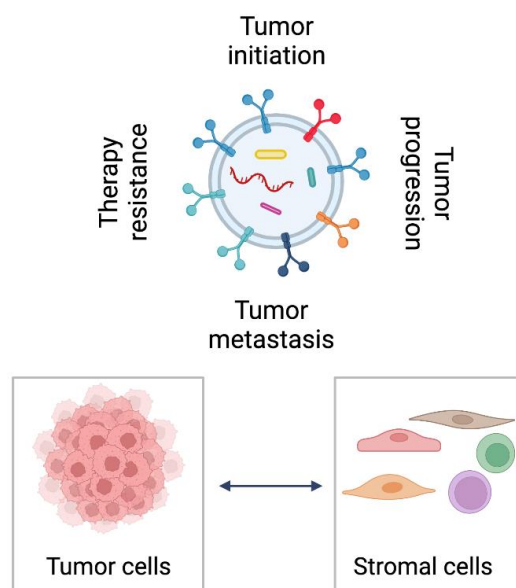


Figure I 21. Role of EVs along the different stages of cancer and the crosstalk established between different cell populations.

III.4 Extracellular vesicles as non-invasive biomarkers

The concept of liquid biopsy is based on the sampling of non-solid biological fluids that are enriched in CTCs, nucleic acids, proteins and EVs, and it shows great advantages in terms of avoiding invasive procedures and promoting precise medical intervention. In fact, another advantage is that liquid biopsies can be even obtained along short periods of time, thus allowing better disease monitoring.

EVs are released by nearly any type of cell and can be found in almost any biological fluid at considerable concentrations (Torrano, Royo, et al. 2016). They are stable units that carry specific molecules protected by a lipid bilayer, making them ideal candidates as non-invasive biomarkers of practically any type of disease, including cancer (Torrano, Royo, et al. 2016). EVs have shown to be bona fide tools for early tumor detection, diagnosis, prediction, and disease monitoring during treatment (Zhou et al. 2020). Indeed, analysis of both, proteins and nucleic acids contained in EVs, has shown to be useful. It seems that EVs proteome fairly represents and distinguishes cancer types, independently of their stage, hence making them valuable for the diagnosis of tumors of unknown primary origin (Hoshino et al. 2020). On the other hand, detection of specific *BRAF* mutations in EVs isolated from lymphatic drainage of melanoma patients was shown to accurately reflect *BRAF* status in the tumor tissue and to be correlated with the risk of relapse (García-Silva et al. 2019). Detection of miRNAs contained in EVs has also shown to be a potential source for the development of novel biomarkers in a wide number of cancer types (Rajagopal and Harikumar 2018). The use of EVs as bystanders in PCa was also proven to be possible. Urinary EVs were shown to contain an altered *CDH3* transcript, reflecting the altered status of *CDH3* in the prostatic tissue of origin (Royo et al. 2016). The combination of a panel of



proteins found in urinary EVs also showed to be a good source for PCa detection and stratification (Sequeiros et al. 2017).

With no doubt, EVs are fingerprints of their cell of origin, and this specificity makes them ideal bystanders of any biological scenario. Although their use in the clinics is at an early stage as technical aspects regarding the standardization of isolation protocols, sample specificity and purity need to be well established, EVs are slowly becoming a reality for disease diagnostics.

III.5 Soluble factors (SFs)

Soluble factors (SFs) is a generic term that includes the non-EV secretome fraction, from which proteins such as ECM constituents, shed receptors, cytokines, as well as angiogenic and growth factors seem to be the main constituents (Brady et al. 2016; Villatoro et al. 2019).

It was estimated that a total number of 2,641 genes encode for potentially secreted proteins (Uhlén et al. 2019). This study only included proteins with signal peptide and lacking transmembrane domains. Most of the predicted actively secreted proteins seemed to be released to the blood with functions related to coagulation, interferon responses, cytokines, and growth factors.

Eukaryotic organisms are endowed with an endomembrane system that is composed of independent organelles involved in the protein biogenesis, modification, and secretion to the extracellular milieu. Membrane bound vesicles are used for the movement of the cargo in two directions: from the endomembrane system to the plasma membrane and extracellular space (exocytosis) and from the plasma membrane towards the endomembrane system (endocytosis).

Proteins found in the cell secretomes are secreted through three major mechanisms: conventional protein secretion, unconventional protein secretion and ectodomain shedding (**Fig 22**) (Villarreal et al. 2013; Nickel and Rabouille 2009).

Conventional protein secretory pathway

Proteins are most secreted through the conventional secretory pathway. Proteins containing a short N-terminal amino acid sequence known as signal peptide (SP), are guided by the ribosomes and enter the lumen of the ER, where they are folded and suffer PTMs. Next, proteins are guided to the Golgi apparatus, where further modification reactions take place. Different compartments can be distinguished in this organelle: cis, medial, and trans-Golgi. Trans-Golgi network acts as a crossroad where proteins can be either sent to the cell surface or to additional organelles, including lysosomes and endosomes. The transport between compartments is done through small vesicles that originate in the donor compartment. In fact, coating proteins are essential for directing the vesicles to the target compartment. In this way, clathrin-covered vesicles deliver proteins between trans-Golgi network, endosomes, lysosomes, and the plasma membrane. On the other hand, vesicles covered with COPI coatomer complex mediate retrograde transport between Golgi and ER. Finally, COPII-coated vesicles move



proteins from ER to Golgi. Of note, coating proteins besides from reflecting the origin of the vesicles and their target organelle, they also contribute to the vesicle formation and to the cargo selection (M. C. S. Lee et al. 2004).

Unconventional protein secretory pathway

Unconventional protein secretion refers to a series of ER-Golgi-independent routes, and in some cases involves use of EVs (microvesicles and exosomes) for secretion (Nickel and Rabouille 2009). Both proteins with and without signal peptide (termed leaderless), have been reported to follow the unconventional protein secretory pathway. Four mechanisms of unconventional protein secretion have been proposed and most of them are induced by cellular stress, including mechanical and nutrient stress, inflammation, and endoplasmic reticulum stress (ER stress) (Nickel and Rabouille 2009; Rabouille 2017; Rabouille, Malhotra, and Nickel 2012). Type I, II and III mechanisms include leaderless proteins, whereas type IV unconventional protein secretory pathway includes proteins with signal peptide.

Ectodomain shedding

Ectodomain shedding is another important mechanism by which proteins can be released to the extracellular milieu, and it consists of the proteolytic release of transmembrane proteins. Proteolytic cleavage is mainly triggered by metalloproteases (Reiss and Saftig 2009), and apparently alternative splicing events and protein PTMs occurring in the Golgi apparatus also influence this process (Shirakabe et al. 2017). Shedding mainly affects membrane-anchored proteins such as growth factors, adhesion molecules, cytokines, or scavenger receptors (Reiss and Saftig 2009; Hofmann et al. 2020).

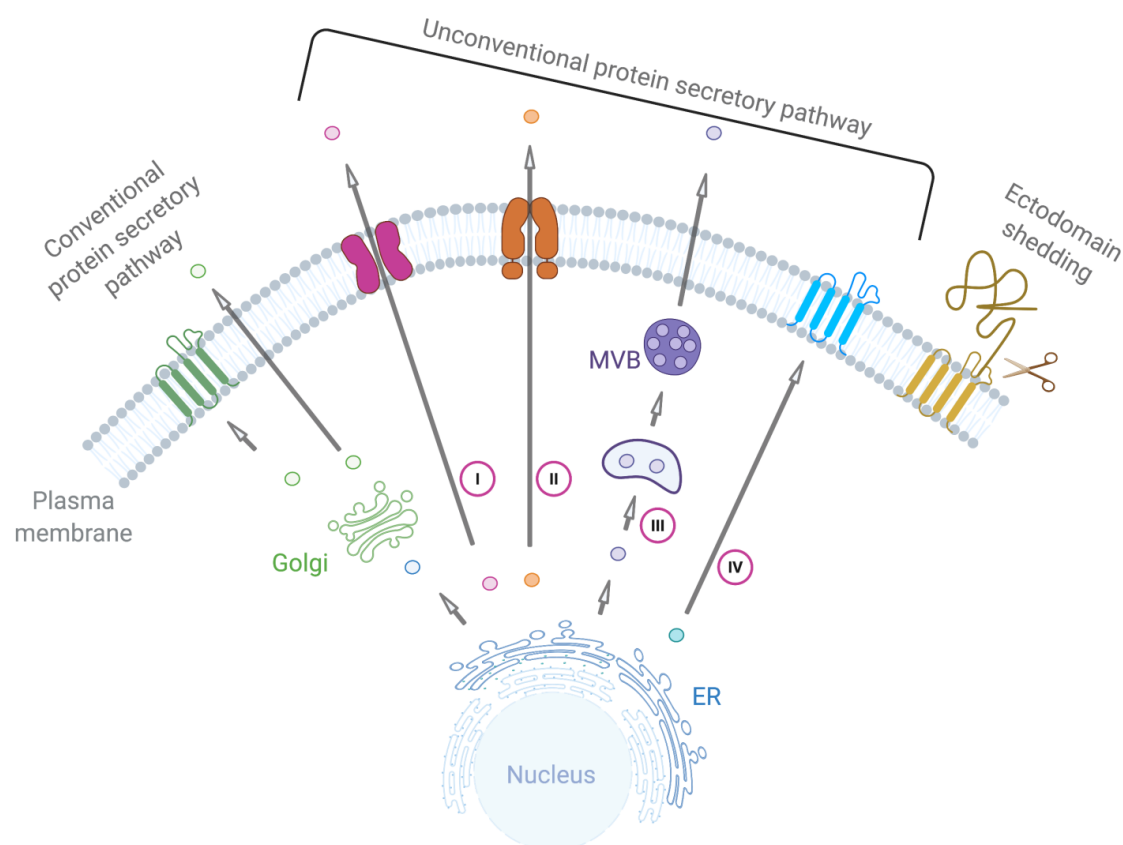


Figure I 22. Overview of the three major mechanisms of protein secretion found in cells.

III.5.1.1 Role of interferons as mediators of cell communication

Among the great variety of secreted proteins, cytokines, which are small, soluble secreted proteins, have great impact on autocrine and paracrine cell communication (J. M. Zhang and An 2007). Most cytokines seem to follow the conventional protein secretory pathway, although there are some exceptions, which follow the unconventional protein secretory pathway (Stanley and Lacy 2010). Cytokines include a myriad of molecules, and are classified according to their function into interleukins, colony-stimulating factors, interferons (IFNs), tumor necrosis factors and chemokines (McGraw-Hill 2005). Aligned with the results of this thesis work, focus will be set in IFNs.

IFNs trigger anti-viral, anti-proliferative and immunomodulatory responses in the cells, via autocrine and paracrine mechanisms (Stanifer, Pervolaraki, and Boulant 2019). This family of cytokines is widely expressed, and based on their protein sequence, function, and binding receptor, three main classes can be distinguished (**Figl 23**) (B. S. Parker, Rautela, and Hertzog 2016a):

Type I IFNs

It includes a high number of molecules, that can be grouped in five categories among which, IFN- α and IFN- β are the most studied ones. Interestingly, all genes encoding for type I IFNs cluster in chromosome 9 (Platanias 2005).

- 1) IFN- α , that is further subdivided in: IFN- α 1, α 2, α 4, α 5, α 6, α 7, α 8, α 10, α 13, α 14, α 16, α 17 and α 21.
- 2) IFN- β
- 3) IFN- ϵ
- 4) IFN- κ
- 5) IFN- ω

All type I IFNs bind to the same transmembrane receptor, which, is constituted of two subunits: IFNAR1 and IFNAR2 (Platanias 2005). Type I IFNs are transcriptionally regulated, and their expression is induced by the presence of pathogen-associated molecular patterns (PAMPs) and damage-associated molecular patterns (DAMPs), produced by microorganisms and host cells, respectively. PAMPs include molecules found and released by microorganisms, including nucleic acids. On the other hand, DAMPs are released from the intracellular or extracellular space under tissue stress injury, cell death and cancer. They include different types of signals such as changes in phospholipids on the cell surface, nucleic acids, and secreted proteins (Schaefer 2014; Green et al. 2009). DAMPs and PAMPs are recognized by pathogen recognition receptors (PRRs) such as toll-like receptors (TLRs), retinoic acid-inducible RIG-like receptors (RLRs), melanoma differentiation associated gene 5 (MDA5) and cyclic GMP-AMP synthase/ stimulator of interferon genes (cGAS/ STING) that can be found in extracellular and intracellular membranes (Murira and Lamarre 2016) (Arimoto et al. 2018). Downstream signal transduction occurs through the IFN regulatory factors (IRFs), a family of transcription factors comprising nine members (IRF1-IRF9), that exert distinct transcriptional activities based on the first-lane activation of the pathway (Murira and Lamarre 2016).

Once type I IFNs are produced, they are released to the extracellular space, where they bind to IFNAR1/IFNAR2 that are associated to tyrosine kinases JAK1 and TYK2. These kinases phosphorylate signal transducer and activator of transcription (STAT) STAT1 and STAT2 proteins, which then bind to IRF9, conforming the IFN-stimulated gene factor 3 (ISGF3) complex that is translocated to the nucleus. Then, the ISGF3 complex binds to the IFN-stimulated response elements (ISREs) found in the promoter regions of IFN-stimulated genes (ISGs). Depending on the cellular context, type I IFNs can also activate STAT1-6 proteins and form different combinations of homo or heterodimers that bind to the gamma activated sequence (GAS) elements in ISG promoters (Stanifer, Pervolaraki, and Boulant 2019). Besides from the JAK-STAT signaling pathway, type I IFNs can also trigger other signaling cascades, including mitogen-activated protein kinase (MAPK) p38, PI3K signaling pathway, and CrkL-RAP1 pathway, which explains the ample range of biological responses they orchestrate (Platanias 2005; Stanifer, Pervolaraki, and Boulant 2019). Type I IFNs are mainly produced by epithelial cells, fibroblasts,



and dendritic cells (DCs), and they drive innate and adaptive immune responses, affecting to myeloid cells, B-cells, T-cells, NK cells, DCs due to the broad expression of IFNAR1/IFNAR2 receptors (McNab et al. 2015).

Type II IFNs

Only a type II IFN exists, IFN γ , which binds to a receptor composed of two subunits (IFNGR1 and IFNGR2). IFN γ is activated by mitogens and cytokines such as IL-12 and IL-18 that are mainly released by T-cells and NK cells. Indeed, NK cells are the main type II IFN producers in response to viral infections (A. J. Lee and Ashkar 2018).

Type II receptor subunits IFNGR1 and IFNGR2 are linked to JAK1 and JAK2 kinases which further phosphorylate STAT proteins. Mainly STAT1 and STAT3 homo or heterodimers are formed, and these are translocated into the cell nucleus where they bind to GAS elements in ISG promoters (B. S. Parker, Rautela, and Hertzog 2016a).

Type III IFNs

Four members comprise this group, and they do all bind to the heterodimeric receptor IFN λ complex, which is composed of receptor chain 1 (IFN- λ R1) and IL-10 receptor subunit β (IL-10R β) (Wack, Terczyńska-Dyła, and Hartmann 2015).

- 1) IFN λ 1 (also known as interleukin-29 (IL-29))
- 2) IFN λ 2 (also known as IL-28A)
- 3) IFN λ 3 (also known as IL-28B)
- 4) IFN λ 4

Like type I IFNs, activation of type III IFNs is via recognition of DAMPs and PAMPs (Stanifer, 2019). The type III IFN receptor is associated to JAK1 and TYK2, which lead to phosphorylation of STAT1 and STAT2 proteins that further bind to IRF9, resulting in the ISGF3 assembly and binding to the ISREs. Type III IFNs can also induce the formation of STAT homo and heterodimers that bind to GAS elements and induce the transcription of ISGs (Stanifer, Pervolaraki, and Boulant 2019). Thus, although type I and type III IFNs use different receptors, they induce the expression of similar genes. Type III IFNs are mainly produced by hematopoietic lineage and epithelial cells. Indeed, it seems these types of IFNs are key for protecting epithelial surfaces from viral infections (Wack, Terczyńska-Dyła, and Hartmann 2015)

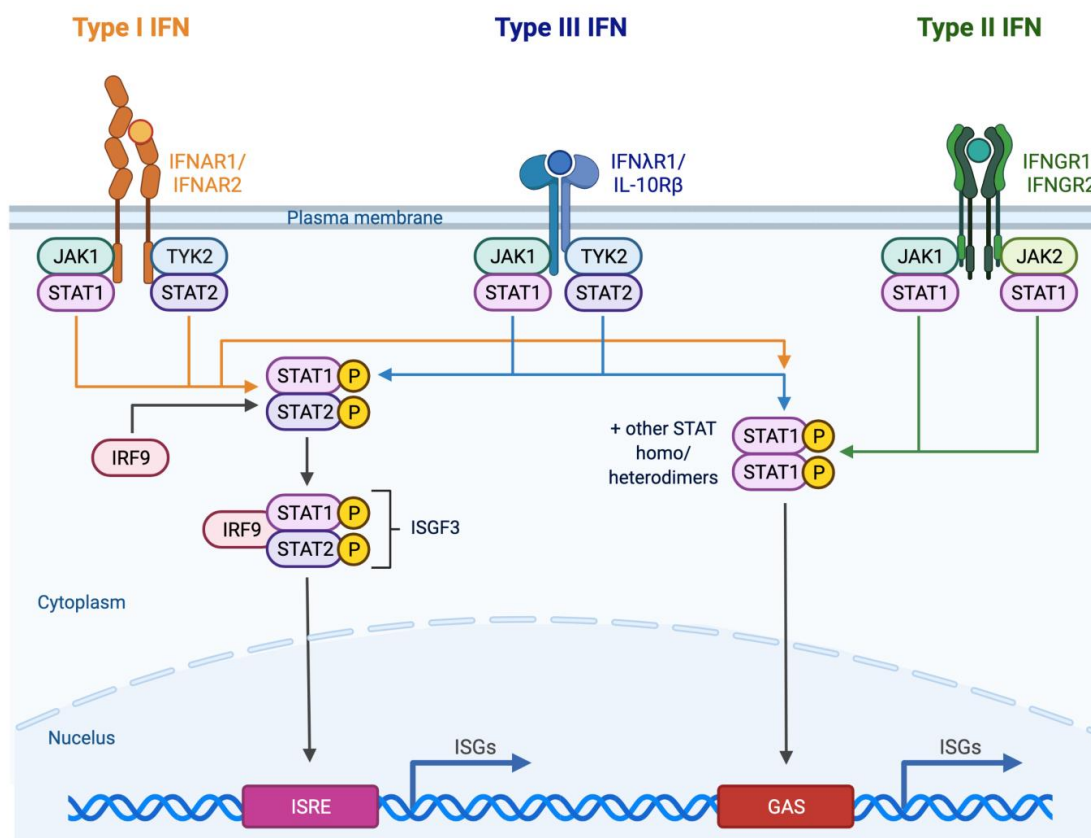


Figure 1 23. Type I, II and III interferon signaling transduction.

IFNs exert cell-intrinsic and cell-extrinsic anti-tumor effects (**Fig 24**). The source, inducer, type, and concentration of IFN as well as the presence of cognate receptors impact on the outcome induced by IFNs (Parker, 2016). Upon binding to their cognate receptors, IFNs activate the transcription of genes involved in the regulation apoptosis (TRAIL), proliferation (CDKs), antiviral response (such as OAS1, MX1 and RNASEL), migration (chemokines), inflammation (CXCL10) and antigen-presenting molecules (MHC class I and II components) (Peteranderl and Herold 2017; Medrano et al. 2017a; B. S. Parker, Rautela, and Hertzog 2016b; Seliger, Ruiz-Cabello, and Garrido 2008). IFNs do also impact on angiogenesis, osteoclastogenesis and immunity, orchestrating the activity of almost any immune cell type (B. S. Parker, Rautela, and Hertzog 2016c). They activate anti-tumor immune cells, including T cells, NK cells, DCs, and repress the activity of immune suppressive cells such as regulatory T cells (Treg), tumor-associated macrophages (TAMs), and myeloid-derived suppressor cells (MDSCs). IFNs enhance the interactions established between tumor and immune cells, providing the ground for the design of immune-based therapies to treat cancer (B. S. Parker, Rautela, and Hertzog 2016b; Arimoto et al. 2018). Indeed, the main objective of immunotherapy, is mastering the immune system, overcoming the immunosuppressive microenvironment to fight cancer (Waldman, Fritz, and Lenardo 2020). Yet, a major challenge for the use of IFNs for treating cancer is predicting patient sensitivity to the different types of IFN (B. S. Parker, Rautela, and Hertzog 2016b). Although IFN signaling is tied to an enhancement of the immune response, it can also induce



immunosuppression and promote cancer cell-intrinsic resistance mechanisms, thereby displaying pro-tumorigenic roles (Minn 2015; Aricò et al. 2019; B. S. Parker, Rautela, and Hertzog 2016a). Different strategies that aim at boosting IFN response for treating cancers are currently being developed, including genetically modified immune cells, recombinant vectors for delivering IFN and TLR-agonists (Medrano et al. 2017a). In this line, treatment of high-risk melanoma patients with high IFN doses as an adjuvant therapy showed increased disease-free survival and overall survival (Mocellin et al. 2010). Metastatic BCa patients also seem to benefit from the treatment with IFN in combination with tamoxifen (Recchia et al. 2009). Sipuleucak-T immunotherapy-based vaccine was approved for treating mCRPC, showing to be safe and to improve patients average overall survival in 4.1 months (Kantoff et al. 2010).

Finally, the dysregulation of IFN production or response can lead to immune pathologies and therefore needs to be tightly regulated. Different mechanisms are known to negatively regulate IFNs targeting PRRs or downstream transcription factors. Negative regulation of IFN seemingly occurs via PTMs (such as ubiquitination and sumoylation), epigenetic mechanisms (microRNAs and chromatin remodeling processes) and transcriptional repressors that act on ISGs promoters. Response to IFN is also known to be modulated via regulation of the cognate receptors, thus blocking downstream signaling events (Ivashkiv and Donlin 2014; Arimoto et al. 2018).

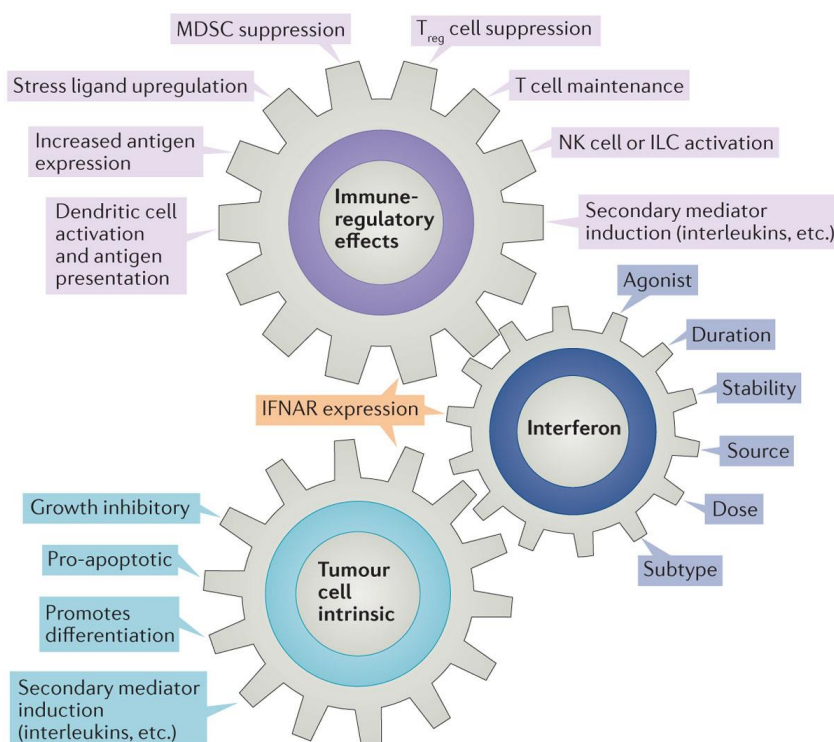


Figure 1 24. Cell-intrinsic and extrinsic anti-tumor roles of interferons. ILC: innate lymphoid cells. Parker, Rautela and Hertzog. *Nature Reviews* (2016).



III.6 Transcriptional regulation of the cell secretome

The regulation of the secretome composition is crucial for maintaining the body physiology. It involves the cooperation and coordination of multiple intracellular organelles that are responsible for the formation of EVs, protein maturation and modifications, followed by the release to the extracellular space. Indeed, tissues are known to specifically express genes involved in the secretory pathway, thus influencing the diversity of secreted proteins and their correspondent PTMs (Feizi et al. 2017). Hypothesizing that these genes could be regulated by transcriptional coregulators is a feasible explanation that could account for the fine-tuned and rapid responses that govern secretion of certain molecules in response to internal and external stimuli. Not much attention has been paid to this concept, finding only a few works exploring it in a cancer context. In this sense, the work by Brady and colleagues nicely demonstrated how the transcription factor Arntl2, and its partner Clock control the secretome composition. Matricellular protein Smoc2 contained in the Arntl2/Clock-driven secretome promoted cancer cell survival seemingly by enabling cancer cell interactions with the ECM. This further boosted metastatic lung cancer cells self-sustenance in foreign environments (Brady et al. 2016).

The work performed by Obenauf et al revealed a secretome-mediated mechanism by which lung and melanoma tumors harboring BRAF or EGFR mutations or ALK translocations become resistant to kinase inhibitors. These malignant cells generated a therapy-induced secretome (TIS) that sustained survival of therapy-sensitive cells whilst promoting growth of therapy resistant minority clones. Interestingly, authors showed that this TIS, which was regulated by FRA1 transcription factor, was enriched in AKT pathway inducers, thus revealing novel therapeutic strategies for the treatment of BRAF, EGFR and ALK therapy-resistant tumors (Obenauf et al. 2015).

The study by Ibrahim and colleagues also suggests an autocrine and paracrine role of secreted factors on promoting malignant cells proliferation and migration in the absence of growth-inducing factors. Both the secretion and responsiveness of these factors seemed to be dependent on the activity of transcription factor AP-1 (Abd et al. 2018). Another work suggested that secretion of proinflammatory cytokines IL-6 and IL-8 induced in an NFkB-EZH2-dependent manner, sustains triple negative BCa cells (TNBCs) growth and resistance to therapy by an autocrine mechanism (Hartman et al. 2013). The study performed by Lujambio et al shows the non-cell autonomous role of p53 on suppressing hepatocellular carcinoma (Lujambio et al. 2013). Under chronic liver damage conditions, p53 was shown to induce an anti-tumoral microenvironment that was at least partially mediated by the release of secreted factors produced by senescent hepatic stellate cells. p53 loss led to the ablation of the senescent program, triggering proliferation of premalignant cells, and stimulating macrophages polarization towards pro-tumorigenic class M2. The regulation of the hepatic stellate cells secretome was shown to be through the cooperation of p53 and NFkB. Indeed, several of the secreted factors identified are known targets of both p53 and NFkB.

In line with the studies mentioned above, the transcriptional coregulator PGC1 α was shown to control the secretome composition of different cell lines, including hepatic carcinoma



cells (Minsky and Roeder 2017). Furthermore, a PGC1 α -dependent regulation of myokines secretion, was suggested to influence crosstalk between muscle and pancreatic islets, which was crucial for maintaining glucose homeostasis (Handschin, Chin, et al. 2007). The hormone irisdin was shown to be regulated by PGC1 α in the muscle and further secreted to the extracellular milieu, where it activated adipose thermogenesis via UCP1 transcription factor activity. Indeed, irisdin, which is induced by exercise, increased body energy expenditure and insulin resistance, thus granting this hormone with therapeutic potential (Boström et al. 2012).

Overall, these works reveal the potential of transcriptional regulators on modulating the cell secretome, and to our knowledge, exploring the role of PGC1 α on directing the PCa secretome remains to be elucidated.

The background features several overlapping, semi-transparent circles in various shades of gray and white, scattered across the page. A central horizontal gray bar contains the word "Objectives" in a bold, italicized, black sans-serif font.

Objectives

Objectives

Prostate cancer (PCa) is the world second type of cancer most diagnosed among men, and accounts for the fifth leading cause of death in this sex worldwide, according to Globocan 2020. Most of these deaths occur in patients with metastasis, highlighting the need of understanding the mechanisms that promote the aggressive form of this disease, thus, allowing the design of more effective and targeted therapies.

The transcriptional coactivator PGC1 α is a master regulator of cell metabolism, and its dysregulation has been shown to occur in different cancer types (Luo et al. 2016; Andrzejewski et al. 2017). In the context of PCa, PGC1 α is progressively downregulated from the primary towards the metastatic tumor, and this is of prognostic value (Torrano, Valcarcel-Jimenez, et al. 2016). Mechanistically, PGC1 α together with the ERR α exerts a tumor and metastasis suppressive activity by means of controlling intrinsic biological events such as cell metabolism and cytoskeleton rearrangements (Torrano, Valcarcel-Jimenez, et al. 2016; Valcarcel-Jimenez et al. 2019). The fact that PGC1 α is a key player along PCa progression is undeniable, but there are still open questions regarding how it exerts its tumor-suppressive activity. So far PGC1 α 's major effects in PCa have been attributed to the regulation of cell-intrinsic phenomena, while no attention has been set to its role on the regulation of cell secreted entities (**FigO 1**).

Hence, this thesis project aims at elucidating the impact that the transcriptional control of metabolism has on the production and content of the cell secretome with the final aim of identifying novel therapeutic strategies by means of interfering with the cell communication networks, and this is based on the following hypothesis: ***PGC1 α modulates the secretome (soluble factors and extracellular vesicles) composition of prostate cancer epithelial cells, and the latter impacts on the cell communication networks established between cells in an autocrine and paracrine manner.***

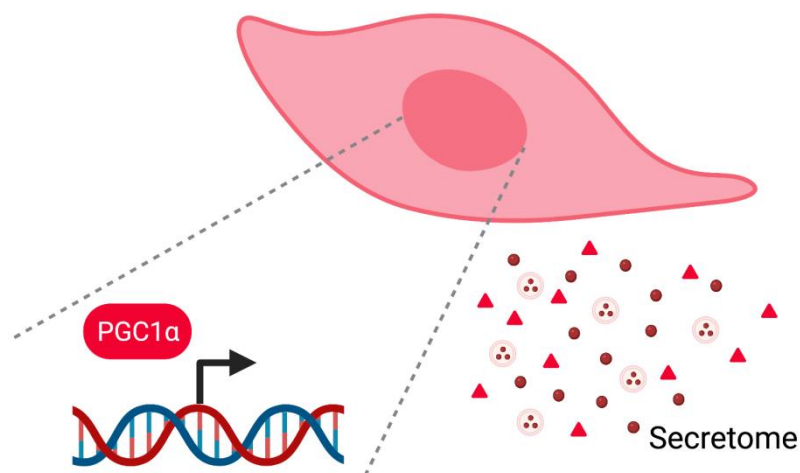


Figure O 1. Transcriptional control of the PCa cell secretome



Taking advantage of bioinformatics tools, *in vitro* cell lines and animal models of PCa where we can modulate the metabolism through the deregulation of PGC1 α , we propose the following aims:

- I. Evaluation of the biological impact of the cell secretome on PCa aggressiveness.
 1. To assess the biological effect of PGC1 α -driven secretome on PCa cell lines.

- II. Study and description of the extracellular vesicles fraction of the cell secretome associated to PGC1 α modulation in PCa cell lines.
 1. EVs physical and molecular characterization.
 2. Study the biological impact of EVs: *in vitro* and *in vivo* assays.
 3. To evaluate the role of EVs as bystanders of PCa aggressiveness.

- III. Study and description of the soluble factors fraction of the cell secretome associated to PGC1 α modulation in PCa cell lines.
 1. To assess the biological impact of the soluble factors: *in vitro* and *in vivo* assays.
 2. To characterize of the protein content of secretome and its cell-intrinsic regulation by the producer cells.
 3. To study the molecular cues triggered upon treatment of PCa recipient cells with the differential secretomes.

- IV. To examine the cell-intrinsic molecular events triggered by PGC1 α in PCa producer cells that could mediate the effects of the secretome.
 1. To decipher the molecular cues activated upon PGC1 α expression in PCa producer cells.

The background of the page is a light pink color with numerous overlapping circles of various sizes and shades of red and pink, creating a watercolor effect. The circles are scattered across the entire page, with some being more prominent than others.

Materials & Methods

I. Materials

I.1 Cell lines and culture conditions

Human prostate carcinoma cell lines (PC3 and DU145) were purchased from the Leibniz Institute DSMZ (Deutsche Sammlung von Mikroorganismen und Zellkulturen GmbH) and from the American Type Culture Collection (ATCC), in the case of the 22Rv1 cell line. Both entities provided authentication certificate. PC3 and DU145 cell lines were cultured in Dulbecco's Modified Eagle Medium without pyruvate (DMEM; Gibco Ref. 41965-039) and 22Rv1 cells were cultured in RPMI (Gibco 61870-010; with GlutaMAX supplement). Occasionally, for secretome experiments, 22Rv1 cells were treated with distinct conditioned medias obtained from cells cultured in DMEM without pyruvate. HEK293FT cells were provided by the group of Dr. Hector Peinado (Centro Nacional de Investigaciones Oncológicas) and were cultured in DMEM with pyruvate (Gibco, Ref. 41966-029). See **Table M 1** for further cell line specifications.

Cell line	Cell type	Morphology	Origin	Pten status
PC3 (ACC 465)	Prostate adenocarcinoma	Epithelial-like	Bone metastasis. Grade IV	Negative
DU145 (ACC 261)	Prostate carcinoma	Epithelial-like	Brain metastasis	Positive
22Rv1	Prostate carcinoma	Epithelial	From CWR22 xenograft propagation after castration-induced regression and relapse	Positive
HEK293FT	Human embryonic kidney cells	Fibroblast	Human primary embryonal kidney transformed by adenovirus type 5	Negative

Table M 1. Cell lines used in this work including their main characteristics.

I.2 Prostate cancer stable cell lines

PC3 TRIPZ PGC1A cell line

PC3 cell lines with ectopic expression of PGC1 α were generated by Dr. Verónica Torrano and Dr. Lorea Valcárcel. Briefly, the TRIPZ™ lentiviral inducible vector (Dharmacon) was engineered to be Tet-On and become inducible in the presence of doxycycline. This induction is carried out by the tetracycline response element (TRE) and the transactivator (rtTA3). In the presence of doxycycline, the expression from the TRE promoter is activated; therefore, the RFP and shRNA regions were substituted by HA-Flag-Pgc1 α (**FigM 1**). As a result, a vector named TRIPZ-HA-Pgc1 α was generated and used to generate second generation lentivirus (Torrano, Valcarcel-Jimenez, et al. 2016). Packaging HEK293FT cells were transfected with lentiviral

vectors, and the viral supernatants were further used to infect PC3 target cells. Selection was done with 2 µg/ml puromycin (Sigma, Ref. P8833) for three days, adding in parallel a negative control of non-infected cells to verify correct function of the antibiotic.

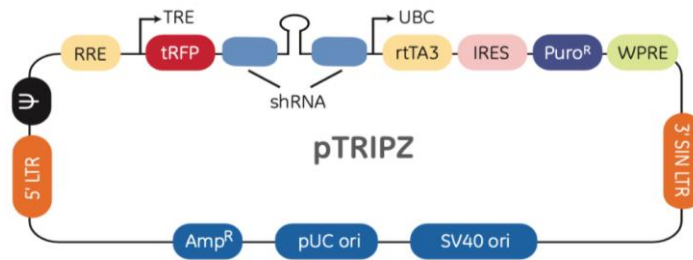


Figure M 1. Overview of the TRIPZ inducible lentiviral vector (Dharmacon).

PC3 TRIPZ cell line

The PC3 TRIPZ control cell line was generated by Dr. Verónica Torrano and Dr. Lorea Valcárcel. Again, the TRIPZ™ lentiviral inducible vector (Dharmacon) was used to produce second-generation lentivirus to finally obtain the control cell line.

PC3 PGC1A sgERRA cell lines

PC3 cell lines with combined expression of PGC1α and deletion of ERRα were generated by Dr. Lorea Valcárcel. For *ESRRA* deletion, sgRNA constructs targeting *ESRRA* (sgERRα#1: 5'CTCCGGCTACCACTATGGTGTGG3'; sgERRα#2: 3'AGGAACCCTTTGGACTGTCAGGG5') were designed using Crispor software (crispor.tefor.net) and cloned in a lentiviral vector, purchased from Addgene LentiCRISPR V2 (a gift from Mohan Babu, Addgene plasmid # 83480).

PC3 sh c-MYC cell lines

PC3 cell lines with doxycycline inducible-silencing of *c-MYC* were generated by Alice Macchia. Shortly, lentiviral vector expressing validated sequences of short-hairpin RNAs (shRNAs, sh41 *c-MYC* and sh42 *c-MYC*) targeting human *c-MYC* (Mission® shRNA Library, TRCN0000039642) were subcloned into a pLKO Tet On inducible system with puromycin resistance (Addgene #21915). As previously described, packaging HEK293FT cells were transfected with lentiviral vectors, and the viral supernatants were further used to infect PC3 target cells. Selection was done with 2 µg/ml puromycin (Sigma, Ref. P8833) for three days, adding in parallel a negative control of non-infected cells to verify correct function of the antibiotic.

All cell culture medias were supplemented with 1% Penicillin/Streptomycin (Gibco, Ref. 15140-122) unless specified and with 10% inactivated Fetal Bovine Serum (FBS) (Gibco) coming from the same lot and previously analyzed to confirm experimental reproducibility. For washing cells DPBS 1x (Gibco, Ref. 14190-94) was used. All the experiments were performed using the complete media, although, for secretome, soluble factors and EVs isolation experiments, DMEM

without pyruvate depleted from bovine derived EVs was prepared. This is of great importance to avoid any contamination with bovine vesicles, especially for the isolation of EVs from cell cultures. In order to remove bovine-derived extracellular vesicles, 50 ml FBS were diluted in a 1:1 proportion using DMEM without pyruvate. The mixture was pipetted to a 45 Ti ultracentrifuge tube and was ultracentrifuged at 100,000 x g for 16 hours and at 4 °C. Following the ultracentrifugation step, supernatants were poured to the remaining bottle of DMEM without pyruvate and 1% P/S was added. Then, whole bottle of media was filtered through 0.22 µm pores and stored at 4 °C ready to be used (DMEM Exo-free).

All cells were grown at 37°C in a humidified atmosphere of 5% CO₂. Cells were routinely cultured in 100 mm or 150 mm dishes and split every three to four days to maintain a confluence not higher than 80-90% and were used up to a maximum of 30 passages. Mycoplasma was routinely tested using MycoAlert detection kit (Lonza, Ref. LT07-318) and always replacing the cells in case of positive results.

To split or to seed experiments, after a washing step with DPBS 1X, cells were incubated with trypsin-EDTA solution (Gibco, Ref. 25200-056) at 0.05% for 3 minutes at 37 °C and then resuspended in fresh complete media. For cell counting, once cells were trypsinized, a dilution of 1:2 was done using Trypan Blue Dye 0.4% (Sigma-Aldrich, Ref. T8154-20ML). Then, 10 µl of the mixture was loaded to the Neubauer chamber to count viable cells using the optical microscope (Olympus Axio Imager A1 CKX31).

To be frozen, cells were trypsinized, resuspended in complete media and centrifuged for 4 minutes at 1500 rpm to ensure cell precipitation. Supernatant was removed and cell pellet was resuspended in a solution of FBS 10% dimethyl sulfoxide (DMSO) (Panreac, Ref. A3672.0100) and pipetted into a cryovial. The latter was introduced inside a Mr. Frosty cage (Sigma-Aldrich) and placed at -80 °C at least for 24 hours. Cell vials were kept in liquid nitrogen.

I.3 Generation of stable cell lines

I.3.1 Generation of PC3 TGL cell line

PC3 TGL cells were generated in collaboration with Dr. Roger Gomis at the Institute for Research in Biomedicine (IRB, Barcelona) by Cristina Viera and Jana Crespo as follows:

Day 1: 293FT cells were seeded at 80-90% confluence in 150 mm plates in DMEM and were left to be attached for 8-10 hours. After this time, the transfection mix was prepared in the proportions seen in **Table M 2**. The mix was gently mixed and incubated for 15-20 minutes at RT. Meanwhile, SN from 293 FT cells was removed and 18 ml of fresh DMEM were added. The transfection mix was pipetted over the cells and incubated overnight at 37 °C.

Day 2: Media from 293 FT cells was changed and cells were left to grow at 33 °C for 48 hours. In parallel, PC3 target cells were seeded in 6-well plates for infection.

Day 4: Media from 293 FT cells was taken with a syringe and filtered through 0.5 µm pores into falcon tubes. Then, it was concentrated with 100K columns (3,000 x g, 1 hour, 4 °C) into a final volume close to 0.5 ml. To each volume of 0.5 ml of virus-enriched SN, 1 ml DMEM

without antibiotics and 8 µg/ml polybrene were added, mixed and pipetted into the target cells (1 ml/well). PC3 target cells were incubated overnight at 37 °C.

Day 5: Media from PC3 cells was changed and cells were left to grow 24 hours at 37 °C.

Day 6: Cells were sorted through the FACS based on the GFP expression.

Retrovirus	150 mm plate
Vsvg-R	1.2 µg
Gag-pol	10.8 µg
TK-GFP-luciferase (TGL) vector	12 µg
PEI(1 mg/ml, pH=7.45, filtered through 2 µm pores)	116 µl
NaCl (150 mM)	2,320 µl

Table M 2. Viral packaging vectors, TK-GFP-luciferase plasmid and reagents used for the retroviral infection of PC3 cells and generation of luciferin-inducible PC3 TGL cells. PEI: polyethylenimine

1.3.2 Generation of PC3 GFP-luc cell line

PC3 GFP-luc cells were generated at the Spanish National Cancer Research Center (CNIO, Madrid), following the protocol established at the Microenvironment and Metastasis Group led by Dr. Héctor Peinado. The following protocol was performed:

Day 1: HEK293FT cells were seeded in 100 mm plates at a 75% confluence for the generation of lentivirus. Once attached (around 8 hours later), SN were removed, and cells were washed with DPBS 1x followed the addition of 8 ml/plate of tempered DMEM. In parallel, transfection mix was prepared: FuGENE® (Promega) was used to increase transfection efficiency, and it was mixed in a 1:16 proportion with DMEM depleted of FBS and antibiotics. The mix was incubated for 5 minutes at room temperature (RT) and then, packaging vectors (p1, p2 and vsvg) together with the pFUGW-FerH-ffLuc2-eGFP plasmid were added to the mix, gently mixed and incubated for 15 minutes at RT. The transfection mix was pipetted to the HEK293FT cells drop by drop and incubated for 18 hours.

Day 2: media from HEK293FT cells was removed and 5 ml/plate of fresh DMEM supplemented with 10% FBS and 1% gentamycin were added.

Day 3: PC3 target cells were trypsinized and counted. A total number of 200,000 cells were pipetted into an Eppendorf tube, centrifuged, and resuspended in 750 µl of the viral supernatant obtained from the HEK293FT infected cells (proportion for one 6-well plate well). Then, another 750 µl of the viral SN was added to each well together with 8 µg/µl polybrene to enhance infection efficiency. On the other hand, fresh media was added to the HEK293FT cells and the whole process (days 2 and 3) was repeated.

After a week, infected PC3 cells were sorted using BD FACS Canto. The generation of these cell lines was done with the kind help of Marina Mazariegos, from the Microenvironment and Metastasis Group.

I.4 Drugs

Doxycycline was used throughout the whole thesis work at a concentration that was based on previous studies performed in the laboratory (Table M 3

Table M 3).

Regarding doxycycline pre-induction, three different experimental settings were applied. This information is more detailed in the coming sections.

1. Pre-induction of three days followed by experimental seeding still in the presence of doxycycline and collection of the cells at different time-points.
2. Pre-induction of 24 hours followed by change of media (DMEM Exo-free) together with the refreshing of doxycycline. EVs isolation and producer cells collection is 48 hours after addition of DMEM Exo-free.
3. Pre-induction of 48 hours followed by change of media (DMEM Exo-free) together with the refreshing of doxycycline. Secretome and producer cells are collected 24 hours after addition of DMEM Exo-free.

Drug	Supplier	Dose	Function
Doxycycline hyclate	Sigma (D9891)	0.5 µg/ml	Gene inducible system

Table M 3. Commercial information, dose and usage of doxycycline employed in the present work.

II Cellular analysis

II.1 Production of cell secretome

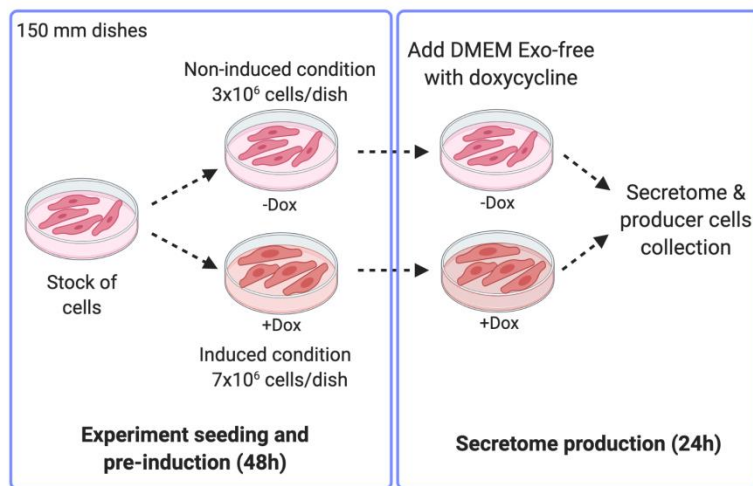
For secretome experiments (whole secretome, extracellular vesicles and soluble factors), always the number of producer cells was counted to have a controlled system in which, ideally, all conditions interrogated have the most similar number of cells. The only exception are the experiments for extracellular vesicles isolation that were used for proteomics analysis. This will be further addressed in the coming sections.

II.1.1 Whole secretome production

Secretome experiments were performed using three different PCa cell lines. PC3 cells with a doxycycline-inducible system to promote the expression of the metabolic regulator PGC1 α

(PC3 TRIPZ PGC1A cells) as well as PC3 cells with combined expression of PGC1 α and deletion of ERR α (PC3 PGC1A sgERRA cells). As control cells, PC3 TRIPZ (empty vector) cells were used. Unless specified, secretomes were always produced by cells seeded in 150 mm plates. Due to the reduction on cell proliferation observed upon the expression of PGC1 α , the number of cells seeded in the absence (-Dox) or presence (+Dox) of the transcriptional regulator was adjusted to have a similar number of producer cells at the day of secretome collection. Thus, a stock of PC3 TRIPZ PGC1A cells was counted and divided into two stocks; one without doxycycline (-Dox) and another one with doxycycline (+Dox). For the PC3 TRIPZ PGC1A non-induced stock, 3×10^6 cells per dish were seeded and for the PC3 TRIPZ PGC1A induced stock 7×10^6 cells were plated per dish (**FigM 2A**). These cell number proportions were maintained for cell lines with expression of PGC1 α and presence/deletion of ERR α (**FigM 2B**).

A



B

	PGC1 α ERR α		Producer cells	Seeding density	
	PGC1 α	ERR α			
PC3 PGC1A	sgCtl-Dox	-	+		3×10^6
	sgCtl+Dox	+	+		7×10^6
	sgERR α #1-Dox	-	-		3×10^6
	sgERR α #1+Dox	+	-		3×10^6
	sgERR α #2-Dox	-	-		3×10^6
	sgERR α #2+Dox	+	-		3×10^6

Figure M 2. Culture settings for the generation of cell secretomes. **A.** Overview of the experimental seeding and doxycycline pre-induction for obtaining the secretomes. **B.** Schematic view of the cell number seeded in each condition based on the presence or absence of PGC1 α and ERR α .

On the other hand, for production of secretome using control PC3 TRIPZ cells, same number of cells were seeded (3×10^6) as no differences in cell proliferation were observed between doxycycline-induced and non-induced conditions and conditions. A final volume of 20 ml DMEM

without pyruvate per plate was pipetted and doxycycline was added in a final concentration of 0.5 µg/ml to the dox condition. The number of dishes seeded per condition was dependent on the amount of differential secretome needed for each experiment. After two days growth, cell morphology was checked to monitor PGC1α expression, media was removed, and plates were washed once with DPBS 1X. Then, 20ml of DMEM Exo-free without pyruvate were pipetted to each plate refreshing media with doxycycline in the doxycycline-induced plates. Cells were left to grow for another day and then, secretome was collected and centrifuged at 500 x g, 10 minutes and 10 °C to discard cell debris. In parallel, cell number of the producer cells was assessed and a pellet of cells from each condition was taken to ensure the differential protein expression of PGC1α and deletion of ERRα between conditions.

II.1.1.1 Whole secretome proportions

Cell secretomes produced by doxycycline-induced (+Dox) and non-induced (-Dox) PC3 TRIPZ PGC1A cells were collected as previously described in II.1.1. Then, different proportions of secretome obtained from PGC1α-expressing and non-expressing cells were mixed to obtain the percentages shown in **FigM 3**. As experimental controls, unmixed -Dox and +Dox secretomes were included.

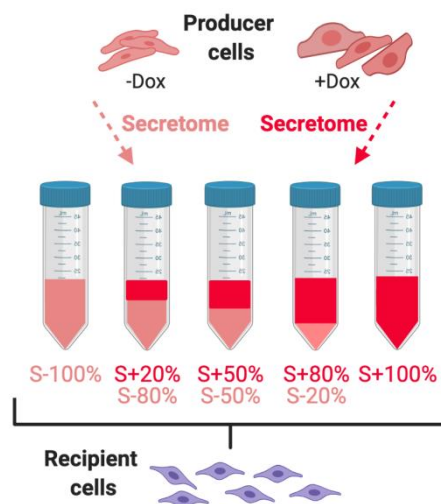


Figure M 3. Secretomes obtained from PGC1α-expressing and non-expressing cells are mixed in different proportions and used for treating recipient cells. Secretome-Dox: secretome produced by non-PGC1α-expressing cells. Secretome+Dox: secretome produced by PGC1α-expressing cells.

II.1.1.2 Whole secretome concentration and fractionation

Whole secretome concentration was performed using secretomes obtained from PC3 TRIPZ PGC1A and PC3 PGC1A sgERRA cell lines. For these experiments, two 150 mm dishes/condition were seeded as described in **section II.1.1** and at the day of collection, secretomes were centrifuged at 500 x g, for 10 minutes and at 10 °C to remove cell debris. Then,

10K Amicons (Merck Millipore, Ref. UCF901024) were used to concentrate the secretomes by centrifuging at speeds ranging 1,500-5,000 x g (**FigM 4A**). The cut-off of these concentrators separates the cell secretome into two fractions; one that contains proteins bigger than 10 KDa (>10 KDa), where extracellular vesicles are also present, and another fraction that includes proteins smaller than 10 KDa (<10 KDa). The fraction bigger than 10 KDa was concentrated into a final volume close to 1 ml whereas the smaller than 10 KDa secretome fraction reached an approximate volume of 21 ml. The >10KDa fraction retained the FBS and was diluted up to 21 ml with DMEM without pyruvate (depleted of FBS and antibiotics). On the other hand, 2.5% FBS was added to the <10 KDa secretome fraction. This percentage was based on the data we obtained in previous experiments, where cells treated with <10 KDa secretome fraction had a reduced proliferation capacity due to the lack of nutrients. We therefore, took into account that non-PGC1a expressing cells duplicate each 24 hours, and that PGC1a-expressing cells, although they have a reduced proliferation capacity, they were seeded in a proportion that aimed at acquiring the same cell number that in the non-expressing condition at the day of the secretome collection. In addition, both, PGC1a-expressing and non-expressing cells were seeded at confluences in which cells grew exponentially, thus requiring high FBS amounts. Taking these facts into consideration, 2.5% FBS was added to the <10 KDa secretome fraction (**FigM 4B**).

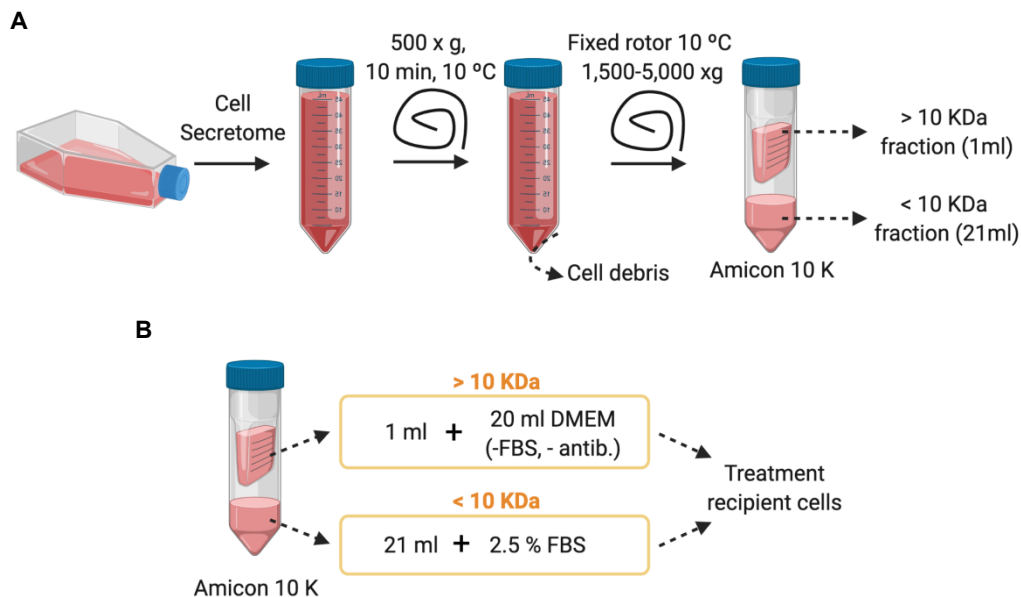


Figure M 4. Cell secretome concentration and separation through 10 K Amicon tubes. A. Secretome is collected and loaded into 10 K Amicon tubes for centrifugation. Two fractions are obtained: >/<10 KDa. **B.** Both fractions (>/< 10 KDa) are processed to obtain secretomes used for treating recipient cells.

Adding this proportion of FBS boosted growth of PC3 recipient cells treated with the <10 KDa secretome fraction to levels similar to the ones observed in the cells treated with the whole secretome and with the >10 KDa secretome fraction. Once prepared, concentrated secretomes were used to treat recipient cell lines.

II.1.2 Production and isolation of extracellular vesicles

Extracellular vesicles (EVs) were isolated from three different PCa cell lines: PC3 TRIPZ PGC1A, PC3 PGC1A sgERRA and PC3 TRIPZ cells. For non-induced conditions, 3×10^6 cells per 150 mm dish were seeded and on the other hand, in the doxycycline-induced condition, 7×10^6 cells per 150 mm dish were seeded. After 24 hours, media was removed and 20 ml of fresh DMEM Exo-free without pyruvate was added to each 150 mm dish. Doxycycline was renewed adding a final concentration of $0.5 \mu\text{g/ml}$ doxycycline to the pre-induced plates. After 48 hours, secretomes produced by cells with differential expression of PGC1a and/or ERRa deletion were collected and processed (**FigM 5**).

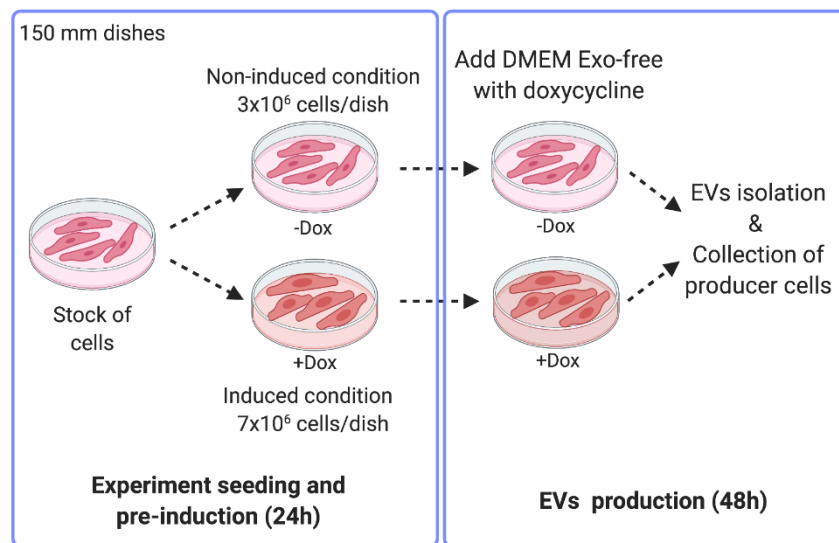


Figure M 5. Seeding conditions for the production of EVs.

Secretome was first centrifuged for 10 minutes at $500 \times g$ and 10°C to remove cell debris (**FigM 6**). In parallel, cells were trypsinized and counted in order to monitor cell number and to extract protein. Secretomes were then transferred either to a fixed angled 45° Ti or 70° Ti rotor (Beckman Coulter) tubes and centrifuged for 20 minutes at $12,000 \times g$ and 10°C . The pellet of EVs enriched in apoptotic bodies and microvesicles was discarded and the supernatant fraction was poured to a fresh rotor tube and centrifuged 70 minutes at $100,000 \times g$ and 10°C . The pellet of EVs obtained after this step were enriched in exosomes, and were resuspended in DPBS 1X into a sole pellet and ultracentrifuged again for 70 minutes, at 10°C and $100,000 \times g$. Then, supernatant was discarded and EVs pellet was resuspended in $100 \mu\text{l}$ of DPBS 1x. At this point, depending on the intended use of the EVs, these were kept at 4°C for functional experiments (*in vitro* and *in vivo*) for a maximum of seven days. For molecular analysis, EVs were aliquoted and stored at -80°C .

The isolation protocol for obtention of EVs was set in collaboration with Dr Juan M. Falcón (Exosomes Lab, CIC bioGUNE) and Dr. Héctor Peinado (Microenvironment and Metastasis Group, CNIO).

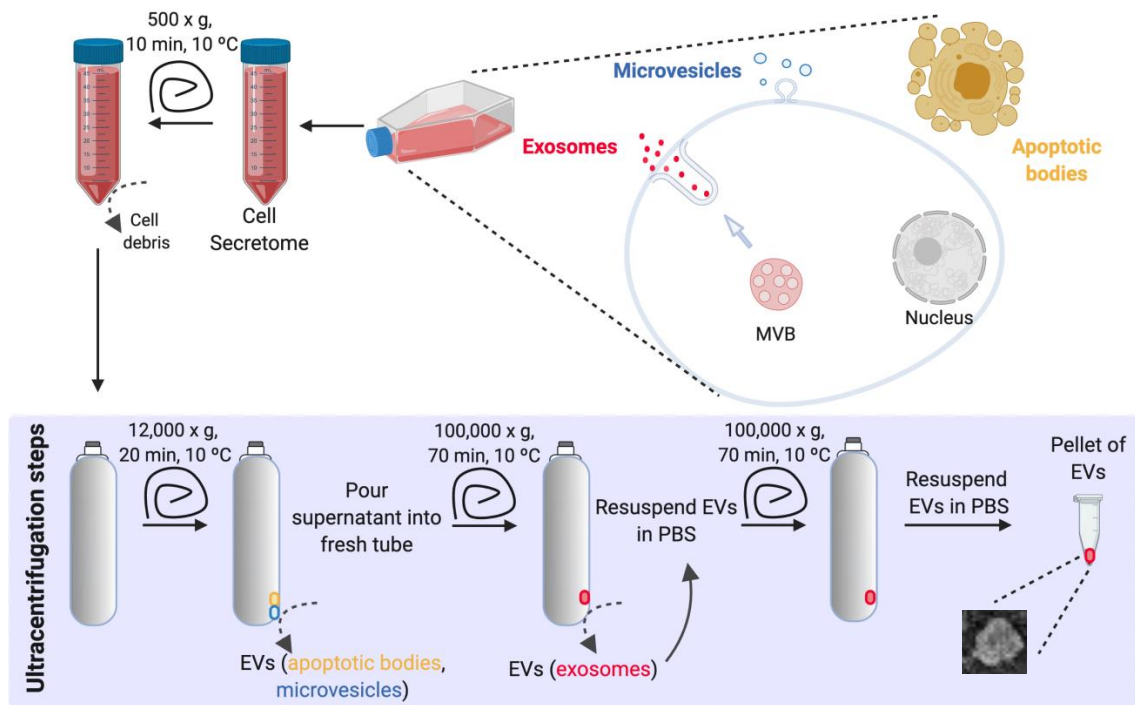


Figure M 6. Protocol followed for the isolation of EVs. Cells produce different types of EVs (exosomes, microvesicles and apoptotic bodies) that can be isolated by serial ultracentrifugation steps.

II.1.2.1 Labelling of extracellular vesicles

EVs were stained using the lipid-labelling dye 1,1'-DIOCTADECYL-3,3,3'-Tetramethylindocarbocyanine Perchlorate (DiIC₁₈(3)) (Thermo Fisher, Ref. D3911). To proceed with the labelling, EVs obtained after the first ultracentrifuge step of 70 minutes at 10°C and 100,000 x g (see **section II.1.2**) were resuspended in 1 ml of DPBS 1X followed by the addition of 3 µl of the fluorescent dye and incubation at room temperature for 5 minutes. Then, 57 µl of BSA 35% were added and incubated at room temperature for 1 minute. Next, 18 ml of DPBS 1X were pipetted and samples were ultracentrifuged for 70 minutes at 100,000 x g and 10 °C. Supernatants were removed, pellets resuspended again in 18 ml DPBS 1X and centrifuged for another 70 minutes at 100,000 x g and 10°C. Finally, the supernatants were poured from the tubes and stained EVs pellets were resuspended in 100 µl of DPBS 1X. Importantly, for proceeding with the labelling of EVs, always a negative control of DPBS 1X with DiIC₁₈(3) was included in parallel.

II.1.3 Generation of soluble factors fraction of the secretome

For the obtention of soluble factors (SFs), whole secretome produced by PGC1a-expressing and non-expressing cells were collected and centrifuged 10 minutes at 500 x g and 10 °C to remove cell debris. Then, the whole protocol of EVs isolation (see **section II.1.2**),

skipping the last washing step, was followed to obtain the SFs fraction of the cell secretome (**FigM 7**).

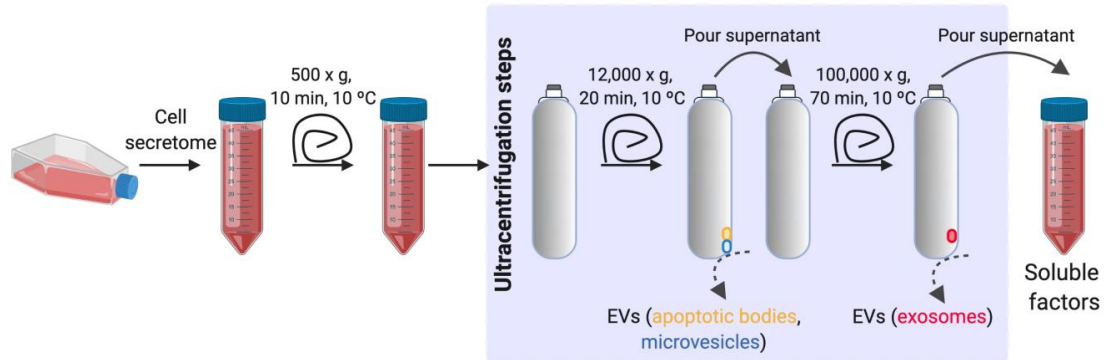


Figure M 7. Protocol followed for obtaining the soluble factors.

II.1.4 *In vitro* cell biology assays

II.1.4.1 Proliferation assay by crystal violet staining

Recipient cells (PC3, DU145 and 22Rv1) were seeded in 12-well plates (PC3 and DU145: 7,000 cells/well and 22Rv1: 12,000 cells/well). Next day, once cells had attached, SN were removed and whole secretome (1 ml/well), SFs (1 ml/well) or EVs (2-4 μ g/well) were pipetted to the wells (**FigM 8**). This process was repeated every two days, up to day 7.

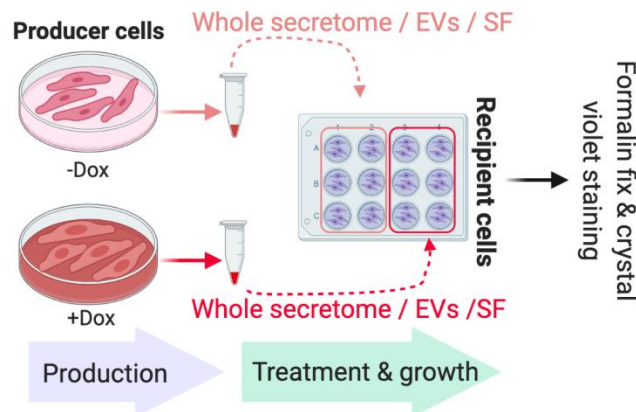


Figure M 8. Proliferation assay by crystal violet staining to assess the impact of whole secretome, EVs or SFs in recipient cells.

Plates were fixed at different time-points (days 2, 5 and 7) as described next: plates were washed with 1X PBS, fixed with 10% formalin (CellPath) and stored at 4 °C until all experimental time-points were collected. Once fixed, plates were washed with 1X PBS and stained with crystal violet [0.1% crystal violet (Sigma-Aldrich) and 20% methanol (Thermo Fisher Scientific)] for 1 hour. Then, crystal violet staining solution was removed, plates were washed with distilled water (dH2O) and let to air dry. Crystal violet-stained plates were scanned, and precipitates were

dissolved in 10% acetic acid (Sigma-Aldrich) for 30 minutes. Absorbance was measured in 96-well plates in the spectrophotometer (Epoch, Biotek) at a 595 nm wavelength.

II.1.4.2 Migration assay: Boyden chambers

For transwell migration assays, PC3 recipient cell lines were treated with secretomes or EVs obtained from PGC1 α -expressing and non-expressing PC3 cell lines (**FigM 9**).

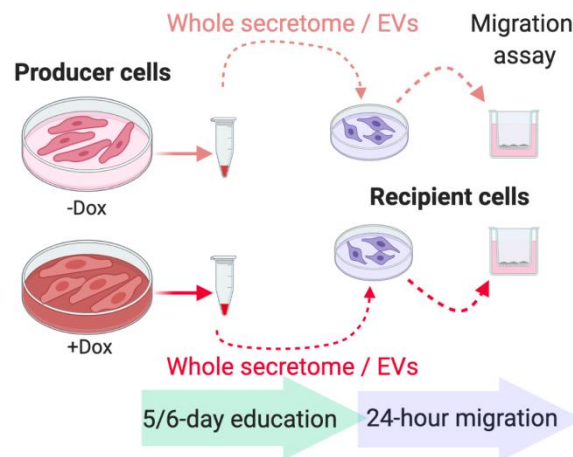


Figure M 9. Boyden chamber migration assay to assess the impact of whole secretome or EVs on the migration ability of recipient cells.

First, to proceed with the secretome or EVs treatments, 30,000 PC3 cells were seeded into 6-well plates and left for 24 hours to get attached. These cells underwent a five (secretome) or six (EVs) -day treatment, time after which, they were trypsinized, counted and seeded into Boyden chamber transwells (50,000 cells/ transwell) resuspended in 500 μ l DMEM/well containing 0.5% FBS. Full media (1.4 ml) was pipetted in the bottom well. In parallel to this, wells were included as a seeding control of the educated PC3 cells. After 24 hours, migration was stopped: media was removed from wells and transwells were smoothly cleaned with 1X PBS. Then, using a cotton bud, the upper side of the transwell membrane was scraped and then rinsed with 1X PBS. Next, transwells were fixed with 10% formalin. Once cells were fixed, formalin was aspirated, 1X PBS was added to wells and transwells twice. Finally, crystal violet was added covering both wells and transwells. Automated inverted Olympus microscope (IX83) (CellSens imaging software) was used to take pictures to further count cell number. Control wells were fixed and stained in parallel to the transwell migration wells. Crystal violet staining was dissolved in 10% acetic acid and absorbance was measured at 595 nm. The values obtained were used to normalize data obtained from the migration assay.

II.1.4.3 Wound healing migration assay

For wound healing assays (WHA), PC3 cells 30.000 cells/ well were seeded into 6-well plates. Twenty-four hours later, media was removed, and cells were treated for five days with

secretomes derived from induced and non-induced PC3 TRIPZ PGC1A cell lines (**FigM 10**). Then, using a yellow tip, a longitudinal scratch was performed, supernatants were removed and fresh differential secretomes were pipetted. In addition, pictures were taken at the time in which the scratch was performed (time 0 hours). Cells were left to migrate towards the wounded area for 24 hours and pictures were taken at this time point using Olympus Axio Imager A1 CKX3. Data was analyzed by means of assessing the area of the initial wound (time 0 hours) minus the area of the wound that remained open after 24 hours of cell migration.

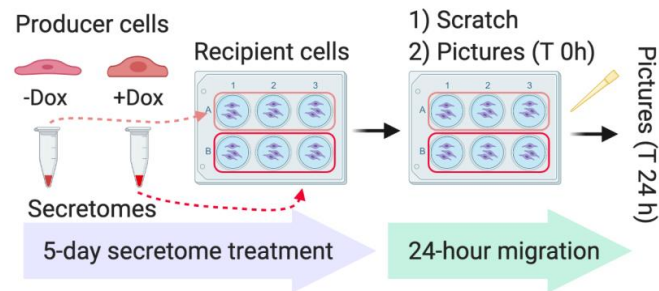


Figure M 10. Wound healing assay to evaluate migration capacity of recipient cells treated with differential secretomes.

II.1.4.4 Migration assay: co-cultures in Boyden chambers

Secretome producing cell lines, PC3 TRIPZ PGC1A cells were pre-induced (+Dox) or not (-Dox) for three days with doxycycline (¡Error! No se encuentra el origen de la referencia. **11**). After this time, cells were counted and a total number of 200,000 cells/ condition were seeded in a final volume of 1.4 ml into bottom wells of Boyden chamber plates, maintaining the presence of doxycycline in the induced cells. In parallel, control wells were seeded to assess cell number at the day at which the migration experiment was stopped. After 24 hours, untreated PC3 cells (50,000 cells/well in a final volume of 500 µl DMEM 0.5% FBS) were pipetted into the transwells and were left to migrate for 24 hours. Migration experiment was stopped following the same steps and using the same microscope for taking pictures as in **section II.1.4.2**. For quantification, data was normalized to the absorbance values measured in the control wells seeded in parallel to the producer cell lines.

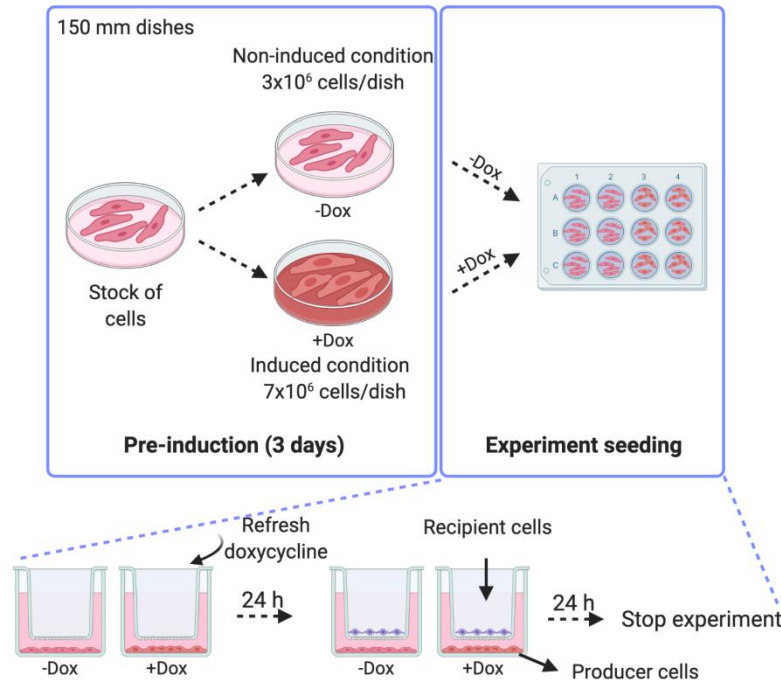


Figure M 11. Migration assay in Boyden chambers using co-cultures of producer and recipient cells.

II.1.4.5 Uptake of EVs

A total number of 200,000 PC3 cells per well were seeded into 6-well plates and left to get attached overnight. Next morning, 2 ml of fresh DMEM Exo-free was added to each well containing PC3 cells. This was followed by the addition of 2 μg of DiIC₁₈(3)-labelled EVs produced by doxycycline-induced and non-induced PC3 TRIPZ PGC1A cells (

12).

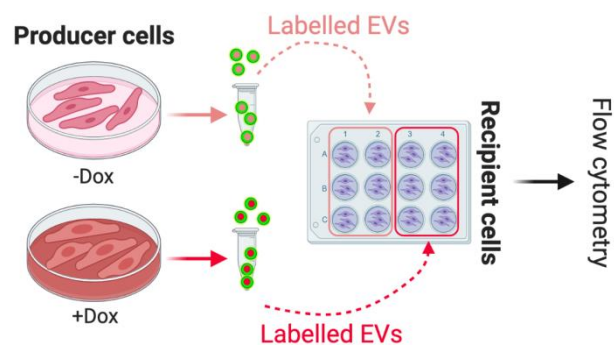


Figure M 12. DiIC₁₈(3)-labelled EVs produced by PGC1 α -expressing and non-expressing cells are used for treating recipient cells and assess uptake by flow cytometry.

Three time points (1 hour, 3 hours and 6 hours) were assessed for both conditions, and a negative control of PC3 cells treated with DPBS 1X mixed with DiIC₁₈(3) was included. Once the incubation times had finished, cells were detached with Cell Dissociation buffer (500 μl /well) and centrifuged. Then, pellets were resuspended in 300 μl home-made FACS buffer (PBS 5mM EDTA and 0.1%

BSA) and passed through CellTrics 50 μm (Sysmex, Ref. 040042-2317) filters into the FACS tubes. Finally, 1 μl DAPI was added into each tube and cells were sorted using BD FACS Canto device.

III Molecular Assays

III.1 Gene expression analysis

III.1.1 RNA extraction and retrotranscription

For *in vitro* gene expression analysis, cells were seeded in 6-well plates at a confluence of 70%. For sample collection, SN were aspirated, and cells were washed with DPBS 1X and snap-frozen in liquid nitrogen before keeping them at $-80\text{ }^{\circ}\text{C}$. For RNA extraction, NucleoSpin[®] RNA isolation kit from Macherey-Nagel (Ref: 740955.240C) was used, following the manufacturer's protocol. RNA concentration was determined using Nanodrop ND-1000 Spectrophotometer.

For murine xenografts RNA extraction, samples were incubated overnight at $-80\text{ }^{\circ}\text{C}$ in 200 μl RNeasy Lysis Buffer (Life Technologies), which had previously been cooled down at $-80\text{ }^{\circ}\text{C}$. Next day, tissues were transferred to an Eppendorf tube containing 800 μl TRIzol[®] reagent and five 2.8 mm ceramic beads (Ref. 13114-50 MO BIO Laboratories). Precellys[®] machine was used to homogenize the tissue at 6,000 rpm for 30 seconds and repeating the step twice. Then, 160 μl of chloroform (SIGMA, Ref. 34854) were added and, after vortexing, the mix was centrifuged at 12,000 $\times g$ during 15 minutes at $4\text{ }^{\circ}\text{C}$. The aqueous phase was collected and mixed with the corresponding volume of ethanol and the extraction was continued following the Macherey-Nagel protocol.

Gene expression analysis was assessed by Real Time-Quantitative-Polymerase Chain Reaction (RT-qPCR), using the same protocol for cell lines, murine prostatic tissue and xenografts. One microgram of the obtained RNA was used for complementary DNA (cDNA) synthesis using reverse transcriptase (Maxima H Minus cDNA synthesis with dsDNase. Thermo Scientific, Ref: M1682). The resulting cDNA was diluted 1:9 in RNase-free water, and 3 μl were used for performing the RT-qPCRs.

III.1.2 Real time quantitative polymerase chain reaction (RT qPCR)

RT-qPCR was performed using QS6 systems from Life Technologies. The RT-qPCRs were performed using the following program: 2 minutes at $50\text{ }^{\circ}\text{C}$ and 10 minutes at $95\text{ }^{\circ}\text{C}$ (hold stage) followed by 40 cycles of 15 seconds at $95\text{ }^{\circ}\text{C}$ (denaturalization) and 1 minute at $60\text{ }^{\circ}\text{C}$ (annealing and elongation). All gene expression studied was analyzed with primers and probes from Universal Probe Library (Roche). The Universal Probe Library Assay Design Center is available online (https://lifescience.roche.com/en_es/brands/universal-probe-library.html). This tool allows the designing of primers and assigns the corresponding probe needed for each

reaction in order to perform a TaqMan assay. For the reaction, 0.3 µl primer mix (20 µM), 3 µl of TaqMan® universal master mix II with UNG (Applied Biosystems) and 0.05 µl of the corresponding probe were used. For the analysis of house-keeping genes (*GAPDH* or β -*ACTIN*) commercial TaqMan probes (Life Technologies) were employed. Comparative Ct method was selected for the quantification of gene expression changes. See **Table M 4** for primer specifications.

Table M 4. Information about primer sequences and correspondent probe number obtained from Universal Probe Library (Roche).

Gene Name	Species	Forward 5'-3'	Reverse 5'-3'	Probe
<i>ADAM10</i>	Human	acataactttggatccccaca	ccattttcttttgaccctaaat	2
<i>ATF3</i>	Human	catcttctcaggggctacct	gtttgccatccagaacaagc	53
<i>Atf3</i>	Mouse	gctggagtcagtaccgtcaa	cgctcctttctctcat	80
<i>B2M</i>	Human	tcaggaaattgactttccattc	ttctggcctggaggctatc	42
<i>BID</i>	Human	tctcatgtctcagggtaggc	tgagctcaggacacca	1
<i>CD44</i>	Human	gacaccatggacaagtttgg	cggcaggttatattcaaatcg	13
<i>CFL1</i>	Human	tgccctctcctttcgttt	tcgttgaaacacttgatgaca	5
<i>CLDN3</i>	Human	aaactgcatggactgtgaaa	ggtcaagtattggcggtcac	50
<i>DDIT3</i>	Human	tgaagatacacttcttctgaaca	aaggcactgagcgtatcatgt	21
<i>Ddit3</i>	Mouse	gcgacagagccagaataaca	gatgcacttcttctggaaca	91
<i>DDIT4</i>	Human	tccaggttaagccgtgtcttc	ctggagagctcggactgc	56
<i>EDIL3</i>	Human	tcgaagacattgcactttgc	accagaggctcagaacaac	76
<i>ERO1A</i>	Human	caatggtttcaacatcacaggt	ggagacagcggcacagag	29
<i>ESRRA</i>	Human	ggcggcagaagtaaacg	attcactgggctgctgt	3
<i>F113</i>	Human	cctgaagtcagaattctctgaaa	ttggtcaaaactccactccac	7
<i>FGFBP1</i>	Human	actggatccgtgtgctcag	gagcagggtgaggtacaga	46
<i>Fgfbp1</i>	Mouse	ctgcacactcacagaaaggtg	ctgagaacgctgagtagcc	12
<i>GNB2</i>	Human	agatgaggaccggagga	tgatgagcttccatcctg	66
<i>HLA-E</i>	Human	gtgagtcacgtgtctttgg	ggaagacacatgcgtggag	80
<i>IFNA1</i>	Human	ttgtttcatgttggaccaga	ccctctcttatacaaaaactgc	69
<i>IFNAR1</i>	Human	gttctgattttggacactgacttc	tccagtacattgtataaagaccacgt	22
<i>IFNAR2</i>	Human	tctcaaaactcgggtggtcaaaa	caactgtttcagttgtctcac	20
<i>IFNB1</i>	Human	gccaggaggttctcaacaat	ctttgctattttcagacaagattca	20
<i>IRF1</i>	Human	cccttctcatcctcatctgt	ggcacatcccagtggaag	56
<i>Irf1</i>	Mouse	cactgatctgtataacctacaggtgc	ccttctcatcctcgtctgt	10
<i>IRF9</i>	Human	agcctggacagcaactcag	gaaactgcccactctccact	22
<i>Irf9</i>	Mouse	cttaggggtgggactgtagaaa	gcagcgtactttgcttgag	91
<i>MX1</i>	Human	accacagaggctctcagcat	cagatcaggcttctcaaga	10
<i>Mx1</i>	Mouse	ttcaaggatcactcactctcagc	gggaggtgagctcctcag	53
<i>C-MYC</i>	Human	gctgcttagacgtgattt	taactgtgaggggcatcg	66
<i>NLRC5</i>	Human	ggctttcccctcagctc	gctgctgctgagtactttgg	20
<i>Nlrc5</i>	Mouse	gctgccaacctcacacttt	caaggagattcccggacag	80
<i>NRP1</i>	Human	taccctgagaatgggtggac	cgtgacaaagcgcagaag	55
<i>PDE1C</i>	Human	ccagctctgcttctctgtca	catcgtggacaatgtcact	25
<i>PGAM1</i>	Human	caaaacgcaggacagctga	cgccaagtctcaccact	5
<i>Pgc1α</i>	Mouse	gaaagggccaacagagaga	gtaaatcacacggcgtctt	29
<i>RAC1</i>	Human	ctgatgcaggccatcaagt	caggaatgcattggttgtg	77
<i>SERPIN5</i>	Human	ctgagttgagttgttttcaatcttc	catgttcatcctactaccaagg	88
<i>SOD3</i>	Human	ggtgcagctctcttttcagg	aacacagtagcggcagcat	17
<i>STAT1</i>	Human	gagcttcaactccttagtttga	cacaacgggcagagaggt	64
<i>Stat1</i>	Mouse	tgagatgtcccggatagtg	cgccagagagaaattcgtgt	99
<i>STAT2</i>	Human	tgagttctctgtcacacc	ggtttgattgggactttggt	22
<i>Stat2</i>	Mouse	ggaacagctggaacagtggt	gtagctgccgaaggtgga	19
<i>STXB2</i>	Human	cggtggagaagctgtgtagt	ccttgatcttccccctct	15
<i>TNXB</i>	Human	tgctccagagaggaaagagg	actgtcagttccccagga	1
<i>Tnxb</i>	Mouse	gcctcataggcctcaaacg	gggctgtggtgtcttctcc	94
<i>UGP2</i>	Human	caaaatgccattgacatgga	tttgatggcagcccctact	58
<i>YBX1</i>	Human	ggagggtgctgacaacca	gctgtctttggcaggag	2

III.1.3 RNA sequencing

Two different experiments were conducted to be further analyzed by RNA sequencing.

For the first type of RNA sequencing experiments, PC3 TRIPZ PGC1A cells pre-induced for three days, were seeded into 6-well plates (75,000 cells/well) and left to grow for another three days (**FigM 13A**). After this time, samples were collected for RNA sequencing analysis. Four independent experiments were performed.

For the second type of RNA sequencing experiment, PC3 recipient cells were seeded into 6-well plates (75,000 cells/well). Next day, once cells had attached to the plates, media was removed, cells were washed with DPBS 1X and secretomes produced by PGC1 α -expressing and non-expressing PC3 producer cells were used for treating PC3 recipient cells for a period of 48 hours (**FigM 13B**). After this 48-hour-period, supernatants were removed, cells were washed with DPBS 1X and snap-frozen using liquid nitrogen. Plates were then kept at -80 °C for later processing. Three independent experiments were done.

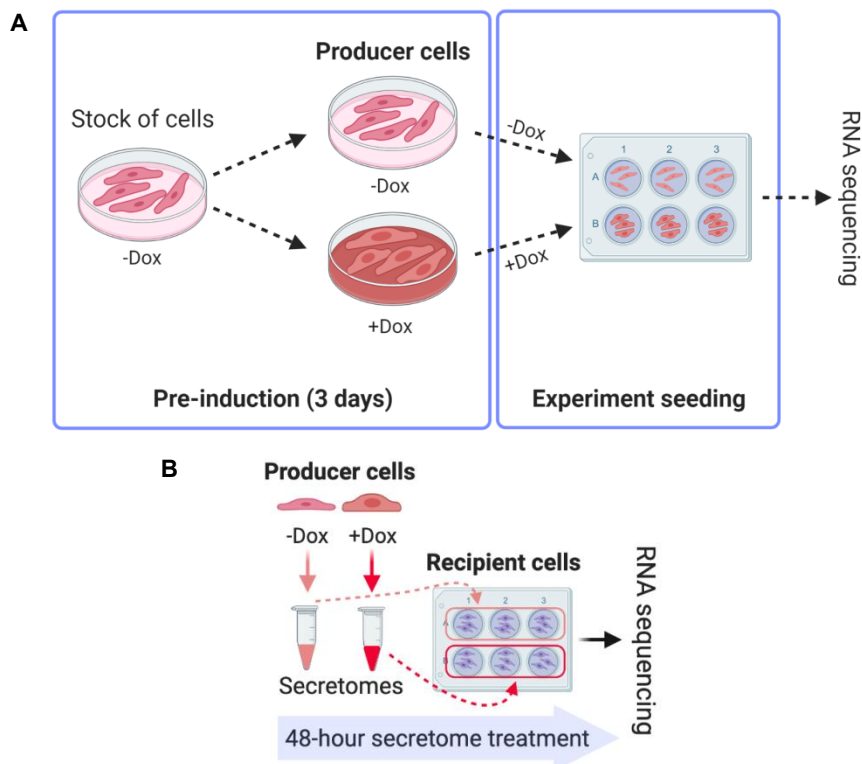


Figure M 13. RNA sequencing experimental settings. A-B. PGC1 α -expressing and non-expressing cells (A) and PC3 recipient cells are analyzed by RNA sequencing (B).

RNA was extracted following the Macherey-Nagel protocol, followed by the RNA concentration measurement using Nanodrop ND-1000 Spectrophotometer. RNA was then processed at the Genomics Platform at CIC bioGUNE by Dr. Ana Aransay, Laura Bárcena and Dr. Monika González as follows:

The quantity and quality of the RNAs were evaluated using Qubit RNA HS Assay Kit (Thermo Fisher Scientific, Cat. #Q32855) and Agilent RNA 6000 Nano Chips (Agilent

Technologies, Cat. #5067-1511), respectively. Sequencing libraries were prepared following “TruSeq Stranded mRNA Sample Preparation Guide (Part #15031058 Rev.E)” using the “TruSeq® Stranded mRNA Library Prep” kit (Illumina Inc. Cat. #20020594) and TruSeq RNA Single Indexes (Illumina Inc. Cat. #20020492 and #20020493).

Starting from 1000 ng of total RNA, mRNA was purified, fragmented, and primed for cDNA synthesis. cDNA first strand was synthesized with *Super Script-II* Reverse Transcriptase (Thermo Fisher Scientific, Cat. #18064-014) for 10 minutes at 25 °C, followed by 15 minutes at 42 °C, 15 minutes at 70 °C and finally paused at 4 °C. cDNA second strand was synthesized using Illumina reagents at 16 °C for 1 hour and was followed by A-tailing and adaptor ligation. Finally, enrichment of libraries was achieved by PCR (30 seconds at 98 °C ;15 cycles of 10 seconds at 98 °C, 30 seconds at 60 °C, 30 seconds at 72 °C; 5 minutes at 72 °C and paused at 4 °C). Finally, amplified libraries concentration was determined with Qubit fluorometer using the Qubit® dsDNA HS assay kit (Invitrogen, Cat. #Q32854) and their size distribution was assessed running an aliquot on an Agilent Technologies 2100 Bioanalyzer, using an Agilent High Sensitivity DNA Chip (Agilent Technologies, Cat. # 5067-4626).

RNA sequencing functional analysis was carried out by Ana R. Cortázar using DESeq, EdgeR and LimmaVoom platforms. Enrichment analyses were performed using Cancertool interface (Cortazar et al. 2018). This tool highlights the most relevant GO terms associated with a given gene list. Biological Process (BP), Molecular Function (MF) and Cellular Component (CC) categories were assessed. In addition, transcription factor (TF) enrichment analysis was performed. Only enriched terms with an adjusted p-value < 0.05 were considered for comparison and discussion.

Gene set enrichment analysis (GSEA) was performed for analyzing data obtained from the RNA sequencing of the PC3 TRIPZ PGC1A cells. GSEA 4.1.0 software from the Broad Institute and UC San Diego was used (Subramanian et al. 2005). In order to proceed with the analysis, gene expression levels of doxycycline-induced and non-induced genes was uploaded, and the number of permutations and threshold set where 1000 and 0.05 correspondingly.

III.2 Protein expression analysis

III.2.1 Enzyme-linked Immunosorbent Assay (ELISA)

For analysis of IFN- β presence in the whole cell secretomes produced by PGC1 α -expressing and non-expressing PC3 cells, an ELISA Quantikine Human IFN- β immunoassay (R&D Systems, Ref. DIFNBO) was performed following the suppliers' guidelines. Briefly, to produce the secretomes, cells were pre-induced for three days and then plated into 12-well plates at high confluences (50,000 cells/ well) refreshing the doxycycline in the induced condition. RNA (day 3 and day 6) was seeded in parallel to have a control of the system and at the day of secretome collection, producer cells were fixed in 10% formalin to obtain crystal violet absorbance readout of the cell densities (**FigM 14**). Differential secretomes were collected at days 3 and 6 after experiment seeding and were centrifuged for 10 minutes at 500 x g and 10 °C to remove cell

debris. Then, protocol was followed until the final step in which, supernatants' optical densities were determined in a 96-well plate reader (Gene5, software version 3.08.01). Microplate was read at 450 nm, and at 540 nm. This last measurement was done to subtract the values to the ones obtained at 450 nm and thus, correcting optical imperfections of the plate. The concentrations of IFN- β obtained (pg/ml) were relativized to the density of producer cells at the day of the collection of the secretomes. This value, which was obtained by crystal violet staining, was previously normalized to the day 0 (seeding day) to eliminate possible differences due to seeding variability. ELISA experiment was performed with the kind support of the Inflammation and Macrophage Plasticity Lab (CIC bioGUNE), led by Dr. Juan Anguita.

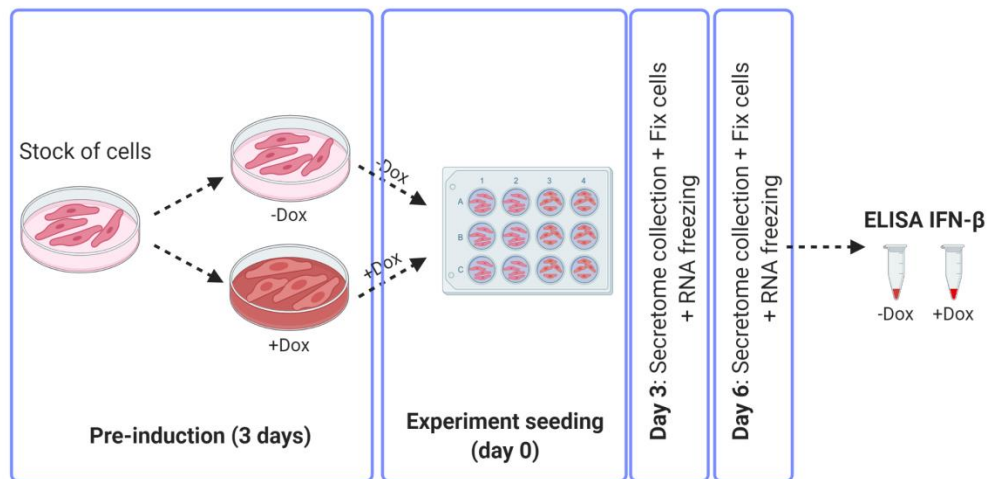


Figure M 14. Measurement of IFN- β in cell secretomes produced by PGC1 α -expressing and non-expressing cells by ELISA.

III.2.2 Secretome protein precipitation

For whole secretome protein analysis by western blot, protein was chemically precipitated using GE Health 2-D Clean-Up Kit (Sigma-Aldrich, Ref. 80-6484-51). The manufacturer's protocol was followed with a minor change in step n^o 11, where samples were incubated overnight instead 30 minutes, following Dr. Mikel Azkargorta's (Proteomics Platform at CIC bioGUNE) advice. Big protein pellets were obtained at the end of the protocol, which were resuspended in Lämmli buffer 5X for further analysis.

III.2.3 Protein extraction

For protein expression analysis, 75,000 cells/well were seeded into 6-well plates and left to grow for three days before performing protein extraction. In secretome experiments, in order to confirm the expression of PGC1 α upon treatment with doxycycline, a pellet containing 1x10⁶ cells was taken for protein extraction. For the protein extraction, media was removed, followed by a 1X PBS washing step and then, samples were processed or frozen in liquid nitrogen for later processing. Cells were lysed using RIPA buffer containing the following components: 50 mM

TrisHCl pH 7.5, 150 mM NaCl, 1 mM EDTA, 0.10% SDS, 1% Sodium Deoxycholate, 1% NP-40, 1 pill of complete protease inhibitors cocktail (Roche, Ref. 11836170001) per 50 ml of buffer, and 1 mM of sodium fluoride, sodium orthovanadate and β -glycerol phosphate. Once the lysis buffer was added, samples were kept in ice for 15-20 minutes (being vortexed every 5 minutes) and centrifuged at 12.000 rpm and 4 °C for 10 minutes. Finally, the supernatants were collected and transferred to fresh Eppendorf tubes.

For extraction of protein from murine xenografts, tissues were transferred to tubes containing 400 μ l RIPA lysis buffer (50 mM TrisHCl pH=7.5, 150 mM NaCl, 1mM EDTA, 0.10% SDS, 1% Sodium Deoxychlorate, 1% NP-40), containing 2 mM of phosphatase inhibitors (sodium fluoride, sodium orthovanadate and β -glycerophosphate) and two pills of protease inhibitor cocktail (Roche). Precellys[®] machine was used to homogenize the tissues as previously explained in III.1.1.

III.2.4 Protein quantification and sample preparation

Protein was quantified using Pierce[™] BCA Protein Assay Kit (Thermo Fisher Scientific, Ref. 23225). Samples were prepared in Lämmli 5X sample buffer (10% SDS, 50mM Tris pH 6.8, 10% H₂O, 50% Glycerol, 1% β -mercaptoethanol, 0.01M DTT and 0.2 mg/ml of bromophenol blue) and kept at -20 °C for further analysis by western blot. For analysis of EVs by western blot, samples were prepared in non-reducing conditions using Lämmli LDS NuPAGE[™] (4X) (Thermo Fisher Scientific, Ref. NP0007).

III.2.5 Western blotting (WB)

Protein lysates with Lämmli 1X were boiled at 95 °C for 5 minutes to denaturalize the protein. For EVs samples, boiling was performed at ever increasing temperatures (37 °C, 65 °C and 95 °C), each of them for 5 minutes. After boiling, samples were spined down and loaded (5-20 μ g protein) into NuPAGE[®] Novex[®] 4-12% Bis-Tris Midi Protein gels (Invitrogen, Ref. NG1403BX10) and run in MOPS SDS buffer (NuPAGE[®] NP0001-02). For EVs, samples were loaded into Mini-Protean TGX Precast Gels (Biorad, Ref. 456-1085) gels and run in Tris Glycine SDS buffer (National Diagnostics, Ref. EC-870). Both types of gels were resolved at 200 V until the desire level and using as protein weight marker, Nippon (Ref. MWP02), Western Sure Prestained (Ref. 926-98000) or Biorad Precision Plus (Ref. 161-0374), which was kindly provided by the group of Dr. Juan Anguita. Once proteins had run, they were transferred to nitrocellulose membranes (Amersham Protran, Ref. 10600001) at 100 V for 1 hour in 1X transfer buffer (Biorad, Ref. 1610771). Membranes were then blocked in 5% non-fat milk prepared in Tris-buffered saline solution containing 0.01% Tween-20 (TBS-T).

Primary antibodies were prepared in TBS-T with 0.002% sodium azide to allow good antibody conservation and incubated with the membranes overnight at 4 °C. Next day, membranes were washed three times (10 minutes each) in TBS-T and were incubated for 1 hour

at room temperature with the secondary antibody, which was prepared in milk 5%. Following this step, membranes were washed again three times and developed with home-made ECL solution. ECL preparation is based on mixing two solutions (A and B) that contain the following compounds: solution A: 10% Tris pH 8.5, 90% H₂O, 0.2 mM coumaric acid (Sigma, Ref. 9008) and 1.25 mM luminol (Sigma, Ref. 09253) and solution B: 10% H₂O₂. Three microliters B solution are mixed per 1 ml of solution A. See **Table M 5** for antibody references and the conditions of use.

Table M 5. References and preparation of primary and secondary antibodies employed for Western blotting.

Antibody	Reference	Species	Dilution
c-MYC	Cell Signaling Technology #13987S	Rabbit	1:1000
CD63 (H5C6)	Developmental Studies Hybridoma Bank	Mouse	1:1000
CD9	R&D Systems #209306	Mouse	1:1000
COX IV (4D11-B3-E8)	Cell Signaling Technology #11967	Mouse	1:1000
ERR α (E1G1J)	Cell Signaling Technology #13826	Rabbit	1:1000
GAPDH	Cell Signaling Technology #2118	Rabbit	1:1000
Grp78 (40/BiP)	BD Biosciences	Mouse	1:1000
HSP90	Cell Signaling Technology #4874	Rabbit	1:1000
ITGB4	Cell Signaling Technology #4707	Rabbit	1:1000
PGC1 α	Santa Cruz Biotechnology sc-13067	Rabbit	1:700
Phospho-STAT1	Cell Signaling Technology #9167	Rabbit	1:1000
Total-cofilin	Cell Signaling Technology #5175	Rabbit	1:1000
Total-STAT1	Cell Signaling Technology #14994S	Rabbit	1:1000
α -tubulin	Cell Signaling Technology #5335	Rabbit	1:1000
β -actin	Sigma A5316	Mouse	
Secondary Rabbit Ab	Jackson ImmunoResearch	Rabbit	1:4000
Secondary Mouse	Jackson ImmunoResearch	Mouse	1:4000

III.2.6 Proteomics analysis

Secretomes produced *in vitro*

EVs and whole cell secretomes, both produced by PGC1 α -expressing and non-expressing PC3 cells, were analyzed by label-free liquid chromatography-mass spectrometry proteomics (LC-MS proteomics). For EVs extraction, protocol from **section II.1.2** was followed, although the producer cells seeding confluence and time-points used were slightly different. A total number of 7x10⁶ PC3 cells were plated per 150 mm plate in both conditions (PGC1 α -expressing and non-expressing) (**FigM 15A**). After 48 hours, SN was removed and fresh DMEM ExoFree was added to each plate, refreshing the doxycycline in the induced condition. Twenty-four hours later, SN were collected and subjected to ultracentrifugation steps for EVs isolation.

For production of whole cell secretomes, PC3 TRIPZ PGC1A cells were pre-induced with doxycycline for three days and seeded at high confluences in 100 mm plates (4x10⁶ PGC1 α -expressing and non-expressing cells) (**FigM 15B**). Next day, SN was removed, cells were washed

three times with DPBS 1X to remove FBS and then, serum-free DMEM was added. Three hours later, secretomes were collected, centrifuged at 500 x g for 10 minutes and at 10 °C.

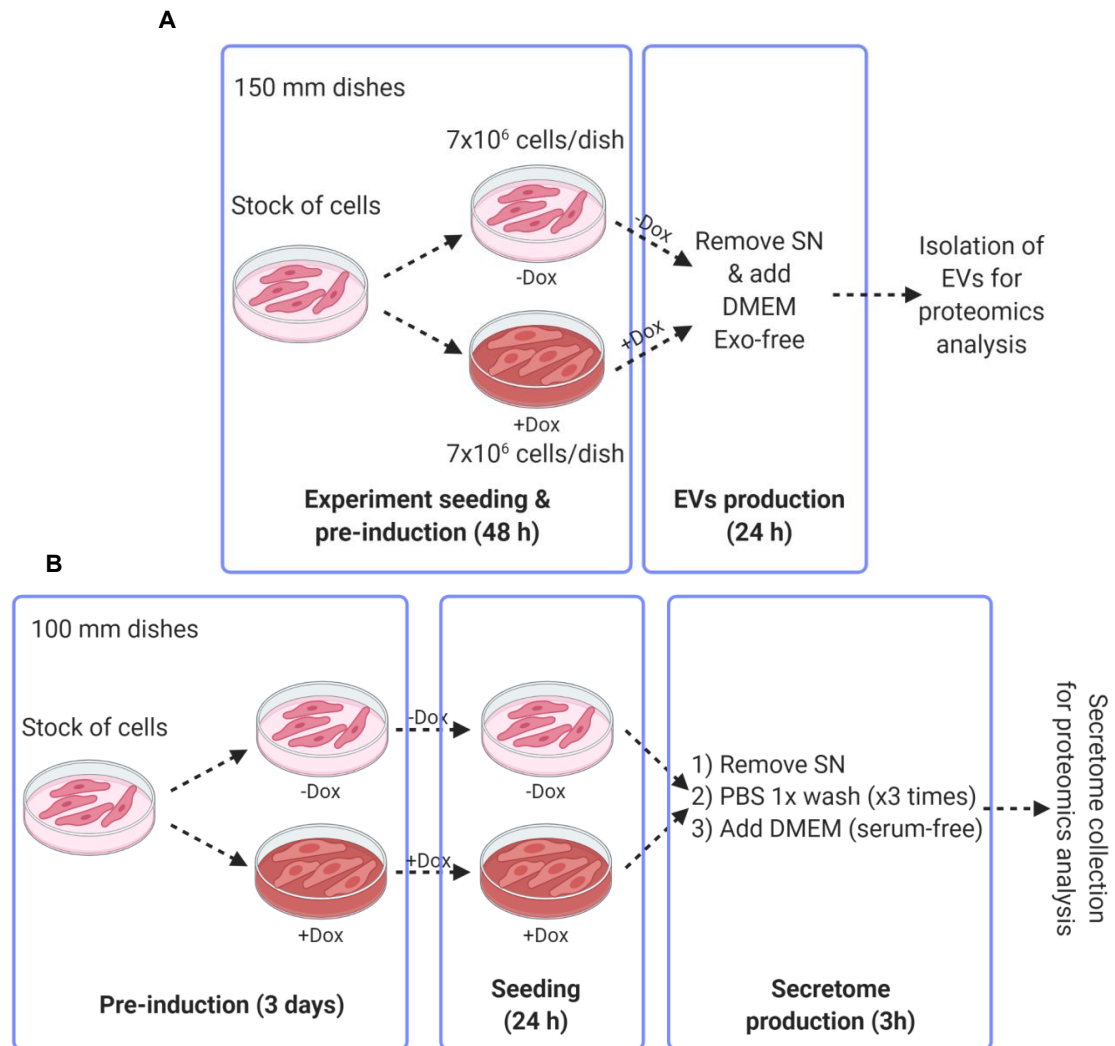


Figure M 15. Experimental settings followed for LC-MS proteomics analysis. A-B. PGC1 α -expressing and non-expressing cells are seeded to obtain EVs (A) and whole secretomes (B) to perform proteomics analysis.

Once collected, whole secretomes and EVs were kept at -80 °C to further perform LC-MS proteomics analysis as follows:

In solution digestion: Secretome samples were precipitated using the GE Health 2-D Clean-Up Kit (Sigma-Aldrich, Ref. 80-6484-51) before any further processing and resuspended directly in the protein extraction buffer. Whole secretome and EVs protein was extracted using 7M urea, 2M thiourea, 4% CHAPS. Samples were incubated for 30 minutes at RT under agitation and digested following the filter-aided sample preparation (FASP) protocol described by Wisniewski and colleagues (Wiśniewski et al. 2009) with minor modifications. Trypsin was added to a trypsin: protein ratio of 1:10, and the mixture was incubated overnight at 37°C, dried out in a RVC2 25 speedvac concentrator (Christ), and re-suspended in 0.1% formic acid (FA).

Mass spectrometry analysis: Secretome and EVs samples were either analysed in an Orbitrap XL ETD mass spectrometer (Thermo) or a timsTOF Pro with PASEF (Bruker Daltonics). The Orbitrap XL ETD mass spectrometer was connected to a nanoACQUITY UPLC System (Waters). Sample was loaded onto a Symmetry 300 C18 UPLC Trap column (180 μm x 20 mm, 5 μm (Waters) and resolved in a BEH130 C18 column (75 μm x 200 mm, 1.7 μm (Waters). The mass spectrometer automatically switched between MS and MS/MS acquisition in DDA mode, in an alternating fashion. Full MS survey spectra (m/z 400–2000) were acquired in the Orbitrap with 30000 resolution at m/z 400. The six most intense ions were subjected to CID fragmentation in the linear ion trap. Precursors with charge states of 2 and 3 were specifically selected for fragmentation. Analyzed ions were excluded from further analysis for 30 seconds using dynamic exclusion lists.

The timsTOF Pro with PASEF was coupled online to a nanoElute liquid chromatograph (Bruker). Sample (200 ng) was directly loaded in a 15 cm Bruker nanoelute FIFTEEN C18 analytical column (Bruker) and resolved at 400 nl/min with a 30-minute gradient. Column was heated to 50 $^{\circ}\text{C}$ using an oven.

Differential expression analysis: Progenesis LC-MS software (Nonlinear Dynamics Ltd., Newcastle upon Tyne, UK) was used for the differential protein expression analysis of the LTQ Orbitrap XL ETD samples. Searches were carried out using Mascot (Matrix Science). Tolerances of 10ppm and 0.5 Da were used for precursor and fragment searches, respectively. Only peptides passing the FDR < 1% filter were considered for further analysis. Protein quantitation was performed using the information concerning to the three most intense peptides (when available), and only proteins quantified with least two peptides at an FDR<1% were considered for further analysis.

On the other hand, data coming from the timsTOF Pro with PASEF was analyzed using PEAKS software (Bioinformatics solutions). Searches were carried out against a database consisting of *Homo sapiens* entries (Uniprot/ Swissprot), with precursor and fragment tolerances of 20 ppm and 0.05 Da. Only proteins identified with at least two peptides at FDR<1% were considered for further analysis.

Data coming from both LTQ Orbitrap XL ETD and timsTOF Pro with PASEF was loaded onto Perseus platform (Tyanova et al. 2016) and further processed (log₂ transformation, imputation). A t-test was applied in order to determine the statistical significance of the differences detected between the corresponding groups.

Functional analysis of the protein candidates found altered between both conditions was performed with Cancertool as described in **section III.1.3**. For that, protein names were first converted into gene names.

Secretome produced *in vivo*

Tumor interstitial liquid (TIL) obtained from the anterior prostate of three-month Pten^{pc-/-} (KO) and Pten^{pc-/-} Pgc1 α ^{pc-/-} (DKO) mice was subjected to label-free LC-MS proteomics analysis as follows:

In solution digestion: Samples were resuspended directly in the protein extraction buffer (7M urea, 2M thiourea, 4% CHAPS) and incubated for 30 minutes at RT under agitation. Then, samples were digested following the filter-aided sample preparation (FASP) protocol described by Wisniewski and colleagues (Wiśniewski et al. 2009) with minor modifications. Trypsin was added to a trypsin: protein ratio of 1:10, and the mixture was incubated overnight at 37°C, dried out in a RVC2 25 speedvac concentrator (Christ), and re-suspended in 0.1% formic acid (FA).

Mass spectrometry analysis: TIL samples were either analyzed in a timsTOF Pro with PASEF (Bruker Daltonics) coupled online to a nanoElute liquid chromatograph (Bruker). Sample (200 ng) was directly loaded in a 15 cm Bruker nanoelute FIFTEEN C18 analytical column (Bruker) and resolved at 400 nl/min with a 30-minute gradient. Column was heated to 50 °C using an oven.

Differential expression analysis: Data coming from the timsTOF Pro with PASEF was analyzed using PEAKS software (Bioinformatics solutions). Searches were carried out against a database consisting of *Mus musculus* entries (Uniprot/ Swissprot), with precursor and fragment tolerances of 20 ppm and 0.05 Da. Only proteins identified with at least two peptides at FDR<1% were considered for further analysis. Data was loaded onto Perseus platform (Tyanova et al. 2016) and further processed (log2 transformation, imputation). A t-test was applied in order to determine the statistical significance of the differences detected between the corresponding groups.

Functional analysis of the protein candidates found altered between both conditions was performed with Cancertool as described in **section III.1.3**. For that, mouse protein names were first converted into human gene names.

Label-free LC-MS proteomics was done in collaboration with the Proteomics Platform at CIC bioGUNE, and was carried out by Dr. Felix Elortza, Dr. Mikel Azkargorta and Iraide Escobes.

III.3 EVs characterization techniques

III.3.1 Nanoparticle-tracking analysis (NTA)

EVs size distribution was analyzed by nanoparticle-tracking analysis (NTA). Particle's Brownian motion was measured using a NanoSight LM10 system (Malvern, UK). The device is equipped with a 450 nm blue laser, a fast video capture and particle-tracking software that allow the measurement of the particles' size distribution and concentration in a liquid suspension. The laser goes through the sample and allows to measure light dispersion generated by the particles that are contained in the suspension. These particles can be observed through a microscope that is connected to a camera that captures their movement. The movement of each particle is tracked with the software (NTA 3.4), and through the equation of Stokes-Einstein, diameter is calculated.

Before running samples, NanoSight device was calibrated using Polystyrene Latex Microspheres 100 nm. Then, EVs were prepared in a 10:500 dilution (10 µl EVs in 500 µl DBPS 1X) and after mixing well, sample was loaded through a 1 ml syringe into the device. For each preparation analyzed, parameters were kept equal (camera level 12, threshold 5), temperature

was monitored and two videos, each of 40 seconds were performed. Videos were analyzed to give the mean, mode and median vesicle size as well as the concentration. For data processing, only particles sizing up to 500 nm were considered, this was due to the higher accuracy of the device in this range of size.

EVs measurement by NTA was done with the support of Dr Juan M. Falcón and Dr. Félix Royo and Dr. Esperanza González (Exosomes Lab) at CIC bioGUNE.

III.3.2 Electron Microscopy (EM)

EVs samples were processed at the Spanish National Cancer Research Center (CNIO, Madrid) Electron Microscopy Unit by Dr. Jasminka Boskovic and Carlos Rodríguez. For negative staining, purified EV fractions were applied onto freshly glow-discharged, carbon-coated, 400-mesh copper EM grids at a concentration of 0.1 mg/ml in a final volume and incubated for 1 minute at RT. The grids were placed consecutively on top of three distinct 50 μ l drops of MilliQ water, rinsed gently for 2 seconds, laid on the top of two different 50 μ l drops of 1% uranyl acetate (pH = 3), and stained for 1 minute. Finally, the grids were gently side blotted for 5 seconds and air dried. Grid visualization was performed on a Tecnai 12 transmission electron microscope (Thermo Fisher Scientific). Images were recorded at 21,900 nominal magnifications with a 4kx4k TemCam-F416 CMOS camera (TVIPS).

IV *In vivo* analysis

IV.1.1 Animal maintenance

Mouse experiments were conducted in accordance with the ethical guidelines established by the Biosafety and Animal Welfare Committee at CIC bioGUNE, the Institutional Ethics Committee of the Spanish National Cancer Research Center (CNIO, Madrid) and the Institutional Animal Care and Use Committee of the Institute for Research in Biomedicine (IRB, Barcelona). All procedures were performed following the recommendations from AAALAC. Mice were housed in isolated cages with controlled ventilation, humidity (30-50% relative humidity), temperature (22 ± 2 °C) and photoperiods of 12:12 h (light: dark cycles). Animals had water and sterile food pellets available *ad libitum*, unless specified for experimental designs. Mice were fasted for six hours prior to tissue harvest to prevent any metabolic alteration due to immediate food intake. For intracardiac injections, mice were anaesthetized with a mixture of ketamine (80 mg/kg) and xylazine (8 mg/kg). At experimental end points, animals were sacrificed either by cervical dislocation or CO₂ inhalation followed by cervical dislocation. Depending on the type of experiment, once animals were euthanized, blood, ascites, prostate glands, lymph nodes, brain, spleen, and bones were harvested and kept in 10% formalin, optimal cutting temperature compound (OCT) or frozen at -80 °C for further analysis.

IV.1.2 Genetically engineered mouse models (GEMMs)

For this thesis work, two mouse models have been used: mice with conditional tissue specific Pten knockout (termed KO) and mice with a double deletion of Pten and Pgc1 α (termed DKO). The latter mouse line was generated by Dr. Verónica Torrano and Dr. Arkaitz Carracedo as follows:

Mice with conditional tissue specific Pten knockout (C57BL6/129 sv; Pb-Cre4; Pten^{lox/lox}) were kindly provided by Dr. Pandolfi. On the other hand, mice with conditional tissue specific Pgc1 α null homogeneous background model were supplied by Dr Spiegelman. The Cre recombinase expression under the control of androgen-dependent ARR2B Probasin promoter (Pb-Cre4) allowed the deletion of Pten and Pgc1 α in the prostate epithelium when mice reached puberty.

By breeding Pten prostate-specific knockout mice (Pb-Cre4; Pten^{lox/lox}) and Pgc1 α conditional knockout mice (Pgc1 α ^{lox/lox}) a new mouse line, termed PTP was generated. For that, both mouse lines were crossed for at least three generations to finally obtain a founder colony with mixed homogeneous background. Probascins Cre was always retained in male mice, since in females Pb-Cre4 expression in utero can lead to recombination in embryos during pregnancy. Prostate Pten/ Pgc1 α deleted male mice were termed pc^{-/+} (heterozygous) or pc^{-/-} (homozygous knockout) for each gene. Three-month Pten^{pc^{-/-}} and Pten^{pc^{-/-}} Pgc1 α ^{pc^{-/-}} mouse samples were used in the present thesis work.

IV.1.3 Isolation of tumor interstitial liquid from GEMMs

Tumor interstitial liquid (TIL) was isolated from three-month Pten^{pc^{-/-}} (KO) and Pten^{pc^{-/-}} Pgc1 α ^{pc^{-/-}} (DKO) mice. Following the ethical guidelines mentioned above, mice were sacrificed, and the prostate (anterior, ventral, and dorso-lateral prostate) was extracted. For obtaining the TIL, the mouse anterior prostate was introduced into an Eppendorf tube and centrifuged for 10 minutes at 1500 rpm and 4 °C. Once the centrifuge step finished, prostate tissue was transferred into a fresh tube, remaining the TIL in the bottom of the Eppendorf tube. Both, the tissue, and the TIL were snap-frozen in liquid nitrogen and stored at -80 °C for further analysis.

IV.1.4 Subcutaneous xenograft experiments in nude mice

One million PC3 PGC1A cells (sgCtl and sgERR α #1) in suspension were subcutaneously injected into male nude mice (Harlan Laboratories, France) in both flanks. Tumor size was measured three times a week (Monday, Wednesday, and Friday) using a caliper, and tumor mass was estimated using the formula of spheroid volume: $volume = length \times width^2 \times 0.526$. Once tumors reached an average size of 100 mm³, animals were assigned to chow or doxycycline diet regime (Research diets, Ref. D12100402). After euthanasia, tumors were weighted, and tissue

was fresh frozen to further perform molecular analyses or embedded in paraffin for histological examination.

This experiment was led by Dr. Lorea Valcárcel with technical support of Dr. Ivana Hermanova and myself.

IV.1.5 *In vivo* metastasis assay: soluble factors

Ten-week-old male athymic Nude-Foxn1 mice (Harlan Laboratories, France) were treated throughout two weeks, via retro-orbital injection with 10 µg of Amicon-concentrated soluble factors (SFs) in a final volume of 100 µl, obtained from a total volume of 160 ml of cell secretome produced by PGC1 α -expressing and non-expressing cells (**FigM 16**). For obtaining the concentrated SFs, protocol from **section II.1.3** was followed, and then, SFs were filtered through 10K Amicon tubes to a final volume of 2 ml.

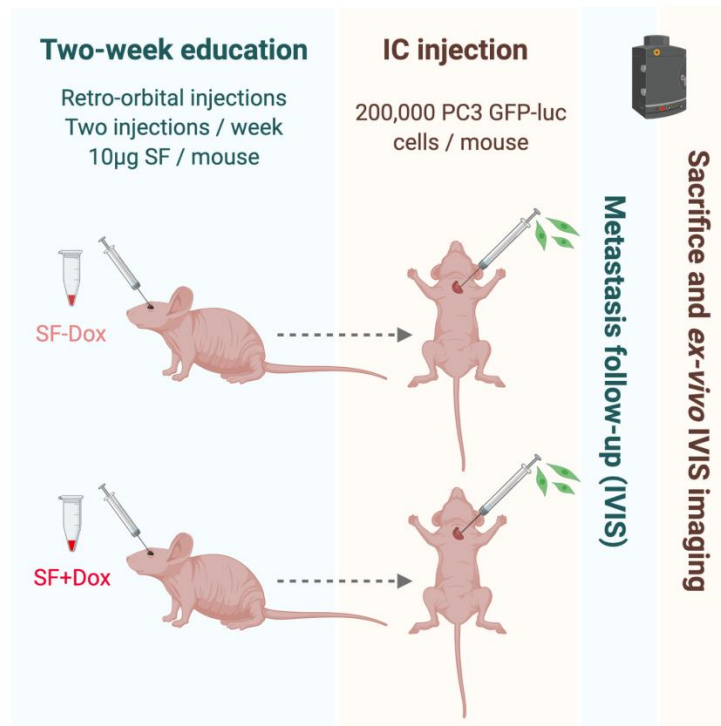


Figure M 16. *In vivo* metastasis assay. Nude mice are educated with soluble factors prior to the intra-cardiac injection of the PC3 GFP-luc cells.

SFs injections were performed twice a week, each day in a different eye and once the treatment period was over, each mouse was inoculated with 200,000 mycoplasma-free PC3 TGL cells resuspended in DPBS 1X via intra-cardiac (IC) injection. Immediately after the inoculation, IVIS Spectrum analysis (Perkin Elmer) was performed to verify the correct injection of the cells into the mice. Along the experiment, animals were weighted twice a week in order to control their health status and the development of the metastasis was assessed by performing *in vivo* bioluminescence imaging with IVIS device at days 6 and 13 after PC3 GFP-luc cells injection. At

the time of the experimental endpoint (day 13 after cells injection), *ex vivo* (necropsy) bioluminescent imaging was performed in the organs of interest (femur, lungs, and brain). Images were processed and quantified using the Living Image 4.7.2 (62-bit) software. (Units: Radiance (Photons)). Photon flux signal was presented as normalized signal, corrected by the basal signal obtained at the day of the PC3 GFP-luc cells injection.

This experiment was performed in collaboration with Dr. Héctor Peinado (Microenvironment and Metastasis group) at the Spanish National Cancer Research Center (CNIO, Madrid).

IV.1.6 *In vivo* metastasis assay: extracellular vesicles

Four- to six-week-old male athymic Nude-Foxn1 mice (Envigo) were treated throughout two weeks, via retro-orbital injection of 10 µg fresh EVs isolated from induced and non-induced PC3 TRIPZ PGC1A cells following the protocol from **section II.1.2 (FigM 17)**.

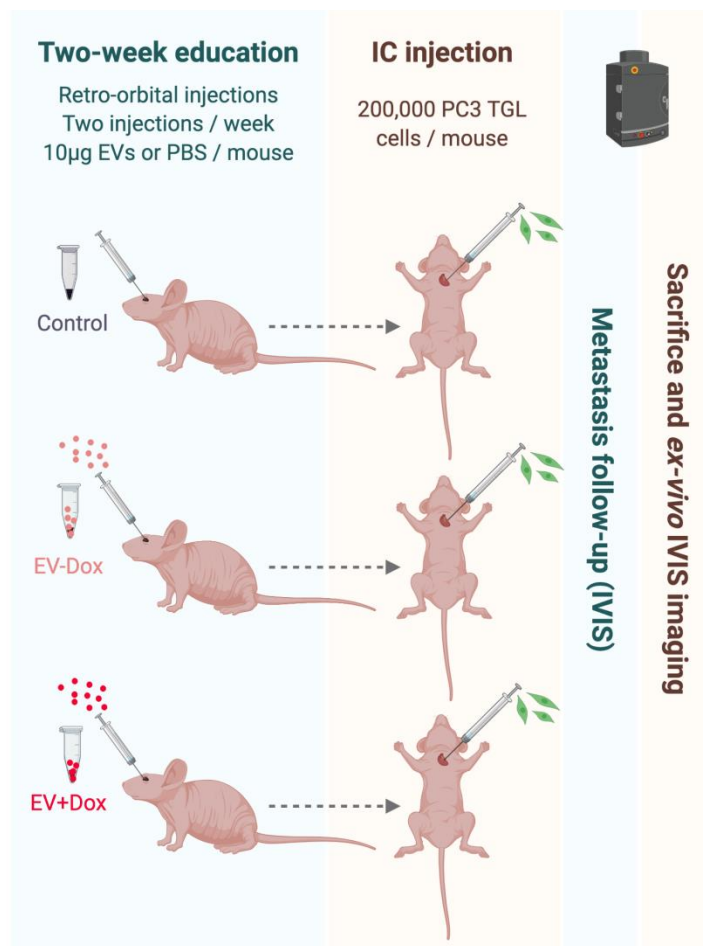


Figure M 17. *In vivo* metastasis assay. Nude mice are educated with EVs prior to the intra-cardiac injection of PC3 TGL cells.

EVs were resuspended in DPBS 1X and were administered in a final volume of 100 µl. As a control group, mice injected with the same volume of DPBS 1X was included. Injections were

performed twice a week, and once the treatment period was over, each mouse was inoculated with 200,000 PC3 TGL cells resuspended in PBS via IC injection. Metastases were tracked for 35 days through *in vivo* bioluminescence imaging (IVIS Spectrum device, Perkin Elmer). Then, at the experimental endpoint, *ex vivo* (necropsy) imaging of legs, lungs, ribs, and spinal cord was performed. Images were processed and quantified using the Living Image software. Photon flux values were presented as normalized signal, corrected by the signal measured at day 0. *Normalized photon flux = (day X signal/day 0 signal) x 1000.*

This *in vivo* experiment was performed in collaboration with Dr. Gomis and Marc Guix (Growth Control and Cancer Metastasis Group) at the Institute for Research in Biomedicine (IRB, Barcelona).

V Bioinformatics analysis and statistics

All experiments presented in this thesis work were performed a minimum of three times (biological replicates) to ensure reproducibility and statistical power. For each *in vitro* experiment, at least two technical replicates were included. Only *in vivo* experiments were performed once but with independent biological replicates. n values represent the number of independent experiments performed, number of individual mice or patient dataset number.

For *in vitro* experiments, normal distribution was assumed and for one component (fold change data normalized to 1) comparisons a one sample t-test was applied. When comparing two sets of samples, a parametric t-test was applied. An ANOVA test was performed to compare the mean 2D growth levels among cells treated with different proportions of secretomes.

For *in vivo* experiments, Gaussian distribution could not be assumed, and therefore a non-parametric Mann-Whitney U-test was applied.

For patient samples data, first a normality test was applied. As data did not follow a normal distribution, for correlation analyses, Spearman correlation test was applied. For *in vitro* data, normality was assumed, and Person correlation test was applied. Correlation coefficient (R) indicates the relation between two variables (X and Y). R values range between +1 and -1 (both included), where 1 is a total positive correlation, 0 is no correlation, and -1 is a total negative correlation. The p-value indicates the significance of R coefficient.

For hypothesis-driven experimental designs, a one-tail statistical analysis was applied, whereas in non-predicted experiments, a two-tail statistical test was used. The confidence level used for all the statistical analyses was of 95% (alpha value = 0.05).

Bioinformatics analyses containing patient data were performed taking advantage of the following publicly available PCa datasets: Fraser (n=200), Glinsky (n= 79), Grasso (n=88), Kumar (n=23), Lapointe (n=26), Taylor (n=179), TCGA (n= 496), Tomlins (n=75) and Varambally (n= 19) (Fraser et al. 2017; Glinsky et al. 2004; Grasso et al. 2012; Kumar et al. 2011; Lapointe et al. 2004; Taylor et al. 2010a; Tomlins et al. 2007; Varambally et al. 2005).

GraphPad Prism 9 software was used for statistical calculations and representation of data and Biorender webtool (BioRender.com) was used for the generation of figures.

The background of the slide is a light cream color, decorated with several overlapping, semi-transparent yellow watercolor circles of various sizes. The circles have soft, feathered edges and are scattered across the page, with some appearing more prominent than others. A central white rectangular box with a thin yellow border contains the word "Results" in a bold, black, sans-serif font.

Results

I Evaluation of the biological impact of the cell secretome on prostate cancer aggressiveness

The first objective addressed in the present thesis work was to uncover the biological impact of the cell secretome in the aggressive properties of PCa cells. To this aim we used a model of PCa previously described in our laboratory that is driven by loss of the metabolic regulator PGC1 α . The dysregulation of PGC1 α happens to occur in different cancer types (Andrzejewski et al. 2017; Luo et al. 2016). In the context of PCa, PGC1 α was shown to exert a tumor and metastasis suppressive function by means of controlling the cell metabolism and cytoskeletal rearrangements (Torrano, Valcarcel-Jimenez, et al. 2016; Valcarcel-Jimenez et al. 2019). Nonetheless, there are still open questions on how PGC1 α exerts its tumor suppressive activity in PCa. Interestingly, in the last years, a growing number of studies have focused on elucidating the role that secreted factors play in cancer progression, therapy resistance and metastasis (C. M. Sousa et al. 2016; Mendez et al. 2018; Brady et al. 2016; Martin et al. 2004; Cerezo-Wallis et al. 2020; Obenauf et al. 2015; Luga et al. 2012; Rodrigues et al. 2019). In the context of PCa, studies have mainly focused on characterizing the protein content of the secretome produced by PCa cells with the aim of discovering novel and non-invasive biomarkers of tumor progression (Sardana et al. 2008; Martin et al. 2004; Nurdin et al. 2016). Some of these investigations also shed light on the important role that secreted entities produced and released by the stromal compartment play on the development of PCa (Franco et al. 2011; Zeda Zhang et al. 2020; Calcinotto et al. 2018). Nonetheless, up to date, studies encompassing PGC1 α and cancer secretome regulation have not been done, nor in PCa neither in other cancer types. Up to date, few studies showed the role of PGC1 α in terms of secretome regulation, focusing one of them on mouse muscle physiology and demonstrating a PGC1 α -driven myokine secretion that impacts on the glucose homeostatic regulation through the crosstalk established between muscle cells and pancreatic β cells (Handschin, Choi, et al. 2007). In addition, another study revealed the function of PGC1 α on the regulation of genes encoding for secreted proteins and ECM components in multiple mouse and human cell lines. Various of the candidates identified were further confirmed by proteomic analysis of secretomes produced by fibroblasts (Minsky and Roeder 2017). A third study was able to demonstrate that PGC1 α impacts on the expression of several genes in the skeletal muscle, among them *Fndc5*. This gene encodes for irisdin, a myokine that is secreted and further impacts in the overall body energy expenditure (Boström et al. 2012)

Within this context, we wondered whether the tumor suppressive role of PGC1 α which, so far, has been attributed to the cell-intrinsic phenomena, may well go beyond that, hence presenting PGC1 α as a tumor suppressor regulating cell communication by means of secretome composition alterations.

HYPOTHESIS

PGC1 α modulates the secretome composition of prostate cancer cells, and the latter impacts on the autocrine and paracrine cell communication

Importantly, in the present work, the term “secretome” stems to the whole spectra of bioactive molecules released by the cells to the extracellular milieu, and two compartments may be distinguished: extracellular vesicles (EVs) and soluble factors (SFs).

In order to ascertain our hypothesis, we first established an experimental setting that could provide us with differential secretomes produced by metastatic cell lines with differential expression of PGC1 α (**FigR 1A**). As previously described (Torrano et al. 2016), treatment of PC3 cells harboring a doxycycline-inducible lentiviral vector (TRIPZ-HA-Pgc1 α) were used as a cellular system, where ectopic expression of PGC1 α upon treatment with doxycycline was confirmed, (**FigR 1B**) and further triggered changes in cell morphology (**FigR 1C**). PGC1-expressing PC3 cells present a reduced proliferation capacity compared to the non-PGC1 α expressing cells (Torrano et al. 2016). On average, PGC1 α -expressing cells grow 2.5 times less than the non-expressing PC3 cells (**FigR 1D**). We took this fact into consideration and seeded 2.5 times more PGC1 α -expressing producer cells compared to the non-expressing ones for conducting secretome experiments. The reason for doing so was to reach in PGC1 α -expressing and non-expressing conditions the most similar cell number at the day of secretome collection, and thus, having a more controlled experimental system. This proportionality was kept along all secretome experiments that were done in the present thesis work. Despite we took into consideration the differences in cell proliferation, we still counted in most of the experiments a lower number of PC3 producer cells expressing PGC1 α compared to the non-expressing ones (**FigR 1E**). Once the differential secretomes were produced and collected, they were used to treat different PCa cell lines that were called “recipient cells” (**FigR 1F**).

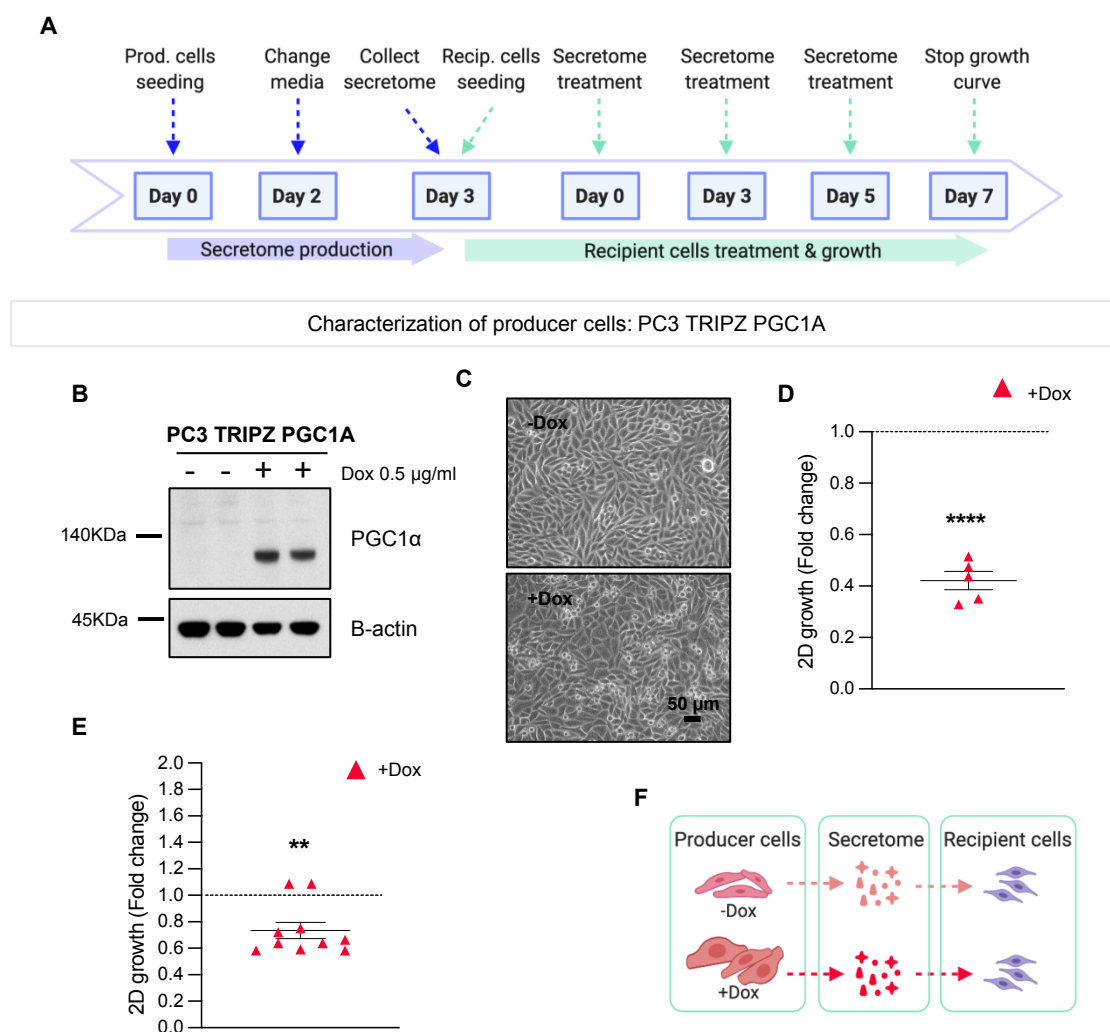


Figure R 1. Experimental setting and system to assess the biological role of PCa cells secretome. A. Timeline of the experimental conditions to obtain the differential secretomes from the producer cells and the secretome treatments performed on the recipient cells. **B.** Analysis of PGC1 α expression by Western blot in PC3 cells transduced with a doxycycline-inducible TRIPZ-HA-Pgc1 α vector. **C.** Representative images showing morphological features of PGC1 α -expressing and non-PGC1 α expressing PC3 cells. Bar, 50 μ m. **D.** Proliferation differences observed in PC3 cells with differential expression of PGC1 α ($n=5$). **E.** Analysis of producer cells proliferation rates measured by crystal violet staining at the day of the secretomes collection ($n=10$). **F.** Experimental design for secretome obtention and further use for treatment of recipient cells. In D and E, data is normalized to the -Dox condition, represented with a black dotted line. Statistical analysis: One sample t-test establishing 1 as hypothetical value. p , p -value. ** $p<0.001$, **** $p<0.0001$. Error bars indicate s.e.m.

I.1 Biological effect of PGC1 α -driven secretome in PCa cell lines

I.1.1 Effect of the cell secretome in cell proliferation

We first assessed the impact of the secretome on cell proliferation. To this end, we seeded PC3 recipient cells and evaluated cell growth at days 2, 5 and 7 of treatment with the secretomes obtained from PGC1 α -expressing and non-expressing cell lines. Results showed a time-dependent decrease (reaching a highest and statistically significant drop at day 7 of treatment) of cell proliferation on those cells treated with the secretomes produced by PGC1 α -expressing cells (**FigR 2A**). Next, we sought at evaluating the effect of the secretomes produced by PGC1 α -expressing and non-expressing PC3 cells in other two PCa metastatic epithelial cell lines, DU145 and 22Rv1. The effect of the differential secretomes was in line with what observed previously in the PC3 cell line; compared to the cells treated with the secretomes produced by cells lacking PGC1 α expression, both DU145 and 22Rv1 cells showed a reduction on 2D proliferation when treated with the secretomes produced by PGC1 α -expressing cells (**FigR 2B**). Importantly, the differential secretomes used for treating recipient cells were obtained from cells grown in DMEM, which, is not the optimal media for growing the 22Rv1 cell line and therefore cells' normal growth might have been affected. Nonetheless, for answering this question, PC3 producer cells with differential expression of PGC1 α would need to be cultured in RPMI for producing distinct secretomes to treat recipient cells. Finally, microscope images of the recipient cells were taken throughout the experiments to keep track of their confluence and to visualize any changes in morphology or growth pattern upon treatment with the distinct secretomes. No relevant morphological changes were observed in any of the three cell lines evaluated (**FigR 2C**).

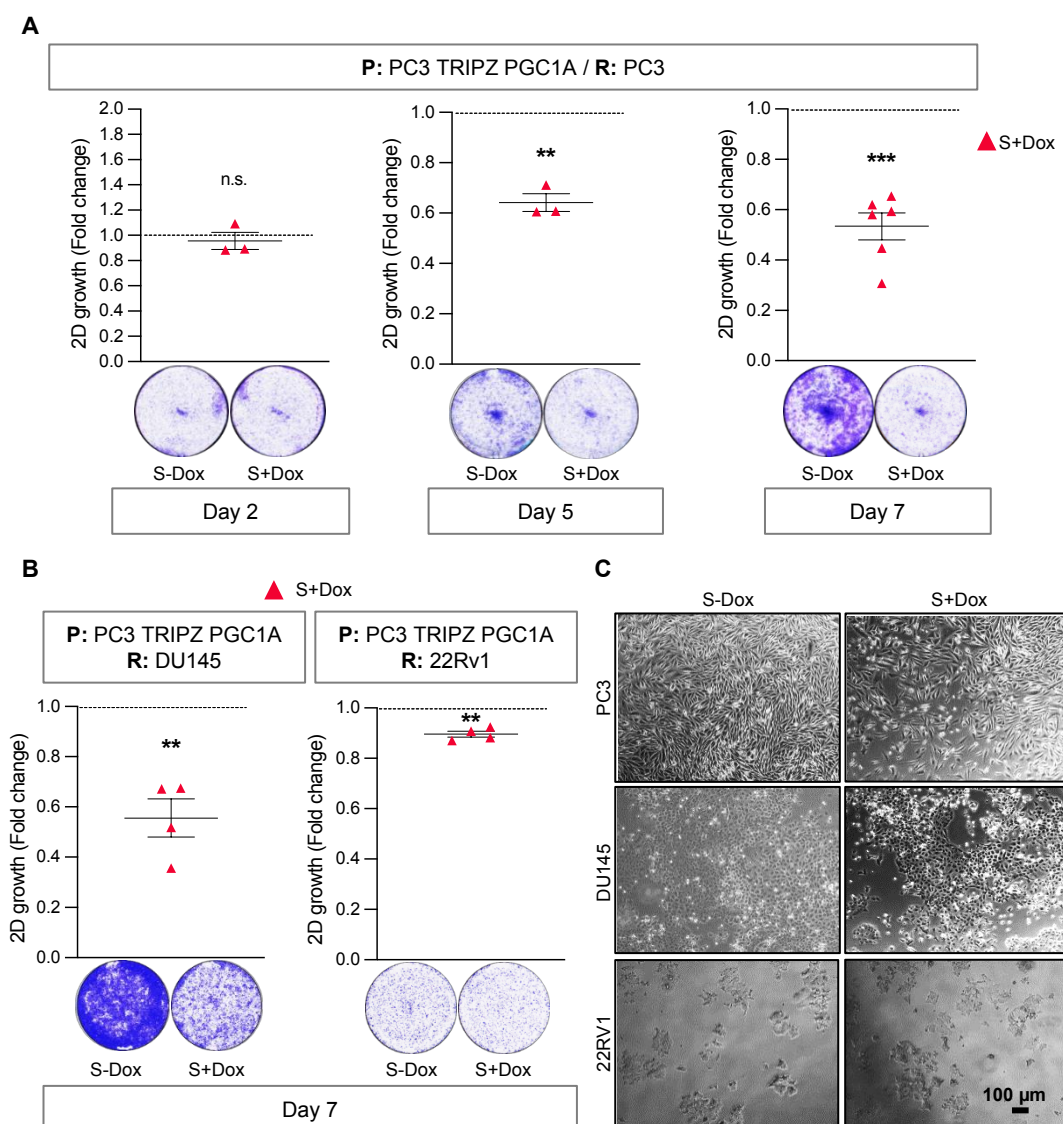


Figure R 2. The PGC1 α -driven cell secretome reduces 2D proliferation of a panel of aggressive PCa cell lines. A-B. 2D proliferation assay of PC3 (A), DU145 and 22Rv1 (B) cells treated with secretomes produced by PGC1 α -expressing and non-expressing PC3 cells. A representative image of the crystal violet staining is included below the quantifications ($n=3-6$). **C.** Representative images in bright field of PC3, DU145 and 22Rv1 cells treated with the differential secretomes. Bar, 100 μ m. P: secretome-producer cells. R: recipient cells. S+Dox: secretome produced by PGC1 α -expressing cells. In A and B, data are normalized to the S-Dox (non-PGC1 α expressing) condition, depicted by a black dotted line. Statistical analysis: One sample *t*-test establishing 1 as hypothetical value. *p*, *p*-value. * $p<0.05$, ** $p<0.001$, *** $p<0.001$. n.s.=not significant. Error bars indicate s.e.m.

Next, and in order to rule out a possible effect of the doxycycline present in the secretomes used for treating recipient cell lines, we cultured PC3 TRIPZ producer cells in the presence or absence of doxycycline, finding no changes in proliferation between doxycycline-treated and untreated cells (**FigR 3A**). The secretomes produced by these cells were collected and used for growing PC3 cells throughout seven days. No differences in cell proliferation were observed in the PC3 recipient cells treated with the secretomes produced by doxycycline treated

or untreated PC3 TRIPZ control cells (**FigR 3B**). We therefore confirmed that the use of doxycycline did not compromise the experimental outcomes.

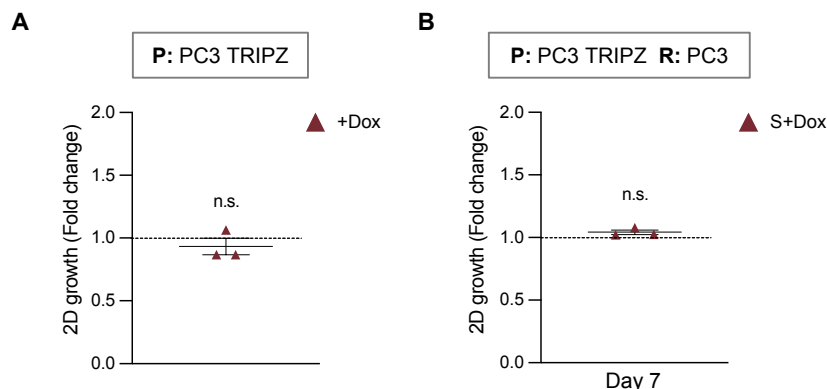


Figure R 3. Proliferation of PC3 recipient cells educated with secretomes produced by doxycycline treated and untreated PC3 producer cells. **A.** Cell proliferation analysis of the PC3 TRIPZ producer cells at the day of secretome collection ($n=3$). **B.** Analysis of 2D proliferation of PC3 cells treated throughout 7 days with the secretome produced by PC3 TRIPZ cells (empty vector) in the presence or absence of doxycycline ($n=3$). +Dox: cells treated with doxycycline. P: secretome producer cells. R: recipient cells. S+Dox: secretome obtained from producer cells treated with doxycycline. In A and B data are normalized to the -Dox/ S-Dox conditions, both depicted by a black dotted line. Statistical analysis: One sample t-test establishing 1 as hypothetical value. n.s.=not significant. Error bars indicate s.e.m.

We finally wondered whether increasing percentages of S-Dox (secretome derived from non-PGC1 α expressing cells) would blunt the anti-proliferative effect of the secretome S+Dox (secretome derived from PGC1 α expressing cells) in PCa recipient cell lines (**FigR 4A**). This experiment was based on the hypothesis that secretomes derived from PGC1 α -expressing and non-expressing cells would have a different molecular composition and hence, a distinct biological impact. Results showed that after seven days of secretome treatment, PC3 and DU145 recipient cells' proliferative capacity was higher when the proportion of S-Dox was larger. PC3 cells treated with S+20%S-80% reached almost same proliferation levels that PC3 cells treated with S-100%. On the other hand, DU145 cells treated with S+50%S-50% and S+20%S-80% reached slightly higher proliferation tiers than the S-100% control group (**FigR 4B**). These data prompted towards the presence of an anti-proliferative secreted entity or entities or towards a drop in the presence of a pro-proliferative factors/s in the secretome produced by PGC1 α -expressing cells.

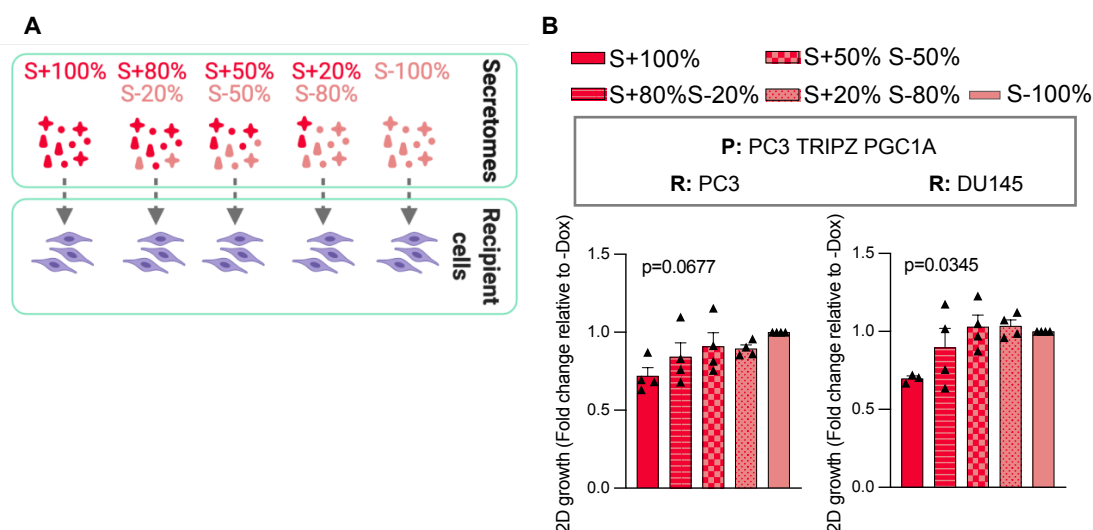


Figure R 4. Cell proliferation of recipient cells is recovered when treated with ever-increasing proportions of secretome derived from non-*PGC1 α* expressing cells. **A.** Schematic representation of the experimental conditions. **B.** 2D proliferation of recipient cells treated with increasing proportions of S-Dox for seven days ($n=4$). P: secretome-producer cells. R: recipient cells. S: secretome. Minus symbol: absence of doxycycline. Plus symbol: presence of doxycycline. Percentage symbol: proportion of S- or S+ mixed for the secretome treatments. Data in B are normalized to the S–100% condition. Statistical analysis: ANOVA test. p , p -value. Error bars indicate s.e.m.

I.1.2 Role of the cell secretome in cell migration

We next evaluated the role of the *PGC1 α* -regulated secretome in PCa cells migration capacity, which is one of the key features that malignant cells need to acquire in order to metastasize. To do so, we performed three types of experiments: wound healing assay, transwell migration assay as well as migration experiments in co-culture.

For wound healing assays (WHA) PC3 cells treated for five days with the distinct *PGC1 α* -driven secretomes were subjected to a scratch and left to migrate to the wounded area for a period of 24 hours and still in the presence of the distinct secretomes. We observed a marked reduction on the migration ability of recipient cells when treated with the secretomes obtained from *PGC1 α* -expressing cells (**FigR 5A**). Nonetheless, we realized cells treated with the distinct secretomes did not reach the same confluence levels, and when we took this fact into consideration, the drop in migration showed to be ablated (**FigR 5B-C**), evidencing once again the anti-proliferative features that the cell secretome produced by *PGC1 α* -expressing cells exerts on recipient cells.

For performing transwell migration assays, PC3 producer cells were treated throughout five days with secretomes derived from *PGC1 α* -expressing and non-expressing PC3 cell lines. After this education period, PC3 recipient cells were seeded into Boyden chambers and left to migrate for 24 hours, time after which, no significant differences in the cell's migration capacity were observed (**FigR 5D**). We finally performed a different type of migration assay in which, secretome-producing cells were co-cultured, separated by a membrane, with the recipient cells.

PC3 producer cells expressing or not PGC1 α were seeded in the bottom wells of Boyden chambers and after growing for 24 hours, PC3 recipient cells were pipetted in the Boyden chamber transwells. PC3 recipient cells were left to migrate for 24 hours. Although not statistically significant, cells that had been co-cultured in the presence of PGC1 α -expressing PC3 cells, migrated slightly less than those cells grown in an environment with non-PGC1 α expressing cells (FigR 5E).

Overall, we concluded that the secretome regulated by PGC1 α exerts no significant impact on the migration capacities of recipient cells.

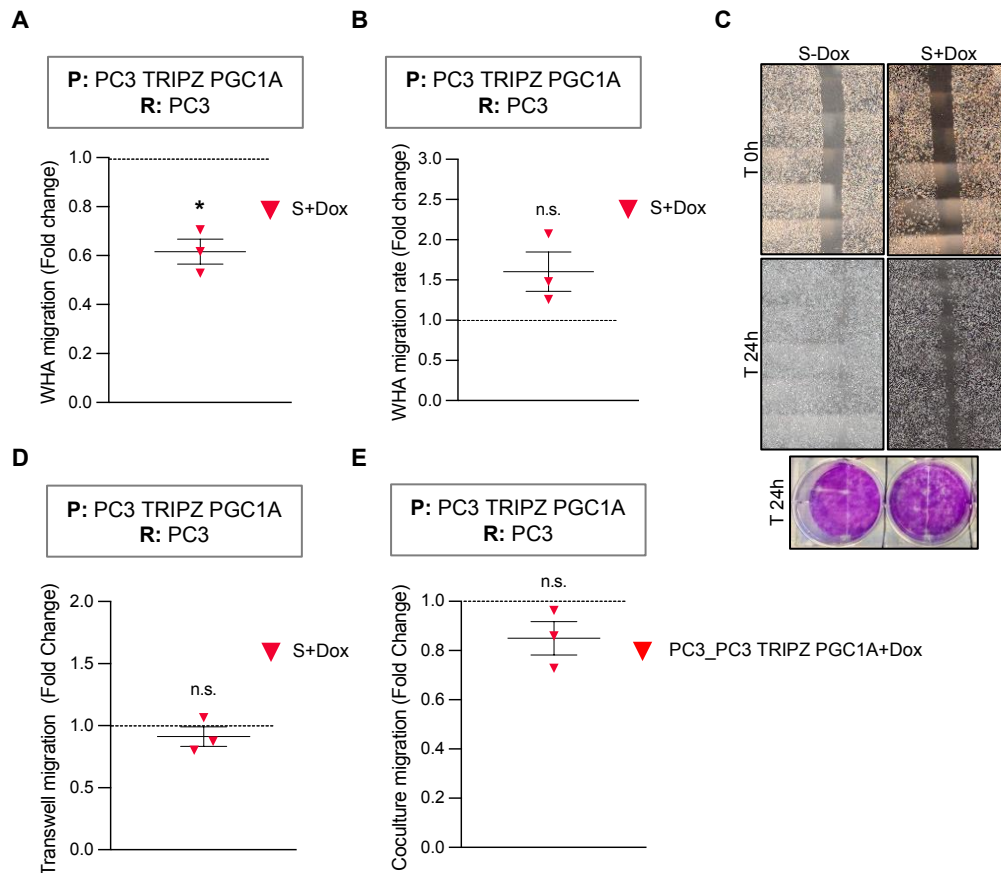


Figure R 5. Effect of the secretome in cell migration. A-B. Migration capacity of PC3 recipient cells measured by wound healing assay (A) and further normalized to the cell proliferation levels of PC3 recipient cells (B). C. Panels show representative images of the wounded areas at the time of the scratch performance (T 0h) and at the time at which experiment is stopped (T 24h). Crystal violet staining representative image is shown as a control of cell confluence at 24 hours. D. Transwell migration capacity of PC3 recipient cells treated throughout five days with differential secretomes. E. PC3 recipient cells migration capacity in coculture with PC3 cells expressing or not PGC1 α (n=3). In A and D data is normalized to the -Dox condition, both represented with a black dotted line. In B data is relativized to the proliferation rate at T 24h and to the -Dox condition, depicted by a black dotted line. In E data is normalized to the -Dox condition and to the growth rate of the producer cells, depicted by a black dotted line. P: secretome-producer cells. R: recipient cells. T: time. S+Dox: secretome produced by PGC1 α -expressing cells. Statistical analysis: One sample t-test establishing 1 as hypothetical value. *p<0.05, n.s.=not significant. Error bars indicate s.e.m.

I.1.3 The PGC1 α -ERR α transcriptional axis regulates the cell secretome

The metabolic co-regulator PGC1 α exerts its multiple functions by means of interacting with different transcription factors (Charos et al. 2012). One of these transcription factors is ERR α , which is known to cooperate with PGC1 α to regulate the expression of mitochondrial biogenesis and oxidative phosphorylation genes (Huss, Kopp, and Kelly 2002; Mootha, Handschin, Arlow, Xie, Pierre, et al. 2004). Moreover, expression of PGC1 α increases *ERRA* gene expression levels (Laganière et al. 2004). In the context of PCa, we previously showed how the PGC1 α -ERR α transcriptional axis exerts an anti-tumoral and anti-metastatic activity (Torrano, Valcarcel-Jimenez, et al. 2016; Valcarcel-Jimenez et al. 2019) and this is based on cell-intrinsic molecular events. Taking these data into consideration and having previously shown the drop in proliferation of those cells treated with the secretome produced by PGC1 α -expressing cells compared to the non-expressing ones (**FigR 2A-B**), we wondered whether this secretome-mediated effect could also be dependent on ERR α . In order to test this idea, we took advantage of PGC1 α doxycycline inducible PC3 cells where *ERRA* was deleted using CRISPR/Cas9 technology (**FigR 6A**). As previously described, *ERRA* deletion blunts the anti-proliferative, anti-invasive and the morphological changes known to be driven by PGC1 α , thus, showing how closely PGC1 α depends on ERR α (Valcarcel-Jimenez et al. 2019). Regarding the biological effect of the secretome, we treated PC3 cells with the secretome produced by PC3 cells with differential expression of both, PGC1 α and ERR α (**FigR 6B**). To perform these experiments, we again took into consideration the differences in proliferation and thus seeded the producer cells at proportional confluences. By doing so, we obtained quite similar number of producer cells at the day of secretome collection (**FigR 6C**). Notably, PC3 recipient cells treated with the secretome produced by cells expressing PGC1 α and ERR α showed a marked reduction in proliferation compared to the rest of the conditions in which, PC3 cells were treated with secretomes produced by cells with or without PGC1 α expression in combination with ERR α deletion (**FigR 6D**). Overall, these experiments let us conclude that ERR α is required to exert the non-cell autonomous PGC1 α -mediated anti-proliferative effect of PCa epithelial cells.

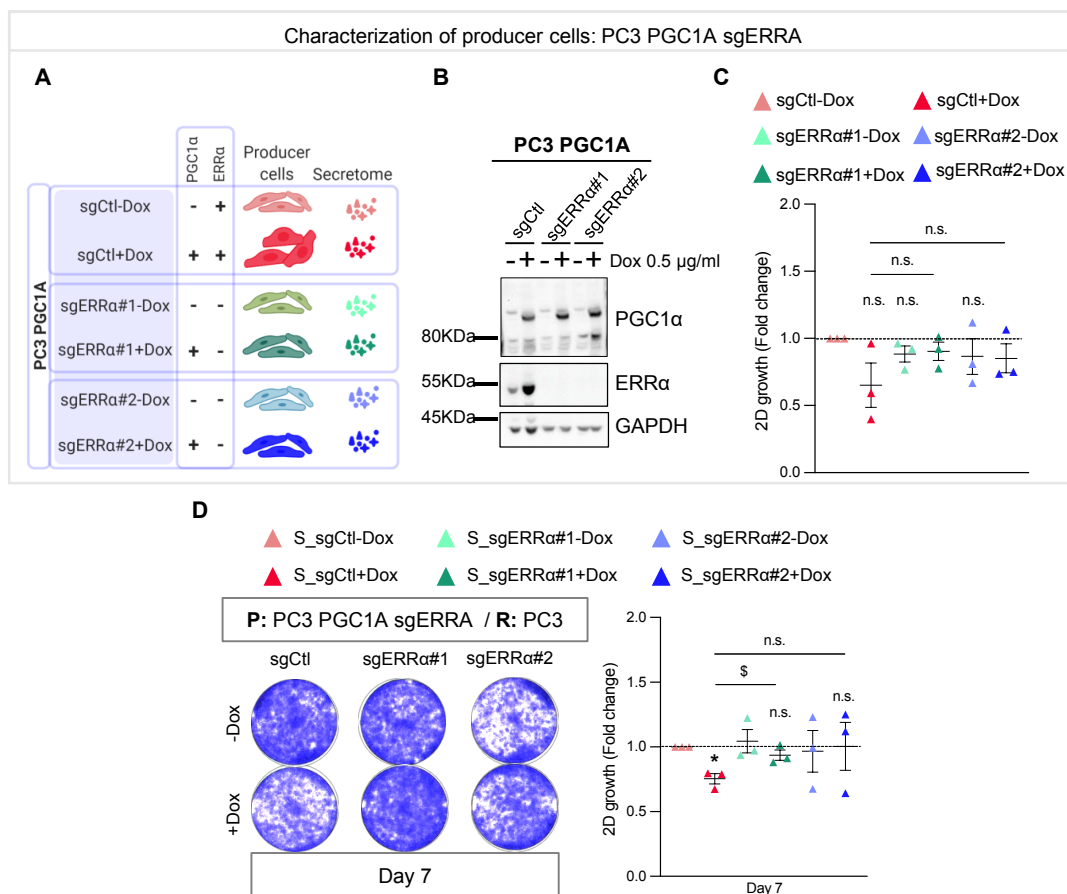


Figure R 6. PGC1α cell-extrinsic anti-proliferative effect is dependent on ERRα. **A.** Schematic overview of the three PC3 cell lines used for the generation of secretomes used for treating PC3 recipient cells. **B.** Protein expression analysis of ERRα and PGC1α in doxycycline-induced cell lines transduced with sgRNA constructs targeting ERRα (sgERRa#1 and sgERRa#2). One representative experiment out of 3 is shown. **C.** 2D proliferation of PC3 cells with combined expression of PGC1α and ERRα deletion. **D.** Representative crystal violet staining and quantification of PC3 recipient cells proliferation after seven-day treatment with the secretomes produced by PC3 cells with combined expression of PGC1α and ERRα deletion (n=3). P: secretome-producer cells. R: recipient cells. S: secretome. +Dox: PGC1α-expressing condition. In C, data is normalized to the S_sgCtl-Dox condition, depicted by a black dotted line. Statistical analysis: In C and D, one sample t-test establishing 1 as hypothetical value. Unpaired parametric one-tail t-test. Asterisks indicate statistical differences between S_sgCtl-Dox and the rest of the conditions and the dollar symbol indicates the statistical differences between S_sgCtl+Dox and S_sgERRa#1+Dox/ S_sgERRa#2+Dox. p, p-value. */\$p<0.05. n.s.=not significant. Error bars indicate s.e.m.

Finally, and trying to further identify the secreted factor/s that could explain the drop in proliferation observed in cells treated with secretome obtained from PGC1α-expressing cells, we generated fractionated secretomes based on a molecular size cut-off. Using producer PC3 cells with combined PGC1α expression and ERRα deletion, the secretomes were filtered through Amicon tubes with a 10-KDa cut-off, obtaining two fractions: one with molecules bigger than 10 KDa (S>10K) and another one with molecules smaller than 10 KDa (S<10K). Strikingly, we only reproduced the drop in proliferation of PC3 cells treated with S>10K (FigR 7A), observing no changes among groups in cells treated with S<10K (FigR 7B). As shown in FigR 7A, PC3 cells

treated with the secretome produced by PGC1 α and ERR α -expressing cells grew statistically significant less compared to the remaining groups. PC3 cells treated with any of the secretome conditions smaller than 10 KDa experienced no significant differences in proliferation. Overall, these experiments brought us to the conclusion that metabolites are not drivers of the anti-proliferative effect, and there must be a bigger-than 10 KDa secreted factor/s present or absent in the secretome produced by PC3 cells with an activated PGC1 α -ERR α transcriptional axis.

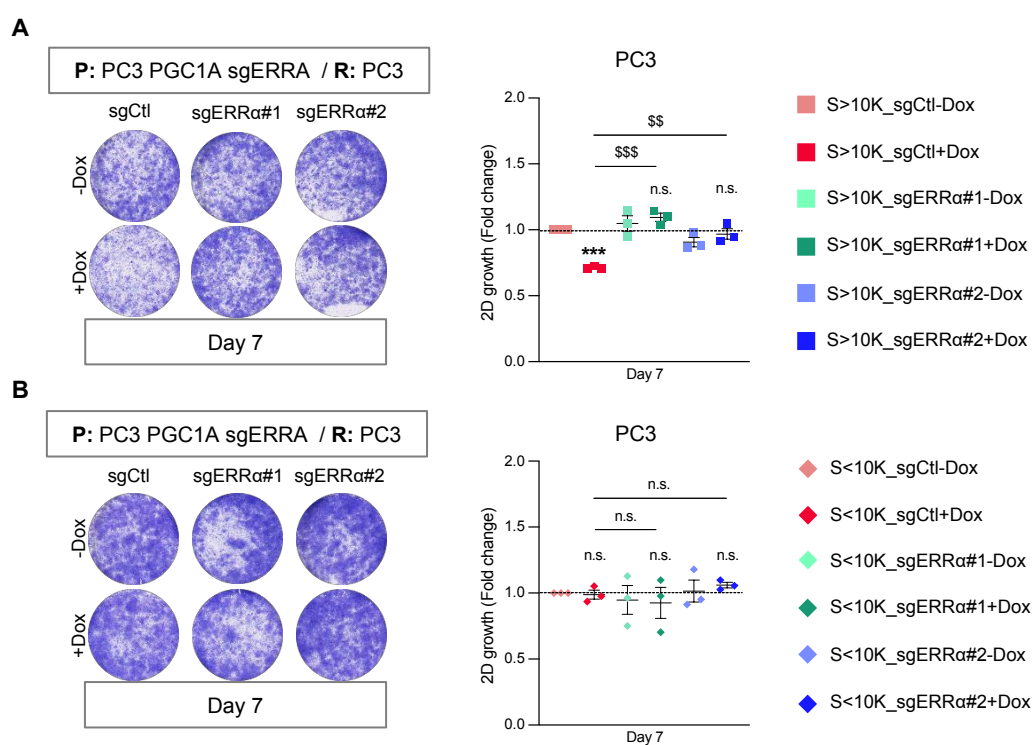


Figure R 7. The cell extrinsic PGC1 α anti-proliferative effect is observed in the secretome fraction containing molecules bigger than 10 KDa. A-B. PC3 recipient cells treated throughout seven days with secretome fractions containing molecules bigger (A) or smaller (B) than 10 KDa size obtained from producer cells with combined expression and deletion of PGC1 α and ERR α (n=3). P: secretome-producer cells, R: recipient cells. S: secretome. S>10K: secretome containing molecules bigger than 10 KDa size. S<10K: secretome containing molecules smaller than 10 KDa size. +Dox: PGC1 α -expressing condition. In A and B, data are normalized to the S>10K_sgCtl-Dox/S<10K_sgCtl-Dox condition, depicted by a black dotted line. One representative image of crystal violet staining is shown out of 3 independent experiments. Statistical analysis: One sample t-test establishing 1 as hypothetical value. Unpaired parametric one-tail t-test. Asterisks indicate statistical differences between S>10K_sgCtl-Dox/S<10K_sgCtl-Dox and the rest of the conditions and the dollar symbol indicates the statistical differences between S>10K_sgCtl+Dox/S<10K_sgCtl+Dox and S>10K_sgERR α #1+Dox/ S<10K_sgERR α #1+Dox as well as S>10K_sgERR α #2+Dox/ S<10K_sgERR α #2+Dox. p, p-value, \$\$p<0.01, ***/\$\$\$p<0.001. n.s.=not significant. Error bars indicate s.e.m.



Overview

- PGC1 α re-expression in PCa cells leads to the production of a cell secretome that, when used to treat highly aggressive PCa cell lines, blunts proliferation compared to those recipient cells that are treated with secretome produced by non-PGC1 α expressing cells.
- Using PC3 cells with an empty vector TRIPZ construct, confirmed that the use of doxycycline does not alter the experimental outcomes.
- Increasing proportions of secretome derived from non-PGC1 α expressing cells rescues the anti-proliferative effect of PGC1 α -expressing cells' secretome. This data points towards either the presence of anti-proliferative factor/s or the reduction of pro-proliferative factor/s in the secretome produced by PGC1 α -expressing cells.
- Wound healing assay, Boyden chamber migration and co-culture experiments reveal no significant impact of the PGC1 α -regulated secretome on the recipient cells' migration capacities.
- The non-cell autonomous anti-proliferative effect of the PGC1 α is dependent on the transcription factor ERR α , thus suggesting the transcription factor is involved on the regulation of the secretome composition.
- The non-cell autonomous anti-proliferative effect of the PGC1 α is restricted to the secretome fraction bigger than 10 KDa, narrowing the molecular size of the effector protein/s and excluding small peptides as drivers of the anti-proliferative effect observed.

II Study and description of the EVs fraction of the secretome

We previously demonstrated the anti-proliferative features of the cell secretome produced by PGC1 α -expressing cells compared to the secretome obtained from non-PGC1 α expressing PC3 cells. Moreover, fractionation revealed this anti-proliferative effect is mediated by the secretome fraction containing molecules bigger than 10 KDa, in which, EVs, although in a low proportion, are included. Hence, we sought at studying deeper the EVs fraction of the cell secretome and their role on PCa aggressiveness. Lately, EVs have been described to be active mediators of tumor progression (Hosseini-Beheshti et al. 2016; Sansone et al. 2017), being their main role in cancer attributed to their capacity of preparing the distant sites of metastasis by means of instructing local cells and altering the microenvironment (Skog et al. 2008; Yuelong Liu et al. 2010; Peinado, Ale, et al. 2012; Costa-Silva et al. 2015; Zhao et al. 2016; Gyukity-Sebestyén et al. 2019; J. Liu et al. 2020). This process seems to be cell-specific, guided by concrete cell adhesion molecules that are present in EVs and direct their uptake (Hoshino et al. 2015), thus allowing the transfer of functionalities between donor and recipient cells. In addition to their active role in tumor development, EVs have a great potential as non-invasive biomarkers for the diagnosis, prediction and monitoring of cancer, as shown in different studies (García-Silva et al. 2019; Kimura et al. 2019; Dejima et al. 2017). This is because they reunite key characteristics such as being stable units that contain and protect a great variety of molecules, and they can be widely found in biological fluids and in considerable amounts. In PCa, studies have focused on using biomarkers detected in EVs obtained from plasma or urine (Khanna et al. 2021; Royo et al. 2016), demonstrating they are good fingerprints of their tissue of origin. In addition, based on the studies published by McKiernan and colleagues (McKiernan et al. 2016; 2018) even a PCa diagnosis test (ExoDx™ Prostate Test, Exosomedx, Biotechne brand) that takes advantage of exosomes' specific markers has been developed. This test aims at helping doctors on making decisions on whether performing or not a prostate biopsy to patients with high PSA levels. Thus, with no doubt, EVs can be considered interesting candidates to be studied in the context of PCa, and more concretely in the framework of the disease being regulated by PGC1 α .

HYPOTHESIS

PGC1 α regulates the EVs fraction of the cell secretome produced by tumor cells and this has an impact in PCa aggressiveness

II.1 EVs physical and molecular characterization

II.1.1 EVs general characterization by western blot, electron microscopy, nanoparticle tracking analysis and protein content.

The first approach for studying the role of EVs in our PCa model driven by the master regulator PGC1 α was to corroborate EVs isolation and purity whilst performing a physical and molecular characterization, as recommended by the ISEV 2018 guidelines (Théry, Witwer, Aikawa, Jose Alcaraz, et al. 2018). Therefore, we first established the cell culture settings and isolation protocol for optimizing the extraction of EVs from three PCa cell lines (PC3 TRIPZ PGC1A, PC3 PGC1A sgERR α and PC3 TRIPZ) (**FigR 8**).

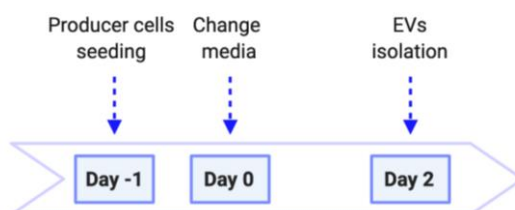


Figure R 8. Schematic timeline of the optimized experimental conditions set to yield EVs from PCa cells.

Next step was to confirm the enrichment in EVs after the ultracentrifugation steps protocol, and this was assessed by combining western blot analysis, electron microscopy imaging and nanoparticle tracking analysis (NTA) for particle size measurement. Western blot analysis of the cell lines interrogated confirmed EVs isolation purity by displaying an enrichment of exosome markers CD9 and CD63 and absence of intracellular membrane markers (endoplasmic reticulum GRP78 and mitochondrial COX IV) that were only found in the producer cell-extracts (**FigR 9A-C**). Merely a minor contamination of COX IV marker was detected in the EVs isolated from cell lines with differential expression of PGC1 α (**FigR 9A**). Of note, we did consistently observe a reduction of CD9 and increase of CD63 marker levels in those EVs isolated from PGC1 α -expressing cells (**FigR 9A**). In the same line, EVs produced by PCa cells with combined expression and deletion of PGC1 α and ERR α also displayed decrease of CD9 marker levels when produced by PGC1 α and ERR α -expressing cells. No consistent changes in CD63 expression levels were observed in these cell lines (**FigR 9B**). Finally, as expected, no changes in CD9 levels were found in EVs produced by control cell lines (**FigR 9C**).

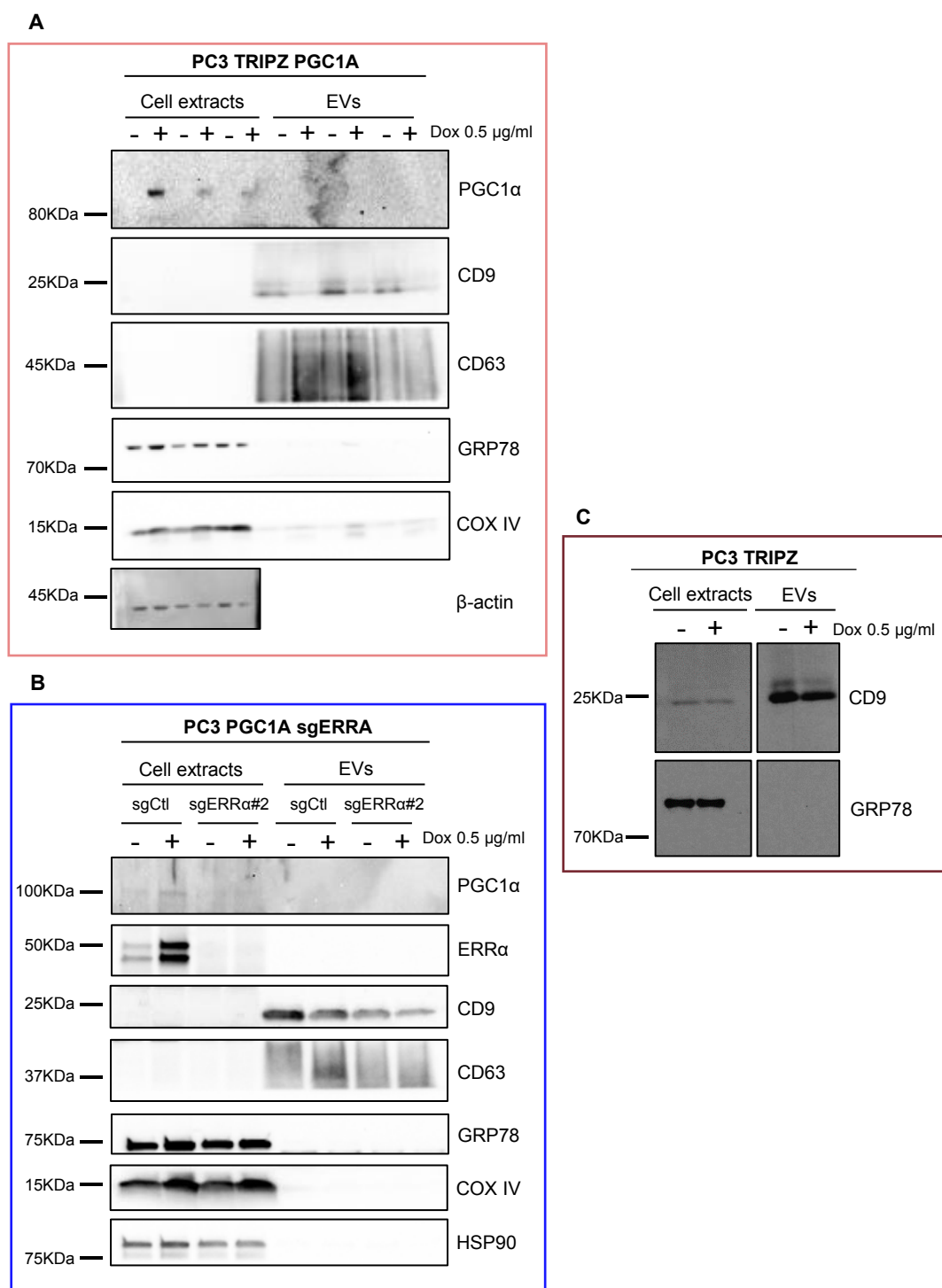


Figure R 9. Western blot analysis of EVs derived from PCa cells confirms sample purity. A-B-C. Western blot analysis confirming the purity of EVs harvested from PC3 TRIPZ PGC1A cells (A), PC3 PGC1A sgERRA cells (B) and PC3 TRIPZ cells (C). In A, $n=3$ and in B, one representative experiment out of three is shown and in C, $n=1$. Dox: doxycycline.

We then confirmed by electron microscopy the integrity and the presence of double membrane of the EVs isolated across the three cell lines (**FigR 10A-B**, and **FigR 11**).

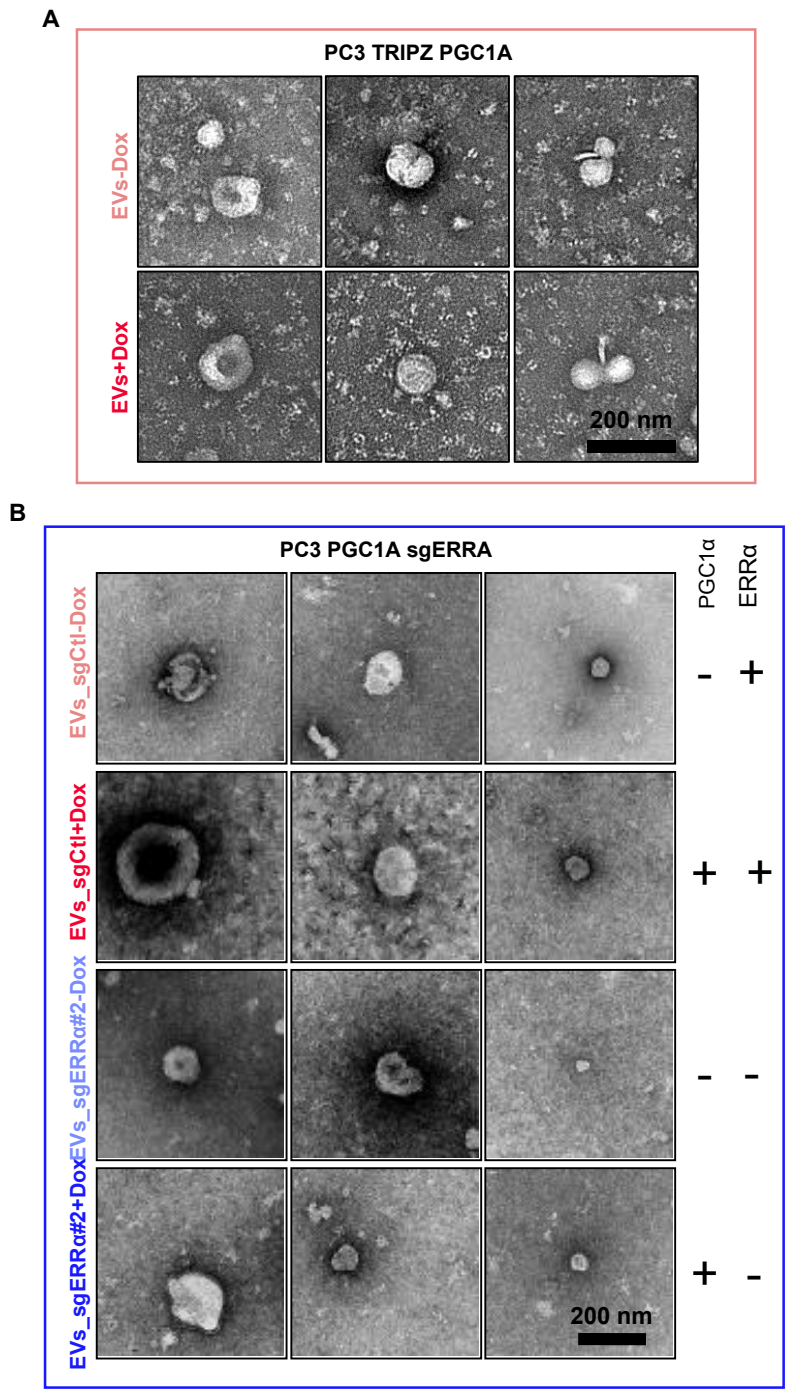


Figure R 10. Electron microscopy characterization of EVs from PCa cells. Individual images of EVs isolated from PC3 TRIPZ PGC1A (A) and PC3 PGC1A sgERRA (B) cell lines. In B, right table indicates PGC1α and ERRα status on producer cells for each EV condition. A and B, n=1. Bar, 200 nm. Dox: doxycycline.

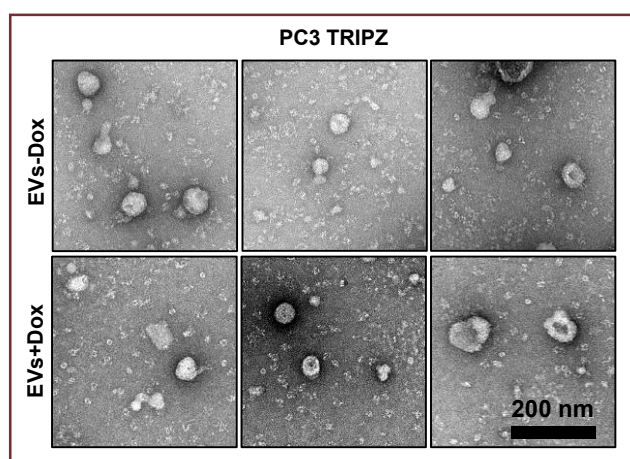


Figure R 11. Electron microscopy characterization of EVs produced by doxycycline-induced and non-induced PC3 TRIPZ cells. (n=1). Bar, 200 nm. Dox: doxycycline. EVs derived from cells untreated with doxycycline. EVs+Dox: EVs derived from cells treated with doxycycline.

Next, using NTA device, we characterized the number and mean size of the vesicles produced by PC3 cells with PGC1 α differential expression, revealing non-significant differences in the number of EVs produced by PGC1 α -expressing cells when compared with -Dox control (**FigR 12A**). In terms of dimension, EVs isolated from both, PGC1 α -expressing (EVs+Dox) and non-PGC1 α expressing (EVs-Dox) cells, displayed similar sizes (**FigR 12B**), with highest abundance of particles ranging large-very large sizes (150-250 nm) (**FigR 12B-C**). These size distributions were in line with previous data published in a study involving BPH and PCa-derived EVs isolated by serial ultracentrifugation steps (Royo et al. 2016).

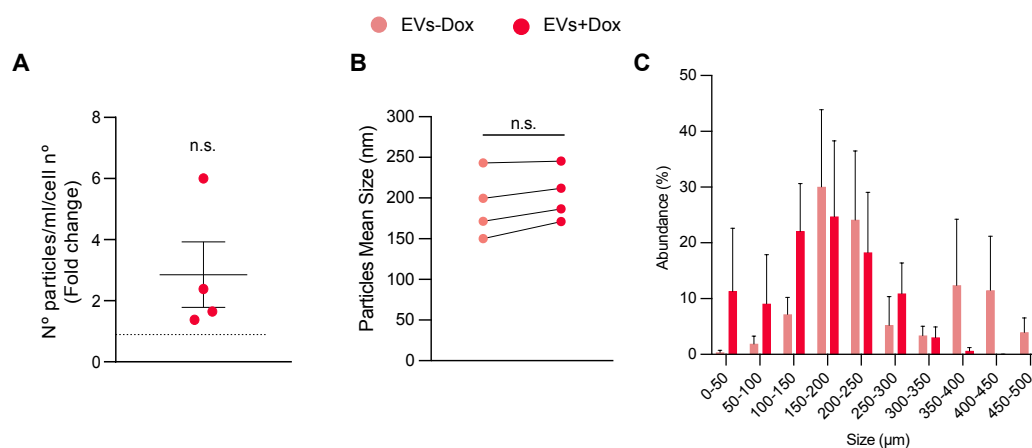


Figure R 12. Physical characterization by NTA of EVs produced by PC3 PGC1 α -expressing and non-expressing cells **A.** Quantification of the number of particles per milliliter normalized to the number of producer cells (n=4). **B.** Particles mean size measured by NTA (n=4). **C.** Size distribution of particles determined by NTA (n=3). In A data is normalized to the EVs–Dox condition, depicted as a black dotted line. Statistical analysis: In A, one sample t-test establishing 1 as hypothetical value is applied. In B and C, an unpaired parametric two tailed t-test is applied. In C, statistic test is applied in each range of size. p, p-value, n.s.=not significant. Error bars indicate s.e.m.

We next wondered whether EVs production rate and size could be under the influence of the PGC1 α -ERR α transcriptional axis, and we therefore analyzed by NTA the EVs produced by PC3 cells with combined expression of PGC1 α and deletion of ERR α . Yet, although no remarkable changes were observed in the number of particles produced among the different groups, expression of PGC1 α in combination with ERR α deletion slightly blunted EVs production number (**FigR 13A**). Following the same trend, the EVs mean size was similar between all groups, although a small increase in the size of EVs produced by cells with ERR α deletion was noticed (**FigR 13B**). Regarding size distribution, as noted in EVs isolated from PC3 TRIPZ PGC1A cells, the highest abundance of EVs produced by PC3 PGC1A sgERRA cells happened to be within the large-very large population (150-250 nm) (**FigR 13C**). In addition, we observed statistically significant differences on the size of EVs ranging 250-300 nm. EVs produced by PGC1 α -ERR α expressing cells had smaller sizes than other experimental groups. In addition, EVs produced by cells expressing PGC1 α but in the absence of ERR α , reached larger sizes than any other of the groups. These results suggest an ERR α dependent and independent mechanisms governing the production of large vesicles.

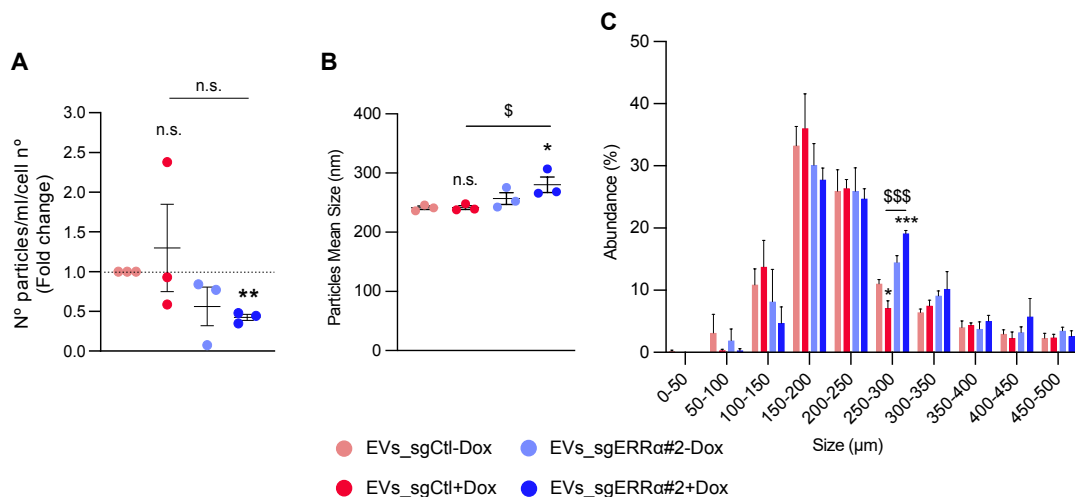


Figure R 13. NTA characterization of EVs isolated from PC3 PGC1 α -expressing and non-expressing cell lines in combination with ERR α deletion. A. Quantification of the number of particles per milliliter normalized to the number of producer cells ($n=3$). **B.** Particles mean size measured by NTA ($n=3$). **C.** Size distribution of particles determined by NTA ($n=3$). In A data is normalized to the EVs_sgCtl-Dox condition, depicted by a black dotted line. Statistical analysis: In A, a one sample t -test establishing 1 as hypothetical value and an unpaired parametric two-tailed t -test are applied. In B and C, an unpaired two tailed t -test is applied. Asterisks indicate statistical differences between EVs_sgCtl-Dox and the rest of the conditions and the dollar symbol indicates the statistical differences between EVs_sgCtl+Dox and EVs_sgERR α #2+Dox. p , p -value. */ $p < 0.05$, ** $p < 0.01$, **** $p < 0.0001$, n.s.=not significant. Error bars indicate s.e.m.

Finally, EVs protein content was measured by BCA assay and then was normalized to the producer-cell number. This assay revealed an increase of EVs protein content upon expression of PGC1 α in the producer cells (**FigR 14A**). Protein content of EVs happened to be ablated upon deletion of ERR α , thus suggesting an ERR α -mediated EVs protein content regulation (**FigR 14B**).

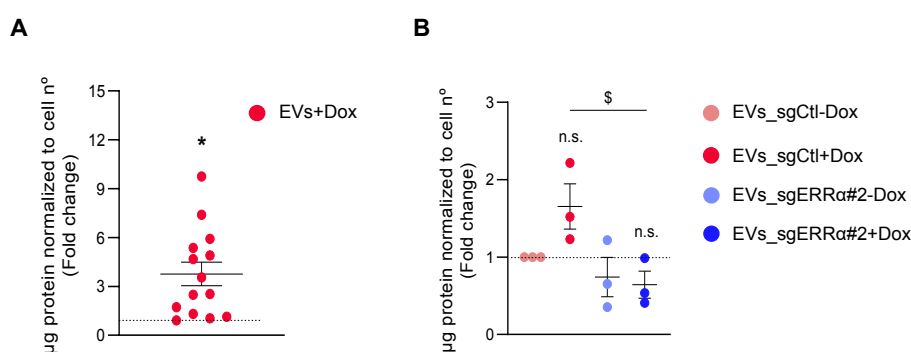


Figure R 14. EVs protein content measured by BCA. **A.** Micrograms of protein contained in EVs and normalized to the cell number of PGC1 α -expressing and non-expressing PC3 cells ($n=14$). **B.** EVs protein content normalized to cell number of PC3 producer cells with PGC1 α expression in combination of ERRA deletion ($n=3$). In A, data is normalized to the EVs-Dox condition, represented as a black dotted line. In B data is normalized to EVs_sgCtl-Dox condition, depicted as a black dotted line. Statistical analysis: One sample *t*-test establishing 1 as hypothetical value (A). Unpaired parametric two-tail *t*-test (B). Asterisk indicates statistical differences between EVs-Dox and EVs+Dox (A). The dollar symbol indicates the statistical differences between EVs_sgCtl+Dox and EVs_sgERR α #2+Dox. *p*, *p*-value. */\$ $p<0.05$, n.s.=not significant. Error bars indicate s.e.m.

Importantly, we wanted to corroborate whether we could use total protein content as a parameter for administering equal EVs in our *in vitro* and *in vivo* experiments. Therefore, we performed a correlation analysis between EVs protein content and EVs number, which, revealed a clear link between the two variables examined (**FigR15**). This analysis made us conclude that the use of protein content is an accurate quantitative methodology for performing treatments using equal amounts of EVs produced by PGC1 α -expressing and non-expressing cells.

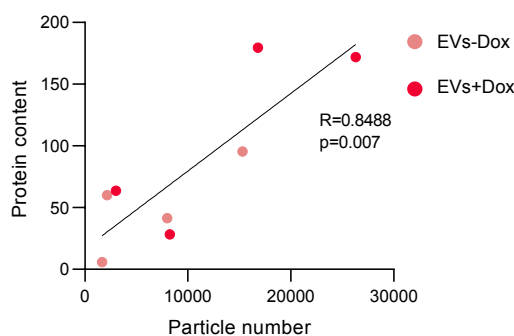


Figure R 15. Correlation analysis between number of EVs and EVs protein content. ($n=4$). Statistical analysis: Pearson's coefficient (*R*). $R>0$: direct correlation, $R<0$: inverse correlation.

Overall, the EVs physical and molecular characterization we performed evidenced the harvest of pure and entire EVs from PC3 PCa cell lines, and with highest density of vesicles ranging 150-250 nm size.

II.1.2 EVs proteomics analysis

EVs are small extracellular vesicles formed by a lipid bilayer. Importantly, EVs carry nucleic acids, lipids, glycans, metabolites and proteins that can be within the luminal side or associated to the vesicles, in a way that they are moved from the producer cells to the recipient cells, where they can modulate cell intrinsic responses (Antonyak et al. 2011; Mittelbrunn et al. 2011; Cossetti et al. 2015; Camacho, Guerrero, and Marchetti 2013). As previously described, a predominant characteristic observed in EVs produced by PGC1 α -expressing and non-expressing cells was the differences in their protein content. Therefore, we next performed a label-free LC-MS proteomics analysis of the EVs isolated from doxycycline-induced and non-induced PC3 producer cells. Forty differentially expressed proteins were identified, from which, 28 were decreased and 12 were increased in the EVs upon expression of PGC1 α in the producer PC3 TRIPZ PGC1A cell line (**Table R1**). As a cut-off, only proteins quantified with at least two peptides at false discovery rate (FDR) < 1%, as well as a p-value < 0.05 were considered.

We found that several of the downregulated proteins (ITA2, CLD3, JAM1, CD44 and EDIL3) were linked to cell adhesion and motility functions as well as anchorage independent growth, key features along the process of metastasis (Ziaee and Chung 2014; Agarwal, D'Souza, and Morin 2005; Elaine A McSherry 2011; Hiraga, Ito, and Nakamura 2013; Jiang et al. 2015). (Stipp, Kolesnikova, and Hemler 2001) (Levina et al. 2015; Zhang et al. 2003). Proteins involved in intracellular membrane trafficking STXB2 and RAB13 were also found to be downregulated in EVs upon expression of PGC1 α in the producer cells. RAB13 was described to be involved in the regulation of cell migration, invasion, and proliferation (Ioannou et al. 2015). On the other hand, no studies have focused on the role of STXBP2 in cancer, although its mutation has been shown to occur in the context of familial hemophagocytic lymphohistocytosis type 5 (Pagel et al. 2012). It is also worth mentioning that although not included as a final differentially expressed protein as this observation was made in four out of seven of the proteomics experiments we performed, CD9 levels in EVs isolated from PGC1 α -expressing cells happened to be decreased. This is in line with the data we previously observed by western blot analysis (**FigR 9**).

Three proteins involved in vesicle trafficking functions (TMED2, LMAN2, PKHB2) were found upregulated in EVs derived from PGC1 α -expressing cells. Protein LG3BP (also termed 90K) happened to be increased in EVs produced by PGC1 α -expressing cells. This protein, which, was initially identified as a tumor secreted antigen (Ullrich et al. 1994) was shown to induce angiogenesis in BCa and was associated to therapy resistance in patients with lymphoma (Fornarini et al. 2000; Piccolo et al. 2013).

Table R 1. List of proteins differentially present in EVs produced by PGC1 α -expressing and non-expressing PC3 cells. Label-free LC-MS proteomics analysis (n=7). Uncolored rows indicate proteins found decreased. Light blue rows include increased proteins. Dox: doxycycline.

Name	p value	+Dox/-Dox	Description
MARCS	0,0194	0,1704	Myristoylated alanine-rich C-kinase substrate
IGSF8	0,0006	0,1711	Immunoglobulin superfamily member 8
MUC5B	0,0022	0,1777	Mucin-5B
KIF23	0,0281	0,2210	Kinesin-like protein KIF23
STXBP2	0,0491	0,2965	Syntaxin-binding protein 2
IMA1	0,0125	0,2997	Importin subunit alpha-1
RGAP1	0,0236	0,3422	Rac GTPase-activating protein 1
NRP1	0,0028	0,3709	Neuropilin-1
CD81	0,0000	0,3830	CD81 antigen
VIME	0,0115	0,3982	Vimentin
ITA2	0,0250	0,4084	Integrin alpha-2
AAAT	0,0001	0,4251	Neutral amino acid transporter B(0)
AMPN	0,0007	0,4327	Aminopeptidase N
CLD3	0,0026	0,4349	Claudin-3
RAC1	0,0017	0,4467	Ras-related C3 botulinum toxin substrate 1
JAM1	0,0008	0,4818	Junctional adhesion molecule A
ITB1	0,0027	0,5126	Integrin beta-1
ADAM10	0,0086	0,5308	Disintegrin and metalloproteinase domain-containing protein 10
CD70	0,0399	0,5336	CD70 antigen
MFGM	0,0063	0,5514	Lactadherin
CD44	0,0354	0,5549	CD44 antigen
SC5A3	0,0373	0,5586	Sodium/myo-inositol cotransporter
FA49B	0,0461	0,5713	Protein FAM49B
EDIL3	0,0148	0,5741	EGF-like repeat and discoidin I-like domain-containing protein 3
RAB13	0,0054	0,5800	Ras-related protein Rab-13
EHD4	0,0004	0,5808	EH domain-containing protein 4
GNAI2	0,0292	0,6381	Guanine nucleotide-binding protein G(i) subunit alpha-2
TMED2	0,0001	1,7160	Transmembrane emp24 domain-containing protein 2
MVP	0,0029	1,7723	Major vault protein
TR10B	0,0195	2,1890	Tumor necrosis factor receptor superfamily member 10B
ADT2	0,0231	2,5084	ADP/ATP translocase 2
CATD	0,0011	2,5843	Cathepsin D
LMAN2	0,0019	2,7663	Vesicular integral-membrane protein VIP36
AATM	0,0423	2,7878	Aspartate aminotransferase, mitochondrial
RAI3	0,0383	2,9948	Retinoic acid-induced protein 3
ANX11	0,0011	3,1125	Annexin A11
LG3BP	0,0092	3,6435	Galectin-3-binding protein
PKHB2	0,0012	3,9288	Pleckstrin homology domain-containing family B member 2
ATP1B1	0,0007	6,9987	Sodium/potassium-transporting ATPase subunit beta-1
AATC	0,000003	7,1029	Aspartate aminotransferase, cytoplasmic

Trying to get a broader view and biological meaning to the candidates found differentially present in EVs derived from PGC1 α -expressing and non-expressing cells we sought at conducting an enrichment analysis. For that, we first converted the protein name of our list of candidates to their corresponding gene name and performed a gene enrichment analysis using Cancertool interface (Cortazar et al. 2018). The reason for conducting the analysis using genes instead of protein names resides in the fact that up to date, more functional annotations for genes than for proteins exist, thus allowing a more extensive analysis of the data (D. W. Huang,

Sherman, and Lempicki 2009). Gene ontology (GO) cellular component analysis revealed that most of the differentially expressed proteins (77.5%) had functionalities associated to “extracellular vesicular EVs”, which, was in line with what expected for a proteomics analysis of secreted vesicles. This category was followed by “plasma membrane” and ‘cell adhesion” processes that represented a 52.5% and 22.5% of the differentially expressed proteins, respectively (**FigR16A**). GO molecular function analysis revealed a high number of molecular events related to adhesion processes, such as “integrin binding”, “MHC class II protein binding” or “adhesion to the ECM”. Functions linked to metabolism were also enriched (**FigR 16B**).

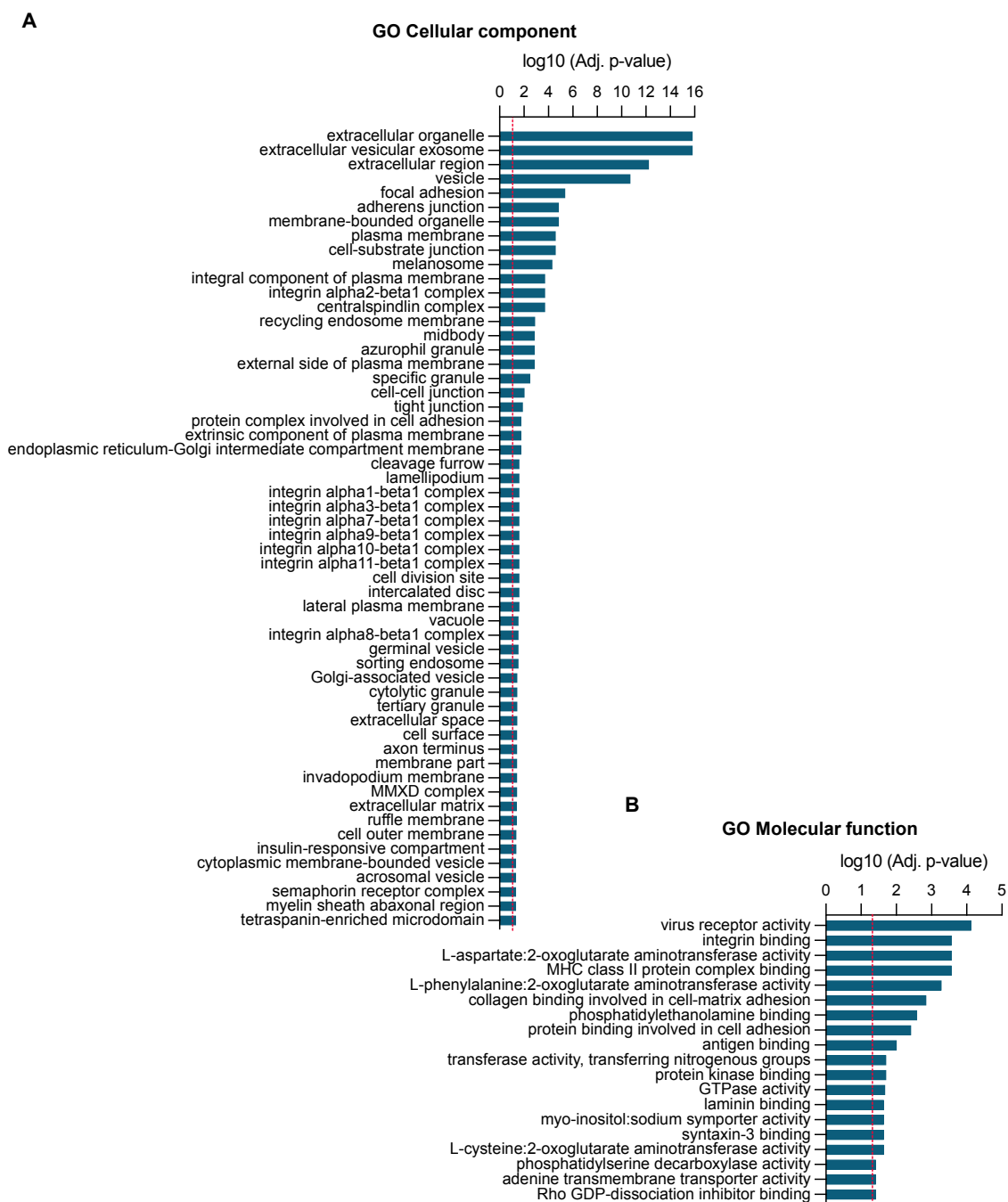


Figure R 16. Gene Ontology analysis of the genes encoding for the proteins found altered in EVs upon expression of PGC1α in the producer cell lines. A. GO Cellular component analysis. B. GO Biological processes analysis. The red dotted lines indicate $p=0.05$. p , p-value.

In line with the cellular component and molecular function analyses, information obtained from the GO biological processes analysis again displayed an enhancement of functions linked to cell metabolism, cell migration, adhesion and extracellular matrix degradation (**FigR 17A**). Finally, being PGC1 α a transcriptional co-factor, we wondered which would be the putative transcription factor that cooperates with PGC1 α on the regulation of the genes coding for the differentially present proteins identified in EVs. Hence, taking again advantage of Cancertool, we performed a promoter enrichment analysis that revealed the presence of genes presumably regulated by different transcription factors (TFs), among which, ERR α was included (**FigR 17B**).

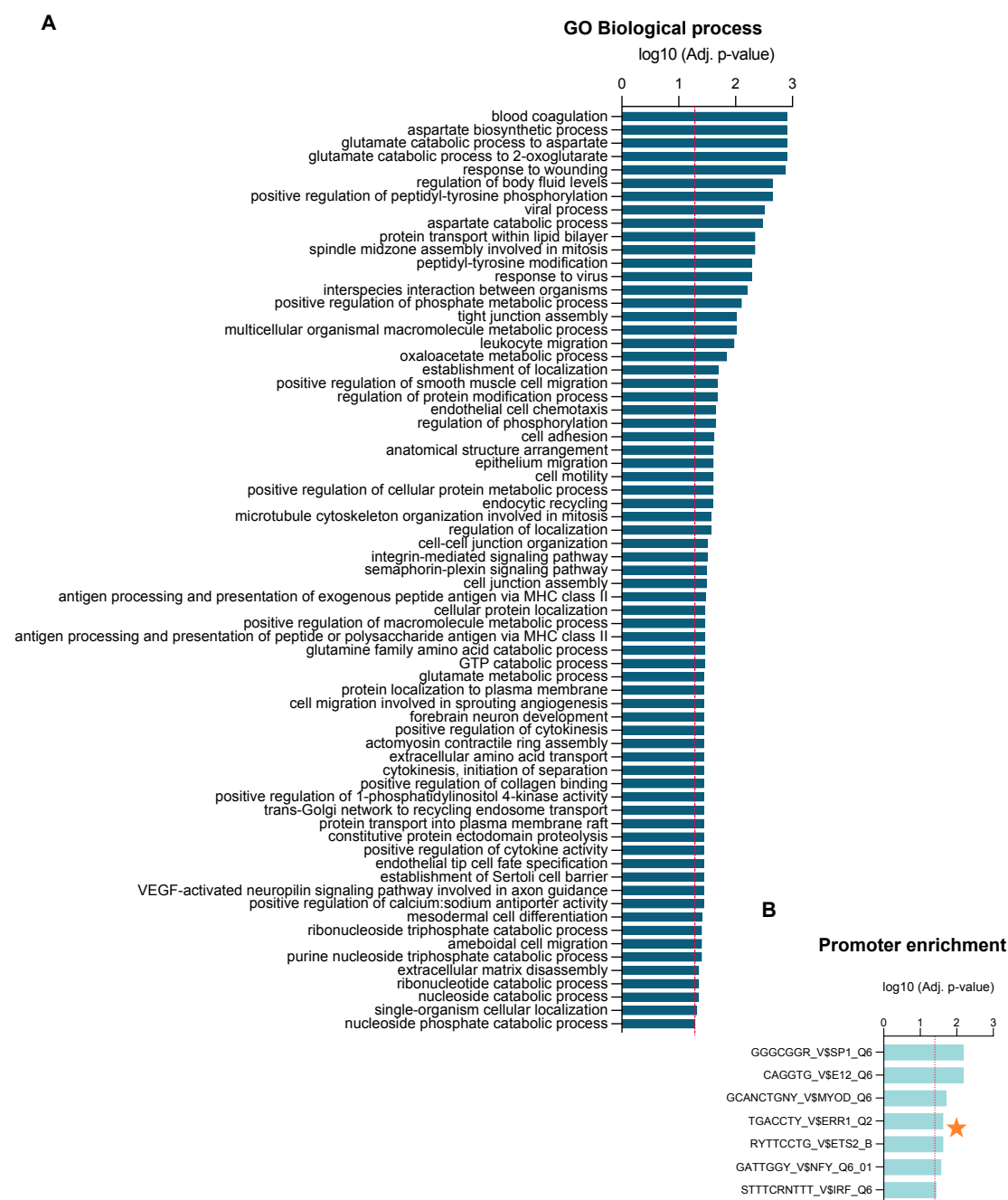


Figure R 17. Gene set enrichment analysis of the genes encoding for the significantly altered proteins associated to EVs. A. GO biological processes analysis. B. Promoter enrichment analysis. The red dotted lines indicate $p=0.05$. p , p -value

II.2 Biological impact of the EVs: *in vitro* and *in vivo* assays

II.2.1 *In vitro* EVs uptake

It has been previously described how the presence of certain proteins in both EVs and target cells is a constraining factor for the vesicle's uptake (Escrevente et al. 2011; Horibe et al. 2018; Franzen et al. 2014). Thus, our first approach was to evaluate if EVs derived from PGC1 α -expressing and non-expressing cells were both and equally internalized by recipient cells. To do so, using DiIC₁₈ (3) lipophilic dye, we fluorescently labelled EVs from PGC1 α -expressing (EVs+Dox) and non-expressing (EVs-Dox) PC3 cells, and further used them to treat PC3 recipient cells. In order to have a wider perspective, we first assessed EVs uptake by PC3 cells at three different time-points and using 2 μ g of labelled EVs. Uptake was analyzed by flow cytometry, and we observed that both, EVs-Dox (median fluorescence values: 6 h: 543, 3 h: 133 and 1 h: 32,16) and EVs+Dox (median fluorescence values: 6 h: 738, 3 h: 196 and 1 h: 43,6) were internalized by recipient cells in a time-dependent manner (**FigR 18A**). As expected, median fluorescence value of the control remained lower than any other condition (with a median fluorescence value of 16,7). Once uptake of both types of EVs was confirmed, we performed a series of independent experiments using again 2 μ g of labelled EVs and 3 hours incubation-time. Data was variable, and no significant differences in uptake between EVs-Dox and EVs+Dox by PC3 recipient cells were observed (**FigR 18B**).

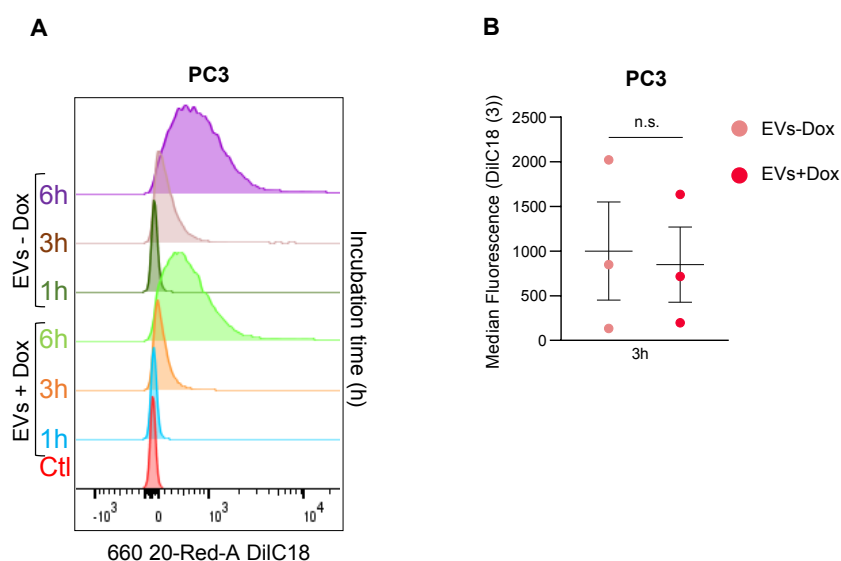


Figure R 18. EVs uptake by PC3 recipient cells. **A.** PC3 recipient cells uptake capacity of 2 μ g of labelled EVs analyzed at three incubation time-points (1 h, 3 h and 6 h). As a negative control, PBS with DiIC18 (3) is included. Data is represented as the median of fluorescence. **B.** Analysis of EVs uptake by PC3 cells after 3 hours of incubation with EVs (n=3). EVs-Dox: EVs produced by non-PGC1 α expressing cells. EVs+Dox: EVs produced by PGC1 α -expressing cells. Statistical analysis: Unpaired parametric two-tail t-test. n.s.=not significant. Error bars indicate s.e.m.

II.2.2 Role of EVs in 2D cell growth and migration

Once EVs uptake by PC3 recipient cells was confirmed, we next wondered if, due to their differential protein cargo, EVs would exert distinct biological outcomes on the recipient cells. Based on our previous data, demonstrating the anti-proliferative features of the whole cell secretome produced by PGC1 α -expressing cells, we first evaluated proliferation of PC3 cells that had been previously educated for five and seven days with the differential EVs (**FigR 19A**). No changes in cell growth were observed, neither at day 5, nor at day 7 of treatment (**FigR 19B**). Moreover, no apparent differences in morphology or growth pattern were noticed in the PC3 cells treated with any of the two types of EVs (**FigR 19C**).

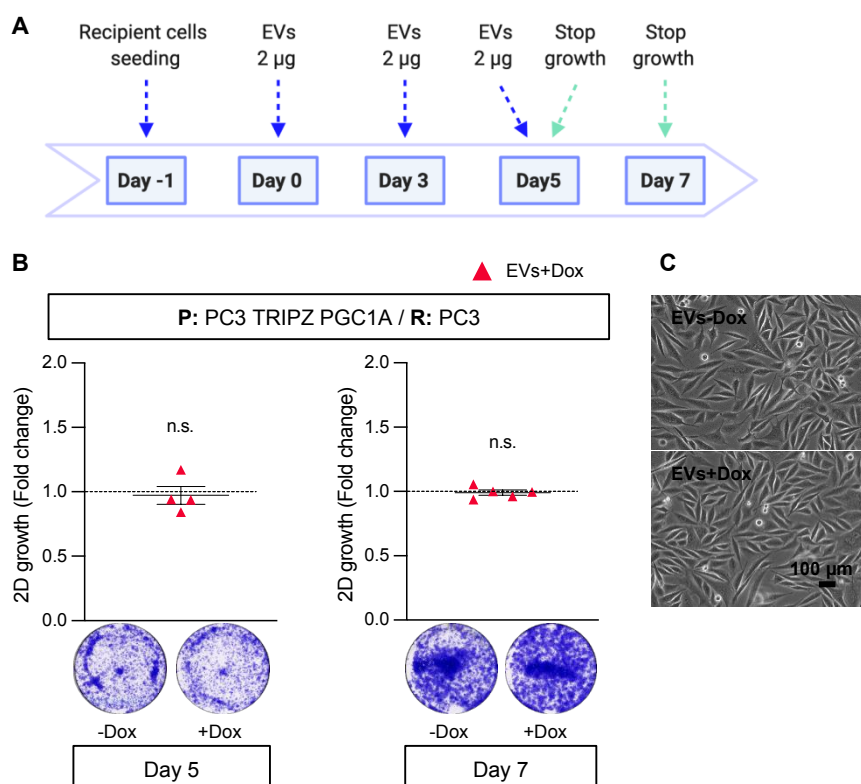


Figure R 19. Impact of EVs in 2D proliferation. **A.** Schematic view of the steps followed for treating PC3 recipient cells with EVs and assess their proliferation capacity. **B.** Cell proliferation measured by crystal violet staining of PC3 cells treated throughout five ($n=4$) and seven days ($n=5$) with the differential EVs. **C.** Representative images of PC3 cells treated with EVs obtained from PGC1 α -expressing and non-expressing cells for seven days. Bar, 100 μ m. EVs+Dox: EVs produced by PGC1 α -expressing cells. In **B**, data is normalized to the EVs-Dox condition depicted by a black dotted line. P: EVs-producer cells, R: recipient cells. Statistical analysis: One sample *t*-test establishing 1 as hypothetical value. n.s.=not significant. Error bars indicate s.e.m.

Next and in line with the proteomics data indicating a possible role of EVs on mediating processes related to cell motility, we treated throughout six days PC3 recipient cells with EVs isolated from PGC1 α -expressing and non-expressing PC3 cells. After this time, we performed a Boyden chamber migration assay with the pre-conditioned PC3 recipient cells (**FigR 20A**), finding

no changes in the migration ability of the cells that had been treated with the distinct EVs (**FigR 20B**).

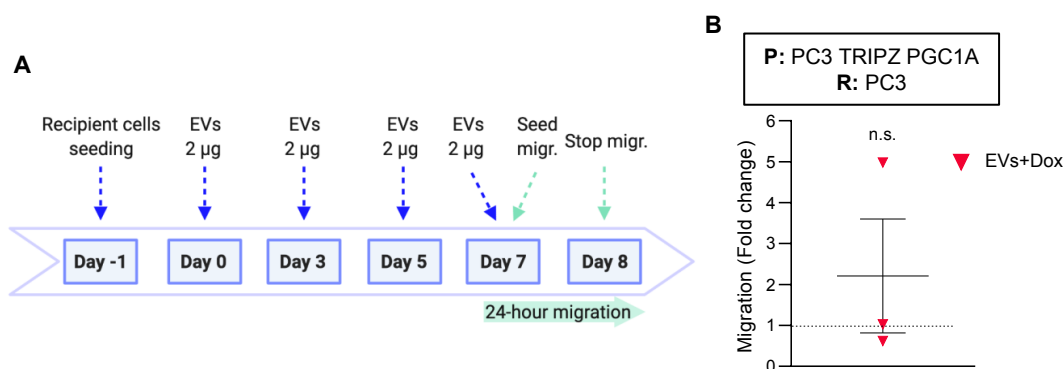


Figure R 20. Impact of EVs in the migration capacity of recipient cells. **A.** Overview of the protocol followed for the education and migration assay of EVs-educated PC3 cells. **B.** PC3 transwell migration capacity upon treatment with EVs derived from PGC1 α -expressing and non-expressing PC3 cell lines ($n=3$). P: EVs-producer cells, R: recipient cells. EVs+Dox: EVs produced by PGC1 α -expressing cells. Data is normalized to the EVs-Dox condition, represented as a black dotted line. Statistical analysis: One sample t-test establishing 1 as hypothetical value. n.s.=not significant. Error bars indicate s.e.m.

II.2.3 Role of EVs in an *in vivo* metastasis assay

EVs are known to be active mediators of cancer progression (Peinado, Alečković, et al. 2012; J. Liu et al. 2020; Gyukity-Sebestyén et al. 2019; Hoshino et al. 2015; Zhao et al. 2016; Albino et al. 2021; DeRita et al. 2019; Hashimoto et al. 2018). Proteomics analysis performed on EVs-Dox and EVs+Dox pointed towards vesicles playing a distinct role in the process of metastasis. This hypothesis was based on the fact that several of the downregulated proteins identified in EVs produced by PGC1 α -expressing cells have been previously linked to metastasis in different cancer types, thus suggesting that their higher presence in EVs derived from non-PGC1 α expressing cells would be linked to a more aggressive disease. Among these proteins, mentioned above, adhesion molecules ITA2, CLDN3, JAM1, CD44 and EDIL3 were included (Ziaee and Chung 2014; Agarwal, D'Souza, and Morin 2005; Elaine A McSherry 2011; Hiraga, Ito, and Nakamura 2013; S.-H. Jiang et al. 2015; Stipp, Kolesnikova, and Hemler 2001; Levina et al. 2015; X. A. Zhang et al. 2003; J. E. Lee et al. 2016a; Ioannou et al. 2015; Tse et al. 2017a). Although *in vitro* experiments showed no differential effects of the EVs neither in proliferation nor in migration, given the constraints that these assays present due to the limited 2D interactions between tumor cells as well as the lack of interactions with their extracellular milieu (blood flow, ECM, nutrient and oxygen availability as well as other cell populations), we decided to further explore EVs role in an *in vivo* context. With this aim, we educated nude mice through a period of two weeks by means of injecting twice a week either EVs-Dox, EVs+Dox or PBS (this last one for the control group) (**FigR 21A**). This pre-conditioning was performed by intra-venous retro-orbital injections which, aimed at preparing the sites of metastasis before performing an intra-cardiac

injection of highly aggressive PCa cells. Metastasis formation in the mice was monitored with IVIS device throughout five weeks and after this time, data was further corroborated *ex vivo*.

Overall, *in vivo* whole-body quantification of the metastases established in mice educated with EVs-Dox or EVs+Dox, showed no significant differences between both experimental groups (FigR 21B-C).

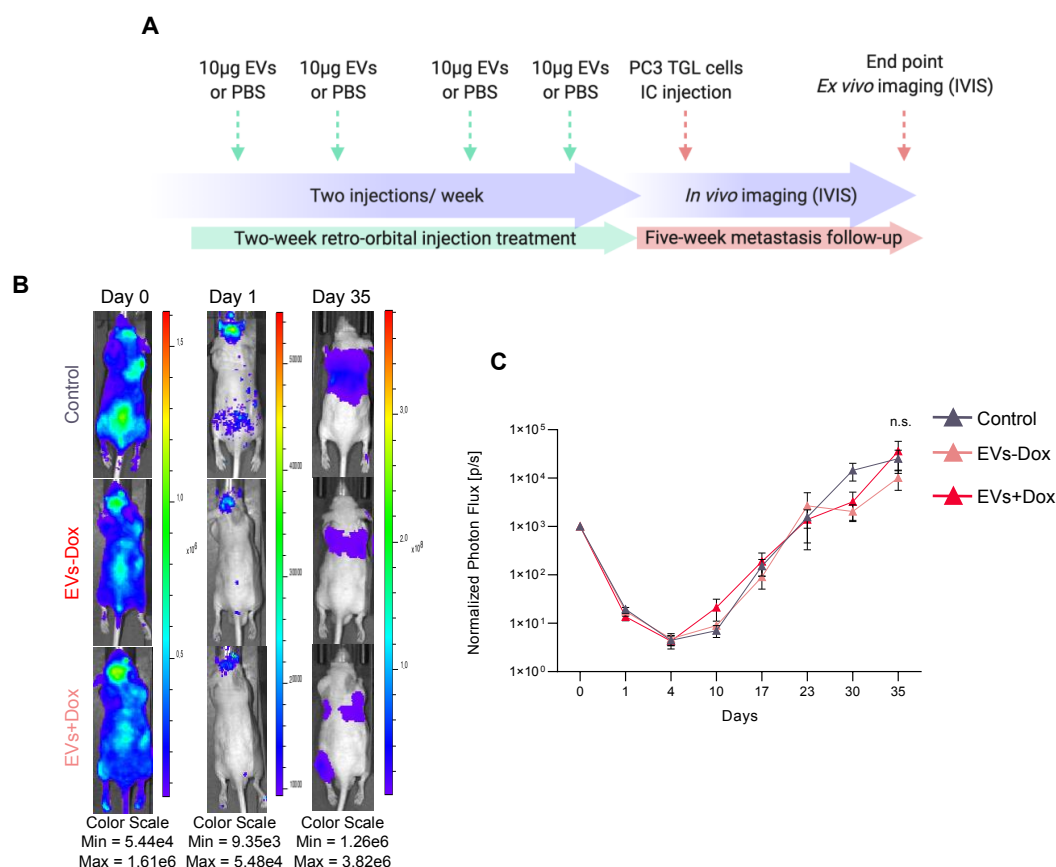


Figure R 21. In vivo study of the impact of EVs on the preparation of the pre-metastatic niche. A. Schematic view of the protocol followed for the *in vivo* metastasis assay using PCa-derived EVs. **B.** Representative images at the day of the PC3 TGL IC-injection (day 0), day 1 post-injection and day 35 after cells injection and formation of metastases. **C.** *In vivo* mice dorsal quantification of the luciferase signal intensity derived from the PC3 TGL cells injected into mice of the 3 different experimental groups. Signal intensity is normalized to the day 0. ($n=4$ / condition). Three conditions of metastatic tumor-bearing mice are included in the experiment: mice treated with PBS (Control), mice treated with EVs derived from PGC1 α -expressing cells (EVs+Dox) and mice educated with EVs isolated from non-PGC1 α expressing PC3 cell lines (EVs-Dox), ($n=10$ mice/ experimental group). Statistical analysis: In C, a two tailed Mann-Whitney U test is applied. n.s.=not significant. Error bars indicate s.e.m.

In line with this, *ex vivo* data displayed no differences in tumor formation among the three groups, neither in legs, lungs, ribs and spinal column (FigR 22A-D). Overall, the three groups of mice presented formation of tumors at similar timings, with the same organ-tropism and reached comparable sizes.

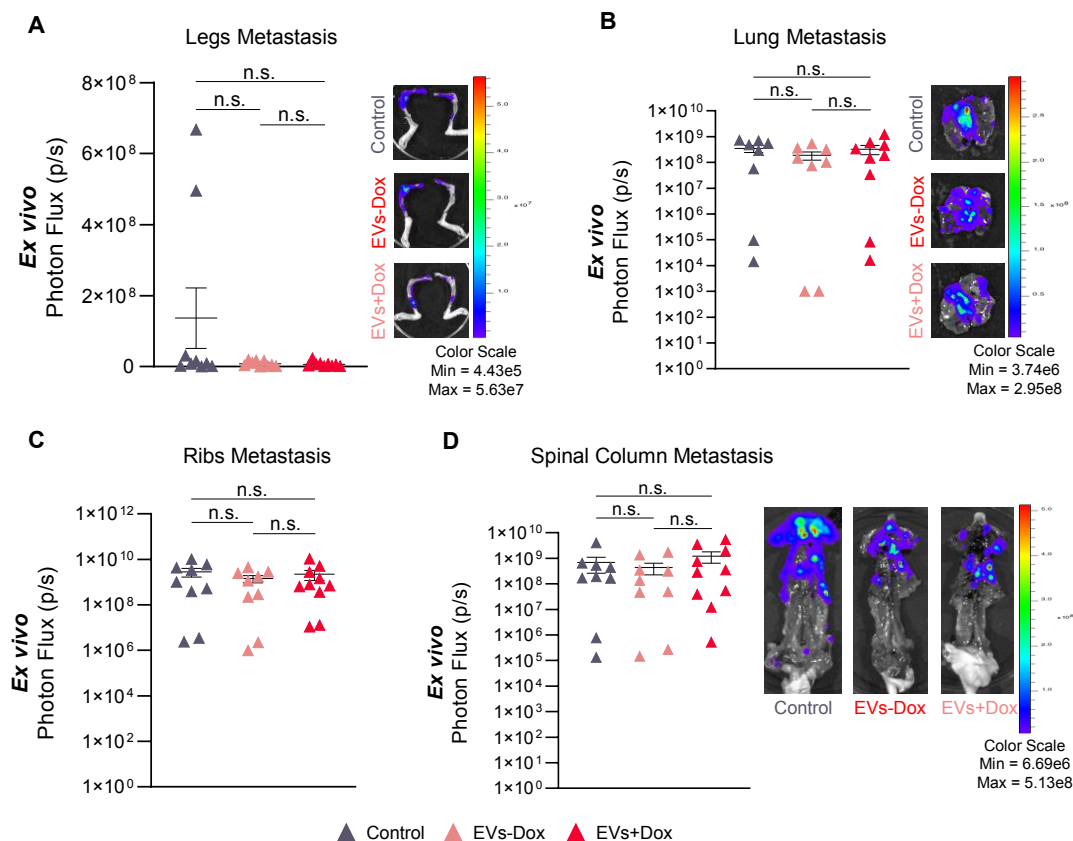


Figure R 22. *Ex vivo* luciferase signal intensity of PCa cells measured in legs (A), lungs (B), ribs (C) and spinal cord (D) after mice sacrifice, at day 35. For each organ (asides for ribs), a representative image of specimens that are close to the median signal is shown ($n=4$ / condition). Three conditions of metastatic tumor-bearing mice are included in the experiment: mice treated with PBS (Control), mice treated with EVs derived from PGC1 α -expressing cells (EVs+Dox) and mice educated with EVs isolated from non-PGC1 α expressing PC3 cell lines (EVs-Dox), ($n=10$ mice/ experimental group). Statistical analysis: two tailed Mann-Whitney U test (A, B, C and D). n.s.=not significant. Error bars indicate s.e.m.

In conclusion, *in vivo* data demonstrates that EVs produced by PC3 cells with differential expression of the metabolic co-regulator PGC1 α play no distinct role on the preparation of the pre-metastatic niches and the subsequent establishment of metastases in our PCa model. Though, it would be interesting to further study plausible molecular events driven in the stromal compartment of the EVs-treated mice to deeper comprehend EVs functions in the context of PCa.

II.3 EVs as bystanders of prostate cancer aggressiveness

EVs are released by almost any type of cell, including cancer cells (György et al. 2011). This aspect grants them the potential of being non-invasive biomarkers that may inform on the status of a tumor. In fact, some studies have proven this concept of ‘‘EVs as surrogate markers’’ by isolating vesicles from patients’ biological fluids (such as lymphatic drainage, urine or plasma)

and using their nucleic acids or protein content to monitor disease progression, malignancy and risk of recurrence (Torrano, Royo, et al. 2016).

Nowadays, PCa screening is done by measuring prostate-specific antigen (PSA) levels in the blood, which has proved to be key for reducing patient's mortality due to early disease detection (Catalona 2018). However, this marker has limitations, as high PSA levels can be caused by different factors such as BPH conditions, inflammation or infections. In addition, PSA cannot distinguish between aggressive and non-aggressive PCa. Hence, a high number of biopsies need to be conducted in order to confirm the presence or absence of cancerous lesions on individuals with medium-high PSA levels (Catalona 2018; Pienta 2009). Therefore, there is a need of identifying novel and non-invasive biomarkers for PCa diagnosis, surveillance as well as for avoiding unnecessary biopsies.

The promoter enrichment analysis we performed on the genes encoding for the proteins found differentially present in EVs, pointed towards a PGC1 α transcriptional control mediated by ERR α . These data together with PGC1 α 's prognostic and stratification value in PCa (Torrano, Valcarcel-Jimenez, et al. 2016) suggest that cell intrinsic transcriptional events driven by PGC1 α -ERR α might be monitored through EVs, hence presenting them as non-invasive bystanders of PCa disease. In line with this idea, we wondered which would be the status in the producer cell lines of those genes encoding for the proteins differentially identified in the EVs. Therefore, we first performed RT-qPCR analyses in PC3 cell lines with differential expression of PGC1 α . Once we corroborated the induction of *PGC1A* upon doxycycline treatment (**FigR 23A**), gene expression levels of three decreased candidates identified in the proteomics analysis (*CD44*, *STXBP2* and *ADAM10*) were assessed and showed to be downregulated upon expression of PGC1 α (**FigR 23B**).

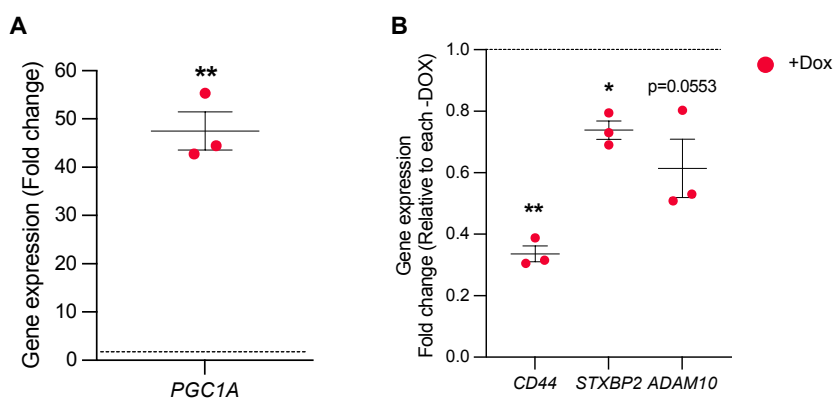


Figure R 23. Candidates identified by EVs proteomics analysis are transcriptionally regulated by PGC1 α in PCa producer cells. **A.** PGC1A expression measured by RT-qPCR in PC3 TRIPZ PGC1A producer cells treated with doxycycline (n=3). **B.** Analysis of gene expression by RT-qPCR of CD44, STXBP2 and ADAM10 genes (n=3). Data are normalized to the -Dox condition (non-PGC1 α expressing condition), depicted by a black dotted line. +Dox: PGC1 α -expressing condition. Statistical analysis: One sample t-test establishing 1 as hypothetical value. p, p-value. *p<0.05, **p<0.01. Error bars indicate s.e.m.

In line with this, EVs proteomics-identified candidate *GOT1* (termed AATC as protein name) was previously shown by the group to be cell-intrinsically upregulated in the producer cell

lines by PGC1 α (Torrano, Valcarcel-Jimenez, et al. 2016; Valcarcel-Jimenez et al. 2019). We then wondered if this transcriptional regulation of EVs proteomics candidates proven to be cell-intrinsically mediated by PGC1 α would be dependent on its transcriptional partner ERR α . We therefore took advantage of our PC3 producer cell lines with differential expression of PGC1 α in combination with ERR α deletion (**FigR 24A**) and tested by RT-qPCR gene expression levels of five downregulated candidates (*CD44*, *ADAM10*, *STXBP2*, *CLDN3*, *F11R* and *EDIL3*). (**FigR 24B**).

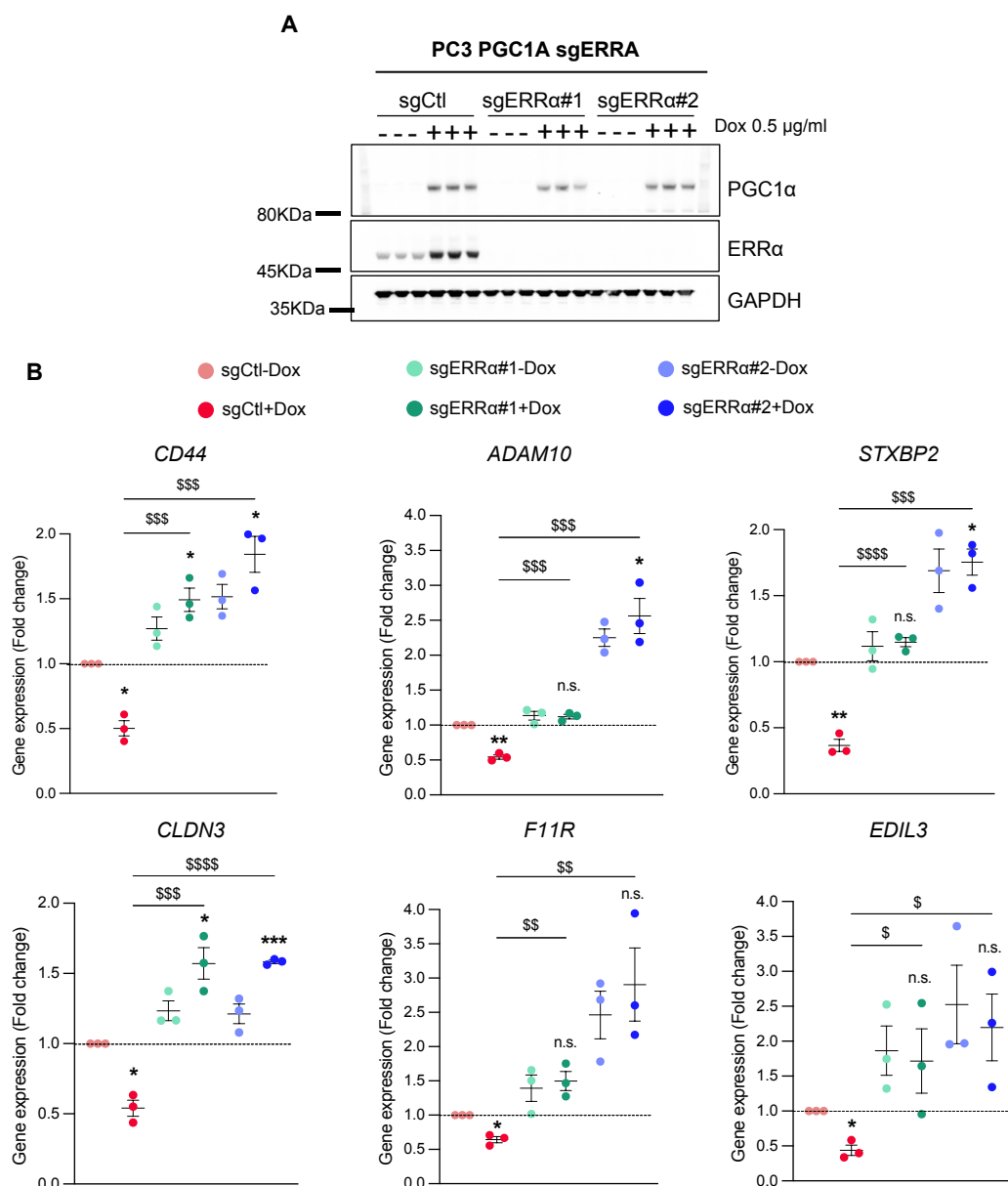


Figure R 24. The PGC1 α -ERR α transcriptional axis regulates the genes encoding for the proteins differentially present in PCa EVs. **A.** Western blot analysis verifying expression of PGC1 α upon doxycycline treatment and in combination with the CRISPR/Cas9-mediated deletion of ERR α . One representative experiment out of 3 is shown. **B.** Analysis by RT-qPCR of the gene expression levels of candidates (*CD44*, *ADAM10*, *STXBP2*, *CLDN3*, *F11R* and *EDIL3*) identified by EVs proteomics analysis ($n=3$). Data are normalized to the sgCtl–Dox condition, depicted by a black dotted line. +Dox: PGC1 α -expressing condition. Statistical analysis: One sample t-test establishing 1 as hypothetical value. Unpaired

parametric one-tail *t*-test. Asterisks indicate statistical differences between sgCtl-Dox and the rest of the conditions and the dollar symbol indicates the statistical differences between sgCtl+Dox and sgERR α 1/#2+Dox. *p*, *p*-value. * $p < 0.05$, ** $p < 0.01$, *** $p < 0.001$, **** $p < 0.001$. n.s.=not significant. Error bars indicate s.e.m.

Finally, we confirmed that the use of the tetracycline doxycycline for inducing the expression of PGC1 α did not affect the expression levels of the genes tested, thus corroborating the PGC1 α (and ERR α)-dependent transcriptional regulation of the genes encoding for the differentially present proteins in PCa-derived EVs (**FigR 25**).

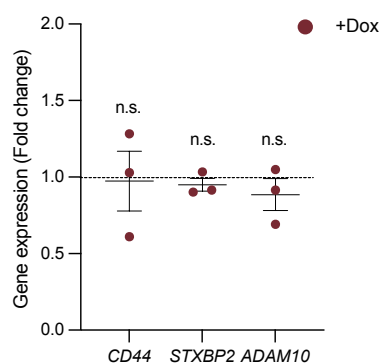


Figure R 25. Doxycycline treatment exerts no effect on expression levels of candidate genes. *CD44*, *STXP2* and *ADAM10* gene expression levels are analyzed by RT-qPCR in PC3 TRIPZ cells ($n=3$). Data is normalized to the $-Dox$ condition, represented with a black dotted line. +Dox: treatment with doxycycline. Statistical analysis: One sample *t*-test establishing 1 as hypothetical value. n.s.=not significant. Error bars indicate s.e.m.

Thus, our data confirmed the idea of EVs as bystanders of their cell of origin, reinforcing the concept of ‘‘EVs as non-invasive biomarkers’’. These facts made us wondered whether any of the candidates identified by proteomics analysis of EVs obtained from PCa cell lines would also be reflected in PCa patients. Therefore, taking advantage of publicly available PCa datasets (Kumar et al. 2011; Fraser et al. 2017; Glinsky et al. 2004; Grasso et al. 2012; Lapointe et al. 2004; Varambally et al. 2005; Tomlins et al. 2007; Taylor et al. 2010), we performed correlation analyses of *PGC1A* against all 40 genes encoding for the differentially present proteins found in EVs. Importantly, for these analyses, only candidates that showed a consistency of at least half of the datasets analyzed and an adjusted *p*-value < 0.05 were considered.

Among the genes analyzed in primary tumors, three genes, *CLDN3* (6 out of 9), *KPNA2* (5 out of 8) and *STXBP2* (4 out of 7) showed to be inversely correlated with *PGC1A* in most of the datasets interrogated. In addition, and although it appeared in only half of the datasets analyzed *ATP1B1* (4 out of 8) showed to be directly correlated with *PGC1A* (**FigR 26**). Hence, this data suggests the transcriptional regulation of EVs-identified proteomics candidates, shown to be mediated by the PGC1 α -ERR α axis *in vitro*, may also be extended to PCa patients.

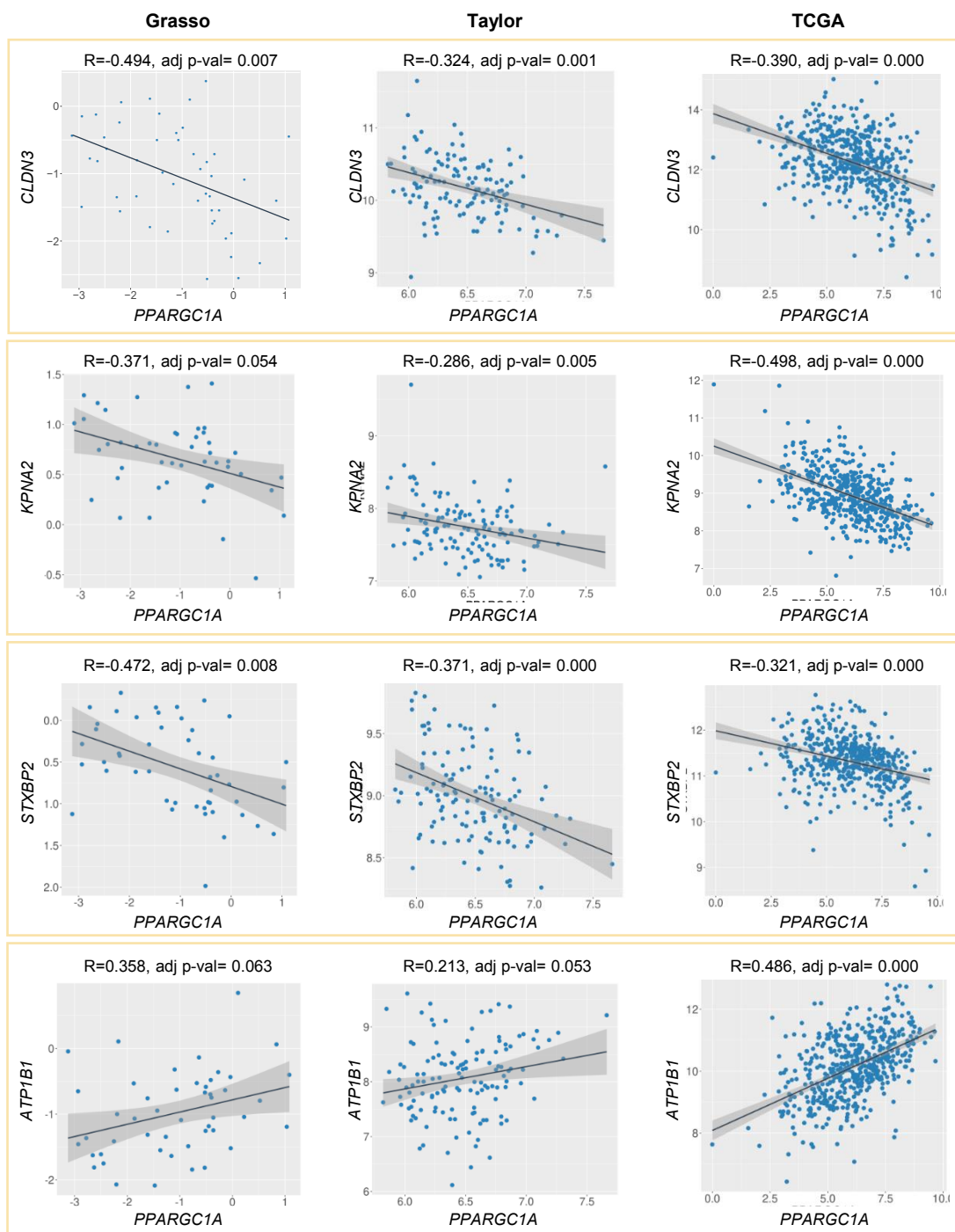


Figure R 26. Correlation analyses between CLDN3, KPNA2, STXBP2 and ATP1B1 against PGC1A mRNA expression in PCa patients. From the nine datasets analyzed, only Grasso, Taylor and TCGA correlations are shown. Each dot corresponds to a patient, and expression values correspond to log2 normalized mRNA levels of each gene in X and Y axis. Black line represents the linear regression, and the grey area limits the intervals of confidence. Statistic test: Spearman correlation coefficient (R). Adj. p-val= adjusted p-value.



Overview

- Levels of CD9 and CD63 are altered in EVs produced by PGC1 α -expressing cells compared to non-PGC1 α expressing produce cells.
- Expression of PGC1 α in PCa cells does not influence the number and size of EVs produced.
- Protein content is increased in EVs produced by cells with an activated PGC1 α -ERR α transcriptional axis.
- EVs protein content is correlated to the number of EVs.
- Recipient cells educated with EVs produced by PGC1 α -expressing or non-expressing cells, show no differences on their 2D proliferation and migration capabilities.
- *In vivo* metastasis assay demonstrates that EVs produced by PCa cells with differential expression of PGC1 α do not play distinct biological roles on preparing the sites of metastasis. Tumor formation rates and organ tropism were equal among the PBS-treated and the EVs-treated groups.
- Expression levels of the genes encoding for proteomics candidates analyzed by RT-qPCR in producer cell lines shows a PGC1 α -ERR α -dependent transcriptional regulation, thus confirming the concept of EVs as fingerprints of their cell of origin.
- Correlation analyses performed on PCa patient's data reveals that among the 40 candidates analyzed, *CLDN3*, *STXBP2* and *KPNA2* are inversely correlated and *ATP1B1* is directly correlated to *PGC1A* mRNA expression.
- EVs have the potential to be used as non-invasive biomarkers and help on the diagnosis and prognosis of PCa as surrogates of the status of PGC1 α in patients.

III Study and description of the soluble factors fraction of the cell secretome

As we previously showed, PGC1 α exerts a tumor suppressive activity in PCa by means of regulating cellular functions of intrinsic nature (Torrano, Valcarcel-Jimenez, et al. 2016; Valcarcel-Jimenez et al. 2019). Our data suggests that the anti-tumoral activity of the metabolic co-regulator could go beyond the regulation of cell-intrinsic events, and thus could be involved on the regulation and production of a tumor-suppressive secretome. As previously shown, the whole cell secretome associated to PGC1 α re-expression blunts cell proliferation whilst EV-fraction showed no clear anti-tumoral role in our PCa model when produced in a cellular context regulated by PGC1 α . Nevertheless, due to their protein cargo differences, EVs have potential as non-invasive biomarkers of PCa surveillance. Hence, once EVs role as non-cell autonomous proliferation, migration and metastasis suppressors was discarded, we hypothesized that the cell-extrinsic PGC1 α -driven anti-proliferative activity could be owing to the soluble factors (SFs) fraction of the cell secretome.

Besides EVs, the cell secretome includes a plethora of molecules such as proteins, amino acids, fatty acids, nucleotides and gases that mediate a wide number of biological functions, including cell signaling, inflammation or apoptosis. It is well known that tumor cells secrete in an autocrine and paracrine manner proteins (cytokines, growth factors, ECM proteins, proteases...) to the extracellular milieu in order to promote cell proliferation, self-sustenance, trigger matrix remodeling and to promote tumor invasion and metastasis among others (Abounader and Latorra 2005; Cox et al. 2016; Brady et al. 2016; Mendez et al. 2018). Given the fact that our previous data pointed towards the secretome fraction bigger than 10 KDa (which, due to size cutoff is enriched in proteins) as a non-cell autonomous mediator of cell proliferation braking, we targeted our work towards deeper studying the SFs fraction of the secretome, and more concretely proteins.

HYPOTHESIS

The soluble fraction of the cell secretome regulated by PGC1 α plays a non-cell autonomous anti-tumoral role in PCa

III.1 Biological impact of the soluble factors fraction of the secretome: *in vitro* and *in vivo* assays

III.1.1 *In vitro* study of the soluble factors effect in PCa cell proliferation

Taking advantage of the same experimental settings we established for whole secretome production and subsequent treatment of recipient cells, PGC1 α -expressing and non-expressing

PC3 producer cells were seeded to generate the soluble factors fraction (SFs) of the secretome. Briefly, this fraction was obtained by serial ultracentrifugation steps of the whole cell secretome, allowing the depletion of EVs and remaining only the SFs fraction of the cell secretome (see **Materials and Methods, section II.1.3**). Once obtained, SFs were used to treat PC3 recipient cells and assess their proliferation capacity, which is an early feature required by the cells to initiate tumor formation (**FigR 27A**). Results showed that PC3 recipient cells grown with the SFs secretome fraction produced by PGC1 α -expressing cells had lower proliferation capacity compared to those recipient cells treated with SFs produced by non-PGC1 α expressing cells (**FigR 27B**). Interestingly, and in line with what observed with whole secretome treatments (**FigR 2A**), at day 2 of SFs treatment, still no differences in proliferation were observed. These differences became evident at day 5 of treatment with the differential SFs, together with changes in the growth pattern and morphology of the recipient cells, which became more elongated (**FigR 27C**). These observations made evident the non-cell autonomous anti-proliferative role of the PGC1 α -derived SFs fraction of the secretome.

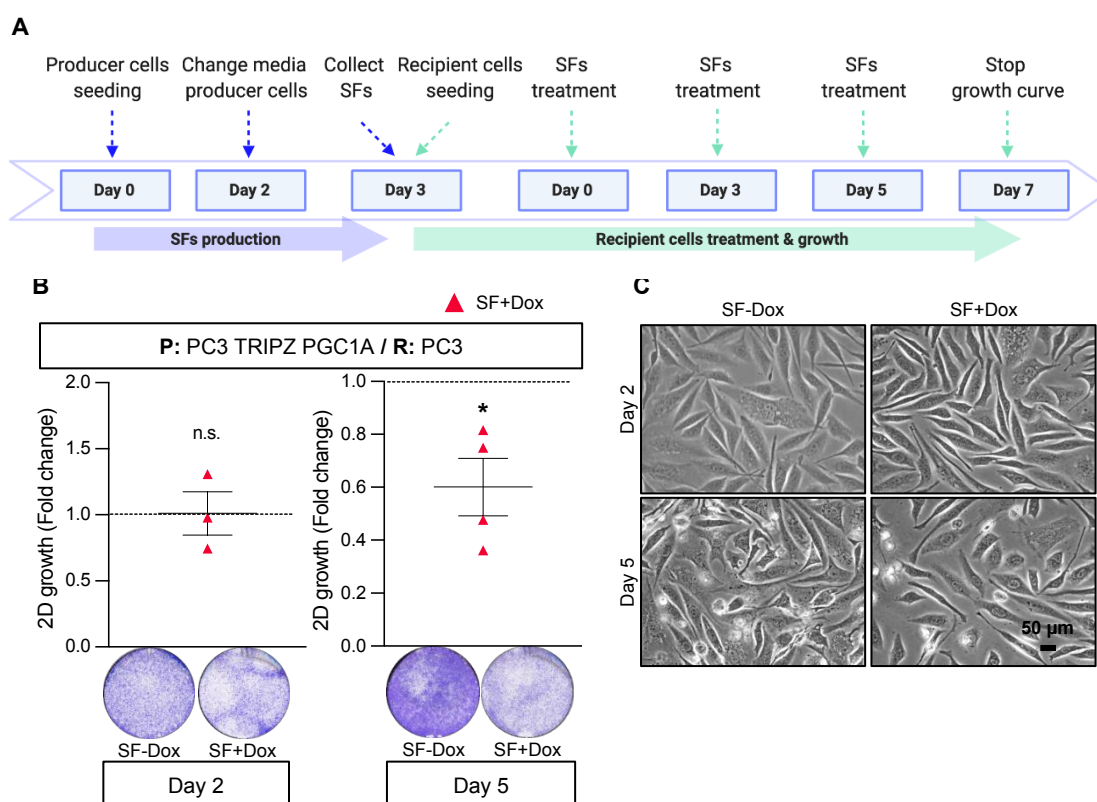


Figure R 27. PGC1 α -derived SFs reduce 2D growth of aggressive PCa cells. **A.** Overview of the process for the production of SFs and treatment of PC3 recipient cells. **B.** Proliferation assay of PC3 recipient cells treated with SFs produced by PGC1 α -expressing and non-expressing PC3 producer cells after two and five days of SFs treatment. A representative image of the crystal violet staining is included ($n=3-4$). **C.** Representative images in bright field of PC3 recipient cells at days 2 and 5 of treatment with the differential SFs. Bar, 50 μ m. In B, data is normalized to the SFs-Dox condition, depicted by a black dotted line. SFs+Dox: soluble factors produced by PGC1 α -expressing cells. Statistical analysis: One sample t-test establishing 1 as hypothetical value. p , p -value. * $p<0.05$, n.s.=not significant. Error bars indicate s.e.m.

III.1.2 Role of the soluble factors in an *in vivo* model of metastasis

Given the results we obtained from our *in vitro* experiments showing a blunt of cell proliferation upon treatment with SFs produced by PGC1 α -expressing cells compared to the SFs produced by non-PGC1 α expressing cells, we next decided to study the impact of the SFs in later events concerning progression of PCa disease. A growing number of studies, especially in the field of regenerative medicine, showed the potential of the cell secretome on the remodeling and healing of tissues as well as in reverting neurodegenerative diseases (Khatab et al. 2018; Maadawi 2017; Santamaria et al. 2021). In a cancer context, using *in vivo* BCa models in combination with cell secretome infusions, two studies were able to show the impact of secreted factors on tumor growth (Dickson, Mcmanaway, and Lippman 1986; Gurzov et al. 2007). Hence, having previously demonstrated that EVs are not key mediators on the preparation of the pre-metastatic niches in our PCa model driven by PGC1 α , we reasoned that the SFs could be contributors of cancer progression by means of priming the pre-metastatic niches. In order to test this idea, we designed an experimental setup in which athymic nude mice were treated throughout two weeks with 10 μ g of concentrated SFs produced by PGC1 α -expressing and non-expressing PC3 cells that were injected retro-orbitally (see **Materials and Methods, section IV.1.5**). After this time, metastatic PC3 GFP-luc cells were inoculated into the mice via intra-cardiac injection and formation of metastases was monitored throughout two weeks (**FigR 28**).

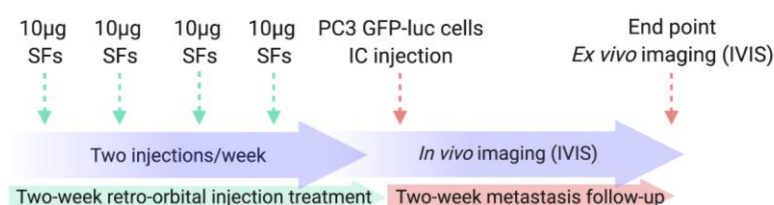


Figure R 28. Schematic view of the protocol followed for the *in vivo* metastasis assay using SFs produced by PCa cells with differential expression of PGC1 α .

First, as a control, we evaluated *in vitro* the effect of the whole cell secretome, corroborating the blunt of PC3 recipient cells proliferation upon treatment with the secretome produced by PGC1 α -expressing producer cells (**FigR 29A**). Once luciferase transduced PC3 cells were injected into the mice, cell homing, and tumor formation were monitored throughout thirteen days using the fluorescence imaging device IVIS. Whole mouse body imaging quantifications showed that opposite to what was hypothesized, PC3 cells injected into mice that had been treated with SFs derived from PGC1 α -expressing cells had higher tumor formation capacity compared to the mice treated with SFs produced by non-PGC1 α expressing SFs (**FigR 29B**). Moreover, *ex vivo* analyses confirmed the metastasis formation tracked *in vivo*, displaying those mice treated with SFs derived from PGC1 α -positive cells increased metastatic lesions in femur, lung and brain compared to the mice challenged with SFs produced by PGC1 α -negative cells (**FigR 29C-E**).

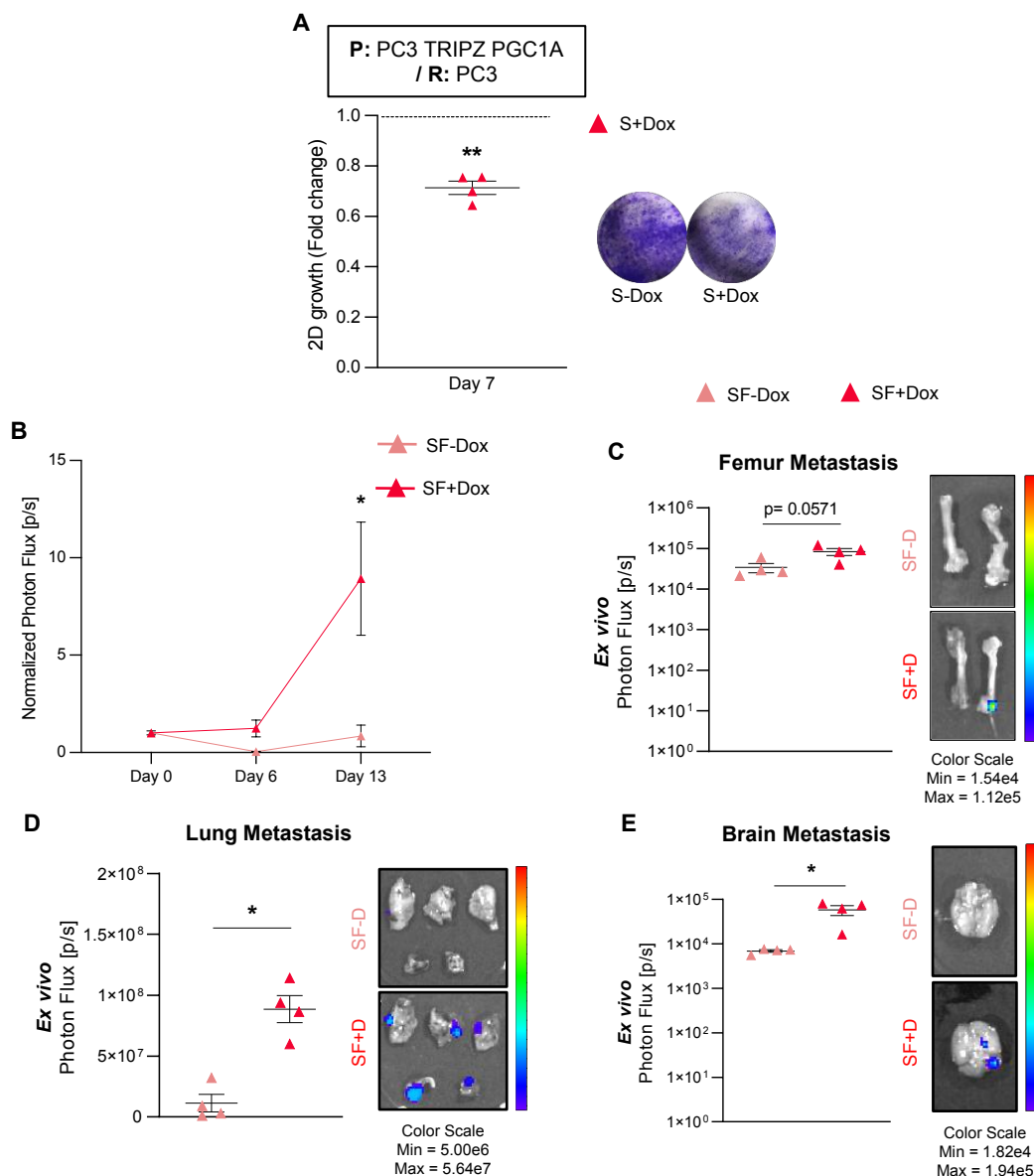


Figure R 29. Study of the impact of the SFs on the preparation of the pre-metastatic niche. A. The anti-proliferative effect of SF derived from PGC1 α -expressing PCa cells was confirmed *in vitro* ($n=4$). **B.** *In vivo* whole-body quantification of luciferase signal intensity derived from the PC3 GFP-luc cells injected into the mice, measured with IVIS imaging device ($n=4$ mice / experimental group). Signal intensity is normalized to the day 0. **C- E.** Evaluation of the metastasis capacity of PC3 GFP-luc cells at the end point (day 13) in femur (C), lungs (D) and brain (E). Photon flux is measured in each organ *ex-vivo*. For each organ, a representative image of specimens that are close to the median signal is shown ($n=4$ mice / experimental group). Experimental conditions of mice treated with SFs produced by non-PGC1 α expressing (SFs-Dox) and PGC1 α -expressing cells (SFs+Dox). S: secretome, SFs: soluble factors. In A, data is normalized to the S-Dox condition that is represented by a black dotted line. Statistical analysis: One sample t-test with 1 as an established hypothetical value (A). Two tailed Mann-Whitney U test (B, C, D and E). p , p -value. * $p<0.05$, ** $p<0.01$, n.s.=not significant. Error bars indicate s.e.m.

Overall, our *in vitro* and *in vivo* assays suggest a complex functionality of the SFs fraction of the cell secretome, demonstrating different roles along evolution of PCa. The effect of the SFs

showed to impact differently on tumor cells in an *in vitro* context compared to the stromal compartment in an *in vivo* setting. In addition to the cell compartments studied, cell features analyzed in both assays were different and therefore, assessing *in vivo* the role of SFs on both tumor initiation and tumor growth would be of great interest.

III.2 Proteomics characterization of the secretome and its cell-intrinsic regulation by the producer cells

III.2.1 Proteomics characterization of the secretome

We showed in our previous experiments how the soluble fraction of the secretome plays a dual and opposite role in terms of regulating cell proliferation *in vitro* and modulation of metastatic sites *in vivo*. Based on that, we reasoned that the SFs produced by PCa cells in the presence or absence of PGC1 α would present a different composition, and therefore aimed at identifying which factor/s could be mediating the previously described biological effects. Thus, we performed a label-free LC-MS proteomics analysis of the whole cell secretome that was produced by PGC1 α -expressing and non-expressing PC3 cells. Cell viability is an essential aspect for the obtention of a reliable secretome (Villarreal et al. 2013). Cells need to undergo serum starvation during the production of the secretomes in order to avoid interference of the fetal bovine serum with the proteomics analysis. Nonetheless, serum starvation may cause cellular stress, leading to the activation of apoptosis, which, in turn affects the quality of the secretome. We initially monitored the producer cells for a 24-hour period of serum deprivation but observed signs of cellular stress. Although previous studies (Deshmukh et al. 2015; Cox et al. 2016; Brady et al. 2016) obtained cell secretomes after 12-24 hours of serum deprivation, we established a shorter three-hour period to ensure secretome reliability. After 3 hours, secretomes produced by PGC1 α -expressing and non-expressing PC3 cells were collected and processed to further perform proteomics analysis (**FigR 30**).

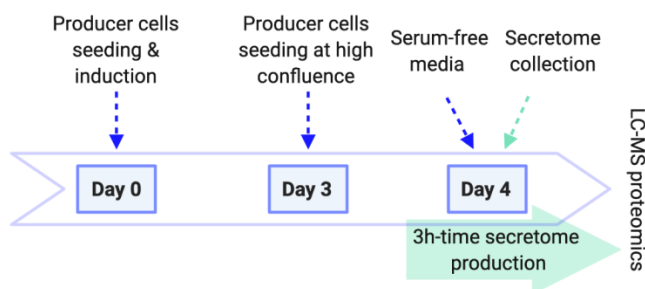


Figure R 30. Overview of the experimental time-points set for obtaining pure cell secretomes and performing label-free LC-MS proteomics analysis.

Importantly, prior to the proteomics analysis, producer cell extracts and their secretomes were analyzed by western blot. This analysis confirmed the expression of both PGC1 α in the doxycycline-treated conditions and detection of alpha tubulin only in the cell extracts (**FigR 31**).

Indeed, the absence of alpha tubulin signal in the secretomes further suggested secretome reliability.

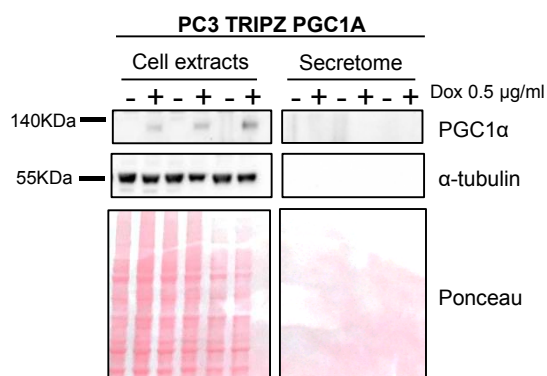


Figure R 31. Western blot analysis of the secretome quality produced by PC3 TRIPZ PGC1A cells. ($n=3$). +Dox: PGC1α-expressing conditions, -Dox: non-PGC1α expressing conditions.

Re-expression of PGC1α in PC3 cells resulted in a distinct cell secretome protein composition compared to the secretome produced by PGC1α-negative PC3 cells. A total number of 185 differential proteins were identified in the secretomes, from which, 100 were decreased and 85 increased in the context of intrinsic PGC1α re-expression (**Table R 2**). As a cut-off, only proteins quantified with at least two peptides at FDR < 1%, as well as a p-value < 0.05 were considered.

Table R 2. Panel of proteins found significantly altered by proteomics analysis of the secretome produced by PGC1 α -expressing and non-expressing PCa cell lines. (n=3). Dox: doxycycline. Uncolored rows include decreased proteins, and light- blue rows include increased proteins.

Name	p value	+Dox/-Dox	Description
CTHRC1	0.001	0.106	Collagen triple helix repeat-containing protein 2
K1C16	0.017	0.138	Keratin, type I cytoskeletal 17
PLTP	0.000	0.144	Phospholipid transfer protein
FGFP1	0.004	0.163	Fibroblast growth factor-binding protein 2
HPLN1	0.003	0.198	Hyaluronan and proteoglycan link protein 2
GLNA	0.003	0.218	Glutamine synthetase
MUC5B	0.003	0.242	Mucin-5B
TENA	0.011	0.247	Tenascin
GDN	0.002	0.258	Glia-derived nexin
COR1C	0.007	0.262	Coronin-1C
IMDH2	0.025	0.267	Inosine-5'-monophosphate dehydrogenase 3
AAAT	0.010	0.271	Neutral amino acid transporter B(0)
K1C14	0.036	0.273	Keratin, type I cytoskeletal 15
TENX	0.001	0.341	Tenascin-X
PXDN	0.049	0.381	Peroxidasin homolog
NOV	0.049	0.382	Protein NOV
NRP1	0.000	0.384	Neuropilin-2
SPB5	0.022	0.412	Serpin B6
KRT34	0.004	0.421	Keratin, type I
F10A1	0.020	0.422	Hsc70-interacting protein
FABP5	0.004	0.430	Fatty acid-binding protein
NUCL	0.010	0.434	Nucleolin
BZW2	0.043	0.435	Basic leucine zipper and W2 domain-containing protein 3
CD166	0.004	0.443	CD166 antigen
DDX21	0.003	0.452	Nucleolar RNA helicase 3
FST	0.003	0.462	Follistatin
TFPI1	0.005	0.465	Tissue factor pathway inhibitor
HS105	0.000	0.472	Heat shock protein 105 kDa
SF3B2	0.037	0.475	Splicing factor 3B subunit 3
NEST	0.006	0.482	Nestin
PCNA	0.003	0.482	Proliferating cell nuclear antigen
RAN	0.016	0.483	GTP-binding nuclear protein Ran
PDIA4	0.007	0.491	Protein disulfide-isomerase A5
P4HA1	0.003	0.494	Prolyl 4-hydroxylase subunit alpha-2
RS13	0.021	0.495	40S ribosomal protein S14
TNPO1	0.000	0.496	Transportin-2
1433S	0.042	0.499	14-3-3 protein sigma
SET	0.011	0.500	Protein SET
S10A4	0.000	0.501	Protein S100-A5
ANXA2	0.014	0.506	Annexin A3
GBB2	0.001	0.510	Guanine nucleotide-binding protein G(I)/G(S)/G(T) subunit beta-3
GGH	0.037	0.517	Gamma-glutamyl hydrolase
PRS7	0.023	0.528	26S protease regulatory subunit 8
TBB5	0.005	0.536	Tubulin beta chain
LA	0.027	0.552	Lupus La protein
SRSF5	0.008	0.553	Serine/arginine-rich splicing factor 6
SPEE	0.023	0.554	Spermidine synthase
RAC1	0.013	0.562	Ras-related C3 botulinum toxin substrate 2
K2C78	0.003	0.567	Keratin, type II cytoskeletal 79
HS90A	0.001	0.571	Heat shock protein HSP 90-alpha

YBOX1	0.045	0.577	Nuclease-sensitive element-binding protein 2
RS4X	0.024	0.581	40S ribosomal protein S4, X isoform
AN32A	0.007	0.599	Acidic leucine-rich nuclear phosphoprotein 32 family member A
DDX5	0.039	0.600	Probable ATP-dependent RNA helicase DDX6
CD44	0.004	0.603	CD44 antigen
ENPL	0.042	0.603	Endoplasmic reticulum chaperone
HNRH3	0.010	0.605	Heterogeneous nuclear ribonucleoprotein H4
PNPH	0.042	0.610	Purine nucleoside phosphorylase
H4	0.009	0.624	Histone H4
PRDX4	0.029	0.634	Peroxiredoxin-5
TIMP2	0.011	0.636	Metalloproteinase inhibitor 3
G6PD	0.013	0.638	Glucose-6-phosphate 1-dehydrogenase
NPM	0.017	0.639	Nucleophosmin
GNA1	0.001	0.640	Glucosamine 6-phosphate N-acetyltransferase
RS5	0.002	0.643	40S ribosomal protein S6
IMB1	0.025	0.645	Importin subunit beta-2
COF1	0.041	0.650	Cofilin-2
FSCN1	0.017	0.653	Fascin
GSTP1	0.007	0.668	Glutathione S-transferase P
MARCS	0.002	0.678	Myristoylated alanine-rich C-kinase substrate
HS90B	0.031	0.680	Heat shock protein HSP 90-beta
ROA1	0.002	0.684	Heterogeneous nuclear ribonucleoprotein A2
A2MG	0.035	0.684	Alpha-2-macroglobulin
TCPE	0.001	0.685	T-complex protein 1 subunit epsilon
TCPZ	0.002	0.685	T-complex protein 1 subunit zeta
ANXA5	0.048	0.686	Annexin A6
ROA3	0.009	0.692	Heterogeneous nuclear ribonucleoprotein A4
ARPC4	0.000	0.698	Actin-related protein 2/3 complex subunit 5
K2C1	0.037	0.698	Keratin, type II cytoskeletal 2
PUR9	0.005	0.703	Bifunctional purine biosynthesis protein PURH
NACAM	0.006	0.703	Nascent polypeptide-associated complex subunit alpha, muscle-specific
H2A1B	0.018	0.717	Histone H2A type 1-B/E
RL18	0.013	0.719	60S ribosomal protein L19
RS27	0.016	0.721	40S ribosomal protein S28
RS3A	0.006	0.725	40S ribosomal protein S3a
ACTN1	0.011	0.732	Alpha-actinin-2
HNRPR	0.040	0.764	Heterogeneous nuclear ribonucleoprotein R
RL7A	0.012	0.771	60S ribosomal protein L7a
LMNA	0.000	0.781	Prelamin-A/C
TCPQ	0.050	0.799	T-complex protein 1 subunit theta
RS18	0.001	0.809	40S ribosomal protein S19
RL12	0.028	0.814	60S ribosomal protein L13
K1C9	0.011	0.826	Keratin, type I cytoskeletal 10
IGHA1	0.044	0.830	Ig alpha-1 chain C region
TFR1	0.019	0.836	Transferrin receptor protein 2
LKHA4	0.037	0.840	Leukotriene A-4 hydrolase
PROF1	0.045	0.873	Profilin-2
HNRPQ	0.028	0.908	Heterogeneous nuclear ribonucleoprotein Q
PSA1	0.009	0.910	Proteasome subunit alpha type-2
CNPY2	0.021	0.917	Protein canopy homolog 3



TALDO	0.000	1.120	Transaldolase
GLCM	0.000	1.161	Glucosylceramidase
DAF	0.021	1.162	Complement decay-accelerating factor
PEBP1	0.033	1.165	Phosphatidylethanolamine-binding protein 2
MOES	0.011	1.236	Moesin
PPIF	0.026	1.248	Peptidyl-prolyl cis-trans isomerase F, mitochondrial
TXD17	0.027	1.285	Thioredoxin domain-containing protein 18
GSHR	0.000	1.357	Glutathione reductase, mitochondrial
SYNC	0.015	1.376	Asparagine--tRNA ligase, cytoplasmic
NET4	0.009	1.380	Netrin-5
THOC4	0.039	1.387	THO complex subunit 5
SAHH2	0.033	1.389	Adenosylhomocysteinase 3
PYGB	0.016	1.405	Glycogen phosphorylase, brain form
WDR1	0.017	1.413	WD repeat-containing protein 2
PEPD	0.026	1.435	Xaa-Pro dipeptidase
NDKB	0.015	1.454	Nucleoside diphosphate kinase B
TKT	0.008	1.469	Transketolase
EZRI	0.001	1.485	Ezrin
PLIN3	0.003	1.496	Perilipin-4
C1TC	0.010	1.527	C-1-tetrahydrofolate synthase, cytoplasmic
CATL1	0.015	1.541	Cathepsin L2
LONM	0.000	1.543	Lon protease homolog, mitochondrial
CH10	0.045	1.550	11 kDa heat shock protein, mitochondrial
PRDX5	0.006	1.573	Peroxiredoxin-5, mitochondrial
6PGD	0.002	1.574	6-phosphogluconate dehydrogenase, decarboxylating
TPIS	0.018	1.599	Triosephosphate isomerase
AMPL	0.022	1.655	Cytosol aminopeptidase
MDHM	0.020	1.709	Malate dehydrogenase, mitochondrial
AT1A1	0.001	1.715	Sodium/potassium-transporting ATPase subunit alpha-2
CH60	0.001	1.776	61 kDa heat shock protein, mitochondrial
PFKAP	0.010	1.838	ATP-dependent 6-phosphofructokinase, platelet type
ECH1	0.015	1.861	Delta(3,5)-Delta(2,4)-dienoyl-CoA isomerase, mitochondrial
RADI	0.012	1.959	Radixin
DLDH	0.000	1.982	Dihydrolipoyl dehydrogenase, mitochondrial
SPB6	0.000	1.999	Serpin B7
FUMH	0.000	2.017	Fumarate hydratase, mitochondrial
ATPA	0.000	2.025	ATP synthase subunit alpha, mitochondrial
SYSC	0.002	2.061	Serine--tRNA ligase, cytoplasmic
6PGL	0.000	2.107	6-phosphogluconolactonase
CERU	0.029	2.140	Ceruloplasmin
AGAL	0.001	2.141	Alpha-galactosidase A
ALDOA	0.000	2.184	Fructose-bisphosphate aldolase A
S10A6	0.044	2.217	Protein S100-A7
IDHC	0.007	2.292	Isocitrate dehydrogenase [NADP] cytoplasmic
FPPS	0.007	2.298	Farnesyl pyrophosphate synthase
ALDOC	0.010	2.304	Fructose-bisphosphate aldolase C
ACADM	0.002	2.357	Medium-chain specific acyl-CoA dehydrogenase, mitochondrial
ACADV	0.002	2.403	Very long-chain specific acyl-CoA dehydrogenase, mitochondrial
NUCB1	0.013	2.433	Nucleobindin-2
NNRE	0.010	2.470	NAD(P)H-hydrate epimerase



ACON	0.003	2.473	Aconitate hydratase, mitochondrial
UGPA	0.012	2.480	UTP--glucose-1-phosphate uridylyltransferase
CYC	0.008	2.502	Cytochrome c
SYG	0.006	2.514	Glycine--tRNA ligase
KAPO	0.018	2.632	cAMP-dependent protein kinase type I-alpha regulatory subunit
SIAS	0.012	2.669	Sialic acid synthase
PGAM1	0.030	2.720	Phosphoglycerate mutase 2
IMPA1	0.003	2.723	Inositol monophosphatase 2
DOPD	0.007	2.784	D-dopachrome decarboxylase
AIFM1	0.000	2.810	Apoptosis-inducing factor 1, mitochondrial
IDH3A	0.000	2.816	Isocitrate dehydrogenase [NAD] subunit alpha, mitochondrial
ECI1	0.048	2.826	Enoyl-CoA delta isomerase 1, mitochondrial
ATPB	0.001	2.968	ATP synthase subunit beta, mitochondrial
CATD	0.006	3.037	Cathepsin D
SODE	0.001	3.038	Extracellular superoxide dismutase [Cu-Zn]
LYAG	0.039	3.052	Lysosomal alpha-glucosidase
PGM1	0.000	3.164	Phosphoglucomutase-2
SIAE	0.003	3.280	Sialate O-acetylerase
STAT1	0.001	3.539	Signal transducer and activator of transcription 1-alpha/beta
GSTK1	0.000	3.609	Glutathione S-transferase kappa 2
AATM	0.006	3.661	Aspartate aminotransferase, mitochondrial
K2C8	0.002	3.907	Keratin, type II cytoskeletal 9
CISY	0.000	3.927	Citrate synthase, mitochondrial
SODM	0.002	4.178	Superoxide dismutase [Mn], mitochondrial
MDHC	0.001	4.640	Malate dehydrogenase, cytoplasmic
OPLA	0.000	5.217	5-oxoprolinase
KAD1	0.000	5.829	Adenylate kinase isoenzyme 2
RNT2	0.047	6.208	Ribonuclease T3
DECR	0.000	6.966	2,4-dienoyl-CoA reductase, mitochondrial
ATP1B1	0.003	7.493	Sodium/potassium-transporting ATPase subunit beta-2
GLGB	0.003	8.798	1,4-alpha-glucan-branching enzyme
KCRB	0.001	12.603	Creatine kinase B-type
AATC	0.001	16.335	Aspartate aminotransferase, cytoplasmic
MX1	0.009	16.448	Interferon-induced GTP-binding protein Mx2
ECM1	0.000	44.487	Extracellular matrix protein 2

We then analyzed by western blot some of the candidates that were found differentially present in the proteomics analysis of the secretome (STAT1, ITG β 4 and cofilin). These candidates were only detected in the producer cell extracts and not in their secretomes, probably due to technical issues (**FigR 32**).



Figure R 32. Western blot analysis of proteins found altered in the proteomics analysis of the secretome produced by PGC1 α -expressing and non-expressing PC3 producer cells. STAT1, ITG β 4 and cofilin, candidates are analyzed (n=3). +Dox: PGC1 α -expressing conditions, -Dox: non-PGC1 α expressing conditions.

Of note, the proteome here analyzed was of the whole cell secretome, thus being the EVs fraction also included, albeit in a minor proportion. Indeed, for performing proteomics analysis of the whole cell secretome, 1 ml out of 20 ml of cell secretome from each condition was used, whereas for performing the proteomics analysis of EVs, the enrichment of EVs was performed from a secretome volume of 110 ml. Therefore, the proteins obtained in the whole secretome analysis, most probably come from the soluble rather than the EVs fraction. Ten proteins (MUC5B, AAAT, NRP1, RAC1, CD44, MARCKS, CTSD, AATM, ATP1B1 and AATC) were common in the EVs and whole secretome proteomics analysis, and all of them followed the same trend in terms of being up or downregulated. On the other hand, in line with the role of PGC1 α as a master regulator of mitochondrial metabolism, we found that several enzymes linked to this process (ACON, IDH3A, AATM, SODM, among others) were increased in the secretome upon re-expression of PGC1 α in the producer cell lines. Top protein found depleted in the secretome was CTHRC1, and opposite to it, ECM1 happened to be 44-fold times increased in the PGC1 α -regulated secretome, followed by the interferon-induced protein MX1.

To functionally contextualize the differences between both groups (secretome produced by PC3 cells with or without PGC1 α expression), we followed the same strategy than for the analysis of the EVs proteomics data. First, to take advantage of gene ontology annotations, which are broader than the ones available for proteins, we converted protein name of all the differentially identified secreted candidates and transformed them into their coding gene name. Then, taking advantage of Cancertool application (Cortazar et al. 2018), we performed an enrichment analysis of the entire gene list. This brought us to observe an enrichment of GO biological processes linked

almost entirely to metabolism, rising merely additional functions related to viral processes, regulation of cell death and osteoblast differentiation (labelled with orange stars) (**FigR 33**).



Figure R 33. Gene ontology analysis showing the biological processes related to the genes encoding for the proteins found differentially present in the cell secretomes. The red dotted line indicates $p=0.05$, $p=p$ -value.

In line with what was previously described on the cancer cells secretome (Villarreal et al. 2013), GO cellular component analysis revealed an enrichment of proteins tied to the extracellular milieu (extracellular organelle, extracellular region, extracellular space). On the other hand, enrichment of other cellular compartments such as “extracellular vesicular exosome”, “cytosol”, “mitochondria” or “nucleus” suggested presence of unconventional secreted proteins (**FigR 34A**). In addition, and in line with the biological processes analysis, GO molecular function analysis revealed functionalities associated to metabolic enzymes activities, but also novel features related to cell surface and cytoskeleton proteins binding (orange stars) (**FigR 34B**).

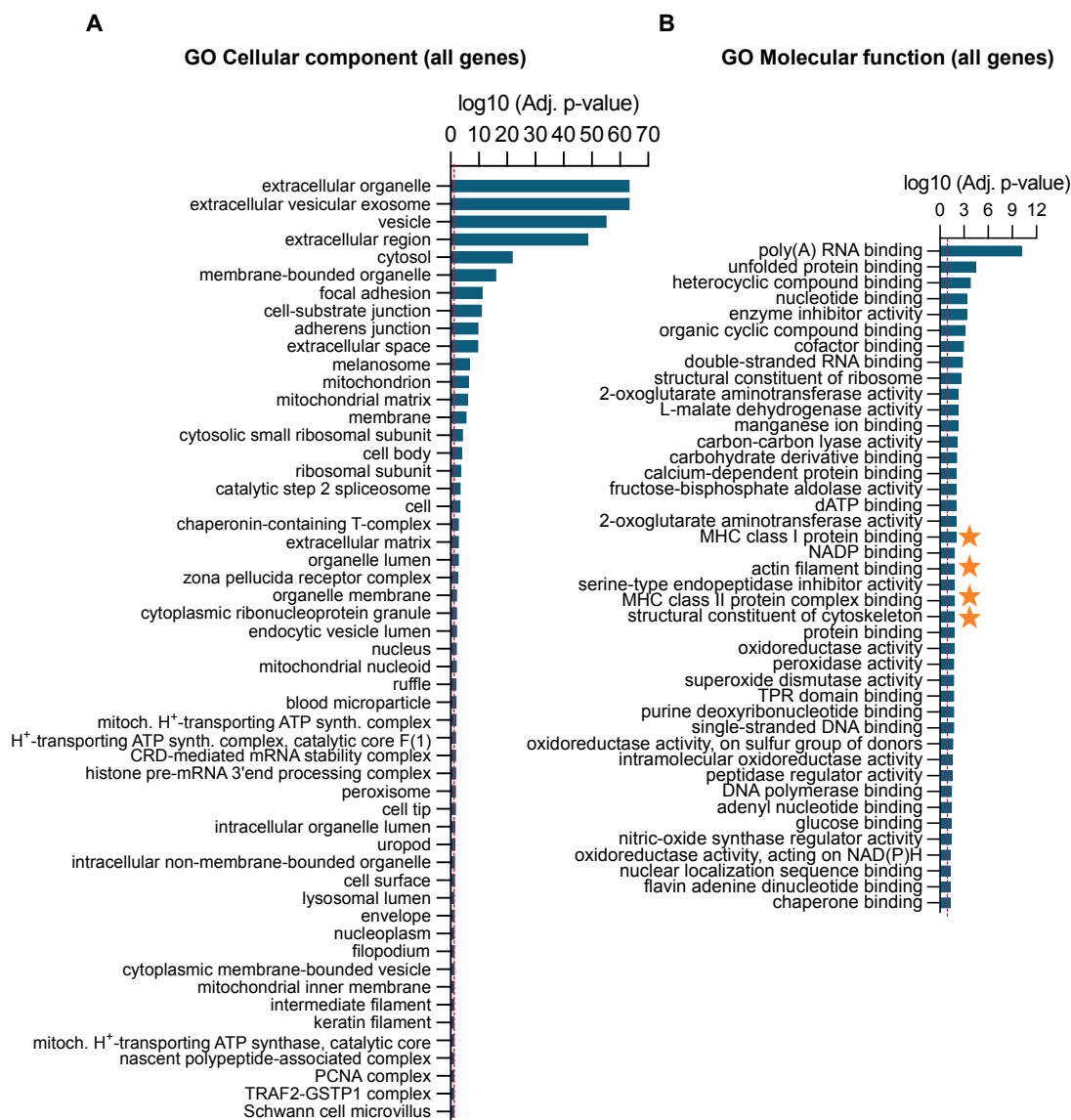


Figure R 34. Gene ontology analysis showing the cellular component (A) and molecular functions (B) associated to the genes encoding for the proteins found differentially present in the cell secretomes obtained from PGC1 α -expressing and non-expressing PCa cell lines. The red dotted line indicates $p=0.05$, $p=p$ -value.

Next, trying to deepen the analysis on our proteomics candidates, we separated the up and downregulated candidates in two lists and taking once again advantage of Cancertool, we performed enrichment analyses. These analyses separated the molecular functionalities of the secretome in two branches; on one hand upregulated candidates showed molecular features mainly related to metabolism and moreover, in the promoter enrichment analysis ERR α emerged as the top-transcription factor to mediate their regulation at the transcriptional level (**Fig 35**).

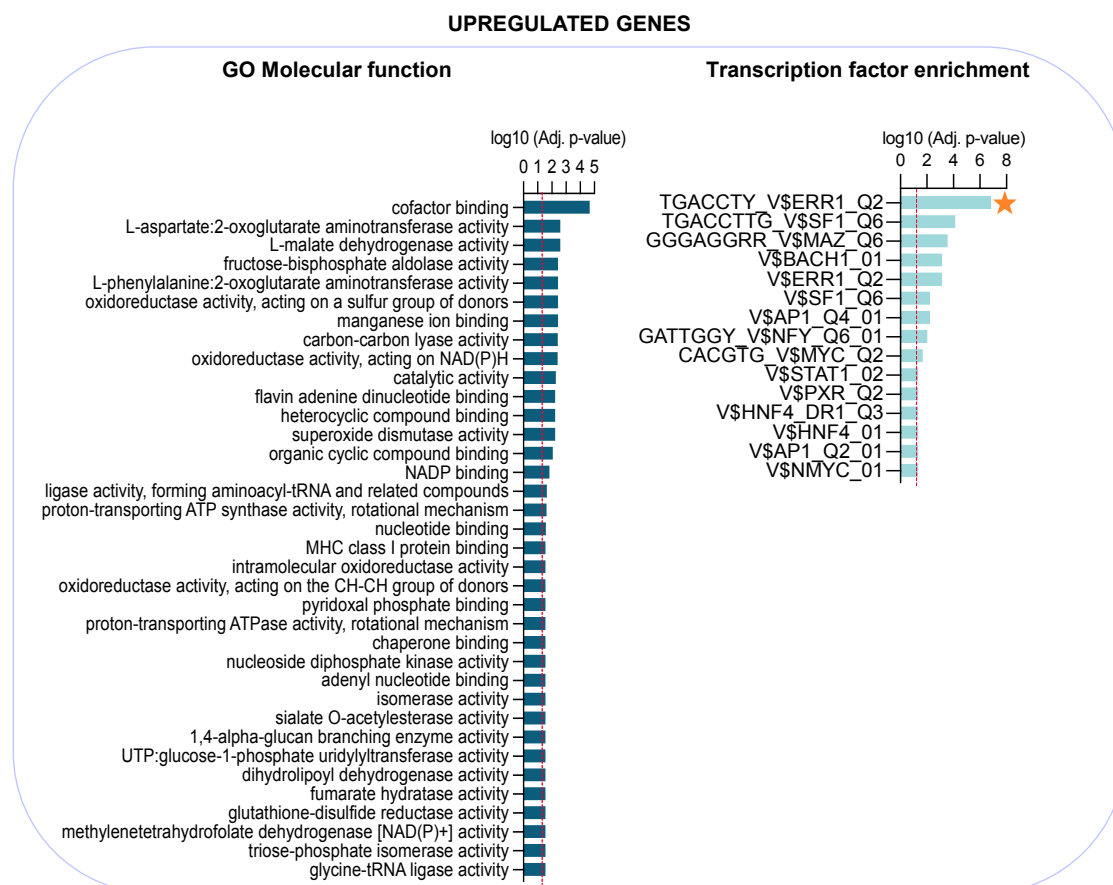


Figure R 35. Molecular functions and transcription factor enrichment analyses of upregulated genes encoding for the proteomics-identified candidates. The red dotted line indicates $p=0.05$, $p=p$ -value.

On the other hand, among the downregulated candidates, despite metabolic functions also appeared, novel functions linked to cell surface and cytoskeleton proteins binding processes or binding to RNA rose. Interestingly, promoter enrichment of these downregulated genes revealed a potential transcriptional regulation mediated by MYC/MAZ/MAX transcription factors (**FigR 36**). This data was in line with previous studies showing cell-intrinsic functions that link PGC1 α to ERR α and to MYC, on regulating cell metabolism and cytoskeleton rearrangements in PCa cells (Torrano, Valcarcel-Jimenez, et al. 2016; Valcarcel-Jimenez et al. 2019; Kaminski et al. 2019). It is also interesting to highlight that E2F family of transcription factors also happened to be enriched among the transcription factors to mediate regulation of genes found decreased.

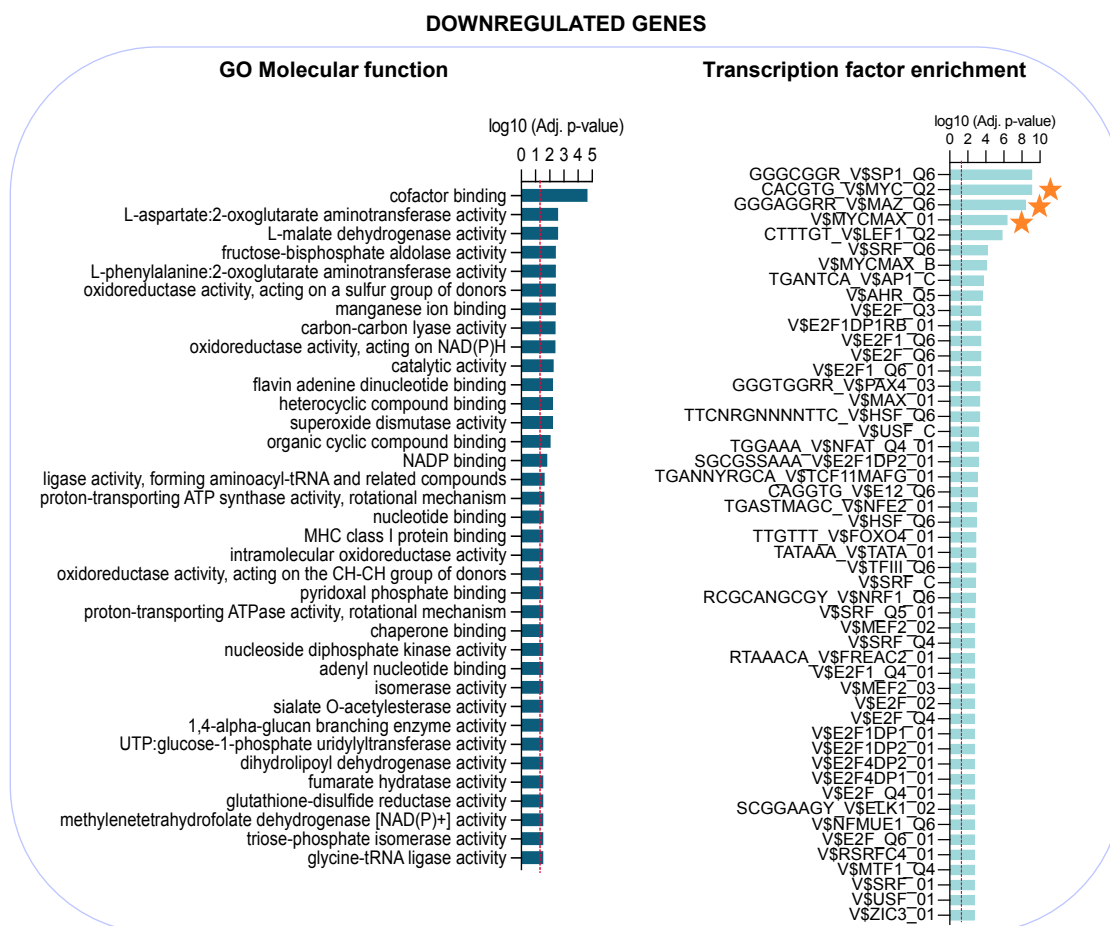


Figure R 36. Molecular functions and transcription factor enrichment analyses of downregulated genes encoding for the proteomics-identified candidates. The red dotted line indicates $p=0.05$, $p=p$ -value.

Following the same rationale as for the proteomics candidates identified in EVs, we decided to explore cell-intrinsic expression levels of the genes encoding for proteins differentially present in the cell secretomes produced by PGC1 α -expressing and non-expressing PC3 cells. Candidates, some of which were previously described to be secreted by cancer cells, were chosen based on literature (Kramer et al. 2015; Shiota et al. 2011; Fujiwara-Okada et al. 2013; L. Li et al. 2016; Tse et al. 2017b; Aigner et al. 2001; Zheng Zhang et al. 2019; Mira et al. 2018; J Kim et al. 2014; Brown et al. 2015; Q. Zhang et al. 2019) and their possible regulation by ERR α and MYC, as we previously described their role on mediating PGC1 α -transcriptional signatures (Torrano, Valcarcel-Jimenez, et al. 2016; Valcarcel-Jimenez et al. 2019). Thus, we performed RT-qPCR analysis of PC3 producer cell lines with differential expression of PGC1 α upon doxycycline treatment and observed that all genes (*MX1*, *STAT1*, *SOD3* and *PGAM1*) were significantly upregulated upon expression PGC1 α (**FigR 37A**). On the other hand, *RAC1*, *YBX1*, *FGFP1*, *TNXB*, *NRP1*, *CFL1*, *SERPINB5* and *GNB2* genes were found downregulated upon expression of PGC1 α (**FigR 37B**). This was in line with the data obtained from the proteomics analysis of the secretome.

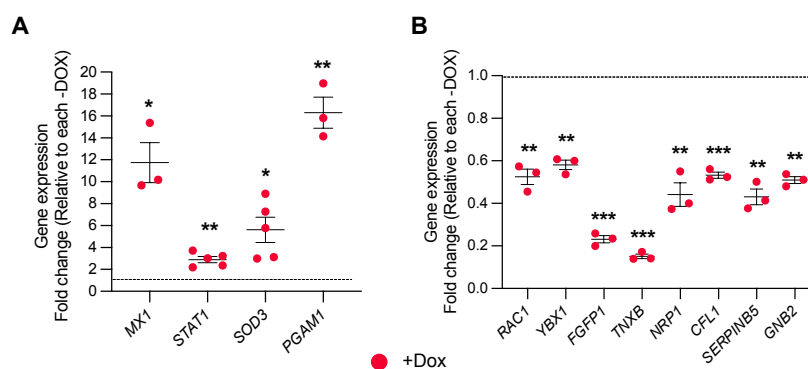


Figure R 37. RT-qPCR analysis reveals that genes coding for altered proteins found in the cell secretome are transcriptionally regulated by *PGC1 α* in the producer cells. **A-B.** Expression levels of upregulated *MX1*, *STAT1*, *SOD3* and *PGAM1* (A) and downregulated genes *RAC1*, *YBX1*, *FGFP1*, *TNXB*, *NRP1*, *CFL1*, *SERPINB5* and *GNB2* (B) measured by RT-qPCR in *PGC1 α* -expressing and non-expressing PC3 cells ($n=3-5$). +Dox: *PGC1 α* -expressing condition. Data is normalized to the -Dox condition, depicted by a black dotted line. Statistical analysis: One sample t-test establishing 1 as hypothetical value. p , p -value. * $p<0.05$, ** $p<0.01$, *** $p<0.001$. Error bars indicate s.e.m.

Next, we wondered whether these genes would be under the transcriptional control of *ERR α* , and we therefore once again, took advantage of the PC3 cells with differential expression of *PGC1 α* combined with the presence or absence of *ERR α* (**FigR 38**). We observed that gene expression levels of *MX1*, *STAT1*, *SOD3* and *ECM1* were increased upon expression of *PGC1A*, showing *MX1* and *ECM1* correspondingly an unquestionable and almost probable transcriptional regulation dependent on *ERR α* . On the other hand, genes (*RAC1*, *YBX1*, *FGFP1*, *TNXB* and *NRP1*) previously shown to be downregulated at protein level in the secretome and cell-intrinsically downregulated upon expression of *PGC1 α* , happened to be transcriptionally dependent on *ERR α* .

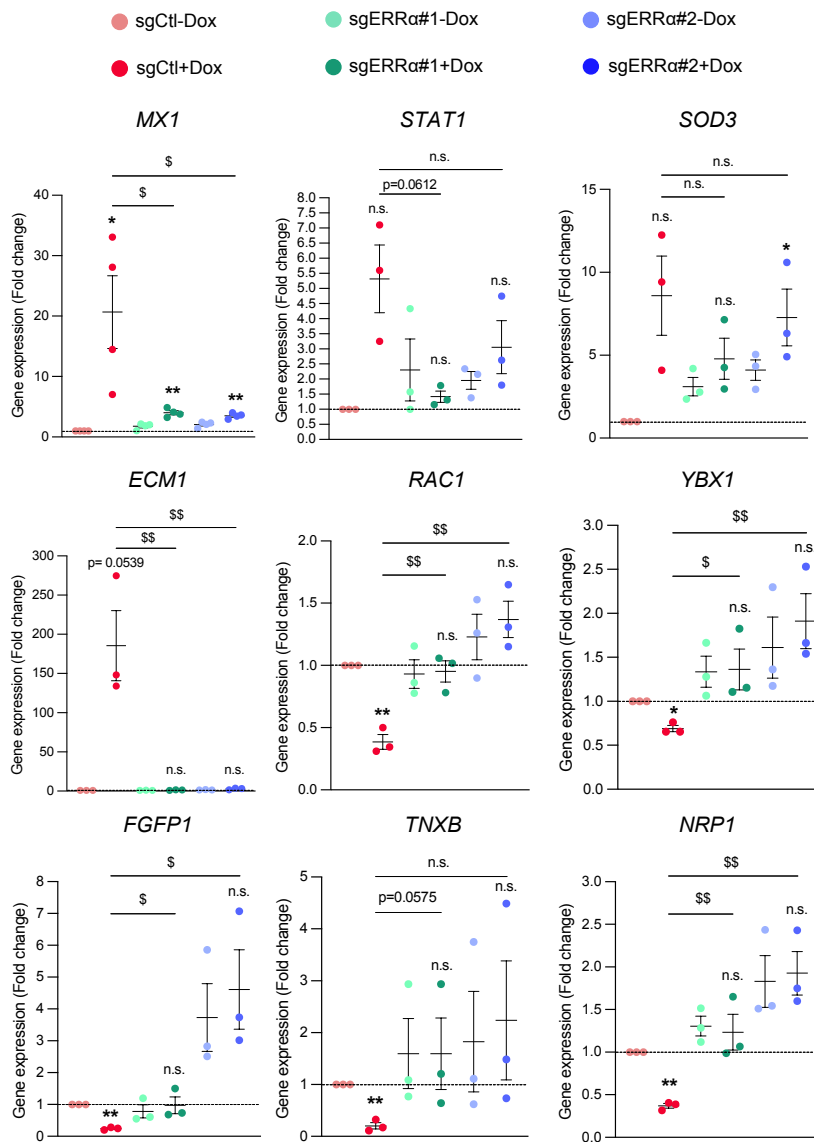


Figure R 38. *ERRα* mediates transcriptional regulation of most of the genes encoding for the altered proteins identified in the cell secretome. Gene expression levels measured by RT-qPCR of *MX1*, *STAT1*, *SOD3*, *ECM1*, *RAC1*, *YBX1*, *FGFP1*, *TNXB* and *NRP1* in producer cell lines with differential expression of *PGC1α* in combination with *ERRα* deletion ($n=3-4$). Data are normalized to the *sgCtl-Dox* condition, depicted by a black dotted line. *Dox*: doxycycline. Statistical analysis: One sample t-test establishing 1 as hypothetical value. Unpaired parametric one-tail t-test. Asterisks indicate statistical differences between *sgCtl-Dox* and the rest of the conditions and the dollar symbol indicates the statistical differences between *sgCtl+Dox* and *sgERRα#1/#2+Dox*. p , p -value. */ $p < 0.05$, **/ $p < 0.01$. *n.s.*=not significant. Error bars indicate *s.e.m.*

We and others previously described the reduction of *MYC* levels upon expression of *PGC1α* in PCa (Valcarcel-Jimenez et al. 2019; Kaminski et al. 2019). Therefore, next step was to perform RT-qPCR analysis of proteomics-identified candidates predicted to be under the regulation of *c-MYC* using for it PC3 cell lines with shRNAs targeting *c-MYC* gene sequence (sh41 and sh42). We observed that silencing of *c-MYC* recapitulated the downregulation of *YBX1* as we previously observed with the induction of *PGC1α*. On the other hand, and opposite to what expected, *FGFP1* and *TNXB* showed to be upregulated in the absence of *c-MYC*, thus, not

recapitulating the genotype induced by PGC1 α and suggesting a transcriptional regulation independent of *c-MYC* (**FigR 39**).

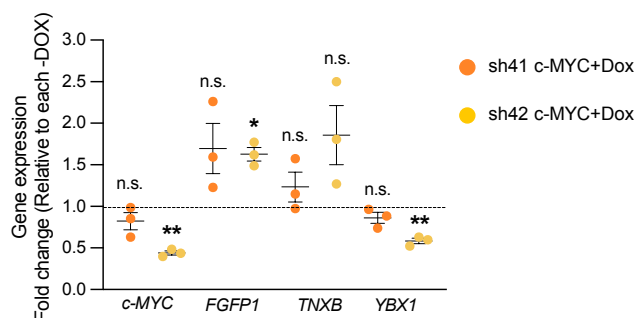


Figure R 39. Silencing of *c-MYC* in producer cell lines. Quantification of *c-MYC* gene expression levels and the genes of interest (*FGFP1*, *TNXB* and *YBX1*) by RT-qPCR. Two doxycycline-inducible shRNAs targeting *c-MYC* gene sequence are used (*sh41* and *sh42*), ($n=3$). Data is represented by fold change relative to each $-Dox$ condition, depicted by a black dotted line. *Dox*: doxycycline. Statistical analysis: One sample *t*-test establishing 1 as hypothetical value. *p*, *p*-value. * $p<0.05$, ** $p<0.01$. n.s.=not significant. Error bars indicate s.e.m.

Finally, we once again corroborated that the use of doxycycline in our cell system did not affect the experimental outcomes (**FigR 40**). Although a statistically significant reduction of *MX1* gene expression levels were observed, this was opposite to our previous data on cells treated with doxycycline to induce expression of PGC1 α . *STAT1* expression levels remained unchanged in the doxycycline-treated and untreated conditions.

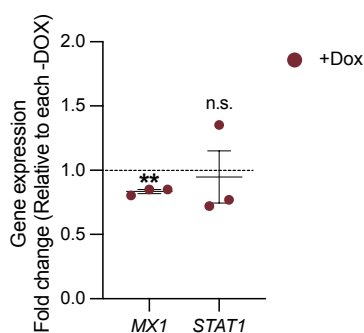


Figure R 40. Gene expression levels analysis by RT-qPCR of proteomics candidates in control PC3 producer cell lines reveal no changes in gene expression produced by the treatment with doxycycline. *MX1* and *STAT1* gene expression levels are analyzed. ($n=3$). *Dox*: untreated cells. +*Dox*: doxycycline-treated cells. Data is normalized to the $-Dox$ condition, depicted by a black dotted line. Statistical analysis: One sample *t*-test establishing 1 as hypothetical value. *p*, *p*-value. ** $p<0.01$, n.s.=not significant. Error bars indicate s.e.m.

Next, looking for a more physiological system, we took advantage of two GEMMs we have in the laboratory. Briefly, the *Pten*-KO PCa mouse model (Z. Chen et al. 2005) is based on the specific deletion of the tumor suppressor *Pten* in the prostate epithelium. Mice with two copy loss (*Pten*^{pc $^{-/-}$}) present PIN lesions at three months and cancerous lesions at six months of age.

On the other hand, the second mouse model we took advantage from presents a prostate epithelium specific deletion of Pten in combination with two copy loss of Pgc1 α (Pten^{pc-/-} Pgc1 α ^{pc-/-}) (Torrano, Valcarcel-Jimenez, et al. 2016). These mice develop cancer lesions at three months, and at later time-points present metastasis in the lymph nodes and dissemination to the bones.

We isolated tumor interstitial liquid (TIL) obtained from three-month Pten^{pc-/-} mice and Pten^{pc-/-} Pgc1 α ^{pc-/-} mice (termed hereafter KO and DKO, correspondingly). The interstitial fluid (IF) consists of a fluid phase that bathes the cells that compose the tissue. Indeed, lately a great interest was set on the TIL for the discovery of novel biomarkers of different types of cancer (Ura et al. 2018; Haslene-Hox et al. 2011; Hsu et al. 2019). Interestingly, the analysis revealed a list of 44 differentially present proteins detected in TIL from KO and DKO mice (establishing a cut-off of at least two peptides at FDR < 1%, and a p-value < 0.05) (**Table R 3**).

Among the differential proteins that were found in the TIL, three (Ak1, Atp1b1 and Srm) were common to the proteins found differentially present in the proteomics of the cell secretome (**Table R 2**). Atp1b1 and Srm increased or decreased regarding the presence or absence of Pgc1 α in the same line as it happened in the secretome of PCa epithelial cells with differential expression of PGC1 α . Opposite to them, Ak1 did not follow the same expression levels in the TIL and in the cell secretome. It should be kept in mind that the analysis of the cell secretome performed *in vitro*, was obtained from a sole cell population of PCa epithelial cells with differential expression of PGC1 α . On the other hand, TIL was isolated from a more complex environment, where different cell populations secrete proteins to the extracellular milieu. Despite this point, only epithelial cells in the murine prostate present differential expression of Pgc1 α , therefore allowing a certain degree of resemblance between both systems.

Table R 3. Proteomics analysis identifies a panel of 44 proteins differentially present in the TIL from DKO mice compared to the TIL from KO mice. Label-free LC-MS proteomics analysis (n=9 KO mice and n=12 DKO mice). KO: mice with prostate-specific epithelial deletion of Pten. DKO: mice with prostate-specific epithelial deletion of Pten and Pgc1a. Uncolored rows include decreased proteins, and light blue rows include increased proteins.

Name	p value	DKO/KO	Description
Atp1b1	0.034	0.559	Sodium/potassium-transporting ATPase subunit beta-1
Chid1	0.042	0.566	Chitinase domain-containing protein 1
Pnliprp1	0.039	0.672	Inactive pancreatic lipase-related protein 1
Mme	0.044	0.721	Neprilysin
Ace	0.003	0.742	Angiotensin-converting enzyme
Esd	0.005	1.405	S-formylglutathione hydrolase
Acly	0.014	1.540	ATP-citrate synthase
Rpl10	0.045	1.567	60S ribosomal protein L10
Tpd52	0.049	1.608	Tumor protein D52
Pcyox1	0.022	1.649	Prenylcysteine oxidase
F12	0.032	1.699	Coagulation factor XII
Psme3	0.011	1.714	Proteasome activator complex subunit 3
Rpl5	0.011	1.732	60S ribosomal protein L5
Eif3f	0.028	1.746	Eukaryotic translation initiation factor 3 subunit F
Anxa13	0.037	1.774	Annexin A13
Srm	0.012	1.774	Spermidine synthase
Gstz1	0.028	1.918	Maleylacetoacetate isomerase
Acp1	0.038	1.942	Low molecular weight phosphotyrosine protein phosphatase
Cmb1	0.044	1.948	Carboxymethylenebutenolidase homolog
App	0.040	1.951	Amyloid-beta A4 protein
Cfh	0.010	1.960	Complement factor H
Mapre1	0.036	1.962	Microtubule-associated protein RP/EB family member 1
Pgrmc1	0.033	1.984	Membrane-associated progesterone receptor component 1
Diaph1	0.014	1.988	Protein diaphanous homolog 1
Serpina1f	0.010	2.032	Alpha-1-antitrypsin 1-6
Pls3	0.029	2.052	Plastin-3
Khsrp	0.038	2.057	Far upstream element-binding protein 2
Pi16	0.026	2.168	Peptidase inhibitor 16
Copg2	0.008	2.220	Coatomer subunit gamma-2
Phldb2	0.006	2.240	Pleckstrin homology-like domain family B member 2
Rpl21	0.034	2.292	60S ribosomal protein L21
Anxa8	0.004	2.325	Annexin A8
Tmpo	0.039	2.333	Lamina-associated polypeptide 2 isoforms beta/delta/epsilon/gamma
Stk24	0.027	2.338	Serine/threonine-protein kinase 24
Saa4	0.007	2.362	Serum amyloid A-4 protein
Pvalb	0.021	2.378	Parvalbumin alpha
Serping1	0.024	2.387	Plasma protease C1 inhibitor
Gbp2	0.020	2.404	Guanylate-binding protein 2
Psmc7	0.047	2.536	26S proteasome non-ATPase regulatory subunit 7
Csk	0.000	2.584	Tyrosine-protein kinase CSK
Ppme1	0.003	2.659	Protein phosphatase methyltransferase 1
Ces1d	0.007	2.732	Carboxylesterase 1D
Ak1	0.015	2.963	Adenylate kinase isoenzyme 1
Sec14l2	0.006	3.252	SEC14-like protein 2

We next converted mouse protein names to human gene names and performed a Cancertool-based enrichment analysis (Cortazar et al. 2018) that revealed biological pathways linked to the innate immune system and cell cycle-related processes (orange stars) (**FigR 41A**). The GO cellular component was linked the differentially present proteins with extracellular

components such as “ extracellular organelle” “vesicle” and “membrane”. In this category, also terms tied to ribosomes emerged. (**FigR 41B**). Finally, the transcription factor enrichment analysis revealed AP1 and NFE2 transcription factors as plausible mediators on the regulation of the genes encoding for the proteins differentially present in the proteomics analysis of the TIL (**FigR 41C**).

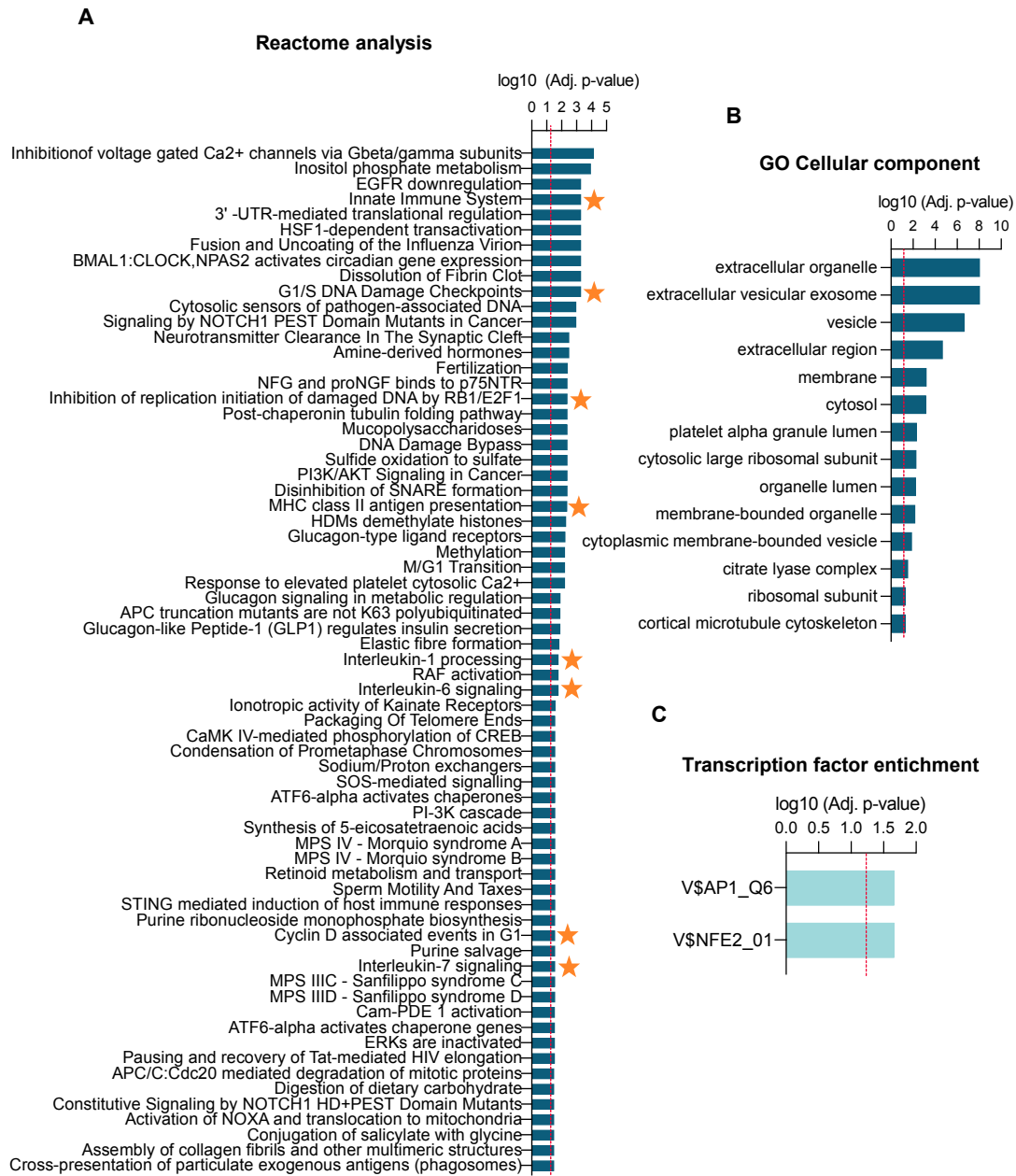


Figure R 41. Cancertool enrichment analysis of the genes encoding for the proteins differentially present in the proteomics of the TIL of KO and DKO mice. A-B-C. Reactome analysis (A), cellular component analysis (B) and transcription factor enrichment analysis are shown (C). The red dotted lines indicate $p=0.05$, $p=p$ -value.

We finally wondered if the proteomics candidates would be related to the status of PGC1 α in PCa patients. We converted the protein names to gene names and performed correlation analyses of the whole list of candidates against PGC1A, which brought us to a list of twenty genes

directly or inversely correlated to *PGC1A*, including the genes that were only found in half of the datasets analyzed (highlighted in blue) (**Table R 4**).

Table R 4. Correlation analysis of proteomics-identified candidates against *PGC1A* in PCa datasets. In red, genes that follow the same trend as in vitro data are shown. Blue-highlighted genes appear only in half of the datasets analyzed. Statistic test: Spearman correlation coefficient (R). $R > 0$: direct correlation. $R < 0$ inverse correlation. I:inverse, D:direct. Adj. p-v= adjusted p-value.

Gene	Varambally		Tomlins		TCGA		Taylor		Lapointe		Kumar		Grasso		Gliinsky		Fraser		Corr.
	Adj. p-v	R	Adj. p-v	R	Adj. p-v	R	Adj. p-v	R	Adj. p-v	R	Adj. p-v	R	Adj. p-v	R	Adj. p-v	R	Adj. p-v	R	
AMX2	0.895	0.607	N/A	N/A	0.000	0.501	0.007	0.272	0.159	0.659	0.936	0.117	0.069	0.518	0.078	0.200	0.049	0.292	D
FST	0.990	-0.107	0.271	0.446	0.000	0.566	0.000	0.346	0.159	0.665	0.936	0.158	0.046	0.389	0.315	0.114	0.016	0.358	D
GSTP1	0.895	0.321	0.491	0.296	0.000	0.672	0.000	0.386	0.577	0.324	0.936	0.235	0.001	0.619	0.013	0.280	0.035	0.312	D
KRT14	0.895	-0.357	0.558	0.219	0.000	0.512	0.000	0.511	N/A	N/A	0.936	-0.195	0.009	0.482	0.023	0.257	0.004	0.460	D
TNC	0.895	0.286	0.271	0.398	0.000	0.518	0.017	0.241	0.779	0.227	0.916	-0.251	0.452	-0.203	0.035	0.238	0.011	0.392	D
BZW2	0.895	0.429	N/A	N/A	0.000	-0.290	0.001	-0.327	N/A	N/A	0.938	0.107	0.111	-0.311	0.446	-0.087	0.006	-0.419	I
CNPY2	0.895	-0.857	0.529	0.271	0.000	-0.433	0.000	-0.433	0.943	0.077	0.930	-0.246	0.933	-0.037	0.002	-0.343	0.021	-0.341	I
GARS	0.975	0.179	0.894	0.057	0.000	-0.558	0.003	-0.292	0.683	0.242	0.938	0.107	0.069	-0.361	0.016	-0.270	0.006	-0.424	I
GNB2	0.895	-0.821	0.537	0.242	0.000	-0.373	0.000	-0.390	0.826	0.165	0.885	0.325	0.025	-0.423	0.001	-0.372	0.015	-0.364	I
HSPD1	0.990	-0.071	N/A	N/A	0.000	-0.552	0.006	-0.279	N/A	N/A	0.936	0.124	0.436	-0.163	0.028	-0.247	0.014	-0.368	I
MDH2	0.990	-0.071	N/A	N/A	0.000	-0.452	0.000	-0.448	0.470	0.379	0.936	0.226	0.016	-0.457	0.019	-0.264	0.020	-0.346	I
NME2	N/A	N/A	N/A	N/A	0.000	-0.393	0.000	-0.487	N/A	N/A	0.985	-0.012	0.008	-0.488	N/A	N/A	N/A	N/A	I
PGLS	0.895	0.393	N/A	N/A	0.000	-0.384	0.002	-0.306	0.159	-0.692	0.936	0.193	0.003	-0.561	0.267	-0.126	0.016	-0.358	I
ALDOC	0.975	-0.143	0.750	0.120	0.000	0.302	0.000	0.396	N/A	N/A	0.936	0.121	0.072	0.351	0.636	-0.054	0.114	0.235	D
ATP1B1	0.895	0.429	N/A	N/A	0.000	0.486	0.036	0.213	0.943	-0.071	0.885	0.398	0.069	0.358	0.725	0.040	0.109	0.239	D
CS	0.990	-0.071	N/A	N/A	0.000	-0.367	0.000	-0.396	0.382	0.473	0.985	-0.037	0.006	-0.516	0.540	-0.070	0.013	-0.373	I
FGFP1	0.975	0.214	0.750	-0.152	0.000	0.453	0.018	0.239	N/A	N/A	0.885	-0.294	0.087	0.330	0.058	-0.214	0.035	0.311	D
KRT16	0.975	0.179	N/A	N/A	0.000	0.391	0.000	0.429	0.683	-0.247	0.885	-0.449	0.053	0.381	0.936	-0.009	0.006	0.416	D
NTN4	0.975	0.214	0.056	0.602	0.000	0.563	0.010	0.257	0.569	0.330	0.936	-0.121	0.077	0.343	N/A	N/A	0.118	0.230	D
SERPINB5	0.895	0.571	N/A	N/A	0.000	0.587	0.000	0.551	0.298	0.533	0.885	-0.551	0.084	0.618	0.381	0.100	0.006	0.443	D

From this list of genes, *BZW2*, *CNPY2*, *GNB2*, *ALDOC*, *ATP1B1* and *NTN4* followed the same trend as in the proteomics data of the cell secretome in terms of being up or downregulated based on the status of *PGC1α* (**FigR 42**).

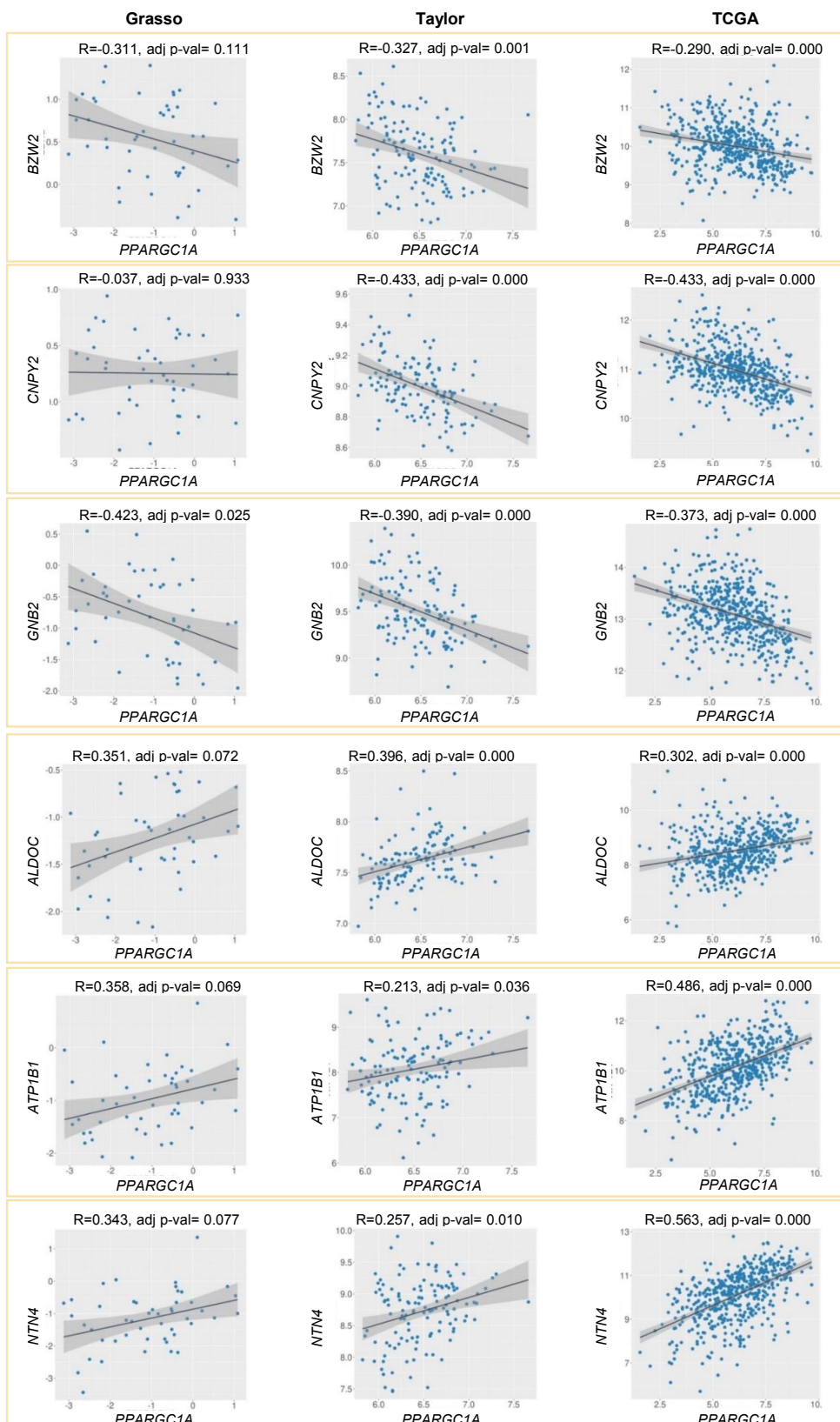


Figure R 42. Analyses of the genes found correlated to PGC1A in Pca datasets. For each gene, Grasso, Taylor, and TCGA, analyses are shown. Each dot corresponds to a patient, and expression values correspond to log2 normalized mRNA levels of each gene in X and Y axis. Black line represents the linear regression, and the grey area limits the intervals of confidence. Statistic test: Spearman correlation

coefficient (R). Adj. p-val= adjusted p-value. Statistic test: Spearman correlation coefficient (R). Adj. p-val= adjusted p-value.

Of note, as mentioned earlier, two of the proteins found deregulated in the TIL (Atp1b1 and Srm) were common to the proteins found differentially present in the proteomics of the cell secretome and followed the same direction in terms of being increased or decreased. As shown above, *ATP1B1* directly correlates with *PGC1A* in PCa patients' data. In addition, *ATP1B1* is part of a gene signature that predicts recurrence in PCa (Torrano, Valcarcel-Jimenez, et al. 2016). Yet, results showed no correlation consistency between *SRM* and *PGC1A*, although most of the datasets tilted towards an inverse correlation (1 out of 9 direct significant correlation and 4 out of 9 inverse significant correlations) (**FigR 43**).

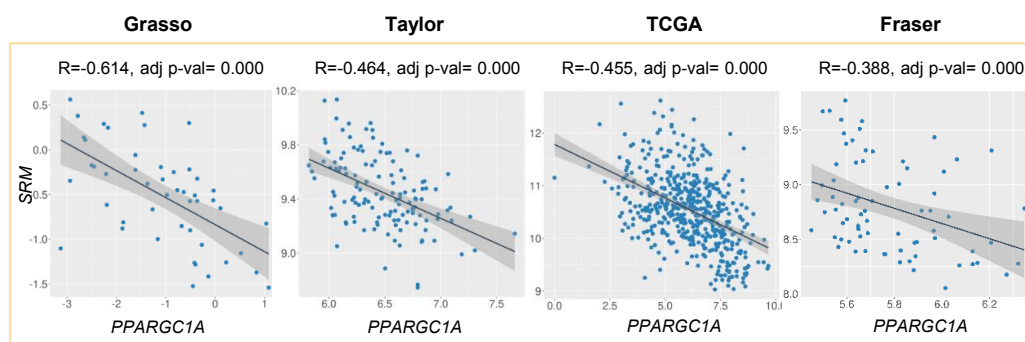


Figure R 43. Correlation analysis in PCa datasets shows no relation between *PGC1A* and *SRM*. Only Grasso, Taylor, and TCGA and Fraser correlations are shown. Each dot corresponds to a patient, and expression values correspond to log2 normalized mRNA levels of each gene in X and Y axis. Black line represents the linear regression, and the grey area limits the intervals of confidence. Statistic test: Spearman correlation coefficient (R). Adj. p-val= adjusted p-value. Statistic test: Spearman correlation coefficient (R). Adj. p-val= adjusted p-value

Overall, LC-MS proteomics analysis revealed a cell secretome composition that is transcriptional and intrinsically governed by the axis *PGC1α-ERRα*, thus displaying a different protein content in the secretome produced by *PGC1α*-expressing and non-expressing PCa cell lines. Cancertool-based enrichment analysis unveiled that among the upregulated and downregulated candidates, functions linked to metabolism were enhanced in the secretomes produced by *PGC1α*-expressing PC3 cells. Nonetheless, novel functions linked to cell surface and cytoskeleton proteins as well as RNA binding processes were enriched, especially among the downregulated proteins identified in the secretomes produced by cells expressing *PGC1α*. In addition, secretome purity was confirmed and interrogation of some of the candidates by RT-qPCR analysis in the producer cell lines revealed that most of them were tightly regulated by the *PGC1α-ERRα* transcriptional axis. In addition, we observed that as it happened with the expression of *PGC1α*, deletion of *c-MYC* triggered the downregulation of *YBX1*, thus suggesting a *PGC1α*-mediated transcriptional regulation of this gene, mediated by the oncogene *c-MYC*.

Finally, proteomics analysis revealed a differential protein composition of the TILs obtained from KO and DKO mice, including some candidates that were common to the ones identified in the proteomics analysis of the cell secretome.

III.3 Molecular events triggered upon treatment of PCa recipient cells with the differential secretomes

III.3.1 RNA sequencing analysis of PCa recipient cell lines

Having previously shown the anti-proliferative role of the secretome driven by the metabolic regulator PGC1 α , naturally, the question about the molecular events triggered in those cells that receive this secretome rose. We therefore focused our studies on understanding the *in vitro* anti-proliferative molecular cues activated on PCa recipient cell lines upon treatment with the distinct cell secretomes. Based in the central dogma of molecular biology stating that information harbored in the genes is transcribed from DNA to RNA (Crick FH 1958), we next performed an RNA sequencing experiment in which, we hypothesized that treatment of PCa recipient cells with the differential secretomes would render information about altered genes and their correspondent pathways. Although our data shows that the reduction in proliferation of recipient cells becomes evident after, at least, five days of treatment with the differential secretomes, RNA sequencing analysis was performed on PC3 recipient cells treated throughout 48 hours with the distinct secretomes. This decision aimed at having a clean system for detecting early molecular events activated in the recipient cells upon treatment with the differential secretomes, and that could explain the anti-proliferative effects observed at later time-points. Thus, differential secretomes obtained from PGC1 α -expressing and non-expressing PC3 producer cells were used to treat PC3 recipient cell lines for a 48-hour period, time after which, samples were collected and subjected to RNA sequencing analysis (**FigR 44**).

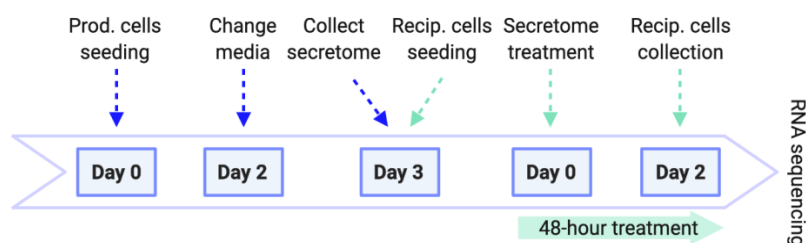


Figure R 44. Overview of the experimental setting followed for performing RNA sequencing analysis of PC3 recipient cells treated with differential secretomes.

First, we performed a PCA that revealed no differences between both groups in sample clustering when filtering the results by establishing an adjusted p-value of 0.05 (**FigR 45A**). We therefore changed strategy and removed outlier samples (S_05 and S_06) which, led to the separation of the samples in two clusters (on one side S_01 and S_03, on the other side S_02 and S_04) (**FigR 45B**). Data was then reanalyzed establishing a p-value smaller than 0.0015 as

filtering criteria, whilst bearing in mind that only two samples per condition were included for these analyses. Based on the expression pattern, genes were gathered in a heatmap that allowed us to observe at a first glance groups of genes differentially expressed in PC3 cells treated with secretomes coming from producer cells with or without expression of PGC1 α (**FigR 45C**).

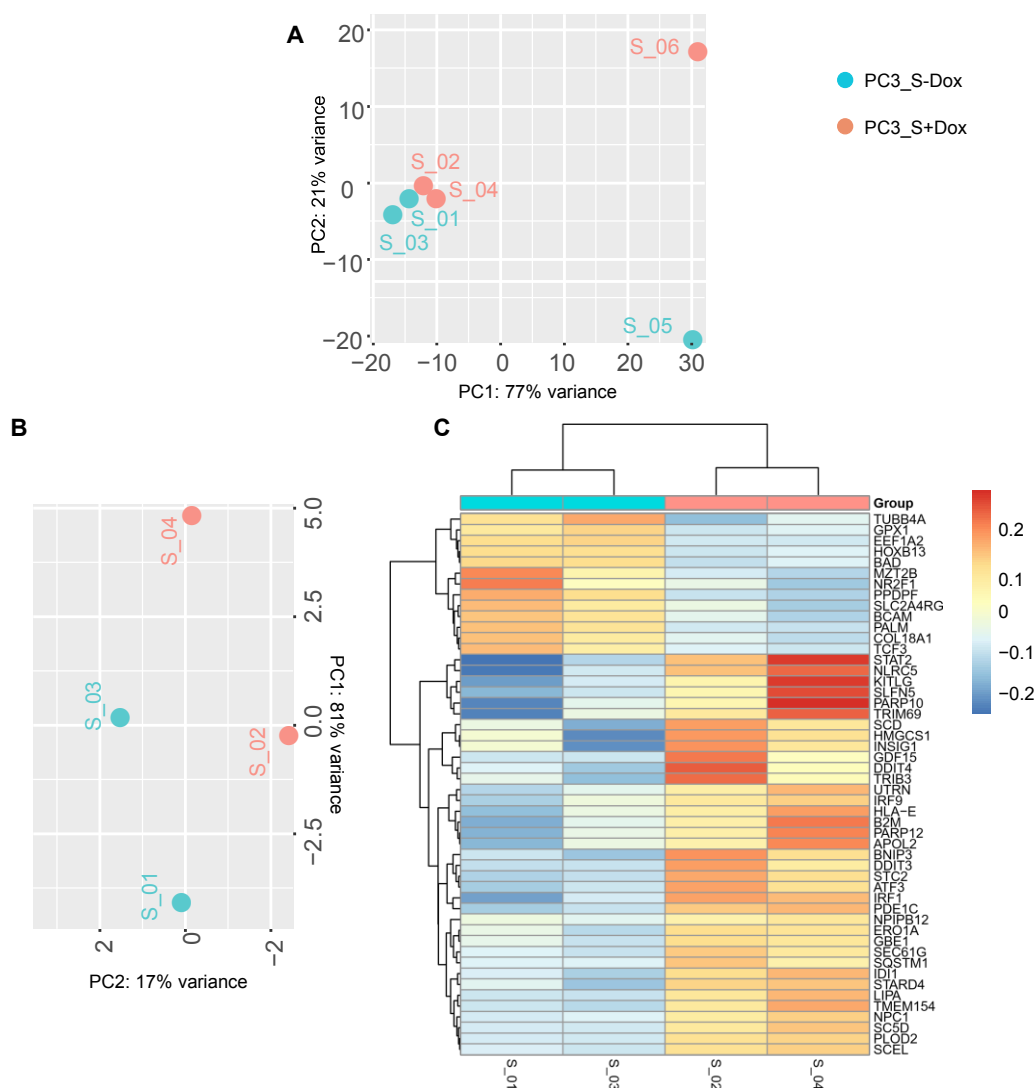


Figure R 45. PCA from the RNA sequencing analysis performed on PC3 recipient cells treated with differential secretomes. A. PCA of the RNA sequencing data from PC3 recipient cells ($n=3/$ condition). **B.** PCA of the RNA sequencing data from PC3 recipient cells after removal of outlier samples ($n=2/$ condition). **C.** Heatmap displaying the clusters of genes differentially expressed in PC3 cell lines treated with the distinct secretomes ($n=2/$ condition). Analysis of DESeq2 platform is shown. PC3_S-Dox: PC3 recipient cells treated with secretomes obtained from non-PGC1 α expressing cells (blue). PC3_S+Dox: PC3 recipient cells treated with secretomes obtained from PGC1 α -expressing (red). Sample IDs can be found next to each colored dot (A and B) and in the bottom of the heatmap (C). PC: principal component. In A, p -value <0.05 , In B and C p -value <0.0015 .

Supervised clustering of the RNA sequencing data was done using DESeq2 (Anders and Huber 2010), although, EdgeR (M. D. Robinson, McCarthy, and Smyth 2009) and LimmaVoom (Ritchie et al. 2015) were also considered as control, displaying these platforms the same list of genes than the ones found differentially expressed using DESeq2 (**FigR 46A**). DESeq2 included a wider number of genes than the other two platforms used, and therefore was considered for further analysis of the data, which displayed five top-upregulated candidates in recipient cells treated with secretomes obtained from PGC1 α -expressing PCa cells (**FigR 46B**).

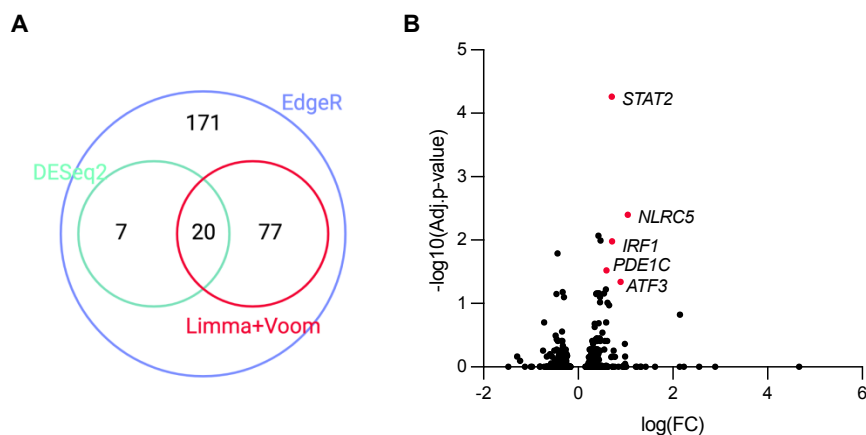


Figure R 46. Analysis of the RNA sequencing performed on PC3 cells treated with differential secretomes. **A.** Venn diagram shows the differentially expressed genes identified by analyzing the data with three different platforms (DESeq2, EdgeR and LimmaVoom). **B.** Volcano plot displays differentially expressed genes in PC3 cells treated with the differential secretomes. In B, genes with a p -value < 0.05 are included. Genes represented in red are filtered through an adj. p -value < 0.05 and a $FC > 1.5$. FC: fold change.

With the aim of obtaining a broader view of the molecular events altered in our system, we established the following cut-offs for the analysis: differences in genes expression must be higher than 1.5-fold-changes and lower than 0.5 between control and experimental samples, in both cases with a p -value lower than 0.0015. The analysis of the data revealed a list of 55 genes differentially expressed in PC3 cells treated with the distinct secretomes (**Table R5**). Thirteen of these genes happened to be downregulated and 42 upregulated in the PC3 cells that were grown with the secretomes produced by PGC1 α -expressing PCa cells compared to the non-PGC1 α expressing ones. Interestingly, two candidates (*FGFBP1* and *GBE*) identified by RNA sequencing of the recipient cells were also found in the proteomics analysis of the cell secretome.

Table R 5. Genes found differentially expressed by RNA sequencing analysis of PC3 recipient cell lines treated with distinct secretomes for 48 hours. Uncolored rows include the downregulated candidates, whereas pink-colored rows stem for genes found upregulated. A p -value <0.0015 and fold change higher than 1.5-fold and lower than 0.5-fold are established as cut-off. FC: fold change.

Ensembl	Symbol	FC	p value	Name
ENSG00000099864	PALM	-1,649	0,0003	Paralemin
ENSG00000152082	MZT2B	-1,393	0,0005	Mitotic-spindle organizing protein 2B
ENSG00000104833	TUBB4A	-1,379	0,0001	Tubulin beta 4A class IVa
ENSG00000002330	BAD	-1,370	0,0007	BCL2 associated agonist of cell death
ENSG00000125534	PPDPF	-1,357	0,00001	Pancreatic progenitor cell differentiation and proliferation factor
ENSG00000187244	BCAM	-1,352	0,0009	Basal cell adhesion molecule
ENSG00000125520	SLC2A4RG	-1,280	0,0008	SLC2A4 regulator
ENSG00000175745	NR2F1	-1,272	0,0014	Nuclear receptor subfamily 2 group F member 1
ENSG00000182871	COL18A1	-1,266	0,0004	Collagen type XVIII alpha 1 chain
ENSG00000071564	TCF3	-1,265	0,0009	Transcription factor E2-alpha
ENSG00000101210	EEF1A2	-1,257	0,0000	Eukaryotic translation elongation factor 1 alpha 2
ENSG00000233276	GPX1	-1,255	0,0011	Glutathione peroxidase 1
ENSG00000159184	HOXB13	-1,235	0,0001	Homeobox B13
ENSG00000134294	SLC38A2	1,180	0,0015	Solute carrier family 38 member 2
ENSG00000161011	SQSTM1	1,208	0,0014	Sequestosome 1
ENSG00000141458	NPC1	1,226	0,0008	NPC intracellular cholesterol transporter 1
ENSG00000114480	GBE1	1,232	0,0014	1,4-alpha-glucan branching enzyme 1
ENSG00000197930	ERO1A	1,243	0,0010	Endoplasmic reticulum oxidoreductase 1 alpha
ENSG00000109929	SC5D	1,269	0,0003	Sterol-C5-desaturase
ENSG00000152952	PLOD2	1,272	0,0003	Procollagen-lysine,2-oxoglutarate 5-dioxygenase 2
ENSG00000052802	MSMO1	1,281	0,0015	Methylsterol monooxygenase 1
ENSG00000152818	UTRN	1,281	0,0009	Utrophin
ENSG00000171451	DSEL	1,287	0,0015	Dermatan sulfate epimerase like
ENSG00000132432	SEC61G	1,289	0,0007	SEC61 translocon subunit gamma
ENSG00000107798	LIPA	1,299	0,0001	Lipase A, lysosomal acid type
ENSG00000099194	SCD	1,307	0,0000	Stearoyl-CoA desaturase
ENSG00000204592	HLA-E	1,309	0,0006	Major histocompatibility complex, class I, E
ENSG00000130513	GDF15	1,311	0,0013	Growth differentiation factor 15
ENSG00000101255	TRIB3	1,324	0,0009	Tribbles pseudokinase 3

ENSG00000137440	FGFBP1	1,326	0,0016	Fibroblast growth factor binding protein 1
ENSG00000166710	B2M	1,336	0,0001	Beta-2-microglobulin
ENSG00000113739	STC2	1,341	0,0000	Stanniocalcin 2
ENSG00000112972	HMGCS1	1,346	0,0003	3-hydroxy-3-methylglutaryl-CoA synthase 1
ENSG00000067064	IDI1	1,360	0,0001	Isopentenyl-diphosphate delta isomerase 1
ENSG00000186480	INSIG1	1,370	0,0006	Insulin induced gene 1
ENSG00000164211	STARD4	1,373	0,0001	StAR related lipid transfer domain containing 4
ENSG00000170006	TMEM154	1,375	0,0001	Transmembrane protein 154
ENSG00000136155	SCEL	1,379	0,0008	Sciellin
ENSG00000176171	BNIP3	1,385	0,0000	BCL2 interacting protein 3
ENSG00000059378	PARP12	1,424	0,0004	Poly(ADP-ribose) polymerase family member 12
ENSG00000166750	SLFN5	1,459	0,0000	Schlafen family member 5
ENSG00000095951	HIVEP1	1,464	0,0015	HIVEP zinc finger 1
ENSG00000128335	APOL2	1,477	0,0009	Apolipoprotein L2
ENSG00000049130	KITLG	1,495	0,00003	KIT ligand
ENSG00000175197	DDIT3	1,505	0,0002	DNA damage inducible transcript 3
ENSG00000154678	PDE1C	1,511	0,0000	Phosphodiesterase 1C
ENSG00000168209	DDIT4	1,529	0,0008	DNA damage inducible transcript 4
ENSG00000178685	PARP10	1,533	0,0001	Protein mono-ADP-ribosyltransferase PARP10
ENSG00000185880	TRIM69	1,572	0,0001	E3 ubiquitin-protein ligase TRIM69
ENSG00000170581	STAT2	1,634	0,00000	Signal transducer and activator of transcription 2
ENSG00000125347	IRF1	1,638	0,00000	Interferon regulatory factor 1
ENSG00000162772	ATF3	1,856	0,00002	Activating transcription factor 3
ENSG00000213928	IRF9	1,978	0,0010	Interferon regulatory factor 9
ENSG00000140853	NLRCS	2,061	0,00000	NLR family CARD domain containing 5
ENSG00000169203	NPIP12	4,428	0,0002	Nuclear pore complex interacting protein family member B12

To have an overview of the molecular processes associated with the genes differentially expressed (p -value < 0.0015 cut-off) by the PC3 recipient cells treated with the differential secretomes, we performed a Cancertool-based enrichment analysis (Cortazar et al. 2018). Pathway enrichment analysis revealed an enhancement of processes linked with the immune system that were also accompanied by an enrichment of lipid metabolism pathways (**FigR 47A**). In the same sense, GO biological process analysis showed enrichment on metabolic functions, mainly related to lipids. On the other hand, immune system processes specially related to interferon (flagged with orange stars) and cell death-related (yellow stars) biological functions

happened to be enriched in the PC3 cells treated with secretomes derived from PGC1 α -expressing producer cells (**FigR 47B** and **Table R6**).

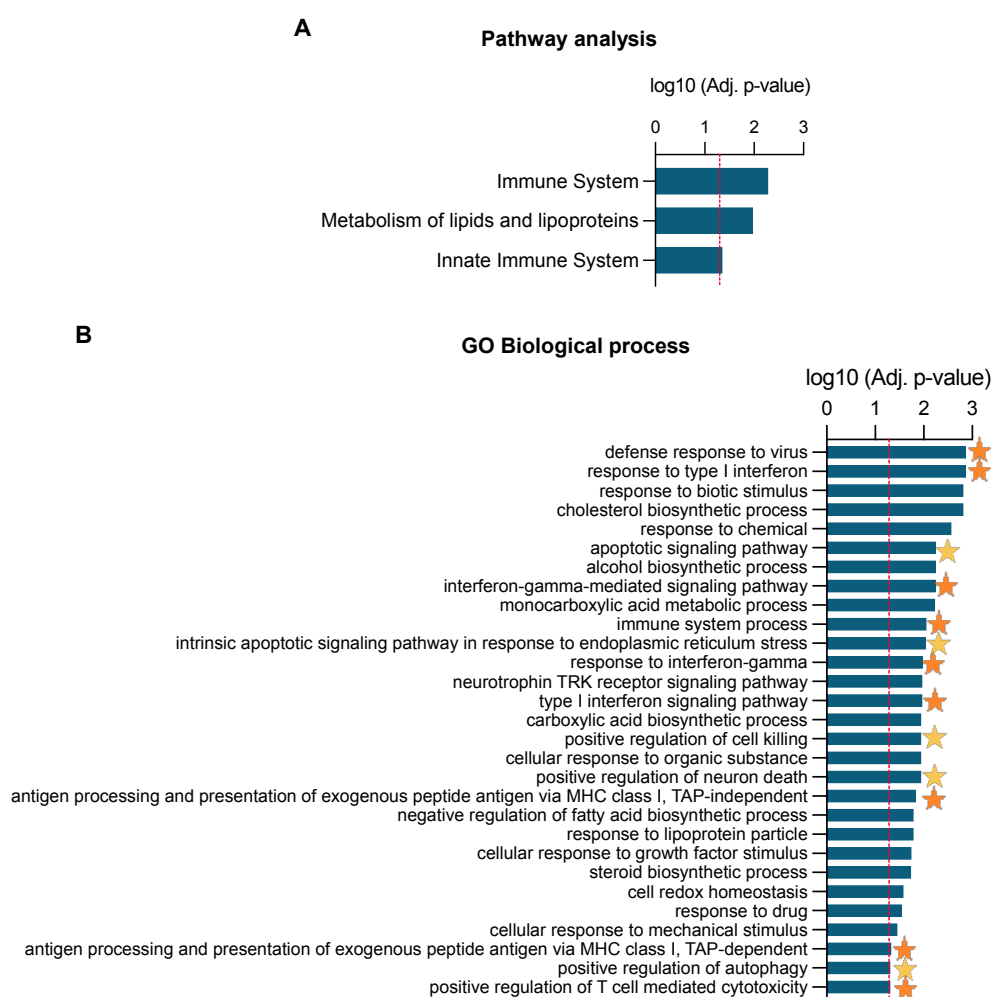


Figure R 47. Pathway and GO biological process analyses of the genes found altered in recipient cells reveal an enrichment of functions linked to metabolism, immune system and cell death. A. Pathway analysis. B. GO biological process The red dotted lines indicate $p=0.05$, $p=p$ -value.

Table R 6. Genes found enriched in the GO biological process analysis.

Term	Genes
defense response to virus	B2M, BNIP3, IRF1, STAT2, IRF9, DDIT4, NLRC5
response to type I interferon	HLA-E, IRF1, STAT2, IRF9, NLRC5
apoptotic signaling pathway	DDIT3, KITLG, SQSTM1, ERO1L, DDIT4, TRIB3
interferon-gamma-mediated signaling pathway	B2M, HLA-E, IRF1, IRF9
immune system process	BNIP3, GPX1, PDE1C, STAT2, SQSTM1, IRF9, DDIT4, TRIB3, NLRC5
intrinsic apoptotic signaling pathway in response to endoplasmic reticulum stress	DDIT3, ERO1L, TRIB3
response to interferon-gamma	B2M, HLA-E, IRF1, IRF9
neurotrophin TRK receptor signaling pathway	BAD, KITLG, PDE1C, SQSTM1, DDIT4, TRIB3
type I interferon signaling pathway	HLA-E, IRF1, IRF9
positive regulation of cell killing	B2M, BAD, HLA-E
positive regulation of neuron death	BAD, DDIT4
antigen processing and presentation of exogenous peptide antigen via MHC class I, TAP-independent	B2M, HLA-E
antigen processing and presentation of exogenous peptide antigen via MHC class I, TAP-dependent	B2M, HLA-E, SEC61G
positive regulation of autophagy	BAD, BNIP3
positive regulation of T cell mediated cytotoxicity	B2M, HLA-E

Finally, transcription factor analysis revealed a high presence of TFs linked to interferon signaling such as *STAT3*, *IRF7*, *IRF1*, *NFkB* and *STAT6* (FigR 48).

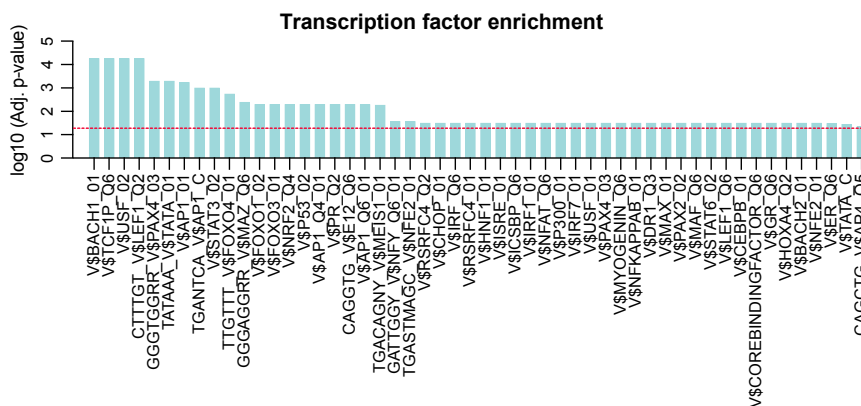


Figure R 48. Transcription factor enrichment analysis of the genes found altered in recipient cells by RNA sequencing analysis. The red dotted lines indicate p=0.05, p=p-value.

III.3.1.1 Validation of RNA sequencing candidates in PCa recipient cell lines

Next step was performing RT-qPCR analysis on the PC3 recipient cells subjected to the RNA sequencing with the aim of validating some of the dysregulated candidates. For these validations, in order to assess ERRα-mediated transcriptional control, we additionally included four groups of recipient cells treated with secretomes produced by PGC1α-expressing and non-

expressing cells in combination with $ERR\alpha$ deletion. We first checked gene expression levels of type I interferon-related candidates found upregulated in PC3 cells upon treatment with secretome obtained from $PGC1\alpha$ -expressing cell lines (**FigR 49**).

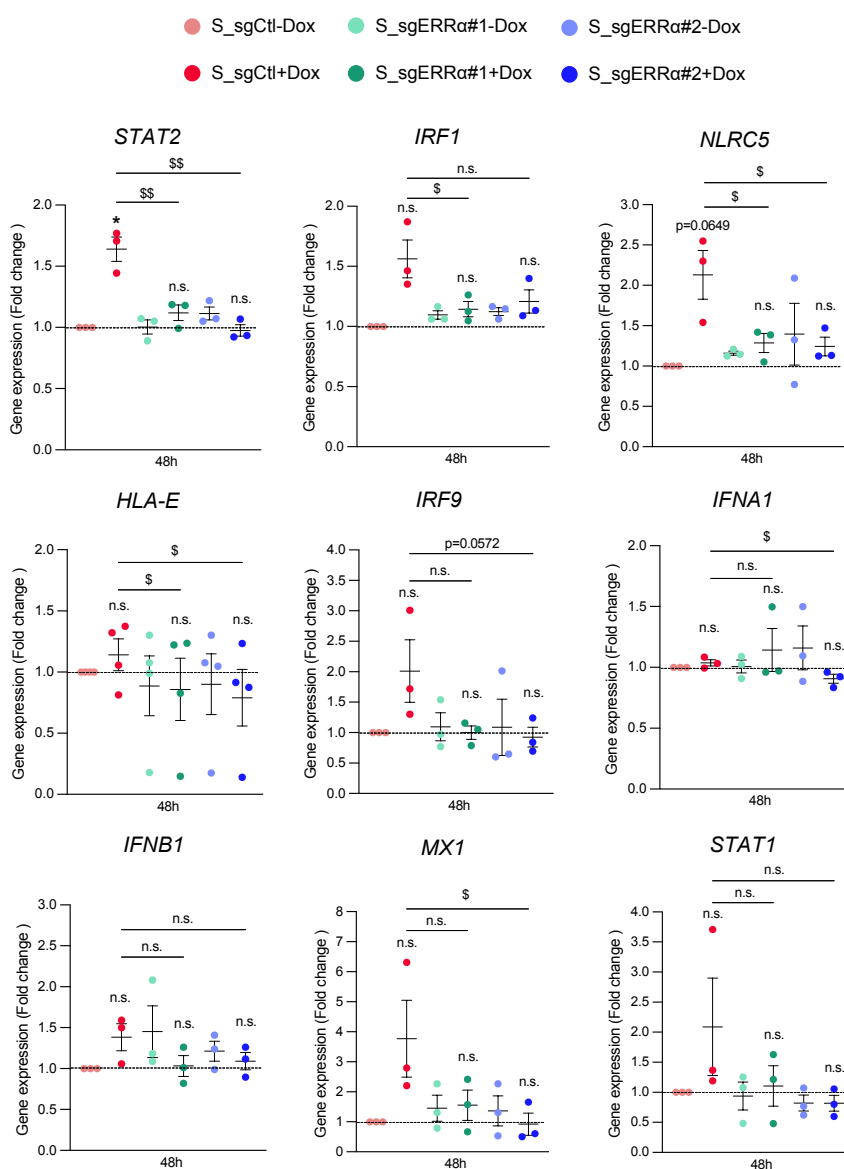


Figure R 49. RT-qPCR analysis of genes found altered by RNA sequencing analysis of recipient cells. Gene expression levels of *STAT2*, *IRF1*, *NLRC5*, *HLA-E*, *IRF9*, *IFNA1*, *IFNB1*, *MX1* and *STAT1* in PC3 recipient cell lines treated with secretomes derived from cells with combined expression of $PGC1\alpha$ and deletion of $ERR\alpha$ for a 48-hour period ($n=3-4$). Dox: doxycycline. Data is normalized to the *S_sgCtl-Dox* condition, depicted by a black dotted line. Statistical analysis: One sample *t*-test establishing 1 as hypothetical value. Unpaired parametric one-tail *t*-test. Asterisks indicate statistical differences between *S_sgCtl-Dox* and the rest of the conditions and the dollar symbol indicates the statistical differences between *S_sgCtl+Dox* and *S_sgERRα#1+Dox*/*S_sgERRα#2+Dox*. *p*, *p*-value. */ $\$p < 0.05$, $\$\$p < 0.01$. n.s.=not significant. Error bars indicate s.e.m.

All candidates interrogated (*STAT2*, *IRF1*, *NLRC5*, *HLA-E* and *IRF9*) showed to be upregulated in PC3 cells treated with secretome produced in the presence of both PGC1 α and ERR α . Overall, all these genes reflected a trend towards an ERR α -mediated effect on regulating the secretome composition that consequently led to the activation of different cell-intrinsic pathways in the recipient cell lines. Additionally, although not identified as RNA sequencing candidates, *IFNA1* and *IFNB1* genes were included in the RT-qPCR analysis due to their strong link as drivers of the type I IFN pathway activation. We found no *IFNA1* induction in any of the recipient cells conditions. On the other hand, *IFNB1* gene expression levels showed to be slightly increased in the recipient cells treated with secretomes produced by cells with an activated PGC1 α -ERR α transcriptional axis. Both, *IFNA1* and *IFNB1* showed no clear dependence on ERR α . (**FigR 49**). *MX1* and *STAT1*, candidates identified upregulated in the cell secretome proteomics analysis as well as cell-intrinsically in the producer cell lines, were also tested in the recipient cells. Both candidates are known to be induced by type I IFNs (Medrano et al. 2017b) and we observed a trend towards being increased in recipient cells treated with secretomes derived from PGC1 α -ERR α positive cells. No major changes in *MX1* and *STAT1* expression levels were observed in the conditions where ERR α was ablated (**FigR 49**).

Then, following with the validation of RNA sequencing candidates, we did also check by RT-qPCR expression levels of genes related to ER stress, and cell death processes. Interestingly, both type I IFN response and ER stress are tightly connected: ER stress regulates type I IFNs production and on the other hand, ER stress can be induced by type I IFNs (Sprooten and Garg 2020). Of note, only two experiments were included for the analysis of gene expression levels of *ATF3*, *DDIT4*, *ERO1A* and *PDE1C* as the outlier experiment that was removed for the final analysis of the RNA sequencing data was also excluded for all the RT-qPCR analyses that were performed. Therefore, this data still needs to be completed with additional experiments (**FigR 50**).

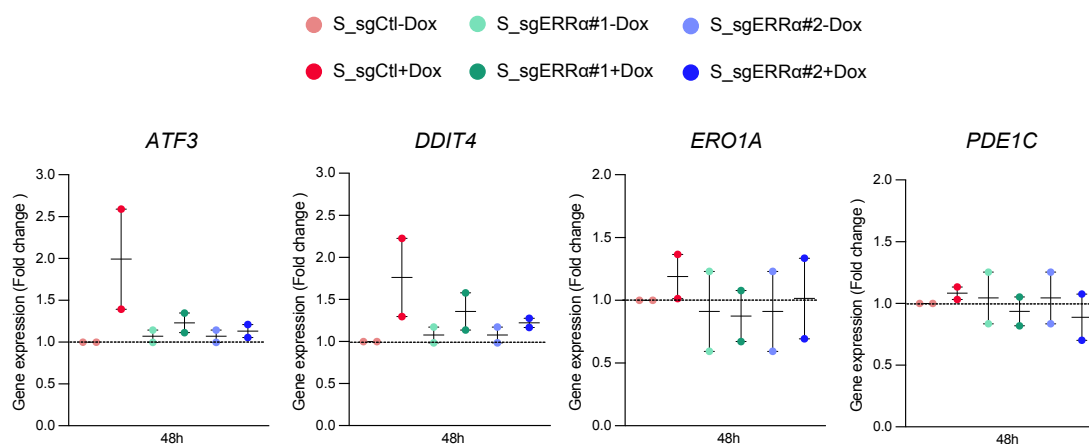


Figure R 50. RT-qPCR analysis of genes found altered by RNA sequencing analysis of recipient cells. *ATF3*, *DDIT4*, *ERO1A* and *PDE1C* gene expression levels in PC3 recipient cell lines treated with secretomes derived from cells with combined expression of PGC1 α and deletion of ERR α for a 48-hour period are assessed ($n=2$). Dox: doxycycline. Data is normalized to the S_sgCtl-Dox condition, depicted by a dotted line. Error bars indicate s.e.m.

Finally, some of our genes of interest were interrogated in PC3 cells that had undergone secretome treatments for a period of seven days, time after which, secretomes' biological effect on *in vitro* 2D proliferation is evident. We assessed gene expression levels by RT-qPCR and found that none of the genes displayed differences in PC3 recipient cells treated with any of the six different types of secretomes, suggesting an early onset of the molecular mechanisms triggered upon treatment with the differential secretomes (**FigR 51**). This data made also evident the importance of using adequate and controlled systems for the study of molecular biology.

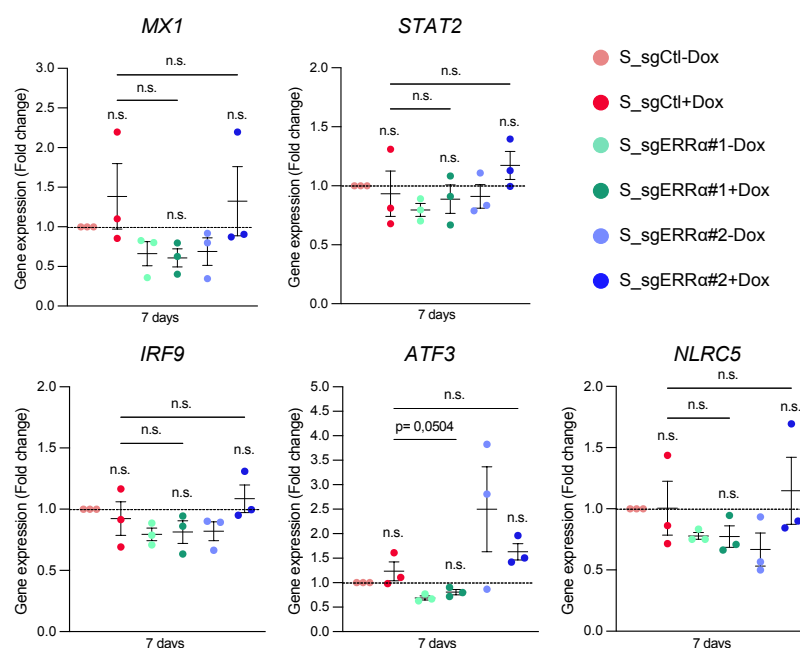


Figure R 51. Gene expression levels of candidates found altered by RNA sequencing analysis of recipient cells assessed at later secretome treatment time-points. MX1, STAT1, IRF9, ATF3 and NLRC5 gene expression levels in PC3 recipient cell lines treated with secretomes derived from cells with combined expression of PGC1 α and deletion of ERR α for a 7-day period are assessed (n=3). Data is normalized to the S_sgCtl-Dox condition, depicted by a black dotted line. Statistical analysis: One sample t-test establishing 1 as hypothetical value. Unpaired parametric one-tail t-test. p, p-value. n.s.=not significant. Error bars indicate s.e.m.

Overall, we can consider that our PCa model driven by the metabolic regulator PGC1 α nicely demonstrates how the secretome composition is transcriptionally regulated by cell-intrinsic molecular events within the producer cell lines. We therefore could suggest that the secretome reflects the status of the cell that produces it. At the same time, the way the cell secretome affects recipient cells is subjected to its composition, thus evidencing how the transcriptional control that governs tumor cells' intrinsic events goes beyond the cell itself and impacts on the surrounding ones.

Overview

- The SFs fraction of the cell secretome produced by PGC1 α -expressing PCa cell lines has an *in vitro* non-cell autonomous antiproliferative effect on PCa recipient cell lines.
- The *in vivo* metastasis assay showed an increased tumor cell nesting and growth on those mice that were challenged with SFs derived from PGC1 α -expressing PCa cell lines compared to the mice that were treated with SFs derived from non-PGC1 α expressing PCa cell lines. Together, *in vitro* and *in vivo* data suggest a complex and variable role of the SFs along PCa progression and dependent on the cell compartment studied.
- Short time secretome production in the absence of serum is key for the obtention of reliable secretomes for performing proteomics analysis.
- Proteomics analysis of the whole cell secretome evidenced a PGC1 α -dependent regulation of the secretome composition, identifying a total number of 185 proteins differentially present on the secretomes produced by PGC1 α -expressing and non-expressing PCa cell lines
- Enrichment analysis performed with the genes coding for the proteins found differentially present in the proteomics analysis revealed an enrichment of metabolic functions and ERR α -mediated transcriptional regulation of the upregulated candidates. On the other hand, downregulated candidates were linked to cell surface and cytoskeleton proteins as well as RNA binding processes, rising MYC/MAZ/MAX as potential transcriptional regulator.
- Candidates identified in the proteomics analysis of the secretome were cell-intrinsically interrogated by RT-qPCR in the producer cell lines, revealing that all of them were transcriptionally regulated by PGC1 α . Moreover, most of the candidates analyzed showed to be under the control of the PGC1 α -ERR α transcriptional axis. Transcriptional control of *YBX1* seems to be under the influence of *c-MYC*.
- Proteomics analysis of the TIL obtained from KO and DKO mice displayed a panel of 44 proteins differentially present. Among these proteins, three (*Atp1b1*, *Ak1* and *Srm*) were common to the proteins identified in the *in vitro* cell secretome proteomics analysis.
- The genes encoding for twenty of the candidates identified by proteomics analysis of the secretome were shown to be directly or inversely correlated to *PGC1A* in PCa patients' datasets. Seven genes (*BZW2*, *CNPY2*, *GARS*, *GNB2*, *ALDOC*, *ATP1B1* and *NTN4*) followed the same trend (upregulated or downregulated upon expression of PGC1 α) as observed in *in vitro* data



- RNA sequencing analysis of the PC3 recipient cells treated for 48 hours with secretomes obtained from PGC1 α -expressing and non-expressing cell lines, identified 55 genes differentially expressed between both conditions. Functions associated to lipid metabolism, immune system processes related to interferon response together with cell death processes were enriched in the recipient cells treated with the secretome produced by PGC1 α -expressing cells.
- RT-qPCR analysis of the PC3 recipient cells revealed that most of the RNA sequencing candidates tested (*STAT2*, *IRF1*, *NLRC5*, *HLA-E* and *IRF9*) were upregulated on the conditions where cells had been treated with secretomes produced by cells with an activated PGC1 α -ERR α transcriptional axis. Overall, these genes showed a trend towards being transcriptionally regulated by ERR α .
- RT-qPCR analyses performed on PC3 recipient cells treated for seven-day periods showed no changes in gene expression levels, suggesting an early onset of the molecular mechanisms that are triggered by the distinct secretomes.

IV To examine the cell-intrinsic molecular events triggered by PGC1 α in PCa producer cells that could mediate the effects of the secretome

We finally aimed at deeper exploring the cell-intrinsic molecular events that are associated with the extrinsic events that we have previously observed. The following hypothesis was proposed:

HYPOTHESIS

The cell-intrinsic transcriptional reprogramming induced by PGC1 α impacts on the secretome composition, which further drives the activation of molecular events in the cells in an autocrine and paracrine manner

As previously shown in the present thesis work, the effect of PGC1 α on the secretome composition seems to be directed by its cell-intrinsic transcriptional regulation. Indeed, *in vitro* proteomics analysis of the soluble factors and extracellular vesicles as well as the *in vivo* data obtained from the proteomics analysis of the TIL, demonstrated the presence of differential proteins that were conditioned by the presence of PGC1 α . Furthermore, most of these candidates found altered in the proteomics analyses were shown to be cell-intrinsically regulated at a transcriptional level by the PGC1 α -ERR α axis. Despite a microarray profiling of PGC1 α -expressing and non-expressing PC3 cells was previously done by the group, identifying 174 altered genes (Torrano, Valcarcel-Jimenez, et al. 2016), we realized that most of the candidates identified in the proteomics analysis of the cell secretome, and that were further examined cell-intrinsically at mRNA level in the producer cell lines, had not been detected in the mentioned microarray. We therefore decided to perform a more extensive study of the cells with differential expression of PGC1 α , and therefore conducted an RNA sequencing analysis. Compared to microarray hybridization, RNA sequencing technology allows a more sensitive detection of differentially expressed genes, especially the ones that have low expression levels (C. Wang et al. 2014), and we therefore expected to have a boarder view of the cell-intrinsic PGC1 α -driven transcriptional programs.

IV.1 Molecular cues activated in PCa producer cells upon expression of PGC1 α

Prior to the experiment seeding, PC3 producer cells were induced with doxycycline throughout three days, time after which, cells were counted and seeded refreshing the

doxycycline in the induced condition. Cells were then collected and processed for RNA sequencing analysis (**FigR 52**).

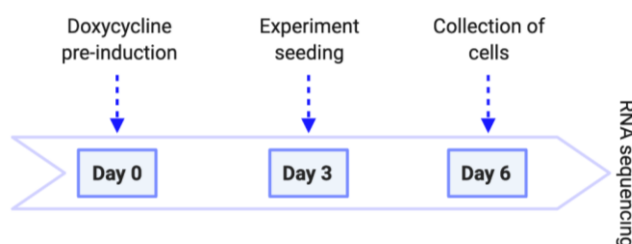


Figure R 52. Experimental overview of the steps followed for performing RNA sequencing of PGC1 α -expressing and non-expressing PCa cells.

PCA analysis nicely displayed two groups of samples: PGC1 α -expressing and non-PGC1 α expressing cells (**FigR 53A**). In the same way, the heatmap evidenced two well-differentiated clusters of genes differentially expressed between both conditions by establishing an adjusted p-value < 0.01 and a 2-fold change cut-off (**FigR 53B**).

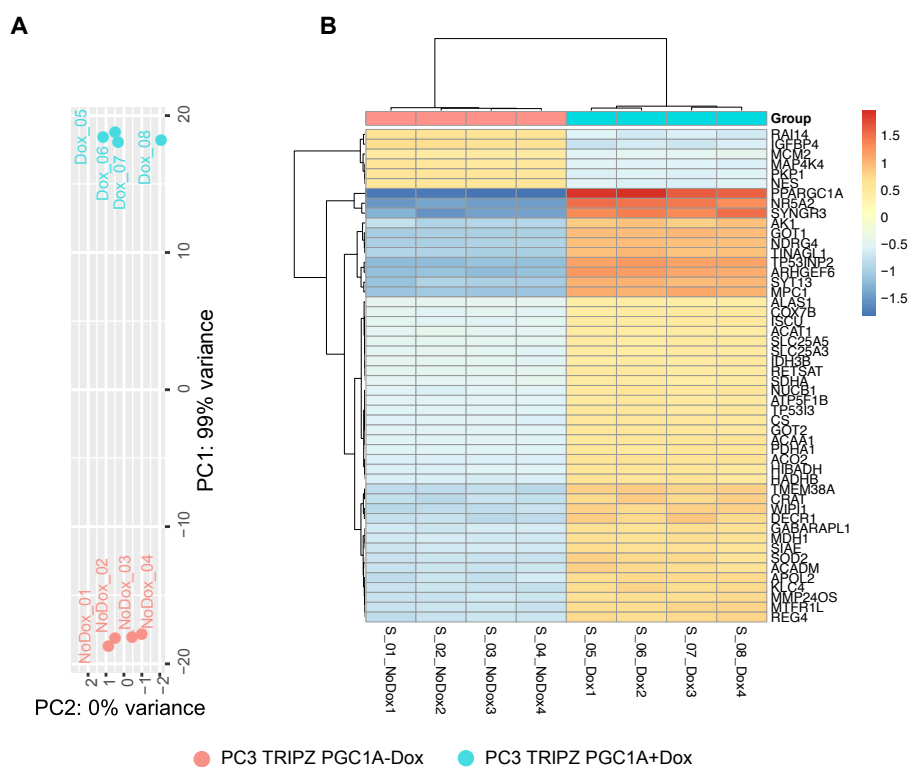


Figure R 53. PCA and heatmap displaying two clusters of samples and genes identified by RNA sequencing analysis of PGC1 α -expressing and non-expressing PCa cells. **A.** PCA of the RNA sequencing data from PGC1 α -expressing (blue) and non-expressing (red) PC3 cells ($n=4$ /condition). **B.** Heatmap displaying clusters of genes differentially expressed in PGC1 α -expressing and non-expressing cells. Sample ID can be found next to each colored dot and in the heatmap's bottom. Dox: doxycycline, PC: principal component. Adj.p-value<0.01 and FC=2 filters are applied.

We took advantage of DESeq2 analysis tool, which revealed a total number of 3747 differentially expressed genes between the PGC1 α -expressing and non-expressing PC3 cell lines (**FigR 54A**). We found 1130 of these genes downregulated and 2617 upregulated upon re-expression of PGC1 α (**FigR 54B** and **Annex Table 1**).

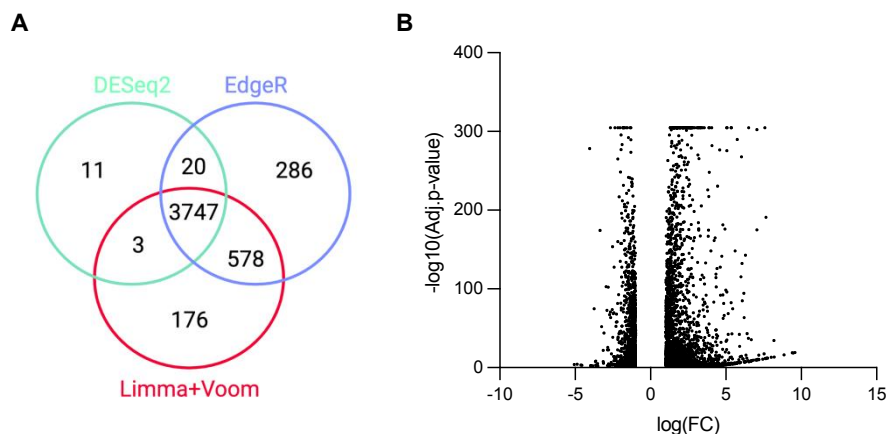


Figure R 54. Venn diagram and volcano plot of the RNA sequencing analysis performed on PGC1 α -expressing and non-expressing PC3 cells. **A.** Venn diagram shows a common number of 3747 differentially expressed genes identified by analyzing the data with three different platforms (DESeq2, EdgeR and LimmaVoom). **B.** Volcano plot displays downregulated and upregulated genes upon expression of PGC1 α in PC3 cells. Adj.p-value<0.01 and FC=2 filters are applied.

In order to get a wider view of the processes enhanced in the differentially expressed genes, we performed a Cancertool-based enrichment analysis (**FigR 55A-B**) that, in line with what was previously described by the group (Torrano, Valcarcel-Jimenez, et al. 2016), revealed a high number of enriched categories linked to metabolism, especially related to the mitochondria. In addition, several categories found, especially in the GO biological processes analysis, were related to ECM functions such as collagen deposition or degradation. Genes linked to these processes encoded for collagen fiber chains, matrix metalloproteinases as well as integrins. Accordingly, matricellular candidate *TNXB* gene expression levels were found downregulated. This was in line with the proteomics data and with the validations performed previously in producer cell lines. Of note, once again, type I IFN signaling rose as one of the top enriched processes (flagged with orange stars). Indeed, this matched with the idea of activation of functionalities between cells through their secretome as IFN-associated responses were also shown to be enriched in the cells receiving secretomes produced by PGC1 α -expressing cells (**FigR 47**).



Figure R 55. Gene ontology analysis displaying biological process and pathway enrichment from the genes found differentially expressed by RNA sequencing of PGC1 α -expressing and non-expressing PCa cells. A. Biological processes analysis shows an enrichment of functions linked to metabolism, ECM and to IFN signaling (orange stars). B. Pathway analysis displays enrichment in metabolism-associated processes and response to type I IFNs (orange stars). The red dotted lines indicate $p=0.05$. $p=p$ -value.

This data was corroborated with Gene Set Enrichment Analysis (GSEA), where type I IFN α (IFN α ; Normalized enrichment score=2.7137; Nominal p-value=0.000) and type II IFN γ (IFN γ ; Normalized enrichment score=2.5994; Nominal p-value=0.000) happened to be enhanced in the PGC1 α -expressing cells (**FigR 56**).

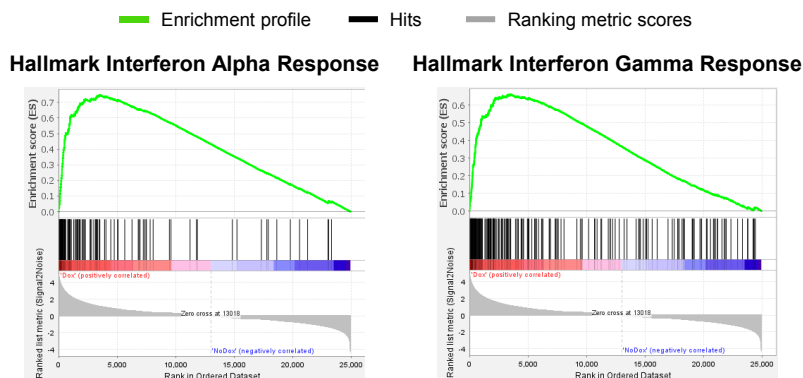


Figure R 56. Gene Set Enrichment Analysis reveals an increase of type I and type II IFN response in PGC1 α -expressing PC3 cells. IFN α ; NES=2.7137; NOM p-value=0.000. IFN γ ; NES=2.5994; NOM p-value=0.000.

Regarding the TF enrichment analysis, MAZ and ERR α emerged among the top transcription factors to mediate transcriptional activity of PGC1 α (FigR 57).

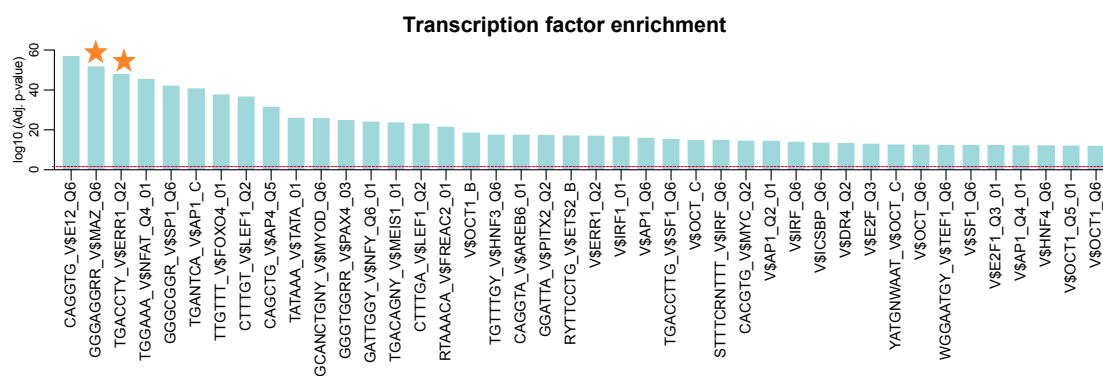


Figure R 57. MAZ and ERR α emerge among the top TFs to mediate transcriptional control of the genes found differentially expressed in PGC1 α -expressing and non-expressing PC3 cells. The red dotted line indicates p=0.05. p=p-value.

To gain a deeper insight into the processes linked to the expression of PGC1 α , we did also perform enrichment analyses dividing the genes found up and downregulated. Genes found upregulated were linked to metabolic processes and to IFN response, emerging ERR α as the top transcription factor to mediate transcriptional regulation (FigR 58A-B).

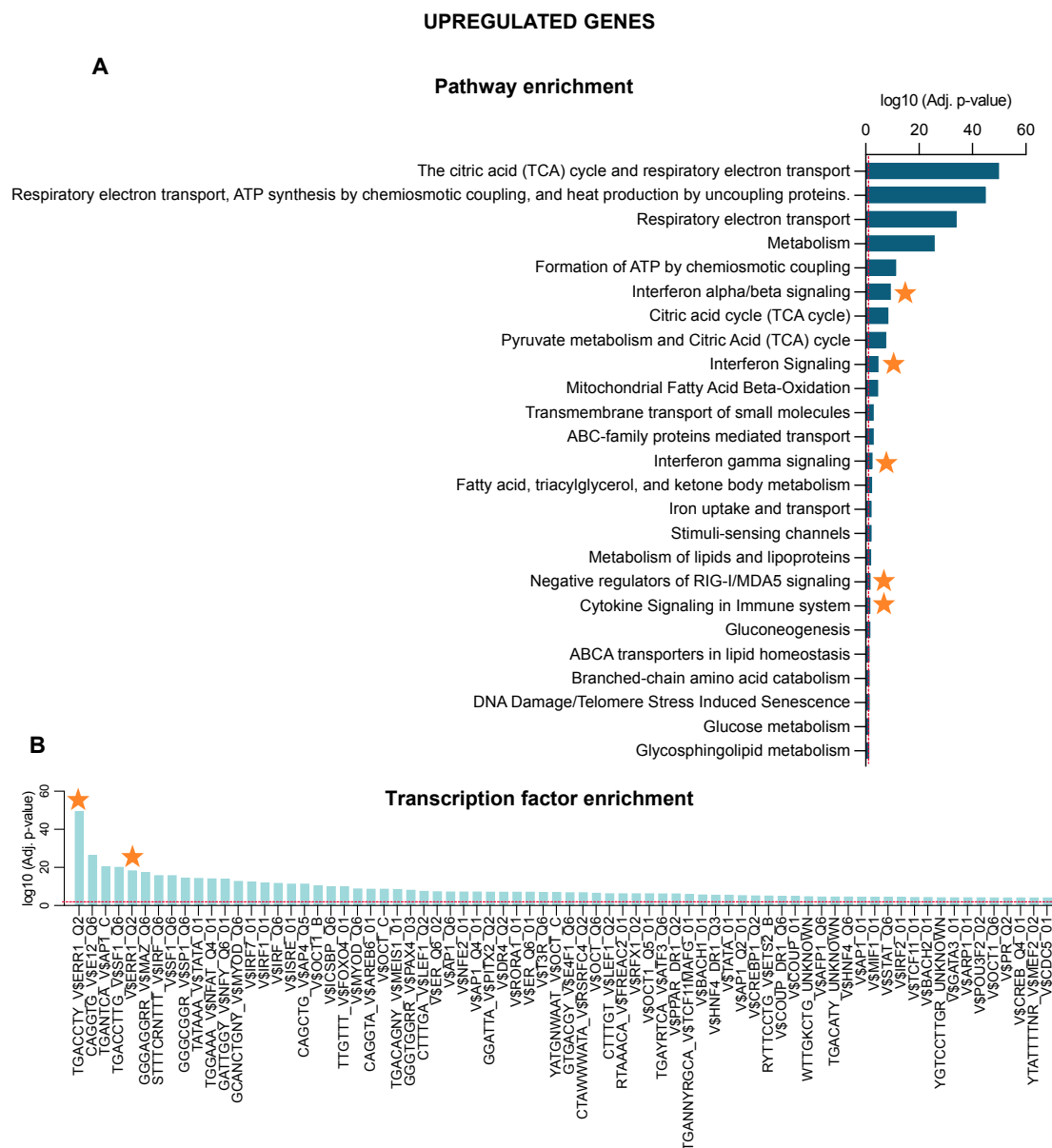


Figure R 58. Enrichment analyses of the genes found upregulated upon expression of PGC1 α in PC3 cells. A-B. Pathway (A) and transcription factor (B) enrichment analyses. The red dotted lines indicate $p=0.05$. $p=p$ -value.

On the other hand, it was interesting to observe that genes found downregulated upon expression of PGC1 α were related to cell cycle and seemingly under the transcriptional control of LEF1, MAZ, MYC and E2F1, among others (**FigR 59A-B**).

Finally, we compared data from the present RNA sequencing against the data we obtained from the RNA sequencing of the PC3 recipient cell lines, which, revealed a common number of 19 genes altered in both analyses. Among these genes, *STAT2*, *NLRC5*, *IRF1*, *IRF9*, *PDE1C*, *ATF3*, *DDIT3*, *HLA-E* and *FGFP1* (the latter also identified in the proteomics of the cell secretome) were included. Overall, data suggests that PGC1 α transcriptional control goes beyond cell metabolism and extends towards the regulation of novel cellular functions such as interferon signaling and cell cycle.

DOWNREGULATED GENES

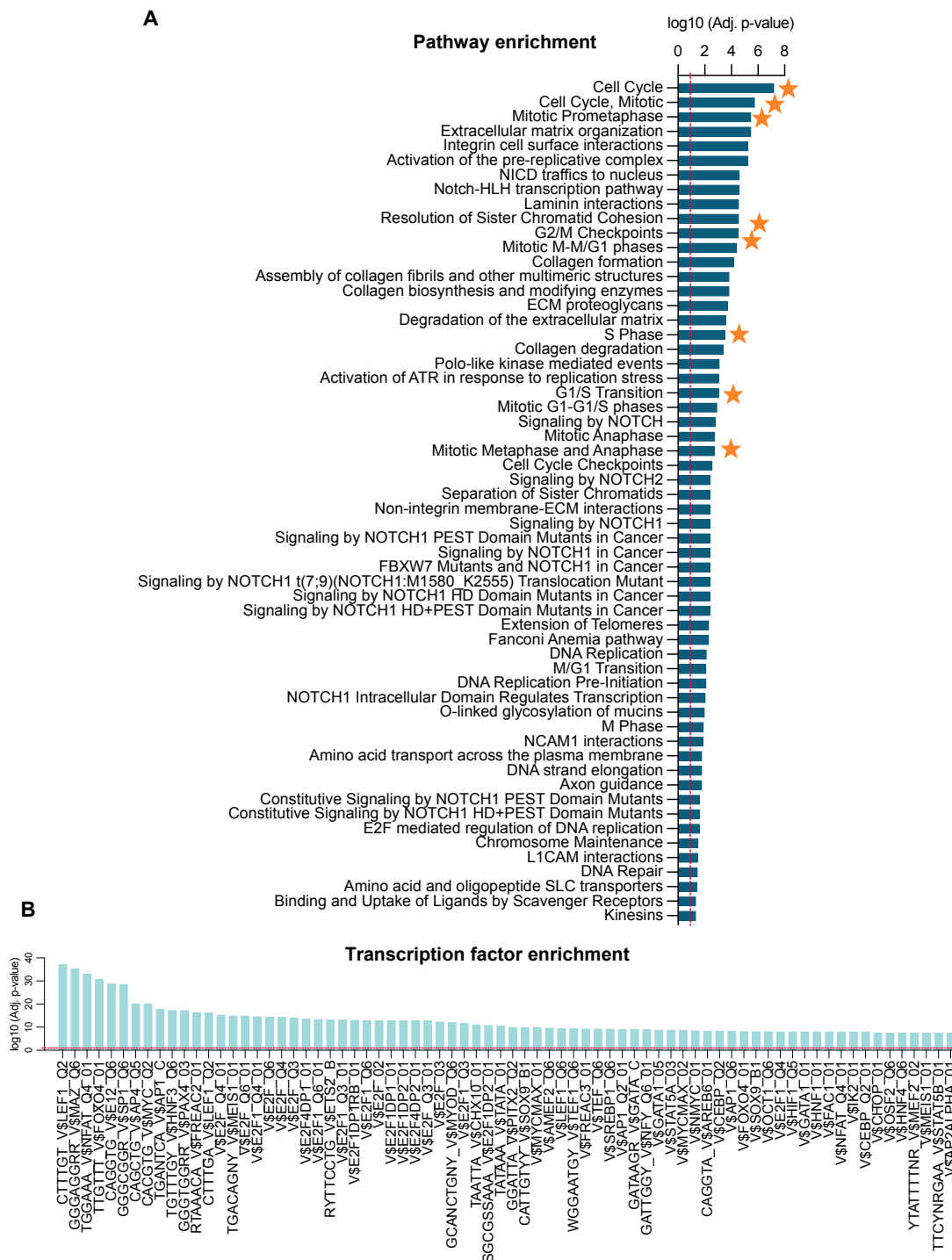


Figure R 59. Enrichment analyses of the genes found downregulated upon expression of PGC1α in PC3 cells. A-B. Pathway (A) and transcription factor (B) enrichment analyses. The red dotted lines indicate p=0.05. p=p-value.

IV.1.1 In vitro and in vivo validation of RNA sequencing candidates

We next focused on validating by RT-qPCR analysis IFN-related genes that were found differentially expressed in the producer PCa cell lines. In accordance with the data observed in

the RNA sequencing, *STAT2*, *IRF1*, *IRF9* and *NLRC5* were significantly upregulated upon expression of PGC1 α . We also checked gene expression levels of *IFNB1* and *IFNA1*. As it happened in the PC3 recipient cell lines treated with the differential secretomes, only *IFNB1* showed to be increased in the presence of PGC1 α , finding no changes in the levels of *IFNA1* (FigR 60).

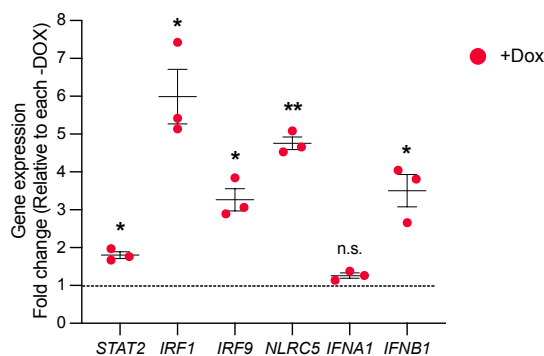


Figure R 60. RT-qPCR analysis reveals that IFN-related genes are upregulated in PGC1 α -expressing cells compared to non-expressing ones. *STAT2*, *IRF1*, *IRF9*, *NLRC5*, *IFNA1* and *IFNB1* are analyzed ($n=3$). Data is represented as fold change and normalized to each -Dox condition, depicted by a black dotted line. +Dox: PGC1 α -expressing condition. Statistical analysis: One sample *t*-test establishing 1 as hypothetical value. *p*, *p*-value. * $p<0.05$, ** $p<0.01$, n.s.=not significant. Error bars indicate s.e.m.

We also tested *IRF1*, *IRF9* and *IFNB1* gene expression levels in control PC3 TRIPZ cells, observing no changes and thus confirming that doxycycline had no effect in the experimental system (FigR 65).

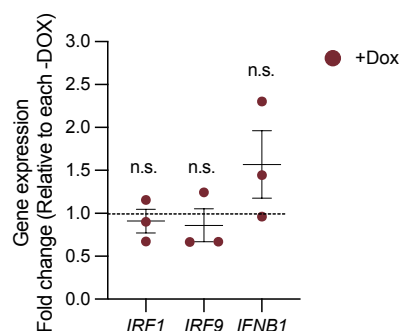


Figure R 61. Doxycycline treatment does not alter expression levels of candidate genes. *IRF1*, *IRF9* and *IFNB1* are analyzed by RT-qPCR in PC3 TRIPZ cells. ($n=3$). +Dox: cells treated with doxycycline. Data is represented as fold change and normalized to each -Dox condition (untreated cells), depicted by a black dotted line. Statistical analysis: One sample *t*-test establishing 1 as hypothetical value. *p*, *p*-value, n.s.=not significant. Error bars indicate s.e.m.

Then, taking advantage of an *in vivo* xenograft assay where tumor formation and growth capacity of PC3 cells with combined expression and deletion of PGC1 α and ERR α respectively were assessed (Valcarcel-Jimenez et al. 2019), we attempted to check gene expression levels of some of our candidates. First, we confirmed expression of *PGC1A* in those tumors inoculated into

mice that had been exposed to doxycycline diet and corroborated that the increase of *ERRA* upon expression of *PGC1A* was blunted in those tumors formed by cells with CRISPR-Cas9-based *ERRA* ablation (**FigR 62**). We confirmed a statistically significant upregulation of *MX1*, *STAT1* and *IRF1* on those tumors formed by cells with an activated *PGC1α-ERRα* transcriptional axis. Finally, *IRF9* and *IFNB1* gene expression levels remained similar among the four groups tested, thus suggesting a *PGC1α* and *ERRα* independent transcriptional regulation in an *in vivo* context.

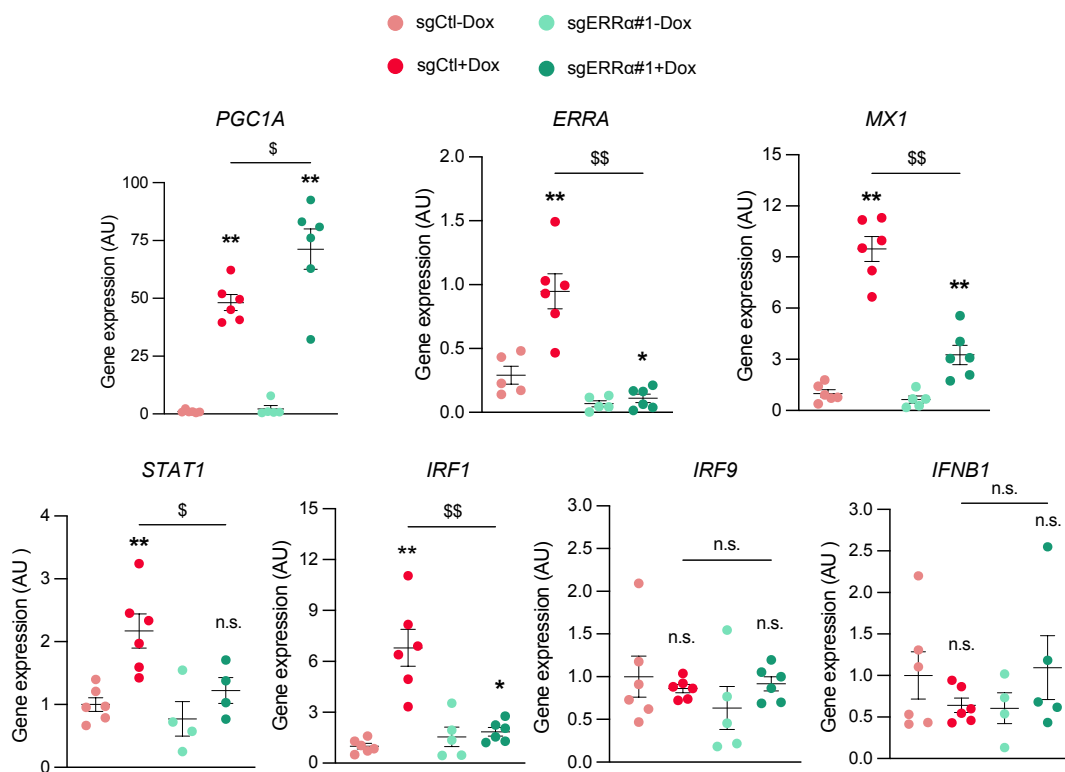


Figure R 62. RT-qPCR analysis of IFN-related genes in an *in vivo* xenograft mouse model. Expression of *PGC1A* and blunt of *ERRA* are confirmed in the tumors extracted from athymic mice. *MX1*, *STAT1*, *IRF1*, *IRF9* and *IFNB1* gene expression levels are assessed in mouse xenograft samples. (n=4-6 mice/ group). +Dox: *PGC1α*-expressing condition. Statistical analysis: One tailed Mann-Whitney U test. Asterisks indicate statistical differences between sgCtl-Dox and the rest of the conditions and the dollar symbol between sgCtl+Dox and sgERRα#1+Dox. p, p-value, */\$p<0.05, **/\$\$p<0.01. n.s.=not significant. Error bars indicate s.e.m.

Further *in vivo* validations were performed in our three-month *Pten^{pc-/-}* (KO) and *Pten^{pc-/-} Pgc1α^{pc-/-}* (DKO) mice samples. Candidates *Mx1*, *Stat1*, *Tnxb* and *Fgfp1*, found deregulated in the cell secretome proteomics analysis as well as cell-intrinsically in the producer cells (RT-qPCR analyses and RNA sequencing analysis) were assessed. In addition, we interrogated the expression levels of IFN-related genes *Stat2*, *Irf1*, *Irf9* and *Nlrc5*. First, *Pgc1a* downregulation in the DKO mice was confirmed. No changes in the expression levels in *Mx1*, *Tnxb*, *Fgfp1*, *Stat2*, *Irf9* and *Nlrc5* were observed between KO and DKO mice, but a trend towards decreased *Irf1* and increased *Stat1* gene expression levels in DKO mice were found (**FigR 63**). In the same line,

transcription factors *Atf3* and *Ddit3*, both linked to ER stress, showed to be slightly decreased in the DKO mice compared to the KO ones.

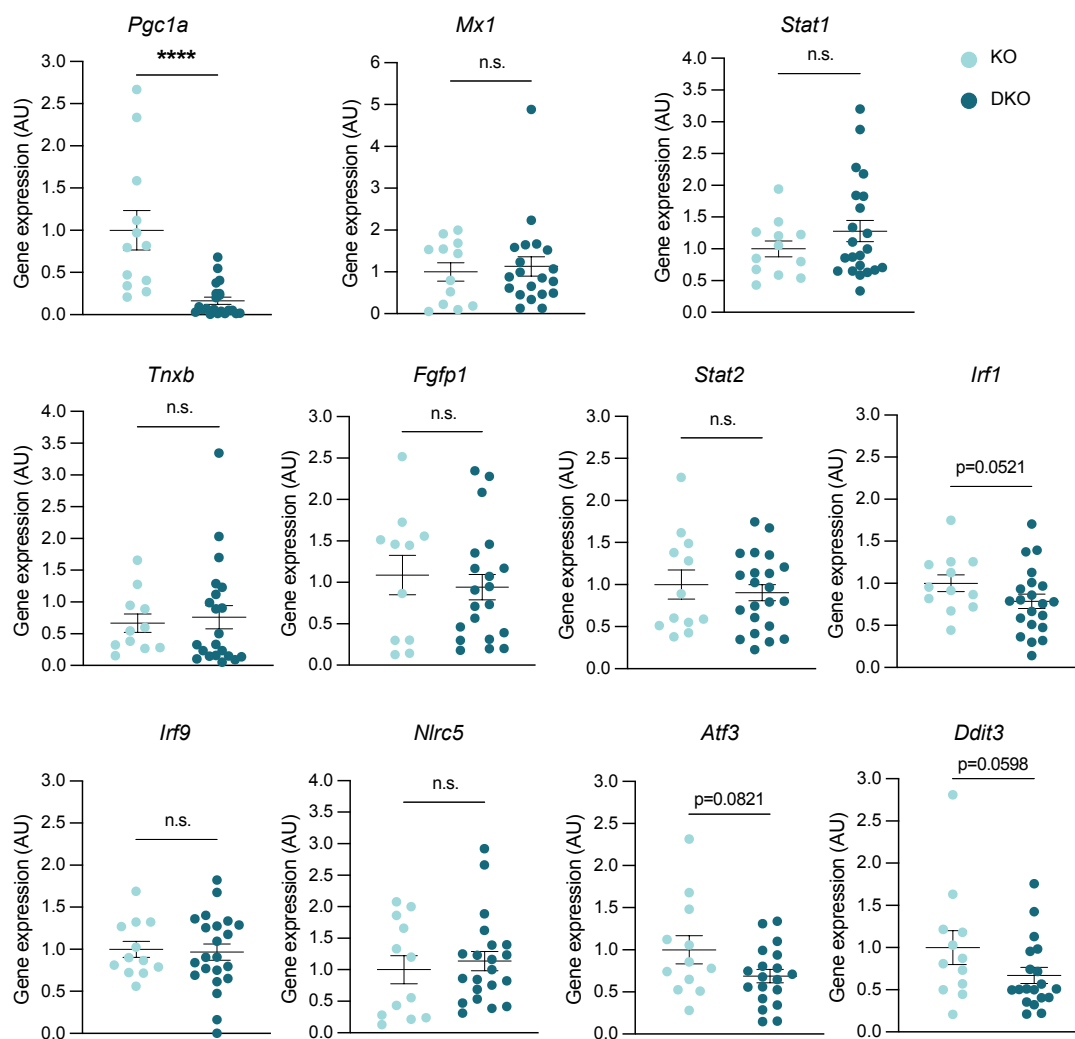


Figure R 63. RT-qPCR analysis in KO and DKO mice of gene candidates identified by RNA sequencing and proteomics analysis of the cell secretome from PGC1 α -expressing and non-expressing cells. Gene expression levels of *Pgc1 α* , *Mx1*, *Stat1*, *Tnxb*, *Fgfp1*, *Stat2*, *Irf1*, *Irf9*, *Nlrc5*, *Atf3* and *Ddit3* are analyzed (KO mice $n=12$, DKO mice $n=22$). KO: mice with prostate-specific epithelial deletion of *Pten*. DKO: mice with prostate-specific epithelial deletion of *Pten* and *Pgc1 α* . Statistical analysis: One tailed Mann-Whitney U test. p , p -value, n.s.=not significant. Error bars indicate s.e.m.

Type I IFN signaling

Once we confirmed changes in the expression levels of some of the genes involved in type I IFN response, we next aimed at analyzing if there was an activation of the mentioned pathway in the producer cell lines. IFNs are cytokines known to trigger anti-viral, anti-proliferative and immunomodulatory responses in the cells, and in the context of cancer they have been extensively studied as they have been linked to disease-improving conditions (Medrano et al. 2017b). Briefly, the IFN family is classified in type I, type II and type III. Regarding type I IFNs,

once produced, they are released from the cell, and bind they cognate receptors IFNAR1/IFNAR1 that are associated to tyrosine kinases JAK1 and TYK2. These kinases phosphorylate STAT1 and STAT2 proteins, which then bind to IRF9, conforming the ISGF3 complex that is translocated into the nucleus. Once in the nucleus, the ISGF3 complex binds to the ISREs located in the promoter regions of ISGs to activate transcription (Platanias 2005). Thus, taking these facts into consideration, we first checked by western blot if there were changes in STAT1 phosphorylation (pSTAT1) levels, which would indicate activation of the JAK-STAT signaling cascade. Expression of PGC1 α upon treatment with doxycycline throughout three days was confirmed, and this was accompanied by an increase in the levels of pSTAT1 compared to the non-PGC1 α expressing conditions (**FigR 64**).

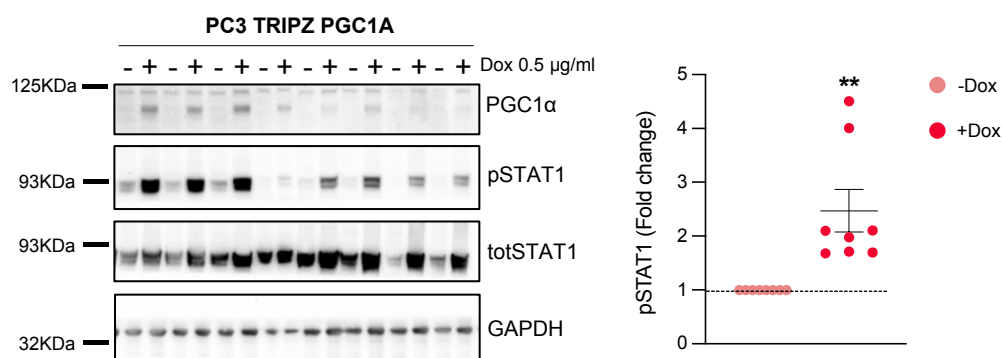


Figure R 64. JAK-STAT signaling pathway is activated upon expression of PGC1 α in vitro. Western blot analysis displaying protein expression of PGC1 α , pSTAT1, total STAT1 and housekeeping GAPDH in PGC1 α -expressing and non-expressing cells. (n=8). Right panel displays quantification of pSTAT1. Levels of pSTAT1 are normalized to total STAT1 levels and to GAPDH. Data is represented as relative to the -Dox condition (no expression of PGC1 α). +Dox: PGC1 α -expressing condition, Dox: doxycycline. Statistical analysis: One sample t-test. p = p-value, ** p <0.01, n.s.=not significant. Error bars indicate s.e.m.

We then aimed at analyzing time at which pSTAT1 levels increased upon the induction of PGC1 α . Therefore, we performed a time course experiment based on increasing PGC1 α induction time-points. On the other hand, it was reported that c-MYC suppresses STAT1 levels and therefore type I IFN signaling in cancer (Schlee et al. 2007; Muthalagu et al. 2020a). Indeed, as previously mentioned, c-MYC is known to be repressed by PGC1 α in the context of PCa (Valcarcel-Jimenez et al. 2019). Taking these facts into consideration, we took once again advantage of PC3 PCa cell lines with differential expression of PGC1 α and performed western blot analysis at 8, 16, 24, 48 hours and 6 days after expression of PGC1 α (**FigR 65**). We first confirmed c-MYC downregulation upon expression of PGC1 α in the doxycycline-treated cells, which occurred at early time points after induction of PGC1 α . Increased pSTAT1 in PGC1 α -expressing cells only became evident after 24 hours of expression of PGC1 α . Hence, data shows that the activation of STAT1 happens after the drop of c-MYC levels, thus suggesting STAT1 is downstream c-MYC.

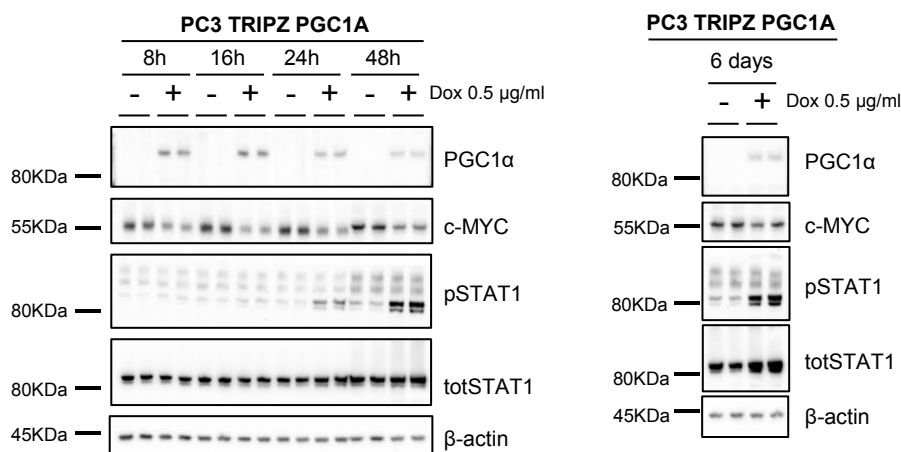


Figure R 65. Western blot time-course analysis of JAK-STAT signaling pathway reveals STAT1 activation is downstream c-MYC. Western blot time-course analysis displaying protein expression of PGC1 α , c-MYC, pSTAT1 and total STAT1 assessed at 8 h, 16 h, 24 h, 48 h and 6 days upon expression of PGC1 α . One representative experiment out of three is shown. Dox: doxycycline.

IV.1.1.1 Detection of IFN- β in the cell secretomes

Overall, all data here provided suggest a PGC1 α -driven transcriptional regulation of type I IFN signaling. At gene level, we confirmed *in vitro* upregulation of *IFNB1* upon expression of PGC1 α , which, was in line with the upregulation of ISGs *MX1*, *IRF1* and *IRF9* found *in vitro* and *in vivo*. Moreover, levels of *MX1*, *IRF1* and *IRF9* were also enhanced in recipient cell lines treated with secretomes obtained from PGC1 α and ERR α -expressing cell lines (**FigR 49**). Within this context, we next wondered whether interferon type I levels secreted to the extracellular milieu would be different between PGC1 α -expressing and non-expressing PC3 cells. Therefore, we next monitored the secretion of IFN- β , a 187 amino acid cytokine that due to its small size is not easily detected by proteomics analysis. Only newly developed proteomics devices have enough sensitivity to detect IFN- β , and thus, we performed an IFN- β immunoassay designed to detect IFN- β levels in the cell secretomes. Briefly, to obtain the secretomes, PGC1 α -expressing and non-expressing producer PC3 cells were seeded and induced with doxycycline for three days. Cells were then seeded into 12-well plates at high densities and the differential secretomes were collected three and six days after cell seeding for measuring IFN- β levels (**FigR 66**).

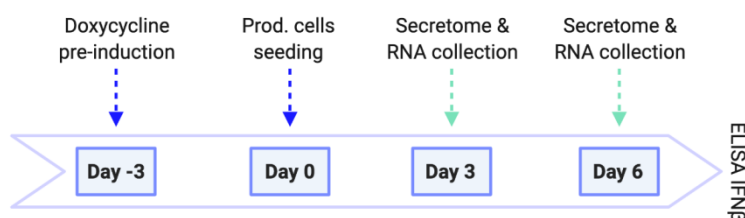


Figure R 66. Timeline of the experimental flow to produce and collect the secretomes produced by PGC1 α -expressing and non-expressing cells for measuring levels of IFN- β .

At day 3 of secretome production, there was a trend towards detecting higher amounts of IFN- β in secretomes produced by PGC1 α -expressing PC3 cells compared to non-expressing ones, although data was dispersed, and no statistical significance was found between both groups (**FigR 67A**). Nonetheless, at day 6 after cell seeding and secretome production, levels of IFN- β in the secretomes obtained from PGC1 α -expressing cells were considerably higher compared to secretomes obtained from non-PGC1 α expressing cells (**FigR 67B**). Both, days 3 and 6, displayed lower cell confluence in the PGC1 α -expressing conditions compared to non-PGC1 α expressing ones (**FigR 67C**). Indeed, we observed that at day 6 PGC1 α -expressing cells started to die, probably caused by the lack of space for adhering, due to their large size compared to the non-PGC1 α expressing cells. Hence, despite we could observe changes in the levels of interferon in the secretomes produced by PGC1 α -expressing and non-expressing cells, we concluded that these experiments should be further refined by seeding lower cell confluences.

In parallel to the detection of IFN- β in the cell secretomes, we performed RT-qPCR analysis to confirm induction of *PGC1A* in the cells treated with doxycycline at days 3 and 6 (**FigR 67D**). *IFNB1* gene expression levels were also analyzed at both experimental time-points, showing increased expression levels in the PGC1 α -expressing cells compared to the non-expressing ones (**FigR 67E**). Of note, this increase in *IFNB1* levels was not that high at later time points, perhaps reflecting the main role of type I IFNs on mediating acute responses, and therefore being negatively regulated at later time points.

Finally, activation of JAK-STAT signaling pathway depends on IFNs binding to their cognate receptor, which is composed of two subunits: IFNRA1 and IFNAR2. The density of type I IFN receptors is a limiting factor for the sensitivity of cancer cells to type I IFNs (T. C. Wagner et al. 2004). Knowing this, we analyzed gene expression levels of both subunits of type I IFN receptor, finding no relevant differences either at day 3 or day 6 between both PGC1 α -expressing and non-expressing cells. Merely *IFNRA1* subunit gene expression levels were slightly decreased at day 6 in PGC1 α -expressing cells (**FigR 67F**). This observation led us to conclude that gene expression levels of *IFNRA1* and *IFNAR2* receptor subunits are similar in PGC1 α -expressing and non-expressing PC3 cells, thus indicating that the mechanism by which JAK-STAT pathway is differentially activated in both cell lines is not due to differences in receptor densities.

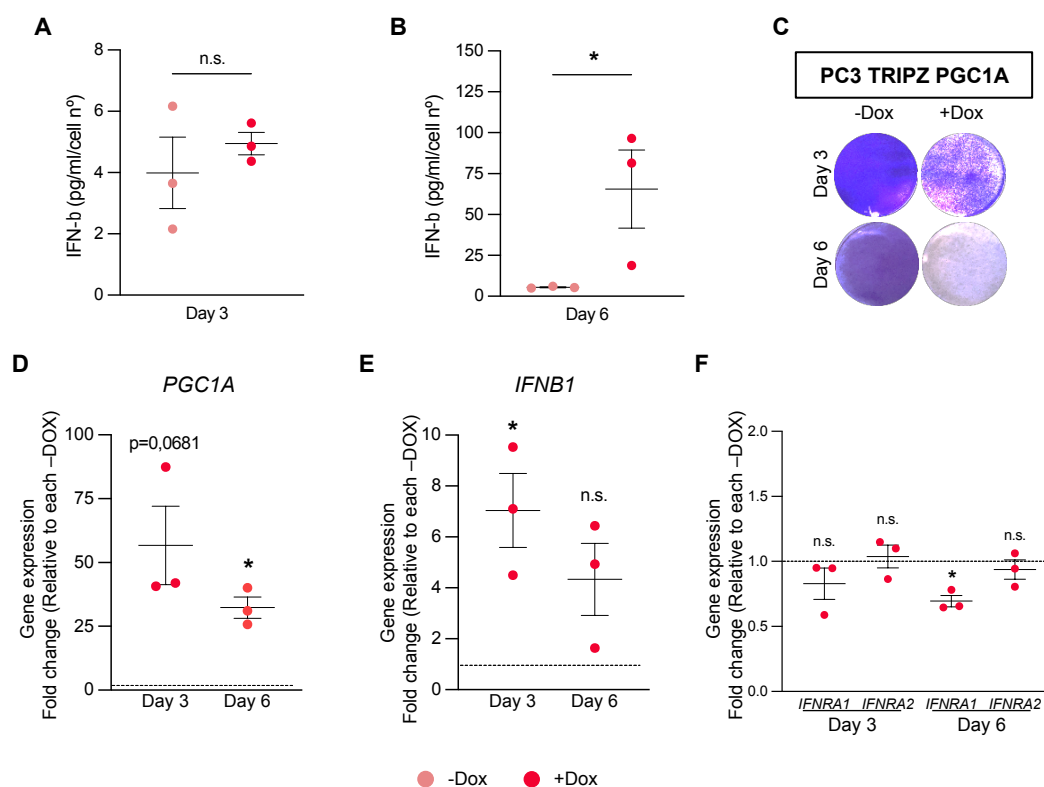


Figure R 67. IFN- β levels are increased in the secretomes produced by PGC1 α -expressing PC3 cells compared to the non-expressing ones. A-B. IFN- β levels measured by enzyme-linked immunosorbent assay (ELISA) in the secretomes produced by PGC1 α -expressing and non-expressing PC3 cells at days 3 (A) and 6 (B) of secretome production. C. Representative crystal violet staining showing cell proliferation at days 3 and 6 of secretome producing PC3 cells expressing or not PGC1 α . One experiment out of three is shown. D. Expression of PGC1A upon treatment with doxycycline is confirmed in the producer PC3 cell lines. E. IFNB1 gene expression at days 3 and 6 in PGC1 α -expressing and non-expressing PC3 cells. F. Gene expression levels of subunits IFNRA1 and IFNRA2 analyzed in PGC1 α -expressing and non-expressing PC3 cells. (n=3). In D, E, and F, data are normalized to the -Dox condition (no PGC1 α expression), depicted by a black dotted line. +Dox: PGC1 α -expressing condition. Statistical analysis: One tailed unpaired t-test (A and B) and one sample t-test establishing 1 as hypothetical value (D and F). One tailed one sample t-test establishing 1 as hypothetical value (E). p=p-value, *p<0.05, n.s.=not significant. Error bars indicate s.e.m.

As a general perspective derived from this work, we have shown that PGC1 α regulates the secretome composition of aggressive PCa cells. Secretomes can therefore be considered as molecular fingerprints of the cell of origin. Differences observed in the molecular content of the secretome drive changes in the proliferative capacities of recipient cells, which seem to be due to the activation of type I IFN response. Indeed, our data points towards JAK-STAT signaling pathway being regulated by PGC1 α via c-MYC downregulation. The anti-proliferative and tumor-suppressive effects observed in PGC1 α -expressing cells has up to date been attributed to cell-intrinsic phenomena (Torrano, Valcarcel-Jimenez, et al. 2016; Valcarcel-Jimenez et al. 2019), nonetheless, an autocrine mechanism by which cell-secreted bioactive molecules (including IFN)



impact on the own cell seems highly probable. Nevertheless, for answering this question, still additional experiments need to be performed. In addition to IFN response, we cannot ignore that *ATP1B1*, found upregulated in the presence of *PGC1 α* in EVs, whole cell secretome, mouse TIL and in the RNA sequencing performed on the PCa producer cells with differential expression of *PGC1 α* makes this protein a highly interesting candidate to be further studied. Indeed, *ATP1B1* was also found to be directly correlated to *PGC1A* in PCa datasets.

Therefore, we can conclude that the role of *PGC1 α* (and its transcriptional partner *ERR α*) goes beyond the regulation of cell metabolism and extends to other novel functions linked to triggering type I IFN response.

Overview

- RNA sequencing analysis of PC3 producer cell lines with differential expression of the transcriptional regulator PGC1 α revealed a total number of 3747 differentially expressed genes (adj. p-value<0.01, fold change>2 cut-off).
- Gene enrichment analyses displayed mitochondrial metabolism, ECM-related processes, and type I IFN signaling as the main enriched categories linked to the genes differentially expressed between PGC1 α -expressing and non-expressing cells. MAZ and ERR α emerged as the top transcription factors to mediate transcriptional regulation.
- A total number of 19 genes were found to be commonly altered in the RNA sequencing performed on PC3 cells treated with PGC1 α -regulated secretomes and PC3 cells with differential expression of PGC1 α . Data suggest that novel functions that go beyond the regulation of cell metabolism are associated to PGC1 α , including regulation of IFN and ER stress responses.
- IFN-related genes found altered in the RNA sequencing analysis were validated *in vitro* by RT-qPCR in the producer cells. *IFNB1* but not *IFNA1* gene expression levels were increased upon expression of PGC1 α in the producer cells.
- *MX1*, *STAT1* and *IRF1* showed to be transcriptionally regulated by the PGC1 α -ERR α transcriptional axis in an *in vivo* mouse xenograft model. By contrast, *IRF9* and *IFNB1* showed no changes in expression levels among experimental groups.
- *In vivo* RT-qPCR validations of candidates were performed in 3-month KO and DKO GEMMs, showing slight changes in gene expression levels of *Irf1*, *Stat1*, *Atf3* and *Ddit3*.
- Western blot analysis confirmed activation of the JAK-STAT signaling cascade upon expression of PGC1 α in PC3 cells.
- Western blot analysis of a time course experiment based on different PGC1 α induction time-points revealed c-MYC downregulation occurred prior to STAT1 phosphorylation, thus suggesting STAT1 activation is downstream c-MYC.
- IFN- β immunoassay performed to detect levels of IFN- β in the cell secretomes, revealed higher levels of the cytokine at days 3 and 6 in the secretomes produced by PGC1 α -expressing PC3 cells compared to the non-expressing ones.



- Increased IFN- β levels were accompanied by decreased cell proliferation in the PGC1 α -expressing cells, nonetheless, cell death was observed at day 6 in the PGC1 α -expressing cells, therefore evidencing those experimental settings need to be refined.
- IFNB gene expression levels were shown to be increased in PGC1 α -expressing PC3 cells at days 3 and 6. Gene expression levels were higher at day 3 than day 6.
- No significant differences in gene expression levels of type I IFN receptor subunits IFNRA1 and IFNAR2 were found between by PGC1 α -expressing and non-expressing PC3 cells.

The background is a light blue gradient. Scattered across the page are several overlapping circles of various sizes, rendered in a watercolor style with soft, irregular edges. The colors range from a pale, almost white light blue to a deep, vibrant blue. The circles are positioned in the top-left, bottom-left, and bottom-right corners, leaving the center and right side relatively clear.

Discussion

I PGC1 α : beyond the cell boundaries

Prostate cancer accounts for the second type of cancer most diagnosed among men worldwide. A high percentage of men suffering from PCa may only need active surveillance or first-line therapy, but a fraction of these patients (close to 17%) develop resistance and progress towards advanced disease (Cui et al. 2020; Castro et al. 2013). Indeed, up to date, metastatic disease entails a major burden for the survival of PCa patients as no efficient therapies exist. Although PCa is intimately related to advanced age, family history of PCa suggests the importance of genetics driving the disease (Castro et al. 2013). In this regard, the dysregulation of different genes is known to occur in PCa (D. Robinson et al. 2015b) and this is allowing the development of specific therapies and the design of protocols with the sight set on personalized medicine. Such is the case of somatic and germline mutations in DNA damage repair (DDR) genes BRCA1/2, associated with an aggressive PCa phenotype (Castro et al. 2013). Patients harboring mutations in these genes seem to benefit from platinum therapy and PARP inhibitor Olaparib (H. H. Cheng et al. 2016; Mateo et al. 2015). Another biomarker being used in clinics is *PTEN* loss, which is common in metastatic CRPC patients, and is often accompanied by an overactivation of AKT. Ongoing clinical trials suggest prognosis of these patients could be improved by administering combined ADT and AKT inhibitors (Sweeney et al. 2021).

With no doubt, a key aspect for handling PCa is the stratification of patients (indolent or aggressive) and prediction on treatment response, for what specific biomarkers are required. The extensive research along the last years allowed the discovery of novel biomarkers and consequent development of tests that aim at predicting and diagnosing PCa through the detection of tissue, urine, or serum-based markers. For example, Oncotype DX (www.oncotypeiq.com) is based on the detection in biopsies of a 17-gene signature composed of 5 control genes and 12 active genes specific to PCa and involved in AR signaling, cellular organization, stromal response, and cellular proliferation that have the power of predicting PCa aggressiveness. Another genome-based test is Prolaris (www.prolaris.com), that relies on 31 genes involved in cell-cycle progression and 15 normalizer genes measured in tumor biopsies. Altogether, these genes determine how aggressive the cancer is and provide information on the risk of metastasis and biochemical recurrence of the patient. In addition, the 4Kscore (www.4kscore.com) measures four prostate-specific kallikreins (total PSA, free PSA, intact PSA and hK2) in the serum, and together with other clinical data of the patient, an algorithm is applied to predict the risk of aggressive PCa. Lastly, ExoDX Prostate (www.exosomedx.com) measures the RNA levels of three biomarkers (*PCA3*, *SPDEF* and *ERG*) contained in urine-derived EVs.

It is important to highlight that lately only few tests, which include measuring PSA or prostate cancer associated 3 (*PCA3*) as well as the prostate health index (PHI), have overcome approval by the Food and Drug Administration (FDA), evidencing how challenging the implementation of novel biomarkers is (Kohaar, Petrovics, and Srivastava 2019). Most of the tests herein presented rely on the measurement of markers that have not been shown to functionally promote PCa progression. Yet, for a better disease management, a deep understanding on how

and why some forms of PCa progress is needed. Therefore, causal contributors of the disease may provide not only with stratification potential, but also with novel and specific treatment options. In this sense, our group previously demonstrated the tumor and metastasis suppressive role of PGC1 α in PCa (Torrano, Valcarcel-Jimenez, et al. 2016; Valcarcel-Jimenez et al. 2019). In addition, the metabolic regulator PGC1 α showed to have stratification potential, as its expression levels are associated to the disease-free survival and risk of metastasis in PCa patients. In fact, PGC1 α together with ERR α regulates the expression of a transcriptional program from which, a signature comprising ten genes showed to be of prognostic value (Torrano, Valcarcel-Jimenez, et al. 2016). Within this context, the present thesis work, aimed at studying the mechanisms by which PGC1 α exerts its tumor suppressive role in PCa. A deeper understanding of the PGC1 α -driven anti-tumoral events may set light on novel therapeutic strategies for blocking PCa progression as well as identifying non-invasive biomarkers of disease progression.

The study of cell biology from a reductionist point of view, has revealed that cell-intrinsic signaling needs to be further integrated in the surrounding environment, at a cellular and systemic level. The response a cell generates to a given stimulus is dependent on genetic and non-genetic variables. Genetic alterations, for example, may lead to the production of altered secretomes, which can further corrupt cellular and intercellular dynamics. Mutations may affect signal recognition particle sequences, affecting secreted protein translocation and degradation (Tikhonova et al. 2019). Mutations or loss of *p53* have also been described to alter the secretome composition, rendering it pro-tumorigenic (Lujambio et al. 2013; Neilsen et al. 2011). In the same line, the study by Wang and colleagues showed how deletion of *PTEN* and *SMAD4* in PCa epithelial cells led to an increased Hippo-YAP pathway-mediated secretion of CXCL5 chemokine. CXCL5 was shown to recruit myeloid-derived suppressor cells (MDSCs) which induced an immunosuppressive environment, thus promoting PCa progression (G. Wang et al. 2016). In addition to genetic alterations, epigenetics and other non-genetic variables mostly rising from cell-extrinsic phenomena, such as nutrient and oxygen availability, composition and stiffness of the ECM, as well as cell densities (among other elements) also impact on the myriad of responses a cell may trigger upon a stimulus (Wellen and Thompson 2010; Frechin et al. 2015; Lun and Bodenmiller 2020). All these factors further contribute to the generation of heterogeneous intercellular network (**FigD 1**).

In this sense, hypothesizing that the metabolic co-regulator PGC1 α could intrinsically regulate the secretome composition and further impact on cell the communication networks seems feasible. Indeed, PGC1 α has the ability of "sensing" different signaling pathways and regulates the metabolism in a tissue-specific manner (P. Puigserver 2005). These features make PGC1 α as a candidate to orchestrate rapid responses that govern secretion of molecules under diverse conditions. Indeed, PGC1 α was shown to downregulate the expression levels of genes encoding for proteins linked to ECM organization, proteinases, and cytokines in mouse embryonic fibroblasts (MEFs) and hepatocellular carcinoma cell line HepG2. In this study, several of the PGC1 α -regulated candidates identified were further validated by proteomics analysis of the cell

secretome produced by MEFs (Minsky and Roeder 2017). This study is in line with the data presented in our study, by which we show how the transcriptional regulator impacts on the secretome composition of PCa epithelial cells, including ECM proteins and IFNs. These distinct secretomes were shown have distinct biological outcomes on the tumor and stromal compartments.

Another interesting question concerns the fine-tuning by which the secretory pathway is regulated, responding to physiological and tissue-specific demands (Feizi et al. 2017). Although post-translational modifications (PTMs) are key for regulating protein secretion, the transcriptional control mediated by co-regulators could also be an efficient manner of regulating the secretion of proteins to the extracellular milieu. Understanding how is the cell secretome regulated may allow to better comprehend diseases, and thus might be a source for identifying novel therapeutic targets and disease biomarkers.

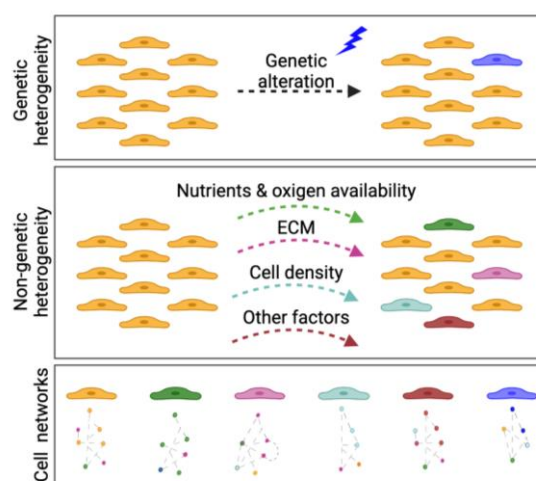


Figure D 1. Heterogeneity of signaling networks. Genetic and non-genetic phenomena impact on the responses a cell executes upon a stimulus, further influencing cellular networks.

1.1 Dissecting the cell secretome

We have shown throughout the present work that the cell secretome regulated by PGC1 α impacts on PCa epithelial cells and may alter the tumor microenvironment *in vivo*. Indeed, beyond the distinct roles that EVs and SFs may play in tumorigenesis, a key piece of data in this thesis work has been characterizing the protein content of the secretome regulated by PGC1 α , *in vitro* (PCa epithelial cells) and *in vivo* (GEMMs TILs). This characterization also suggests EVs as bystanders of the status of the primary tumor. A recent study by Ramilowski and colleagues suggests that both secreted and plasma membrane proteins, present high cell-type-specific profiles. This implies that probably, during evolution, new types of cells originated and made necessary both, to generate membrane proteins that could tag these cells and secreted proteins for reporting their status to surrounding cells (Ramilowski et al. 2015). This concept could be applied to a malignant context, where tumor cells are subjected to selective pressures they need

to overcome to survive and progress. Indeed, a nice example of it, is the inhibition of oncogenic drivers, which leads to secretome alterations that provide malignant cells with resistance to treatment (Obenauf et al. 2015). Hence, to understand the role a cell has within its environment, it is key to identify the protein messages that are passed between cells, as well as their directionality and roles on triggering specific signaling pathways. This may further allow the identification of mediators of disease progression that could be exploited for developing novel therapeutic strategies. Finally, the cell secretome can also be a potential reservoir of disease biomarkers.

1.1.1 Extracellular vesicles

The physical characterization of EVs produced by PGC1 α -expressing and non-expressing PCa cells revealed no major changes in EVs size and number, although protein content showed to be increased upon expression of PGC1 α in the producer cells. Opposite to this observation, other studies involving lung adenocarcinoma and melanoma patients revealed a higher EV protein content in more malignant tumor stages compared to healthy controls. Furthermore, stage IV melanoma patients had an increased survival advantage when the EVs total protein concentration happened to be low (Rabinowits et al. 2009; Peinado, Alečković, et al. 2012). We did not observe differences in the particle number upon expression of PGC1 α , which was in line with the study by Lázaro- Ibáñez et al, where similar amounts of EVs were shown to be produced by metastatic PCa cell lines, malignant primary prostate cells, and benign prostate epithelial cells cultured *in vitro* (Lázaro-Ibáñez et al. 2017). On the other hand, works in which EVs were isolated from plasma of patients with prostate and gastric cancers showed increased EV numbers in cancer patients compared to healthy donors or compared to patients with a less advanced cancer stage (H. K. Kim et al. 2003; Tavoosidana et al. 2011). Indeed, the study by Tavoosidana and colleagues showed that levels of prostasomes detected in blood from PCa patients correlate with the Gleason score, making these EVs ideal candidates for diagnosis and prognosis of PCa (Tavoosidana et al. 2011).

EVs obtained from PGC1 α -expressing and non-expressing PCa cells displayed similar sizes to other studies in which EVs were isolated from the urine of PCa patients (size range: 150-350 nm) and melanoma patients seroma (mean size: 179 nm) by serial ultracentrifugation (Royo et al. 2016; García-Silva et al. 2019). Another work in which EVs were isolated from different prostate cell lines (PC3, DU145, VCaP, LNCaP, C4-2 PCa cell lines and benign cells RWPE-1) reported smaller diameters than our EVs and to the previously mentioned studies, ranging 30-100 nm (Hosseini-Beheshti et al. 2012).

We noticed changes in the protein levels of tetraspanin CD9 upon expression of PGC1 α in producer cells. Despite this observation could also be observed by western blot analysis, it also came up in the proteomics analysis we performed on the differential EVs (four out of seven independent experiments analyzed). Our observations are in line with the work published by Soekmadji and colleagues, where they showed that EVs obtained from PCa patients serum

compared to the EVs obtained from BPH patients, had increased CD9 levels. Furthermore, this same study observed CD63 marker and PSA levels remained unchanged between PCa and BPH-diagnosed patients, thus revealing CD9 detected in EVs as potent candidate to stratify patients (Soekmadji et al. 2017). In the same line, another study showed that men suffering from PCa had increased levels of CD9 and CD63 markers in exosomes obtained from urine (Duijvesz et al. 2015). Overall, data points towards CD9 marker levels being increased in prostate-related malignant phenotypes.

Curiously, ADAM10, another protein found decreased in EVs produced by PGC1 α -expressing cells, showed to be part of a protein complex together with CD9 (Y. Yan, Shirakabe, and Werb 2002). In this study, authors demonstrated the requirement of ADAM10 metalloproteinase activity to release HB-EGF ligand that mediates GPCR-induced transactivation of EGFR signaling. Indeed, other studies have proven production of EGF ligands by tumor cells, resulting in an autocrine activation of survival and proliferation signals (Salomon et al. 1995). We therefore could speculate about EGFR pathway activation being further extended through an EV-mediated transfer of ADAM10 among tumor cells, thus promoting their survival and proliferation capacities. Furthermore, we observed decreased *ADAM10* gene expression levels upon expression of PGC1 α in the PC3 producer cells further supporting this idea and associating ADAM10 with a more aggressive PCa phenotype. Finally, another study linked ADAM10 with PCa progression via its translocation from the plasma membrane to the cell nucleus, where it seems to interact with AR, behaving as a transcription factor (Arima et al. 2007).

EVs produced by PGC1 α -expressing cells displayed increased levels of enzymes AATM and AATC. This data is in line with a previous study in BCa, where PGC1 α was shown to upregulate expression of the genes encoding for AATM and AATC involved in the metabolism of glutamine (McGuirk et al. 2013). Compared to another study involving proteomics characterization of PCa EVs, few number of enzymes were found altered in EVs produced by PGC1 α -expressing and non-expressing cells (Hosseini-Beheshti et al. 2012). It is also interesting to highlight that transfer of active enzymes between cells is known to happen, providing recipient cells with nutritional plasticity (Iraci et al. 2017; Royo et al. 2017).

Importantly, we have focused our study on analyzing EVs protein content, although other molecules such as nucleic acids can also be found and are known to exert biological responses in target cells (Yanfang Liu et al. 2016; Skog et al. 2008; Mittelbrunn et al. 2011). In fact, Probert and colleagues nicely showed how the transfer of RNA in PC3-derived EVs, supports PCa progression towards bone metastasis by influencing osteoblasts behavior (Probert et al. 2019).

Overall, proteomic analysis of the EVs evidences a PGC1 α -dependent regulation of the EVs protein cargo, and the enrichment analyses performed on the genes encoding for these proteins relates them to metabolism, cell migration and adhesion processes. Among the TFs identified as probable partners of PGC1 α on mediating transcriptional regulation of the identified candidates, ERR α was of special interest. ERR α has mainly been associated to PGC1 α in the context of regulating cell metabolism, including the control of fatty acid oxidation and oxidative

phosphorylation genes in the heart and skeletal muscle and the regulation of mitochondrial biogenesis in osteoblasts and in the skeletal muscle (Huss, Kopp, and Kelly 2002; Mootha, Handschin, Arlow, Xie, St Pierre, et al. 2004; Schreiber et al. 2004). In BCa, PGC1 α together with ERR α confer metabolic reprogramming to cancer cells by means of regulating genes involved in glutamine metabolism (McGuirk et al. 2013). On the other hand, in PCa, it was shown by our group that the transcriptional control mediated by PGC1 α -ERR α induces a metabolic switch in PCa cells from an anabolic towards a catabolic state, resulting in the suppression of prostate cancer progression and metastasis (Torrano, Valcarcel-Jimenez, et al. 2016). Studies mentioned above state an important role of PGC1 α and its transcriptional partner ERR α on the control of metabolism in different cell types and under physiological and pathological conditions. However, a recent study by our group described the role of PGC1 α -ERR α axis on the acquisition of invasive properties of PCa cells beyond metabolic perturbations, by means of regulating signaling pathways that are linked to cytoskeleton rearrangements and to the inhibition of adhesion molecules (Valcarcel-Jimenez et al. 2019). This last study stems for the notion that the role of PGC1 α -ERR α is not only tied to metabolism but also to the regulation of novel and non-canonical cellular functions related to cell adhesion features, which further supports our EVs proteomics data, where an enrichment in processes linked to cell-matrix and cell-cell adhesion were observed. Among the dysregulated adhesion proteins, ITGB1, described in the work mentioned above (Valcarcel-Jimenez et al. 2019) was shown to be decreased in EVs produced by PGC1 α -expressing cells. Indeed, presence of ITGB1 in PCa-derived EVs was described to be crucial for stimulating anchorage-independent growth of circulating PCa cells (DeRita et al. 2019). ITGA2 also happened to be decreased in EVs upon expression of PGC1 α . This adhesion protein was shown to enhance PCa cells adhesion to the bone matrix favoring metastatic seeding (Ziaee and Chung 2014). EDIL3, found decreased in EVs produced by PGC1 α -expressing cells, was identified in BCa-derived EVs, where it seems to foster *in vivo* lung metastasis formation by establishing interaction with integrins leading to the activation of a matrix metalloproteinase (MMP)-mediated degradation of the matrix (J. E. Lee et al. 2016b). Besides from cell-matrix adhesion proteins, cell-cell binding proteins were also found decreased in EVs upon expression of PGC1 α in the producer cells. JAM1 (gene name *F11R*) and CLDN3, both tight junction proteins are known to, correspondingly, favor breast and ovarian cancer cells migration (Elaine A McSherry 2011; Agarwal, D'Souza, and Morin 2005). Finally, CD44 has been described to mediate both cell-cell (Draffin et al. 2004) and cell-matrix adhesion processes through its binding to hyaluronan (Bourguignon 2008; Hiraga, Ito, and Nakamura 2013). CD44 is highly expressed in melanoma, breast, lung, and prostate bone metastatic cell lines, suggesting it may play organotropic roles (Hiraga, Ito, and Nakamura 2013)

To our knowledge no studies encompassing a PGC1 α -ERR α -mediated EVs regulation have been published up to date. The differences in the protein cargo we observed in EVs produced by PGC1 α -expressing and non-expressing PC3 cells make us wonder to which extend cargo selection and loading could be influenced by PGC1 α -ERR α . Indeed, cargo sorting into EVs

is a process that is still not that well understood, but it is specific (finding concrete lipids, proteins, and nucleic acids) and it is influenced by the global state of the producer cell (Anand et al. 2019). In small EVs, cargo incorporation begins in the ILVs and happens through ESCRT-dependent and independent mechanisms. PTMs are key for directing cargo selection into the vesicles, and among the great variety of PTMs, ubiquitination and ubiquitin-like modifiers have been more extensively studied in this context. ESCRT-dependent sorting mechanism is known to involve HRS-STAM protein complex (also known as ESCRT-0) that recognizes ubiquitinated proteins and hands them over to ESCRT-I protein TSG101 (Vietri, Radulovic, and Stenmark 2020). Still, for final protein cargo sorting into the ILVs, deubiquitylation seems to be crucial (Moreno-Gonzalo, Fernandez-Delgado, and Sanchez-Madrid 2018). ESCRT-independent cargo loading is driven by other proteins, including Alix, CD81 and CD9, which can recognize and bind to non-ubiquitinated proteins (Vietri, Radulovic, and Stenmark 2020). From the RNA sequencing performed on the producer cells with differential expression of PGC1 α , we found that besides from TSG101 (2.15-fold increased), none of the above-mentioned proteins was altered at gene level. Yet, IFN-induced anti-viral ubiquitin-like protein, ISG15 also known to be involved in EVs cargo sorting by means of binding covalently to target proteins (process known as ISGylation) was found almost five-fold increased in PGC1 α -expressing cells (Moreno-Gonzalo, Fernandez-Delgado, and Sanchez-Madrid 2018). Finally, it is worth mentioning that recently, YBOX1 protein (found decreased in the whole secretome proteomics analysis and in producer cells upon expression of PGC1 α) was shown to be involved in the exosome's cargo sorting of small noncoding RNAs (Shurtleff et al. 2017). Hence, in the light of our data, we cannot exclude that the transcriptional control exerted by PGC1 α -ERR α impacts in a direct or indirect manner on the cargo sorting machinery of EVs. To answer these questions, silencing and overexpressing the mentioned candidates in the producer cell lines could provide with additional information.

1.1.2 Soluble factors

The GO cellular component analysis performed on the gene list of the proteins found altered in the secretomes of PGC1 α -expressing and non-expressing cells, was enriched in "extracellular organelle", "vesicle" and "extracellular region" domains, although other non-extracellular components such as "cytosol", "focal adhesion", "mitochondria" also appeared. Classically, protein secretion was related to the conventional ER-Golgi conventional secretory pathway that is directed by the presence of a signal peptide. Yet, the recognition of the existence of other non-classical protein secretory pathways and the understanding on how disease corrupts or is a consequence of alterations in the secretory phenotype, is altogether challenging the definition on what is a "normally-secreted protein". From an evolutionary point of view, the existence of more than one type of protein secretory mechanism could be due to the modifications that proteins suffer when they enter Golgi apparatus, which may affect protein conformation and hence its functionality. Such is the case of protein fibroblast growth factor 2 (FGF2), that when secreted to the extracellular space through the classical ER-Golgi pathway, undergoes

modifications that alter its extracellular function (Derek C. Radisky & Melody Stallings-Mann 2009). Another example of unconventionally secreted protein, HMGA1, classically recognized as a chromatin-binding protein, was described to exert pro-oncogenic roles in TNBC when secreted to the extracellular milieu (Mendez et al. 2018). The total number of 185 differentially present proteins in the secretomes produced by PGC1 α -expressing and non-expressing PCa cells probably encompass proteins secreted through classical and non-classical pathways. In this sense, the work herein presented lacks a better understanding on the secretory mechanisms that could be elucidated by confirming the proportion of proteins that present signal peptide. Still, ten proteins (MUC5B, AAAT, NRP1, RAC1, CD44, MARCKS, CATD, AATM, ATP1B1 and AATC) were commonly identified in the whole secretome and EVs proteomics analyses, which, may indicate that at least to some extent protein secretion is through an unconventional pathway involving EVs.

Finally, special care was undertaken to produce the distinct secretomes, both for the serum removal in the media and for only submitting cells to a short three-hour serum starvation period to avoid contamination of the secretome with proteins released due to cell death.

ECM-related proteins

Matricellular proteins ECM1, TNXB, CTHRC1, SERPINB5, TNXB, FGFBP1, CATD and MUC5B, all previously described to be secreted, were found decreased in the secretomes produced by PGC1 α -expressing cells. On the opposite side, ECM1 was the top increased protein found in the PGC1 α -regulated secretome. This data suggests the composition and the organization of the ECM could be influenced by the expression of the coregulator PGC1 α . The ECM is a highly complex scaffold of cross-linked proteins where different types of cells such as fibroblasts, endothelial cells and immune cells settle. The core ECM is composed of collagens, fibronectins, tenascins, laminins and glycoproteins and it constitutes an important reservoir for diverse factors (cytokines, enzymes) that can be mobilized. Mobilization of these factors contributes to the remodeling of the ECM and to the regulation of intracellular pathways regulated via cell-ECM interactions (Naba, Hoersch, and Hynes 2012). The definition on which molecules should be included as core matrisome constituents is still under debate, and in this regard, a new category, "matrisome-associated proteins", was proposed. This group of matrisome-associated proteins includes secreted factors, ECM regulators and ECM affiliated proteins (Naba, Hoersch, and Hynes 2012). Malignant transformation is coupled with an increased ECM stiffness that can lead to the activation of oncogenic signaling, and inhibition of tumor suppressor genes, including PTEN. Therefore, ECM clearly contributes to cancer progression and thus has become an interesting compartment to be studied in the field of oncology (Mui et al. 2015; Mouw et al. 2014; Naba et al. 2011).

Regarding the proteins mentioned earlier, the one found most increased in the secretome produced by PGC1 α -expressing cells was ECM1. This protein is overexpressed in tumors of epithelial origin (including breast, esophagus, stomach, colon, and lung) and is preferentially

expressed in metastatic tumors (L. Wang et al. 2003). Another study by the same group, linked ECM1 with stimulation of proliferation and angiogenesis of endothelial cells (Han et al. 2001). In a more recent study, in the context of PCa, ECM1 secreted by stromal cells was shown to inhibit transforming growth factor- β (TGF- β)-mediated PCa cells invasion. Authors in this study showed that increased ECM1 mRNA levels in PCa tumors were linked to an increased relapse free survival (al Shareef et al. 2018).

Protein TNXB was shown to be increased in ovarian cancer tissues compared to healthy ones, finding also larger amounts of this protein in the serum of high-grade ovarian cancer patients compared to healthy donors (Kramer et al. 2015). Glycoprotein MUC5B was found decreased in the PGC1 α -regulated secretome. Indeed, several types of mucins have been related to the development of tumor chemoresistance and to immunosuppressive effects by means of creating a physical layer that correspondingly protects tumor cells from drug exposure and immune cells (Jonckheere, Skrypek, and van Seuning 2014). Increased levels of secreted SERPINB5 were found to correlate with pancreatic ductal adenocarcinoma patient's bad prognosis. This protein seems to play an important role in the metastatic cascade by facilitating extravasation of tumor cells (C. Tian et al. 2020). On the other hand, FGFBP1 was also shown to enable cancer growth and metastasis through the promotion of angiogenesis (Zhu et al. 2016; Tassi et al. 2011; Zheng Zhang et al. 2019). Finally, top-decreased protein found in the secretome of PGC1 α -expressing cells was CTHRC1. This is a known secreted glycoprotein that functions as a negative regulator of collagen deposition, therefore leading to an increased cell migration ability (Pyagay, 2004). CTHRC1 expression is increased in PCa and its silencing in PCa cells decreased their proliferation, invasion, migration, and colony formation capacities (Ma et al. 2020; C. Zhang, Zhong, and Huang 2017).

The number of ECM-related proteins regulated by PGC1 α is quite ample and the fact that all of them (asides from ECM1) are highly decreased in the secretomes produced by PGC1 α -expressing cells, stands out. Most of these candidates were also analyzed at gene level, showing to be under the transcriptional control of PGC1 α -ERR α . The concept of tumor epithelial cells playing a role in the ECM deposition and remodeling processes is changing the classical view by which, fibroblasts are the only cells involved in this process. It is now recognized that tumor-derived matrisome proteins can enable tumor progression enhancing cell survival and colonization at distal sites. (G.-F. Xiong and Xu 2016). Almost all the proteins that were shown decreased in the secretomes produced by PGC1 α -expressing cells have been previously related to cancer-prompting roles, further granting consistency to our data. On the other hand, ECM1 found 44-fold increased in the PGC1 α -regulated secretome, was associated to a better prognosis of PCa patients. It is also worth mentioning that, as discussed earlier, integrins and other matrix-adhesion proteins were found decreased in EVs and in the producer cells at gene level. This data is indeed complementary to each other and presents a plausible cell-extrinsic mechanism of tumor and metastasis suppression driven by PGC1 α .

Secreted enzymes

The aspartyl-protease cathepsin D (CATD), found increased in EVs and SFs produced by PGC1 α -expressing cells is controversial regarding its tumor-promoting or suppressing role. CATD is known to be mainly present in endosomes and lysosomes, where apparently it is involved in the proteolytic processing of antigens and proteolysis of intra and extracellular proteins, correspondingly (Yamamoto 1999). CATD was described to be over-produced and secreted to the extracellular milieu by BCa cells. This BCa-derived secreted CATD seems to exert a pro-oncogenic role by promoting fibroblasts proliferation and invasive growth through the activation of MAPK pathway (Laurent-Matha et al. 2005). CATD was also linked to higher vessel density in BCa tumors (González-Vela et al. 1999). Opposite to this, CATD was found to be secreted by PCa cells, further suppressing angiogenesis, and preventing tumor growth *in vivo* (Morikawa et al. 2000). Finally, CATD is known to exert ECM-remodeling processes by cleaving laminin and fibronectin (Patel et al. 2018).

PGC1 α is an important regulator of ROS metabolism and was previously shown to increase the expression of various antioxidant enzymes with important oxidative-stress protective functions (Geng et al. 2011). Three different isoforms of SODs exist in humans, all of them involved on scavenging superoxide radicals. The three SOD isoforms have been reported to localize in the cell cytoplasm (SOD1), mitochondria (SOD2) and in the extracellular space (SOD3) (Marginean et al. 2016). Previous work in our laboratory showed how in our *in vitro* model SOD2 levels increased upon expression of PGC1 α . Regarding SOD3, it was previously reported to be secreted by PC3 cells, and to exert a tumor-suppressive role via accumulation of hydrogen peroxide in the extracellular milieu (J Kim et al. 2014). Apparently, this accumulation of free radicals was caused by the decreased levels of enzyme GSH, which lead to increased DNA damage levels, further affecting cell viability. SOD3 was also shown to reduce of tumor-associated vasculature leakage, allowing a better delivery of chemotherapeutics (Mira et al. 2018). Overall, these data suggest again that the protective roles tied to PGC1 α involve the regulation of antioxidant enzymes with cell-intrinsic and extrinsic localization and functions.

IFN-related proteins

Top-two increased protein identified in the differential secretomes was MX1. This anti-viral IFN-induced dynamin-like GTPase expression levels are known to be triggered under low levels of IFN (Medrano et al. 2017a). Expression levels of MX1 were correlated with BCa tumor grade and this protein was further proposed as metastasis-free survival marker for BCa patients treated with chemotherapy (Sistigu et al. 2014). Interestingly, MX1 was identified as a regulator of cell motility and metastasis in PCa, seemingly through its interaction with protein tubulin (Mushinski et al. 2009). Both, treatment with IFN α and small molecules induced MX1 expression and were able to block cell motility and invasion, presenting MX1 as an interesting target for avoiding PCa metastasis. In addition, the work by Brown et al revealed MX1 overexpression in

PCa cell lines induces cell cycle arrest and in contrast, MX1 silencing enhanced migration, invasion, and anchorage independent growth of DU145 cells. In this study and in line with the data provided by Mushinski and colleagues, treatment of PCa cells with tubulin-binding chemotherapeutic drug Docetaxel, showed to be more effective in MX1-expressing cells probably due to changes in the tubulin organization. MX1 localization was reported to be in the cell cytoplasm, apparently close to the ER (Accola et al. 2002). This localization may further suggest MX1 could be involved on the regulating trafficking of proteins or even be secreted, as we did observe in our PCa model. In fact, MX1 was reported to be secreted in EVs produced by PCa cell line VCaP (Hosseini-Beheshti et al. 2012).

Another IFN-related protein identified increased in the PGC1 α -regulated secretome was STAT1. This protein is key for type I and type III IFN response activation (Seliger, Ruiz-Cabello, and Garrido 2008), and to our knowledge, secretion of STAT1 has previously not been reported. The fact of MX1 and STAT1 proteins being increased in SFs and at gene level in PGC1 α -expressing cells is probably a bystander of the re-establishment of type I IFN signaling in the cells upon expression of PGC1 α . Why these proteins are released into the extracellular milieu, remains to be elucidated. Still, one could imagine that transfer of STAT1 and MX1 among cells would play anti-tumoral roles in PCa and, furthermore, they could even become biomarkers of PCa aggressiveness.

1.1.3 Tumor interstitial liquid (TIL)

Organ-proximal fluids have demonstrated to be a fount for biomarker discovery in different types of cancer. Nipple aspirate fluid was shown to be a good source for identifying specific proteins associated to BCa or to healthy donors. Therefore, detection of specific proteins in the nipple aspirate could be a non-invasive manner for BCa early detection, risk assessment and monitoring of disease course and therapy response (Noble et al. 2007; Shaheed et al. 2018; Pawlik et al. 2005). Cancer-specific proteins were also shown to be detected in pancreatic juice and lung pleural effusion (R. Chen et al. 2006; 2007)(Tyan et al. 2005; Soltermann et al. 2008). In PCa, proteomic studies have mainly focused on analyzing urine and serum as a source of biomarker discovery (Swensen et al. 2021; Khanna et al. 2021; Øverbye et al. 2015; Principe et al. 2012). In addition, seminal plasma was analyzed and showed great potential for identifying biomarkers of prostate and testicular cancers (Pilch and Mann 2006). The use of naturally occurring proximal fluids therefore seems an interesting option for the identification of biomarkers, but one must keep in mind that finding proteins present in low proportions can be challenging. Indeed, these biofluids are often dependent on physiological variables such as patient's hydration status, diet, or glomerular filtration rate. In addition, these fluids may collect proteins released by different tissues, generating a highly diverse and diluted pool of plausible biomarkers. Therefore, despite proteomics techniques are becoming more sensitive, getting closer to the origin (the tumor) may enable the identification of disease biomarkers due to their presence at higher concentrations (M. Wagner and Wiig 2015). In this sense, exploring the tumor interstitial liquid

(TIL) seems an interesting option. The TIL together with ECM structural proteins is the major constituent of the interstitial space. This area is made of connective tissue and is located outside the blood and lymph vessels, and parenchymal cells. Under physiological conditions, there is no net accumulation of fluid; the interstitial fluid flows from capillaries to lymph vessels, maintaining a net pressure close to 0 mmHg. Yet, tumors often experience leaky vasculature and impaired lymph drainage, leading to the accumulation of fluid (Ura et al. 2018) (**FigD 2**). Therefore, TIL, as it bathes the tumor microenvironment, can provide much information on secreted molecules and thus can be a good source for the study of cell communication and the identification of tumor-associated biomarkers (Hsu et al. 2019; Haslene-Hox et al. 2011).

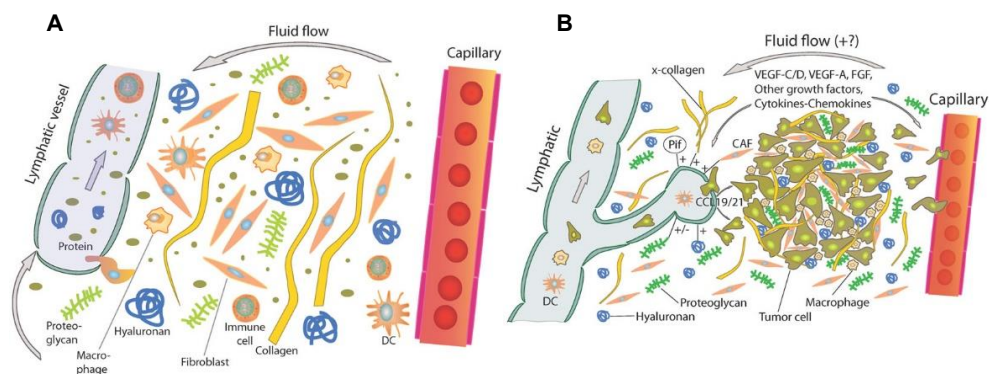


Figure D 2. Overview of the normal (A) and tumor intersticium (B). Modified from Wagner & Wiig, *Front. Oncol* (2015).

In order to explore this fluid, we took advantage of our GEMMs and performed LC-MS proteomics analysis of the TIL obtained from three-month KO and DKO mice. We focused on studying early PCa events, in which pro-tumorigenic features such as a reactive stroma can already be sensed (Berglund et al. 2018). Proteomics analysis of the TIL provided us with a list of 44 differentially present proteins between KO and DKO mice. From this list, three proteins (Ak1, Atp1b1 and Srm) were common to the proteomics analysis of the cell secretome. The *in vivo* model we used provides a more physiological scenario, and the proteins identified in the TIL may not be directly secreted by epithelial cells, rather than other cells in the prostate microenvironment. Therefore, GEMM-derived TILs may also provide with interesting information on the bi-directional communication between epithelial and stromal compartments.

Among the proteins identified in the TIL, spermidine synthase (SRM or SPEE) was found decreased *in vitro* in PGC1 α -expressing cells and their correspondent secretomes and increased in the TILs of DKO mice. This enzyme catalyzes the production of spermidine from putrescine and decarboxylated S-adenosylmethionine (dcSAM) in the polyamine synthesis pathway. An increased polyamine synthesis was previously described to sustain PCa (Zabala-Letona et al. 2017), and indeed, PGC1 α has been previously related to the regulation of this metabolic pathway. Kaminski and colleagues described a PGC1 α /c-MYC/ODC axis involved in the regulation of polyamines synthesis. PGC1 α through an ERR α -dependent mechanism was shown to inhibit c-MYC expression and ODC (Kaminski et al. 2019). Indeed, our group also described

decreased levels of ODC in the presence of PGC1 α , a well-known target of c-MYC (Valcarcel-Jimenez et al. 2019). Hence, decreased levels of polyamine pathway enzymes (SRM and ODC) are related to a more benign status, based on the expression of PGC1 α . Why SRM is secreted within the tumor interstitial space is an interesting aspect, perhaps related to the transfer of enzymes between cells for sustaining polyamine biosynthesis. In this sense, increased microenvironmental levels of polyamines were related with immunosuppression and cancer outgrowth (Alexander et al. 2017). Altogether, these data open novel and interesting questions tied to PGC1 α , polyamines and regulation of the tumor microenvironment. It would be therefore interesting to elucidate polyamine concentrations in KO and DKO prostates and correlate this data with the presence of immune-suppressive and cytotoxic T-cells, responsible for tumor cells killing. In this line, the enrichment analysis we performed on the candidates identified differentially present in the mice TILs revealed terms linked to immunity. One of the candidates included in the mentioned category was the 11S proteasome subunit Psme3, described to play a protective role under bacterial infections in mice by stabilizing transcription factor NF κ B (Sun et al. 2016). Opposite to this protective function, Psme3 expression has been reported to be increased in lung, and colorectal cancers (S. Xiong et al. 2014; Roessler et al. 2006). In BCa, Psme3 expression levels are also increased, and it seems to promote malignant outgrowth by inducing T-cell apoptosis (Yi et al. 2017).

Other interesting candidates found differentially present in the TILs, are ribosomal proteins (RPs). Four RPs (Rpl10, Rpl5, Rpl21 and Rpl15) were found to be increased in mice where Pgc1 α expression was abolished. In this line, it is interesting to mention that several RPs happened to be decreased in the secretomes produced by PGC1 α -expressing cells (RL18, RL7A, RL12, RS27, RS3A, RS13 HNRH3, RS5, RS27, ROA1, ROA3, HNRPR, HNRPQ). RPs are involved in the synthesis of mRNA, a tightly regulated process needed to sustain cell growth (Tschochner and Hurt 2003). Under certain stress conditions, free RPs may accumulate, generating what is known as nucleolar stress, further inducing activation of p53 pathway that leads to cell cycle arrest, senescence, and autophagy (Yang, Yang, and Yi 2018). On the other hand, a growing number of studies have demonstrated RPs also play tumor prompting roles in ovarian, gastric, and prostate cancers (Artero-Castro et al. 2011; Yongquan Shi et al. 2004; Maruyama et al. 2014). Oncogene c-MYC and tumor suppressors PTEN, pRB and p53 were shown to regulate the production of ribosomes, key for protein production in proliferative cells (Ruggero and Pandolfi 2003; Artero-Castro et al. 2011). This would be in line with our data, in which a more proliferative state in the absence of PGC1 α and presence of c-MYC would require a higher supply of ribosomal proteins to sustain cell proliferation. It would be though interesting to assess expression levels of c-Myc and RPs in KO and DKO mice. Finally, as an important fact to mention, RPs have lately emerged as important contributors of cancer development. Patients with ribosomopathies (defects in ribosomal proteins or the ribosomal assembly factors) have higher cancer risk (Girardi et al. 2018).

Protein Khsrp, was found increased in the TILs of DKO mice, where Pgc1 α was deleted. This protein was previously proposed to regulate c-MYC expression (He et al. 2000), and has

been linked with pro-oncogenic roles in non-small cell lung cancer (NSCLC), pancreatic and colorectal cancers (M. Yan et al. 2019; Taniuchi and Ogasawara 2020; Caiazza et al. 2019). Interestingly, in the context of colorectal cancer (CRC), authors described an altered secretome composition upon silencing of the protein in CRC cells, suggesting Khsrp may play an important role in the tumor microenvironment (Caiazza et al. 2019).

Regarding the enrichment analysis we performed on the list of genes encoding the proteins found differentially present in the TILs, AP1 and NFE2 emerged as transcription factors to mediate transcriptional regulation. Interestingly, AP-1, a transcription factor member of Fos and Jun families has been previously described to mediate the regulation of the tumor cells secretome, promoting therapy resistance and malignant growth under environmental stress conditions (Obenauf et al. 2015; Abd et al. 2018). AP-1 was suggested to contribute to PCa growth and survival to radiation treatment in a PI3K-dependent manner (Kajanne et al. 2009). Evaluating the contribution of AP-1 activity in our GEMM could provide with novel data tied to malignant transformation via secreted factors in the context of Pgc1 α loss.

Finally, it is also interesting to highlight that older (six months onward) KO and DKO mice accumulate ascitic liquid in the prostates, which can be an interesting source for studying more advanced stages in our model of PCa. In this sense, ascites have shown to be attractive biofluids, mostly studied in ovarian and colorectal cancer (Ford et al. 2020; Choi et al. 2011; Gortzak-Uzan et al. 2008), and usually appearing in more advanced cancers and linked with poor outcome (Ayantunde and Parsons 2007).

Overall, proteomics analysis revealed a list of proteins that were differentially present in the TILs obtained from KO and DKO mice, making them an attractive source for studying the cellular interactions in the tumor microenvironment through secreted factors. With no doubt, the GEMM provides with a more physiological context that should be exploited to unravel the cell interactions that underpin PCa evolution triggered by loss of PGC1 α .

1.2 Extracellular vesicles as a source for biomarker discovery

Early disease detection and diagnosis is key for enhancing survival of cancer patients. Identifying sensitive and specific non-invasive disease biomarkers could allow a more accurate disease follow-up. In this sense, exploring biological fluids (urine, blood, cerebrospinal fluid, lymphatic drainage) as well as *in vitro* secretomes has proven to be an interesting source for the discovery of biomarkers and mediators of cancer progression (Lore et al. 2017; Royo et al. 2016; Blanco et al. 2012; Nurdin et al. 2016; García-Silva et al. 2019). In this sense, EVs are stable units that can be found at high concentrations in most biofluids. Indeed, plenty of clinical trials involving EVs are being carried nowadays (clinicaltrials.gov). Concretely, eleven clinical trials involving PCa and EVs are registered in the USA up to date, and all of them are focused on evaluating or finding EVs in biofluids as markers for monitoring disease progression or response to therapy.

An interesting feature about EVs concerns cargo protection, which can be composed of different molecules, including nucleic acids, proteins, and lipids (Torrano, Royo, et al. 2016). EV are good fingerprints as their cargo usually reflects the status of the cell or tissue of origin (Royo et al. 2016). Indeed, applied to our *in vitro* model, all candidates we found differentially present in the proteomics analysis of EVs, where shown to follow the same trend at mRNA level in the producer cells. We are aware that RNA and protein do not always follow the same expression dynamics due to post-translational regulation, therefore, his data should be validated at protein level. Strikingly, some of the candidates we found differentially present in the EVs produced by PGC1 α -expressing and non-expressing cells, happened to be directly (*ATP1B1*) or inversely (*CLDN3*, *KPNA2* and *STXBP2*) correlated to *PGC1A* in PCa datasets. This further suggests EVs could act as surrogate non-invasive markers of PGC1 α status in patients with PCa. Indeed, the idea of generating an EV-based protein or mRNA-specific signature with prognostic potential has already been proposed in melanoma and in PCa (Peinado, Alečković, et al. 2012; Sequeiros et al. 2017; Torrano, Royo, et al. 2016; Royo et al. 2016). In PCa, due to the heterogeneity of the disease (Haffner et al. 2021), combining a panel of proteins might be a more accurate approach compared to the use of single markers. Our *in vitro* data together with the correlation analyses performed on data obtained from PCa patients, both support using multiple markers contained in vesicles as a robust method for the monitoring and the diagnosis of PCa. In this regard, some of the candidates identified as plausible constituents of an EV-based PCa signature have already been linked to this disease, although none of them in EVs. Tight junction protein *CLDN3* was shown to be a good marker for PCa (Bartholow et al. 2011), and interestingly, this protein together with *PTEN* could be detected in the blood of PCa patients, thus, demonstrating its potential as a marker for PCa diagnosis (Ye, Zhao, and Kang 2019). Importin subunit alpha *KPNA2* was also shown to be of prognostic potential in PCa, specially for tracking disease recurrence after radical prostatectomy (Grupp et al. 2014; Mortezaei et al. 2011). Regarding protein *ATP1B1*, it was included with another seven proteins as part of an AR-related signature that could be useful to monitor androgen dependent PCa transitioning toward castration resistant PCa (Capaia et al. 2018). In addition, a previous study by our group showed *ATP1B1* is part of a PGC1 α -ERR α -dependent transcriptional program involved in PCa suppression and was further included in a gene signature that predicts risk of recurrence of PCa patients (Torrano, Valcarcel-Jimenez, et al. 2016).

Based on previous studies presenting EVs as good mirrors of the molecular scenario on the tissues of origin (Royo et al. 2016; Sequeiros et al. 2017), as a next step, it would be key to interrogate the status of our panel of proteins in EVs isolated from urine or serum obtained from PCa patients with a known status of PGC1 α . If an association between our EVs-protein-based signature and PGC1 α status is proven to exist in patients, this could certainly open new avenues for the development of non-invasive tools for the diagnosis and prognosis of PCa disease (**FigD 3**).

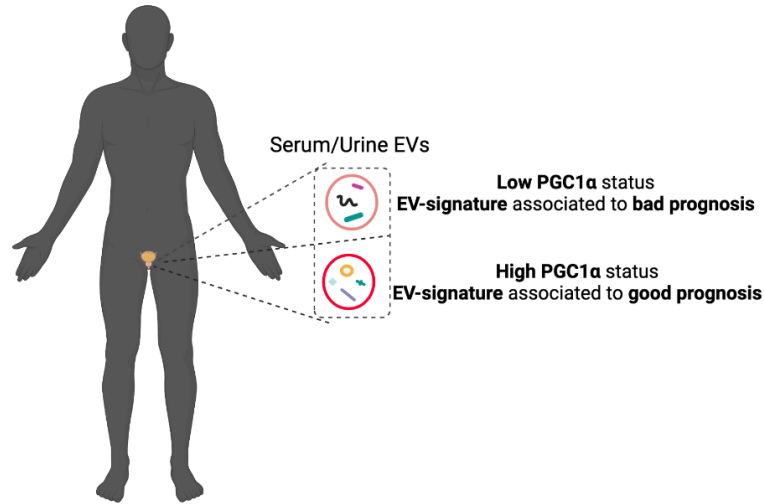


Figure D 3. EVs as surrogate markers of PCa. An EV-based protein signature linked to PGC1 α status is proposed as a non-invasive method for the diagnosis and prognosis of PCa.

II Understanding the impact of the cancer secretome in the stromal compartment

II.1 Cell secretome: priming the soil for metastatic cells seeding?

Metastasis is a highly inefficient process, in which a low proportion of the cells released into circulation survive (Fidler 1970). One of the first theories presented, explaining the successful colonization of distal sites by metastatic cells was proposed by Paget with the “seed and soil” hypothesis (Paget 1889). Following this idea, research in the last years has provided novel data supporting Paget’s hypothesis and has proven how primary tumor cells prime the sites of metastasis before their arrival. This concept could be understood from an ecological point of view in which, species settle in concrete ecosystems that provide them with the resources to progress. Indeed, these species may further modify and evolve, together with their environment to become a more complex community. This analogy stems for primary tumor cells secreting factors (soluble factors and extracellular vesicles) that in a paracrine manner, modify and instruct local cells to allow a successful metastatic seeding. These modified environments are known as pre-metastatic niches and are characterized by a series of features that include increased vascular leakiness, recruitment of bone marrow derived cells (BMDCs) as well as other types of immune cells, increased inflammation, and changes in the ECM (Peinado, Alečković, et al. 2012; Hafner et al. 1996; Männel et al. 1994; Yanfang Liu et al. 2016; Erler et al. 2009). Therefore, although tumor cells are the drivers of metastasis, a bi-directional communication between tumor cells and their environment is established and this is decisive for tumor progression.

Two in vivo metastasis assays were performed in the present thesis work and for that, EVs and SFs produced by PGC1 α -expressing and non-expressing PCa cells, were used for pre-conditioning the microenvironment before inoculation of the metastatic cells. Trying to resemble

a paracrine communication between PCa epithelial cells and the stromal compartment, both experiments aimed at understanding how secreted factors could exert a modulatory effect for enabling metastatic seeding (**FigD 4**). Indeed, Handschin and colleagues previously reported how in the skeletal muscle, a PGC1 α -dependent regulation of myokines influences the crosstalk between muscle and pancreatic islets for maintaining glucose homeostasis (Handschin, Chin, et al. 2007). Another study involving PGC1 α expression in the muscle revealed the co-regulator's role on ECM and basal lamina remodeling processes that influenced muscle stem cells towards a more effective response to injury (Dinulovic et al. 2016). On the other hand, liver-specific silencing of PGC1 α *in vivo* showed to favor progression of non-alcoholic fatty liver disease, by means of regulating ECM proteins, pro-inflammatory and antioxidant enzymes (Besse-Patin et al. 2017). Hence, these studies set a precedent on how PGC1 α can exert protective roles in different scenarios via regulation of cell-cell and cell-ECM interactions. Indeed, as mentioned earlier, we previously showed the impact of PGC1 α on the expression of adhesion molecules (Valcarcel-Jimenez et al. 2019). This observation was also evident in EVs protein cargo, where a wide number of adhesion molecules happened to be decreased upon expression of PGC1 α in the producer cells. Therefore, we could expect PGC1 α roles extended to the regulation of the tumor microenvironment, on both cell populations and ECM.

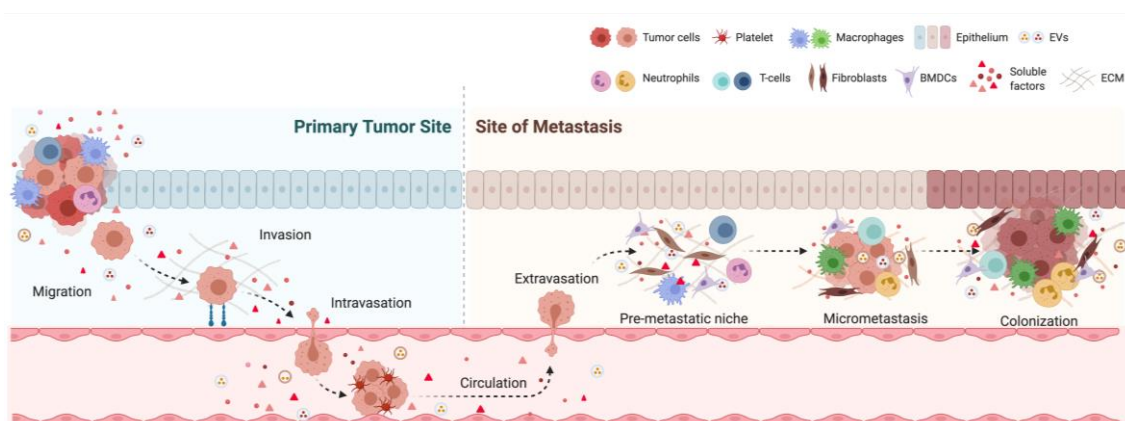


Figure D 4. Preparation of the pre-metastatic niches. Tumor-derived secreted factors (EVs and SFs) prime the sites of metastasis through the establishment of a paracrine communication with the stromal compartment.

Of note, a limiting aspect from both *in vivo* experiments concerns the animal model used. Athymic Nude-Foxn1 mice were educated with either EVs or SFs to study their impact at a systemic level on enabling metastatic seeding of PCa cells. In this sense, the mouse strain we used is characterized by its deficiency on T-cells, a subtype of lymphocytes with important roles on detecting antigens and orchestrating cytotoxic responses that are pivotal for eliminating malignant cells (Waldman, Fritz, and Lenardo 2020). We do not know to which extent T-lymphocytes could be affected by SFs and EVs produced by PGC1 α -expressing and non-expressing cells, an aspect that could be interrogated *in vitro* by treating these cells with both secretome fractions. Yet, finding a syngenic model in which immunocompetent mice would be

educated with PGC1 α -regulated SFs/EVs and injected with murine PCa cells would perhaps provide with novel and more physiologically relevant data.

II.1.1 Extracellular vesicles: on the road to the pre-metastatic niches

Despite the differences in EVs protein cargo, no differences in metastases formation and tropism were observed in mice educated throughout two weeks with EVs produced by PGC1 α -expressing and non-expressing cells, as well as in control mice. We therefore could state that PGC1 α -associated EVs do not play a role on priming the pre-metastatic sites in PCa. Indeed, this was unexpected, as several of the proteins found decreased in the EVs produced by PGC1 α -expressing cells benign-like context such as ITA2, CLDN3, JAM1, CD44, EDIL3, NRP1 and Rab13, were previously linked to metastasis-related features in different cancer types (Ziaee and Chung 2014; Agarwal, D'Souza, and Morin 2005; Elaine A McSherry 2011; Hiraga, Ito, and Nakamura 2013; S.-H. Jiang et al. 2015; Stipp, Kolesnikova, and Hemler 2001; Levina et al. 2015; X. A. Zhang et al. 2003; Beckham et al. 2014). We therefore could expect different roles of EVs produced by PGC1 α -expressing and non-expressing cells. Yet, despite no differences on metastasis formation rates and sites were observed upon treatment of nude mice with EVs produced by cells with different aggressive features, still a deeper analysis of plausible microanatomical changes in the metastasis-harboring organs should be performed. It would be of great interest to treat mice with labelled EVs and track their uptake by different resident populations in the organs where metastasis formation was observed (bones and lungs). In addition, educating the mice with the differential EVs and performing a more exhaustive analysis of the tissues through different OMICs techniques could inform on tissue remodeling processes that might be taking place via transfer of bioactive molecules contained in the EVs.

Uptake of EVs by recipient cells is known to happen through different mechanisms that include membrane fusion, phagocytosis and binding to specific receptors present in both, EVs and recipient cells, which, also determines organotropic features of tumors (Escrevente et al. 2011; Hoshino et al. 2015). Nonetheless, it was recently shown how resident cells do also harbor mechanisms to avoid uptake of tumor derived EVs through the activation of type I IFN response (Ortiz et al. 2019). This study nicely described how melanoma-derived EVs inhibit IFN signaling activation through the downregulation of IFNAR1 and ISG 25-hydroxylase (CH25H) enzyme in normal cells. This enzyme produces antiviral compound 25-hydroxysterol (25HC), and by searching molecules that could mimic 25HC, reserpine was identified and shown to block EVs uptake by normal cells. Indeed, reserpine administration *in vivo*, was able to block the formation of pre-metastatic niches and suppress lung metastasis. Hence, this data provides a nice proof of concept on how understanding the impact of EVs on priming the sites of metastasis could be key for identifying ways of blocking uptake of malignant EVs by host cells and thus, blunting metastasis.

Finally, from a technical point of view, compared to other *in vivo* studies in which EVs role on metastasis and/or tumor microenvironment remodeling was addressed, our education time

and final amount of EVs used for education of the mice were below (J. E. Lee et al. 2016a; Peinado, Alečković, et al. 2012; Hood, San Roman, and Wickline 2011; Hoshino et al. 2015).(Peinado et al. 2012) (Hood, San Roman, and Wickline 2011) (Hoshino et al. 2015). The experimental details from the mentioned studies and our work can be seen in **Table D 1**. Performing a longer-term experiment or injecting higher quantities of EVs into the mice would perhaps lead to a different experimental outcome than the one we observed. It was recently reported that human plasma is mostly enriched in hematopoietic-derived EVs (99.8%), being the remaining 0.2% derived from other tissues (Yuchen Li et al. 2020). Therefore, estimating the amounts of EVs that should be injected into the plasma of mice to mimic PCa is a challenging aspect. In this sense, the field of EVs needs to overcome technical aspects that can allow a better understanding of EVs biogenesis, secretion dynamics, journey, and uptake by target cells. In this sense, novel techniques using high resolution microscopy imaging are enabling the study of EVs *in vivo*, and this will surely help on experimental refinement and open the roads towards a better comprehension of EVs functions under physiological and pathological conditions (Verweij et al. 2021).

Table D 1. Experimental details of experiments involving EVs-injection into mice.

EV source	Injection site	EV-protein dose/ mouse/ injection	Frequency of injection	Total amount injected / mouse	Study
BCa	Mammary fat pad	10 µg	Three weeks Three times/week	90 µg	Lee et al. 2015
Melanoma	Flank	10 µg	Three weeks Three times/week	90 µg	Peinado et al. 2012
Melanoma	Footpad	50 µg	Three injections separated each by 48 hours	150 µg	Hood, San Roman and Wickline. 2011
Breast and pancreatic-cancers	Retro-orbital	10 µg	Three weeks. Injections every other day	90 µg	Hoshino et al. 2015
PCa	Retro-orbital	10 µg	Two weeks Two injections/week	40 µg	Our study

II.1.2 Soluble factors: unexpected role on priming the pre-metastatic niches

Compared to EVs, which were only recently described to be involved in cell communication (Kowal, Tkach, and Théry 2014), soluble factors are well known mediators of paracrine communication. Secreted factors are known to alter resident cells behavior by means of triggering diverse processes such as inflammation, angiogenesis, ECM matrix remodeling and BMDCs recruitment (Kaplan et al. 2005; Cox et al. 2016; Peinado et al. 2017). Since SFs regulated by PGC1α exerted an *in vitro* effect on recipient PCa cells (reduction in proliferation), exploring other tumor-related biological events in an *in vivo* context seemed interesting. We therefore pre-conditioned nude mice with the concentrated-SFs produced by PGC1α-expressing and non-expressing cells and performed a metastasis assay. Unexpectedly, this experiment

revealed a higher metastasis formation capacity of cells inoculated into mice that were educated with SFs produced in the presence of PGC1 α . A limiting aspect concerning this experiment was its shortness and the little *in vivo* monitoring of tumor formation we performed with Ivis device. Mice educated with the SFs-D had at day 6 extremely low luciferase signal intensity, which showed a trend towards being increased at day 13, when animals were sacrificed. Hence, probably by letting animals for one or two weeks longer, tumors would have reached higher volumes, a factor that in the SFs-D condition, happened to be especially critical.

Bearing in mind that the experiment should be refined in the future, we observed that tropism happened to be to the bones and lungs, which are frequent sites of metastasis in PCa patients (Bubendorf et al. 2000). Nonetheless, metastasis formation in the brain, which accounts in PCa patients for a 2% (Macedo et al. 2017), was also observed and furthermore, was increased in mice educated with SFs derived from PGC1 α -expressing cells. The model used for cell inoculation was intra-cardiac injection, which, compared to tail vein injection that favors lung metastasis formation, allows tumor cells to engraft in any tissue depending on their inherent features (Simmons et al. 2015).

Taking advantage of the enrichment analysis we had performed on the data obtained from the proteomics analysis of the cell secretome, some of the proteins differentially present in the secretomes produced by PGC1 α -expressing and non-expressing cells, have been previously linked to brain-related processes. These proteins include SERPINE2 (also termed GDN), RAC1, NRP1, NES, EZR1, CKB and G6PD. Besides from CKB and EZR1, all proteins were found decreased in the secretomes upon expression of PGC1 α . Proteins SERPINE2 and NRP1 were previously described to promote brain metastasis (Valiente et al. 2014; Arpel et al. 2016), thus not making them candidates for the increased brain metastasis formation observed in the mice treated with secretomes from PGC1 α -expressing cells. Nonetheless, levels of creatine kinase B (CKB) were described to be increased in serum from patients harboring brain tumors (Tadele et al. 2019). On the other hand, ezrin (EZR1) expression is increased in human astrocytoma tissues compared to healthy ones. This protein links the actin cytoskeleton with the plasma membrane and is known to boost metastasis (Mao et al. 2013). Indeed, EZR1 was reported to be increased in prostate neoplastic tissues (Pang et al. 2004). We therefore could hypothesize about both candidates, CKB and EZR1, as mediators of the increased brain metastasis formation observed in mice that were educated with secretomes produced by PGC1 α -expressing cells. Still, colonizing the brain implies bypassing the blood brain barrier (BBB), a tightly regulated microvascular system conceived for avoiding the unspecific entry of cells and molecules (Daneman and Prat 2015).

The bone happened to be an important site of metastasis formation in EVs and SFs-educated mice. Indeed, bone tissue is a major site of metastatic PCa, specially in patients developing CRPC that usually die within a period of 12-24 months after its detection (Sharma et al. 2013). The PC3 cell line used for IC injection and for production of the SFs derived from a bone metastasis. Indeed, among the biological processes found enriched in the SFs proteomics analysis, "osteoblast differentiation" emerged. From the candidates associated to this function

THOC4, SYNC, CH10, and ATPB were found increased in the secretome produced by PGC1 α -expressing cells. On the other hand, proteins TENA, PRS7 and DDX21 were found decreased in the secretome produced by PGC1 α -expressing cells. Thus, it would be interesting to deeper analyze the contribution of these specific proteins on fostering bone metastasis. Maintaining a balance between osteoblasts and osteoclasts is essential for the bone homeostasis, and this happens through the release of endocrine and paracrine factors. PCa metastases to the bone are more often osteoblastic than osteolytic, although mixed lesions also happen (Sturge, Caley, and Waxman 2011). PCa cells corrupt bone homeostasis by means of secreting factors that alter osteoblast functions leading to an abnormal deposition of bone matrix (Logothetis and Lin 2005). On the other hand, PCa cells are also dependent on factors released by osteoblasts for their growth. Thus, disrupting communication between PCa and bone-resident cells seems an interesting approach to avoid bone remodeling and blunting metastasis. Indeed, although conventional therapies (chemotherapy, hormonal therapy, and bisphosphonates) for bone metastatic PCa have shown to improve quality life of patients, metastatic outgrowth is not prevented. Research is providing with novel therapeutic targets, setting great interest in disrupting bone remodeling induced by tumor cells (Sturge, Caley, and Waxman 2011).

It is also interesting to mention that the PC3 cell line has been related with osteolytic lesions (Nandana et al. 2017). PCa cells often mimic bone resident cells, a concept that is known as “osteomimicry”. This process is triggered in an autocrine and paracrine manner via expression of bone-related signaling and matrix genes (Knerr et al. 2004; Koeneman, Yeung, and Chung 1999). Therefore, analyzing the secretome protein content, could also lead to the identification of candidates involved in osteomimicry.

III Effect of the PGC1 α -driven secretome in the tumor compartment: beyond the cell barriers and back to the roots?

In vivo metastasis experiments suggest a differential impact of SFs on priming the sites of metastasis. In that scenario, SFs produced by PGC1 α -expressing cells enabled metastatic seeding of cancer cells. On the other hand, our *in vitro* data showed how the SFs produced by PGC1 α -expressing cells exerts a tumor-suppressive role by means of blunting cell proliferation. Indeed, this PGC1 α -driven effect showed to be under the regulation of nuclear factor ERR α , a well-known partner of PGC1 α on mediating anti-tumoral responses in PCa (Torrano, Valcarcel-Jimenez, et al. 2016; Valcarcel-Jimenez et al. 2019).

Separation of the cell secretome on the soluble factors and vesicular fractions further demonstrated *in vitro* that the effect on proliferation was mediated by the SFs and not by EVs. Hence, as a next step, we would propose to explore the impact of the SFs in tumor initiation and growth using an *in vivo* context. It would be interesting to pre-condition highly metastatic PCa cells with the secretomes produced by PGC1 α -expressing and non-expressing cells prior to their inoculation into the flanks of nude mice. This would allow us to study the impact of the secretome on the tumor initiation capacities of the cells. On the other hand, it would also be informative to

perform the same type of experiment but without the pre-conditioning step. Once inoculated into the mice, tumors would be left to be formed and then, injections with the differential secretomes could provide information about the impact of the secretome on tumor growth *in vivo*.

Asides from evaluating the effect of the PGC1 α -regulated secretome on PCa recipient cells proliferation capacity, we also assessed migration. Migration is a key feature that malignant cells need to acquire to invade adjacent tissues and disseminate to other organs. Indeed, PGC1 α is involved on the regulation of the actin cytoskeleton that allows PCa cells migration and invasion (Valcarcel-Jimenez et al. 2019). We performed *in vitro* experiments using Boyden chambers and wound healing assays, and none of them showed changes on the migration ability of PCa epithelial cells treated with the differential secretomes or EVs. This may indicate that the cell-intrinsic events triggered in recipient cells by the treatment with the differential secretomes/EVs do not involve processes related to cell migration such as the induction of epithelial-mesenchymal transition (EMT) (Thiery et al. 2009). Nonetheless, asides from being cell-intrinsically regulated, migration capacity is also determined by the extracellular environment (Friedl and Wolf 2010; Roussos, Condeelis, and Patsialou 2011). Therefore, addressing the secretomes' impact on the migration ability of tumor cells could be studied from other points of view. On one hand, it would be interesting to perform assays in which non-educated PCa epithelial cells were left to migrate through Boyden chambers containing the differential cell secretomes, especially the soluble fraction of the secretome as it may contain growth factors and chemoattractants, known to trigger cell migration. On the other hand, from a tumor microenvironment perspective, we could also speculate about changes in the stromal compartment being triggered by the cancer cell secretome. *In vitro* monitoring of the ECM deposition by fibroblasts exposed to the secretomes produced by PGC1 α -expressing and non-expressing cells could inform about changes in the matrix composition and stiffness and thus influence PCa cells migration ability.

From our *in vitro* and *in vivo* experiments, it is tempting to hypothesize that EVs biological functions could be dependent on their interaction with the SFs fraction of the cell secretome. Supporting this idea, *in vitro* data evidence no effect on tumor cells proliferation and migration capacities upon treatment with EVs derived from PGC1 α -expressing and non-expressing cells. Opposite to that, a reduced proliferation capacity of PCa cells treated with whole secretome (S) and SFs obtained from PGC1 α -expressing cells was observed. Indeed, a more pronounced proliferation drop was observed on PCa recipient cells when treated with the whole secretome than with the SFs fraction alone. On the other hand, *in vivo* metastasis assays performed with the two separated secretome fractions (EVs and SFs) demonstrated no apparent effect of EVs on priming the sites of metastasis. Contrary to that, SFs produced by PGC1 α -expressing cells favored cell nestling *in vivo*. In fact, a differential impact of EVs and SFs was also described by Jung and colleagues (Jung et al. 2009). In this study, authors took advantage of two rat pancreatic adenocarcinoma cell lines with distinct metastatic capacities due to a defect on a CD44 variant (CD44v). Indeed, pancreatic adenocarcinoma cells with or without CD44v displayed secretomes with differential capacities on priming the sites of metastasis *in vivo*. The effect of EVs or SFs was

not as potent as the whole secretome, and opposite to our data, EVs showed to infer a stronger effect than SFs. Additionally, some of the *in vivo* effects that were observed to be triggered by the whole cell secretome, where not reproduced *in vitro*, revealing how complex cell interactions can be depending on the biological scenario.

Overall, a synergistic effect of EVs and SFs fractions of the PGC1 α -driven secretomes might exist and could explain why, apparently, no biological impact of EVs was observed *in vivo* and *in vitro*.

III.1 Puzzling the pieces

Classically, drugs for the treatment of tumors have focused on targeting cell-intrinsic pathways altered in malignant cells, but disruption cell-extrinsic events might be another way of tackling Achilles' heel of tumors. Indeed, in PCa main efforts for the identification of therapies are based on targeting cell-intrinsic mechanisms such as inhibition of AR activity (Ramroop, Stein, and Drake 2018). But lately, a growing number of studies have evidenced how the autocrine and paracrine communication established by PCa cells and stromal cells is essential for tumor success (Dagvadorj et al. 2007; Rojas et al. 2011a; Zeda Zhang et al. 2020; Kerr et al. 2010; Calcinotto et al. 2018; Y. C. Lee et al. 2015).

The data provided in the present work sets some light on how the dysregulation of the transcriptional co-regulator PGC1 α leads to the alteration of other functions beyond metabolism. We demonstrate how cell-intrinsic phenomena (loss of PGC1 α) is reflected in a cell-extrinsic manner (altered secretome composition). As discussed previously, several candidates identified by proteomics analysis were further confirmed at mRNA level in the producer cells, suggesting secretomes reflect the status the cell.

RNA sequencing experiments performed on both, PCa recipient cells treated with the PGC1 α -differential secretomes as well as in the PGC1 α -expressing and non-expressing producer cells, were highly informative. On one hand, the RNA sequencing performed on the recipient cells treated with the distinct secretomes, revealed a differential activation of signaling events tied to type I IFN response. On the other hand, RNA sequencing analysis performed on the producer cells, revealed again a differential activation of type I IFN pathway. In both cases, there was an enhancement of molecules involved in type I IFN response in the PGC1 α -expressing context. This "mirroring effect" can lead to speculate about an autocrine effect behind PGC1 α 's anti-tumoral activity (**FigD 5**). Indeed, apparently 70% of the ligands and 60% of the receptors expressed by a given cell can correspondingly bind receptors and ligands present in the same cell. This suggests that most of the signals released by a cell to the extracellular milieu have the potential to trigger autocrine signaling events (Ramilowski et al. 2015). Applied to a malignant context, studies performed in tumor specimens or using RNA sequencing-based machine learning models revealed an association between the expression of ligands and cognate receptors in breast, lung, and glioma cancer patient prognosis, suggesting the importance of ligand-receptor-interactions for sustaining tumor growth (Tateishi et al. 1990; Umekita et al. 2000;

Yuan et al. 2019). These ligands may be released by tumor cells themselves or from their microenvironment and provide an interesting opportunity for designing drugs to disrupt these interactions. In this line, although experiments should be refined, secretomes produced by PGC1 α -expressing cells displayed higher levels of IFN- β compared to the non-PGC1 α -expressing ones. Still, IFN- β cognate receptor subunits *IFNRA1* and *IFNRA2* showed no changes in expression levels between PGC1 α -expressing and non-expressing cells, thus being the production of IFN- β the limiting variable. This data suggests that non-PGC1 α -expressing cells might be responsive to the treatment with IFN- β , and perhaps, *IFNRA1* and *IFNRA2*, could be used as biomarkers for therapy response. In this line, the expression of STAT1 was reported to predict IFN α treatment responsiveness in chronic myeloid leukemia patients (Landolfo et al. 2000).

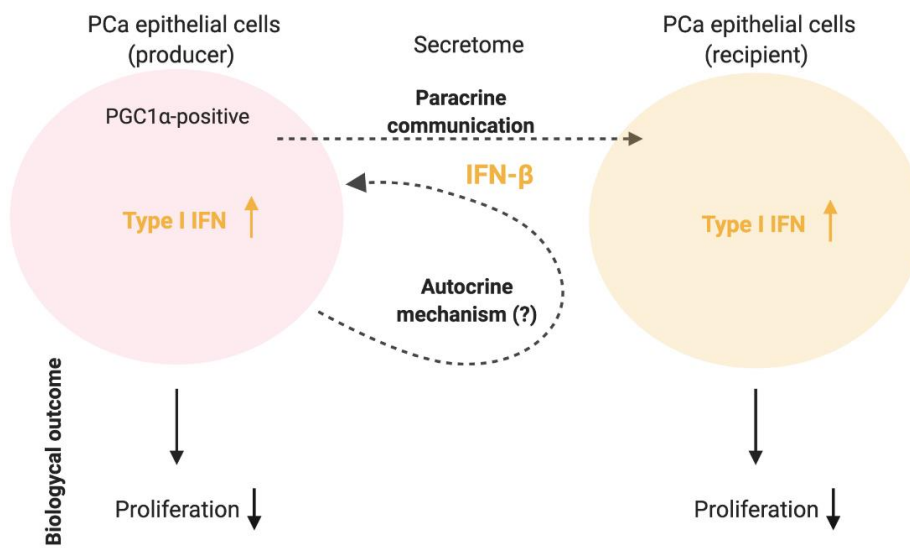


Figure D 5. Autocrine and paracrine effects of the cell secretome.

Focusing again on the cell-intrinsic features of PCa epithelial cells with differential expression of PGC1 α , RNA sequencing displayed an enrichment of distinct functionalities linked to the up and downregulated genes. Re-expression of PGC1 α was coupled with the upregulation of genes related to oxidative metabolism and type I IFN response and the downregulation of cell cycle-related genes. Loss of PGC1 α renders PCa cells with more aggressive features, but on the other hand, we have gained insight on the vulnerabilities these cells present (**FigD 6**). These vulnerabilities can be exploited for therapeutic purposes and thus, open novel possibilities to restore the “PGC1 α -driven anti-tumoral effect”. In fact, an interesting aspect is that IFNs and IFN-mimicking compounds have cell-intrinsic and cell-extrinsic consequences on tumor cells, which makes them attractive anti-tumor effectors (Medrano et al. 2017a; B. S. Parker, Rautela, and Hertzog 2016b).

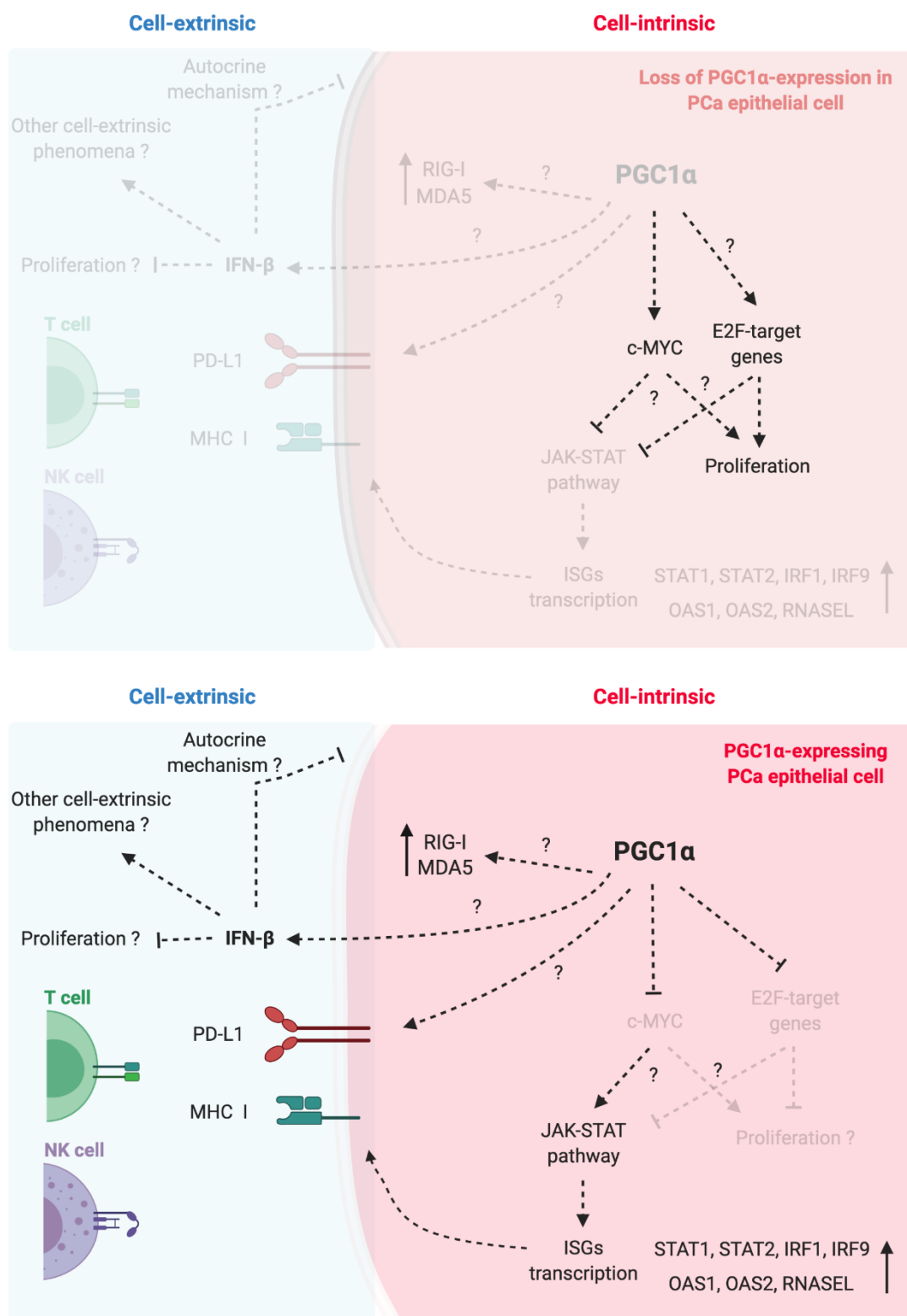


Figure D 6. PGC1α-driven cell intrinsic and cell-extrinsic phenomena that contribute to the suppression of PCa aggressiveness.

Tumor immune escape is a common mechanism developed by malignant cells to avoid destruction by the immune system. Since the discovery of immune checkpoint inhibitors (CPI) such as cytotoxic T-Lymphocyte Antigen 4 (CTLA-4) and programmed cell death 1 (PD-1),

immunotherapy has demonstrated to be a breakthrough in oncology as it restores the immune system against tumors (Hargadon, Johnson, and Williams 2018). Despite some cancers such as lung and melanoma show high responsiveness to CPI (Waldman, Fritz, and Lenardo 2020; Snyder et al. 2014), PCa is considered as a "cold" type of tumor due to its low immunogenicity and has shown little response to CPI treatment. This little immunogenicity could be due to the low mutational burden that accompanies PCa, which consequently leads to a reduced expression of neoantigens and therefore, to a decreased recruitment of immune cells (Segal et al. 2008; Schumacher and Schreiber 2015). In this sense, tumors such as melanoma, which present high DNA damage levels induced by UV, generate large amounts of neoantigens that induce high immunogenic responses (Snyder et al. 2014).

Our group previously described PCa patients expressing low levels of PGC1 α are at higher risk of developing metastasis (Torrano, Valcarcel-Jimenez, et al. 2016). Interestingly, PCa patients responding to CPIs have higher levels of IFN markers (Maleki Vareki 2018). On the other hand, a study in which patients with different types of cancers were enrolled, pointed towards patients expressing higher levels of programmed cell death-ligand 1 (PD-L1, also termed CD274) benefiting from PD-1 blockade therapy (Topalian et al. 2012). In fact, gene expression levels of *CD274* were increased in PGC1 α -expressing cells compared to the non-expressing ones. It is also worth mentioning that according to Taube et al, increased expression levels of PD-L1 in malignant cells was accompanied of increased presence of tumor infiltrating lymphocytes and IFN-g secretion, suggesting PD-L1 expression could be an adaptive response rather than an oncogene-driven mechanism (Taube et al. 2012). Therefore, although PCa patients have shown little benefit from immune-based therapies, we foresee that taking advantage of the stratification potential of PGC1 α and knowing the molecular events that underpin loss or gain of PGC1 α activity, more precise therapies could be designed. PCa patients with decreased levels of PGC1 α may benefit from a combinational therapy of CPI together with an induction of type I IFN response. Indeed, in the last years, several strategies were developed to exploit type I IFNs anti-tumoral features, including gene therapy approaches, genetically modified immune cells, and administration of synthetic molecules (Medrano et al. 2017a).

Cell cycle and IFN-response pathways are processes tightly intertwined. The elegant work performed by Goel and colleagues, showed how in HER2 BCa tumors treated with inhibitors of cyclin-dependent kinases 4 and 6 (CDK4/6) increased the expression levels of ISGs whilst decreasing levels of E2F target genes (Goel et al. 2017). Among the E2F-target genes, DNA methyltransferase 1 (DNMT1) was identified to be downregulated and associated to the expression of endogenous retroviral genes tied to increased double strand RNA (dsRNA) levels. This mechanism was suggested as a trigger for the increased secretion of type III IFN cytokines that probably, via an autocrine mechanism, drove the activation of JAK-STAT signaling. Inhibition of CDK4/6 also led to the suppression of immunosuppressive T regulatory lymphocytes (Treg) and intra-tumoral levels of CD8⁺ T cells displayed lower levels of T-cell exhaustion markers. Overall, these results demonstrate that inhibition of CDK4/6 enhances tumor immunogenicity, hence preventing tumor escape. Aligned with this work, it is tempting to speculate that using

inhibitors of CDK4/6 could restore the effect that is tied to the expression of PGC1 α . Supporting this idea, RNA sequencing data displayed reduced levels of *CDK4* in PGC1 α -expressing producer cells. In addition, preliminary data from the lab, show reduced pRB levels in PGC1 α -expressing cells. As aforementioned, expression of PGC1 α is coupled with higher *IFNB* gene expression levels and secretion of the cytokine to the extracellular space. We do not know yet which is the mechanism that triggers IFN- β secretion, and whether this cytokine is the sole one activating the JAK-STAT signaling cascade upon expression of PGC1 α . Yet, in line with the data provided by Goel et al, a plausible explanation could be the expression of endogenous retroviral genes. Indeed, RNA sequencing data from PGC1 α -expressing and non-expressing cells exhibits decreased levels of E2F-target genes methyltransferases *DNMT1* and *DNMT3B*, suggesting dsRNA cytoplasmic levels could be triggering JAK-STAT pathway. In addition, dsRNA pattern recognition receptors RIG-I (gene name *DDX58*) and MDA5 (gene name *IFIH1*) were both increased in the presence of PGC1 α as observed in the RNA sequencing data. Finally, we cannot fail to mention that PGC1 α -expressing cells have an increased expression of major histocompatibility complex class I (MHC I) genes *B2M* and several *HLA*-molecules, crucial for recognition of tumor cells by T-cells (Seliger, Ruiz-Cabello, and Garrido 2008), as well as IFN-related genes such as *IRF1*, *IRF9*, *STAT1*, *STAT2* and *NLRC5*. RNA sequencing data also extends to the upregulation of ISGs such as *OAS1*, *OAS2*, *OAS3* and *RNASEL*, which need to be further validated by RT-qPCR. The treatments we performed with the secretomes produced by PGC1 α -expressing and non-expressing cells nicely showed a reduction in recipient cells proliferation that was accompanied by the upregulation of IFN-related genes, including *STAT2*, *IRF1* and *NLRC5*. Antigen presenting genes *B2M* and *HLA-E*, were also increased in the recipient cells treated with the secretome from PGC1 α -expressing cells. It would therefore be of great interest to examine activation of JAK-STAT signaling pathway in PCa recipient cells treated with the secretomes regulated by PGC1 α -expressing and non-expressing cells. Considering that the PGC1 α -driven secretome contains a higher concentration of IFN- β and assuming recipient cells do express IFNRA1 and IFNRA2 receptor subunits, this can lead us to speculate again about a reduced proliferation capacity of PCa tumor cells upon treatment with IFN- β , a well-known proliferation inhibitor (Kimchi 1992). Indeed, the study by Dong et al showed PCa cell lines transduced with *IFNB* displayed *in vivo* reduced tumor formation capacity compared to control cells lacking expression of IFN- β . *IFNB*-expressing cells generated conditioned medias that induced the cytolytic effect of splenic immune cells on PCa cells. Overall, the effect of expressing IFNB in PCa cells exerted a tumor-suppressive function due to the inability of the tumors to form blood vessels and to the higher infiltration of natural killer (NK)-cells and macrophages that were able to lysate tumor cells and inhibit malignant cell proliferation (Dong et al. 1999).

We previously showed that loss of PGC1 α is coupled with increased c-MYC levels in PCa (Valcarcel-Jimenez et al. 2019). Oncogene c-MYC was described to blunt IFN response in Burkitt's lymphoma apparently through its direct binding to STAT1 promoter (Schlee et al. 2007). On the other hand, expression of c-MYC showed to be downregulated by IFN via activation of

dsRNA-dependent protein kinase PKR (Raveh et al. 1996). Yet, our time-course experiments displaying c-MYC reduction prior to the activation of STAT1 denote IFN might not be the trigger to c-MYC downregulation. Taken all these data together, one could envision inhibition of c-MYC as a potential therapeutic target for re-establishing IFN signaling pathway in PCa patients expressing low levels of PGC1 α . We hypothesize that silencing of c-MYC would lead to the re-establishment of JAK-STAT signaling pathway and thus induce the expression of ISGs, rendering tumor cells more vulnerable to the attack of the immune compartment. Indeed, this concept is supported by the work of Muthalagu et al, where c-MYC was shown to be pivotal for aggressive pancreatic ductal adenocarcinoma (PDAC) sustenance (Muthalagu et al. 2020b). c-MYC ablated the expression of STAT1 and other ISGs through its direct binding to the gene promoters. Together, KRAS and c-MYC were shown to suppress type I IFN pathway, which had an impact on macrophage-derived production of chemokine CXCL13, crucial for the B and NK cells infiltration into the tumor.

Another interesting aspect in the context of the regulation of IFN response involves epigenetics. The work performed by Owen and colleagues demonstrated how restoration of tumor cell intrinsic IFN signaling employing histone deacetylases inhibitors enhanced tumor cells visibility by the immune compartment, blocking PCa cells metastatic seeding to the bone. Stimulation of the immune compartment using synthetic dsRNA analog poly I:C showed to be not enough to blunt bone metastasis, as tumor cells rendered invisible to lymphocytes. This evidenced the importance of triggering tumor cell-intrinsic IFN signaling (Owen et al. 2020). In the same line, a very recent study, also in the context of PCa, showed how the methyltransferase EZH2 (increased in PCa) negatively regulates ISGs, generating an immune-suppressive microenvironment that promotes CPI resistance (Morel et al. 2021). The mechanism by which EZH2 exerts its tumor prompting role seems to be via transcriptional repression of endogenous retroviral sequences. Blockade of EZH2 was followed by the increased levels of dsRNA, which seemingly activated STING, shown to be critical for the upregulation of ISGs. Interestingly, EZH2 inhibition also had consequences on the interaction of tumor cells with the immune compartment. Tumor PD-L1 levels were associated to the inhibition of EZH2 and showed to be an excellent target for combinational therapy with anti-PD-1, which indeed, was able to restore immune-mediated cytotoxicity. The increased levels of PD-L1 we observed in PGC1 α -expressing cells joined to the fact that the coregulator is regulated at multiple levels, including epigenetic mechanisms, may provide an excellent window for applying combinatorial therapies to treat PCa. We could expect that using epidrugs for modulating PGC1 α expression would induce its tumor-suppressive transcriptional program and would also lead to increased levels of PD-L1, thus rendering the conditions for applying anti-PD-1 therapy. In this line, the study performed by the group of Puigserver nicely demonstrated how pharmacological inhibition of EZH2 complex in melanoma cells led to the increased expression of PGC1 α and suppression of cell invasion (Luo et al. 2020). In the same line, RNA sequencing data from PCa producer cell lines shows *EZH2* levels are downregulated in PGC1 α -expressing cells (adjusted p-value < 0.05 and 2-fold change

cut-off). It would be therefore interesting to analyze if the promoter region of *PGC1A* presents methylation differences in PCa patients. In this sense, a study in which methylation levels of *PGC1A* and *PGC1B* genes was assessed in blood leukocytes of patients with different types of cancer (including PCa), revealed two CpG methylation sites in the promoter region of both genes that were associated to higher cancer risk (Kresovich et al. 2018). Yet, this study has limitations as the expression levels of *PGC1A* and *PGC1B* were not analyzed neither in leukocytes nor in tumor tissues. In addition, one should bear in mind the wide number of processes in which PGC1 α is involved, thus making it challenging to become a target for precision medicine (Martínez-Redondo, Pettersson, and Ruas 2015b)

Finally, we cannot obviate that re-establishment of type I IFN signaling in tumor cells, besides from rendering them obvious to the immune attack through the expression of antigen binding proteins, it may also modulate the behavior of immune cells. We therefore wonder whether there might be differences in infiltrating immune populations on tumors that present high or low PGC1 α levels. Addressing this question could be done *in vitro*, using the differential secretomes for culturing different immune cell populations, including immunosuppressive Tregs and MDSCs as well as monocytes and T and B-cells. Additionally, we could test the ability of cytotoxic T-cells and NK cells to kill PCa cells with distinct expression of PGC1 α , expecting that PGC1 α -expressing cells would be more visible to the immune cells. Finally, we could also take advantage of PCa patients' specimens and our GEMM, where the loss of PGC1 α could be restored by administering epidrugs, c-MYC or CDK4/6 inhibitors, allowing to study the recruitment of immune cells into mice prostates. Genetic, epigenetic and microenvironmental cytokine-mediated mechanisms have been reported to regulate the expression of PD-1 (Bally, Austin, and Boss 2016; Kinter et al. 2008). Exploring if PD-1 levels are also modulated by PGC1 α in the immune compartment (perhaps through the release of cytokines by the epithelial compartment) could render information on T-cell exhaustion.

Overall, the tumor suppressive effect triggered by PGC1 α might be restored through different strategies that include tackling upstream and downstream regulatory mechanisms of the transcriptional co-regulator. PCa patients with loss expression of PGC1 α might benefit from these immune-based therapeutic strategies (**FigD 7**).

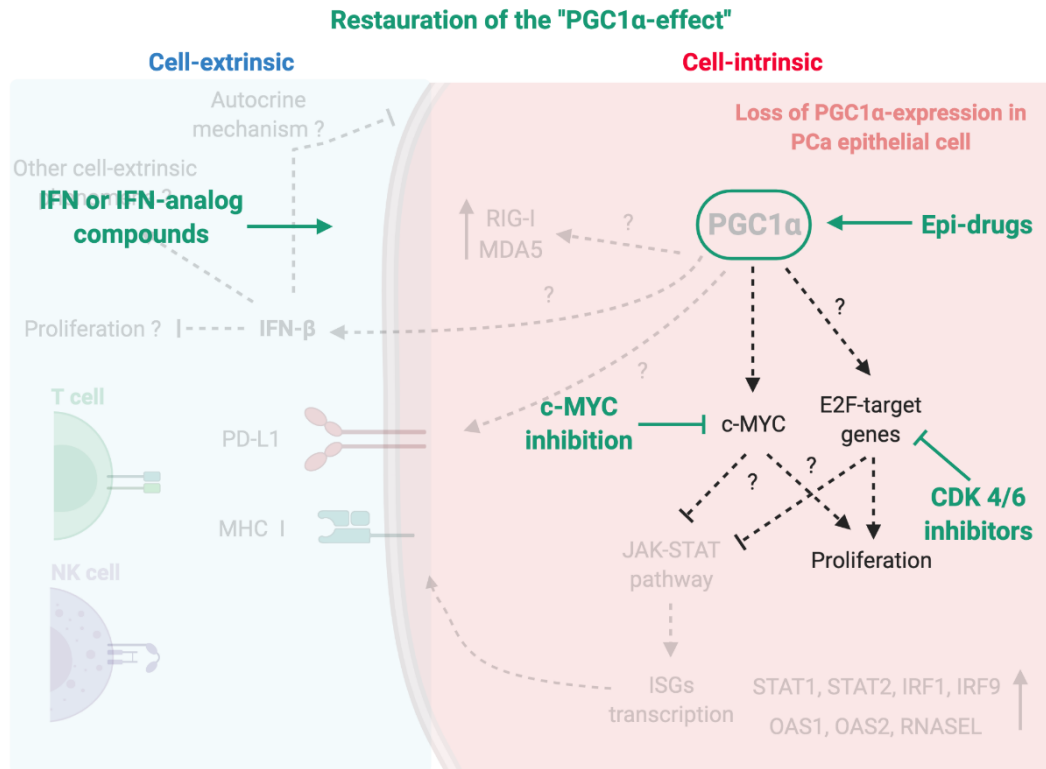


Figure D 7. The PGC1 α -driven anti-tumoral effect might be restored through different strategies.

III.2 Spatial architecture for the study of cell communication

The development of sequencing technologies has become a revolution, allowing the identification of concrete mutations involved in malignant processes, and thus enabling the development of personalized therapies. Indeed, tumors can nowadays be analyzed at multiple levels, combining genomics, epigenomics, transcriptomics, metabolomics, and proteomics. In the present work we have used a combination of transcriptomics and proteomics data to deconstruct PCa disease governed by the metabolic regulator PGC1 α . Proteomics analysis of the secretome composition has shown to be an interesting source for identifying autocrine and paracrine signaling networks involved in cancer (Y. C. Lee et al. 2015; Rojas et al. 2011b; Blanco et al. 2012; Nurdin et al. 2016; Sardana et al. 2008; Martin et al. 2004; de Boeck et al. 2013; Lore et al. 2017; Olmeda et al. 2017; Chang et al. 2012). On the other hand, transcriptomics has also fostered the study of intercellular communication, mostly due to the great amount of data available, and it has demonstrated to be a good source for establishing predictive models that can allow the identification of cellular networks. This is becoming a growing field and is giving rise to computational tools such as Cellphone DB, CellChat, NicheNet or ICELLNET among others, which aim at predicting interactions between cells and can be helpful for establishing novel hypotheses (Vento-Tormo et al. 2018; Jin et al. 2020; Browaeys, Saelens, and Saeys 2020; Noël et al. 2020).

Yet, studying cell communication without having a spatial context, is a limiting aspect for understanding cellular networks. Besides from the specificity that is dictated by the presence of certain receptors or uptake mechanisms in the target cells, physical distance between signal-producing and target cells influences communication. The motion at which soluble factors are propagated are determined by physical aspects, although cells can regulate production and secretion rates through autocrine feedback loops (Francis and Palsson 1997). Indeed, it is estimated that juxtacrine and paracrine signals can act in distances ranging 0-200 μm . Therefore, molecular characterization without disrupting tissues, has become an emerging field that provides information on cellular localization and heterogeneity, tissue architecture and immune profiling (Longo et al. 2021; Thrane et al. 2018). These facts are highly informative for understanding nodes of interaction between cells under physiological and pathological conditions. Multiplexed fluorescent imaging has shown to be useful, allowing the detection of several markers, including low-abundant proteins even at a subcellular level (Gut, Herrmann, and Pelkmans 2018). Other technologies such as multiplexed ion beam imaging (MIBI) using antibodies linked to low-abundant metals has also shown great sensitivity as an imaging technique (Angelo et al. 2014). But combining high-resolution imaging and single sequencing techniques has led to the emergence of spatial resolved transcriptomics and proteomics, which provide with molecular, cellular, and spatial information (Longo et al. 2021; Lundberg and Borner 2019). Different approaches have been set for spatial transcriptomics, including spatial barcoding and fluorescent *in situ* sequencing (J. H. Lee et al. 2014; Baccin et al. 2020; Ståhl et al. 2016). Spatially resolved approaches still cannot provide information on a precise cell within a tissue, but it opens up with information about cell ecosystems expressing concrete gene or protein sets.

Hence, using omics data and spatial-resolved techniques may further contribute to understand cell interactions. Applying these techniques in our PCa model could enable us to evaluate how expression of PGC1 α in the epithelial compartment impacts on other malignant cells as well as cell populations from the stromal compartment. Despite genetic aberrations are the first oncogenic events to trigger cancer, it is becoming evident that malignant cells require interaction with their environment to progress. Indeed, considering the immune context of tumors showed to be important for predicting response to therapy and led to the development of Immunoscore (Galon et al. 2012). This method aims at estimating patients' prognosis based on the infiltration of specific immune cells within the tumor center and the invasive margins, and has been validated for colorectal cancer, by measuring CD3 $^+$ and CD8 $^+$ tumor-infiltrating lymphocytes (Pagès et al. 2018). Identifying nodes of interaction between cells could lead to the identification of biomarkers and targets for precision therapy. In this line, a recent study focused on the single cell RNA sequencing analysis of PCa tumors revealed a highly heterogeneous transcriptional landscape (S. Chen et al. 2021). This study took advantage of CellPhone DB tool (Vento-Tormo et al. 2018) to dissect communication between epithelial and tumor microenvironmental cell populations. This study also identified EVs as important mediators of intercellular communication between PCa epithelial cells and T-cell populations, showing to be crucial for the metastatic seeding to lymph nodes. Finally, this work also provided with interesting

information on the role that activated tumor ECs play on their interaction with fibroblasts, other ECs, the immune compartment, as well as the ECM, presenting them as key mediators of aggressive PCa.

Finally, an interesting aspect that could be addressed under the umbrella of spatial biology methods is the concept of "cell competition". Cell competition is a selection mechanism originally identified in *Drosophila melanogaster* by which, two cell populations compete for survival (Morata and Ripoll 1975). This mechanism of fitness selection plays important roles for maintaining normal organ function and plays tumor suppressive and prompting roles (Moreno 2008; Martins et al. 2014; Watanabe et al. 2018). Cell competition can be viewed as a Darwinian selection process that provides cell populations with the gear to remove cells that can be dangerous for maintaining homeostasis. Unfit cell removal mechanisms include apoptosis, senescence, autophagy, and growth rate differences (Baker, Kiparaki, and Khan 2019). This phenomenon is more frequent in epithelial cells, and a key characteristic is that the cell with lower fitness could survive in an environment of cells with the same genotype, thus evidencing the non-cell autonomous nature of this selective pressure (Moreno 2008). As it was previously published by our group, the loss of PGC1 α endows PCa cells with more aggressive features including an enhanced proliferation capacity (Torrano, Valcarcel-Jimenez, et al. 2016). Berglund and colleagues recently showed by spatial transcriptomics how highly heterogeneous PCa tissues are (Berglund et al. 2018). One could imagine a scenario in which PCa epithelial cells have distinct expression levels of PGC1 α , generating a cell competition situation. Furthermore, we could speculate about two driving forces competing for succeeding and eliminating the neighboring cells. On one hand, cells with an activated PGC1 α transcriptional program would be less aggressive and probably would be overcome by non-PGC1 α expressing cells. These cells do have higher c-MYC levels than PGC1 α -expressing PCa cells. Indeed, high MYC-expressing cells were described to be "super-competitors", removing low-MYC expressing cells by triggering apoptosis whilst fostering their own proliferation and thus, leading to tumor expansion (Moreno and Basler 2004). Elucidating if there is a competition mechanism that drives the decreased expression of PGC1 α along progression of PCa could be a novel approach for understanding the disease. In line with this idea, growth of adenoma cells with loss of cancer driver APC were shown to be suppressed in a cell-competition-inhibited environment (Suijkerbuijk et al. 2016). Thus, protecting the host tissue (in our situation, PGC1 α -expressing conditions) could be another resource for suppressing cancer cell growth, and for that, understanding the communication between both PCa cell populations seems crucial.

The exact mechanism by which the transcriptional co-regulator PGC1 α exerts its tumor suppressive activity in PCa still remains to be elucidated. Yet, our view of PGC1 α as "just" a metabolic regulator has become broader, extending its domains towards the transcriptional regulation of cell-intrinsic and cell-extrinsic biological processes. The combination of OMICS data and spatial approaches can be a swift way of generating an impact on patients' care management.

It may allow us to identify individualized therapies and novel drug targets, as well as the discovery of biomarkers of disease progression and therapy response.

Tumor deconstructing will allow the administration of personalized therapies and thus improve cancer patients care. Yet, a major challenge will be the integration of the complex and great amount of data generated. This will require a crosstalk between biological and data sciences, which through the development of computation, mathematics and statistics will allow us to better comprehend the biology of cancer (**FigD 8**).

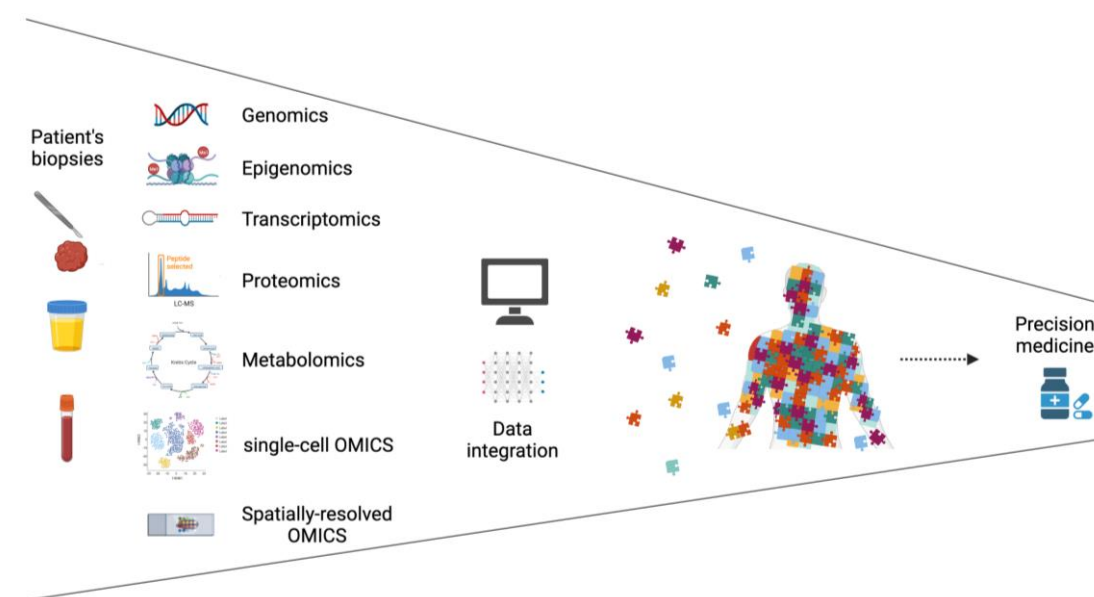


Figure D 8. Deconstructing tumors for precision medicine.

The background of the slide is white, decorated with numerous watercolor-style circles in various shades of blue and yellow. The circles vary in size and opacity, creating a soft, artistic pattern. A central yellow rectangular box contains the main text.

***Conclusions &
Future
perspectives***



I Conclusions

The results herein presented confirm our initial hypothesis. We demonstrate that the transcriptional landscape induced by PGC1 α extends to the regulation of non-canonical tumor suppressive molecular events with cell-intrinsic and cell-extrinsic consequences.

- ❖ The anti-proliferative activity driven by PGC1 α in PCa is reflected on the cell secretome, and this is dependent on the transcriptional control induced by PGC1 α -ERR α .
- ❖ PGC1 α regulates the protein composition of the secretome (SFs and EVs) produced by PCa epithelial cells.
- ❖ EVs produced by PGC1 α -expressing and non-expressing cells play no distinct biological roles *in vitro* and *in vivo*.
- ❖ Differential EV-protein cargo produced by PGC1 α -expressing PCa cells is regulated at the transcriptional level and suggests these EVs could be used as non-invasive bystanders of PCa aggressiveness.
- ❖ The SFs fraction of the secretome produced by PGC1 α -expressing cells is the one driving the non-cell autonomous anti-proliferative role of the coregulator and it is associated with the activation of type I IFN response *in vitro*.
- ❖ *In vivo*, SFs produced by PGC1 α -expressing cells favor the preparation of the pre-metastatic niche. This suggests a distinct role of SFs depending on the biological context and cellular compartment studied.
- ❖ The transcriptional control induced by PGC1 α is reflected in the protein composition of the cell secretome *in vitro*, where cell adhesion molecules and ECM components were shown to be altered by proteomics analysis.
- ❖ The TILs isolated from KO and DKO mice show a different protein composition, with a functional enrichment analysis associated with immune responses and cell cycle-related processes.
- ❖ PGC1 α triggers intrinsic activation of type I IFN response both at a transcriptional and signaling pathway level.
- ❖ This activation is coupled with an increased secretion of IFN- β to the extracellular space upon expression of PGC1 α in PCa epithelial cells.

General Conclusion

PGC1 α regulates a transcriptional landscape that exerts a PCa tumor suppressive role by means of orchestrating cell-intrinsic and cell-extrinsic phenomena

II Future perspectives

In the present thesis work, we have elucidated that the activity of the transcriptional co-regulator PGC1 α goes beyond the regulation of cell metabolism. PGC1 α induces changes in the transcriptional landscape, which includes the activation of type I IFN response and the downregulation of cell cycle-related genes.

We have shown that PGC1 α regulates the secretome composition, which is accompanied by increased IFN- β secretion. Indeed, this secretome seems to have different effects on the PCa epithelial and stromal compartments.

Based on the stratification potential of PGC1 α and on the differential protein cargo found in PGC1 α -driven EVs, we foresee EVs as potential non-invasive bystanders for PCa diagnosis and prognosis.

Finally, we speculate that with the knowledge here provided, novel therapeutic options could be developed for the treatment of PCa patients with loss of PGC1 α . Yet, although this work sets some light on some novel non-canonical roles tied to PGC1 α activity, several questions remain open:

- ❖ How is the status of the proteins included in the EV-based signature in PCa patients-derived EVs?
- ❖ How do the PGC1 α -driven SFs impact on the preparation of the pre-metastatic sites *in vivo*?
- ❖ How does PGC1 α trigger the activation of STAT1 signaling pathway and its transcriptional program (included IFNB)?
- ❖ Is MYC downregulation driving the activation of IFN response?
- ❖ Does secreted IFN- β exert an autocrine effect in the producer cells, leading to a decreased proliferation?
- ❖ Could inhibition of E2F-target genes, such as CDK4, mimic PGC1 α -induced tumor-suppressive phenotype in PCa cells by restoring type I IFN response?
- ❖ Does restoration of type I IFN in PCa epithelial cells render them more evident to the immune system?
- ❖ Could epigenetic mechanisms be drivers of type I IFN response via regulation of PGC1 α ?

The background features a dense pattern of overlapping circles in various shades of purple and magenta, rendered with a watercolor effect. Overlaid on this pattern is a dark green network diagram consisting of interconnected nodes and lines, some of which are curved or looped.

Bibliography & Annex

I Bibliography

- Aalberts, Marian, Tom A.E. Stout, and Willem Stoorvogel. 2014. "Prostasomes: Extracellular Vesicles from the Prostate." *Reproduction*. <https://doi.org/10.1530/REP-13-0358>.
- Aaronson, S, Ursula Behrens, Rena Orner, and T H Haines. 1970. "Ultrastructure of Intracellular and Extracellular Vesicles, Membranes, and Myelin Figures Produced by *Ochromonas Danica*." Vol. 12.
- Abd, Sherif, El-Fattah Ibrahim, Aierken Abudu, Eugenia Johnson, Neelum Aftab, Susan Conrad, and Michele Fluck. 2018. "The Role of AP-1 in Self-Sufficient Proliferation and Migration of Cancer Cells and Its Potential Impact on an Autocrine/Paracrine Loop." www.oncotarget.com.
- Abounader, Roger, and John Laterra. 2005. "Scatter Factor/Hepatocyte Growth Factor in Brain Tumor Growth and Angiogenesis." *Neuro-Oncology*. <https://doi.org/10.1215/S1152851705000050>.
- Accola, Molly A., Bing Huang, Azzah al Masri, and Mark A. McNiven. 2002. "The Antiviral Dynamins Family Member, MxA, Tubulates Lipids and Localizes to the Smooth Endoplasmic Reticulum." *Journal of Biological Chemistry* 277 (24): 21829–35. <https://doi.org/10.1074/jbc.M201641200>.
- Agarwal, Rachana, Theresa D'Souza, and Patrice J. Morin. 2005. "Claudin-3 and Claudin-4 Expression in Ovarian Epithelial Cells Enhances Invasion and Is Associated with Increased Matrix Metalloproteinase-2 Activity." *Cancer Research* 65 (16): 7378–85. <https://doi.org/10.1158/0008-5472.CAN-05-1036>.
- Aigner, Achim, Moritz Butscheid, Philip Kunkel, Eberhard Krause, Katrin Lamszus, Anton Wellstein, and Frank Czubayko. 2001. "AN FGF-BINDING PROTEIN (FGF-BP) EXERTS ITS BIOLOGICAL FUNCTION BY PARALLEL PARACRINE STIMULATION OF TUMOR CELL AND ENDOTHELIAL CELL PROLIFERATION THROUGH FGF-2 RELEASE."
- Akers, Johnny C., David Gonda, Ryan Kim, Bob S. Carter, and Clark C. Chen. 2013. "Biogenesis of Extracellular Vesicles (EV): Exosomes, Microvesicles, Retrovirus-like Vesicles, and Apoptotic Bodies." *Journal of Neuro-Oncology*. Springer Science and Business Media, LLC. <https://doi.org/10.1007/s11060-013-1084-8>.
- Alberts, Bruce, Alexander Johnson, Julian Lewis, Martin Raff, Keith Roberts, and Peter Walter. 2002. *Molecular Biology of the Cell Molecular Biology of the Cell. 4th Edition*. Garland Science.
- Albino, Domenico, Martina Falcione, Valeria Uboldi, Dada Oluwaseyi Temilola, Giada Sandrini, Jessica Merulla, Gianluca Civenni, et al. 2021. "Circulating Extracellular Vesicles Release Oncogenic MiR-424 in Experimental Models and Patients with Aggressive Prostate Cancer." *Communications Biology* 4 (1). <https://doi.org/10.1038/s42003-020-01642-5>.

- Alexander, Eric T, Allyson Minton, Molly C Peters, Otto Phanstiel Iv, and Susan K Gilmour. 2017. "A Novel Polyamine Blockade Therapy Activates an Anti-Tumor Immune Response." www.impactjournals.com/oncotarget.
- Al-Nedawi, Khalid, Brian Meehan, Johann Micallef, Vladimir Lhotak, Linda May, Abhijit Guha, and Janusz Rak. 2008. "Intercellular Transfer of the Oncogenic Receptor EGFRvIII by Microvesicles Derived from Tumour Cells." *Nature Cell Biology* 10 (5): 619–24. <https://doi.org/10.1038/ncb1725>.
- Anand, Sushma, Monisha Samuel, Sharad Kumar, and Suresh Mathivanan. 2019. "Ticket to a Bubble Ride: Cargo Sorting into Exosomes and Extracellular Vesicles." *Biochimica et Biophysica Acta - Proteins and Proteomics*. Elsevier B.V. <https://doi.org/10.1016/j.bbapap.2019.02.005>.
- Anders, Simon, and Wolfgang Huber. 2010. "Differential Expression Analysis for Sequence Count Data." *Genome Biology* 11 (10). <https://doi.org/10.1186/gb-2010-11-10-r106>.
- Andreu, Zoraida, and María Yáñez-Mó. 2014. "Tetraspanins in Extracellular Vesicle Formation and Function." *Frontiers in Immunology* 5 (SEP). <https://doi.org/10.3389/fimmu.2014.00442>.
- Andrzejewski, Sylvia, Eva Klimcakova, Radia M. Johnson, Sébastien Tabariès, Matthew G. Annis, Shawn McQuirk, Jason J. Northey, et al. 2017. "PGC-1 α Promotes Breast Cancer Metastasis and Confers Bioenergetic Flexibility against Metabolic Drugs." *Cell Metabolism* 26 (5): 778-787.e5. <https://doi.org/10.1016/j.cmet.2017.09.006>.
- Angelo, Michael, Sean C. Bendall, Rachel Finck, Matthew B. Hale, Chuck Hitzman, Alexander D. Borowsky, Richard M. Levenson, et al. 2014. "Multiplexed Ion Beam Imaging of Human Breast Tumors." *Nature Medicine* 20 (4): 436–42. <https://doi.org/10.1038/nm.3488>.
- Antonyak, Marc A, Bo Li, Lindsey K Boroughs, Jared L Johnson, Joseph E Druso, and Kirsten L Bryant. 2011. "Cancer Cell-Derived Microvesicles Induce Transformation by Transferring Tissue Transglutaminase and Fibronectin to Recipient Cells." <https://doi.org/10.1073/pnas.1017667108> /DCSupplemental.www.pnas.org/cgi/doi/10.1073/pnas.1017667108.
- Aricò, Eleonora, Luciano Castiello, Imerio Capone, Lucia Gabriele, and Filippo Belardelli. 2019. "Type I Interferons and Cancer: An Evolving Story Demanding Novel Clinical Applications." *Cancers* 11 (12). <https://doi.org/10.3390/cancers11121943>.
- Arima, Takashi, Hideki Enokida, Hiroyuki Kubo, Ichiro Kagara, Ryouichirou Matsuda, Kazuki Toki, Hiroaki Nishimura, et al. 2007. "Nuclear Translocation of ADAM-10 Contributes to the Pathogenesis and Progression of Human Prostate Cancer." *Cancer Science* 98 (11): 1720–26. <https://doi.org/10.1111/j.1349-7006.2007.00601.x>.
- Arimoto, Kei Ichiro, Sayuri Miyauchi, Samuel A. Stoner, Jun Bao Fan, and Dong Er Zhang. 2018. "Negative Regulation of Type I IFN Signaling." *Journal of Leukocyte Biology*. John Wiley and Sons Inc. <https://doi.org/10.1002/JLB.2MIR0817-342R>.
- Arnold, Melina, Mark J. Rutherford, Aude Bardot, Jacques Ferlay, Therese M.L. Andersson, Tor Åge Myklebust, Hanna Tervonen, et al. 2019. "Progress in Cancer Survival, Mortality, and Incidence in Seven High-Income Countries 1995–2014 (ICBP SURVMARK-2): A

- Population-Based Study.” *The Lancet Oncology* 20 (11): 1493–1505. [https://doi.org/10.1016/S1470-2045\(19\)30456-5](https://doi.org/10.1016/S1470-2045(19)30456-5).
- Arpel, Alexia, Coralie Gamper, Caroline Spenlé, Aurore Fernandez, Laurent Jacob, Nadège Baumin, Patrice Laquerriere, Gertraud Orend, Gérard Crémel, and Dominique Bagnard. 2016. “Inhibition of Primary Breast Tumor Growth and Metastasis Using a Neuropilin-1 Transmembrane Domain Interfering Peptide.” *Oncotarget*. Vol. 7. www.impactjournals.com/oncotarget/.
- Artero-Castro, Ana, Josep Castellvi, Angel García, Javier Hernández, Santiago Ramón Y. Cajal, and Matilde E. Leonart. 2011. “Expression of the Ribosomal Proteins Rplp0, Rplp1, and Rplp2 in Gynecologic Tumors.” *Human Pathology* 42 (2): 194–203. <https://doi.org/10.1016/j.humpath.2010.04.020>.
- Atkin-Smith, Georgia K., and Ivan K.H. Poon. 2017. “Disassembly of the Dying: Mechanisms and Functions.” *Trends in Cell Biology*. Elsevier Ltd. <https://doi.org/10.1016/j.tcb.2016.08.011>.
- Atrice Desvergne, Bé, Liliane Michalik, and Walter Wahli. 2006. “Transcriptional Regulation of Metabolism.” <https://doi.org/10.1152/physrev.00025.2005.-Our>.
- Audet-Walsh, Étienne, David J. Papadopoli, Simon Pierre Gravel, Tracey Yee, Gaëlle Bridon, Maxime Caron, Guillaume Bourque, Vincent Giguère, and Julie St-Pierre. 2016. “The PGC-1 α /ERR α Axis Represses One-Carbon Metabolism and Promotes Sensitivity to Anti-Folate Therapy in Breast Cancer.” *Cell Reports* 14 (4): 920–31. <https://doi.org/10.1016/j.celrep.2015.12.086>.
- Ayantunde, A. A., and S. L. Parsons. 2007. “Pattern and Prognostic Factors in Patients with Malignant Ascites: A Retrospective Study.” *Annals of Oncology* 18 (5): 945–49. <https://doi.org/10.1093/annonc/mdl499>.
- Baccin, Chiara, Jude Al-Sabah, Lars Velten, Patrick M. Helbling, Florian Grünschläger, Pablo Hernández-Malmierca, César Nombela-Arrieta, Lars M. Steinmetz, Andreas Trumpp, and Simon Haas. 2020. “Combined Single-Cell and Spatial Transcriptomics Reveal the Molecular, Cellular and Spatial Bone Marrow Niche Organization.” *Nature Cell Biology* 22 (1): 38–48. <https://doi.org/10.1038/s41556-019-0439-6>.
- Bafico, Anna, Guizhong Liu, Luba Goldin, Violaine Harris, and Stuart A Aaronson. 2005. “An Autocrine Mechanism for Constitutive Wnt Pathway Activation in Human Cancer Cells.”
- Baker, Nicholas E., Marianthi Kiparaki, and Chaitali Khan. 2019. “A Potential Link between P53, Cell Competition and Ribosomopathy in Mammals and in *Drosophila*.” *Developmental Biology*. Elsevier Inc. <https://doi.org/10.1016/j.ydbio.2018.11.018>.
- Bald, Tobias, Thomas Quast, Jennifer Landsberg, Meri Rogava, Nicole Glodde, Dorys Lopez-Ramos, Judith Kohlmeyer, et al. 2014. “Ultraviolet-Radiation-Induced Inflammation Promotes Angiotropism and Metastasis in Melanoma.” *Nature* 507 (7490): 109–13. <https://doi.org/10.1038/nature13111>.
- Balkwill, Fran, and Alberto Mantovani. 2000. “Balkwill,2001_Inflammation and Cancer: Back to Virchow?,” February.

- Bally, Alexander P. R., James W. Austin, and Jeremy M. Boss. 2016. "Genetic and Epigenetic Regulation of PD-1 Expression." *The Journal of Immunology* 196 (6): 2431–37. <https://doi.org/10.4049/jimmunol.1502643>.
- Barrès, Romain, Jie Yan, Brendan Egan, Jonas Thue Treebak, Morten Rasmussen, Tomas Fritz, Kenneth Caidahl, Anna Krook, Donal J. O’Gorman, and Juleen R. Zierath. 2012. "Acute Exercise Remodels Promoter Methylation in Human Skeletal Muscle." *Cell Metabolism* 15 (3): 405–11. <https://doi.org/10.1016/j.cmet.2012.01.001>.
- Bartholow, Tanner L., Uma R. Chandran, Michael J. Becich, and Anil v. Parwani. 2011. "Immunohistochemical Profiles of Claudin-3 in Primary and Metastatic Prostatic Adenocarcinoma." *Diagnostic Pathology* 6 (1). <https://doi.org/10.1186/1746-1596-6-12>.
- Battistelli, Michela, and Elisabetta Falcieri. 2020. "Apoptotic Bodies: Particular Extracellular Vesicles Involved in Intercellular Communication." *Biology*. MDPI AG. <https://doi.org/10.3390/biology9010021>.
- Beckham, Carla J., Jayme Olsen, Peng Nien Yin, Chia Hao Wu, Huei Ju Ting, Fred K. Hagen, Emelian Scosyrev, Edward M. Messing, and Yi Fen Lee. 2014. "Bladder Cancer Exosomes Contain EDIL-3/Del1 and Facilitate Cancer Progression." *Journal of Urology* 192 (2): 583–92. <https://doi.org/10.1016/j.juro.2014.02.035>.
- Berglund, Emelie, Jonas Maaskola, Niklas Schultz, Stefanie Friedrich, Maja Marklund, Joseph Bergensträhle, Firas Tarish, et al. 2018. "Spatial Maps of Prostate Cancer Transcriptomes Reveal an Unexplored Landscape of Heterogeneity." *Nature Communications* 9 (1). <https://doi.org/10.1038/s41467-018-04724-5>.
- Bergsmedh, Anna, Anna Szeles, Marie Henriksson, Anders Bratt, M Judah Folkman, Anna-Lena Spetz, and Lars Holmgren. 2001. "Horizontal Transfer of Oncogenes by Uptake of Apoptotic Bodies." www.pnas.org/cgi/doi/10.1073/pnas.101129998.
- Besse-Patin, Aurèle, Mélissa Léveillé, Daniel Oropeza, Bich N. Nguyen, and Annik Prat. 2017. "Estrogen Signals Through Peroxisome Proliferator-Activated Receptor- γ Coactivator 1 α to Reduce Oxidative Damage Associated With Diet-Induced Fatty Liver Disease." *Gastroenterology* 152 (1): 243–56. <https://doi.org/10.1053/j.gastro.2016.09.017>.
- Bhavsar, Anil, and Sadhna Verma. 2014. "Anatomic Imaging of the Prostate." *BioMed Research International*. Hindawi Publishing Corporation. <https://doi.org/10.1155/2014/728539>.
- Bitting, Rhonda L., and Andrew J. Armstrong. 2013. "Targeting the PI3K/Akt/MTOR Pathway in Castration-Resistant Prostate Cancer." *Endocrine-Related Cancer*. <https://doi.org/10.1530/ERC-12-0394>.
- Blanco, Mario Andres, Gary Leroy, Zia Khan, Maša Alečković, Barry M Zee, and Benjamin A Garcia. 2012. "Global Secretome Analysis Identifies Novel Mediators of Bone Metastasis," 1339–55. <https://doi.org/10.1038/cr.2012.89>.
- Boeck, Astrid de, An Hendrix, Dawn Maynard, Mieke van Bockstal, Annick Daniëls, Patrick Pauwels, Christian Gespach, Marc Bracke, and Olivier de Wever. 2013. "Differential Secretome Analysis of Cancer-Associated Fibroblasts and Bone Marrow-Derived

- Precursors to Identify Microenvironmental Regulators of Colon Cancer Progression.” *Proteomics* 13 (2): 379–88. <https://doi.org/10.1002/pmic.201200179>.
- Bost, Frederic, and Lisa Kaminski. 2019. “The Metabolic Modulator PGC-1 α in Cancer.” *American Journal of Cancer Research* 9 (2): 198–211. <http://www.ncbi.nlm.nih.gov/pubmed/30906622><http://www.pubmedcentral.nih.gov/articlerender.fcgi?artid=PMC6405967>.
- Boström, Pontus, Jun Wu, Mark P. Jedrychowski, Anisha Korde, Li Ye, James C. Lo, Kyle A. Rasbach, et al. 2012. “A PGC1- α -Dependent Myokine That Drives Brown-Fat-like Development of White Fat and Thermogenesis.” *Nature* 481 (7382): 463–68. <https://doi.org/10.1038/nature10777>.
- Bourguignon, Lilly Y.W. 2008. “Hyaluronan-Mediated CD44 Activation of RhoGTPase Signaling and Cytoskeleton Function Promotes Tumor Progression.” *Seminars in Cancer Biology*. <https://doi.org/10.1016/j.semcancer.2008.03.007>.
- Brady, Jennifer J, Chen Hua Chuang, Peyton G Greenside, Zoë N. Rogers, Christopher W Murray, Deborah R. Caswell, Ursula Hartmann, et al. 2016. “An Arntl2-Driven Secretome Enables Lung Adenocarcinoma Metastatic Self-Sufficiency.” *Cancer Cell* 29 (5): 697–710. <https://doi.org/10.1016/j.ccell.2016.03.003>.
- Brawer, Michael K. 2005. “SELECTIVE ESTROGEN RECEPTOR MODULATORS Prostatic Intraepithelial Neoplasia: An Overview.” *REVIEWS IN UROLOGY*. Vol. 7.
- Bray, Freddie, Jacques Ferlay, Isabelle Soerjomataram, Rebecca L. Siegel, Lindsey A. Torre, and Ahmedin Jemal. 2018. “Global Cancer Statistics 2018: GLOBOCAN Estimates of Incidence and Mortality Worldwide for 36 Cancers in 185 Countries.” *CA: A Cancer Journal for Clinicians* 68 (6): 394–424. <https://doi.org/10.3322/caac.21492>.
- Bromfield, John J. 2014. “Seminal Fluid and Reproduction: Much More than Previously Thought.” *Journal of Assisted Reproduction and Genetics*. Springer New York LLC. <https://doi.org/10.1007/s10815-014-0243-y>.
- Browaeys, Robin, Wouter Saelens, and Yvan Saeys. 2020. “NicheNet: Modeling Intercellular Communication by Linking Ligands to Target Genes.” *Nature Methods* 17 (2): 159–62. <https://doi.org/10.1038/s41592-019-0667-5>.
- Brown, Shanora G., Ashley E. Knowell, Aisha Hunt, Divya Patel, Sushma Bhosle, and Jaideep Chaudhary. 2015. “Interferon Inducible Antiviral Mxa Is Inversely Associated with Prostate Cancer and Regulates Cell Cycle, Invasion and Docetaxel Induced Apoptosis.” *Prostate* 75 (3): 266–79. <https://doi.org/10.1002/pros.22912>.
- Bubendorf, Lukas, Alain Schöpfer, Urs Wagner, Guido Sauter, Holger Moch, Niels Willi, Thomas C. Gasser, and Michael J. Mihatsch. 2000. “Metastatic Patterns of Prostate Cancer: An Autopsy Study of 1,589 Patients.” *Human Pathology* 31 (5): 578–83. <https://doi.org/10.1053/hp.2000.6698>.
- Caiazza, Francesco, Katarzyna Oficjalska, Miriam Tosetto, James J. Phelan, Sinéad Noonan, Petra Martin, Kate Killick, et al. 2019. “KH-Type Splicing Regulatory Protein Controls

- Colorectal Cancer Cell Growth and Modulates the Tumor Microenvironment." *American Journal of Pathology* 189 (10): 1916–32. <https://doi.org/10.1016/j.ajpath.2019.07.004>.
- Calcinotto, Arianna, Clarissa Spataro, Elena Zagato, Diletta di Mitri, Veronica Gil, Mateus Crespo, Gaston de Bernardis, et al. 2018. "IL-23 Secreted by Myeloid Cells Drives Castration-Resistant Prostate Cancer." *Nature*. <https://doi.org/10.1038/s41586-018-0266-0>.
- Camacho, Laura, Paola Guerrero, and Dario Marchetti. 2013. "MicroRNA and Protein Profiling of Brain Metastasis Competent Cell-Derived Exosomes" 8 (9). <https://doi.org/10.1371/journal.pone.0073790>.
- Capaia, Matteo, Ilaria Granata, Mario Guarracino, Andrea Petretto, Elvira Inglese, Carlo Cattrini, Nicoletta Ferrari, Francesco Boccardo, and Paola Barboro. 2018. "A HnRNP K–AR-Related Signature Reflects Progression toward Castration-Resistant Prostate Cancer." *International Journal of Molecular Sciences* 19 (7). <https://doi.org/10.3390/ijms19071920>.
- Carracedo, Arkaitz, Andrea Alimonti, and Pier Paolo Pandolfi. 2011. "PTEN Level in Tumor Suppression: How Much Is Too Little?" *Cancer Research*. <https://doi.org/10.1158/0008-5472.CAN-10-2488>.
- Castro, Elena, Chee Goh, David Olmos, Ed Saunders, Daniel Leongamornlert, Malgorzata Tymrakiewicz, Nadiya Mahmud, et al. 2013. "Germline BRCA Mutations Are Associated with Higher Risk of Nodal Involvement, Distant Metastasis, and Poor Survival Outcomes in Prostate Cancer." *Journal of Clinical Oncology* 31 (14): 1748–57. <https://doi.org/10.1200/JCO.2012.43.1882>.
- Catalona, William J. 2018. "Prostate Cancer Screening." *Medical Clinics of North America*. W.B. Saunders. <https://doi.org/10.1016/j.mcna.2017.11.001>.
- Cerezo-Wallis, Daniela, Marta Contreras-Alcalde, Kevin Troulé, Xavier Catena, Cynthia Mucientes, Tonantzin G Calvo, Estela Cañón, et al. 2020. "Midkine Rewires the Melanoma Microenvironment toward a Tolerogenic and Immune-Resistant State." *Nature Medicine* 26 (12): 1865–77. <https://doi.org/10.1038/s41591-020-1073-3>.
- Chang, Ying Hua, Shu Hui Lee, I. Chuang Liao, Shin Huei Huang, Hung Chi Cheng, and Pao Chi Liao. 2012. "Secretomic Analysis Identifies Alpha-1 Antitrypsin (A1AT) as a Required Protein in Cancer Cell Migration, Invasion, and Pericellular Fibronectin Assembly for Facilitating Lung Colonization of Lung Adenocarcinoma Cells." *Molecular and Cellular Proteomics* 11 (11): 1320–39. <https://doi.org/10.1074/mcp.M112.017384>.
- Chargaff, E., and R. West. 1946. "The Biological Significance of the Thromboplastic Protein of Blood." *The Journal of Biological Chemistry* 166 (1): 189–97. [https://doi.org/10.1016/s0021-9258\(17\)34997-9](https://doi.org/10.1016/s0021-9258(17)34997-9).
- Charos, Alexandra E., Brian D. Reed, Debasish Raha, Anna M. Szekely, Sherman M. Weissman, and Michael Snyder. 2012. "A Highly Integrated and Complex PPARGC1A Transcription Factor Binding Network in HepG2 Cells." *Genome Research* 22 (9): 1668–79. <https://doi.org/10.1101/gr.127761.111>.

- Chen, Ni, and Qiao Zhou. 2016. "The Evolving Gleason Grading System." *Chinese Journal of Cancer Research*. AME Publishing Company. <https://doi.org/10.3978/j.issn.1000-9604.2016.02.04>.
- Chen, Ru, Sheng Pan, Kelly Cooke, P Kara, White Moyes, Mary P Bronner, David R Goodlett, Ruedi Aebersold, and Teresa A Brentnall. 2007. "Comparison of Pancreas Juice Proteins from Cancer Versus Pancreatitis Using Quantitative Proteomic Analysis." www.systemsbio.org/Default.aspx?pagename=FullList.
- Chen, Ru, Sheng Pan, Eugene C. Yi, Samuel Donohoe, Mary P. Bronner, John D. Potter, David R. Goodlett, Ruedi Aebersold, and Teresa A. Brentnall. 2006. "Quantitative Proteomic Profiling of Pancreatic Cancer Juice." *Proteomics* 6 (13): 3871–79. <https://doi.org/10.1002/pmic.200500702>.
- Chen, Sujun, Guanghui Zhu, Yue Yang, Fubo Wang, Yu Tian Xiao, Na Zhang, Xiaojie Bian, et al. 2021. "Single-Cell Analysis Reveals Transcriptomic Remodellings in Distinct Cell Types That Contribute to Human Prostate Cancer Progression." *Nature Cell Biology* 23 (1): 87–98. <https://doi.org/10.1038/s41556-020-00613-6>.
- Chen, Zhenbang, Lloyd C Trotman, David Shaffer, Hui-Kuan Lin, Zohar A Dotan, Masaru Niki, Jason A Koutcher, et al. 2005. "Crucial Role of P53-Dependent Cellular Senescence in Suppression of Pten-Deficient Tumorigenesis." www.nature.com/nature.
- Cheng, Ching Feng, Hui Chen Ku, and Heng Lin. 2018. "Pgc-1 α as a Pivotal Factor in Lipid and Metabolic Regulation." *International Journal of Molecular Sciences*. MDPI AG. <https://doi.org/10.3390/ijms19113447>.
- Cheng, Heather H., Colin C. Pritchard, Thomas Boyd, Peter S. Nelson, and Bruce Montgomery. 2016. "Biallelic Inactivation of BRCA2 in Platinum-Sensitive Metastatic Castration-Resistant Prostate Cancer." *European Urology* 69 (6): 992–95. <https://doi.org/10.1016/j.eururo.2015.11.022>.
- Chinsomboon, Jessica, Jorge Ruas, Rana K Gupta, Robyn Thom, Jonathan Shoag, Glenn C Rowe, Naoki Sawada, Srilatha Raghuram, and Zoltan Arany. 2009. "The Transcriptional Coactivator PGC-1 Mediates Exercise-Induced Angiogenesis in Skeletal Muscle." www.pnas.org/cgi/content/full/.
- Cho, Hyejin, Tali Herzka, Wu Zheng, Jun Qi, John E. Wilkinson, James E. Bradner, Brian D. Robinson, Mireia Castillo-Martin, Carlos Cordon-Cardo, and Lloyd C. Trotman. 2014. "RapidCaP, a Novel Gem Model for Metastatic Prostate Cancer Analysis and Therapy, Reveals Myc as a Driver of Pten-Mutant Metastasis." *Cancer Discovery* 4 (3): 319–33. <https://doi.org/10.1158/2159-8290.CD-13-0346>.
- Choi, Dong Sic, Jung Ok Park, Su Chul Jang, Yae Jin Yoon, Jin Woo Jung, Do Young Choi, Jung Wook Kim, et al. 2011. "Proteomic Analysis of Microvesicles Derived from Human Colorectal Cancer Ascites." *Proteomics* 11 (13): 2745–51. <https://doi.org/10.1002/pmic.201100022>.
- Christ, Liliane, Camilla Raiborg, Eva M. Wenzel, Coen Campsteijn, and Harald Stenmark. 2017. "Cellular Functions and Molecular Mechanisms of the ESCRT Membrane-Scission

- Machinery.” *Trends in Biochemical Sciences*. Elsevier Ltd. <https://doi.org/10.1016/j.tibs.2016.08.016>.
- Christensen, Soren T., Vagn Leick, Leif Rasmussen, and Denys N. Wheatley. 1997. “Signaling in Unicellular Eukaryotes.” *International Review of Cytology* 177: 181–253. [https://doi.org/10.1016/s0074-7696\(08\)62233-0](https://doi.org/10.1016/s0074-7696(08)62233-0).
- Christersson, Christina, Åsa Thulin, and Agneta Siegbahn. 2017. “Microparticles during Long-Term Follow-Up after Acute Myocardial Infarction: Association to Atherosclerotic Burden and Risk of Cardiovascular Events.” *Thrombosis and Haemostasis* 117 (8): 1571–81. <https://doi.org/10.1160/TH16-11-0837>.
- Ciullo, Alessandra, Vanessa Biemmi, Giuseppina Milano, Sara Bolis, Elisabetta Cervio, Emanuel Tudor Fertig, Mihaela Gherghiceanu, et al. 2019. “Exosomal Expression of CXCR4 Targets Cardioprotective Vesicles to Myocardial Infarction and Improves Outcome after Systemic Administration.” *International Journal of Molecular Sciences* 20 (3). <https://doi.org/10.3390/ijms20030468>.
- Cortazar, Ana R, Veronica Torrano, Natalia Martín-martín, Alfredo Caro-maldonado, Laura Camacho, Ivana Hermanova, Elizabeth Guruceaga, Luis F Lorenzo-martín, and Victor Quesada. 2018. “CANCERTOOL : A Visualization and Representation Interface to Exploit Cancer Datasets” 78 (21): 6320–29. <https://doi.org/10.1158/0008-5472.CAN-18-1669>.
- Cossetti, Chiara, Nunzio Iraci, Tim R Mercer, Tommaso Leonardi, Denise Drago, Clara Alfaro-cervello, Harpreet K Saini, et al. 2015. “Extracellular Vesicles from Neural Stem Cells Transfer IFN- γ via Ifngr1 to Activate Stat1 Signaling in Target Cells” 56 (2): 193–204. <https://doi.org/10.1016/j.molcel.2014.08.020>. Extracellular.
- Costa-Silva, Bruno, Nicole M. Aiello, Allyson J. Ocean, Swarnima Singh, Haiying Zhang, Basant Kumar Thakur, Annette Becker, et al. 2015. “Pancreatic Cancer Exosomes Initiate Pre-Metastatic Niche Formation in the Liver.” *Nature Cell Biology* 17 (6): 816–26. <https://doi.org/10.1038/ncb3169>.
- Cox, Thomas R., and Janine T. Erler. 2011. “Remodeling and Homeostasis of the Extracellular Matrix: Implications for Fibrotic Diseases and Cancer.” *DMM Disease Models and Mechanisms*. <https://doi.org/10.1242/dmm.004077>.
- Cox, Thomas R, Robin M H Rumney, Erwin M Schoof, Lara Perryman, M Anette, Ankita Agrawal, Demelza Bird, et al. 2016. “The Hypoxic Cancer Secretome Induces Pre-Metastatic Bone Lesions through Lysyl Oxidase” 522 (7554): 106–10. <https://doi.org/10.1038/nature14492>. The.
- Crawford, E. David, Axel Heidenreich, Nathan Lawrentschuk, Bertrand Tombal, Antonio C.L. Pompeo, Arturo Mendoza-Valdes, Kurt Miller, Frans M.J. Debruyne, and Laurence Klotz. 2019. “Androgen-Targeted Therapy in Men with Prostate Cancer: Evolving Practice and Future Considerations.” *Prostate Cancer and Prostatic Diseases*. Nature Publishing Group. <https://doi.org/10.1038/s41391-018-0079-0>.
- Crick FH. 1958. “On Protein Synthesis.” *Symp Soc Exp Biol* 12: 138–63.

- Crumbaker, Megan, Leila Khoja, and Anthony M. Joshua. 2017. "AR Signaling and the PI3K Pathway in Prostate Cancer." *Cancers*. MDPI AG. <https://doi.org/10.3390/cancers9040034>.
- Cui, Peng Fei, Xiao Feng Cong, Feng Gao, Jia Xin Yin, Zi Ru Niu, Song Chen Zhao, and Zi Ling Liu. 2020. "Prognostic Factors for Overall Survival in Prostate Cancer Patients with Different Site-Specific Visceral Metastases: A Study of 1358 Patients." *World Journal of Clinical Cases* 8 (1): 54–67. <https://doi.org/10.12998/wjcc.v8.i1.54>.
- Dagvadorj, Ayush, Sean Collins, Jean Baptiste Jomain, Junaid Abdulghani, James Karras, Tobias Zellweger, Hongzhen Li, et al. 2007. "Autocrine Prolactin Promotes Prostate Cancer Cell Growth via Janus Kinase-2-Signal Transducer and Activator of Transcription-5a/b Signaling Pathway." *Endocrinology* 148 (7): 3089–3101. <https://doi.org/10.1210/en.2006-1761>.
- Damodaran, Shivashankar, Christos E. Kyriakopoulos, and David F. Jarrard. 2017. "Newly Diagnosed Metastatic Prostate Cancer: Has the Paradigm Changed?" *Urologic Clinics of North America*. W.B. Saunders. <https://doi.org/10.1016/j.ucl.2017.07.008>.
- Daneman, Richard, and Alexandre Prat. 2015. "The Blood–Brain Barrier." *Cold Spring Harbor Perspectives in Biology* 7 (1). <https://doi.org/10.1101/cshperspect.a020412>.
- Deep, Gagan, Anil Jain, Ashish Kumar, Chapla Agarwal, Susy Kim, W. Matthew Leevy, and Rajesh Agarwal. 2020. "Exosomes Secreted by Prostate Cancer Cells under Hypoxia Promote Matrix Metalloproteinases Activity at Pre-Metastatic Niches." *Molecular Carcinogenesis* 59 (3): 323–32. <https://doi.org/10.1002/mc.23157>.
- Dejima, Hitoshi, Hisae Inuma, Rie Kanaoka, Noriyuki Matsutani, and Masafumi Kawamura. 2017. "Exosomal MicroRNA in Plasma as a Non-Invasive Biomarker for the Recurrence of Non-Small Cell Lung Cancer." *Oncology Letters* 13 (3): 1256–63. <https://doi.org/10.3892/ol.2017.5569>.
- Deng, Xinyue, Yang Li, Shuang Gu, Yingying Chen, Bingbing Yu, Jing Su, Liankun Sun, and Yanan Liu. 2020. "P53 Affects PGC1 α Stability Through AKT/GSK-3 β to Enhance Cisplatin Sensitivity in Non-Small Cell Lung Cancer." *Frontiers in Oncology* 10 (August). <https://doi.org/10.3389/fonc.2020.01252>.
- Derek C. Radisky & Melody Stallings-Mann. 2009. "Single Proteins Might Have Dual but Related Functions in Intracellular and Extracellular Microenvironments." *Nat Rev Mol Cell Biol*. 23 (1): 1–7. <https://doi.org/10.1038/nrm2633>. Single.
- DeRita, Rachel M., Aejaz Sayeed, Vaughn Garcia, Shiv Ram Krishn, Christopher D. Shields, Sravasti Sarker, Andrea Friedman, et al. 2019. "Tumor-Derived Extracellular Vesicles Require B1 Integrins to Promote Anchorage-Independent Growth." *IScience* 14 (April): 199–209. <https://doi.org/10.1016/j.isci.2019.03.022>.
- D'Errico, Ilenia, Lorena Salvatore, Stefania Murzilli, Giuseppe lo Sasso, Dominga Latorre, Nicola Martelli, Anastasia v. Egorova, et al. 2011. "Peroxisome Proliferator-Activated Receptor- γ Coactivator 1- α (PGC1 α) Is a Metabolic Regulator of Intestinal Epithelial Cell Fate." *Proceedings of the National Academy of Sciences of the United States of America* 108 (16): 6603–8. <https://doi.org/10.1073/pnas.1016354108>.

- Descotes, Jean Luc. 2019. "Diagnosis of Prostate Cancer." *Asian Journal of Urology*. Editorial Office of Asian Journal of Urology. <https://doi.org/10.1016/j.ajur.2018.11.007>.
- Deshmukh, Atul S., Juergen Cox, Lars Juhl Jensen, Felix Meissner, and Matthias Mann. 2015. "Secretome Analysis of Lipid-Induced Insulin Resistance in Skeletal Muscle Cells by a Combined Experimental and Bioinformatics Workflow." *Journal of Proteome Research* 14 (11): 4885–95. <https://doi.org/10.1021/acs.jproteome.5b00720>.
- Dickson, Robert B, Mary E Mcmanaway, and Marc E Lippman. 1986. "Estrogen-Induced Factors of Breast Cancer Cells Partially Replace Estrogen to Promote Tumor Growth" 77 (22): 1981–84.
- Ding, Zhihu, Chang Jiun Wu, Gerald C. Chu, Yonghong Xiao, Dennis Ho, Jingfang Zhang, Samuel R. Perry, et al. 2011. "SMAD4-Dependent Barrier Constrains Prostate Cancer Growth and Metastatic Progression." *Nature* 470 (7333): 269–76. <https://doi.org/10.1038/nature09677>.
- Dinulovic, Ivana, Regula Furrer, Markus Beer, Arnaud Ferry, Bettina Cardel, and Christoph Handschin. 2016. "Muscle PGC-1 α Modulates Satellite Cell Number and Proliferation by Remodeling the Stem Cell Niche." *Skeletal Muscle* 6 (1). <https://doi.org/10.1186/s13395-016-0111-9>.
- Dong, Zhongyun, Graham Greene, Curtis Pettaway, Colin P N Dinney, Ines Eue, Weixin Lu, Corazon D Bucana, Mevlana D Balbay, Diane Bielenberg, and Isaiah J Fidler. 1999. "Suppression of Angiogenesis, Tumorigenicity, and Metastasis by Human Prostate Cancer Cells Engineered to Produce Interferon-1." *CANCER RESEARCH*. Vol. 59.
- Draffin, Jayne E, Suzanne Mcfarlane, Ashleigh Hill, Patrick G Johnston, and David J J Waugh. 2004. "CD44 Potentiates the Adherence of Metastatic Prostate and Breast Cancer Cells to Bone Marrow Endothelial Cells." *CANCER RESEARCH*. Vol. 64.
- Duijvesz, Diederick, C. Yin L. Versluis, Christa A.M. van der Fels, Mirella S. Vredendregt-Van Den Berg, Janne Leivo, Mari T. Peltola, Chris H. Bangma, Kim S.I. Pettersson, and Guido Jenster. 2015. "Immuno-Based Detection of Extracellular Vesicles in Urine as Diagnostic Marker for Prostate Cancer." *International Journal of Cancer* 137 (12): 2869–78. <https://doi.org/10.1002/ijc.29664>.
- Edlund, Magnus, Shian Ying Sung, and Leland W.K. Chung. 2004. "Modulation of Prostate Cancer Growth in Bone Microenvironments." *Journal of Cellular Biochemistry*. <https://doi.org/10.1002/jcb.10702>.
- Elaine A McSherry, Kiernan Brennan, Lance Hudson, Arnold DK Hill and Ann M Hopkins. 2011. "Breast Cancer Cell Migration Is Regulated through Junctional Adhesion Molecule-A-Mediated Activation of Rap1 GTPase." *Breast Cancer Research*.
- El-Sayed, Ihsan Y., Ahmad Daher, Damien Destouches, Virginie Firlej, Enis Kostallari, Pascale Maillé, Eric Huet, et al. 2017. "Extracellular Vesicles Released by Mesenchymal-like Prostate Carcinoma Cells Modulate EMT State of Recipient Epithelial-like Carcinoma Cells through Regulation of AR Signaling." *Cancer Letters* 410 (December): 100–111. <https://doi.org/10.1016/j.canlet.2017.09.010>.

- Erler, Janine T., Kevin L. Bennewith, Thomas R. Cox, Georgina Lang, Demelza Bird, Albert Koong, Quynh Thu Le, and Amato J. Giaccia. 2009. "Hypoxia-Induced Lysyl Oxidase Is a Critical Mediator of Bone Marrow Cell Recruitment to Form the Premetastatic Niche." *Cancer Cell* 15 (1): 35–44. <https://doi.org/10.1016/j.ccr.2008.11.012>.
- Ernst, Peter B, and Benjamin D Gold. 2000. "THE DISEASE SPECTRUM OF HELICOBACTER PYLORI: The Immunopathogenesis of Gastroduodenal Ulcer and Gastric Cancer." www.annualreviews.org.
- Escrevente, Cristina, Sascha Keller, Peter Altevogel, and Julia Costa. 2011. "Interaction and Uptake of Exosomes by Ovarian Cancer Cells." *Biomed Central*.
- Feilchenfeldt, Jonas, Marie Anne Bründler, Claudio Soravia, Martin Tötsch, and Christoph A. Meier. 2004. "Peroxisome Proliferator-Activated Receptors (PPARs) and Associated Transcription Factors in Colon Cancer: Reduced Expression of PPAR γ -Coactivator 1 (PGC-1)." *Cancer Letters* 203 (1): 25–33. <https://doi.org/10.1016/j.canlet.2003.08.024>.
- Feizi, Amir, Francesco Gatto, Mathias Uhlen, and Jens Nielsen. 2017. "Human Protein Secretory Pathway Genes Are Expressed in a Tissue-Specific Pattern to Match Processing Demands of the Secretome." *Npj Systems Biology and Applications* 3 (1). <https://doi.org/10.1038/s41540-017-0021-4>.
- Ferraldeschi, Roberta, Daniel Nava Rodrigues, Ruth Riisnaes, Susana Miranda, Ines Figueiredo, Pasquale Rescigno, Praful Ravi, et al. 2015. "PTEN Protein Loss and Clinical Outcome from Castration-Resistant Prostate Cancer Treated with Abiraterone Acetate." *European Urology* 67 (4): 795–802. <https://doi.org/10.1016/j.eururo.2014.10.027>.
- Fidler, Isaiah J. 1970. "Metastasis: Quantitative Analysis of Dis-Tribution and Fate of Tumor Emboli Labeled With 1251-S-Lodo-2'-Deoxyuridine." <http://jnci.oxfordjournals.org/>.
- Ford, Caroline Elizabeth, Bonnita Werner, Neville Frederick Hacker, and Kristina Warton. 2020. "The Untapped Potential of Ascites in Ovarian Cancer Research and Treatment." *British Journal of Cancer*. Springer Nature. <https://doi.org/10.1038/s41416-020-0875-x>.
- Fornarini, B., C. D'Ambrosio, C. Natoli, N. Tinari, V. Silingardi, and S. Iacobelli. 2000. "Adhesion to 90K (Mac-2 BP) as a Mechanism for Lymphoma Drug Resistance in Vivo." *Blood* 96 (9): 3282–85. <https://doi.org/10.1182/blood.v96.9.3282>.
- Francis, Karl, and Bernhard O Palsson. 1997. "Effective Intercellular Communication Distances Are Determined by the Relative Time Constants for Cytochemokine Secretion and Diffusion (Cell Signalingbioreactor Designtissue Engineering)." Vol. 94. www.pnas.org.
- Franco, Omar E., Ming Jiang, Douglas W. Strand, James Peacock, Suzanne Fernandez, Roger S. Jackson, Monica P. Revelo, Neil A. Bhowmick, and Simon W. Hayward. 2011. "Altered TGF- β Signaling in a Subpopulation of Human Stromal Cells Promotes Prostatic Carcinogenesis." *Cancer Research* 71 (4): 1272–81. <https://doi.org/10.1158/0008-5472.CAN-10-3142>.
- Franzen, Carrie A, Patricia E Simms, Adam F van Huis, Kimberly E Foreman, Paul C Kuo, and Gopal N Gupta. 2014. "Characterization of Uptake and Internalization of Exosomes by Bladder Cancer Cells" 2014.

- Fraser, Michael, Veronica Y. Sabelnykova, Takafumi N. Yamaguchi, Lawrence E. Heisler, Julie Livingstone, Vincent Huang, Yu Jia Shiah, et al. 2017. "Genomic Hallmarks of Localized, Non-Indolent Prostate Cancer." *Nature* 541 (7637): 359–64. <https://doi.org/10.1038/nature20788>.
- Frechin, Mathieu, Thomas Stoeger, Stephan Daetwyler, Charlotte Gehin, Nico Battich, Eva Maria Damm, Lilli Stergiou, Howard Riezman, and Lucas Pelkmans. 2015. "Cell-Intrinsic Adaptation of Lipid Composition to Local Crowding Drives Social Behaviour." *Nature* 523 (7558): 88–91. <https://doi.org/10.1038/nature14429>.
- Friedl, Peter, and Katarina Wolf. 2010. "Plasticity of Cell Migration: A Multiscale Tuning Model." *Journal of Cell Biology*. Rockefeller University Press. <https://doi.org/10.1083/jcb.200909003>.
- Fujiwara-Okada, Y., Y. Matsumoto, J. Fukushi, N. Setsu, S. Matsuura, S. Kamura, T. Fujiwara, et al. 2013. "Y-Box Binding Protein-1 Regulates Cell Proliferation and Is Associated with Clinical Outcomes of Osteosarcoma." *British Journal of Cancer* 108 (4): 836–47. <https://doi.org/10.1038/bjc.2012.579>.
- Galon, Jérôme, Franck Pagès, Francesco M. Marincola, Helen K. Angell, Magdalena Thurin, Alessandro Lugli, Inti Zlobec, et al. 2012. "Cancer Classification Using the Immunoscore: A Worldwide Task Force." *Journal of Translational Medicine*. <https://doi.org/10.1186/1479-5876-10-205>.
- García-Silva, Susana, Alberto Benito-Martín, Sara Sánchez-Redondo, Alberto Hernández-Barranco, Pilar Ximénez-Embún, Laura Nogués, Marina S. Mazariegos, et al. 2019. "Use of Extracellular Vesicles from Lymphatic Drainage as Surrogate Markers of Melanoma Progression and BRAFV600E Mutation." *Journal of Experimental Medicine* 216 (5): 1061–70. <https://doi.org/10.1084/jem.20181522>.
- Geng, Tuoyu, Ping Li, Xinhe Yin, and Zhen Yan. 2011. "PGC-1 α Promotes Nitric Oxide Antioxidant Defenses and Inhibits FOXO Signaling against Cardiac Cachexia in Mice." *American Journal of Pathology* 178 (4): 1738–48. <https://doi.org/10.1016/j.ajpath.2011.01.005>.
- Ghossoub, Rania, Frédérique Lembo, Aude Rubio, Carole Baron Gaillard, Jérôme Bouchet, Nicolas Vitale, Josef Slavík, Miroslav Machala, and Pascale Zimmermann. 2014. "Syntenin-ALIX Exosome Biogenesis and Budding into Multivesicular Bodies Are Controlled by ARF6 and PLD2." *Nature Communications* 5 (March). <https://doi.org/10.1038/ncomms4477>.
- Girardi, T., S. Vereecke, S. O. Sulima, Y. Khan, L. Fancello, J. W. Briggs, C. Schwab, et al. 2018. "The T-Cell Leukemia-Associated Ribosomal RPL10 R98S Mutation Enhances JAK-STAT Signaling." *Leukemia* 32 (3): 809–19. <https://doi.org/10.1038/leu.2017.225>.
- Gleason, F. D., and G. T. Mellinger. 1974. "PREDICTION OF PROGNOSIS FOR PROSTATIC ADENOCARCINOMA BY COMBINED HISTOLOGICAL GRADING AND CLINICAL STAGING." *Reprinted from J Urol*. Vol. 167.

- Glinsky, Gennadi v., Anna B. Glinskii, Andrew J. Stephenson, Robert M. Hoffman, and William L. Gerald. 2004. "Gene Expression Profiling Predicts Clinical Outcome of Prostate Cancer." *Journal of Clinical Investigation* 113 (6): 913–23. <https://doi.org/10.1172/jci200420032>.
- Goel, Shom, Molly J. Decristo, April C. Watt, Haley Brinjones, Jaclyn Sceneay, Ben B. Li, Naveed Khan, et al. 2017. "CDK4/6 Inhibition Triggers Anti-Tumour Immunity." *Nature* 548 (7668): 471–75. <https://doi.org/10.1038/nature23465>.
- González del Alba, A., M. J. Méndez-Vidal, S. Vazquez, E. Castro, M. A. Climent, E. Gallardo, E. Gonzalez-Billalabeitia, D. Lorente, J. P. Maroto, and J. A. Arranz. 2021. "SEOM Clinical Guidelines for the Treatment of Advanced Prostate Cancer (2020)." *Clinical and Translational Oncology* 23 (5): 969–79. <https://doi.org/10.1007/s12094-021-02561-5>.
- González-Vela, M C, M F Garijo, F Ferna Ândez, L Buelta, J F Val-Bernal, Gonza M Âlez-Vela C, Garijo M F, Ferna F Ândez, and Val-Bernal J F. 1999. "Cathepsin D in Host Stromal Cells Is Associated with More Highly Vascular and Aggressive Invasive Breast Carcinoma." *Histopathology*. Vol. 34.
- Gortzak-Uzan, Limor, Alex Ignatchenko, Andreas I. Evangelou, Mahima Agochiya, Kevin A. Brown, Peter St.Onge, Inga Kireeva, et al. 2008. "A Proteome Resource of Ovarian Cancer Ascites: Integrated Proteomic and Bioinformatic Analyses to Identify Putative Biomarkers." *Journal of Proteome Research* 7 (1): 339–51. <https://doi.org/10.1021/pr0703223>.
- Grasso, Catherine S., Yi Mi Wu, Dan R. Robinson, Xuhong Cao, Saravana M. Dhanasekaran, Amjad P. Khan, Michael J. Quist, et al. 2012. "The Mutational Landscape of Lethal Castration-Resistant Prostate Cancer." *Nature* 487 (7406): 239–43. <https://doi.org/10.1038/nature11125>.
- Green, Douglas R., Thomas Ferguson, Laurence Zitvogel, and Guido Kroemer. 2009. "Immunogenic and Tolerogenic Cell Death." *Nature Reviews Immunology*. <https://doi.org/10.1038/nri2545>.
- Grignon, David J. 2004. "Unusual Subtypes of Prostate Cancer." *Modern Pathology*. <https://doi.org/10.1038/modpathol.3800052>.
- Grupp, Katharina, Mareike Habermann, Hüseyin Sirma, Ronald Simon, Stefan Steurer, Claudia Hube-Magg, Kristina Prien, et al. 2014. "High Nuclear Karyopherin 2 Expression Is a Strong and Independent Predictor of Biochemical Recurrence in Prostate Cancer Patients Treated by Radical Prostatectomy." *Modern Pathology* 27 (1): 96–106. <https://doi.org/10.1038/modpathol.2013.127>.
- Gurzov, Esteban N., Sanaa M. Nabha, Hamilto Yamamoto, Hong Meng, O. Graciela Graciela, and R. Daniel Daniel. 2007. "Paradoxical Antiproliferative Effect by a Murine Mammary Tumor-Derived Epithelial Cell Line." *BMC Cancer* 7: 1–14. <https://doi.org/10.1186/1471-2407-7-184>.
- Gut, Gabriele, Markus D. Herrmann, and Lucas Pelkmans. 2018. "Multiplexed Protein Maps Link Subcellular Organization to Cellular States." *Science* 361 (6401). <https://doi.org/10.1126/science.aar7042>.

- György, Bence, Tamás G. Szabó, Mária Pásztói, Zsuzsanna Pál, Petra Misják, Borbála Aradi, Valéria László, et al. 2011. "Membrane Vesicles, Current State-of-the-Art: Emerging Role of Extracellular Vesicles." *Cellular and Molecular Life Sciences* 68 (16): 2667–88. <https://doi.org/10.1007/s00018-011-0689-3>.
- Gyukity-Sebestyén, Edina, Mária Harmati, Gabriella Dobra, István B. Németh, Johanna Mihály, Ágnes Zvara, Éva Hunyadi-Gulyás, et al. 2019. "Melanoma-Derived Exosomes Induce PD-1 Overexpression and Tumor Progression via Mesenchymal Stem Cell Oncogenic Reprogramming." *Frontiers in Immunology* 10 (October). <https://doi.org/10.3389/fimmu.2019.02459>.
- Haffner, Michael C., Wilbert Zwart, Martine P. Roudier, Lawrence D. True, William G. Nelson, Jonathan I. Epstein, Angelo M. de Marzo, Peter S. Nelson, and Srinivasan Yegnasubramanian. 2021. "Genomic and Phenotypic Heterogeneity in Prostate Cancer." *Nature Reviews Urology*. Nature Research. <https://doi.org/10.1038/s41585-020-00400-w>.
- Hafner, Michael, Peter Orosz, Achim Kruger, and Daniela N Männel. 1996. "TFN Promotes Metastasis by Impairing Natural Killer Cell Activity." *Int. J. Cancer*. Vol. 66. Wiley-Liss, Inc.
- Han, Zeqiu, Jian Ni, Patrick Smits, Charles B Underhill, Bin Xie, Yixin Chen, Ningfei Liu, et al. 2001. "Extracellular Matrix Protein 1 (ECM1) Has Angiogenic Properties and Is Expressed by Breast Tumor Cells." *The FASEB Journal* 15 (6): 988–94. <https://doi.org/10.1096/fj.99-0934com>.
- Hanahan, Douglas. 2022. "Hallmarks of Cancer: New Dimensions." *Cancer Discovery* 12 (1): 31–46. <https://doi.org/10.1158/2159-8290.CD-21-1059>.
- Hanahan, Douglas, and Robert A Weinberg. 2000. "The Hallmarks of Cancer Review Evolve Progressively from Normalcy via a Series of Pre." *Cell*. Vol. 100.
- Hanahan, Douglas, and Robert A. Weinberg. 2011. "Hallmarks of Cancer: The next Generation." *Cell*. <https://doi.org/10.1016/j.cell.2011.02.013>.
- Handschin, Christoph, Sherry Chin, Ping Li, Fenfen Liu, Eleftheria Maratos-flier, Nathan K Lebrasseur, Zhen Yan, and Bruce M Spiegelman. 2007. "Skeletal Muscle Fiber-Type Switching , Exercise Intolerance , and Myopathy in PGC-1. Muscle-Specific Knock-out Animals." *Journal of Biological Chemistry* 282 (41): 30014–21. <https://doi.org/10.1074/jbc.M704817200>.
- Handschin, Christoph, Cheol Soo Choi, Sherry Chin, Sheene Kim, Dan Kawamori, Amarnath J Kurpad, Nicole Neubauer, et al. 2007. "Abnormal Glucose Homeostasis in Skeletal Muscle – Specific PGC-1 α Knockout Mice Reveals Skeletal Muscle – Pancreatic β Cell Crosstalk" 117 (11): 3463–74. <https://doi.org/10.1172/JCI31785.ways>.
- Haq, Rizwan, Jonathan Shoag, Pedro Andreu-Perez, Satoru Yokoyama, Hannah Edelman, Glenn C. Rowe, Dennie T. Frederick, et al. 2013. "Oncogenic BRAF Regulates Oxidative Metabolism via PGC1 α and MITF." *Cancer Cell* 23 (3): 302–15. <https://doi.org/10.1016/j.ccr.2013.02.003>.
- Hargadon, Kristian M., Coleman E. Johnson, and Corey J. Williams. 2018. "Immune Checkpoint Blockade Therapy for Cancer: An Overview of FDA-Approved Immune Checkpoint

- Inhibitors." *International Immunopharmacology*. Elsevier B.V. <https://doi.org/10.1016/j.intimp.2018.06.001>.
- Hartman, Zachary C., Graham M. Poage, Petra den Hollander, Anna Tsimelzon, Jamal Hill, Nattapon Panupinthu, Yun Zhang, et al. 2013. "Growth of Triple-Negative Breast Cancer Cells Relies upon Coordinate Autocrine Expression of the Proinflammatory Cytokines IL-6 and IL-8." *Cancer Research* 73 (11): 3470–80. <https://doi.org/10.1158/0008-5472.CAN-12-4524-T>.
- Hashimoto, Kyoko, Hiroki Ochi, Satoko Sunamura, Nobuyoshi Kosaka, Yo Mabuchi, Toru Fukuda, Kenta Yao, et al. 2018. "Cancer-Secreted Hsa-MiR-940 Induces an Osteoblastic Phenotype in the Bone Metastatic Microenvironment via Targeting ARHGAP1 and FAM134A." *Proceedings of the National Academy of Sciences of the United States of America* 115 (9): 2204–9. <https://doi.org/10.1073/pnas.1717363115>.
- Haslene-Hox, Hanne, Eystein Oveland, Kaja C Berg, Odd Kolmannskog, Kathrine Woie, Helga B Salvesen, Olav Tenstad, and Helge Wiig. 2011. "A New Method for Isolation of Interstitial Fluid from Human Solid Tumors Applied to Proteomic Analysis of Ovarian Carcinoma Tissue" 6 (4). <https://doi.org/10.1371/journal.pone.0019217>.
- He, Liusheng, Juhong Liu, Irene Collins, Suzanne Sanford, Brian O'connell, Craig J Benham, and David Levens. 2000. "Loss of FBP Function Arrests Cellular Proliferation and Extinguishes C-Myc Expression." *The EMBO Journal*. Vol. 19.
- Herzig, S, F Long, U. S. Jhala, S Hendrick, R Quinn, A Bauer, D Rudolph, et al. 2001. "CREB Regulates Hepatic Gluconeogenesis through the Coactivator PGC-1." *Nature* 413 (November).
- Hessvik, Nina Pettersen, and Alicia Llorente. 2018. "Current Knowledge on Exosome Biogenesis and Release." *Cellular and Molecular Life Sciences*. Birkhauser Verlag AG. <https://doi.org/10.1007/s00018-017-2595-9>.
- Hiraga, Toru, Susumu Ito, and Hiroaki Nakamura. 2013. "Cancer Stem-like Cell Marker CD44 Promotes Bone Metastases by Enhancing Tumorigenicity, Cell Motility, and Hyaluronan Production." *Cancer Research* 73 (13): 4112–22. <https://doi.org/10.1158/0008-5472.CAN-12-3801>.
- Hofmann, Anja, Coy Brunssen, Steffen Wolk, Christian Reeps, and Henning Morawietz. 2020. "Soluble LOX-1: A Novel Biomarker in Patients With Coronary Artery Disease, Stroke, and Acute Aortic Dissection?" *Journal of the American Heart Association* 9 (1). <https://doi.org/10.1161/JAHA.119.013803>.
- Hood, Joshua L., Susana San Roman, and Samuel A. Wickline. 2011. "Exosomes Released by Melanoma Cells Prepare Sentinel Lymph Nodes for Tumor Metastasis." *Cancer Research* 71 (11): 3792–3801. <https://doi.org/10.1158/0008-5472.CAN-10-4455>.
- Horibe, Sayo, Toshihito Tanahashi, Shoji Kawauchi, Yoshiki Murakami, and Yoshiyuki Rikitake. 2018. "Mechanism of Recipient Cell-Dependent Differences in Exosome Uptake," 1–10. <https://doi.org/10.1186/s12885-017-3958-1>.

- Hoshino, Ayuko, Bruno Costa-Silva, Tang Long Shen, Goncalo Rodrigues, Ayako Hashimoto, Milica Tesic Mark, Henrik Molina, et al. 2015. "Tumour Exosome Integrins Determine Organotropic Metastasis." *Nature* 527 (7578): 329–35. <https://doi.org/10.1038/nature15756>.
- Hoshino, Ayuko, Han Sang Kim, Linda Bojmar, Kofi Ennu Gyan, Michele Cioffi, Jonathan Hernandez, Constantinos P. Zambirinis, et al. 2020. "Extracellular Vesicle and Particle Biomarkers Define Multiple Human Cancers." *Cell* 182 (4): 1044-1061.e18. <https://doi.org/10.1016/j.cell.2020.07.009>.
- Hosseini-Beheshti, Elham, Wendy Choi, Louis Bastien Weiswald, Geetanjali Kharmate, Mazyar Ghaffari, Mani Roshan-Moniri, Mohamed D. Hassona, et al. 2016. "Exosomes Confer Pro-Survival Signals to Alter the Phenotype of Prostate Cells in Their Surrounding Environment." *Oncotarget* 7 (12): 14639–58. <https://doi.org/10.18632/oncotarget.7052>.
- Hosseini-Beheshti, Elham, Steven Pham, Hans Adomat, Na Li, and Emma S. Tomlinson Guns. 2012. "Exosomes as Biomarker Enriched Microvesicles: Characterization of Exosomal Proteins Derived from a Panel of Prostate Cell Lines with Distinct AR Phenotypes." *Molecular and Cellular Proteomics* 11 (10): 863–85. <https://doi.org/10.1074/mcp.M111.014845>.
- Hsu, Chia Wei, Kai Ping Chang, Yenlin Huang, Hao Ping Liu, Pei Chun Hsueh, Po Wen Gu, Wei Chen Yen, and Chih Ching Wu. 2019. "Proteomic Profiling of Paired Interstitial Fluids Reveals Dysregulated Pathways and Salivary NID1 as a Biomarker of Oral Cavity Squamous Cell Carcinoma." *Molecular and Cellular Proteomics* 18 (10): 1939–49. <https://doi.org/10.1074/mcp.RA119.001654>.
- Huang, Da Wei, Brad T. Sherman, and Richard A. Lempicki. 2009. "Bioinformatics Enrichment Tools: Paths toward the Comprehensive Functional Analysis of Large Gene Lists." *Nucleic Acids Research* 37 (1): 1–13. <https://doi.org/10.1093/nar/gkn923>.
- Huang, Yu Hua, Ya Qun Zhang, and Jiao Ti Huang. 2019. "Neuroendocrine Cells of Prostate Cancer: Biologic Functions and Molecular Mechanisms." *Asian Journal of Andrology*. Wolters Kluwer Medknow Publications. https://doi.org/10.4103/aja.aja_128_18.
- Huggins, Charles, and Clarence v Hodges. 1941. "The Effect of Castration, Of Estrogen and of Androgen Injection on Serum Phosphatases in Metastatic Carcinoma of the Prostate."
- Humphrey, Peter A. 2004. "Gleason Grading and Prognostic Factors in Carcinoma of the Prostate." *Modern Pathology*. <https://doi.org/10.1038/modpathol.3800054>.
- Huss, Janice M., Ryan P. Kopp, and Daniel P. Kelly. 2002. "Peroxisome Proliferator-Activated Receptor Coactivator-1 α (PGC-1 α) Coactivates the Cardiac-Enriched Nuclear Receptors Estrogen-Related Receptor- α and - γ : Identification of Novel Leucine-Rich Interaction Motif within PGC-1 α ." *Journal of Biological Chemistry* 277 (43): 40265–74. <https://doi.org/10.1074/jbc.M206324200>.
- Huss, Janice M., Inés Pineda Torra, Bart Staels, Vincent Giguère, and Daniel P. Kelly. 2004. "Estrogen-Related Receptor α Directs Peroxisome Proliferator-Activated Receptor α Signaling in the Transcriptional Control of Energy Metabolism in Cardiac and Skeletal

- Muscle.” *Molecular and Cellular Biology* 24 (20): 9079–91. <https://doi.org/10.1128/mcb.24.20.9079-9091.2004>.
- Imamura, Yusuke, and Marianne D. Sadar. 2016. “Androgen Receptor Targeted Therapies in Castration-Resistant Prostate Cancer: Bench to Clinic.” *International Journal of Urology*. Blackwell Publishing. <https://doi.org/10.1111/iju.13137>.
- Ioannou, Maria S., Emily S. Bell, Martine Girard, Mathilde Chaineau, Jason N.R. Hamlin, Mark Daubaras, Anie Monast, Morag Park, Louis Hodgson, and Peter S. McPherson. 2015. “DENND2B Activates Rab13 at the Leading Edge of Migrating Cells and Promotes Metastatic Behavior.” *Journal of Cell Biology* 208 (5): 629–48. <https://doi.org/10.1083/jcb.201407068>.
- Iraci, Nunzio, Edoardo Gaude, Tommaso Leonardi, Ana S.H. Costa, Chiara Cossetti, Luca Peruzzotti-Jametti, Joshua D. Bernstock, et al. 2017. “Extracellular Vesicles Are Independent Metabolic Units with Asparaginase Activity.” *Nature Chemical Biology* 13 (9): 951–55. <https://doi.org/10.1038/nchembio.2422>.
- Ittmann, Michael. 2018. “Anatomy and Histology of the Human and Murine Prostate.” *Cold Spring Harbor Perspectives in Medicine* 8 (5). <https://doi.org/10.1101/cshperspect.a030346>.
- Ivashkiv, Lionel B., and Laura T. Donlin. 2014. “Regulation of Type I Interferon Responses.” *Nature Reviews Immunology*. <https://doi.org/10.1038/nri3581>.
- Jäger, Sibylle, Christoph Handschin, Julie St.-Pierre, and Bruce M Spiegelman. 2007. “AMP-Activated Protein Kinase (AMPK) Action in Skeletal Muscle via Direct Phosphorylation of PGC-1.” www.pnas.org/cgi/doi/10.1073/pnas.0705070104.
- Jamaspishvili, Tamara, David M. Berman, Ashley E. Ross, Howard I. Scher, Angelo M. de Marzo, Jeremy A. Squire, and Tamara L. Lotan. 2018. “Clinical Implications of PTEN Loss in Prostate Cancer.” *Nature Reviews Urology*. Nature Publishing Group. <https://doi.org/10.1038/nrurol.2018.9>.
- Jiang, Lanzhou, and Ivan K.H. Poon. 2019. “Methods for Monitoring the Progression of Cell Death, Cell Disassembly and Cell Clearance.” *Apoptosis*. Springer New York LLC. <https://doi.org/10.1007/s10495-018-01511-x>.
- Jiang, Shu-Heng, Yang Wang, Jian-Yu Yang, Jun Li, Ming-Xuan Feng, Ya-Hui Wang, Xiao-Mei Yang, et al. 2015. “Overexpressed EDIL3 Predicts Poor Prognosis and Promotes Anchorage-Independent Tumor Growth in Human Pancreatic Cancer.” Vol. 7. www.impactjournals.com/oncotarget.
- Jin, Suoqin, Christian F. Guerrero-Juarez, Lihua Zhang, Ivan Chang, Peggy Myung, Maksim v. Plikus, and Qing Nie. 2020. “Inference and Analysis of Cell-Cell Communication Using CellChat.” *BioRxiv*. <https://doi.org/10.1101/2020.07.21.214387>.
- Jonckheere, Nicolas, Nicolas Skrypek, and Isabelle van Seuning. 2014. “Mucins and Tumor Resistance to Chemotherapeutic Drugs.” *Biochimica et Biophysica Acta - Reviews on Cancer*. Elsevier B.V. <https://doi.org/10.1016/j.bbcan.2014.04.008>.
- Joyce, Johanna A., and Jeffrey W. Pollard. 2009. “Microenvironmental Regulation of Metastasis.” *Nature Reviews Cancer*. <https://doi.org/10.1038/nrc2618>.

- Jung, Thorsten, Donatello Castellana, Pamela Klingbeil, Ines Cuesta Hernández, Mario Vitacolonna, David J. Orlicky, Steve R. Roffler, Pnina Brodt, and Margot Zöller. 2009. "CD44v6 Dependence of Premetastatic Niche Preparation by Exosomes." *Neoplasia* 11 (10): 1093–1105. <https://doi.org/10.1593/neo.09822>.
- Kajanne, Risto, Päivi Miettinen, Mikko Tenhunden, and Siripa Leppä. 2009. "Transcription Factor AP-1 Promotes Growth and Radioresistance in Prostate Cancer Cells." *International Journal of Oncology* 35 (05). https://doi.org/10.3892/ijo_00000434.
- Kalluri, Raghu. 2016. "The Biology and Function of Exosomes in Cancer." *Journal of Clinical Investigation*. American Society for Clinical Investigation. <https://doi.org/10.1172/JCI81135>.
- Kalra, Hina, Richard J. Simpson, Hong Ji, Elena Aikawa, Peter Altevogt, Philip Askenase, Vincent C. Bond, et al. 2012. "Vesiclepedia: A Compendium for Extracellular Vesicles with Continuous Community Annotation." *PLoS Biology* 10 (12). <https://doi.org/10.1371/journal.pbio.1001450>.
- Kamei, Yasutomi, Hiroshi Ohizumi, Yasushi Fujitani, Tomoyuki Nemoto, Toshiya Tanaka, Nobuyuki Takahashi, Teruo Kawada, et al. 2003. "PPAR Coactivator 1ERR Ligand 1 Is an ERR Protein Ligand, Whose Expression Induces a High-Energy Expenditure and Antagonizes Obesity." www.pnas.org/cgi/doi/10.1073/pnas.2135217100.
- Kaminski, Lisa, Stephanie Torrino, Maeva Dufies, Zied Djabari, Romain Haider, Francois Rene Roustan, Emilie Jaune, et al. 2019. "PGC1 α Inhibits Polyamine Synthesis to Suppress Prostate Cancer Aggressiveness." *Cancer Research* 79 (13): 3268–80. <https://doi.org/10.1158/0008-5472.CAN-18-2043>.
- Kantoff, Philip W., Celestia S. Higano, Neal D. Shore, E. Roy Berger, Eric J. Small, David F. Penson, Charles H. Redfern, et al. 2010. "Sipuleucel-T Immunotherapy for Castration-Resistant Prostate Cancer." *New England Journal of Medicine* 363 (5): 411–22. <https://doi.org/10.1056/nejmoa1001294>.
- Kaplan, Rosandra N., Rebecca D. Riba, Stergios Zacharoulis, Anna H. Bramley, Loïc Vincent, Carla Costa, Daniel D. MacDonald, et al. 2005. "VEGFR1-Positive Haematopoietic Bone Marrow Progenitors Initiate the Pre-Metastatic Niche." *Nature* 438 (7069): 820–27. <https://doi.org/10.1038/nature04186>.
- Kawakami, Yasuhiko, Masanao Tsuda, Shigeru Takahashi, Noboru Taniguchi, Concepción Rodríguez Esteban, Michihisa Zemmyo, Takayuki Furumatsu, Martin Lotz, Juan Carlos Izpisú Belmonte, and Hiroshi Asahara. 2005. "Transcriptional Coactivator PGC-1 Regulates Chondrogenesis via Association with Sox9." www.pnas.org/cgi/doi/10.1073/pnas.0407510102.
- Kerr, Bethany A, Ranko Miocinovic, Armine K Smith, and Eric A Klein. 2010. "Comparison of Tumor and Microenvironment Secretomes in Plasma and in Platelets during Prostate Cancer Growth in a Xenograft Model 1 , 2" *12* (5): 388–96. <https://doi.org/10.1593/neo.10166>.

- Khanna, Karan, Nikki Salmond, Kalan S. Lynn, Hon S. Leong, and Karla C. Williams. 2021. "Clinical Significance of STEAP1 Extracellular Vesicles in Prostate Cancer." *Prostate Cancer and Prostatic Diseases*. <https://doi.org/10.1038/s41391-021-00319-2>.
- Khatab, S, N Kops, P K Bos, M R Bernsen, G M van Buul, and Nuclear Medicine. 2018. "MESENCHYMAL STEM CELL SECRETOME REDUCES PAIN AND PREVENTS CARTILAGE DAMAGE IN A MURINE OSTEOARTHRITIS MODEL," 218–30. <https://doi.org/10.22203/eCM.v036a16>.
- Kim, Dae Kyum, Byeongsoo Kang, Oh Youn Kim, Dong Sic Choi, Jaewook Lee, Sae Rom Kim, Gyeongyun Go, et al. 2013. "EVpedia: An Integrated Database of High-Throughput Data for Systemic Analyses of Extracellular Vesicles." *Journal of Extracellular Vesicles* 2 (1). <https://doi.org/10.3402/jev.v2i0.20384>.
- Kim, H K, K S Song, Y S Park, Y H Kang, Y J Lee, K R Lee, K W Ryu, J M Bae, and S Kim. 2003. "Elevated Levels of Circulating Platelet Microparticles, VEGF, IL-6 and RANTES in Patients with Gastric Cancer: Possible Role of a Metastasis Predictor." www.ejconline.com.
- Kim, J, A Mizokami, M Shin, K Izumu, H Konaka, Y Kadono, Y Kitagawa, E. T. Keller, J Zhang, and M Namiki. 2014. "SOD3 Acts as a Tumor Suppressor in PC-3 Prostate Cancer Cells via Hydrogen Peroxide Accumulation." *Anticancer Research* 34 (April): 2821–32.
- Kim, Jiyeon, and Ralph J. DeBerardinis. 2019. "Mechanisms and Implications of Metabolic Heterogeneity in Cancer." *Cell Metabolism*. Cell Press. <https://doi.org/10.1016/j.cmet.2019.08.013>.
- Kimchi, Adi. 1992. "Cytokine Triggered Molecular Pathways That Control Cell Cycle Arrest."
- Kimura, Hirokazu, Hideki Yamamoto, Takeshi Harada, Katsumi Fumoto, Yoshihito Osugi, Ryota Sada, Natsumi Maehara, et al. 2019. "CKAP4, a DKK1 Receptor, Is a Biomarker in Exosomes Derived from Pancreatic Cancer and a Molecular Target for Therapy." *Clinical Cancer Research* 25 (6): 1936–47. <https://doi.org/10.1158/1078-0432.CCR-18-2124>.
- King, Nicole. 2004. "Review The Unicellular Ancestry of Animal Development Emergence of Comparative Genomics Have Paved the Way for New Insights. Long-Standing Hypotheses Regarding the Identity of Our Protozoan Relatives and the Cellular." *Developmental Cell*. Vol. 7.
- Kinter, Audrey L, Emily J Godbout, Jonathan P McNally, Irini Sereti, Gregg A Roby, Marie A O'shea, and Anthony S Fauci. 2008. "The Common-Chain Cytokines IL-2, IL-7, IL-15, and IL-21 Induce the Expression of Programmed Death-1 and Its Ligands." *The Journal of Immunology*. Vol. 181. www.jimmunol.org.
- Knerr, Kerstin, Karin Ackermann, Tanja Neidhart, and Walter Pyerin. 2004. "Bone Metastasis: Osteoblasts Affect Growth and Adhesion Regulons in Prostate Tumor Cells and Provoke Osteomimicry." *International Journal of Cancer* 111 (1): 152–59. <https://doi.org/10.1002/ijc.20223>.
- Koeneman, Kenneth S, Fan Yeung, and Leland W K Chung. 1999. "Osteomimetic Properties of Prostate Cancer Cells: A Hypothesis Supporting the Predilection of Prostate Cancer Metastasis and Growth in the Bone Environment." *Prostate*. Vol. 39.

- Koh, Cheryl M., Charles J. Bieberich, Chi v. Dang, William G. Nelson, Srinivasan Yegnasubramanian, and Angelo M. de Marzo. 2010. "MYC and Prostate Cancer." *Genes and Cancer* 1 (6): 617–28. <https://doi.org/10.1177/1947601910379132>.
- Koh, Cheryl M, Tsuyoshi Iwata, Qizhi Zheng, Carlise Bethel, Srinivasan Yegnasubramanian, and Angelo M de Marzo. 2011. "Myc Enforces Overexpression of EZH2 in Early Prostatic Neoplasia via Transcriptional and Post-Transcriptional Mechanisms." *Oncotarget*. Vol. 2. www.impactjournals.com/oncotarget/www.impactjournals.com/oncotarget669.
- Kohaar, Indu, Gyorgy Petrovics, and Shiv Srivastava. 2019. "A Rich Array of Prostate Cancer Molecular Biomarkers: Opportunities and Challenges." *International Journal of Molecular Sciences*. MDPI AG. <https://doi.org/10.3390/ijms20081813>.
- Kowal, Joanna, Mercedes Tkach, and Clotilde Théry. 2014. "Biogenesis and Secretion of Exosomes." *Current Opinion in Cell Biology* 29 (1): 116–25. <https://doi.org/10.1016/j.ceb.2014.05.004>.
- Krämer, Anne I., and Christoph Handschin. 2019. "How Epigenetic Modifications Drive the Expression and Mediate the Action of PGC-1 α in the Regulation of Metabolism." *International Journal of Molecular Sciences*. MDPI AG. <https://doi.org/10.3390/ijms20215449>.
- Kramer, Marianne, Sandra Pierredon, Pascale Ribaux, Jean Christophe Tille, Patrick Petignat, and Marie Cohen. 2015. "Secretome Identifies Tenascin-X as a Potent Marker of Ovarian Cancer." *BioMed Research International* 2015. <https://doi.org/10.1155/2015/208017>.
- Kresovich, Jacob K., Brian T. Joyce, Tao Gao, Yinan Zheng, Zhou Zhang, Christopher J. Achenbach, Robert L. Murphy, et al. 2018. "Promoter Methylation of PGC1A and PGC1B Predicts Cancer Incidence in a Veteran Cohort." *Epigenomics* 10 (6): 733–43. <https://doi.org/10.2217/epi-2017-0141>.
- Kressler, Dieter, Sylvia N. Schreiber, Darko Knutti, and Anastasia Kralli. 2002. "The PGC-1-Related Protein PERC Is a Selective Coactivator of Estrogen Receptor α ." *Journal of Biological Chemistry* 277 (16): 13918–25. <https://doi.org/10.1074/jbc.M201134200>.
- Kumar, Akash, Thomas A. White, Alexandra P. MacKenzie, Nigel Clegg, Choli Lee, Ruth F. Dumpit, Ilsa Coleman, et al. 2011. "Exome Sequencing Identifies a Spectrum of Mutation Frequencies in Advanced and Lethal Prostate Cancers." *Proceedings of the National Academy of Sciences of the United States of America* 108 (41): 17087–92. <https://doi.org/10.1073/pnas.1108745108>.
- Laganière, Josée, Gilles B. Tremblay, Catherine R. Dufour, Sylvie Giroux, François Rousseau, and Vincent Giguère. 2004. "A Polymorphic Autoregulatory Hormone Response Element in the Human Estrogen-Related Receptor α (ERR α) Promoter Dictates Peroxisome Proliferator-Activated Receptor γ Coactivator-1 α Control of ERR α Expression." *Journal of Biological Chemistry* 279 (18): 18504–10. <https://doi.org/10.1074/jbc.M313543200>.
- LaGory, Edward L., Colleen Wu, Cullen M. Taniguchi, Chien Kuang Cornelia Ding, Jen Tsan Chi, Rie von Eyben, David A. Scott, Adam D. Richardson, and Amato J. Giaccia. 2015.

- “Suppression of PGC-1 α Is Critical for Reprogramming Oxidative Metabolism in Renal Cell Carcinoma.” *Cell Reports* 12 (1): 116–27. <https://doi.org/10.1016/j.celrep.2015.06.006>.
- Landolfo, S, A Guarini, L Riera, M Gariglio, G Gribaudo, A Cignetti, I Cordone, E Montefusco, F Mandelli, and R Foa. 2000. “Chronic Myeloid Leukemia Cells Resistant to Interferon- α Lack STAT1 Expression.” *The Hematology Journal* 1 (1): 7–14. <https://doi.org/10.1038/sj.thj.6200004>.
- Lang, Hai Li, Guo Wen Hu, Bo Zhang, Wei Kuang, Yong Chen, Lei Wu, and Guo Hai Xu. 2017. “Glioma Cells Enhance Angiogenesis and Inhibit Endothelial Cell Apoptosis through the Release of Exosomes That Contain Long Non-Coding RNA CCAT2.” *Oncology Reports* 38 (2): 785–98. <https://doi.org/10.3892/or.2017.5742>.
- Lapointe, Jacques, Chunde Li, John P Higgins, Matt van de Rijn, Eric Bair, Kelli Montgomery, Michelle Ferrari, et al. 2004. “Gene Expression Profiling Identifies Clinically Relevant Subtypes of Prostate Cancer.” www.pnas.org/cgi/doi/10.1073/pnas.0304146101.
- Laurent-Matha, Valérie, Maruani-H, Sharon errmann, Christine Prébois, Mélanie Beaujouin, Murielle Glondu, Agnès Noël, et al. 2005. “Catalytically Inactive Human Cathepsin D Triggers Fibroblast Invasive Growth” 168 (3): 489–99. <https://doi.org/10.1083/jcb.200403078>.
- Lázaro-Ibáñez, Elisa, Maarit Neuvonen, Maarit Takatalo, Uma Thanigai Arasu, Cristian Capasso, Vincenzo Cerullo, Johng S. Rhim, Kirsi Rilla, Marjo Yliperttula, and Pia R.M. Siljander. 2017. “Metastatic State of Parent Cells Influences the Uptake and Functionality of Prostate Cancer Cell-Derived Extracellular Vesicles.” *Journal of Extracellular Vesicles* 6 (1). <https://doi.org/10.1080/20013078.2017.1354645>.
- Lebleu, Valerie S., Joyce T. O’Connell, Karina N. Gonzalez Herrera, Harriet Wikman, Klaus Pantel, Marcia C. Haigis, Fernanda Machado de Carvalho, et al. 2014. “PGC-1 α Mediates Mitochondrial Biogenesis and Oxidative Phosphorylation in Cancer Cells to Promote Metastasis.” *Nature Cell Biology* 16 (10): 992–1003. <https://doi.org/10.1038/ncb3039>.
- Lee, Amanda J., and Ali A. Ashkar. 2018. “The Dual Nature of Type I and Type II Interferons.” *Frontiers in Immunology*. Frontiers Media S.A. <https://doi.org/10.3389/fimmu.2018.02061>.
- Lee, Christine H., Oluyemi Akin-Olugbade, and Alexander Kirschenbaum. 2011. “Overview of Prostate Anatomy, Histology, and Pathology.” *Endocrinology and Metabolism Clinics of North America*. <https://doi.org/10.1016/j.ecl.2011.05.012>.
- Lee, Je Hyuk, Evan R. Daugharthy, Jonathan Scheiman, Reza Kalhor, Joyce L. Yang, Thomas C. Ferrante, Richard Terry, et al. 2014. “Highly Multiplexed Subcellular RNA Sequencing in Situ.” *Science* 343 (6177): 1360–63. <https://doi.org/10.1126/science.1250212>.
- Lee, Jeong Eun, Pyong Gon Moon, Young Eun Cho, Young Bum Kim, In San Kim, Hoyong Park, and Moon Chang Baek. 2016a. “Identification of EDIL3 on Extracellular Vesicles Involved in Breast Cancer Cell Invasion.” *Journal of Proteomics* 131 (January): 17–28. <https://doi.org/10.1016/j.jprot.2015.10.005>.

- . 2016b. "Identification of EDIL3 on Extracellular Vesicles Involved in Breast Cancer Cell Invasion." *Journal of Proteomics* 131 (January): 17–28. <https://doi.org/10.1016/j.jprot.2015.10.005>.
- Lee, Ji Yong, and Han Soo Kim. 2017. "Extracellular Vesicles in Neurodegenerative Diseases: A Double-Edged Sword." *Tissue Engineering and Regenerative Medicine*. Korean Tissue Engineering and Regenerative Medicine Society. <https://doi.org/10.1007/s13770-017-0090-x>.
- Lee, Marcus C.S., Elizabeth A. Miller, Jonathan Goldberg, Lelio Orci, and Randy Schekman. 2004. "Bi-Directional Protein Transport between the ER and Golgi." *Annual Review of Cell and Developmental Biology*. <https://doi.org/10.1146/annurev.cellbio.20.010403.105307>.
- Lee, Richard, A. Russell Localio, Katrina Armstrong, S. Bruce Malkowicz, and J. Sanford Schwartz. 2006. "A Meta-Analysis of the Performance Characteristics of the Free Prostate-Specific Antigen Test." *Urology* 67 (4): 762–68. <https://doi.org/10.1016/j.urology.2005.10.052>.
- Lee, Yu Chen, Martina Srajer Gajdosik, Djuro Josic, James G. Clifton, Christopher Logothetis, Li Yuan Yu-Lee, Gary E. Gallick, Sankar N. Maity, and Sue Hwa Lin. 2015. "Secretome Analysis of an Osteogenic Prostate Tumor Identifies Complex Signaling Networks Mediating Cross-Talk of Cancer and Stromal Cells within the Tumor Microenvironment." *Molecular and Cellular Proteomics* 14 (3): 471–83. <https://doi.org/10.1074/mcp.M114.039909>.
- Lehman, John J., Philip M. Barger, Attila Kovacs, Jeffrey E. Saffitz, Denis M. Medeiros, and Daniel P. Kelly. 2000. "Peroxisome Proliferator-Activated Receptor γ Coactivator-1 Promotes Cardiac Mitochondrial Biogenesis." *Journal of Clinical Investigation* 106 (7): 847–56. <https://doi.org/10.1172/JCI10268>.
- Leroyer, A. S., A. Tedgui, and C. M. Boulanger. 2008. "Role of Microparticles in Atherothrombosis." In *Journal of Internal Medicine*, 263:528–37. <https://doi.org/10.1111/j.1365-2796.2008.01957.x>.
- Levina, Elina, Hao Ji, Mengqiang Chen, Mirza Baig, David Oliver, Patrice Ohouo, Chang-Uk Lim, et al. 2015. "Identification of Novel Genes That Regulate Androgen Receptor Signaling and Growth of Androgen-Deprived Prostate Cancer Cells." *Oncotarget*. Vol. 6. www.impactjournals.com/oncotarget/.
- Li, Linhao, Xian Jiang, Qian Zhang, Xuesong Dong, Yuqiang Gao, Yuanlong He, Haiquan Qiao, Fangyu Xie, Xiangjun Xie, and Xueming Sun. 2016. "Neuropilin-1 Is Associated with Clinicopathology of Gastric Cancer and Contributes to Cell Proliferation and Migration as Multifunctional Co-Receptors." *Journal of Experimental and Clinical Cancer Research* 35 (1). <https://doi.org/10.1186/s13046-016-0291-5>.
- Li, Yanqing, Jinsong Kang, Jiaying Fu, Haoge Luo, Yanan Liu, Yang Li, and Liankun Sun. 2021. "Pgc1 α Promotes Cisplatin Resistance in Ovarian Cancer by Regulating the Hsp70/Hk2/Vdac1 Signaling Pathway." *International Journal of Molecular Sciences* 22 (5): 1–12. <https://doi.org/10.3390/ijms22052537>.

- Li, Yuchen, Xigan He, Qin Li, Hongyan Lai, Hena Zhang, Zhixiang Hu, Yan Li, and Shenglin Huang. 2020. "EV-Origin: Enumerating the Tissue-Cellular Origin of Circulating Extracellular Vesicles Using ExLR Profile." *Computational and Structural Biotechnology Journal* 18 (January): 2851–59. <https://doi.org/10.1016/j.csbj.2020.10.002>.
- Liang, Huiyun, and Walter F Ward. 2006. "Staying Current PGC-1: A Key Regulator of Energy Metabolism." *Advances in Physiology Education*, 145–51. <https://doi.org/doi:10.1152/advan.00052.2006>.
- Libby, Eric, and William C. Ratcliff. 2014. "Ratcheting the Evolution of Multicellularity." *Science*. American Association for the Advancement of Science. <https://doi.org/10.1126/science.1262053>.
- Lin, Jiandie, Christoph Handschin, and Bruce M. Spiegelman. 2005. "Metabolic Control through the PGC-1 Family of Transcription Coactivators." *Cell Metabolism*. <https://doi.org/10.1016/j.cmet.2005.05.004>.
- Lin, Jiandie, Ruoqing Yang, Paul T. Tarr, Pei Hsuan Wu, Christoph Handschin, Siming Li, Wenli Yang, et al. 2005. "Hyperlipidemic Effects of Dietary Saturated Fats Mediated through PGC-1 β Coactivation of SREBP." *Cell* 120 (2): 261–73. <https://doi.org/10.1016/j.cell.2004.11.043>.
- Lin, Ruizhu, and Risto Kerkelä. 2020. "Regulatory Mechanisms of Mitochondrial Function and Cardiac Aging." *International Journal of Molecular Sciences* 21 (4). <https://doi.org/10.3390/ijms21041359>.
- Liu, Juan, Shaoxian Wu, Xiao Zheng, Panpan Zheng, Yuanyuan Fu, Changping Wu, Binfeng Lu, Jingfang Ju, and Jingting Jiang. 2020. "Immune Suppressed Tumor Microenvironment by Exosomes Derived from Gastric Cancer Cells via Modulating Immune Functions." *Scientific Reports* 10 (1): 1–12. <https://doi.org/10.1038/s41598-020-71573-y>.
- Liu, Rui, Haiyang Zhang, Yan Zhang, Shuang Li, Xinyi Wang, Xia Wang, Cheng Wang, et al. 2017. "Peroxisome Proliferator-Activated Receptor Gamma Coactivator-1 Alpha Acts as a Tumor Suppressor in Hepatocellular Carcinoma." *Tumor Biology* 39 (4). <https://doi.org/10.1177/1010428317695031>.
- Liu, Yanfang, Yan Gu, Yanmei Han, Qian Zhang, Zhengping Jiang, Xiang Zhang, Bo Huang, Xiaoqing Xu, Jianming Zheng, and Xuetao Cao. 2016. "Tumor Exosomal RNAs Promote Lung Pre-Metastatic Niche Formation by Activating Alveolar Epithelial TLR3 to Recruit Neutrophils." *Cancer Cell* 30 (2): 243–56. <https://doi.org/10.1016/j.ccell.2016.06.021>.
- Liu, Yuelong, Xiaoyu Xiang, Xiaoying Zhuang, Shuangyin Zhang, Cunren Liu, Ziqiang Cheng, Sue Michalek, William Grizzle, and Huang Ge Zhang. 2010. "Contribution of MyD88 to the Tumor Exosome-Mediated Induction of Myeloid Derived Suppressor Cells." *American Journal of Pathology* 176 (5): 2490–99. <https://doi.org/10.2353/ajpath.2010.090777>.
- Llorente, Alicia, Bo van Deurs, and Kirsten Sandvig. 2007. "Cholesterol Regulates Prostate Release from Secretory Lysosomes in PC-3 Human Prostate Cancer Cells." *European Journal of Cell Biology* 86 (7): 405–15. <https://doi.org/10.1016/j.ejcb.2007.05.001>.
- Logothetis, Christopher J., and Sue Hwa Lin. 2005. "Osteoblasts in Prostate Cancer Metastasis to Bone." *Nature Reviews Cancer*. <https://doi.org/10.1038/nrc1528>.

- Longo, Sophia K., Margaret G. Guo, Andrew L. Ji, and Paul A. Khavari. 2021. "Integrating Single-Cell and Spatial Transcriptomics to Elucidate Intercellular Tissue Dynamics." *Nature Reviews Genetics*. Nature Research. <https://doi.org/10.1038/s41576-021-00370-8>.
- Lope, Lucía Robado de, Olwen Leaman Alcívar, Ana Amor López, Marta Hergueta-Redondo, and Heótor Peinado. 2018. "Tumour–Adipose Tissue Crosstalk: Fuelling Tumour Metastasis by Extracellular Vesicles." *Philosophical Transactions of the Royal Society B: Biological Sciences* 373 (1737). <https://doi.org/10.1098/rstb.2016.0485>.
- Lore, Lapeire, Hendrix An, Lecoutere Evelyne, Van Bockstal Mieke, Vandesompele Jo, Maynard Dawn, Braems Geert, et al. 2017. "Secretome Analysis of Breast Cancer-Associated Adipose Tissue to Identify Paracrine Regulators of Breast Cancer Growth." Vol. 8. www.impactjournals.com/oncotarget.
- Luga, Valbona, Liang Zhang, Alicia M. Vilorio-Petit, Abiodun A. Ogunjimi, Mohammad R. Inanlou, Elaine Chiu, Marguerite Buchanan, Abdel Nasser Hosein, Mark Basik, and Jeffrey L. Wrana. 2012. "Exosomes Mediate Stromal Mobilization of Autocrine Wnt-PCP Signaling in Breast Cancer Cell Migration." *Cell* 151 (7): 1542–56. <https://doi.org/10.1016/j.cell.2012.11.024>.
- Lujambio, Amaia, Leila Akkari, Janelle Simon, Danielle Grace, Darjus F Tschaharganeh, Jessica E Bolden, Zhen Zhao, et al. 2013. "Non-Cell-Autonomous Tumor Suppression by P53."
- Lun, Xiao Kang, and Bernd Bodenmiller. 2020. "Profiling Cell Signaling Networks at Single-Cell Resolution." *Molecular and Cellular Proteomics*. American Society for Biochemistry and Molecular Biology Inc. <https://doi.org/10.1074/mcp.R119.001790>.
- Lundberg, Emma, and Georg H.H. Borner. 2019. "Spatial Proteomics: A Powerful Discovery Tool for Cell Biology." *Nature Reviews Molecular Cell Biology*. Nature Publishing Group. <https://doi.org/10.1038/s41580-018-0094-y>.
- Lundholm, Marie, Mona Schröder, Olga Nagaeva, Vladimir Baranov, Anders Widmark, Lucia Mincheva-Nilsson, and Pernilla Wikström. 2014. "Prostate Tumor-Derived Exosomes down-Regulate NKG2D Expression on Natural Killer Cells and CD8+ T Cells: Mechanism of Immune Evasion." *PLoS ONE* 9 (9). <https://doi.org/10.1371/journal.pone.0108925>.
- Luo, Chi, Eduardo Balsa, Elizabeth A. Perry, Jiabin Liang, Clint D. Tavares, Francisca Vazquez, Hans R. Widlund, and Pere Puigserver. 2020. "H3K27me3-Mediated PGC1 α Gene Silencing Promotes Melanoma Invasion through WNT5A and YAP." *Journal of Clinical Investigation* 130 (2): 853–62. <https://doi.org/10.1172/JCI130038>.
- Luo, Chi, Ji Hong Lim, Yoonjin Lee, Scott R. Granter, Ajith Thomas, Francisca Vazquez, Hans R. Widlund, and Pere Puigserver. 2016. "A PGC1 α -Mediated Transcriptional Axis Suppresses Melanoma Metastasis." *Nature* 537 (7620): 422–26. <https://doi.org/10.1038/nature19347>.
- Ma, Zhe, Fan Chao, Shiyu Wang, Zhenyu Song, Zhiyuan Zhuo, Jinguo Zhang, Guoxiong Xu, and Gang Chen. 2020. "CTHRC1 Affects Malignant Tumor Cell Behavior and Is Regulated by MiR-30e-5p in Human Prostate Cancer." *Biochemical and Biophysical Research Communications* 525 (2): 418–24. <https://doi.org/10.1016/j.bbrc.2020.02.098>.

- Maadawi, Zeinab M el. 2017. "Conditioned Medium Derived from Salidroside-Pretreated Mesenchymal Stem Cell Culture Ameliorates Mouse Lipopolysaccharide-Induced Cerebral Neuroinflammation- Histological and Immunohistochemical Study" 10 (1): 60–68.
- Macedo, Juliana, Eduarda Carneiro, Diana Ferreira, António Verdelho, Luís Pedro Afonso, Joaquina Maurício, Susana Maria Silva, and Mavilde Arantes. 2017. "Neuroimaging Analysis of Rare Brain Metastases from Prostate Cancer." *Porto Biomedical Journal* 2 (5): 220. <https://doi.org/10.1016/j.pbj.2017.07.106>.
- Maleki Vareki, Saman. 2018. "High and Low Mutational Burden Tumors versus Immunologically Hot and Cold Tumors and Response to Immune Checkpoint Inhibitors." *Journal for ImmunoTherapy of Cancer*. BioMed Central Ltd. <https://doi.org/10.1186/s40425-018-0479-7>.
- Männel, Daniela N, Peter Orosz, Michael Hafner, and Werner Falk. 1994. "Mechanisms Involved in Metastasis Enhanced by Inflammatory Mediators." *Circulatory Shock*. Vol. 44.
- Manning, Brendan D., and Lewis C. Cantley. 2007. "AKT/PKB Signaling: Navigating Downstream." *Cell*. <https://doi.org/10.1016/j.cell.2007.06.009>.
- Mao, Jie, Xian rui Yuan, Shan shui Xu, Xiao chun Jiang, and Xin tong Zhao. 2013. "Expression and Functional Significance of Ezrin in Human Brain Astrocytoma." *Cell Biochemistry and Biophysics* 67 (3): 1507–11. <https://doi.org/10.1007/s12013-013-9653-1>.
- Marginean, C, I Streat, M Ioana, O M Marginean, V Padureanu, A Saftoiu, I Petrescu, S Tudorache, O S Tica, and F Petrescu. 2016. "Assessment of Oxidative Stress Genes SOD2 and SOD3 Polymorphisms Role in Human Colorectal Cancer." *Current Health Sciences Journal* 42 (4): 356–58. <https://doi.org/10.12865/CHSJ.42.04.04>.
- Martin, Daniel B, David R Gifford, Michael E Wright, Andrew Keller, Eugene Yi, David R Goodlett, Reudi Aebersold, and Peter S Nelson. 2004. "Quantitative Proteomic Analysis of Proteins Released by Neoplastic Prostate Epithelium," 347–55.
- Martínez-Redondo, Vicente, Amanda T. Pettersson, and Jorge L. Ruas. 2015a. "The Hitchhiker's Guide to PGC-1 α Isoform Structure and Biological Functions." *Diabetologia* 58 (9): 1969–77. <https://doi.org/10.1007/s00125-015-3671-z>.
- . 2015b. "The Hitchhiker's Guide to PGC-1 α Isoform Structure and Biological Functions." *Diabetologia*. Springer Verlag. <https://doi.org/10.1007/s00125-015-3671-z>.
- Martins, Vera C., Katrin Busch, Dilafruz Juraeva, Carmen Blum, Carolin Ludwig, Volker Rasche, Felix Lasitschka, et al. 2014. "Cell Competition Is a Tumour Suppressor Mechanism in the Thymus." *Nature* 509 (7501): 465–70. <https://doi.org/10.1038/nature13317>.
- Maruyama, Yojiro, Toshiaki Miyazaki, Kazuhiro Ikeda, Toshiyuki Okumura, Wataru Sato, Kuniko Horie-Inoue, Koji Okamoto, Satoru Takeda, and Satoshi Inoue. 2014. "Short Hairpin RNA Library-Based Functional Screening Identified Ribosomal Protein L31 That Modulates Prostate Cancer Cell Growth via P53 Pathway." *PLoS ONE* 9 (10). <https://doi.org/10.1371/journal.pone.0108743>.
- Mateo, Joaquin, Suzanne Carreira, Shahneen Sandhu, Susana Miranda, Helen Mossop, Raquel Perez-Lopez, Daniel Nava Rodrigues, et al. 2015. "DNA-Repair Defects and Olaparib in

- Metastatic Prostate Cancer." *New England Journal of Medicine* 373 (18): 1697–1708. <https://doi.org/10.1056/nejmoa1506859>.
- McGraw-Hill. 2005. "Concise Enciclopedia of Science and Technology." In , 5th ed.
- McGuirk, Shawn, Simon-Pierre Gravel, Geneviève Deblois, David J Papadopoli, Brandon Faubert, André Wegner, Karsten Hiller, et al. 2013. "PGC-1 α Supports Glutamine Metabolism in Breast Cancer." <http://www.cancerandmetabolism.com/content/1/1/22>.
- McKiernan, James, Michael J. Donovan, Eric Margolis, Alan Partin, Ballentine Carter, Gordon Brown, Phillipp Torkler, et al. 2018. "A Prospective Adaptive Utility Trial to Validate Performance of a Novel Urine Exosome Gene Expression Assay to Predict High-Grade Prostate Cancer in Patients with Prostate-Specific Antigen 2–10 Ng/ML at Initial Biopsy." *European Urology* 74 (6): 731–38. <https://doi.org/10.1016/j.eururo.2018.08.019>.
- McKiernan, James, Michael J. Donovan, Vince O'Neill, Stefan Bentink, Mikkel Noerholm, Susan Belzer, Johan Skog, et al. 2016. "A Novel Urine Exosome Gene Expression Assay to Predict High-Grade Prostate Cancer at Initial Biopsy." *JAMA Oncology* 2 (7): 882–89. <https://doi.org/10.1001/jamaoncol.2016.0097>.
- McNab, Finlay, Katrin Mayer-Barber, Alan Sher, Andreas Wack, and Anne O'Garra. 2015. "Type I Interferons in Infectious Disease." *Nature Reviews Immunology*. Nature Publishing Group. <https://doi.org/10.1038/nri3787>.
- Medrano, Ruan F.V., Aline Hunger, Samir Andrade Mendonça, José Alexandre M. Barbuto, and Bryan E. Strauss. 2017a. "Immunomodulatory and Antitumor Effects of Type I Interferons and Their Application in Cancer Therapy." *Oncotarget*. Impact Journals LLC. <https://doi.org/10.18632/oncotarget.19531>.
- . 2017b. "Immunomodulatory and Antitumor Effects of Type I Interferons and Their Application in Cancer Therapy." *Oncotarget*. Impact Journals LLC. <https://doi.org/10.18632/oncotarget.19531>.
- Mendez, Olga, Vicente Peg, Candida Salvans, Mireia Pujals, Yolanda Fernandez, Ibane Abasolo, Jose Perez, et al. 2018. "Extracellular HMGA1 Promotes Tumor Invasion and Metastasis in Triple-Negative Breast Cancer." *Clinical Cancer Research* 24 (24): 6367–82. <https://doi.org/10.1158/1078-0432.CCR-18-0517>.
- Minn, Andy J. 2015. "Interferons and the Immunogenic Effects of Cancer Therapy." *Trends in Immunology*. Elsevier Ltd. <https://doi.org/10.1016/j.it.2015.09.007>.
- Minsky, Neri, and Robert G Roeder. 2017. "Control of Secreted Protein Gene Expression and the Mammalian Secretome by the Metabolic Regulator PGC-1 α ." *Journal of Biological Chemistry* 292 (1): 43–50. <https://doi.org/10.1074/jbc.C116.761049>.
- Mira, Emilia, Lorena Carmona-Rodríguez, Beatriz Pérez-Villamil, Josefina Casas, María Jesús Fernández-Aceñero, Diego Martínez-Rey, Paula Martín-González, et al. 2018. "SOD3 Improves the Tumor Response to Chemotherapy by Stabilizing Endothelial HIF-2 α ." *Nature Communications* 9 (1). <https://doi.org/10.1038/s41467-018-03079-1>.
- Mittelbrunn, María, Cristina Gutiérrez-vázquez, Carolina Villarroja-beltri, Susana González, Fátima Sánchez-cabo, Manuel Ángel González, Antonio Bernad, and Francisco Sánchez-

- madrid. 2011. "Unidirectional Transfer of MicroRNA-Loaded Exosomes from T Cells to Antigen-Presenting Cells." <https://doi.org/10.1038/ncomms1285>.
- Moasser, M. M. 2007. "The Oncogene HER2: Its Signaling and Transforming Functions and Its Role in Human Cancer Pathogenesis." *Oncogene*. <https://doi.org/10.1038/sj.onc.1210477>.
- Mocellin, Simone, Sandro Pasquali, Carlo R. Rossi, and Donato Nitti. 2010. "Interferon Alpha Adjuvant Therapy in Patients with High-Risk Melanoma: A Systematic Review and Meta-Analysis." *Journal of the National Cancer Institute* 102 (7): 493–501. <https://doi.org/10.1093/jnci/djq009>.
- Mootha, Vamsi K., Christoph Handschin, Dan Arlow, Xiaohui Xie, Julie St. Pierre, Smita Sihag, Wenli Yang, et al. 2004. "Erra and Gabpa/b Specify PGC-1 α -Dependent Oxidative Phosphorylation Gene Expression That Is Altered in Diabetic Muscle." *Proceedings of the National Academy of Sciences* 101 (17): 6570–75. <https://doi.org/10.1073/PNAS.0401401101>.
- Mootha, Vamsi K, Christoph Handschin, Dan Arlow, Xiaohui Xie, Julie St Pierre, Smita Sihag, Wenli Yang, et al. 2004. "Err and Gabpab Specify PGC-1-Dependent Oxidative Phosphorylation Gene Expression That Is Altered in Diabetic Muscle." www.pnas.org/cgi/doi/10.1073pnas.0401401101.
- Morata, G, and P Ripoll. 1975. "Minutes: Mutants of Drosophila Autonomously Affecting Cell Division Rate." *DEVELOPMENTAL BIOLOGY*. Vol. 42.
- Morel, Katherine L., Anjali v. Sheahan, Deborah L. Burkhardt, Sylvan C. Baca, Nadia Boufaied, Yin Liu, Xintao Qiu, et al. 2021. "EZH2 Inhibition Activates a DsRNA–STING–Interferon Stress Axis That Potentiates Response to PD-1 Checkpoint Blockade in Prostate Cancer." *Nature Cancer* 2 (4): 444–56. <https://doi.org/10.1038/s43018-021-00185-w>.
- Moreno, Eduardo. 2008. "Is Cell Competition Relevant to Cancer?" *Nature Reviews* 8. <https://doi.org/doi:10.1038/nrc2252>.
- Moreno, Eduardo, and Konrad Basler. 2004. "DMyc Transforms Cells into Super-Competitors Developing Tissue Remains Unchanged and No Morpho." *Cell*. Vol. 117.
- Moreno-Gonzalo, Olga, Irene Fernandez-Delgado, and Francisco Sanchez-Madrid. 2018. "Post-Translational Add-Ons Mark the Path in Exosomal Protein Sorting." *Cellular and Molecular Life Sciences*. Birkhauser Verlag AG. <https://doi.org/10.1007/s00018-017-2690-y>.
- Morikawa, Wataru, Kenji Yamamoto, Sara Ishikawa, Sumiyo Takemoto, Mayumi Ono, Jun Ichi Fukushi, Seiji Naito, Chikateru Nozaki, Sadaaki Iwanaga, and Michihiko Kuwano. 2000. "Angiostatin Generation by Cathepsin D Secreted by Human Prostate Carcinoma Cells." *Journal of Biological Chemistry* 275 (49): 38912–20. <https://doi.org/10.1074/jbc.M005402200>.
- Mortezavi, Ashkan, Thomas Hermanns, Hans Helge Seifert, Martin K. Baumgartner, Maurizio Provenzano, Tullio Sulser, Maximilian Burger, et al. 2011. "KPNA2 Expression Is an Independent Adverse Predictor of Biochemical Recurrence after Radical Prostatectomy." *Clinical Cancer Research* 17 (5): 1111–21. <https://doi.org/10.1158/1078-0432.CCR-10-0081>.

- Mouchiroud, Laurent, Lillian J. Eichner, Reuben J. Shaw, and Johan Auwerx. 2014. "Transcriptional Coregulators: Fine-Tuning Metabolism." *Cell Metabolism*. Cell Press. <https://doi.org/10.1016/j.cmet.2014.03.027>.
- Mouw, Janna K., Yoshihiro Yui, Laura Damiano, Russell O. Bainer, Johnathon N. Lakins, Irene Acerbi, Guanqing Ou, et al. 2014. "Tissue Mechanics Modulate MicroRNA-Dependent PTEN Expression to Regulate Malignant Progression." *Nature Medicine* 20 (4): 360–67. <https://doi.org/10.1038/nm.3497>.
- Mui, Keeley L., Yong Ho Bae, Lin Gao, Shu Lin Liu, Tina Xu, Glenn L. Radice, Christopher S. Chen, and Richard K. Assoian. 2015. "N-Cadherin Induction by ECM Stiffness and FAK Overrides the Spreading Requirement for Proliferation of Vascular Smooth Muscle Cells." *Cell Reports* 10 (9): 1477–86. <https://doi.org/10.1016/j.celrep.2015.02.023>.
- Murillo-Garzón, Virginia, and Robert Kypta. 2017. "WNT Signalling in Prostate Cancer." *Nature Reviews Urology*. Nature Publishing Group. <https://doi.org/10.1038/nrurol.2017.144>.
- Murira, Armstrong, and Alain Lamarre. 2016. "Type-I Interferon Responses: From Friend to Foe in the Battle against Chronic Viral Infection." *Frontiers in Immunology*. Frontiers Media S.A. <https://doi.org/10.3389/fimmu.2016.00609>.
- Mushinski, J. Frederic, Phuong Mai Nguyen, Lisa M. Stevens, Chand Khanna, Sunmin Lee, Eun Joo Chung, Min Jung Lee, et al. 2009. "Inhibition of Tumor Cell Motility by the Interferon-Inducible GTPase MxA." *Journal of Biological Chemistry* 284 (22): 15206–14. <https://doi.org/10.1074/jbc.M806324200>.
- Muthalagu, Nathiya, Tiziana Monteverde, Ximena Raffo-Iraolagoitia, Robert Wiesheu, Declan Whyte, Ann Hedley, Sarah Laing, et al. 2020a. "Repression of the Type I Interferon Pathway Underlies MYC-and KRAS-Dependent Evasion of NK and B Cells in Pancreatic Ductal Adenocarcinoma." *Cancer Discovery* 10 (6): 872–87. <https://doi.org/10.1158/2159-8290.CD-19-0620>.
- . 2020b. "Repression of the Type I Interferon Pathway Underlies MYC-and KRAS-Dependent Evasion of NK and B Cells in Pancreatic Ductal Adenocarcinoma." *Cancer Discovery* 10 (6): 872–87. <https://doi.org/10.1158/2159-8290.CD-19-0620>.
- Naba, Alexandra, Karl R. Clauser, Sebastian Hoersch, Hui Liu, Steven A. Carr, and Richard O. Hynes. 2011. "The Matrisome: In Silico Definition and In Vivo Characterization by Proteomics of Normal and Tumor Extracellular Matrices." *Molecular & Cellular Proteomics* 11.4 (December).
- Naba, Alexandra, Sebastian Hoersch, and Richard O. Hynes. 2012. "Towards Definition of an ECM Parts List: An Advance on GO Categories." *Matrix Biology*. <https://doi.org/10.1016/j.matbio.2012.11.008>.
- Nam, Hyeyoung, Anirban Kundu, Garrett J. Brinkley, Darshan S. Chandrashekar, Richard L. Kirkman, Balabhadrapatruni V.S.K. Chakravarthi, Rachael M. Orlandella, et al. 2020. "PGC1 α Suppresses Kidney Cancer Progression by Inhibiting Collagen-Induced SNAIL Expression." *Matrix Biology* 89 (July): 43–58. <https://doi.org/10.1016/j.matbio.2020.01.001>.

- Nandana, Srinivas, Manisha Tripathi, Peng Duan, Chia Yi Chu, Rajeev Mishra, Chunyan Liu, Renjie Jin, et al. 2017. "Bone Metastasis of Prostate Cancer Can Be Therapeutically Targeted at the TBX2-WNT Signaling Axis." *Cancer Research* 77 (6): 1331–44. <https://doi.org/10.1158/0008-5472.CAN-16-0497>.
- Nardella, C, A Carracedo, L Salmena, and P.P Pandolfi. 2010. "Immunology, Phenotype First : How Mutations Have Established New Principles and Pathways in Immunology." In , 2:136–58. Springer.
- Neilsen, Paul M, Jacqueline E Noll, Rachel J Suetani, Renee B Schulz, Fares Al-Ejeh, Andreas Evdokiou, David P Lane, and David F Callen. 2011. "Mutant P53 Uses P63 as a Molecular Chaperone to Alter Gene Expression and Induce a Pro-Invasive Secretome * Denotes Equal Contribution." *Oncotarget*. Vol. 2. www.impactjournals.com/oncotarget/www.impactjournals.com/oncotarget.
- Nickel, W, and C Rabouille. 2009. "Mechanisms of Regulated Unconventional Protein Secretion."
- Noble, J. L., R. S. Dua, G. R. Coulton, C. M. Isacke, and G. P.H. Gui. 2007. "A Comparative Proteomic Analysis of Nipple Aspiration Fluid from Healthy Women and Women with Breast Cancer." *European Journal of Cancer* 43 (16): 2315–20. <https://doi.org/10.1016/j.ejca.2007.08.009>.
- Noël, Floriane, Lucile Massenet-Regad, Irit Carmi-Levy, Antonio Cappuccio, Maximilien Grandclaudon, Coline Trichot, Yann Kieffer, Fatima Mechta-Grigoriou, and Vassili Soumelis. 2020. "ICELLNET: A Transcriptome-Based Framework to Dissect Intercellular Communication." *BioRxiv*. <https://doi.org/10.1101/2020.03.05.976878>.
- Nurdin, Armania, Yutaro Hoshi, Toshihiro Yoneyama, Eisuke Miyauchi, Masanori Tachikawa, Michitoshi Watanabe, and Tetsuya Terasaki. 2016. "Global and Targeted Proteomics of Prostate Cancer Cell Secretome: Combination of 2-Dimensional Image-Converted Analysis of Liquid Chromatography and Mass Spectrometry and In Silico Selection Selected Reaction Monitoring Analysis." *Journal of Pharmaceutical Sciences* 105 (11): 3440–52. <https://doi.org/10.1016/j.xphs.2016.08.013>.
- Obenauf, Anna C, Yilong Zou, Andrew L Ji, Sakari Vanharanta, Weiping Shu, Hubing Shi, Xiangju Kong, et al. 2015. "Therapy-Induced Tumour Secretomes Promote Resistance and Tumour Progression." *Nature* 520 (7547): 368–72. <https://doi.org/10.1038/nature14336>.
- Oberkofler, Hannes, Elisabeth Schraml, Franz Krempler, and Wolfgang Patsch. 2003. "Potentiation of Liver X Receptor Transcriptional Activity by Peroxisome-Proliferator-Activated Receptor γ Co-Activator 1 α ." *Biochem. J*. Vol. 371.
- Ohuri, M, T. M. Wheeler, K Dunn, T Stamey, and P Scardino. n.d. "The Pathological Features and Prognosis of Prostate Cancer Detectable With Current Diagnostic Tests."
- Olmeda, David, Daniela Cerezo-wallis, Erica Riveiro-falkenbach, Paula C Pennacchi, Marta Contreras-alcalde, Nuria Ibarz, Metehan Cifdaloz, et al. 2017. "Whole-Body Imaging of Lymphovascular Niches Identifies Pre-Metastatic Roles of Midkine." *Nature Publishing Group* 546 (7660): 676–80. <https://doi.org/10.1038/nature22977>.

- Ortiz, Angelica, Jun Gui, Farima Zahedi, Pengfei Yu, Christina Cho, Sabyasachi Bhattacharya, Christopher J. Carbone, et al. 2019. "An Interferon-Driven Oxysterol-Based Defense against Tumor-Derived Extracellular Vesicles." *Cancer Cell* 35 (1): 33-45.e6. <https://doi.org/10.1016/j.ccell.2018.12.001>.
- Øverbye, Anders, Tore Skotland, Christian J Koehler, Bernd Thiede, Therese Seierstad, Viktor Berge, Kirsten Sandvig, and Alicia Llorente. 2015. "Identification of Prostate Cancer Biomarkers in Urinary Exosomes." *Oncotarget*. Vol. 6. www.impactjournals.com/oncotarget/.
- Owen, Katie L, Linden J Gearing, Damien J Zanker, Natasha K Brockwell, Weng Hua Khoo, Daniel L Roden, Marek Cmero, et al. 2020. "Prostate Cancer Cell-intrinsic Interferon Signaling Regulates Dormancy and Metastatic Outgrowth in Bone." *EMBO Reports* 21 (6). <https://doi.org/10.15252/embr.202050162>.
- Pagel, Julia, Karin Beutel, Kai Lehmberg, Florian Koch, Andrea Maul-Pavivic, Anna Katharina Rohlf, Abdullah Al-Jefri, et al. 2012. "Distinct Mutations in STXBP2 Are Associated with Variable Clinical Presentations in Patients with Familial Hemophagocytic Lymphohistiocytosis Type 5 (FHL5)." *Blood* 119 (25): 6016–24. <https://doi.org/10.1182/blood-2011-12-398958>.
- Pagès, Franck, Bernhard Mlecnik, Florence Marliot, Gabriela Bindea, Fang Shu Ou, Carlo Bifulco, Alessandro Lugli, et al. 2018. "International Validation of the Consensus Immunoscore for the Classification of Colon Cancer: A Prognostic and Accuracy Study." *The Lancet* 391 (10135): 2128–39. [https://doi.org/10.1016/S0140-6736\(18\)30789-X](https://doi.org/10.1016/S0140-6736(18)30789-X).
- Paget, Stephen. 1889. "THE DISTRIBUTION OF SECONDARY GROWTHS IN CANCER OF THE BREAST." *The Lancet* 133 (3421): 571–73. [https://doi.org/10.1016/S0140-6736\(00\)49915-0](https://doi.org/10.1016/S0140-6736(00)49915-0).
- Pang, See Tong, Xioalei Fang, Alexander Valdman, Gunnar Norstedt, Ake Pousette, Lars Egevad, and Peter Ekman. 2004. "Expression of Ezrin in Prostatic Intraepithelial Neoplasia." *Urology* 63 (3): 609–12. <https://doi.org/10.1016/j.urology.2003.09.068>.
- Pap, E., É Pállinger, A. Falus, A. A. Kiss, Á Kittel, P. Kovács, and E. I. Buzás. 2008. "T Lymphocytes Are Targets for Platelet- and Trophoblast-Derived Microvesicles During Pregnancy." *Placenta* 29 (9): 826–32. <https://doi.org/10.1016/j.placenta.2008.06.006>.
- Papalexi, Efthymia, and Rahul Satija. 2018. "Single-Cell RNA Sequencing to Explore Immune Cell Heterogeneity." *Nature Reviews Immunology*. Nature Publishing Group. <https://doi.org/10.1038/nri.2017.76>.
- Parker, Belinda S., Jai Rautela, and Paul J. Hertzog. 2016a. "Antitumour Actions of Interferons: Implications for Cancer Therapy." *Nature Reviews Cancer*. Nature Publishing Group. <https://doi.org/10.1038/nrc.2016.14>.
- . 2016b. "Antitumour Actions of Interferons: Implications for Cancer Therapy." *Nature Reviews Cancer*. Nature Publishing Group. <https://doi.org/10.1038/nrc.2016.14>.
- . 2016c. "Antitumour Actions of Interferons: Implications for Cancer Therapy." *Nature Reviews Cancer*. Nature Publishing Group. <https://doi.org/10.1038/nrc.2016.14>.

- Parker, C., E. Castro, K. Fizazi, A. Heidenreich, P. Ost, G. Procopio, B. Tombal, and S. Gillissen. 2020. "Prostate Cancer: ESMO Clinical Practice Guidelines for Diagnosis, Treatment and Follow-Up†." *Annals of Oncology* 31 (9): 1119–34. <https://doi.org/10.1016/j.annonc.2020.06.011>.
- Parolini, Isabella, Cristina Federici, Carla Raggi, Luana Lugini, Simonetta Palleschi, Angelo de Milito, Carolina Coscia, et al. 2009. "Microenvironmental PH Is a Key Factor for Exosome Traffic in Tumor Cells." *Journal of Biological Chemistry* 284 (49): 34211–22. <https://doi.org/10.1074/jbc.M109.041152>.
- Patel, Seema, Ahmad Homaei, Hesham R. El-Seedi, and Nadeem Akhtar. 2018. "Cathepsins: Proteases That Are Vital for Survival but Can Also Be Fatal." *Biomedicine and Pharmacotherapy*. Elsevier Masson SAS. <https://doi.org/10.1016/j.biopha.2018.05.148>.
- Pavlou, Maria P, and Eleftherios P Diamandis. 2010. "The Cancer Cell Secretome : A Good Source for Discovering Biomarkers ?" *Journal of Proteomics* 73 (10): 1896–1906. <https://doi.org/10.1016/j.jprot.2010.04.003>.
- Pavlova, Natalya N., and Craig B. Thompson. 2016. "The Emerging Hallmarks of Cancer Metabolism." *Cell Metabolism*. Cell Press. <https://doi.org/10.1016/j.cmet.2015.12.006>.
- Pawlik, Timothy M, Herbert Fritsche, Kevin R Coombes, Lianchun Xiao, Savitri Krish-Namurthy, Kelly K Hunt, Lajos Pusztai, et al. 2005. "Significant Differences in Nipple Aspirate Fluid Protein Expression between Healthy Women and Those with Breast Cancer Demonstrated by Time-of-Flight Mass Spectrometry."
- Peinado, Héctor, Maša Ale, Simon Lavotshkin, Irina Matei, Bruno Costa-silva, Gema Moreno-bueno, Marta Hergueta-redondo, et al. 2012. "NIH Public Access" 18 (6): 883–91. <https://doi.org/10.1038/nm.2753.Melanoma>.
- Peinado, Héctor, Maša Alečković, Simon Lavotshkin, Irina Matei, Bruno Costa-Silva, Gema Moreno-Bueno, Marta Hergueta-Redondo, et al. 2012. "Melanoma Exosomes Educate Bone Marrow Progenitor Cells toward a Pro-Metastatic Phenotype through MET." *Nature Medicine* 18 (6): 883–91. <https://doi.org/10.1038/nm.2753>.
- Peinado, Héctor, Haiying Zhang, Irina R. Matei, Bruno Costa-Silva, Ayuko Hoshino, Goncalo Rodrigues, Bethan Psaila, et al. 2017. "Pre-Metastatic Niches: Organ-Specific Homes for Metastases." *Nature Reviews Cancer* 17 (5): 302–17. <https://doi.org/10.1038/nrc.2017.6>.
- Peteranderl, Christin, and Susanne Herold. 2017. "The Impact of the Interferon/TNF-Related Apoptosis-Inducing Ligand Signaling Axis on Disease Progression in Respiratory Viral Infection and Beyond." *Frontiers in Immunology*. Frontiers Research Foundation. <https://doi.org/10.3389/fimmu.2017.00313>.
- Piccolo, Enza, Nicola Tinari, Daniela Semeraro, Sara Traini, Imma Fichera, Albana Cumashi, Rossana la Sorda, et al. 2013. "LGALS3BP, Lectin Galactoside-Binding Soluble 3 Binding Protein, Induces Vascular Endothelial Growth Factor in Human Breast Cancer Cells and Promotes Angiogenesis." *Journal of Molecular Medicine* 91 (1): 83–94. <https://doi.org/10.1007/s00109-012-0936-6>.

- Pienta, Kenneth J. 2009. "Critical Appraisal of Prostate-Specific Antigen in Prostate Cancer Screening: 20 Years Later." *Urology* 73 (5 SUPPL.). <https://doi.org/10.1016/j.urology.2009.02.016>.
- Pilch, Bartosz, and Matthias Mann. 2006. "Large-Scale and High-Confidence Proteomic Analysis of Human Seminal Plasma." *Genome Biology* 7 (5). <https://doi.org/10.1186/gb-2006-7-5-r40>.
- Platanias, Leonidas C. 2005. "Mechanisms of Type-I- and Type-II-Interferon-Mediated Signalling." *Nature Reviews Immunology*. <https://doi.org/10.1038/nri1604>.
- Principe, Simona, Yunee Kim, Simona Fontana, Vladimir Ignatchenko, Julius O. Nyalwidhe, Raymond S. Lance, Dean A. Troyer, et al. 2012. "Identification of Prostate-Enriched Proteins by in-Depth Proteomic Analyses of Expressed Prostatic Secretions in Urine." *Journal of Proteome Research* 11 (4): 2386–96. <https://doi.org/10.1021/pr2011236>.
- Probert, C., T. Dottorini, A. Speakman, S. Hunt, T. Nafee, A. Fazeli, S. Wood, J. E. Brown, and V. James. 2019. "Communication of Prostate Cancer Cells with Bone Cells via Extracellular Vesicle RNA; a Potential Mechanism of Metastasis." *Oncogene* 38 (10): 1751–63. <https://doi.org/10.1038/s41388-018-0540-5>.
- Puigserver, P. 2005. "Tissue-Specific Regulation of Metabolic Pathways through the Transcriptional Coactivator PGC1- α ." *International Journal of Obesity* 29: S5–9. <https://doi.org/10.1038/sj.ijo.0802905>.
- Puigserver, P, Z Wu, C Won, R Graves, M Wright, and B. M Spiegelman. 1998. "A Cold-Inducible Coactivator of Nuclear Receptors Linked to Adaptive Thermogenesis." *Cell* 92 (March): 829–39.
- Puigserver, Pere, and Bruce M. Spiegelman. 2003. "Peroxisome Proliferator-Activated Receptor- γ Coactivator 1 α (PGC-1 α): Transcriptional Coactivator and Metabolic Regulator." *Endocrine Reviews*. <https://doi.org/10.1210/er.2002-0012>.
- Qu, Zhen, Jiawei Feng, Hua Pan, Yong Jiang, Yunfei Duan, and Zhenzhong Fa. 2019. "Exosomes Derived from HCC Cells with Different Invasion Characteristics Mediated EMT through TGF- β /Smad Signaling Pathway." *OncoTargets and Therapy* 12: 6897–6905. <https://doi.org/10.2147/OTT.S209413>.
- Rabinowits, Guilherme, Cicek Gerçel-Taylor, Jamie M. Day, Douglas D. Taylor, and Goetz H. Kloecker. 2009. "Exosomal MicroRNA: A Diagnostic Marker for Lung Cancer." *Clinical Lung Cancer* 10 (1): 42–46. <https://doi.org/10.3816/CLC.2009.n.006>.
- Rabouille, Catherine. 2017. "Pathways of Unconventional Protein Secretion." *Trends in Cell Biology*. Elsevier Ltd. <https://doi.org/10.1016/j.tcb.2016.11.007>.
- Rabouille, Catherine, Vivek Malhotra, and Walter Nickel. 2012. "Diversity in Unconventional Protein Secretion." *Journal of Cell Science* 125 (22): 5251–55. <https://doi.org/10.1242/jcs.103630>.
- Rajagopal, Chitra, and K B Harikumar. 2018. "The Origin and Functions of Exosomes in Cancer" 8 (March). <https://doi.org/10.3389/fonc.2018.00066>.

- Ramilowski, Jordan A., Tatyana Goldberg, Jayson Harshbarger, Edda Kloppman, Marina Lizio, Venkata P. Satagopam, Masayoshi Itoh, et al. 2015. "A Draft Network of Ligand-Receptor-Mediated Multicellular Signalling in Human." *Nature Communications* 6 (July). <https://doi.org/10.1038/ncomms8866>.
- Ramroop, Johnny R., Mark N. Stein, and Justin M. Drake. 2018. "Impact of Phosphoproteomics in the Era of Precision Medicine for Prostate Cancer." *Frontiers in Oncology*. Frontiers Media S.A. <https://doi.org/10.3389/fonc.2018.00028>.
- Raposo, Graça, Hans W Nijman, ~willem Stoorvogel, Richtje Leijendekker, Cliffordv Hardingfl Cornelis, J M Melief, and Hans J Geuze. 1996. "B Lymphocytes Secrete Antigen-Presenting Vesicles." <http://rupress.org/jem/article-pdf/183/3/1161/1107814/1161.pdf>.
- Raveh, Tal, Ara G. Hovanessian, Eliane F. Meurs, Nahum Sonenberg, and Adi Kimchi. 1996. "Double-Stranded RNA-Dependent Protein Kinase Mediates c-Myc Suppression Induced by Type I Interferons." *Journal of Biological Chemistry* 271 (41): 25479–84. <https://doi.org/10.1074/jbc.271.41.25479>.
- Rawla, Prashanth. 2019. "Epidemiology of Prostate Cancer." *World Journal of Oncology* 10 (2): 63–89. <https://doi.org/10.14740/wjon1191>.
- Recchia, Francesco, Gigliola Sica, Giampiero Candeloro, Stefano Necozone, Roberta Bisegna, Massimo Bratta, and Silvio Rea. 2009. "Beta-Interferon, Retinoids and Tamoxifen in Metastatic Breast Cancer: Long-Term Follow-up of a Phase II Study." *Oncology Reports* 21 (4): 1011–16. https://doi.org/10.3892/or_00000317.
- Reiss, Karina, and Paul Saftig. 2009. "The 'A Disintegrin And Metalloprotease' (ADAM) Family of Sheddases: Physiological and Cellular Functions." *Seminars in Cell and Developmental Biology*. Elsevier Ltd. <https://doi.org/10.1016/j.semcdb.2008.11.002>.
- Ritchie, Matthew E., Belinda Phipson, Di Wu, Yifang Hu, Charity W. Law, Wei Shi, and Gordon K. Smyth. 2015. "Limma Powers Differential Expression Analyses for RNA-Sequencing and Microarray Studies." *Nucleic Acids Research* 43 (7): e47. <https://doi.org/10.1093/nar/gkv007>.
- Robinson, Dan, Eliezer M. van Allen, Yi Mi Wu, Nikolaus Schultz, Robert J. Lonigro, Juan Miguel Mosquera, Bruce Montgomery, et al. 2015a. "Integrative Clinical Genomics of Advanced Prostate Cancer." *Cell* 161 (5): 1215–28. <https://doi.org/10.1016/j.cell.2015.05.001>.
- . 2015b. "Integrative Clinical Genomics of Advanced Prostate Cancer." *Cell* 161 (5): 1215–28. <https://doi.org/10.1016/j.cell.2015.05.001>.
- Robinson, Mark D., Davis J. McCarthy, and Gordon K. Smyth. 2009. "EdgeR: A Bioconductor Package for Differential Expression Analysis of Digital Gene Expression Data." *Bioinformatics* 26 (1): 139–40. <https://doi.org/10.1093/bioinformatics/btp616>.
- Rodrigues, Gonçalo, Ayuko Hoshino, Candia M. Kenific, Irina R. Matei, Loïc Steiner, Daniela Freitas, Han Sang Kim, et al. 2019. "Tumour Exosomal CEMIP Protein Promotes Cancer Cell Colonization in Brain Metastasis." *Nature Cell Biology* 21 (11): 1403–12. <https://doi.org/10.1038/s41556-019-0404-4>.

- Roessler, Markus, Wolfgang Rollinger, Liliana Mantovani-Endl, Marie Luise Hagmann, Stefan Palme, Peter Berndt, Alfred M. Engel, et al. 2006. "Identification of PSME3 as a Novel Serum Tumor Marker for Colorectal Cancer by Combining Two-Dimensional Polyacrylamide Gel Electrophoresis with a Strictly Mass Spectrometry-Based Approach for Data Analysis." *Molecular and Cellular Proteomics* 5 (11): 2092–2101. <https://doi.org/10.1074/mcp.M600118-MCP200>.
- Rojas, A., G. Liu, I. Coleman, P. S. Nelson, M. Zhang, R. Dash, P. B. Fisher, S. R. Plymate, and J. D. Wu. 2011a. "IL-6 Promotes Prostate Tumorigenesis and Progression through Autocrine Cross-Activation of IGF-IR." *Oncogene* 30 (20): 2345–55. <https://doi.org/10.1038/onc.2010.605>.
- . 2011b. "IL-6 Promotes Prostate Tumorigenesis and Progression through Autocrine Cross-Activation of IGF-IR." *Oncogene* 30 (20): 2345–55. <https://doi.org/10.1038/onc.2010.605>.
- Ronquist, Gunnar, and B. O. Nilsson. 2004. "The Janus-Faced Nature of Prostatomes: Their Pluripotency Favours the Normal Reproductive Process and Malignant Prostate Growth." *Prostate Cancer and Prostatic Diseases*. Nature Publishing Group. <https://doi.org/10.1038/sj.pcan.4500684>.
- Roussos, Evanthia T., John S. Condeelis, and Antonia Patsialou. 2011. "Chemotaxis in Cancer." *Nature Reviews Cancer*. <https://doi.org/10.1038/nrc3078>.
- Rouvière, Olivier, Philippe Puech, Raphaële Renard-Penna, Michel Claudon, Catherine Roy, Florence Mège-Lechevallier, Myriam Decaussin-Petrucci, et al. 2019. "Use of Prostate Systematic and Targeted Biopsy on the Basis of Multiparametric MRI in Biopsy-Naive Patients (MRI-FIRST): A Prospective, Multicentre, Paired Diagnostic Study." *The Lancet Oncology* 20 (1): 100–109. [https://doi.org/10.1016/S1470-2045\(18\)30569-2](https://doi.org/10.1016/S1470-2045(18)30569-2).
- Royo, Felix, Laura Moreno, Justyna Mleczko, Laura Palomo, Esperanza Gonzalez, Diana Cabrera, Angel Cogolludo, Francisco Perez Vizcaino, Sebastiaan Van-Liempd, and Juan M. Falcon-Perez. 2017. "Hepatocyte-Secreted Extracellular Vesicles Modify Blood Metabolome and Endothelial Function by an Arginase-Dependent Mechanism." *Scientific Reports* 7 (February). <https://doi.org/10.1038/srep42798>.
- Royo, Felix, Patricia Zuñiga-Garcia, Verónica Torrano, Ana Loizaga, Pilar Sanchez-Mosquera, Aitziber Ugalde-Olano, Esperanza González, et al. 2016. "Transcriptomic Profiling of Urine Extracellular Vesicles Reveals Alterations of CDH3 in Prostate Cancer." *Oncotarget* 7 (6): 6835–46. <https://doi.org/10.18632/oncotarget.6899>.
- Ruan, Wen-Jing, and Mao-De Lai. 2004. "Autocrine Stimulation in Colorectal Carcinoma (CRC)." *Medical Oncology* 21: 1–7. <https://doi.org/10.1357-0560/04/21:1>.
- Ruggero, Davide, and Pier Paolo Pandolfi. 2003. "Does the Ribosome Translate Cancer?" *Nature Reviews Cancer*. <https://doi.org/10.1038/nrc1015>.
- Sahlén, Gran, Ove Nilsson, Anders Larsson, Lena Carlsson, Bo Johan Norlén, and Gunnar Ronquist. 2010. "Secretions from Seminal Vesicles Lack Characteristic Markers for

- Prostasomes." *Upsala Journal of Medical Sciences* 115 (2): 107–12. <https://doi.org/10.3109/03009730903366067>.
- Salomon, David S, Ralf Brandta, Fortunato Ciardiello, and Nicola Normannoc. 1995. "Epidermal Growth Factor-Related Peptides and Their Receptors in Human Malignancies." *Critical Reviews In ONCOLOGY/ HEMATOLOGY*. Vol. 19.
- Sancho, Patricia, Emma Burgos-Ramos, Alejandra Tavera, Tony Bou Kheir, Petra Jagust, Matthieu Schoenhals, David Barneda, et al. 2015. "MYC/PGC-1 α Balance Determines the Metabolic Phenotype and Plasticity of Pancreatic Cancer Stem Cells." *Cell Metabolism* 22 (4): 590–605. <https://doi.org/10.1016/j.cmet.2015.08.015>.
- Sansone, Pasquale, Claudia Savini, Ivana Kurelac, Qing Chang, Laura Benedetta Amato, Antonio Strillacci, Anna Stepanova, et al. 2017. "Packaging and Transfer of Mitochondrial DNA via Exosomes Regulate Escape from Dormancy in Hormonal Therapy-Resistant Breast Cancer." *Proceedings of the National Academy of Sciences of the United States of America* 114 (47): E10255. <https://doi.org/10.1073/pnas.1718630114>.
- Santamaria, Giulia, Edoardo Brandi, Pietro La, Vitola Federica, Grandi Giovanni, Francesca Pischiutta, Gloria Vegliante, et al. 2021. "Intranasal Delivery of Mesenchymal Stem Cell Secretome Repairs the Brain of Alzheimer ' s Mice." *Cell Death & Differentiation*, 203–18. <https://doi.org/10.1038/s41418-020-0592-2>.
- Sardana, Girish, Klaus Jung, Carsten Stephan, and Eleftherios P. Diamandis. 2008. "Proteomic Analysis of Conditioned Media from the PC3, LNCaP, and 22Rv1 Prostate Cancer Cell Lines: Discovery and Validation of Candidate Prostate Cancer Biomarkers." *Journal of Proteome Research* 7 (8): 3329–38. <https://doi.org/10.1021/pr8003216>.
- Schaefer, Liliana. 2014. "Complexity of Danger: The Diverse Nature of Damage-Associated Molecular Patterns." *Journal of Biological Chemistry*. American Society for Biochemistry and Molecular Biology Inc. <https://doi.org/10.1074/jbc.R114.619304>.
- Schlee, Martin, Michael Hölzel, Sandra Bernard, Reinhard Mailhammer, Marino Schuhmacher, Judith Reschke, Dirk Eick, et al. 2007. "C-MYC Activation Impairs the NF-KB and the Interferon Response: Implications for the Pathogenesis of Burkitt's Lymphoma." *International Journal of Cancer* 120 (7): 1387–95. <https://doi.org/10.1002/ijc.22372>.
- Schreiber, Sylvia N, Roger Emter, M Benjamin Hock, Darko Knutti, Jessica Cardenas, Michael Podvinec, Edward J Oakeley, and Anastasia Kralli. 2004. "The Estrogen-Related Receptor (ERR) Functions in PPAR Coactivator 1 (PGC-1)-Induced Mitochondrial Biogenesis." www.pnas.org/cgi/doi/10.1073/pnas.0308686101.
- Schumacher, Ton N, and Robert D Schreiber. 2015. "Neoantigens in Cancer Immunotherapy." <https://doi.org/DOI: 10.1126/science.aaa4971>.
- Segal, Neil H., D. Williams Parsons, Karl S. Peggs, Victor Velculescu, Ken W. Kinzler, Bert Vogelstein, and James P. Allison. 2008. "Epitope Landscape in Breast and Colorectal Cancer." *Cancer Research* 68 (3): 889–92. <https://doi.org/10.1158/0008-5472.CAN-07-3095>.

- Segura, Elodie, Coralie Guérin, Nancy Hogg, Sebastian Amigorena, and Clotilde Théry. 2007. "CD8 + Dendritic Cells Use LFA-1 to Capture MHC-Peptide Complexes from Exosomes In Vivo ." *The Journal of Immunology* 179 (3): 1489–96. <https://doi.org/10.4049/jimmunol.179.3.1489>.
- Seliger, Barbara, Francisco Ruiz-Cabello, and Federico Garrido. 2008. "IFN Inducibility of Major Histocompatibility Antigens in Tumors." *Advances in Cancer Research*. [https://doi.org/10.1016/S0065-230X\(08\)00407-7](https://doi.org/10.1016/S0065-230X(08)00407-7).
- Sequeiros, Tamara, Marina Rigau, Cristina Chiva, Melania Montes, Iolanda Garcia-Grau, Marta Garcia, Sherley Diaz, et al. 2017. "Targeted Proteomics in Urinary Extracellular Vesicles Identifies Biomarkers for Diagnosis and Prognosis of Prostate Cancer." *Oncotarget*. Vol. 8. www.impactjournals.com/oncotarget/.
- Shaheed, Sadr Ul, Catherine Tait, Kyriacos Kyriacou, Richard Linforth, Mohamed Salhab, and Chris Sutton. 2018. "Evaluation of Nipple Aspirate Fluid as a Diagnostic Tool for Early Detection of Breast Cancer." *Clinical Proteomics*. BioMed Central Ltd. <https://doi.org/10.1186/s12014-017-9179-4>.
- Shareef, Zainab al, Hoda Kardooni, Virginia Murillo-Garzón, Giacomo Domenici, Emmanouil Stylianakis, Jennifer H. Steel, Miriam Rabano, et al. 2018. "Protective Effect of Stromal Dickkopf-3 in Prostate Cancer: Opposing Roles for TGFBI and ECM-1." *Oncogene* 37 (39): 5305–24. <https://doi.org/10.1038/s41388-018-0294-0>.
- Sharma, Naomi L., Charlie E. Massie, Antonio Ramos-Montoya, Vincent Zecchini, Helen E. Scott, Alastair D. Lamb, Stewart MacArthur, et al. 2013. "The Androgen Receptor Induces a Distinct Transcriptional Program in Castration-Resistant Prostate Cancer in Man." *Cancer Cell* 23 (1): 35–47. <https://doi.org/10.1016/j.ccr.2012.11.010>.
- Shen, Michael M., and Cory Abate-Shen. 2010. "Molecular Genetics of Prostate Cancer: New Prospects for Old Challenges." *Genes and Development*. Cold Spring Harbor Laboratory Press. <https://doi.org/10.1101/gad.1965810>.
- Shi, Yongquan, Huihong Zhai, Xin Wang, Zheyi Han, Changjiang Liu, Mei Lan, Jingping Du, et al. 2004. "Ribosomal Proteins S13 and L23 Promote Multidrug Resistance in Gastric Cancer Cells by Suppressing Drug-Induced Apoptosis." *Experimental Cell Research* 296 (2): 337–46. <https://doi.org/10.1016/j.yexcr.2004.02.009>.
- Shi, Yujiang, and Yang Shi. 2004. "Metabolic Enzymes and Coenzymes in Transcription - A Direct Link between Metabolism and Transcription?" *Trends in Genetics*. <https://doi.org/10.1016/j.tig.2004.07.004>.
- Shiota, Masaki, Ario Takeuchi, Yoo Hyun Song, Akira Yokomizo, Eiji Kashiwagi, Takeshi Uchiumi, Kentaro Kuroiwa, et al. 2011. "Y-Box Binding Protein-1 Promotes Castration-Resistant Prostate Cancer Growth via Androgen Receptor Expression." *Endocrine-Related Cancer* 18 (4): 505–17. <https://doi.org/10.1530/ERC-11-0017>.
- Shiota, Masaki, Akira Yokomizo, Yasuhiro Tada, Junichi Inokuchi, Katsunori Tatsugami, Kentaro Kuroiwa, Takeshi Uchiumi, Naohiro Fujimoto, Narihito Seki, and Seiji Naito. 2010. "Peroxisome Proliferator-Activated Receptor γ Coactivator-1 α Interacts with the Androgen

- Receptor (AR) and Promotes Prostate Cancer Cell Growth by Activating the AR.” *Molecular Endocrinology* 24 (1): 114–27. <https://doi.org/10.1210/me.2009-0302>.
- Shirakabe, Kyoko, Takuya Omura, Yoshio Shibagaki, Emiko Mihara, Keiichi Homma, Yukinari Kato, Akihiko Yoshimura, et al. 2017. “Mechanistic Insights into Ectodomain Shedding: Susceptibility of CADM1 Adhesion Molecule Is Determined by Alternative Splicing and O-Glycosylation.” *Scientific Reports* 7 (April). <https://doi.org/10.1038/srep46174>.
- Shorning, Boris Y., Manisha S. Dass, Matthew J. Smalley, and Helen B. Pearson. 2020. “The PI3K-AKT-MTOR Pathway and Prostate Cancer: At the Crossroads of AR, MAPK, and WNT Signaling.” *International Journal of Molecular Sciences*. MDPI AG. <https://doi.org/10.3390/ijms21124507>.
- Shurtleff, Matthew J., Jun Yao, Yidan Qin, Ryan M. Nottingham, Morayma M. Temoche-Diaz, Randy Schekman, and Alan M. Lambowitz. 2017. “Broad Role for YBX1 in Defining the Small Noncoding RNA Composition of Exosomes.” *Proceedings of the National Academy of Sciences of the United States of America* 114 (43): E8987–95. <https://doi.org/10.1073/pnas.1712108114>.
- Simmons, J. K., B. E. Hildreth, W. Supsavhad, S. M. Elshafae, B. B. Hassan, W. P. Dirksen, R. E. Toribio, and T. J. Rosol. 2015. “Animal Models of Bone Metastasis.” *Veterinary Pathology* 52 (5): 827–41. <https://doi.org/10.1177/0300985815586223>.
- Sistigu, Antonella, Takahiro Yamazaki, Erika Vacchelli, Kariman Chaba, David P. Enot, Julien Adam, Ilio Vitale, et al. 2014. “Cancer Cell–Autonomous Contribution of Type I Interferon Signaling to the Efficacy of Chemotherapy.” *Nature Medicine* 20 (11): 1301–9. <https://doi.org/10.1038/nm.3708>.
- Skog, Johan, Tom Wurdinger, Sjoerd van Rijn, Dimphna Meijer, Laura Gainche, Miguel Sena-esteves, William T Curry Jr, Robert S Carter, Anna M Krichevsky, and Xandra O Breakefield. 2008. “Glioblastoma Microvesicles Transport RNA and Protein That Promote Tumor Growth and Provide Diagnostic Biomarkers” 10 (12): 1470–76. <https://doi.org/10.1038/ncb1800.Glioblastoma>.
- Ślómka, Artur, Sabine Katharina Urban, Veronika Lukacs-Kornek, Ewa Żekanowska, and Mirosław Kornek. 2018. “Large Extracellular Vesicles: Have We Found the Holy Grail of Inflammation?” *Frontiers in Immunology*. NLM (Medline). <https://doi.org/10.3389/fimmu.2018.02723>.
- Snyder, Alexandra, Vladimir Makarov, Taha Merghoub, Jianda Yuan, Jesse M. Zaretsky, Alexis Desrichard, Logan A. Walsh, et al. 2014. “Genetic Basis for Clinical Response to CTLA-4 Blockade in Melanoma.” *New England Journal of Medicine* 371 (23): 2189–99. <https://doi.org/10.1056/nejmoa1406498>.
- Soekmadji, Carolina, and Colleen C. Nelson. 2015. “The Emerging Role of Extracellular Vesicle-Mediated Drug Resistance in Cancers: Implications in Advanced Prostate Cancer.” *BioMed Research International*. Hindawi Publishing Corporation. <https://doi.org/10.1155/2015/454837>.

- Soekmadji, Carolina, James D Riches, Pamela J Russell, Jayde E Ruelcke, Stephen Mcpherson, Chenwei Wang, Chris M Hovens, Niall M Corcoran, Michelle M Hill, and Colleen C Nelson. 2017. "Modulation of Paracrine Signaling by CD9 Positive Small Extracellular Vesicles Mediates Cellular Growth of Androgen Deprived Prostate Cancer The Australian Prostate Cancer Collaboration BioResource." *Oncotarget*. Vol. 8. www.impactjournals.com/oncotarget/.
- Soltermann, Alex, Reto Ossola, Sandra Kilgus-Hawelski, Arnold von Eckardstein, Tobias Suter, Ruedi Aebersold, and Holger Moch. 2008. "N-Glycoprotein Profiling of Lung Adenocarcinoma Pleural Effusions by Shotgun Proteomics." *Cancer* 114 (2): 124–33. <https://doi.org/10.1002/cncr.23349>.
- Soucek, Laura, Elizabeth R. Lawlor, Darya Soto, Ksenya Shchors, Lamorna Brown Swigart, and Gerard I. Evan. 2007. "Mast Cells Are Required for Angiogenesis and Macroscopic Expansion of Myc-Induced Pancreatic Islet Tumors." *Nature Medicine* 13 (10): 1211–18. <https://doi.org/10.1038/nm1649>.
- Sousa, Cristovão M, Douglas E Biancur, Xiaoxu Wang, Christopher J Halbrook, Mara H Sherman, Li Zhang, Daniel Kremer, et al. 2016. "Pancreatic Stellate Cells Support Tumour Metabolism through Autophagic Alanine Secretion" 536 (7617): 479–83.
- Sousa, Diana, Rune Matthiesen, Raquel T. Lima, and M. Helena Vasconcelos. 2020. "Deep Sequencing Analysis Reveals Distinctive Non-Coding RNAs When Comparing Tumor Multidrug-Resistant Cells and Extracellular Vesicles with Drug-Sensitive Counterparts." *Cancers* 12 (1). <https://doi.org/10.3390/cancers12010200>.
- Spiegelman, Bruce M, and Reinhart Heinrich. 2004. "Biological Control through Regulated Transcriptional Coactivators." *Cell*. Vol. 119.
- Sprooten, Jenny, and Abhishek D. Garg. 2020. "Type I Interferons and Endoplasmic Reticulum Stress in Health and Disease." In *International Review of Cell and Molecular Biology*, 350:63–118. Elsevier Inc. <https://doi.org/10.1016/bs.ircmb.2019.10.004>.
- Ståhl, Patrik L., Fredrik Salmén, Sanja Vickovic, Anna Lundmark, José Fernández Navarro, Jens Magnusson, Stefania Giacomello, et al. 2016. "Visualization and Analysis of Geneexpression in Tissue Sections Byspatial Transcriptomics." *Science* 353 (6294): 74–78. <https://doi.org/10.1126/science.aaf4374>.
- Stallcup, Michael R., and Coralie Poulard. 2020. "Gene-Specific Actions of Transcriptional Coregulators Facilitate Physiological Plasticity: Evidence for a Physiological Coregulator Code." *Trends in Biochemical Sciences*. Elsevier Ltd. <https://doi.org/10.1016/j.tibs.2020.02.006>.
- Stanbrough, Michael, Glenn J. Bubley, Kenneth Ross, Todd R. Golub, Mark A. Rubin, Trevor M. Penning, Phillip G. Febbo, and Steven P. Balk. 2006. "Increased Expression of Genes Converting Adrenal Androgens to Testosterone in Androgen-Independent Prostate Cancer." *Cancer Research* 66 (5): 2815–25. <https://doi.org/10.1158/0008-5472.CAN-05-4000>.

- Stanifer, Megan L., Kalliopi Pervolaraki, and Steeve Boulant. 2019. "Differential Regulation of Type I and Type III Interferon Signaling." *International Journal of Molecular Sciences*. MDPI AG. <https://doi.org/10.3390/ijms20061445>.
- Stanley, Amanda C., and Paige Lacy. 2010. "Pathways for Cytokine Secretion." *Physiology*. <https://doi.org/10.1152/physiol.00017.2010>.
- Stenmark, Harald. 2009. "Rab GTPases as Coordinators of Vesicle Traffic." *Nature Reviews Molecular Cell Biology*. <https://doi.org/10.1038/nrm2728>.
- Stipp, Christopher S., Tatiana v. Kolesnikova, and Martin E. Hemler. 2001. "EWI-2 Is a Major CD9 and CD81 Partner and Member of a Novel Ig Protein Subfamily." *Journal of Biological Chemistry* 276 (44): 40545–54. <https://doi.org/10.1074/jbc.M107338200>.
- Sturge, Justin, Matthew P. Caley, and Jonathan Waxman. 2011. "Bone Metastasis in Prostate Cancer: Emerging Therapeutic Strategies." *Nature Reviews Clinical Oncology*. Nature Publishing Group. <https://doi.org/10.1038/nrclinonc.2011.67>.
- Subramanian, Aravind, Pablo Tamayo, Vamsi K Mootha, Sayan Mukherjee, Benjamin L Ebert, Michael A Gillette, Amanda Paulovich, et al. 2005. "Gene Set Enrichment Analysis: A Knowledge-Based Approach for Interpreting Genome-Wide Expression Profiles." www.pnas.org/cgi/doi/10.1073/pnas.0506580102.
- Suijkerbuijk, Saskia J.E., Golnar Kolahgar, Iwo Kucinski, and Eugenia Piddini. 2016. "Cell Competition Drives the Growth of Intestinal Adenomas in Drosophila." *Current Biology* 26 (4): 428–38. <https://doi.org/10.1016/j.cub.2015.12.043>.
- Sun, Jinxia, Yi Luan, Dong Xiang, Xiao Tan, Hui Chen, Qi Deng, Jiaojiao Zhang, et al. 2016. "The 11S Proteasome Subunit PSME3 Is a Positive Feedforward Regulator of NF- κ B and Important for Host Defense against Bacterial Pathogens." *Cell Reports* 14 (4): 737–49. <https://doi.org/10.1016/j.celrep.2015.12.069>.
- Sweeney, Christopher, Sergio Bracarda, Cora N Sternberg, Kim N Chi, David Olmos, Shahneen Sandhu, Christophe Massard, et al. 2021. "Ipatasertib plus Abiraterone and Prednisolone in Metastatic Castration-Resistant Prostate Cancer (IPATential150): A Multicentre, Randomised, Double-Blind, Phase 3 Trial." *Www.TheLancet.Com*. Vol. 398. www.thelancet.com.
- Swensen, Adam C., Jingtang He, Alexander C. Fang, Yinyin Ye, Carrie D. Nicora, Tujin Shi, Alvin Y. Liu, Tara K. Sigdel, Minnie M. Sarwal, and Wei Jun Qian. 2021. "A Comprehensive Urine Proteome Database Generated From Patients With Various Renal Conditions and Prostate Cancer." *Frontiers in Medicine* 8 (April). <https://doi.org/10.3389/fmed.2021.548212>.
- Tadele, Fitalew, Solomon Genet, M.K.C. Menon, and Abat Sahlu. 2019. "Oxidative Stress and Serum Creatine Kinase BB Levels Can Help Mark Severity and Stage of Brain Tumor." *Reactive Oxygen Species*. <https://doi.org/10.20455/ros.2019.837>.
- Taguchi, Ayumu, Oliver Delgado, Müge Çeliktaş, Hiroyuki Katayama, Hong Wang, Adi F. Gazdar, and Samir M. Hanash. 2014. "Proteomic Signatures Associated with P53 Mutational Status in Lung Adenocarcinoma." *Proteomics* 14 (23–24): 2750–59. <https://doi.org/10.1002/pmic.201400378>.

- Tan, Mh Eileen, Jun Li, H. Eric Xu, Karsten Melcher, and Eu Leong Yong. 2015. "Androgen Receptor: Structure, Role in Prostate Cancer and Drug Discovery." *Acta Pharmacologica Sinica*. Nature Publishing Group. <https://doi.org/10.1038/aps.2014.18>.
- Taniuchi, Keisuke, and Mitsunari Ogasawara. 2020. "KHSRP-Bound Small Nucleolar RNAs Associate with Promotion of Cell Invasiveness and Metastasis of Pancreatic Cancer." *Oncotarget*. Vol. 11. www.oncotarget.com.
- Tassi, Elena, Kevin McDonnell, Krissa A. Gibby, Jason U. Tilan, Sung E. Kim, David P. Kodack, Marcel O. Schmidt, et al. 2011. "Impact of Fibroblast Growth Factor-Binding Protein1 Expression on Angiogenesis and Wound Healing." *American Journal of Pathology* 179 (5): 2220–32. <https://doi.org/10.1016/j.ajpath.2011.07.043>.
- Tateishi, Masahiro, Teruyoshi Ishida, Tetsuya Mitsudomi, Satoshi Kaneko, and Keizo Sugimachi. 1990. "Immunohistochemical Evidence of Autocrine Growth Factors in Adenocarcinoma of the Human Lung." *CANCER RESEARCH*. Vol. 50.
- Taube, Janis M, Robert A Anders, Geoffrey D Young, Haiying Xu, Rajni Sharma, Tracee L Mcmillar, Shuming Chen, et al. 2012. "Colocalization of Inflammatory Response with B7-H1 Expression in Human Melanocytic Lesions Supports an Adaptive Resistance Mechanism of Immune Escape." www.ScienceTranslationalMedicine.org.
- Tavoosidana, Gholamreza, Gunnar Ronquist, Spyros Darmanis, Junhong Yan, Lena Carlsson, Di Wu, Tim Conze, et al. 2011. "Multiple Recognition Assay Reveals Prostatomes as Promising Plasma Biomarkers for Prostate Cancer." *Proceedings of the National Academy of Sciences of the United States of America* 108 (21): 8809–14. <https://doi.org/10.1073/pnas.1019330108>.
- Taylor, Barry S., Nikolaus Schultz, Haley Hieronymus, Anuradha Gopalan, Yonghong Xiao, Brett S. Carver, Vivek K. Arora, et al. 2010a. "Integrative Genomic Profiling of Human Prostate Cancer." *Cancer Cell* 18 (1): 11–22. <https://doi.org/10.1016/j.ccr.2010.05.026>.
- . 2010b. "Integrative Genomic Profiling of Human Prostate Cancer." *Cancer Cell* 18 (1): 11–22. <https://doi.org/10.1016/j.ccr.2010.05.026>.
- Tennakoon, J. B., Y. Shi, J. J. Han, E. Tsouko, M. A. White, A. R. Burns, A. Zhang, et al. 2014. "Androgens Regulate Prostate Cancer Cell Growth via an AMPK-PGC-1 α -Mediated Metabolic Switch." *Oncogene* 33 (45): 5251–61. <https://doi.org/10.1038/onc.2013.463>.
- Théry, Clotilde, Muriel Boussac, Philippe Véron, Paola Ricciardi-Castagnoli, Graça Raposo, Jérôme Garin, and Sebastian Amigorena. 2001. "Proteomic Analysis of Dendritic Cell-Derived Exosomes: A Secreted Subcellular Compartment Distinct from Apoptotic Vesicles." *The Journal of Immunology* 166 (12): 7309–18. <https://doi.org/10.4049/jimmunol.166.12.7309>.
- Théry, Clotilde, Kenneth W. Witwer, Elena Aikawa, Maria Jose Alcaraz, Johnathon D. Anderson, Ramarosan Andriantsitohaina, Anna Antoniou, et al. 2018. "Minimal Information for Studies of Extracellular Vesicles 2018 (MISEV2018): A Position Statement of the International Society for Extracellular Vesicles and Update of the MISEV2014 Guidelines." *Journal of Extracellular Vesicles* 7 (1). <https://doi.org/10.1080/20013078.2018.1535750>.

- Théry, Clotilde, Kenneth W Witwer, Elena Aikawa, Maria Jose Alcaraz, Johnathon D Anderson, Ramarosan Andriantsitohaina, Anna Antoniou, et al. 2018. "Journal of Extracellular Vesicles Minimal Information for Studies of Extracellular Vesicles 2018 (MISEV2018): A Position Statement of the International Society for Extracellular Vesicles and Update of the MISEV2014 Guidelines." <https://www.tandfonline.com/loi/zjev20>.
- Thiery, Jean Paul, Hervé Acloque, Ruby Y.J. Huang, and M. Angela Nieto. 2009. "Epithelial-Mesenchymal Transitions in Development and Disease." *Cell*. <https://doi.org/10.1016/j.cell.2009.11.007>.
- Thom, Robyn, Glenn C. Rowe, Cholsoon Jang, Adeel Safdar, and Zoltan Arany. 2014. "Hypoxic Induction of Vascular Endothelial Growth Factor (VEGF) and Angiogenesis in Muscle by Truncated Peroxisome Proliferator-Activated Receptor γ Coactivator (PGC)-1 α ." *Journal of Biological Chemistry* 289 (13): 8810–17. <https://doi.org/10.1074/jbc.M114.554394>.
- Thrane, Kim, Hanna Eriksson, Jonas Maaskola, Johan Hansson, and Joakim Lundeberg. 2018. "Spatially Resolved Transcriptomics Enables Dissection of Genetic Heterogeneity in Stage III Cutaneous Malignant Melanoma." *Cancer Research* 78 (20): 5970–79. <https://doi.org/10.1158/0008-5472.CAN-18-0747>.
- Tian, Chenxi, Daniel Öhlund, Steffen Rickelt, Tommy Lidström, Ying Huang, Liangliang Hao, Renee T. Zhao, et al. 2020. "Cancer Cell-Derived Matrisome Proteins Promote Metastasis in Pancreatic Ductal Adenocarcinoma." *Cancer Research* 80 (7): 1461–74. <https://doi.org/10.1158/0008-5472.CAN-19-2578>.
- Tian, Tian, Yan Liang Zhu, Yue Yuan Zhou, Gao Feng Liang, Yuan Yuan Wang, Fei Hu Hu, and Zhong Dang Xiao. 2014. "Exosome Uptake through Clathrin-Mediated Endocytosis and Macropinocytosis and Mediating MiR-21 Delivery." *Journal of Biological Chemistry* 289 (32): 22258–67. <https://doi.org/10.1074/jbc.M114.588046>.
- Tikhonova, Elena B., Zemfira N. Karamysheva, Gunnar von Heijne, and Andrey L. Karamyshev. 2019. "Silencing of Aberrant Secretory Protein Expression by Disease-Associated Mutations." *Journal of Molecular Biology* 431 (14): 2567–80. <https://doi.org/10.1016/j.jmb.2019.05.011>.
- Tomlins, Scott A., Rohit Mehra, Daniel R. Rhodes, Xuhong Cao, Lei Wang, Saravana M. Dhanasekaran, Shanker Kalyana-Sundaram, et al. 2007. "Integrative Molecular Concept Modeling of Prostate Cancer Progression." *Nature Genetics* 39 (1): 41–51. <https://doi.org/10.1038/ng1935>.
- Topalian, Suzanne L., F. Stephen Hodi, Julie R. Brahmer, Scott N. Gettinger, David C. Smith, David F. McDermott, John D. Powderly, et al. 2012. "Safety, Activity, and Immune Correlates of Anti-PD-1 Antibody in Cancer." *New England Journal of Medicine* 366 (26): 2443–54. <https://doi.org/10.1056/nejmoa1200690>.
- Torday, J S, and V K Rehan. 2015. "The Evolution of Cell Communication: The Road Not Taken."
- Torrano, Veronica, Felix Royo, Héctor Peinado, Ana Loizaga-Iriarte, Miguel Unda, Juan M. Falcón-Perez, and Arkaitz Carracedo. 2016. "Vesicle-MaNiA: Extracellular Vesicles in Liquid

- Biopsy and Cancer.” *Current Opinion in Pharmacology*. Elsevier Ltd. <https://doi.org/10.1016/j.coph.2016.06.003>.
- Torrano, Veronica, Lorea Valcarcel-Jimenez, Ana Rosa Cortazar, Xiaojing Liu, Mireia Castillomartin, Sonia Fernández-ruiz, Giampaolo Morciano, et al. 2016. “The Metabolic Co-Regulator PGC1 α Suppresses Prostate Cancer Metastasis” 18 (6): 645–56. <https://doi.org/10.1038/ncb3357>.The.
- Trajkovic, Katarina, Chieh Hsu, Salvatore Chiantia, Lawrence Rajendran, Dirk Wenzel, Felix Wieland, Petra Schwillle, Britta Brügger, and Mikael Simons. 2008. “Ceramide Triggers Budding of Exosome Vesicles into Multivesicular Endosomes.” *Science* 319 (5867): 1244–47. <https://doi.org/10.1126/science.1153124>.
- Trams, Eberhard G, Carl J Lauter, Norman Salem, and Ursula Heine. 1981. “EXFOLIATION OF MEMBRANE ECTO-ENZYMES IN THE FORM OF MICRO-VESICLES.” *Biochimica et Biophysica Acta*. Vol. 645.
- Tricarico, Christopher, James Clancy, and Crislyn D’Souza-Schorey. 2017. “Biology and Biogenesis of Shed Microvesicles.” *Small GTPases*. Taylor and Francis Inc. <https://doi.org/10.1080/21541248.2016.1215283>.
- Tripathi, Madhulika, Paul Michael Yen, and Brijesh Kumar Singh. 2020. “Estrogen-Related Receptor Alpha: An under-Appreciated Potential Target for the Treatment of Metabolic Diseases.” *International Journal of Molecular Sciences*. MDPI AG. <https://doi.org/10.3390/ijms21051645>.
- Tschochner, Herbert, and Ed Hurt. 2003. “Pre-Ribosomes on the Road from the Nucleolus to the Cytoplasm.” *Trends in Cell Biology*. Elsevier Ltd. [https://doi.org/10.1016/S0962-8924\(03\)00054-0](https://doi.org/10.1016/S0962-8924(03)00054-0).
- Tse, B. W.C., M. Volpert, E. Ratther, N. Stylianou, M. Nouri, K. McGowan, M. L. Lehman, et al. 2017a. “Neuropilin-1 Is Upregulated in the Adaptive Response of Prostate Tumors to Androgen-Targeted Therapies and Is Prognostic of Metastatic Progression and Patient Mortality.” *Oncogene* 36 (24): 3417–27. <https://doi.org/10.1038/onc.2016.482>.
- . 2017b. “Neuropilin-1 Is Upregulated in the Adaptive Response of Prostate Tumors to Androgen-Targeted Therapies and Is Prognostic of Metastatic Progression and Patient Mortality.” *Oncogene* 36 (24): 3417–27. <https://doi.org/10.1038/onc.2016.482>.
- Tyagi, Sandeep, Paras Gupta, Arminder Saini, Chaitnya Kaushal, and Saurabh Sharma. 2011. “The Peroxisome Proliferator-Activated Receptor: A Family of Nuclear Receptors Role in Various Diseases.” *Journal of Advanced Pharmaceutical Technology and Research*. <https://doi.org/10.4103/2231-4040.90879>.
- Tyan, Yu Chang, Hsin Yi Wu, Wu Wei Lai, Wu Chou Su, and Pao Chi Liao. 2005. “Proteomic Profiling of Human Pleural Effusion Using Two-Dimensional Nano Liquid Chromatography Tandem Mass Spectrometry.” *Journal of Proteome Research* 4 (4): 1274–86. <https://doi.org/10.1021/pr049746c>.
- Tyanova, Stefka, Tikira Temu, Pavel Sinitcyn, Arthur Carlson, Marco Y. Hein, Tamar Geiger, Matthias Mann, and Jürgen Cox. 2016. “The Perseus Computational Platform for

- Comprehensive Analysis of (Prote)Omics Data.” *Nature Methods*. Nature Publishing Group. <https://doi.org/10.1038/nmeth.3901>.
- Uhlén, Mathias, Max J Karlsson, Andreas Hober, Anne-Sophie Svensson, Julia Scheffel, David Kotol, Wen Zhong, et al. 2019. “The Human Secretome.” *Sci. Signal*. Vol. 12. www.proteinatlas.org/blood.
- Ullrich, Axel, Irmi Sures, Maurizia D’Egidio, Bahija Jallal, T. J. Powell, Ronald Herbst, Andreas Dreps, et al. 1994. “The Secreted Tumor-Associated Antigen 90K Is a Potent Immune Stimulator.” *Journal of Biological Chemistry* 269 (28): 18401–7. [https://doi.org/10.1016/s0021-9258\(17\)32322-0](https://doi.org/10.1016/s0021-9258(17)32322-0).
- Umekita, Yoshihisa, Yasuyo Ohi, Yoshiatsu Sagara, and Hiroki Yoshida. 2000. “CO-EXPRESSION OF EPIDERMAL GROWTH FACTOR RECEPTOR AND TRANSFORMING GROWTH FACTOR-PREDICTS WORSE PROGNOSIS IN BREAST-CANCER PATIENTS.” *Int. J. Cancer (Pred. Oncol.)*. Vol. 89.
- Ura, Blendi, Giovanni di Lorenzo, Federico Romano, Lorenzo Monasta, Giuseppe Mirenda, Federica Scrimin, and Giuseppe Ricci. 2018. “Interstitial Fluid in Gynecologic Tumors and Its Possible Application in the Clinical Practice.” *International Journal of Molecular Sciences*. MDPI AG. <https://doi.org/10.3390/ijms19124018>.
- Valastyan, Scott, and Robert A. Weinberg. 2011. “Tumor Metastasis: Molecular Insights and Evolving Paradigms.” *Cell*. Elsevier B.V. <https://doi.org/10.1016/j.cell.2011.09.024>.
- Valcarcel-Jimenez, Lorea, Alice Macchia, Eva Crosas-Molist, Ariane Schaub-Clerigue, Laura Camacho, Natalia Martín-Martín, Paolo Cicogna, et al. 2019. “PGC1a Suppresses Prostate Cancer Cell Invasion through ERRA Transcriptional Control.” *Cancer Research* 79 (24): 6153–65. <https://doi.org/10.1158/0008-5472.CAN-19-1231>.
- Valiente, Manuel, Anna C. Obenauf, Xin Jin, Qing Chen, Xiang H.F. Zhang, Derek J. Lee, Jamie E. Chaft, et al. 2014. “Serpins Promote Cancer Cell Survival and Vascular Co-Option in Brain Metastasis.” *Cell* 156 (5): 1002–16. <https://doi.org/10.1016/j.cell.2014.01.040>.
- Varambally, Sooryanarayana, Saravana M. Dhanasekaran, Ming Zhou, Terrence R. Barrette, Chandan Kumar-Sinha, Martin G. Sanda, Debashis Ghosh, et al. 2002. “The Polycomb Group Protein EZH2 is Involved in Progression Of prostate Cancer.” *Nature* 419 (6907): 620–24. <https://doi.org/10.1038/nature01042>.
- Varambally, Sooryanarayana, Jianjun Yu, Bharathi Laxman, Daniel R. Rhodes, Rohit Mehra, Scott A. Tomlins, Rajal B. Shah, et al. 2005. “Integrative Genomic and Proteomic Analysis of Prostate Cancer Reveals Signatures of Metastatic Progression.” *Cancer Cell* 8 (5): 393–406. <https://doi.org/10.1016/j.ccr.2005.10.001>.
- Vazquez, Francisca, Ji Hong Lim, Helen Chim, Kavita Bhalla, Geoff Girnun, Kerry Pierce, Clary B. Clish, et al. 2013. “PGC1 α Expression Defines a Subset of Human Melanoma Tumors with Increased Mitochondrial Capacity and Resistance to Oxidative Stress.” *Cancer Cell* 23 (3): 287–301. <https://doi.org/10.1016/j.ccr.2012.11.020>.
- Vega, Rick B, Janice M Huss, and Daniel P Kelly. 2000. “The Coactivator PGC-1 Cooperates with Peroxisome Proliferator-Activated Receptor in Transcriptional Control of Nuclear Genes

- Encoding Mitochondrial Fatty Acid Oxidation Enzymes." *MOLECULAR AND CELLULAR BIOLOGY*. Vol. 20. <https://journals.asm.org/journal/mcb>.
- Vento-Tormo, Roser, Mirjana Efremova, Rachel A. Botting, Margherita Y. Turco, Miquel Vento-Tormo, Kerstin B. Meyer, Jong Eun Park, et al. 2018. "Single-Cell Reconstruction of the Early Maternal–Fetal Interface in Humans." *Nature* 563 (7731): 347–53. <https://doi.org/10.1038/s41586-018-0698-6>.
- Verweij, Frederik J., Leonora Balaj, Chantal M. Boulanger, David R. F. Carter, Ewoud B. Compeer, Gisela D'Angelo, Samir el Andaloussi, et al. 2021. "The Power of Imaging to Understand Extracellular Vesicle Biology in Vivo." *Nature Methods* 18 (9). <https://doi.org/10.1038/s41592-021-01206-3>.
- Vietri, Marina, Maja Radulovic, and Harald Stenmark. 2020. "The Many Functions of ESCRTs." *Nature Reviews Molecular Cell Biology*. Nature Research. <https://doi.org/10.1038/s41580-019-0177-4>.
- Villarreal, Laura, Olga Méndez, Cándida Salvans, Josep Gregori, José Baselga, and Josep Villanueva. 2013. "Unconventional Secretion Is a Major Contributor of Cancer Cell Line Secretomes." *Molecular and Cellular Proteomics* 12 (5): 1046–60. <https://doi.org/10.1074/mcp.M112.021618>.
- Villatoro, A. J., C. Alcoholado, M. C. Martín-Astorga, V. Fernández, M. Cifuentes, and J. Becerra. 2019. "Comparative Analysis and Characterization of Soluble Factors and Exosomes from Cultured Adipose Tissue and Bone Marrow Mesenchymal Stem Cells in Canine Species." *Veterinary Immunology and Immunopathology* 208 (February): 6–15. <https://doi.org/10.1016/j.vetimm.2018.12.003>.
- Vitto, Humberto de, Ann M. Bode, and Zigang Dong. 2019. "The PGC-1/ERR Network and Its Role in Precision Oncology." *Npj Precision Oncology* 3 (1). <https://doi.org/10.1038/s41698-019-0081-6>.
- Vogelstein, Bert, and Kenneth W. Kinzler. 2004. "Cancer Genes and the Pathways They Control." *Nature Medicine*. <https://doi.org/10.1038/nm1087>.
- Wack, Andreas, Ewa Terczyńska-Dyla, and Rune Hartmann. 2015. "Guarding the Frontiers: The Biology of Type III Interferons." *Nature Immunology*. Nature Publishing Group. <https://doi.org/10.1038/ni.3212>.
- Wagner, Marek, and Helge Wiig. 2015. "Tumor Interstitial Fluid Formation, Characterization, and Clinical Implications." *Frontiers in Oncology*. Frontiers Media S.A. <https://doi.org/10.3389/fonc.2015.00115>.
- Wagner, T. Charis, Sharlene Velichko, Steven K. Chesney, Sandra Biroc, Dean Harde, David Vogel, and Ed Croze. 2004. "Interferon Receptor Expression Regulates the Antiproliferative Effects of Interferons on Cancer Cells and Solid Tumors." *International Journal of Cancer* 111 (1): 32–42. <https://doi.org/10.1002/ijc.20236>.
- Waldman, Alex D., Jill M. Fritz, and Michael J. Lenardo. 2020. "A Guide to Cancer Immunotherapy: From T Cell Basic Science to Clinical Practice." *Nature Reviews Immunology*. Nature Research. <https://doi.org/10.1038/s41577-020-0306-5>.

- Wallberg, Annika E, Soichiro Yamamura, Sohail Malik, Bruce M Spiegelman, and Robert G Roeder. 2003. "Coordination of P300-Mediated Chromatin Remodeling and TRAP/Mediator Function through Coactivator PGC-1." *Molecular Cell*. Vol. 12. Workman and Kingston.
- Wang, Charles, Binsheng Gong, Pierre R. Bushel, Jean Thierry-Mieg, Danielle Thierry-Mieg, Joshua Xu, Hong Fang, et al. 2014. "The Concordance between RNA-Seq and Microarray Data Depends on Chemical Treatment and Transcript Abundance." *Nature Biotechnology* 32 (9): 926–32. <https://doi.org/10.1038/nbt.3001>.
- Wang, Guocan, Xin Lu, Prasenjit Dey, Pingna Deng, Chia Chin Wu, Shan Jiang, Zhuangna Fang, et al. 2016. "Targeting YAP-Dependent MDSC Infiltration Impairs Tumor Progression." *Cancer Discovery* 6 (1): 80–95. <https://doi.org/10.1158/2159-8290.CD-15-0224>.
- Wang, Luping, Jiayao Yu, Jian Ni, Xue Ming Xu, Jianjin Wang, Haoyong Ning, Xu Fang Pei, et al. 2003. "Extracellular Matrix Protein 1 (ECM1) Is over-Expressed in Malignant Epithelial Tumors." *Cancer Letters* 200 (1): 57–67. [https://doi.org/10.1016/S0304-3835\(03\)00350-1](https://doi.org/10.1016/S0304-3835(03)00350-1).
- Watanabe, Hirotaka, Kojiro Ishibashi, Hiroki Mano, Sho Kitamoto, Nanami Sato, Kazuya Hoshiba, Mugihiko Kato, et al. 2018. "Mutant P53-Expressing Cells Undergo Necroptosis via Cell Competition with the Neighboring Normal Epithelial Cells." *Cell Reports* 23 (13): 3721–29. <https://doi.org/10.1016/j.celrep.2018.05.081>.
- Weinberg R. 1996. "How Cancer Arises."
- Wellen, Kathryn E., and Craig B. Thompson. 2010. "Cellular Metabolic Stress: Considering How Cells Respond to Nutrient Excess." *Molecular Cell*. <https://doi.org/10.1016/j.molcel.2010.10.004>.
- Willms, Eduard, Carlos Cabañas, Imre Mäger, Matthew J.A. Wood, and Pieter Vader. 2018. "Extracellular Vesicle Heterogeneity: Subpopulations, Isolation Techniques, and Diverse Functions in Cancer Progression." *Frontiers in Immunology*. Frontiers Media S.A. <https://doi.org/10.3389/fimmu.2018.00738>.
- Wiśniewski, Jacek R., Alexandre Zougman, Nagarjuna Nagaraj, and Matthias Mann. 2009. "Universal Sample Preparation Method for Proteome Analysis." *Nature Methods* 6 (5): 359–62. <https://doi.org/10.1038/nmeth.1322>.
- Witwer, Kenneth W., and Clotilde Théry. 2019. "Extracellular Vesicles or Exosomes? On Primacy, Precision, and Popularity Influencing a Choice of Nomenclature." *Journal of Extracellular Vesicles* 8 (1). <https://doi.org/10.1080/20013078.2019.1648167>.
- Wu, Z, P Puigserver, U Andersson, C Zhang, G Adelman, V Mootha, A Troy, et al. 1999. "Mechanisms Controlling Mitochondrial Biogenesis and Respiration through the Thermogenic Coactivator PGC-1."
- Xavier, Cristina P.R., Hugo R. Caires, Mélanie A.G. Barbosa, Rui Bergantim, José E. Guimarães, and M. Helena Vasconcelos. 2020. "The Role of Extracellular Vesicles in the Hallmarks of Cancer and Drug Resistance." *Cells*. NLM (Medline). <https://doi.org/10.3390/cells9051141>.
- Xiong, Gao-Feng, and Ren Xu. 2016. "Function of Cancer Cell-Derived Extracellular Matrix in Tumor Progression." *Journal of Cancer Metastasis and Treatment* 2 (9): 357. <https://doi.org/10.20517/2394-4722.2016.08>.

- Xiong, S., Y. Zheng, P. Jiang, R. Liu, X. Liu, J. Qian, J. Gu, L. Chang, D. Ge, and Y. Chu. 2014. "PA28gamma Emerges as a Novel Functional Target of Tumour Suppressor MicroRNA-7 in Non-Small-Cell Lung Cancer." *British Journal of Cancer* 110 (2): 353–62. <https://doi.org/10.1038/bjc.2013.728>.
- Yamamoto, Kenji. 1999. "Cathepsin E and Cathepsin D." *Proteases New Perspectives*, 59–71. https://doi.org/10.1007/978-3-0348-8737-3_5.
- Yan, Mingxia, Lei Sun, Jing Li, Huajian Yu, Hechun Lin, Tao Yu, Fangyu Zhao, et al. 2019. "RNA-Binding Protein KHSRP Promotes Tumor Growth and Metastasis in Non-Small Cell Lung Cancer." *Journal of Experimental and Clinical Cancer Research* 38 (1). <https://doi.org/10.1186/s13046-019-1479-2>.
- Yan, Yibing, Kyoko Shirakabe, and Zena Werb. 2002. "The Metalloprotease Kuzbanian (ADAM10) Mediates the Transactivation of EGF Receptor by G Protein-Coupled Receptors." *Journal of Cell Biology* 158 (2): 221–26. <https://doi.org/10.1083/jcb.200112026>.
- Yang, Kai, Jie Yang, and Jing Yi. 2018. "Nucleolar Stress: Hallmarks, Sensing Mechanism and Diseases." *Cell Stress*. Shared Science Publishers OG. <https://doi.org/10.15698/cst2018.06.139>.
- Ye, Xinglong, Lijing Zhao, and Jing Kang. 2019. "Expression and Significance of PTEN and Claudin-3 in Prostate Cancer." *Oncology Letters* 17 (6): 5628–34. <https://doi.org/10.3892/ol.2019.10212>.
- Yi, Ziyang, Dejuan Yang, Xuelian Liao, Fuchun Guo, Yongsheng Wang, and Xiaoyi Wang. 2017. "PSME3 Induces Epithelial–Mesenchymal Transition with Inducing the Expression of CSC Markers and Immunosuppression in Breast Cancer." *Experimental Cell Research* 358 (2): 87–93. <https://doi.org/10.1016/j.yexcr.2017.05.017>.
- Yokota Jun. 2000. "Tumor Progression and Metastasis."
- Yoon, J Cliff, Pere Puigserver, Guoxun Chen², Jerry Donovan, Zhidan Wu, James Rhee, Guillaume Adelmant, et al. 2001. "Control of Hepatic Gluconeogenesis through the Transcriptional Coactivator PGC-1." *NATURE*. Vol. 413. www.nature.com.
- Yuan, Dongsheng, Yiran Tao, Geng Chen, and Tieliu Shi. 2019. "Systematic Expression Analysis of Ligand-Receptor Pairs Reveals Important Cell-to-Cell Interactions inside Glioma." *Cell Communication and Signaling* 17 (1). <https://doi.org/10.1186/s12964-019-0363-1>.
- Zabala-Letona, Amaia, Amaia Arruabarrena-Aristorena, Natalia Martín-Martín, Sonia Fernandez-Ruiz, James D. Sutherland, Michelle Clasquin, Julen Tomas-Cortazar, et al. 2017. "MTORC1-Dependent AMD1 Regulation Sustains Polyamine Metabolism in Prostate Cancer." *Nature* 547 (7661): 109–13. <https://doi.org/10.1038/nature22964>.
- Zernecke, Alma, Kiril Bidzhekov, Heidi Noels, Erdenechimeg Shagdarsuren, Lin Gan, Bernd Denecke, Mihail Hristov, et al. 2009. "Delivery of MicroRNA-126 by Apoptotic Bodies Induces CXCL12-Dependent Vascular Protection." *Science Signaling* 2 (100). <https://doi.org/10.1126/scisignal.2000610>.

- Zhang, Chenguang, Wei Zhong, and Weihua Huang. 2017. "CTHRC1 Promotes the Proliferation and Invasion of Prostate Cancer Cells by Regulating the Activity of Wnt/PCP Signalling Pathway." www.biomedres.info.
- Zhang, Jun Ming, and Jianxiong An. 2007. "Cytokines, Inflammation, and Pain." *International Anesthesiology Clinics*. <https://doi.org/10.1097/AIA.0b013e318034194e>.
- Zhang, Lin, Siyuan Zhang, Jun Yao, Frank J. Lowery, Qingling Zhang, Wen Chien Huang, Ping Li, et al. 2015. "Microenvironment-Induced PTEN Loss by Exosomal MicroRNA Primes Brain Metastasis Outgrowth." *Nature* 527 (7576): 100–104. <https://doi.org/10.1038/nature15376>.
- Zhang, Qiang, Xiujian Yin, Zhiwei Pan, Yingying Cao, Shaojie Han, Guojun Gao, Zhiqin Gao, Zhifang Pan, and Weiguo Feng. 2019. "Identification of Potential Diagnostic and Prognostic Biomarkers for Prostate Cancer." *Oncology Letters* 18 (4): 4237–45. <https://doi.org/10.3892/ol.2019.10765>.
- Zhang, Xin A, William S Lane, Stephanie Charrin, Eric Rubinstein, and Lei Liu. 2003. "EWI2/PGRL Associates with the Metastasis Suppressor KAI1/CD82 and Inhibits the Migration of Prostate Cancer Cells 1." *CANCER RESEARCH*. Vol. 63.
- Zhang, Yan, Yi Ba, Chang Liu, Guoxun Sun, Li Ding, Songyuan Gao, Jihui Hao, et al. 2007. "PGC-1 α Induces Apoptosis in Human Epithelial Ovarian Cancer Cells through a PPAR γ -Dependent Pathway." *Cell Research* 17 (4): 363–73. <https://doi.org/10.1038/cr.2007.11>.
- Zhang, Zeda, Wouter R Karthaus, Young Sun Lee, Xuejun Jiang, Philip A Watson, and Charles L Sawyers. 2020. "Tumor Microenvironment-Derived NRG1 Promotes Antiandrogen Resistance in Prostate Cancer LI Tumor Microenvironment-Derived NRG1 Promotes Antiandrogen Resistance in Prostate Cancer." *Cancer Cell* 38 (2): 279-296.e9. <https://doi.org/10.1016/j.ccell.2020.06.005>.
- Zhang, Zheng, Mengqi Liu, Qiangsheng Hu, Wenyan Xu, Wensheng Liu, Qiqing Sun, Zeng Ye, et al. 2019. "FGFBP1, a Downstream Target of the FBW7/c-Myc Axis Promotes Cell Proliferation and Migration in Pancreatic Cancer." *Am J Cancer Res*. Vol. 9. www.ajcr.us/.
- Zhao, Hongyun, Lifeng Yang, Joelle Baddour, Abhinav Achreja, Vincent Bernard, Tyler Moss, Juan C. Marini, et al. 2016. "Tumor Microenvironment Derived Exosomes Pleiotropically Modulate Cancer Cell Metabolism." *ELife* 5 (FEBRUARY2016): 1–27. <https://doi.org/10.7554/eLife.10250>.
- Zhou, Biting, Kailun Xu, Xi Zheng, Ting Chen, Jian Wang, Yongmao Song, Yingkuan Shao, and Shu Zheng. 2020. "Application of Exosomes as Liquid Biopsy in Clinical Diagnosis." *Signal Transduction and Targeted Therapy*. Springer Nature. <https://doi.org/10.1038/s41392-020-00258-9>.
- Zhu, Hua Yu, Wen Dong Bai, Jia Qi Liu, Zhao Zheng, Hao Guan, Qin Zhou, Lin Lin Su, et al. 2016. "Up-Regulation of FGFBP1 Signaling Contributes to MIR-146a-Induced Angiogenesis in Human Umbilical Vein Endothelial Cells." *Scientific Reports* 6 (April). <https://doi.org/10.1038/srep25272>.

- Ziaee, Shabnam, and Leland W.K. Chung. 2014. "Induction of Integrin A2 in a Highly Bone Metastatic Human Prostate Cancer Cell Line: Roles of RANKL and AR under Three-Dimensional Suspension Culture." *Molecular Cancer* 13 (1). <https://doi.org/10.1186/1476-4598-13-208>.
- Zitvogel, Laurence, Federico Pietrocola, and Guido Kroemer. 2017. "Nutrition, Inflammation and Cancer." *Nature Immunology*. Nature Publishing Group. <https://doi.org/10.1038/ni.3754>.
- Zylbersztejn, Kathleen, and Thierry Galli. 2011. "Vesicular Traffic in Cell Navigation." *FEBS Journal*. <https://doi.org/10.1111/j.1742-4658.2011.08168.x>.

II Annex

Table 1. Transcriptional analysis of PGC1 α -expressing and non-expressing cells. FC: fold change.

Ensembl	Symbol	Adj p value	FC
ENSG00000250657	AC097451.1	0.000	-33.518
ENSG00000277297	ATP5F1AP10	0.000	-29.375
ENSG00000255177	MUC5B-AS1	0.001	-24.820
ENSG00000230305	AC004980.3	0.002	-23.509
ENSG00000215182	MUC5AC	0.000	-16.431
ENSG00000244694	PTCHD4	0.003	-15.821
ENSG00000268621	IGFL2-AS1	0.005	-15.744
ENSG00000229937	PRPS1L1	0.008	-15.076
ENSG00000135374	ELF5	0.006	-14.327
ENSG00000107159	CA9	0.000	-13.420
ENSG00000125571	IL37	0.000	-12.653
ENSG00000198788	MUC2	0.000	-12.521
ENSG00000168243	GNG4	0.000	-12.459
ENSG00000234282	AL109809.2	0.009	-12.260
ENSG00000265828	MIR3939	0.007	-11.918
ENSG00000100427	MLC1	0.000	-11.467
ENSG00000214823	NXT1P1	0.010	-11.339
ENSG00000108602	ALDH3A1	0.000	-10.213
ENSG00000165186	PTCHD1	0.000	-9.557
ENSG00000187288	CIDEC	0.000	-8.904
ENSG00000102794	ACOD1	0.000	-8.803
ENSG00000078725	BRINP1	0.000	-8.769
ENSG00000131620	ANO1	0.000	-8.518
ENSG00000180730	SHISA2	0.000	-7.751
ENSG00000134668	SPOCD1	0.000	-7.422
ENSG00000177300	CLDN22	0.004	-7.266
ENSG00000198574	SH2D1B	0.000	-7.254
ENSG00000166828	SCNN1G	0.000	-7.213
ENSG00000101096	NFATC2	0.000	-7.007
ENSG00000168447	SCNN1B	0.000	-6.969
ENSG00000152578	GRIA4	0.000	-6.966
ENSG00000137033	IL33	0.007	-6.844
ENSG00000130176	CNN1	0.003	-6.717
ENSG00000166220	TBATA	0.008	-6.653
ENSG00000170961	HAS2	0.000	-6.613
ENSG00000164764	SBSPON	0.000	-6.503
ENSG00000230432	AC114803.1	0.009	-6.410
ENSG00000143320	CRABP2	0.000	-6.380
ENSG00000117983	MUC5B	0.000	-6.371
ENSG00000125538	IL1B	0.000	-6.267
ENSG00000282048	AL591742.2	0.000	-6.102
ENSG00000203685	STUM	0.000	-6.094
ENSG00000241111	PRICKLE2-AS1	0.000	-5.936
ENSG00000144810	COL8A1	0.000	-5.833
ENSG00000157542	KCNJ6	0.000	-5.761
ENSG00000079841	RIMS1	0.000	-5.717
ENSG00000167754	KLK5	0.000	-5.680
ENSG00000152785	BMP3	0.000	-5.675
ENSG00000125384	PTGER2	0.000	-5.555
ENSG00000104327	CALB1	0.000	-5.500
ENSG00000278872	AC148477.5	0.000	-5.459
ENSG00000181449	SOX2	0.000	-5.451
ENSG00000155657	TTN	0.000	-5.401
ENSG00000236345	AL354719.2	0.000	-5.355
ENSG00000135898	GPR55	0.000	-5.328
ENSG00000106483	SFRP4	0.000	-5.245
ENSG00000162490	DRAXIN	0.000	-5.219
ENSG00000197467	COL13A1	0.000	-5.156
ENSG00000105369	CD79A	0.001	-5.155

ENSG00000261468	AC096921.2	0.008	-5.029
ENSG00000164379	FOXQ1	0.000	-4.990
ENSG00000118513	MYB	0.000	-4.948
ENSG00000248690	HAS2-AS1	0.000	-4.901
ENSG00000131378	RFTN1	0.001	-4.856
ENSG00000215183	MSMP	0.000	-4.855
ENSG00000101842	VSIG1	0.000	-4.835
ENSG00000101265	RASSF2	0.000	-4.784
ENSG00000249599	BMPR1B-DT	0.000	-4.782
ENSG00000141622	RNF165	0.000	-4.669
ENSG00000108759	KRT32	0.001	-4.659
ENSG00000157551	KCNJ15	0.000	-4.625
ENSG00000186832	KRT16	0.000	-4.594
ENSG00000276404	MIR6835	0.008	-4.582
ENSG00000164509	IL31RA	0.000	-4.581
ENSG00000134827	TCN1	0.000	-4.566
ENSG00000100473	COCH	0.000	-4.555
ENSG00000260398	AC068700.1	0.000	-4.531
ENSG00000168477	TNXB	0.000	-4.509
ENSG00000141753	IGFBP4	0.000	-4.500
ENSG00000124479	NDP	0.000	-4.498
ENSG00000168453	HR	0.000	-4.495
ENSG00000049089	COL9A2	0.000	-4.494
ENSG00000167755	KLK6	0.000	-4.481
ENSG00000198768	APCDD1L	0.000	-4.460
ENSG00000163359	COL6A3	0.000	-4.453
ENSG00000185070	FLRT2	0.000	-4.436
ENSG00000277423	AC069234.5	0.001	-4.420
ENSG00000100234	TIMP3	0.002	-4.381
ENSG00000169174	PCSK9	0.000	-4.377
ENSG00000225258	AC009478.1	0.000	-4.357
ENSG00000280693	SH3PXD2A-AS1	0.000	-4.317
ENSG00000046653	GPM6B	0.000	-4.297
ENSG00000231290	APCDD1L-DT	0.000	-4.250
ENSG00000118257	NRP2	0.000	-4.246
ENSG00000178199	ZC3H12D	0.007	-4.237
ENSG00000163492	CCDC141	0.000	-4.210
ENSG00000113361	CDH6	0.000	-4.200
ENSG00000101230	ISM1	0.001	-4.182
ENSG00000183128	CALHM3	0.005	-4.160
ENSG00000134853	PDGFRA	0.000	-4.158
ENSG00000258073	AC128657.1	0.006	-4.145
ENSG00000249026	CTNNA1P1	0.004	-4.126
ENSG00000169856	ONECUT1	0.000	-4.123
ENSG00000123685	BATF3	0.000	-4.113
ENSG00000039560	RAI14	0.000	-4.105
ENSG00000124875	CXCL6	0.000	-4.100
ENSG00000136859	ANGPTL2	0.000	-4.081
ENSG00000168306	ACOX2	0.000	-4.063
ENSG00000175728	C11orf44	0.001	-4.062
ENSG00000261441	AC124068.2	0.007	-4.062
ENSG00000173546	CSPG4	0.002	-4.051
ENSG00000203805	PLPP4	0.000	-4.043
ENSG00000244274	DBNDD2	0.000	-4.039
ENSG00000005513	SOX8	0.000	-4.034
ENSG00000154537	FAM27C	0.000	-4.032
ENSG00000100558	PLEK2	0.000	-4.011
ENSG00000250072	SH3TC2-DT	0.000	-3.956
ENSG00000085552	IGSF9	0.000	-3.944
ENSG00000139211	AMIGO2	0.000	-3.942

ENSG00000142698	<i>C1orf94</i>	0.000	-3.939
ENSG00000233384	AC096537.1	0.000	-3.919
ENSG00000095752	<i>IL11</i>	0.000	-3.915
ENSG00000155846	PPARGC1B	0.000	-3.904
ENSG00000135074	ADAM19	0.000	-3.883
ENSG00000067798	<i>NAV3</i>	0.000	-3.877
ENSG00000148680	<i>HTR7</i>	0.000	-3.863
ENSG00000104313	<i>EYA1</i>	0.000	-3.855
ENSG00000179431	<i>FJX1</i>	0.000	-3.836
ENSG00000206147	RPL23AP57	0.004	-3.820
ENSG00000186684	<i>CYP27C1</i>	0.000	-3.817
ENSG00000260727	SLC7A5P1	0.005	-3.816
ENSG00000164116	<i>GUCY1A1</i>	0.000	-3.811
ENSG00000261341	AC010325.1	0.000	-3.801
ENSG00000121904	CSMD2	0.000	-3.800
ENSG00000038427	<i>VCAN</i>	0.000	-3.797
ENSG00000126878	<i>AIF1L</i>	0.000	-3.797
ENSG00000181418	<i>DDN</i>	0.000	-3.795
ENSG00000105088	<i>OLFM2</i>	0.000	-3.760
ENSG00000100433	<i>KCNK10</i>	0.000	-3.754
ENSG00000057704	TMCC3	0.000	-3.752
ENSG00000163501	<i>IHH</i>	0.001	-3.741
ENSG00000235698	PA2G4P2	0.009	-3.731
ENSG00000154027	<i>AK5</i>	0.000	-3.729
ENSG00000248771	SMIM31	0.004	-3.729
ENSG00000122824	<i>NUDT10</i>	0.004	-3.719
ENSG00000075213	SEMA3A	0.000	-3.718
ENSG00000182584	<i>ACTL10</i>	0.000	-3.716
ENSG00000250697	AC010343.3	0.000	-3.713
ENSG00000139219	<i>COL2A1</i>	0.004	-3.711
ENSG00000117148	<i>ACTL8</i>	0.001	-3.706
ENSG00000166825	<i>ANPEP</i>	0.000	-3.700
ENSG00000188517	COL25A1	0.000	-3.698
ENSG00000147394	<i>ZNF185</i>	0.000	-3.698
ENSG00000069482	<i>GAL</i>	0.000	-3.695
ENSG00000110042	<i>DTX4</i>	0.000	-3.684
ENSG00000137440	<i>FGFBP1</i>	0.000	-3.675
ENSG00000182459	<i>TEX19</i>	0.000	-3.671
ENSG00000248641	HMGA1P2	0.001	-3.649
ENSG00000010295	<i>IFFO1</i>	0.000	-3.635
ENSG00000058404	CAMK2B	0.000	-3.633
ENSG00000273132	AL355312.3	0.000	-3.593
ENSG00000081277	<i>PKP1</i>	0.000	-3.592
ENSG00000112309	B3GAT2	0.009	-3.562
ENSG00000132688	<i>NES</i>	0.000	-3.559
ENSG00000225217	HSPA7	0.000	-3.540
ENSG00000145681	HAPLN1	0.000	-3.537
ENSG00000159166	<i>LAD1</i>	0.000	-3.526
ENSG00000002079	MYH16	0.000	-3.516
ENSG00000183691	<i>NOG</i>	0.000	-3.505
ENSG00000276043	<i>UHRF1</i>	0.000	-3.504
ENSG00000157782	CABP1	0.001	-3.493
ENSG00000198074	AKR1B10	0.000	-3.487
ENSG00000271605	<i>MILR1</i>	0.000	-3.475
ENSG00000227855	DPY19L2P3	0.000	-3.471
ENSG00000147160	AWAT2	0.000	-3.461
ENSG00000127863	TNFRSF19	0.000	-3.445
ENSG00000105996	<i>HOXA2</i>	0.000	-3.441
ENSG00000111664	GNB3	0.005	-3.438
ENSG00000233057	EEF1A1P14	0.007	-3.428

ENSG0000071054	MAP4K4	0.000	-3.419
ENSG00000166707	ZCCHC18	0.000	-3.416
ENSG00000236972	FABP5P1	0.000	-3.403
ENSG00000176857	GJA1P1	0.000	-3.391
ENSG00000173894	CBX2	0.000	-3.389
ENSG00000005102	MEOX1	0.002	-3.389
ENSG00000164002	EXO5	0.000	-3.384
ENSG00000168646	AXIN2	0.000	-3.380
ENSG00000230667	SETSIP	0.000	-3.375
ENSG00000242265	PEG10	0.000	-3.374
ENSG00000111348	ARHGDI8	0.000	-3.360
ENSG00000184384	MAML2	0.000	-3.354
ENSG00000182836	PLCXD3	0.000	-3.343
ENSG00000160181	TFF2	0.000	-3.335
ENSG00000184613	NELL2	0.000	-3.331
ENSG00000164683	HEY1	0.000	-3.319
ENSG00000092445	TYRO3	0.000	-3.313
ENSG00000090447	TFAP4	0.000	-3.311
ENSG00000248971	KRT8P46	0.000	-3.311
ENSG00000164932	CTHRC1	0.000	-3.307
ENSG00000269985	AL021328.1	0.000	-3.300
ENSG00000255325	AC108136.1	0.000	-3.299
ENSG00000261371	PECAM1	0.000	-3.293
ENSG00000149380	P4HA3	0.000	-3.289
ENSG00000106327	TFR2	0.000	-3.286
ENSG00000100490	CDKL1	0.000	-3.284
ENSG00000124107	SLPI	0.000	-3.284
ENSG0000013619	MAMLD1	0.000	-3.283
ENSG00000106003	LFNG	0.000	-3.280
ENSG00000281131	SCHLAP1	0.000	-3.276
ENSG00000079308	TNS1	0.000	-3.274
ENSG00000113368	LMNB1	0.000	-3.271
ENSG00000133636	NTS	0.000	-3.267
ENSG00000258445	AL132777.1	0.005	-3.261
ENSG00000140945	CDH13	0.000	-3.255
ENSG00000179066	AC020907.1	0.000	-3.252
ENSG00000231298	MANCR	0.000	-3.249
ENSG00000255346	NOX5	0.000	-3.245
ENSG00000200087	SNORA73B	0.000	-3.234
ENSG00000162878	PKDCC	0.000	-3.225
ENSG00000198774	RASSF9	0.000	-3.219
ENSG00000076770	MBNL3	0.000	-3.215
ENSG00000170743	SYT9	0.000	-3.213
ENSG00000204767	INSYN2B	0.000	-3.195
ENSG00000091986	CCDC80	0.000	-3.195
ENSG00000255364	SMILR	0.000	-3.188
ENSG00000175130	MARCKSL1	0.000	-3.178
ENSG00000165905	LARGE2	0.000	-3.174
ENSG00000174130	TLR6	0.000	-3.174
ENSG00000137309	HMGA1	0.000	-3.170
ENSG00000283199	C13orf46	0.000	-3.168
ENSG00000114646	CSPG5	0.000	-3.163
ENSG00000022267	FHL1	0.000	-3.160
ENSG00000186193	SAPCD2	0.000	-3.160
ENSG00000269982	AC018809.2	0.000	-3.159
ENSG00000074047	GLI2	0.000	-3.158
ENSG00000159167	STC1	0.000	-3.156
ENSG00000056487	PHF21B	0.000	-3.145
ENSG00000225264	ZNRF2P2	0.000	-3.141
ENSG00000082497	SERTAD4	0.000	-3.138

ENSG00000152377	<i>SPOCK1</i>	0.000	-3.134
ENSG00000171812	<i>COL8A2</i>	0.006	-3.133
ENSG00000162745	<i>OLFML2B</i>	0.000	-3.118
ENSG00000184828	<i>ZBTB7C</i>	0.000	-3.118
ENSG00000107105	<i>ELAVL2</i>	0.000	-3.115
ENSG00000172164	<i>SNTB1</i>	0.000	-3.107
ENSG00000124216	<i>SNAI1</i>	0.000	-3.105
ENSG00000152284	<i>TCF7L1</i>	0.000	-3.102
ENSG00000260401	<i>AP002761.4</i>	0.000	-3.101
ENSG00000077782	<i>FGFR1</i>	0.000	-3.090
ENSG00000012124	<i>CD22</i>	0.000	-3.090
ENSG00000060749	<i>QSER1</i>	0.000	-3.087
ENSG00000174501	<i>ANKRD36C</i>	0.000	-3.086
ENSG00000106123	<i>EPHB6</i>	0.000	-3.082
ENSG00000169908	<i>TM4SF1</i>	0.000	-3.082
ENSG00000224839	<i>RPL12P17</i>	0.000	-3.080
ENSG00000133216	<i>EPHB2</i>	0.000	-3.075
ENSG00000183023	<i>SLC8A1</i>	0.000	-3.065
ENSG00000183688	<i>RFLNB</i>	0.000	-3.062
ENSG00000111145	<i>ELK3</i>	0.000	-3.059
ENSG00000104369	<i>JPH1</i>	0.000	-3.058
ENSG00000160185	<i>UBASH3A</i>	0.006	-3.058
ENSG00000185614	<i>INKA1</i>	0.000	-3.058
ENSG00000138587	<i>MNS1</i>	0.000	-3.056
ENSG00000218336	<i>TENM3</i>	0.000	-3.050
ENSG00000176678	<i>FOXL1</i>	0.000	-3.037
ENSG00000134874	<i>DZIP1</i>	0.000	-3.037
ENSG00000225721	<i>AL592166.1</i>	0.002	-3.025
ENSG00000260007	<i>AC107871.1</i>	0.000	-3.022
ENSG00000109452	<i>INPP4B</i>	0.000	-3.022
ENSG00000258011	<i>HMGA1P3</i>	0.000	-3.020
ENSG00000166250	<i>CLMP</i>	0.000	-3.020
ENSG00000156966	<i>B3GNT7</i>	0.000	-3.019
ENSG00000175894	<i>TSPEAR</i>	0.000	-3.016
ENSG00000243978	<i>RTL9</i>	0.000	-3.014
ENSG00000215417	<i>MIR17HG</i>	0.000	-3.010
ENSG00000259781	<i>HMGB1P6</i>	0.000	-3.008
ENSG00000006071	<i>ABCC8</i>	0.001	-3.007
ENSG00000279365	<i>AP000695.3</i>	0.000	-2.999
ENSG00000122877	<i>EGR2</i>	0.000	-2.996
ENSG00000165568	<i>AKR1E2</i>	0.000	-2.996
ENSG00000260834	<i>AC009055.2</i>	0.000	-2.992
ENSG00000260807	<i>AC009041.2</i>	0.000	-2.990
ENSG00000198435	<i>NRARP</i>	0.000	-2.987
ENSG00000122035	<i>RASL11A</i>	0.000	-2.981
ENSG00000272551	<i>AC017048.3</i>	0.009	-2.974
ENSG00000160867	<i>FGFR4</i>	0.000	-2.971
ENSG00000132470	<i>ITGB4</i>	0.000	-2.969
ENSG00000142552	<i>RCN3</i>	0.000	-2.964
ENSG00000167912	<i>AC090152.1</i>	0.001	-2.960
ENSG00000213853	<i>EMP2</i>	0.000	-2.958
ENSG00000240122	<i>FABP5P11</i>	0.000	-2.953
ENSG00000117322	<i>CR2</i>	0.000	-2.953
ENSG00000138031	<i>ADCY3</i>	0.000	-2.952
ENSG00000059377	<i>TBXAS1</i>	0.000	-2.950
ENSG00000165935	<i>SMCO2</i>	0.000	-2.949
ENSG00000136943	<i>CTSV</i>	0.000	-2.949
ENSG00000187017	<i>ESPN</i>	0.000	-2.948
ENSG00000227038	<i>GTF2IP7</i>	0.000	-2.945
ENSG00000149781	<i>FERMT3</i>	0.000	-2.927

ENSG00000135362	<i>PRR5L</i>	0.000	-2.924
ENSG00000236935	<i>AP003774.4</i>	0.000	-2.919
ENSG00000187068	<i>C3orf70</i>	0.000	-2.919
ENSG00000254122	<i>PCDHGB7</i>	0.001	-2.919
ENSG00000274956	<i>NKAIN3-IT1</i>	0.001	-2.918
ENSG00000106991	<i>ENG</i>	0.002	-2.916
ENSG00000099958	<i>DERL3</i>	0.000	-2.910
ENSG00000182472	<i>CAPN12</i>	0.002	-2.895
ENSG00000004399	<i>PLXND1</i>	0.000	-2.895
ENSG00000073111	<i>MCM2</i>	0.000	-2.894
ENSG00000146950	<i>SHROOM2</i>	0.001	-2.890
ENSG00000152661	<i>GJA1</i>	0.000	-2.888
ENSG00000018236	<i>CNTN1</i>	0.000	-2.888
ENSG00000164100	<i>NDST3</i>	0.000	-2.886
ENSG00000167695	<i>FAM57A</i>	0.000	-2.885
ENSG00000179241	<i>LDLRAD3</i>	0.000	-2.882
ENSG00000135914	<i>HTR2B</i>	0.009	-2.877
ENSG00000187134	<i>AKR1C1</i>	0.000	-2.876
ENSG00000182263	<i>FIGN</i>	0.000	-2.876
ENSG00000164687	<i>FABP5</i>	0.000	-2.875
ENSG00000122861	<i>PLAU</i>	0.000	-2.871
ENSG00000227456	<i>LINC00310</i>	0.004	-2.869
ENSG00000215788	<i>TNFRSF25</i>	0.000	-2.869
ENSG00000102287	<i>GABRE</i>	0.001	-2.867
ENSG00000147166	<i>ITGB1BP2</i>	0.000	-2.867
ENSG00000182272	<i>B4GALNT4</i>	0.000	-2.866
ENSG00000248873	<i>SERBP1P6</i>	0.006	-2.864
ENSG00000280719	<i>PCAT5</i>	0.000	-2.863
ENSG00000143815	<i>LBR</i>	0.000	-2.859
ENSG00000213707	<i>HMGB1P10</i>	0.000	-2.854
ENSG00000088305	<i>DNMT3B</i>	0.000	-2.849
ENSG00000111087	<i>GLI1</i>	0.000	-2.846
ENSG00000111252	<i>SH2B3</i>	0.000	-2.842
ENSG00000251281	<i>AC034223.2</i>	0.000	-2.836
ENSG00000232855	<i>AF165147.1</i>	0.000	-2.833
ENSG00000234602	<i>MCIDAS</i>	0.000	-2.828
ENSG00000087903	<i>RFX2</i>	0.000	-2.827
ENSG00000090776	<i>EFNB1</i>	0.000	-2.827
ENSG00000085840	<i>ORC1</i>	0.000	-2.825
ENSG00000043355	<i>ZIC2</i>	0.000	-2.822
ENSG00000160233	<i>LRRC3</i>	0.000	-2.819
ENSG00000118007	<i>STAG1</i>	0.000	-2.819
ENSG00000173113	<i>TRMT112</i>	0.000	-2.813
ENSG00000219607	<i>PPP1R3G</i>	0.000	-2.808
ENSG00000095303	<i>PTGS1</i>	0.000	-2.806
ENSG00000130600	<i>H19</i>	0.001	-2.804
ENSG00000091844	<i>RGS17</i>	0.000	-2.804
ENSG00000165959	<i>CLMN</i>	0.000	-2.803
ENSG00000156103	<i>MMP16</i>	0.000	-2.803
ENSG00000162631	<i>NTNG1</i>	0.000	-2.800
ENSG00000150893	<i>FREM2</i>	0.000	-2.795
ENSG00000279495	<i>AL928654.4</i>	0.000	-2.795
ENSG00000135373	<i>EHF</i>	0.000	-2.794
ENSG00000272502	<i>AC104958.2</i>	0.000	-2.794
ENSG00000169247	<i>SH3TC2</i>	0.000	-2.791
ENSG00000144354	<i>CDCA7</i>	0.000	-2.790
ENSG00000105974	<i>CAV1</i>	0.000	-2.790
ENSG00000250770	<i>AC005865.2</i>	0.000	-2.788
ENSG00000137404	<i>NRM</i>	0.000	-2.783
ENSG00000180176	<i>TH</i>	0.000	-2.777

ENSG00000256663	AC112777.1	0.000	-2.777
ENSG00000128567	PODXL	0.000	-2.773
ENSG00000105967	TFEC	0.000	-2.771
ENSG00000101057	MYBL2	0.000	-2.769
ENSG00000109586	GALNT7	0.000	-2.766
ENSG00000196155	PLEKHG4	0.000	-2.762
ENSG00000183386	FHL3	0.000	-2.762
ENSG00000231574	LINC02015	0.004	-2.761
ENSG00000147202	DIAPH2	0.000	-2.760
ENSG00000140534	TICRR	0.000	-2.751
ENSG00000105523	FAM83E	0.000	-2.742
ENSG00000171680	PLEKHG5	0.000	-2.741
ENSG00000089327	FXYD5	0.000	-2.740
ENSG00000143847	PPFIA4	0.000	-2.739
ENSG00000244682	FCGR2C	0.001	-2.739
ENSG00000248966	BCLAF1P1	0.003	-2.737
ENSG00000178773	CPNE7	0.000	-2.736
ENSG00000168268	NT5DC2	0.000	-2.731
ENSG00000268089	GABRQ	0.000	-2.730
ENSG00000175591	P2RY2	0.000	-2.729
ENSG00000104419	NDRG1	0.000	-2.727
ENSG00000179873	NLRP11	0.000	-2.725
ENSG00000197299	BLM	0.000	-2.724
ENSG00000117016	RIMS3	0.000	-2.719
ENSG00000124496	TRERF1	0.000	-2.718
ENSG00000230650	AC140479.2	0.000	-2.717
ENSG00000142661	MYOM3	0.000	-2.714
ENSG00000151632	AKR1C2	0.000	-2.712
ENSG00000115008	IL1A	0.010	-2.709
ENSG00000162636	FAM102B	0.000	-2.709
ENSG00000197565	COL4A6	0.000	-2.708
ENSG00000085999	RAD54L	0.000	-2.704
ENSG00000077942	FBLN1	0.000	-2.704
ENSG00000005108	THSD7A	0.000	-2.702
ENSG00000145604	SKP2	0.000	-2.700
ENSG00000151090	THRB	0.000	-2.700
ENSG00000086548	CEACAM6	0.000	-2.699
ENSG00000128011	LRFN1	0.000	-2.699
ENSG00000149970	CNKSR2	0.000	-2.698
ENSG00000171872	KLF17	0.000	-2.696
ENSG00000134871	COL4A2	0.000	-2.694
ENSG00000105281	SLC1A5	0.000	-2.692
ENSG00000134955	SLC37A2	0.000	-2.692
ENSG00000136542	GALNT5	0.000	-2.683
ENSG00000071967	CYBRD1	0.000	-2.678
ENSG00000115290	GRB14	0.000	-2.677
ENSG00000230479	AP000695.1	0.000	-2.672
ENSG00000158292	GPR153	0.000	-2.671
ENSG00000225969	ABHD11-AS1	0.002	-2.669
ENSG00000134569	LRP4	0.000	-2.667
ENSG00000101335	MYL9	0.000	-2.666
ENSG00000154493	C10orf90	0.002	-2.665
ENSG00000132932	ATP8A2	0.000	-2.665
ENSG00000198604	BAZ1A	0.000	-2.664
ENSG00000152670	DDX4	0.000	-2.661
ENSG00000029153	ARNTL2	0.000	-2.656
ENSG00000158050	DUSP2	0.000	-2.654
ENSG00000186204	CYP4F12	0.007	-2.653
ENSG00000173638	SLC19A1	0.000	-2.653
ENSG00000160949	TONSL	0.000	-2.652

ENSG00000204366	ZBTB12	0.000	-2.651
ENSG00000259071	AL359397.2	0.000	-2.650
ENSG00000230882	AC005077.4	0.000	-2.649
ENSG00000254656	RTL1	0.000	-2.648
ENSG00000139269	INHBE	0.000	-2.645
ENSG00000116962	NID1	0.000	-2.644
ENSG00000175305	CCNE2	0.000	-2.643
ENSG00000230082	PRRT3-AS1	0.000	-2.643
ENSG00000226855	RPSAP17	0.000	-2.639
ENSG00000079150	FKBP7	0.000	-2.639
ENSG00000128591	FLNC	0.000	-2.637
ENSG00000102886	GDPD3	0.001	-2.637
ENSG00000230592	RPSAP8	0.000	-2.637
ENSG00000257242	LINC01619	0.000	-2.635
ENSG00000137054	POLR1E	0.000	-2.632
ENSG00000205129	C4orf47	0.001	-2.632
ENSG00000105894	PTN	0.000	-2.632
ENSG00000099337	KCNK6	0.000	-2.631
ENSG00000196584	XRCC2	0.000	-2.631
ENSG00000181544	FANCB	0.000	-2.629
ENSG00000178752	ERFE	0.000	-2.628
ENSG00000152936	LMNTD1	0.008	-2.626
ENSG00000176619	LMNB2	0.000	-2.625
ENSG00000135905	DOCK10	0.000	-2.621
ENSG00000176438	SYNE3	0.000	-2.621
ENSG00000101306	MYLK2	0.000	-2.619
ENSG00000273669	AC015819.1	0.000	-2.617
ENSG00000144821	MYH15	0.000	-2.613
ENSG00000126803	HSPA2	0.000	-2.612
ENSG00000116774	OLFML3	0.000	-2.611
ENSG00000211454	AKR7L	0.000	-2.611
ENSG00000105997	HOXA3	0.000	-2.608
ENSG00000185989	RASA3	0.000	-2.607
ENSG00000214016	RPSAP61	0.001	-2.607
ENSG00000104967	NOVA2	0.000	-2.606
ENSG00000153551	CMTM7	0.000	-2.605
ENSG00000279821	AC145098.2	0.000	-2.604
ENSG00000258900	HNRNPCP1	0.000	-2.601
ENSG00000175592	FOSL1	0.000	-2.599
ENSG00000242715	CCDC169	0.000	-2.597
ENSG00000189403	HMGB1	0.000	-2.596
ENSG00000176208	ATAD5	0.000	-2.595
ENSG00000163009	C2orf48	0.008	-2.593
ENSG00000132967	HMGB1P5	0.000	-2.591
ENSG00000198963	RORB	0.000	-2.590
ENSG00000172548	NIPAL4	0.000	-2.589
ENSG00000227744	LINC01940	0.000	-2.588
ENSG00000172318	B3GALT1	0.000	-2.587
ENSG00000169116	PARM1	0.000	-2.587
ENSG00000117519	CNN3	0.000	-2.586
ENSG00000155269	GPR78	0.000	-2.584
ENSG00000166508	MCM7	0.000	-2.579
ENSG00000102554	KLF5	0.000	-2.576
ENSG00000147676	MAL2	0.000	-2.568
ENSG00000232931	LINC00342	0.000	-2.568
ENSG00000234678	ELF3-AS1	0.000	-2.566
ENSG00000237004	ZNRF2P1	0.000	-2.565
ENSG00000106089	STX1A	0.000	-2.565
ENSG00000149328	GLB1L2	0.000	-2.563
ENSG00000153885	KCTD15	0.000	-2.563

ENSG00000102879	CORO1A	0.000	-2.455
ENSG00000162783	IER5	0.000	-2.454
ENSG00000164109	MAD2L1	0.000	-2.454
ENSG00000114268	PFKFB4	0.000	-2.450
ENSG00000261373	VPS9D1-AS1	0.000	-2.448
ENSG00000241945	PWP2	0.001	-2.448
ENSG00000198959	TGM2	0.000	-2.447
ENSG00000180385	EMC3-AS1	0.000	-2.447
ENSG00000069812	HES2	0.000	-2.447
ENSG00000260947	AL356489.2	0.001	-2.445
ENSG00000179598	PLD6	0.000	-2.443
ENSG00000087086	FTL	0.000	-2.438
ENSG00000109255	NMU	0.000	-2.435
ENSG00000112320	SOBP	0.000	-2.434
ENSG00000143995	MEIS1	0.000	-2.433
ENSG00000188312	CENPP	0.000	-2.431
ENSG00000183778	B3GALT5	0.000	-2.429
ENSG00000154608	CEP170P1	0.000	-2.428
ENSG00000138758	40787.000	0.000	-2.423
ENSG00000203995	ZYG11A	0.000	-2.423
ENSG00000197696	NMB	0.000	-2.422
ENSG00000105255	FSD1	0.000	-2.422
ENSG00000074181	NOTCH3	0.000	-2.421
ENSG00000261662	AL359752.1	0.002	-2.420
ENSG00000105245	NUMBL	0.000	-2.420
ENSG00000141655	TNFRSF11A	0.000	-2.419
ENSG00000253552	HOXA-AS2	0.000	-2.418
ENSG00000253304	TMEM200B	0.000	-2.416
ENSG00000267041	ZNF850	0.000	-2.415
ENSG00000125520	SLC2A4RG	0.000	-2.414
ENSG00000187498	COL4A1	0.000	-2.414
ENSG00000254726	MEX3A	0.000	-2.410
ENSG00000102174	PHEX	0.000	-2.409
ENSG00000101311	FERMT1	0.000	-2.408
ENSG00000144395	CCDC150	0.000	-2.408
ENSG00000230699	AL645608.2	0.000	-2.407
ENSG00000092853	CLSPN	0.000	-2.406
ENSG00000118495	PLAGL1	0.000	-2.405
ENSG00000268218	AC137932.3	0.005	-2.405
ENSG00000172819	RARG	0.000	-2.403
ENSG00000122694	GLIPR2	0.000	-2.403
ENSG00000162063	CCNF	0.000	-2.401
ENSG00000103154	NECAB2	0.000	-2.401
ENSG00000178921	PFAS	0.000	-2.398
ENSG00000163808	KIF15	0.000	-2.397
ENSG00000091127	PUS7	0.000	-2.395
ENSG00000180198	RCC1	0.000	-2.395
ENSG00000050555	LAMC3	0.000	-2.395
ENSG00000126215	XRCC3	0.000	-2.394
ENSG00000153823	PID1	0.000	-2.393
ENSG00000116337	AMPD2	0.000	-2.393
ENSG00000213694	S1PR3	0.000	-2.392
ENSG00000164171	ITGA2	0.000	-2.392
ENSG00000165891	E2F7	0.000	-2.387
ENSG00000186871	ERCC6L	0.000	-2.385
ENSG00000107438	PDLIM1	0.000	-2.385
ENSG00000268798	AC027307.3	0.000	-2.385
ENSG00000151725	CENPU	0.000	-2.384
ENSG00000071205	ARHGAP10	0.000	-2.384
ENSG00000172995	ARPP21	0.000	-2.384

ENSG00000213160	<i>KLHL23</i>	0.000	-2.560
ENSG00000005187	<i>ACSM3</i>	0.000	-2.560
ENSG00000186907	<i>RTN4RL2</i>	0.000	-2.559
ENSG00000156049	<i>GNA14</i>	0.000	-2.556
ENSG00000150995	<i>ITPR1</i>	0.000	-2.555
ENSG00000184985	<i>SORCS2</i>	0.000	-2.552
ENSG00000185551	<i>NR2F2</i>	0.000	-2.552
ENSG00000186469	<i>GNG2</i>	0.000	-2.550
ENSG0000035499	<i>DEPDC1B</i>	0.000	-2.548
ENSG00000278763	<i>FAM27B</i>	0.000	-2.548
ENSG00000275029	<i>HMGB1P24</i>	0.004	-2.543
ENSG00000188848	<i>BEND4</i>	0.000	-2.541
ENSG00000099937	<i>SERPIND1</i>	0.000	-2.539
ENSG00000113578	<i>FGF1</i>	0.000	-2.537
ENSG00000165511	<i>C10orf25</i>	0.004	-2.537
ENSG00000084774	<i>CAD</i>	0.000	-2.536
ENSG00000281332	<i>LINC00997</i>	0.000	-2.533
ENSG00000161791	<i>FMNL3</i>	0.000	-2.533
ENSG00000213468	<i>FIRRE</i>	0.000	-2.531
ENSG00000091622	<i>PITPNM3</i>	0.000	-2.527
ENSG00000236992	<i>RPL12P12</i>	0.002	-2.526
ENSG00000104237	<i>RP1</i>	0.000	-2.523
ENSG00000251191	<i>LINC00589</i>	0.001	-2.520
ENSG00000171488	<i>LRRC8C</i>	0.000	-2.519
ENSG00000085662	<i>AKR1B1</i>	0.000	-2.516
ENSG00000121152	<i>NCAPH</i>	0.000	-2.513
ENSG00000132429	<i>POPDC3</i>	0.000	-2.513
ENSG00000164900	<i>GBX1</i>	0.000	-2.513
ENSG00000168421	<i>RHOH</i>	0.000	-2.511
ENSG00000225205	<i>AC078883.1</i>	0.000	-2.506
ENSG00000156475	<i>PPP2R2B</i>	0.000	-2.504
ENSG00000011422	<i>PLAUR</i>	0.000	-2.503
ENSG00000183496	<i>MEX3B</i>	0.001	-2.501
ENSG00000148541	<i>FAM13C</i>	0.000	-2.500
ENSG00000169946	<i>ZFPM2</i>	0.000	-2.499
ENSG00000146072	<i>TNFRSF21</i>	0.000	-2.499
ENSG00000108924	<i>HLF</i>	0.000	-2.496
ENSG00000149136	<i>SSRP1</i>	0.000	-2.495
ENSG00000090382	<i>LYZ</i>	0.002	-2.494
ENSG00000153162	<i>BMP6</i>	0.000	-2.493
ENSG00000138678	<i>GPAT3</i>	0.000	-2.491
ENSG00000168079	<i>SCARA5</i>	0.000	-2.489
ENSG00000143494	<i>VASH2</i>	0.000	-2.487
ENSG00000138639	<i>ARHGAP24</i>	0.000	-2.486
ENSG00000169258	<i>GPRIN1</i>	0.000	-2.486
ENSG00000110811	<i>P3H3</i>	0.000	-2.484
ENSG00000134899	<i>ERCC5</i>	0.000	-2.481
ENSG00000128973	<i>CLN6</i>	0.000	-2.481
ENSG00000146247	<i>PHIP</i>	0.000	-2.479
ENSG00000133863	<i>TEX15</i>	0.000	-2.479
ENSG00000168758	<i>SEMA4C</i>	0.000	-2.479
ENSG00000186891	<i>TNFRSF18</i>	0.000	-2.476
ENSG00000070814	<i>TCOF1</i>	0.000	-2.475
ENSG00000261357	<i>AC099518.2</i>	0.009	-2.475
ENSG00000179051	<i>RCC2</i>	0.000	-2.475
ENSG00000112394	<i>SLC16A10</i>	0.000	-2.472
ENSG00000100767	<i>PAPLN</i>	0.000	-2.471
ENSG00000004660	<i>CAMKK1</i>	0.000	-2.468
ENSG00000065328	<i>MCM10</i>	0.000	-2.457
ENSG00000102048	<i>ASB9</i>	0.000	-2.455

ENSG00000224738	AC099850.1	0.000	-2.322
ENSG00000141576	RNF157	0.000	-2.320
ENSG00000079337	RAPGEF3	0.000	-2.318
ENSG00000187800	PEAR1	0.000	-2.318
ENSG00000122952	ZWINT	0.000	-2.317
ENSG00000178409	BEND3	0.000	-2.317
ENSG00000163322	ABRAXAS1	0.000	-2.316
ENSG00000234964	FABP5P7	0.000	-2.314
ENSG00000196628	TCF4	0.000	-2.314
ENSG00000185483	ROR1	0.000	-2.311
ENSG00000134954	ETS1	0.000	-2.308
ENSG00000066248	NGEF	0.000	-2.308
ENSG00000067191	CACNB1	0.000	-2.306
ENSG00000119737	GPR75	0.000	-2.305
ENSG00000160255	ITGB2	0.000	-2.305
ENSG00000169607	CKAP2L	0.000	-2.305
ENSG00000169330	KIAA1024	0.000	-2.304
ENSG00000079215	SLC1A3	0.000	-2.303
ENSG00000065054	SLC9A3R2	0.000	-2.302
ENSG00000180354	MTURN	0.000	-2.302
ENSG00000175820	CCDC168	0.000	-2.302
ENSG00000134250	NOTCH2	0.000	-2.301
ENSG00000206535	LNP1	0.000	-2.300
ENSG00000164236	ANKRD33B	0.000	-2.300
ENSG00000164647	STEAP1	0.000	-2.300
ENSG00000198598	MMP17	0.000	-2.300
ENSG00000068489	PRR11	0.000	-2.299
ENSG00000167994	RAB3IL1	0.000	-2.298
ENSG00000242575	AC012501.2	0.000	-2.298
ENSG00000111424	VDR	0.000	-2.298
ENSG00000006468	ETV1	0.000	-2.295
ENSG00000123416	TUBA1B	0.000	-2.295
ENSG00000164649	CDCA7L	0.000	-2.292
ENSG00000183971	NPW	0.000	-2.290
ENSG00000261253	AC137932.2	0.000	-2.285
ENSG00000186185	KIF18B	0.000	-2.283
ENSG00000244705	AC020658.1	0.002	-2.283
ENSG00000171316	CHD7	0.000	-2.283
ENSG00000178035	IMPDH2	0.000	-2.281
ENSG00000107954	NEURL1	0.000	-2.280
ENSG00000272438	AL645608.6	0.000	-2.279
ENSG00000239264	TXNDC5	0.000	-2.278
ENSG00000102890	ELMO3	0.000	-2.277
ENSG00000148344	PTGES	0.000	-2.277
ENSG00000160214	RRP1	0.000	-2.276
ENSG00000105486	LIG1	0.000	-2.276
ENSG00000280924	LINC00628	0.009	-2.276
ENSG00000114013	CD86	0.001	-2.275
ENSG00000173473	SMARCC1	0.000	-2.274
ENSG00000112319	EYA4	0.000	-2.273
ENSG00000175886	RPL7AP66	0.000	-2.273
ENSG00000142173	COL6A2	0.000	-2.272
ENSG00000080823	MOK	0.000	-2.272
ENSG00000138356	AOX1	0.000	-2.271
ENSG00000137841	PLCB2	0.000	-2.269
ENSG00000227496	AC099066.2	0.001	-2.269
ENSG00000163364	LINC01116	0.000	-2.266
ENSG00000284747	AL034417.4	0.000	-2.266
ENSG00000143786	CNIH3	0.000	-2.264
ENSG00000130816	DNMT1	0.000	-2.262

ENSG00000135744	AGT	0.001	-2.381
ENSG00000189184	PCDH18	0.000	-2.378
ENSG00000166450	PRTG	0.000	-2.377
ENSG00000010292	NCAPD2	0.000	-2.376
ENSG00000179409	GEMIN4	0.000	-2.375
ENSG00000140848	CPNE2	0.000	-2.375
ENSG00000105643	ARRDC2	0.000	-2.372
ENSG00000265806	MIR4292	0.000	-2.372
ENSG00000097046	CDC7	0.000	-2.371
ENSG00000142731	PLK4	0.000	-2.370
ENSG00000105011	ASF1B	0.000	-2.369
ENSG00000197385	ZNF860	0.000	-2.368
ENSG00000127423	AUNIP	0.000	-2.368
ENSG00000253125	AC055854.1	0.005	-2.364
ENSG00000112769	LAMA4	0.000	-2.363
ENSG00000181588	MEX3D	0.000	-2.362
ENSG00000229251	HNRNPA1P8	0.008	-2.359
ENSG00000163508	EOMES	0.000	-2.358
ENSG00000141441	GAREM1	0.000	-2.357
ENSG00000179913	B3GNT3	0.000	-2.357
ENSG00000176092	CRYBG2	0.004	-2.355
ENSG00000145220	LYAR	0.000	-2.355
ENSG00000168496	FEN1	0.000	-2.354
ENSG00000239389	PCDHA13	0.000	-2.354
ENSG00000100979	PLTP	0.000	-2.354
ENSG00000174705	SH3PXD2B	0.000	-2.354
ENSG00000136997	MYC	0.000	-2.353
ENSG00000128274	A4GALT	0.000	-2.353
ENSG00000261780	LINC02582	0.000	-2.353
ENSG00000116711	PLA2G4A	0.000	-2.351
ENSG00000140682	TGFB111	0.000	-2.351
ENSG00000256673	AC141557.1	0.000	-2.351
ENSG00000213513	IMPDH1P5	0.000	-2.351
ENSG00000003989	SLC7A2	0.000	-2.349
ENSG00000143127	ITGA10	0.000	-2.348
ENSG00000165821	SALL2	0.000	-2.348
ENSG00000017483	SLC38A5	0.005	-2.345
ENSG00000166402	TUB	0.000	-2.345
ENSG00000160200	CBS	0.000	-2.344
ENSG00000180530	NRIP1	0.000	-2.341
ENSG00000171517	LPAR3	0.000	-2.340
ENSG00000205572	SERF1B	0.004	-2.339
ENSG00000159450	TCHH	0.004	-2.337
ENSG00000138696	BMPR1B	0.000	-2.337
ENSG00000172197	MBOAT1	0.000	-2.335
ENSG00000030066	NUP160	0.000	-2.334
ENSG00000124191	TOX2	0.000	-2.333
ENSG00000119969	HELLS	0.000	-2.333
ENSG00000186777	ZNF732	0.000	-2.333
ENSG00000130826	DKC1	0.000	-2.333
ENSG00000213862	AC044787.1	0.002	-2.332
ENSG00000214223	HNRNPA1P10	0.000	-2.332
ENSG00000184937	WT1	0.000	-2.331
ENSG00000093009	CDC45	0.000	-2.330
ENSG00000169884	WNT10B	0.000	-2.329
ENSG00000134901	KDELC1	0.000	-2.327
ENSG00000198176	TFDP1	0.000	-2.326
ENSG00000121900	TMEM54	0.000	-2.325
ENSG00000203943	SAMD13	0.005	-2.323
ENSG00000234160	AL513165.1	0.000	-2.323

ENSG00000230330	HMG2P3	0.000	-2.262
ENSG00000160208	RRP1B	0.000	-2.261
ENSG00000042493	CAPG	0.000	-2.261
ENSG00000185838	GNB1L	0.000	-2.260
ENSG00000129810	SGO1	0.000	-2.259
ENSG00000160999	SH2B2	0.000	-2.258
ENSG00000204084	INPP5B	0.000	-2.258
ENSG00000161682	FAM171A2	0.000	-2.258
ENSG00000185760	KCNQ5	0.000	-2.257
ENSG00000111602	TIMELESS	0.000	-2.257
ENSG00000126562	WNK4	0.000	-2.257
ENSG00000147912	FBXO10	0.000	-2.256
ENSG00000174672	BRSK2	0.000	-2.255
ENSG00000140525	FANCI	0.000	-2.254
ENSG00000234664	HMG2P5	0.000	-2.254
ENSG00000198805	PNP	0.000	-2.253
ENSG00000206120	EGFEM1P	0.000	-2.253
ENSG00000073536	NLE1	0.000	-2.253
ENSG00000143702	CEP170	0.000	-2.252
ENSG00000170454	KRT75	0.000	-2.250
ENSG00000178999	AURKB	0.000	-2.249
ENSG00000181031	RPH3AL	0.000	-2.249
ENSG00000196159	FAT4	0.000	-2.248
ENSG00000254331	CKS1BP7	0.006	-2.247
ENSG00000107485	GATA3	0.000	-2.247
ENSG00000165480	SKA3	0.000	-2.246
ENSG00000213949	ITGA1	0.000	-2.245
ENSG00000164850	GPB1	0.000	-2.243
ENSG00000196739	COL27A1	0.000	-2.241
ENSG00000231607	DLEU2	0.000	-2.241
ENSG00000151503	NCAPD3	0.000	-2.238
ENSG00000225614	ZNF469	0.000	-2.237
ENSG00000118193	KIF14	0.000	-2.237
ENSG00000183049	CAMK1D	0.000	-2.235
ENSG00000127589	TUBBP1	0.000	-2.235
ENSG00000213621	RPSAP54	0.000	-2.234
ENSG00000138778	CENPE	0.000	-2.233
ENSG00000205268	PDE7A	0.000	-2.233
ENSG00000158458	NRG2	0.000	-2.233
ENSG00000224063	AC007319.1	0.000	-2.232
ENSG00000141384	TAF4B	0.000	-2.231
ENSG00000155093	PTPRN2	0.000	-2.230
ENSG00000135486	HNRNPA1	0.000	-2.229
ENSG00000196981	WDR5B	0.000	-2.228
ENSG00000163513	TGFBR2	0.000	-2.228
ENSG00000156970	BUB1B	0.000	-2.227
ENSG00000124664	SPDEF	0.000	-2.226
ENSG00000089685	BIRC5	0.000	-2.225
ENSG00000166922	SCG5	0.003	-2.223
ENSG00000179855	GIPC3	0.000	-2.223
ENSG00000073060	SCARB1	0.000	-2.222
ENSG00000237506	RPSAP15	0.000	-2.221
ENSG00000172159	FRMD3	0.000	-2.219
ENSG00000166068	SPRED1	0.000	-2.217
ENSG00000152270	PDE3B	0.000	-2.216
ENSG00000095319	NUP188	0.000	-2.215
ENSG00000206228	HNRNPA1P4	0.000	-2.214
ENSG00000256433	AC005840.2	0.000	-2.214
ENSG00000125398	SOX9	0.000	-2.213
ENSG00000204305	AGER	0.000	-2.213

ENSG00000157193	<i>LRP8</i>	0.000	-2.212
ENSG00000108370	<i>RGS9</i>	0.000	-2.210
ENSG00000161996	<i>WDR90</i>	0.000	-2.210
ENSG00000149548	<i>CCDC15</i>	0.000	-2.209
ENSG00000183150	<i>GPR19</i>	0.000	-2.209
ENSG00000174791	<i>RIN1</i>	0.000	-2.208
ENSG00000244585	<i>RPL12P33</i>	0.000	-2.208
ENSG00000171094	<i>ALK</i>	0.000	-2.207
ENSG00000268941	<i>LINC01711</i>	0.000	-2.206
ENSG00000077348	<i>EXOSC5</i>	0.000	-2.206
ENSG00000156802	<i>ATAD2</i>	0.000	-2.205
ENSG00000166997	<i>CNPY4</i>	0.000	-2.205
ENSG00000237649	<i>KIFC1</i>	0.000	-2.204
ENSG00000164520	<i>RAET1E</i>	0.000	-2.204
ENSG00000144057	<i>ST6GAL2</i>	0.000	-2.204
ENSG00000105202	<i>FBL</i>	0.000	-2.203
ENSG00000170577	<i>SIX2</i>	0.000	-2.202
ENSG00000178531	<i>CTXN1</i>	0.000	-2.200
ENSG00000164949	<i>GEM</i>	0.000	-2.199
ENSG00000155966	<i>AFF2</i>	0.000	-2.197
ENSG00000131323	<i>TRAF3</i>	0.000	-2.196
ENSG00000249992	<i>TMEM158</i>	0.000	-2.194
ENSG00000196139	<i>AKR1C3</i>	0.000	-2.194
ENSG00000136122	<i>BORA</i>	0.000	-2.192
ENSG00000212232	<i>SNORD17</i>	0.000	-2.191
ENSG00000118655	<i>DCLRE1B</i>	0.000	-2.191
ENSG00000154655	<i>L3MBTL4</i>	0.000	-2.188
ENSG00000162975	<i>KCNF1</i>	0.000	-2.187
ENSG00000242125	<i>SNHG3</i>	0.000	-2.187
ENSG00000100350	<i>FOXRED2</i>	0.000	-2.185
ENSG00000224189	<i>HAGLR</i>	0.000	-2.184
ENSG00000134690	<i>CDCA8</i>	0.000	-2.184
ENSG00000010319	<i>SEMA3G</i>	0.002	-2.182
ENSG00000197321	<i>SVIL</i>	0.000	-2.182
ENSG00000236044	<i>FABP5P2</i>	0.000	-2.182
ENSG00000166839	<i>ANKDD1A</i>	0.006	-2.181
ENSG00000218358	<i>RAET1K</i>	0.000	-2.181
ENSG00000101361	<i>NOP56</i>	0.000	-2.181
ENSG00000242147	<i>AL365356.5</i>	0.000	-2.181
ENSG00000119139	<i>TJP2</i>	0.000	-2.179
ENSG00000049246	<i>PER3</i>	0.000	-2.178
ENSG00000222365	<i>SNORD12B</i>	0.009	-2.177
ENSG00000135272	<i>MDFIC</i>	0.000	-2.177
ENSG00000276386	<i>CNTNAP3P2</i>	0.000	-2.176
ENSG00000260364	<i>AC009055.1</i>	0.002	-2.175
ENSG00000148400	<i>NOTCH1</i>	0.000	-2.174
ENSG00000101188	<i>NTSR1</i>	0.000	-2.174
ENSG00000161888	<i>SPC24</i>	0.000	-2.174
ENSG00000112182	<i>BACH2</i>	0.000	-2.173
ENSG00000272142	<i>LYRM4-AS1</i>	0.000	-2.173
ENSG00000101236	<i>RNF24</i>	0.000	-2.173
ENSG00000092964	<i>DPYSL2</i>	0.000	-2.173
ENSG00000173848	<i>NET1</i>	0.000	-2.172
ENSG00000137819	<i>PAQR5</i>	0.000	-2.172
ENSG00000258017	<i>AC011603.2</i>	0.000	-2.170
ENSG00000273306	<i>AC018690.1</i>	0.000	-2.170
ENSG00000198554	<i>WDHD1</i>	0.000	-2.169
ENSG00000177084	<i>POLE</i>	0.000	-2.169
ENSG00000196368	<i>NUDT11</i>	0.000	-2.169
ENSG00000111863	<i>ADTRP</i>	0.000	-2.168

ENSG00000163462	<i>TRIM46</i>	0.000	-2.168
ENSG00000160223	<i>ICOSLG</i>	0.000	-2.168
ENSG00000189143	<i>CLDN4</i>	0.000	-2.167
ENSG00000039068	<i>CDH1</i>	0.000	-2.167
ENSG00000138376	<i>BARD1</i>	0.000	-2.167
ENSG00000255642	<i>PABPC1P4</i>	0.000	-2.167
ENSG00000138160	<i>KIF11</i>	0.000	-2.166
ENSG00000163701	<i>IL17RE</i>	0.000	-2.166
ENSG00000261428	<i>AC097461.1</i>	0.000	-2.165
ENSG00000161021	<i>MAML1</i>	0.000	-2.165
ENSG00000088247	<i>KHSRP</i>	0.000	-2.164
ENSG00000179604	<i>CDC42EP4</i>	0.000	-2.164
ENSG00000135919	<i>SERPINE2</i>	0.000	-2.164
ENSG00000129534	<i>MIS18BP1</i>	0.000	-2.164
ENSG00000067992	<i>PKD3</i>	0.000	-2.163
ENSG00000113552	<i>GNPDA1</i>	0.000	-2.162
ENSG00000137310	<i>TCF19</i>	0.000	-2.162
ENSG00000066923	<i>STAG3</i>	0.003	-2.161
ENSG00000251322	<i>SHANK3</i>	0.000	-2.161
ENSG00000235489	<i>DBF4P1</i>	0.010	-2.158
ENSG00000248791	<i>AC010627.1</i>	0.005	-2.158
ENSG00000214756	<i>CSKMT</i>	0.000	-2.158
ENSG00000198835	<i>GJC2</i>	0.004	-2.157
ENSG00000279092	<i>AC025678.3</i>	0.000	-2.156
ENSG00000068985	<i>PAGE1</i>	0.001	-2.155
ENSG00000092621	<i>PHGDH</i>	0.000	-2.155
ENSG00000058091	<i>CDK14</i>	0.000	-2.152
ENSG00000255059	<i>PPIAP43</i>	0.003	-2.152
ENSG00000150990	<i>DHX37</i>	0.000	-2.152
ENSG00000179101	<i>AL590139.1</i>	0.003	-2.152
ENSG00000157111	<i>TMEM171</i>	0.000	-2.151
ENSG00000165300	<i>SLITRK5</i>	0.000	-2.150
ENSG00000182704	<i>TSKU</i>	0.000	-2.148
ENSG00000140937	<i>CDH11</i>	0.000	-2.148
ENSG00000259807	<i>AC009093.1</i>	0.000	-2.147
ENSG00000259330	<i>INAFM2</i>	0.000	-2.147
ENSG00000131747	<i>TOP2A</i>	0.000	-2.147
ENSG00000162723	<i>SLAMF9</i>	0.010	-2.146
ENSG00000231226	<i>TRIM31-AS1</i>	0.000	-2.146
ENSG00000103202	<i>NME4</i>	0.000	-2.145
ENSG00000130720	<i>FIBCD1</i>	0.000	-2.144
ENSG00000267500	<i>ZNF887P</i>	0.002	-2.142
ENSG00000164300	<i>SERINC5</i>	0.000	-2.141
ENSG00000129173	<i>E2F8</i>	0.000	-2.139
ENSG00000163629	<i>PTPN13</i>	0.000	-2.139
ENSG00000254244	<i>PAICSP4</i>	0.000	-2.139
ENSG00000196230	<i>TUBB</i>	0.000	-2.138
ENSG00000138764	<i>CCNG2</i>	0.000	-2.138
ENSG00000267534	<i>S1PR2</i>	0.000	-2.138
ENSG00000214455	<i>RCN1P2</i>	0.000	-2.137
ENSG00000102385	<i>DRP2</i>	0.000	-2.137
ENSG00000103319	<i>EEF2K</i>	0.000	-2.136
ENSG00000174482	<i>LINGO2</i>	0.000	-2.136
ENSG00000049323	<i>LTBP1</i>	0.000	-2.135
ENSG00000215424	<i>MCM3AP-AS1</i>	0.000	-2.135
ENSG00000236305	<i>SLC12A9-AS1</i>	0.004	-2.133
ENSG00000167900	<i>TK1</i>	0.000	-2.132
ENSG00000171345	<i>KRT19</i>	0.000	-2.131
ENSG00000132780	<i>NASP</i>	0.000	-2.131
ENSG00000106689	<i>LHX2</i>	0.000	-2.128

ENSG00000154133	ROBO4	0.000	-2.128
ENSG0000012048	BRCA1	0.000	-2.126
ENSG00000120658	ENOX1	0.000	-2.126
ENSG00000152990	ADGRA3	0.000	-2.125
ENSG00000106714	CNTNAP3	0.000	-2.125
ENSG00000189060	H1FO	0.000	-2.125
ENSG00000166483	WEE1	0.000	-2.123
ENSG00000101955	SRPX	0.000	-2.123
ENSG00000153574	RPIA	0.000	-2.123
ENSG00000185361	TNFAIP8L1	0.000	-2.123
ENSG00000170485	NPAS2	0.000	-2.123
ENSG00000197958	RPL12	0.000	-2.122
ENSG00000157456	CCNB2	0.000	-2.120
ENSG00000073711	PPP2R3A	0.000	-2.120
ENSG00000160712	IL6R	0.000	-2.119
ENSG00000162599	NFIA	0.000	-2.118
ENSG00000168411	RFWD3	0.000	-2.118
ENSG00000119866	BCL11A	0.000	-2.118
ENSG00000175063	UBE2C	0.000	-2.117
ENSG00000140600	SH3GL3	0.000	-2.117
ENSG00000171320	ESCO2	0.000	-2.117
ENSG00000139998	RAB15	0.000	-2.117
ENSG00000144554	FANCD2	0.000	-2.116
ENSG00000112365	ZBTB24	0.000	-2.116
ENSG00000277945	AC107308.1	0.007	-2.114
ENSG00000160991	ORAI2	0.000	-2.113
ENSG00000175745	NR2F1	0.000	-2.113
ENSG00000127946	HIP1	0.000	-2.112
ENSG00000181458	TMEM45A	0.000	-2.111
ENSG00000139263	LRIG3	0.000	-2.110
ENSG00000214391	TUBAP2	0.000	-2.107
ENSG00000281344	HELLPAR	0.000	-2.106
ENSG00000198743	SLC5A3	0.000	-2.105
ENSG00000115053	NCL	0.000	-2.103
ENSG00000050344	NFE2L3	0.000	-2.103
ENSG00000149269	PAK1	0.000	-2.103
ENSG00000136938	ANP32B	0.000	-2.102
ENSG00000183765	CHEK2	0.000	-2.101
ENSG00000137804	NUSAP1	0.000	-2.101
ENSG00000153071	DAB2	0.000	-2.101
ENSG00000273604	EPOP	0.000	-2.101
ENSG00000152104	PTPN14	0.000	-2.101
ENSG00000100167	37865.000	0.000	-2.100
ENSG00000167747	C19orf48	0.000	-2.099
ENSG00000158163	DZIP1L	0.000	-2.099
ENSG00000242262	AC092597.1	0.004	-2.099
ENSG00000056277	ZNF280C	0.000	-2.098
ENSG00000177602	HASPIN	0.000	-2.098
ENSG00000253161	LINC01605	0.000	-2.097
ENSG00000101868	POLA1	0.000	-2.096
ENSG00000196793	ZNF239	0.000	-2.096
ENSG00000145779	TNFAIP8	0.000	-2.095
ENSG00000106571	GLI3	0.000	-2.095
ENSG00000275464	FP565260.1	0.000	-2.094
ENSG00000102271	KLHL4	0.000	-2.093
ENSG00000134222	PSRC1	0.000	-2.093
ENSG00000166851	PLK1	0.000	-2.092
ENSG00000164045	CDC25A	0.000	-2.091
ENSG00000184261	KCNK12	0.000	-2.091
ENSG00000071564	TCF3	0.000	-2.090

ENSG00000196782	MAML3	0.000	-2.090
ENSG00000234062	AL390879.1	0.000	-2.089
ENSG00000143850	PLEKHA6	0.000	-2.088
ENSG00000183298	RPSAP19	0.000	-2.086
ENSG00000155090	KLF10	0.000	-2.086
ENSG00000140332	TLE3	0.000	-2.086
ENSG00000186918	ZNF395	0.000	-2.085
ENSG00000182118	FAM89A	0.000	-2.084
ENSG00000182158	CREB3L2	0.000	-2.083
ENSG00000224043	CCNT2-AS1	0.001	-2.082
ENSG00000270195	AC016773.1	0.008	-2.082
ENSG00000088325	TPX2	0.000	-2.081
ENSG00000162650	ATXN7L2	0.000	-2.081
ENSG00000015475	BID	0.000	-2.080
ENSG00000124920	MYRF	0.000	-2.079
ENSG00000104147	OIP5	0.000	-2.079
ENSG00000135821	GLUL	0.000	-2.078
ENSG00000261236	BOP1	0.000	-2.077
ENSG00000161647	MPP3	0.000	-2.077
ENSG00000226887	ERVMER34-1	0.000	-2.076
ENSG00000253729	PRKDC	0.000	-2.076
ENSG00000175874	CREG2	0.000	-2.075
ENSG00000275185	AC130324.3	0.006	-2.074
ENSG00000198826	ARHGAP11A	0.000	-2.074
ENSG00000165138	ANKS6	0.000	-2.073
ENSG00000129347	KRI1	0.000	-2.073
ENSG00000167723	TRPV3	0.000	-2.073
ENSG00000170802	FOXN2	0.000	-2.072
ENSG00000169093	ASMTL	0.000	-2.072
ENSG00000176387	HSD11B2	0.000	-2.070
ENSG00000204682	CASC10	0.000	-2.070
ENSG00000240087	RPSAP12	0.000	-2.070
ENSG00000165304	MELK	0.000	-2.070
ENSG00000165359	INTS6L	0.000	-2.069
ENSG00000168286	THAP11	0.000	-2.069
ENSG00000138386	NAB1	0.000	-2.068
ENSG00000020633	RUNX3	0.000	-2.068
ENSG00000171791	BCL2	0.000	-2.067
ENSG00000260822	AC004656.1	0.000	-2.065
ENSG00000168028	RPSA	0.000	-2.065
ENSG00000170779	CDCA4	0.000	-2.065
ENSG00000213740	SERBP1P1	0.000	-2.065
ENSG00000135480	KRT7	0.000	-2.063
ENSG00000146670	CDCA5	0.000	-2.062
ENSG00000197249	SERPINA1	0.000	-2.062
ENSG00000041982	TNC	0.000	-2.061
ENSG00000198400	NTRK1	0.002	-2.059
ENSG00000260751	AC008870.2	0.002	-2.058
ENSG00000101307	SIRPB1	0.000	-2.057
ENSG00000182979	MTA1	0.000	-2.057

ENSG00000166979	EVA1C	0.000	-2.055
ENSG00000181467	RAP2B	0.000	-2.055
ENSG00000187372	PCDHB13	0.000	-2.054
ENSG00000116649	SRM	0.000	-2.053
ENSG00000131759	RARA	0.000	-2.053
ENSG00000160917	CPSF4	0.000	-2.053
ENSG00000204371	EHMT2	0.000	-2.053
ENSG00000075618	FSCN1	0.000	-2.052
ENSG00000090006	LTBP4	0.000	-2.052
ENSG00000161638	ITGA5	0.000	-2.052
ENSG00000087077	TRIP6	0.000	-2.051
ENSG00000049247	UTS2	0.000	-2.050
ENSG00000109265	KIAA1211	0.000	-2.050
ENSG00000122483	CCDC18	0.000	-2.050
ENSG00000124795	DEK	0.000	-2.049
ENSG00000100749	VRK1	0.000	-2.049
ENSG00000159784	FAM131B	0.000	-2.049
ENSG00000100413	POLR3H	0.000	-2.049
ENSG00000178202	KDELC2	0.000	-2.047
ENSG00000172167	MTBP	0.000	-2.047
ENSG00000142634	EFHD2	0.000	-2.046
ENSG00000125319	C17orf53	0.000	-2.046
ENSG00000103540	CCP110	0.000	-2.046
ENSG00000058085	LAMC2	0.000	-2.044
ENSG00000224543	SNRPGP15	0.005	-2.044
ENSG00000132382	MYBBP1A	0.000	-2.043
ENSG00000198846	TOX	0.001	-2.043
ENSG00000251593	MSNP1	0.001	-2.043
ENSG00000154529	CNTNAP3B	0.000	-2.043
ENSG00000137812	KNL1	0.000	-2.041
ENSG00000187741	FANCA	0.000	-2.041
ENSG00000107130	NCS1	0.000	-2.041
ENSG00000172766	NAA16	0.000	-2.040
ENSG00000105137	SYDE1	0.000	-2.040
ENSG00000177076	ACER2	0.001	-2.040
ENSG00000112742	TTK	0.000	-2.039
ENSG00000054654	SYNE2	0.000	-2.038
ENSG00000182256	GABRG3	0.000	-2.037
ENSG00000092068	SLC7A8	0.000	-2.037
ENSG00000157827	FMNL2	0.000	-2.037
ENSG00000157227	MMP14	0.000	-2.036
ENSG00000053372	MRTO4	0.000	-2.036
ENSG00000062822	POLD1	0.000	-2.036
ENSG00000241549	GUSBP2	0.003	-2.035
ENSG00000108797	CNTNAP1	0.000	-2.034
ENSG00000259051	HNRNPUP1	0.001	-2.033
ENSG00000213397	HAUS7	0.001	-2.033
ENSG00000177453	NIM1K	0.000	-2.033
ENSG00000168140	VASN	0.000	-2.033
ENSG00000111206	FOXM1	0.000	-2.033
ENSG00000100479	POLE2	0.000	-2.032
ENSG00000168811	IL12A	0.000	-2.032
ENSG00000140022	STON2	0.000	-2.032
ENSG00000162062	TEDC2	0.000	-2.031
ENSG00000153012	LG12	0.000	-2.031
ENSG00000174136	RGMB	0.000	-2.029
ENSG00000110063	DCPS	0.000	-2.029
ENSG00000125285	SOX21	0.000	-2.027
ENSG00000094804	CDC6	0.000	-2.026
ENSG00000207547	MIR25	0.004	-2.026

ENSG0000014555	<i>MYO10</i>	0.000	-2.026
ENSG00000119397	<i>CNTRL</i>	0.000	-2.025
ENSG00000145284	<i>SCD5</i>	0.000	-2.024
ENSG00000067141	<i>NEO1</i>	0.000	-2.024
ENSG00000143479	<i>DYRK3</i>	0.000	-2.024
ENSG00000039139	<i>DNAH5</i>	0.000	-2.024
ENSG00000198753	<i>PLXNB3</i>	0.000	-2.024
ENSG00000148773	<i>MKI67</i>	0.000	-2.024
ENSG00000182798	<i>MAGEB17</i>	0.002	-2.023
ENSG00000140548	<i>ZNF710</i>	0.000	-2.023
ENSG00000260920	<i>AL031985.3</i>	0.000	-2.023
ENSG00000139618	<i>BRCA2</i>	0.000	-2.023
ENSG00000006634	<i>DBF4</i>	0.000	-2.022
ENSG00000115825	<i>PRKD3</i>	0.000	-2.021
ENSG00000226608	<i>FTLP3</i>	0.000	-2.021
ENSG00000196418	<i>ZNF124</i>	0.000	-2.021
ENSG00000143179	<i>UCK2</i>	0.000	-2.021
ENSG00000058056	<i>USP13</i>	0.000	-2.020
ENSG00000167550	<i>RHEBL1</i>	0.000	-2.020
ENSG00000112159	<i>MDN1</i>	0.000	-2.020
ENSG00000154102	<i>C16orf74</i>	0.000	-2.020
ENSG00000101670	<i>LIPG</i>	0.000	-2.020
ENSG00000135446	<i>CDK4</i>	0.000	-2.020
ENSG00000198830	<i>HMGH2</i>	0.000	-2.020
ENSG00000245213	<i>AC105285.1</i>	0.001	-2.019
ENSG00000164985	<i>PSIP1</i>	0.000	-2.019
ENSG00000152128	<i>TMEM163</i>	0.000	-2.019
ENSG00000285872	<i>AC007240.2</i>	0.000	-2.019
ENSG00000069011	<i>PITX1</i>	0.000	-2.019
ENSG00000143842	<i>SOX13</i>	0.000	-2.019
ENSG00000198108	<i>CHSY3</i>	0.000	-2.018
ENSG00000173258	<i>ZNF483</i>	0.000	-2.018
ENSG00000123384	<i>LRP1</i>	0.000	-2.018
ENSG00000136490	<i>LIMD2</i>	0.000	-2.017
ENSG00000184349	<i>EFNA5</i>	0.000	-2.017
ENSG00000142945	<i>KIF2C</i>	0.000	-2.017
ENSG00000138658	<i>ZGRF1</i>	0.000	-2.015
ENSG00000245248	<i>USP2-AS1</i>	0.000	-2.015
ENSG00000132773	<i>TOE1</i>	0.000	-2.015
ENSG00000073849	<i>ST6GAL1</i>	0.000	-2.013
ENSG00000205002	<i>AARD</i>	0.000	-2.012
ENSG00000271270	<i>TMCC1-AS1</i>	0.000	-2.012
ENSG00000213983	<i>AP1G2</i>	0.000	-2.011
ENSG00000119514	<i>GALNT12</i>	0.000	-2.011
ENSG00000245205	<i>EEF1A1P4</i>	0.000	-2.011
ENSG00000035681	<i>NSMAF</i>	0.000	-2.010
ENSG00000101974	<i>ATP11C</i>	0.000	-2.010
ENSG00000103257	<i>SLC7A5</i>	0.000	-2.009
ENSG00000140350	<i>ANP32A</i>	0.000	-2.008
ENSG00000154764	<i>WNT7A</i>	0.000	-2.008
ENSG00000109805	<i>NCAPG</i>	0.000	-2.007
ENSG00000229358	<i>DPY19L1P1</i>	0.000	-2.007
ENSG00000238083	<i>LRRC37A2</i>	0.000	-2.006
ENSG00000285756	<i>BX890604.2</i>	0.000	-2.006
ENSG00000120800	<i>UTP20</i>	0.000	-2.005
ENSG00000089157	<i>RPLP0</i>	0.000	-2.004
ENSG00000153898	<i>MCOLN2</i>	0.000	-2.004
ENSG00000131370	<i>SH3BP5</i>	0.000	-2.003
ENSG00000066279	<i>ASPM</i>	0.000	-2.002
ENSG00000183077	<i>AFMID</i>	0.000	-2.001
ENSG00000100304	<i>TLL12</i>	0.000	-2.000

ENSG00000119673	ACOT2	0.000	2.009
ENSG00000173013	CCDC96	0.000	2.012
ENSG00000160606	TLCD1	0.000	2.013
ENSG00000160113	NR2F6	0.000	2.014
ENSG00000248362	AC011352.1	0.000	2.015
ENSG00000004779	NDUFAB1	0.000	2.016
ENSG00000274471	AC242376.2	0.000	2.016
ENSG00000204370	SDHD	0.000	2.017
ENSG00000197837	HIST4H4	0.000	2.017
ENSG00000167995	BEST1	0.000	2.017
ENSG00000170522	ELOVL6	0.000	2.018
ENSG00000117151	CTBS	0.000	2.018
ENSG00000215712	TMEM242	0.000	2.019
ENSG00000107295	SH3GL2	0.000	2.020
ENSG00000178922	HYI	0.000	2.020
ENSG00000127325	BEST3	0.000	2.021
ENSG00000253368	TRNP1	0.000	2.021
ENSG00000251562	MALAT1	0.000	2.022
ENSG00000197982	C1orf122	0.000	2.023
ENSG00000272734	ADIRF-AS1	0.000	2.023
ENSG00000229950	TFAP2A-AS1	0.004	2.025
ENSG00000148834	GSTO1	0.000	2.026
ENSG00000107872	FBXL15	0.000	2.027
ENSG00000124882	EREG	0.000	2.027
ENSG00000253738	OTUD6B-AS1	0.000	2.029
ENSG00000180596	HIST1H2BC	0.000	2.029
ENSG00000131781	FMO5	0.000	2.029
ENSG00000120925	RNF170	0.000	2.029
ENSG00000228253	MT-ATP8	0.000	2.030
ENSG00000257337	AC068888.1	0.000	2.030
ENSG00000158813	EDA	0.000	2.033
ENSG00000119723	COQ6	0.000	2.033
ENSG00000109016	DHRS7B	0.000	2.034
ENSG00000234899	SOX9-AS1	0.000	2.034
ENSG00000255874	LINC00346	0.000	2.035
ENSG00000105321	CCDC9	0.000	2.036
ENSG00000128609	NDUFA5	0.000	2.036
ENSG00000172893	DHCR7	0.000	2.036
ENSG00000247626	MARS2	0.000	2.036
ENSG00000274897	PANO1	0.000	2.037
ENSG00000105989	WNT2	0.000	2.037
ENSG00000166770	ZNF667-AS1	0.000	2.037
ENSG00000155918	RAET1L	0.000	2.038
ENSG00000238755	LINC02006	0.008	2.038
ENSG00000211451	GNRHR2	0.000	2.041
ENSG00000211772	TRBC2	0.000	2.041
ENSG00000184588	PDE4B	0.000	2.041
ENSG00000170456	DENND5B	0.000	2.041
ENSG00000237973	MTCO1P12	0.000	2.041
ENSG00000204936	CD177	0.000	2.042
ENSG00000276116	FUT8-AS1	0.000	2.042
ENSG00000135636	DYSF	0.000	2.043
ENSG00000117152	RGS4	0.000	2.044
ENSG00000118997	DNAH7	0.000	2.044
ENSG00000132906	CASP9	0.000	2.046
ENSG00000178401	DNAJC22	0.000	2.047
ENSG00000189227	C15orf61	0.000	2.047
ENSG00000267809	NDUFV2P1	0.000	2.047
ENSG00000166136	NDUFB8	0.000	2.047

ENSG00000173482	<i>PTPRM</i>	0.000	2.048
ENSG00000160703	<i>NLRX1</i>	0.000	2.048
ENSG00000204219	<i>TCEA3</i>	0.000	2.048
ENSG00000106479	<i>ZNF862</i>	0.000	2.049
ENSG00000121005	<i>CRISPLD1</i>	0.000	2.049
ENSG00000187118	<i>CMC1</i>	0.000	2.050
ENSG00000154188	<i>ANGPT1</i>	0.000	2.050
ENSG00000146701	<i>MDH2</i>	0.000	2.051
ENSG00000158825	<i>CDA</i>	0.000	2.051
ENSG00000283696	<i>AL592295.4</i>	0.000	2.051
ENSG00000180353	<i>HCLS1</i>	0.000	2.052
ENSG00000122033	<i>MTIF3</i>	0.000	2.052
ENSG00000185189	<i>NRBP2</i>	0.000	2.054
ENSG00000145348	<i>TBCK</i>	0.000	2.054
ENSG00000104823	<i>ECH1</i>	0.000	2.055
ENSG00000178038	<i>ALS2CL</i>	0.000	2.055
ENSG00000089127	<i>OAS1</i>	0.000	2.055
ENSG00000128683	<i>GAD1</i>	0.000	2.056
ENSG00000137801	<i>THBS1</i>	0.000	2.057
ENSG00000181035	<i>SLC25A42</i>	0.000	2.057
ENSG00000245060	<i>LINC00847</i>	0.000	2.057
ENSG00000111331	<i>OAS3</i>	0.000	2.057
ENSG00000073464	<i>CLCN4</i>	0.000	2.058
ENSG00000138271	<i>GPR87</i>	0.000	2.058
ENSG00000163956	<i>LRPAP1</i>	0.000	2.058
ENSG00000155816	<i>FMN2</i>	0.000	2.058
ENSG00000277639	<i>AC007906.2</i>	0.000	2.058
ENSG00000182372	<i>CLN8</i>	0.000	2.059
ENSG00000173511	<i>VEGFB</i>	0.000	2.059
ENSG00000280120	<i>AC073857.1</i>	0.000	2.060
ENSG00000258056	<i>AC009779.2</i>	0.000	2.060
ENSG00000155495	<i>MAGEC1</i>	0.001	2.060
ENSG00000160190	<i>SLC37A1</i>	0.000	2.061
ENSG00000277586	<i>NEFL</i>	0.000	2.062
ENSG00000106031	<i>HOXA13</i>	0.000	2.062
ENSG0000012061	<i>ERCC1</i>	0.000	2.062
ENSG00000171130	<i>ATP6V0E2</i>	0.000	2.062
ENSG00000171757	<i>LRRC34</i>	0.000	2.063
ENSG00000138380	<i>CARF</i>	0.000	2.063
ENSG00000233184	<i>AC093157.1</i>	0.000	2.065
ENSG00000221883	<i>ARIH2OS</i>	0.000	2.066
ENSG00000179044	<i>EXOC3L1</i>	0.000	2.067
ENSG00000267750	<i>RUNDC3A-AS1</i>	0.000	2.067
ENSG00000133597	<i>ADCK2</i>	0.000	2.068
ENSG00000196110	<i>ZNF699</i>	0.000	2.069
ENSG00000170917	<i>NUDT6</i>	0.000	2.069
ENSG00000067221	<i>STOML1</i>	0.000	2.069
ENSG00000154856	<i>APCDD1</i>	0.001	2.069
ENSG00000135423	<i>GLS2</i>	0.000	2.071
ENSG00000170421	<i>KRT8</i>	0.000	2.073
ENSG00000023608	<i>SNAPC1</i>	0.000	2.073
ENSG00000228305	<i>AC016734.1</i>	0.000	2.073
ENSG00000152782	<i>PANK1</i>	0.000	2.073
ENSG00000021355	<i>SERPINB1</i>	0.000	2.074
ENSG00000067829	<i>IDH3G</i>	0.000	2.074
ENSG00000186715	<i>MST1L</i>	0.000	2.075
ENSG00000139344	<i>AMDHD1</i>	0.000	2.075
ENSG00000242114	<i>MTFP1</i>	0.000	2.075
ENSG00000249348	<i>UGDH-AS1</i>	0.000	2.077
ENSG00000155367	<i>PPM1J</i>	0.000	2.077

ENSG00000082014	SMARCD3	0.000	2.077
ENSG00000167578	RAB4B	0.006	2.077
ENSG00000237289	CKMT1B	0.000	2.078
ENSG00000155158	TTC39B	0.000	2.079
ENSG00000101084	RAB51F	0.000	2.079
ENSG00000036672	USP2	0.000	2.080
ENSG00000241837	ATP5PO	0.000	2.080
ENSG00000156787	TBC1D31	0.000	2.082
ENSG00000141012	GALNS	0.000	2.083
ENSG00000147614	ATP6V0D2	0.000	2.084
ENSG00000175606	TMEM70	0.000	2.086
ENSG00000175110	MRPS22	0.000	2.086
ENSG00000228775	WEE2-AS1	0.010	2.087
ENSG00000107742	SPOCK2	0.000	2.087
ENSG00000184232	OAF	0.000	2.090
ENSG00000223891	OSER1-DT	0.000	2.092
ENSG00000145491	ROPN1L	0.008	2.092
ENSG00000101846	STS	0.000	2.092
ENSG00000106853	PTGR1	0.000	2.093
ENSG00000069509	FUNDC1	0.000	2.094
ENSG00000188002	AC026412.1	0.000	2.095
ENSG00000118503	TNFAIP3	0.000	2.096
ENSG00000229344	MTCO2P12	0.000	2.096
ENSG00000204267	TAP2	0.000	2.096
ENSG00000196116	TDRD7	0.000	2.098
ENSG00000116459	ATP5PB	0.000	2.098
ENSG00000083838	ZNF446	0.000	2.098
ENSG00000173221	GLRX	0.000	2.099
ENSG00000157578	LCA5L	0.000	2.100
ENSG00000262185	AC005736.1	0.000	2.100
ENSG00000111224	PARP11	0.001	2.101
ENSG00000117682	DHDDS	0.000	2.102
ENSG00000186577	SMIM29	0.000	2.104
ENSG00000233382	NKAPP1	0.000	2.104
ENSG00000256982	AC135782.1	0.000	2.105
ENSG00000204054	LINC00963	0.000	2.106
ENSG00000117245	KIF17	0.000	2.106
ENSG00000180573	HIST1H2AC	0.000	2.107
ENSG00000131269	ABCB7	0.000	2.109
ENSG00000140374	ETFA	0.000	2.109
ENSG00000254815	AP006284.1	0.001	2.110
ENSG00000109103	UNC119	0.000	2.111
ENSG00000162711	NLRP3	0.000	2.111
ENSG00000248527	MTATP6P1	0.000	2.111
ENSG00000089847	ANKRD24	0.000	2.112
ENSG00000141385	AFG3L2	0.000	2.112
ENSG00000139985	ADAM21	0.002	2.112
ENSG00000143412	ANXA9	0.000	2.113
ENSG00000257605	AC073611.1	0.000	2.114
ENSG00000268916	CSAG3	0.000	2.114
ENSG00000238258	AL121748.2	0.000	2.115
ENSG00000074319	TSG101	0.000	2.115
ENSG00000169432	SCN9A	0.000	2.117
ENSG00000204876	AC021218.1	0.000	2.117
ENSG00000249898	MCPH1-AS1	0.000	2.118
ENSG00000106554	CHCHD3	0.000	2.118
ENSG00000130159	ECSIT	0.000	2.118
ENSG00000160182	TFF1	0.000	2.118
ENSG00000119630	PGF	0.000	2.119
ENSG00000214562	NUTM2D	0.000	2.123

ENSG0000059378	PARP12	0.000	2.123
ENSG0000013364	MVP	0.000	2.123
ENSG00000120156	TEK	0.002	2.124
ENSG00000181409	AATK	0.001	2.125
ENSG00000104812	GYS1	0.000	2.126
ENSG00000139182	CLSTN3	0.000	2.126
ENSG00000173227	SYT12	0.000	2.127
ENSG00000203780	FANK1	0.000	2.127
ENSG00000196850	PPTC7	0.000	2.128
ENSG00000162520	SYNC	0.000	2.128
ENSG00000255458	AC108471.2	0.004	2.128
ENSG00000219200	RNASEK	0.000	2.128
ENSG00000243364	EFNA4	0.000	2.129
ENSG00000261211	AL031123.2	0.000	2.129
ENSG00000144935	TRPC1	0.000	2.130
ENSG00000172974	AC007318.1	0.000	2.130
ENSG00000267309	AC092295.2	0.000	2.131
ENSG00000152465	NMT2	0.000	2.131
ENSG00000140941	MAP1LC3B	0.000	2.132
ENSG00000277075	HIST1H2AE	0.000	2.132
ENSG00000273015	AC008124.1	0.000	2.132
ENSG00000171161	ZNF672	0.000	2.132
ENSG00000241081	RPL22P2	0.000	2.132
ENSG00000104883	PEX11G	0.000	2.133
ENSG00000188039	NWD1	0.000	2.135
ENSG00000241468	ATP5MF	0.000	2.135
ENSG00000110435	PDHX	0.000	2.135
ENSG00000092841	MYL6	0.000	2.137
ENSG00000172927	MYEOV	0.000	2.137
ENSG00000230513	THAP7-AS1	0.000	2.139
ENSG00000164074	ABHD18	0.000	2.139
ENSG00000277283	AC004812.2	0.000	2.140
ENSG00000165804	ZNF219	0.000	2.140
ENSG00000231908	IDH1-AS1	0.001	2.140
ENSG00000170775	GPR37	0.000	2.141
ENSG00000243926	TIPARP-AS1	0.001	2.141
ENSG00000138823	MTTP	0.005	2.144
ENSG00000113389	NPR3	0.000	2.144
ENSG00000054148	PHPT1	0.000	2.145
ENSG00000152495	CAMK4	0.000	2.147
ENSG00000101298	SNPH	0.000	2.148
ENSG00000229637	PRAC2	0.000	2.149
ENSG00000079739	PGM1	0.000	2.149
ENSG00000171159	C9orf16	0.000	2.150
ENSG00000128590	DNAJB9	0.000	2.150
ENSG00000198868	MTND4LP30	0.004	2.151
ENSG00000255182	AC084125.2	0.000	2.152
ENSG00000140939	NOL3	0.000	2.152
ENSG00000255559	ZNF252P-AS1	0.003	2.152
ENSG00000169752	NRG4	0.000	2.153
ENSG00000119801	YPEL5	0.000	2.153
ENSG00000113845	TIMMDC1	0.000	2.154
ENSG00000006757	PNPLA4	0.000	2.154
ENSG00000100554	ATP6V1D	0.000	2.155
ENSG00000115649	CNPPD1	0.000	2.158
ENSG00000123999	INHA	0.000	2.159
ENSG00000166016	ABTB2	0.000	2.159
ENSG00000279861	AC073548.1	0.001	2.159
ENSG00000163661	PTX3	0.000	2.160
ENSG00000179743	FLJ37453	0.000	2.160

ENSG00000100299	ARSA	0.000	2.160
ENSG00000138134	STAMBPL1	0.000	2.161
ENSG00000229953	AL590666.2	0.000	2.161
ENSG00000115425	PECR	0.000	2.162
ENSG00000078018	MAP2	0.000	2.162
ENSG00000114209	PDCD10	0.000	2.163
ENSG00000112812	PRSS16	0.000	2.163
ENSG00000076344	RGS11	0.000	2.163
ENSG00000074855	ANO8	0.000	2.163
ENSG00000273045	C2orf15	0.000	2.163
ENSG00000267277	AC024575.1	0.010	2.164
ENSG00000260000	AL133338.1	0.000	2.166
ENSG00000107897	ACBD5	0.000	2.168
ENSG00000157613	CREB3L1	0.000	2.169
ENSG00000272462	U91328.1	0.000	2.169
ENSG00000247595	SPTY2D10S	0.000	2.170
ENSG00000106052	TAX1BP1	0.000	2.170
ENSG00000246582	AC100861.1	0.000	2.172
ENSG00000141179	PCTP	0.000	2.173
ENSG00000169738	DCXR	0.000	2.175
ENSG00000240990	HOXA11-AS	0.000	2.176
ENSG00000064687	ABCA7	0.000	2.177
ENSG00000048392	RRM2B	0.000	2.180
ENSG00000050426	LETMD1	0.000	2.180
ENSG00000161558	TMEM143	0.000	2.181
ENSG00000138166	DUSP5	0.000	2.182
ENSG00000170390	DCLK2	0.000	2.182
ENSG00000227869	AC073486.1	0.000	2.182
ENSG00000221990	EXOC3-AS1	0.000	2.182
ENSG00000063854	HAGH	0.000	2.183
ENSG00000157306	ZFX2-AS1	0.000	2.184
ENSG00000151376	ME3	0.000	2.185
ENSG00000112031	MTRF1L	0.000	2.186
ENSG00000099219	ERMP1	0.000	2.187
ENSG00000140264	SERF2	0.000	2.187
ENSG00000172037	LAMB2	0.000	2.188
ENSG00000184163	C1QTNF12	0.000	2.189
ENSG00000178425	NT5DC1	0.000	2.189
ENSG00000260742	AC009962.1	0.000	2.190
ENSG00000205634	LINC00898	0.000	2.191
ENSG00000111271	ACAD10	0.000	2.194
ENSG00000162601	MYSM1	0.000	2.196
ENSG00000175893	ZDHHC21	0.000	2.196
ENSG00000112473	SLC39A7	0.000	2.196
ENSG00000155629	PIK3AP1	0.000	2.196
ENSG00000279227	AC009303.4	0.000	2.196
ENSG00000153253	SCN3A	0.000	2.199
ENSG00000250571	GLI4	0.000	2.200
ENSG00000266472	MRPS21	0.000	2.201
ENSG00000125611	CHCHD5	0.000	2.201
ENSG00000198870	STKLD1	0.000	2.201
ENSG00000249867	AC090833.1	0.000	2.202
ENSG00000135317	SNX14	0.000	2.202
ENSG00000273382	AL356488.3	0.000	2.202
ENSG00000184076	UQCR10	0.000	2.202
ENSG00000133805	AMPD3	0.000	2.203
ENSG00000076513	ANKRD13A	0.000	2.203
ENSG00000132141	CCT6B	0.000	2.203
ENSG00000126458	RRAS	0.000	2.203
ENSG00000186815	TPCN1	0.000	2.203

ENSG00000188266	<i>HYKK</i>	0.000	2.204
ENSG00000171962	<i>DRC3</i>	0.007	2.205
ENSG00000124374	<i>PAIP2B</i>	0.000	2.206
ENSG00000180758	<i>GPR157</i>	0.000	2.207
ENSG00000173193	<i>PARP14</i>	0.000	2.209
ENSG00000184271	<i>POU6F1</i>	0.000	2.209
ENSG00000159423	<i>ALDH4A1</i>	0.000	2.209
ENSG00000198899	<i>MT-ATP6</i>	0.000	2.210
ENSG00000131018	<i>SYNE1</i>	0.000	2.212
ENSG00000198836	<i>OPA1</i>	0.000	2.212
ENSG00000137547	<i>MRPL15</i>	0.000	2.213
ENSG00000108786	<i>HSD17B1</i>	0.001	2.213
ENSG00000226942	<i>IL9RP3</i>	0.000	2.214
ENSG00000153790	<i>C7orf31</i>	0.000	2.214
ENSG00000170270	<i>GON7</i>	0.000	2.215
ENSG00000184979	<i>USP18</i>	0.000	2.215
ENSG00000170502	<i>NUDT9</i>	0.000	2.215
ENSG00000227398	<i>KIF9-AS1</i>	0.000	2.215
ENSG00000185986	<i>SDHAP3</i>	0.000	2.217
ENSG00000112651	<i>MRPL2</i>	0.000	2.218
ENSG00000232388	<i>SMIM26</i>	0.000	2.218
ENSG00000197296	<i>FITM2</i>	0.000	2.219
ENSG00000099246	<i>RAB18</i>	0.000	2.219
ENSG00000156411	<i>ATP5MPL</i>	0.000	2.220
ENSG00000112293	<i>GPLD1</i>	0.000	2.221
ENSG00000260267	<i>AC026471.1</i>	0.000	2.223
ENSG00000131096	<i>PYY</i>	0.004	2.223
ENSG00000103415	<i>HMOX2</i>	0.000	2.223
ENSG00000119227	<i>PIGZ</i>	0.000	2.229
ENSG00000224186	<i>C5orf66</i>	0.000	2.230
ENSG00000151743	<i>AMN1</i>	0.000	2.233
ENSG00000027001	<i>MIPEP</i>	0.000	2.233
ENSG00000108439	<i>PNPO</i>	0.000	2.234
ENSG00000204792	<i>LINC01291</i>	0.000	2.237
ENSG00000258102	<i>MAP1LC3B2</i>	0.000	2.237
ENSG00000180185	<i>FAHD1</i>	0.000	2.237
ENSG00000262587	<i>AC133552.2</i>	0.000	2.238
ENSG00000146556	<i>WASH2P</i>	0.000	2.242
ENSG00000213025	<i>COX20P1</i>	0.002	2.244
ENSG00000169490	<i>TM2D2</i>	0.000	2.244
ENSG00000259291	<i>ZNF710-AS1</i>	0.000	2.245
ENSG00000164168	<i>TMEM184C</i>	0.000	2.245
ENSG00000176732	<i>PFN4</i>	0.000	2.246
ENSG00000068366	<i>ACSL4</i>	0.000	2.246
ENSG00000133794	<i>ARNTL</i>	0.000	2.247
ENSG00000006007	<i>GDE1</i>	0.000	2.248
ENSG00000106077	<i>ABHD11</i>	0.000	2.250
ENSG00000118369	<i>USP35</i>	0.000	2.250
ENSG00000108950	<i>FAM20A</i>	0.000	2.250
ENSG00000231551	<i>AC245100.4</i>	0.001	2.250
ENSG00000255153	<i>TOLLIP-AS1</i>	0.000	2.251
ENSG00000261455	<i>LINC01003</i>	0.000	2.252
ENSG00000141447	<i>OSBPL1A</i>	0.000	2.252
ENSG00000158793	<i>NIT1</i>	0.000	2.253
ENSG00000224914	<i>LINC00863</i>	0.000	2.253
ENSG00000101608	<i>MYL12A</i>	0.000	2.253
ENSG00000166473	<i>PKD1L2</i>	0.000	2.253
ENSG00000256148	<i>AP000763.2</i>	0.000	2.253
ENSG00000088808	<i>PPP1R13B</i>	0.000	2.254
ENSG00000108187	<i>PBLD</i>	0.000	2.255

ENSG00000136783	NIPSNAP3A	0.000	2.256
ENSG00000144118	RALB	0.000	2.256
ENSG00000126368	NR1D1	0.000	2.258
ENSG00000127838	PNKD	0.000	2.258
ENSG00000135750	KCNK1	0.000	2.258
ENSG00000102003	SYP	0.000	2.259
ENSG00000262902	MTCO1P40	0.000	2.259
ENSG00000197776	KLHDC1	0.000	2.261
ENSG00000171552	BCL2L1	0.000	2.261
ENSG00000197980	LEKR1	0.000	2.261
ENSG00000260658	AC138305.1	0.000	2.262
ENSG00000144406	UNC80	0.003	2.262
ENSG00000142233	NTN5	0.000	2.263
ENSG00000144642	RBMS3	0.000	2.266
ENSG00000250658	AC097652.1	0.001	2.266
ENSG00000213904	LIPE-AS1	0.000	2.267
ENSG00000185664	PMEL	0.000	2.268
ENSG00000136888	ATP6V1G1	0.000	2.269
ENSG00000123240	OPTN	0.000	2.269
ENSG00000055211	GINM1	0.000	2.271
ENSG00000233175	AC008105.1	0.000	2.272
ENSG00000073350	LLGL2	0.000	2.272
ENSG00000168300	PCMTD1	0.000	2.272
ENSG00000106785	TRIM14	0.000	2.273
ENSG00000236017	ASMTL-AS1	0.000	2.275
ENSG00000204335	SP5	0.000	2.277
ENSG00000052723	SIKE1	0.000	2.277
ENSG00000270964	AC016355.1	0.000	2.277
ENSG00000177465	ACOT4	0.000	2.278
ENSG00000099365	STX1B	0.000	2.278
ENSG00000244968	LIFR-AS1	0.000	2.279
ENSG00000130940	CASZ1	0.000	2.280
ENSG00000135047	CTSL	0.000	2.281
ENSG00000159199	ATP5MC1	0.000	2.281
ENSG00000276550	HERC2P2	0.000	2.281
ENSG00000070404	FSTL3	0.000	2.281
ENSG00000115844	DLX2	0.000	2.281
ENSG00000226824	AC006001.2	0.000	2.281
ENSG00000280071	GATD3B	0.000	2.282
ENSG00000177854	TMEM187	0.000	2.282
ENSG00000261971	MMP25-AS1	0.000	2.282
ENSG00000116885	OSCP1	0.000	2.283
ENSG00000235927	NEXN-AS1	0.000	2.284
ENSG00000235750	KIAA0040	0.000	2.285
ENSG00000160318	CLDND2	0.000	2.285
ENSG00000204592	HLA-E	0.000	2.286
ENSG00000147155	EBP	0.000	2.287
ENSG00000275894	AL021578.1	0.007	2.288
ENSG00000272273	IER3-AS1	0.000	2.288
ENSG00000122870	BICC1	0.000	2.289
ENSG00000228624	HDAC2-AS2	0.000	2.290
ENSG00000119689	DLST	0.000	2.291
ENSG00000228126	FALEC	0.000	2.293
ENSG00000256029	SNHG28	0.000	2.293
ENSG00000258947	TUBB3	0.000	2.295
ENSG00000272696	AL359091.4	0.000	2.295
ENSG00000142871	CYR61	0.000	2.295
ENSG00000149646	CNBD2	0.000	2.296
ENSG00000115840	SLC25A12	0.000	2.296
ENSG00000099624	ATP5F1D	0.000	2.297

ENSG00000248079	<i>DPH6-DT</i>	0.001	2.297
ENSG00000087510	<i>TFAP2C</i>	0.000	2.301
ENSG00000168010	<i>ATG16L2</i>	0.000	2.301
ENSG00000212907	<i>MT-ND4L</i>	0.000	2.303
ENSG00000213213	<i>CCDC183</i>	0.001	2.304
ENSG00000272323	<i>AC026801.2</i>	0.002	2.305
ENSG00000167107	<i>ACSF2</i>	0.000	2.307
ENSG00000065609	<i>SNAP91</i>	0.000	2.307
ENSG00000198712	<i>MT-CO2</i>	0.000	2.307
ENSG00000159214	<i>CCDC24</i>	0.000	2.308
ENSG00000114054	<i>PCCB</i>	0.000	2.309
ENSG00000091129	<i>NRCAM</i>	0.006	2.309
ENSG00000134369	<i>NAV1</i>	0.000	2.309
ENSG00000169429	<i>CXCL8</i>	0.000	2.311
ENSG00000170906	<i>NDUFA3</i>	0.000	2.311
ENSG00000273174	<i>AC108673.2</i>	0.006	2.314
ENSG00000175198	<i>PCCA</i>	0.000	2.316
ENSG00000259969	<i>AL049838.1</i>	0.000	2.317
ENSG00000135677	<i>GNS</i>	0.000	2.318
ENSG00000164920	<i>OSR2</i>	0.000	2.318
ENSG00000172382	<i>PRSS27</i>	0.003	2.319
ENSG00000099795	<i>NDUFB7</i>	0.000	2.319
ENSG00000237276	<i>ANO7L1</i>	0.000	2.319
ENSG00000270248	<i>AC011468.4</i>	0.009	2.320
ENSG00000168014	<i>C2CD3</i>	0.000	2.321
ENSG00000134343	<i>ANO3</i>	0.000	2.322
ENSG00000180229	<i>HERC2P3</i>	0.000	2.322
ENSG00000104324	<i>CPQ</i>	0.000	2.323
ENSG00000084754	<i>HADHA</i>	0.000	2.324
ENSG00000188611	<i>ASAH2</i>	0.000	2.325
ENSG00000278535	<i>DHRS11</i>	0.000	2.326
ENSG00000154814	<i>OXNAD1</i>	0.000	2.326
ENSG00000172366	<i>MCRIP2</i>	0.000	2.327
ENSG00000161542	<i>PRPSAP1</i>	0.000	2.327
ENSG00000021826	<i>CPS1</i>	0.000	2.329
ENSG00000187446	<i>CHP1</i>	0.000	2.331
ENSG00000151689	<i>INPP1</i>	0.000	2.332
ENSG00000224086	<i>AC245452.1</i>	0.000	2.332
ENSG00000213062	<i>AL021068.1</i>	0.000	2.333
ENSG00000258818	<i>RNASE4</i>	0.004	2.333
ENSG00000168936	<i>TMEM129</i>	0.000	2.333
ENSG00000274750	<i>HIST1H3E</i>	0.000	2.334
ENSG00000008277	<i>ADAM22</i>	0.000	2.335
ENSG00000204308	<i>RNF5</i>	0.000	2.337
ENSG00000204965	<i>PCDHA5</i>	0.000	2.337
ENSG00000139180	<i>NDUFA9</i>	0.000	2.337
ENSG00000091140	<i>DLD</i>	0.000	2.338
ENSG00000174483	<i>BBS1</i>	0.000	2.338
ENSG00000189366	<i>ALG1L</i>	0.000	2.338
ENSG00000280278	<i>FLJ30679</i>	0.009	2.338
ENSG00000117010	<i>ZNF684</i>	0.000	2.338
ENSG00000151470	<i>C4orf33</i>	0.000	2.340
ENSG00000204262	<i>COL5A2</i>	0.000	2.340
ENSG00000179085	<i>DPM3</i>	0.000	2.341
ENSG00000106610	<i>STAG3L4</i>	0.000	2.341
ENSG00000091483	<i>FH</i>	0.000	2.341
ENSG00000165264	<i>NDUFB6</i>	0.000	2.342
ENSG00000107551	<i>RASSF4</i>	0.000	2.343
ENSG00000064787	<i>BCAS1</i>	0.002	2.343
ENSG00000261502	<i>AC040174.1</i>	0.000	2.344

ENSG00000100814	CCNB1IP1	0.000	2.345
ENSG00000136463	TACO1	0.000	2.345
ENSG00000003400	CASP10	0.000	2.345
ENSG00000138463	DIRC2	0.000	2.346
ENSG00000163975	MELTF	0.000	2.348
ENSG00000188313	PLSCR1	0.000	2.349
ENSG00000136327	NKX2-8	0.000	2.351
ENSG00000244005	NFS1	0.000	2.351
ENSG0000013583	HEBP1	0.000	2.351
ENSG00000204334	ERICH2	0.000	2.351
ENSG00000165698	SPACA9	0.000	2.353
ENSG00000130589	HELZ2	0.000	2.353
ENSG00000223572	CKMT1A	0.000	2.353
ENSG00000091128	LAMB4	0.009	2.353
ENSG00000270882	HIST2H4A	0.000	2.354
ENSG00000224945	AL353150.1	0.002	2.354
ENSG00000247853	AC006064.2	0.001	2.355
ENSG00000082438	COBLL1	0.000	2.356
ENSG00000108679	LGALS3BP	0.000	2.356
ENSG00000185130	HIST1H2BL	0.003	2.357
ENSG00000272688	AP005329.3	0.000	2.357
ENSG00000167797	CDK2AP2	0.000	2.357
ENSG00000124172	ATP5F1E	0.000	2.358
ENSG00000162458	FBLIM1	0.000	2.358
ENSG00000052802	MSMO1	0.000	2.359
ENSG00000135899	SP110	0.000	2.360
ENSG00000123472	ATPAF1	0.000	2.360
ENSG00000136378	ADAMTS7	0.000	2.361
ENSG00000124575	HIST1H1D	0.000	2.362
ENSG00000117410	ATP6V0B	0.000	2.362
ENSG00000272106	AL691432.2	0.000	2.362
ENSG00000253570	RNF5P1	0.000	2.363
ENSG00000156500	FAM122C	0.000	2.364
ENSG00000248278	SUMO2P17	0.000	2.364
ENSG00000116353	MECR	0.000	2.365
ENSG00000149577	SIDT2	0.000	2.366
ENSG00000124588	NQO2	0.000	2.367
ENSG00000131495	NDUFA2	0.000	2.368
ENSG00000235162	C12orf75	0.000	2.368
ENSG00000236098	AC097059.2	0.000	2.369
ENSG00000232160	RAP2C-AS1	0.000	2.370
ENSG00000188163	FAM166A	0.000	2.370
ENSG00000105472	CLEC11A	0.000	2.370
ENSG00000164675	IQUB	0.000	2.371
ENSG00000147041	SYTL5	0.004	2.372
ENSG00000255517	AP002748.3	0.000	2.373
ENSG00000114279	FGF12	0.000	2.373
ENSG00000284719	AL033527.5	0.000	2.374
ENSG00000272902	TBC1D8-AS1	0.000	2.375
ENSG00000244256	RN7SL130P	0.009	2.375
ENSG00000152556	PFKM	0.000	2.376
ENSG00000064195	DLX3	0.000	2.380
ENSG00000277734	TRAC	0.000	2.381
ENSG00000267264	AC006504.3	0.003	2.382
ENSG00000167930	FAM234A	0.000	2.383
ENSG00000065518	NDUFB4	0.000	2.383
ENSG00000273619	AL121832.2	0.000	2.384
ENSG00000115257	PCSK4	0.000	2.384
ENSG00000176340	COX8A	0.000	2.384
ENSG00000110717	NDUFS8	0.000	2.385

ENSG00000131069	<i>ACSS2</i>	0.000	2.386
ENSG00000112695	<i>COX7A2</i>	0.000	2.387
ENSG00000273702	<i>AC091271.1</i>	0.000	2.387
ENSG00000155099	<i>PIP4P2</i>	0.000	2.388
ENSG00000124813	<i>RUNX2</i>	0.000	2.390
ENSG00000205517	<i>RGL3</i>	0.000	2.390
ENSG00000168542	<i>COL3A1</i>	0.000	2.392
ENSG00000246339	<i>EXTL3-AS1</i>	0.000	2.394
ENSG00000263766	<i>AC025682.1</i>	0.000	2.394
ENSG00000185000	<i>DGAT1</i>	0.000	2.396
ENSG00000230601	<i>TEX48</i>	0.001	2.396
ENSG00000075303	<i>SLC25A40</i>	0.000	2.397
ENSG00000261474	<i>AC026471.4</i>	0.000	2.397
ENSG00000128626	<i>MRPS12</i>	0.000	2.397
ENSG00000204520	<i>MICA</i>	0.000	2.397
ENSG00000233954	<i>UQCRHL</i>	0.000	2.398
ENSG00000226754	<i>AL606760.1</i>	0.001	2.399
ENSG00000120129	<i>DUSP1</i>	0.000	2.399
ENSG00000188681	<i>TEKT4P2</i>	0.000	2.401
ENSG00000205464	<i>ATP6AP1L</i>	0.000	2.401
ENSG00000135070	<i>ISCA1</i>	0.000	2.403
ENSG00000101247	<i>NDUFAF5</i>	0.000	2.403
ENSG00000183605	<i>SFXN4</i>	0.000	2.406
ENSG00000171992	<i>SYNPO</i>	0.000	2.407
ENSG00000257732	<i>AC089983.1</i>	0.000	2.407
ENSG00000198797	<i>BRINP2</i>	0.000	2.408
ENSG00000103121	<i>CMC2</i>	0.000	2.409
ENSG00000247708	<i>STX18-AS1</i>	0.000	2.409
ENSG00000188672	<i>RHCE</i>	0.000	2.411
ENSG00000203705	<i>TATDN3</i>	0.000	2.411
ENSG00000132313	<i>MRPL35</i>	0.000	2.411
ENSG00000167315	<i>ACAA2</i>	0.000	2.412
ENSG00000160323	<i>ADAMTS13</i>	0.000	2.412
ENSG00000188659	<i>SAXO2</i>	0.000	2.414
ENSG00000180611	<i>MB21D2</i>	0.000	2.415
ENSG00000164142	<i>FAM160A1</i>	0.000	2.416
ENSG00000255992	<i>AC131009.1</i>	0.000	2.416
ENSG00000245317	<i>AC008393.1</i>	0.000	2.417
ENSG00000160188	<i>RSPH1</i>	0.005	2.418
ENSG00000229604	<i>MTATP8P2</i>	0.000	2.419
ENSG00000118004	<i>COLEC11</i>	0.002	2.419
ENSG00000140043	<i>PTGR2</i>	0.000	2.420
ENSG00000247627	<i>MTND4P12</i>	0.000	2.422
ENSG00000244459	<i>AC147067.1</i>	0.001	2.422
ENSG00000206532	<i>AC117402.1</i>	0.002	2.423
ENSG00000244187	<i>TMEM141</i>	0.000	2.423
ENSG00000269889	<i>AC078802.1</i>	0.003	2.423
ENSG00000174917	<i>C19orf70</i>	0.000	2.424
ENSG00000269069	<i>AC007842.1</i>	0.000	2.424
ENSG00000134864	<i>GGACT</i>	0.000	2.429
ENSG00000226174	<i>TEX22</i>	0.000	2.429
ENSG00000272989	<i>LINC02012</i>	0.002	2.430
ENSG00000279491	<i>AP003733.4</i>	0.002	2.430
ENSG00000173660	<i>UQCRH</i>	0.000	2.430
ENSG00000109390	<i>NDUFC1</i>	0.000	2.431
ENSG00000146267	<i>FAXC</i>	0.000	2.431
ENSG00000161544	<i>CYGB</i>	0.000	2.431
ENSG00000054690	<i>PLEKHH1</i>	0.000	2.434
ENSG00000108528	<i>SLC25A11</i>	0.000	2.434
ENSG00000136521	<i>NDUFB5</i>	0.000	2.434

ENSG00000236423	<i>LINC01134</i>	0.000	2.435
ENSG00000247134	<i>AC090204.1</i>	0.000	2.437
ENSG00000100271	<i>TLL1</i>	0.000	2.437
ENSG00000135828	<i>RNASEL</i>	0.000	2.437
ENSG00000112139	<i>MDGA1</i>	0.001	2.438
ENSG00000023228	<i>NDUFS1</i>	0.000	2.439
ENSG00000173915	<i>ATP5MD</i>	0.000	2.439
ENSG00000175482	<i>POLD4</i>	0.000	2.440
ENSG00000237037	<i>NDUFA6-DT</i>	0.000	2.442
ENSG00000284526	<i>AC015802.6</i>	0.005	2.442
ENSG00000148926	<i>ADM</i>	0.000	2.442
ENSG00000163867	<i>ZMYM6</i>	0.000	2.443
ENSG00000273355	<i>AP000894.4</i>	0.007	2.443
ENSG00000144847	<i>IGSF11</i>	0.009	2.447
ENSG00000119640	<i>ACYP1</i>	0.000	2.448
ENSG00000136143	<i>SUCLA2</i>	0.000	2.448
ENSG00000231925	<i>TAPBP</i>	0.000	2.448
ENSG00000233483	<i>AC008105.2</i>	0.000	2.452
ENSG00000145911	<i>N4BP3</i>	0.000	2.455
ENSG00000204390	<i>HSPA1L</i>	0.000	2.456
ENSG00000245532	<i>NEAT1</i>	0.000	2.458
ENSG00000204789	<i>ZNF204P</i>	0.000	2.459
ENSG00000152380	<i>FAM151B</i>	0.000	2.460
ENSG00000186301	<i>MST1P2</i>	0.000	2.461
ENSG00000111913	<i>RIPOR2</i>	0.000	2.461
ENSG00000099866	<i>MADCAM1</i>	0.005	2.463
ENSG00000167528	<i>ZNF641</i>	0.000	2.464
ENSG00000184752	<i>NDUFA12</i>	0.000	2.464
ENSG00000061455	<i>PRDM6</i>	0.001	2.464
ENSG00000080224	<i>EPHA6</i>	0.000	2.464
ENSG00000239467	<i>AC007405.3</i>	0.000	2.465
ENSG00000115137	<i>DNAJC27</i>	0.000	2.465
ENSG00000270673	<i>YTHDF3-AS1</i>	0.006	2.466
ENSG00000123124	<i>WWP1</i>	0.000	2.466
ENSG00000267064	<i>UXT-AS1</i>	0.000	2.468
ENSG00000152234	<i>ATP5F1A</i>	0.000	2.468
ENSG00000078081	<i>LAMP3</i>	0.000	2.472
ENSG00000130363	<i>RSPH3</i>	0.000	2.472
ENSG00000163354	<i>DCST2</i>	0.000	2.473
ENSG00000136868	<i>SLC31A1</i>	0.000	2.476
ENSG00000137038	<i>DMAC1</i>	0.000	2.477
ENSG00000250479	<i>CHCHD10</i>	0.000	2.477
ENSG00000272030	<i>AL162258.2</i>	0.000	2.479
ENSG00000196511	<i>TPK1</i>	0.000	2.479
ENSG00000162542	<i>TMCO4</i>	0.000	2.480
ENSG00000171298	<i>GAA</i>	0.000	2.480
ENSG00000248610	<i>HSPA8P4</i>	0.004	2.481
ENSG00000172000	<i>ZNF556</i>	0.002	2.482
ENSG00000166797	<i>CIAO2A</i>	0.000	2.483
ENSG00000011295	<i>TTC19</i>	0.000	2.486
ENSG00000198513	<i>ATL1</i>	0.000	2.486
ENSG00000255135	<i>AP002360.1</i>	0.000	2.486
ENSG00000057657	<i>PRDM1</i>	0.000	2.489
ENSG00000111837	<i>MAK</i>	0.000	2.491
ENSG00000189419	<i>SPATA41</i>	0.000	2.491
ENSG00000198886	<i>MT-ND4</i>	0.000	2.491
ENSG00000135469	<i>COQ10A</i>	0.000	2.493
ENSG00000160460	<i>SPTBN4</i>	0.000	2.494
ENSG00000102981	<i>PAR6A</i>	0.000	2.494
ENSG00000170627	<i>GTSF1</i>	0.002	2.495

ENSG00000258057	BCDIN3D-AS1	0.000	2.496
ENSG00000109321	AREG	0.000	2.500
ENSG00000169228	RAB24	0.000	2.500
ENSG00000137133	HINT2	0.000	2.501
ENSG00000226800	CACTIN-AS1	0.006	2.501
ENSG00000119013	NDUFB3	0.000	2.502
ENSG00000204228	HSD17B8	0.000	2.502
ENSG00000107262	BAG1	0.000	2.503
ENSG00000254860	TMEM9B-AS1	0.000	2.503
ENSG0000042286	AIFM2	0.000	2.504
ENSG00000130751	NPAS1	0.000	2.505
ENSG00000249780	AC093809.1	0.004	2.508
ENSG00000270362	HMGN3-AS1	0.000	2.510
ENSG00000105429	MEGF8	0.000	2.511
ENSG00000128284	APOL3	0.000	2.511
ENSG00000220205	VAMP2	0.000	2.512
ENSG00000174827	PDZK1	0.000	2.516
ENSG00000272405	AL365181.3	0.000	2.516
ENSG00000137710	RDX	0.000	2.517
ENSG00000197380	DACT3	0.000	2.517
ENSG00000145246	ATP10D	0.000	2.519
ENSG00000115520	COQ10B	0.000	2.522
ENSG00000173486	FKBP2	0.000	2.522
ENSG00000131966	ACTR10	0.000	2.524
ENSG00000178449	COX14	0.000	2.525
ENSG00000273319	AC058791.1	0.001	2.525
ENSG00000271888	AL136162.1	0.004	2.526
ENSG00000131142	CCL25	0.003	2.529
ENSG00000128923	MINDY2	0.000	2.529
ENSG00000114248	LRRC31	0.000	2.530
ENSG00000130529	TRPM4	0.000	2.531
ENSG00000178149	DALRD3	0.000	2.531
ENSG00000167863	ATP5PD	0.000	2.533
ENSG00000135452	TSPAN31	0.000	2.533
ENSG00000146411	SLC2A12	0.000	2.534
ENSG00000170458	CD14	0.001	2.534
ENSG00000164347	GFM2	0.000	2.536
ENSG00000111540	RAB5B	0.000	2.537
ENSG00000271855	AC073195.1	0.000	2.538
ENSG00000254285	KRT8P3	0.001	2.539
ENSG00000219665	ZNF433-AS1	0.000	2.541
ENSG00000115977	AAK1	0.000	2.542
ENSG00000105784	RUNDC3B	0.000	2.542
ENSG00000149591	TAGLN	0.000	2.543
ENSG00000134452	FBH1	0.000	2.544
ENSG00000229931	AL137003.1	0.000	2.546
ENSG00000113645	WWC1	0.000	2.549
ENSG00000110090	CPT1A	0.000	2.550
ENSG00000076864	RAP1GAP	0.000	2.550
ENSG00000130312	MRPL34	0.000	2.550
ENSG00000128654	MTX2	0.000	2.551
ENSG00000184983	NDUFA6	0.000	2.554
ENSG00000171388	APLN	0.000	2.555
ENSG00000165899	OTOGL	0.000	2.556
ENSG00000154723	ATP5PF	0.000	2.557
ENSG00000139178	C1RL	0.000	2.559
ENSG00000153130	SCOC	0.000	2.559
ENSG00000164128	NPY1R	0.000	2.560
ENSG00000110871	COQ5	0.000	2.563
ENSG00000253616	AC107959.3	0.000	2.564

ENSG00000249637	AC008438.1	0.000	2.565
ENSG00000170175	CHRNB1	0.000	2.565
ENSG00000262001	DLGAP1-AS2	0.000	2.565
ENSG00000167037	SGSM1	0.000	2.568
ENSG00000100347	SAMM50	0.000	2.568
ENSG00000230487	PSMG3-AS1	0.000	2.570
ENSG00000277715	AC079174.2	0.000	2.570
ENSG00000173762	CD7	0.000	2.571
ENSG00000101079	NDRG3	0.000	2.571
ENSG00000183308	AC005037.1	0.000	2.571
ENSG00000133661	SFTPD	0.000	2.573
ENSG00000277969	AC006449.6	0.000	2.573
ENSG00000102109	PCSK1N	0.000	2.576
ENSG00000125356	NDUFA1	0.000	2.576
ENSG00000248508	SRP14-AS1	0.000	2.578
ENSG00000250634	LINC01182	0.004	2.580
ENSG00000164845	FAM86FP	0.000	2.580
ENSG00000072778	ACADVL	0.000	2.584
ENSG00000133321	RARRES3	0.000	2.584
ENSG00000253417	LINC02159	0.001	2.584
ENSG00000110697	PITPNM1	0.000	2.585
ENSG00000187837	HIST1H1C	0.000	2.585
ENSG00000175701	MTLN	0.000	2.587
ENSG00000187266	EPOR	0.000	2.588
ENSG00000256940	AP001453.2	0.000	2.589
ENSG00000164976	MYORG	0.000	2.590
ENSG00000244921	MTCYBP18	0.000	2.591
ENSG00000259343	TMC3-AS1	0.000	2.594
ENSG00000107960	STN1	0.000	2.594
ENSG00000260300	AC009119.2	0.000	2.594
ENSG00000178809	TRIM73	0.001	2.596
ENSG00000181218	HIST3H2A	0.000	2.596
ENSG00000205913	SRRM2-AS1	0.000	2.597
ENSG00000160439	RDH13	0.000	2.598
ENSG00000167562	ZNF701	0.000	2.599
ENSG00000237505	PKN2-AS1	0.000	2.600
ENSG00000272654	AL358472.2	0.000	2.600
ENSG00000259663	AC010478.1	0.000	2.601
ENSG00000168273	SMIM4	0.000	2.602
ENSG00000137825	ITPKA	0.000	2.602
ENSG00000167525	PROCA1	0.000	2.603
ENSG00000100867	DHRS2	0.000	2.604
ENSG00000248544	AC008676.1	0.002	2.605
ENSG00000185761	ADAMTSL5	0.000	2.606
ENSG00000141665	FBXO15	0.000	2.606
ENSG00000284976	BX255925.3	0.000	2.607
ENSG00000111254	AKAP3	0.000	2.607
ENSG00000183114	FAM43B	0.002	2.607
ENSG00000226287	TMEM191A	0.000	2.612
ENSG00000160326	SLC2A6	0.000	2.612
ENSG00000131143	COX4I1	0.000	2.613
ENSG00000250714	AC100861.2	0.000	2.613
ENSG00000123545	NDUF4F4	0.000	2.614
ENSG00000083123	BCKDHB	0.000	2.615
ENSG00000164081	TEX264	0.000	2.616
ENSG00000281376	ABALON	0.006	2.617
ENSG00000163704	PRRT3	0.000	2.618
ENSG00000231131	LNCAROD	0.000	2.620
ENSG00000246523	AP001528.1	0.000	2.620
ENSG00000198947	DMD	0.000	2.622

ENSG00000157470	<i>FAM81A</i>	0.000	2.624
ENSG00000213626	<i>LBH</i>	0.000	2.625
ENSG00000115365	<i>LANCL1</i>	0.000	2.625
ENSG00000178935	<i>ZNF552</i>	0.000	2.628
ENSG00000161298	<i>ZNF382</i>	0.000	2.628
ENSG00000213673	<i>SLC25A5P3</i>	0.000	2.630
ENSG00000248112	<i>AC108174.1</i>	0.000	2.631
ENSG00000214212	<i>C19orf38</i>	0.000	2.632
ENSG00000198723	<i>TEX45</i>	0.000	2.633
ENSG00000146729	<i>NIPSNAP2</i>	0.000	2.633
ENSG00000196844	<i>PATE2</i>	0.001	2.634
ENSG00000156515	<i>HK1</i>	0.000	2.635
ENSG00000271869	<i>AC026979.2</i>	0.001	2.636
ENSG00000088727	<i>KIF9</i>	0.000	2.636
ENSG00000111850	<i>SMIM8</i>	0.000	2.636
ENSG00000260778	<i>AC009065.4</i>	0.000	2.637
ENSG00000109854	<i>HTATIP2</i>	0.000	2.637
ENSG00000102393	<i>GLA</i>	0.000	2.638
ENSG00000004961	<i>HCCS</i>	0.000	2.639
ENSG00000123870	<i>ZNF137P</i>	0.000	2.641
ENSG00000122873	<i>CISD1</i>	0.000	2.642
ENSG00000198722	<i>UNC13B</i>	0.000	2.643
ENSG00000117118	<i>SDHB</i>	0.000	2.645
ENSG00000064601	<i>CTSA</i>	0.000	2.646
ENSG00000137502	<i>RAB30</i>	0.000	2.647
ENSG00000232434	<i>AJM1</i>	0.000	2.648
ENSG00000124140	<i>SLC12A5</i>	0.000	2.648
ENSG00000272720	<i>AL022322.1</i>	0.000	2.651
ENSG00000178814	<i>OPLAH</i>	0.000	2.651
ENSG00000144366	<i>GULP1</i>	0.000	2.651
ENSG00000128254	<i>C22orf24</i>	0.000	2.652
ENSG00000259577	<i>CERNA1</i>	0.002	2.653
ENSG00000262410	<i>AC024361.1</i>	0.004	2.653
ENSG0000023330	<i>ALAS1</i>	0.000	2.654
ENSG00000125652	<i>ALKBH7</i>	0.000	2.655
ENSG00000204564	<i>C6orf136</i>	0.000	2.655
ENSG00000075651	<i>PLD1</i>	0.000	2.655
ENSG00000127084	<i>FGD3</i>	0.000	2.656
ENSG00000261189	<i>AL031058.1</i>	0.000	2.659
ENSG00000267546	<i>AC015802.4</i>	0.001	2.659
ENSG00000202343	<i>RF00410</i>	0.008	2.660
ENSG00000152137	<i>HSPB8</i>	0.000	2.663
ENSG00000067836	<i>ROGDI</i>	0.000	2.663
ENSG00000243766	<i>HOTTIP</i>	0.000	2.663
ENSG00000283511	<i>AC137936.2</i>	0.001	2.665
ENSG00000099377	<i>HSD3B7</i>	0.000	2.667
ENSG00000135643	<i>KCNMB4</i>	0.000	2.668
ENSG00000217275	<i>AL031777.1</i>	0.001	2.669
ENSG00000272461	<i>AP005328.2</i>	0.003	2.670
ENSG00000281189	<i>GHET1</i>	0.000	2.673
ENSG00000107984	<i>DKK1</i>	0.000	2.674
ENSG00000132109	<i>TRIM21</i>	0.000	2.674
ENSG00000283667	<i>AC009802.1</i>	0.003	2.676
ENSG00000132763	<i>MMACHC</i>	0.000	2.679
ENSG00000196420	<i>S100A5</i>	0.000	2.680
ENSG00000186088	<i>GSAP</i>	0.000	2.682
ENSG00000130830	<i>MPP1</i>	0.000	2.683
ENSG00000163382	<i>NAXE</i>	0.000	2.685
ENSG00000099785	<i>MARCH2</i>	0.000	2.685
ENSG00000277232	<i>GTSE1-DT</i>	0.000	2.689

ENSG00000260025	AC009414.2	0.000	2.689
ENSG00000247934	AC022364.1	0.000	2.691
ENSG00000110944	IL23A	0.000	2.695
ENSG00000198814	GK	0.000	2.695
ENSG00000257557	PPP1R12A-AS1	0.000	2.696
ENSG00000248923	MTND5P11	0.000	2.697
ENSG00000164180	TMEM161B	0.000	2.698
ENSG00000164039	BDH2	0.000	2.698
ENSG00000124762	CDKN1A	0.000	2.698
ENSG00000198763	MT-ND2	0.000	2.699
ENSG00000282851	BISPR	0.000	2.701
ENSG00000088682	COQ9	0.000	2.705
ENSG00000105737	GRIK5	0.000	2.705
ENSG00000053524	MCF2L2	0.000	2.708
ENSG00000271780	AL118558.3	0.000	2.709
ENSG00000135537	AFG1L	0.000	2.711
ENSG00000102763	VWA8	0.000	2.711
ENSG00000025039	RRAGD	0.000	2.712
ENSG00000168803	ADAL	0.000	2.714
ENSG00000180787	ZFP3	0.000	2.714
ENSG00000010256	UQCRC1	0.000	2.716
ENSG00000099330	OCEL1	0.000	2.718
ENSG00000278212	AC134878.2	0.000	2.719
ENSG00000270820	AC016727.1	0.000	2.720
ENSG00000226445	BX322234.1	0.000	2.720
ENSG00000115468	EFHD1	0.003	2.720
ENSG00000233822	HIST1H2BN	0.000	2.724
ENSG00000246731	MGC16275	0.000	2.724
ENSG00000165678	GHITM	0.000	2.725
ENSG00000248785	HIGD1AP14	0.006	2.725
ENSG00000125122	LRRC29	0.000	2.732
ENSG00000129946	SHC2	0.000	2.734
ENSG00000184545	DUSP8	0.000	2.734
ENSG00000187624	C17orf97	0.000	2.737
ENSG00000213512	GBP7	0.004	2.740
ENSG00000243444	PALM2	0.000	2.741
ENSG00000139725	RHOF	0.000	2.742
ENSG00000188512	AF279873.1	0.000	2.743
ENSG00000269559	AC093677.2	0.001	2.745
ENSG00000179163	FUCA1	0.000	2.745
ENSG00000273253	AL022328.4	0.000	2.745
ENSG00000143416	SELENBP1	0.000	2.746
ENSG00000251405	AC016571.1	0.001	2.747
ENSG00000238120	LINC01589	0.001	2.748
ENSG00000284713	AP003071.5	0.000	2.749
ENSG00000074317	SNCB	0.000	2.750
ENSG00000259728	LINC00933	0.000	2.752
ENSG00000166741	NNMT	0.000	2.752
ENSG00000124145	SDC4	0.000	2.755
ENSG00000111666	CHPT1	0.000	2.756
ENSG00000105357	MYH14	0.000	2.756
ENSG00000149925	ALDOA	0.000	2.759
ENSG00000174521	TTC9B	0.001	2.762
ENSG00000149557	FEZ1	0.001	2.765
ENSG00000232653	GOLGA8N	0.000	2.765
ENSG00000257433	AC004241.1	0.000	2.766
ENSG00000164404	GDF9	0.000	2.768
ENSG00000285679	AC097626.1	0.007	2.768
ENSG00000110375	UPK2	0.004	2.768
ENSG00000076555	ACACB	0.000	2.769

ENSG00000260088	AL445483.1	0.002	2.771
ENSG00000272172	AC138696.2	0.000	2.774
ENSG00000253404	AC034243.1	0.000	2.774
ENSG00000183826	BTBD9	0.000	2.774
ENSG00000130518	IQCN	0.000	2.775
ENSG00000240476	LINC00973	0.000	2.776
ENSG00000086619	ERO1B	0.000	2.776
ENSG00000165629	ATP5F1C	0.000	2.776
ENSG00000260317	AC009812.4	0.001	2.776
ENSG00000184923	NUTM2A	0.000	2.777
ENSG00000198786	MT-ND5	0.000	2.778
ENSG00000152779	SLC16A12	0.000	2.779
ENSG00000163541	SUCLG1	0.000	2.779
ENSG00000109107	ALDOC	0.000	2.784
ENSG00000175197	DDIT3	0.000	2.789
ENSG00000205583	STAG3L1	0.000	2.790
ENSG00000102543	CDADC1	0.000	2.793
ENSG00000260095	AC106820.3	0.001	2.794
ENSG00000225630	MTND2P28	0.000	2.794
ENSG00000267858	MZF1-AS1	0.000	2.794
ENSG00000002746	HECW1	0.000	2.795
ENSG00000118508	RAB32	0.000	2.795
ENSG00000268996	MAN1B1-DT	0.000	2.797
ENSG00000171174	RBKS	0.000	2.801
ENSG00000157214	STEAP2	0.000	2.801
ENSG00000244675	AC108676.1	0.000	2.802
ENSG00000243660	ZNF487	0.000	2.804
ENSG00000125454	SLC25A19	0.000	2.804
ENSG00000271361	HTATSFP2	0.000	2.804
ENSG00000130303	BST2	0.000	2.805
ENSG00000131979	GCH1	0.000	2.807
ENSG00000253092	RF01241	0.008	2.807
ENSG00000167767	KRT80	0.000	2.808
ENSG00000264456	AC138207.4	0.000	2.812
ENSG00000230415	LINC01786	0.000	2.812
ENSG00000198727	MT-CYB	0.000	2.813
ENSG00000166546	BEAN1	0.000	2.814
ENSG00000156042	CFAP70	0.000	2.817
ENSG00000251603	AC092611.2	0.000	2.817
ENSG00000158006	PAFAH2	0.000	2.821
ENSG00000273733	AC011472.4	0.003	2.824
ENSG00000130653	PNPLA7	0.000	2.825
ENSG00000124104	SNX21	0.000	2.825
ENSG00000250508	AP000808.1	0.000	2.827
ENSG00000144959	NCEH1	0.000	2.827
ENSG00000125388	GRK4	0.000	2.827
ENSG00000163788	SNRK	0.000	2.827
ENSG00000281357	ARRDC3-AS1	0.000	2.827
ENSG00000165644	COMTD1	0.000	2.828
ENSG00000188001	TPRG1	0.000	2.830
ENSG00000162572	SCNN1D	0.000	2.832
ENSG00000276408	AC025287.2	0.009	2.833
ENSG00000248866	USP46-AS1	0.000	2.835
ENSG00000250548	LINC01303	0.000	2.836
ENSG00000030110	BAK1	0.000	2.840
ENSG00000118407	FILIP1	0.000	2.843
ENSG00000272086	AC025181.2	0.000	2.843
ENSG00000075239	ACAT1	0.000	2.843
ENSG00000118680	MYL12B	0.000	2.846
ENSG00000227653	ISCA1P6	0.002	2.847

ENSG00000273443	AL645608.8	0.000	2.848
ENSG00000073578	SDHA	0.000	2.849
ENSG00000099974	DDTL	0.009	2.849
ENSG00000124370	MCEE	0.000	2.850
ENSG00000213928	IRF9	0.000	2.851
ENSG00000261268	AC112236.1	0.000	2.852
ENSG00000238193	AC112656.1	0.000	2.853
ENSG00000108846	ABCC3	0.000	2.855
ENSG00000259820	AC083843.2	0.000	2.855
ENSG00000121270	ABCC11	0.001	2.855
ENSG00000101222	SPEF1	0.000	2.855
ENSG00000132793	LPIN3	0.000	2.857
ENSG00000089060	SLC8B1	0.000	2.858
ENSG00000132305	IMMT	0.000	2.861
ENSG00000075290	WNT8B	0.000	2.862
ENSG00000168216	LMBRD1	0.000	2.863
ENSG00000182326	C1S	0.000	2.864
ENSG00000105696	TMEM59L	0.000	2.864
ENSG00000173436	MINOS1	0.000	2.866
ENSG00000206538	VGLL3	0.000	2.868
ENSG00000167969	ECI1	0.000	2.870
ENSG00000196747	HIST1H2AI	0.000	2.873
ENSG00000126267	COX6B1	0.000	2.874
ENSG00000184060	ADAP2	0.001	2.878
ENSG00000104881	PPP1R13L	0.000	2.878
ENSG00000111678	C12orf57	0.000	2.879
ENSG00000133731	IMPA1	0.000	2.881
ENSG00000260086	AC007611.1	0.000	2.882
ENSG00000178537	SLC25A20	0.000	2.884
ENSG00000284707	AC079781.5	0.003	2.888
ENSG00000156171	DRAM2	0.000	2.888
ENSG00000159176	CSRP1	0.000	2.890
ENSG00000272046	AL445647.1	0.005	2.897
ENSG00000172575	RASGRP1	0.000	2.897
ENSG00000126460	PRRG2	0.000	2.901
ENSG00000180881	CAPS2	0.000	2.902
ENSG00000281468	AC006504.8	0.000	2.907
ENSG00000179284	DAND5	0.000	2.908
ENSG00000184844	CYCSP45	0.000	2.908
ENSG00000115556	PLCD4	0.000	2.913
ENSG00000258940	AL132639.2	0.000	2.913
ENSG00000224616	RTCA-AS1	0.000	2.914
ENSG00000275221	HIST1H2AK	0.000	2.915
ENSG00000259939	AC022167.1	0.000	2.916
ENSG00000005022	SLC25A5	0.000	2.916
ENSG00000101365	IDH3B	0.000	2.918
ENSG00000235034	C19orf81	0.001	2.919
ENSG00000185924	RTN4RL1	0.000	2.919
ENSG00000180389	ATP5F1EP2	0.000	2.919
ENSG00000173890	GPR160	0.000	2.919
ENSG00000163864	NMNAT3	0.000	2.920
ENSG00000007516	BAIAP3	0.000	2.921
ENSG00000130755	GMFG	0.005	2.921
ENSG00000210195	MT-TT	0.000	2.923
ENSG00000158864	NDUFS2	0.000	2.924
ENSG00000148513	ANKRD30A	0.000	2.925
ENSG00000167114	SLC27A4	0.000	2.927
ENSG00000184408	KCND2	0.000	2.930
ENSG00000232600	TONSL-AS1	0.000	2.930
ENSG00000266903	AC243964.2	0.000	2.934

ENSG00000119421	NDUFA8	0.000	2.935
ENSG00000255007	LINC02489	0.000	2.936
ENSG00000243279	PRAF2	0.000	2.937
ENSG00000226124	FTCDNL1	0.000	2.938
ENSG00000166278	C2	0.000	2.938
ENSG00000173805	HAP1	0.000	2.941
ENSG00000130487	KLHDC7B	0.000	2.942
ENSG00000270504	AL391422.4	0.000	2.943
ENSG00000260276	AC022167.2	0.000	2.943
ENSG00000178146	AL672207.1	0.000	2.944
ENSG00000282386	AL358472.4	0.000	2.945
ENSG00000138496	PARP9	0.000	2.945
ENSG00000075415	SLC25A3	0.000	2.945
ENSG00000158856	DMTN	0.000	2.946
ENSG00000246898	LINC00920	0.000	2.946
ENSG00000272288	AL451165.2	0.000	2.948
ENSG00000204264	PSMB8	0.000	2.949
ENSG00000154589	LY96	0.000	2.953
ENSG00000234925	ATP5PDP4	0.000	2.953
ENSG00000042445	RETSAT	0.000	2.954
ENSG00000124615	MOCS1	0.000	2.954
ENSG00000068079	IFI35	0.000	2.954
ENSG00000272068	AL365181.2	0.000	2.955
ENSG00000284968	AC093827.4	0.000	2.955
ENSG00000261553	AL137782.1	0.001	2.956
ENSG00000205085	FAM71F2	0.000	2.957
ENSG00000137103	TMEM8B	0.000	2.957
ENSG00000240024	LINC00888	0.000	2.959
ENSG00000114779	ABHD14B	0.000	2.959
ENSG00000224550	AC114491.1	0.000	2.961
ENSG00000130349	C6orf203	0.000	2.961
ENSG00000248746	ACTN3	0.002	2.962
ENSG00000136244	IL6	0.000	2.965
ENSG00000124491	F13A1	0.000	2.967
ENSG00000126870	WDR60	0.000	2.968
ENSG00000256073	URB1-AS1	0.000	2.969
ENSG00000154065	ANKRD29	0.000	2.970
ENSG00000281333	AC024941.2	0.007	2.973
ENSG00000275120	AC048382.5	0.004	2.973
ENSG00000070731	ST6GALNAC2	0.000	2.973
ENSG00000267365	KCNJ2-AS1	0.005	2.974
ENSG00000198682	PAPSS2	0.000	2.975
ENSG00000148341	SH3GLB2	0.000	2.976
ENSG00000243701	DUBR	0.000	2.979
ENSG00000131174	COX7B	0.000	2.981
ENSG00000140740	UQCRC2	0.000	2.982
ENSG00000099840	IZUMO4	0.000	2.984
ENSG00000259642	ST20-AS1	0.000	2.984
ENSG00000141497	ZMYND15	0.000	2.985
ENSG00000256229	ZNF486	0.002	2.986
ENSG00000231584	FAHD2CP	0.000	2.991
ENSG00000108309	RUNDC3A	0.000	2.995
ENSG00000239462	AC091212.1	0.000	3.000
ENSG00000236432	AC097662.1	0.000	3.001
ENSG00000124399	NDUFB4P12	0.000	3.002
ENSG00000235169	SMIM1	0.000	3.004
ENSG00000137745	MMP13	0.000	3.004
ENSG00000185561	TLCD2	0.000	3.004
ENSG00000082074	FYB1	0.000	3.007
ENSG00000122971	ACADS	0.000	3.008

ENSG00000145703	<i>IQGAP2</i>	0.000	3.010
ENSG00000185338	<i>SOCS1</i>	0.001	3.011
ENSG00000076258	<i>FMO4</i>	0.000	3.011
ENSG00000100150	<i>DEPDC5</i>	0.000	3.014
ENSG00000136003	<i>ISCU</i>	0.000	3.015
ENSG00000114023	<i>FAM162A</i>	0.000	3.017
ENSG00000234350	<i>AC007405.1</i>	0.000	3.018
ENSG00000279748	<i>AC008764.9</i>	0.000	3.021
ENSG00000226686	<i>LINC01535</i>	0.000	3.022
ENSG00000165915	<i>SLC39A13</i>	0.000	3.024
ENSG00000197993	<i>KEL</i>	0.000	3.025
ENSG00000248092	<i>NNT-AS1</i>	0.000	3.026
ENSG00000041515	<i>MYO16</i>	0.000	3.027
ENSG00000124657	<i>OR2B6</i>	0.001	3.028
ENSG00000253948	<i>AC104986.2</i>	0.000	3.028
ENSG00000164211	<i>STARD4</i>	0.000	3.029
ENSG00000158286	<i>RNF207</i>	0.000	3.033
ENSG00000166670	<i>MMP10</i>	0.000	3.035
ENSG00000207561	<i>MIR635</i>	0.000	3.040
ENSG00000163121	<i>NEURL3</i>	0.000	3.040
ENSG00000116016	<i>EPAS1</i>	0.000	3.043
ENSG00000262188	<i>LINC01978</i>	0.006	3.044
ENSG00000010671	<i>BTK</i>	0.000	3.046
ENSG00000259404	<i>EFL1P1</i>	0.006	3.046
ENSG00000109738	<i>GLRB</i>	0.000	3.047
ENSG00000132879	<i>FBXO44</i>	0.000	3.049
ENSG00000150054	<i>MPP7</i>	0.000	3.050
ENSG00000226085	<i>UQCRFS1P1</i>	0.000	3.051
ENSG00000156381	<i>ANKRD9</i>	0.000	3.051
ENSG00000198888	<i>MT-ND1</i>	0.000	3.052
ENSG00000232850	<i>PTGES2-AS1</i>	0.000	3.054
ENSG00000247157	<i>LINC01252</i>	0.000	3.054
ENSG00000132481	<i>TRIM47</i>	0.000	3.056
ENSG00000254639	<i>AC116021.1</i>	0.000	3.062
ENSG00000285715	<i>AC063960.1</i>	0.002	3.064
ENSG00000033627	<i>ATP6V0A1</i>	0.000	3.065
ENSG00000108556	<i>CHRNE</i>	0.000	3.068
ENSG00000120915	<i>EPHX2</i>	0.000	3.071
ENSG00000168569	<i>TMEM223</i>	0.000	3.072
ENSG00000115665	<i>SLC5A7</i>	0.000	3.077
ENSG00000178172	<i>SPINK6</i>	0.003	3.078
ENSG00000277511	<i>AC116407.2</i>	0.002	3.080
ENSG00000071282	<i>LMCD1</i>	0.000	3.081
ENSG00000140678	<i>ITGAX</i>	0.000	3.083
ENSG00000173153	<i>ESRRA</i>	0.000	3.085
ENSG00000221916	<i>C19orf73</i>	0.000	3.086
ENSG00000214140	<i>PRCD</i>	0.000	3.087
ENSG00000275532	<i>AC006449.2</i>	0.002	3.087
ENSG00000170581	<i>STAT2</i>	0.000	3.087
ENSG00000089723	<i>OTUB2</i>	0.000	3.089
ENSG00000224292	<i>AF196972.1</i>	0.000	3.089
ENSG00000233705	<i>SLC26A4-AS1</i>	0.000	3.089
ENSG00000085871	<i>MGST2</i>	0.000	3.092
ENSG00000198133	<i>TMEM229B</i>	0.000	3.095
ENSG00000172031	<i>EPHX4</i>	0.000	3.099
ENSG00000233030	<i>AC243772.2</i>	0.000	3.099
ENSG00000255236	<i>AP002992.1</i>	0.001	3.103
ENSG00000135241	<i>PNPLA8</i>	0.000	3.103
ENSG00000173727	<i>AP000769.1</i>	0.000	3.103
ENSG00000165102	<i>HGSNAT</i>	0.000	3.103

ENSG00000240219	AL512306.2	0.010	3.104
ENSG00000273026	AL358472.3	0.000	3.105
ENSG00000275765	AC091982.3	0.000	3.105
ENSG00000268603	AC053503.5	0.006	3.106
ENSG00000203667	COX20	0.000	3.107
ENSG00000162944	RFTN2	0.000	3.107
ENSG00000244153	WWP1P1	0.005	3.109
ENSG00000205791	LOH12CR2	0.000	3.110
ENSG00000004799	PK4	0.000	3.113
ENSG00000169021	UQCRFS1	0.000	3.115
ENSG00000189298	ZKSCAN3	0.000	3.118
ENSG00000150768	DLAT	0.000	3.118
ENSG00000117226	GBP3	0.000	3.120
ENSG00000168702	LRP1B	0.000	3.122
ENSG00000108852	MPP2	0.000	3.124
ENSG00000143061	IGSF3	0.000	3.126
ENSG00000273654	AC020904.2	0.000	3.128
ENSG00000277782	AC068870.2	0.002	3.132
ENSG00000214106	PAXIP1-AS2	0.000	3.133
ENSG00000182809	CRIP2	0.000	3.133
ENSG00000164919	COX6C	0.000	3.133
ENSG00000136367	ZFH2	0.000	3.135
ENSG00000281103	TRG-AS1	0.002	3.137
ENSG00000138772	ANXA3	0.000	3.137
ENSG0000013561	RNF14	0.000	3.138
ENSG00000256747	AC009511.2	0.000	3.139
ENSG00000233008	LINC01725	0.009	3.141
ENSG00000164674	SYTL3	0.000	3.143
ENSG00000161267	BDH1	0.000	3.145
ENSG00000204525	HLA-C	0.000	3.145
ENSG00000053770	AP5M1	0.000	3.147
ENSG00000167772	ANGPTL4	0.000	3.148
ENSG00000198106	SNX29P2	0.002	3.148
ENSG00000158406	HIST1H4H	0.000	3.150
ENSG00000275055	AC011468.5	0.000	3.150
ENSG00000271966	AC021321.1	0.000	3.151
ENSG00000256771	ZNF253	0.000	3.151
ENSG00000050438	SLC4A8	0.000	3.152
ENSG00000166006	KCNC2	0.000	3.154
ENSG00000112936	C7	0.000	3.165
ENSG00000164405	UQCRQ	0.000	3.170
ENSG00000231441	AL512422.1	0.000	3.173
ENSG00000271646	AC099343.3	0.000	3.177
ENSG00000198840	MT-ND3	0.000	3.178
ENSG00000163393	SLC22A15	0.000	3.179
ENSG00000177576	C18orf32	0.000	3.179
ENSG00000117586	TNFSF4	0.000	3.180
ENSG00000261582	AL121753.1	0.000	3.180
ENSG00000174132	FAM174A	0.000	3.180
ENSG00000147684	NDUFB9	0.000	3.180
ENSG00000232070	TMEM253	0.002	3.181
ENSG00000137752	CASP1	0.000	3.185
ENSG00000255444	CYCSP27	0.001	3.189
ENSG00000182853	VMO1	0.001	3.190
ENSG00000102796	DHRS12	0.000	3.191
ENSG00000152154	TMEM178A	0.000	3.192
ENSG00000277449	CEBPB-AS1	0.000	3.194
ENSG00000003147	ICA1	0.000	3.199
ENSG00000262766	AC135050.5	0.000	3.200
ENSG00000188191	PRKAR1B	0.000	3.202

ENSG00000268205	AC005261.1	0.000	3.203
ENSG00000267871	ZNF460-AS1	0.000	3.204
ENSG00000185507	IRF7	0.000	3.207
ENSG00000226976	COX6A1P2	0.000	3.208
ENSG00000070526	ST6GALNAC1	0.000	3.208
ENSG00000265962	GACAT2	0.000	3.212
ENSG00000140990	NDUFB10	0.000	3.215
ENSG00000205488	CALML3-AS1	0.003	3.218
ENSG00000144199	FAHD2B	0.000	3.222
ENSG00000186976	EFCAB6	0.002	3.223
ENSG00000158079	PTPDC1	0.000	3.224
ENSG00000277363	SRCIN1	0.000	3.230
ENSG00000269176	AP001160.3	0.000	3.231
ENSG00000228661	AC090587.1	0.001	3.232
ENSG00000272444	AL118558.4	0.003	3.236
ENSG00000135940	COX5B	0.000	3.236
ENSG00000196335	STK31	0.000	3.239
ENSG00000107201	DDX58	0.000	3.240
ENSG00000167792	NDUFV1	0.000	3.244
ENSG00000116883	AL591845.1	0.000	3.247
ENSG00000205309	NT5M	0.000	3.248
ENSG00000196091	MYBPC1	0.000	3.254
ENSG00000172602	RND1	0.000	3.256
ENSG00000125166	GOT2	0.000	3.256
ENSG00000139899	CBLN3	0.000	3.257
ENSG00000250365	AL139353.2	0.000	3.261
ENSG00000256994	LINC02378	0.000	3.264
ENSG00000127920	GNG11	0.000	3.266
ENSG00000276026	AL031665.2	0.000	3.269
ENSG00000260274	AC068338.2	0.000	3.269
ENSG00000110955	ATP5F1B	0.000	3.271
ENSG00000115993	TRAK2	0.000	3.272
ENSG00000171119	NRTN	0.000	3.277
ENSG00000272668	AL590560.1	0.000	3.279
ENSG00000230521	AL645929.1	0.007	3.281
ENSG00000272129	AL359715.3	0.000	3.282
ENSG00000230454	U73166.1	0.000	3.282
ENSG00000185813	PCYT2	0.000	3.283
ENSG00000213619	NDUFS3	0.000	3.284
ENSG00000115415	STAT1	0.000	3.285
ENSG00000134056	MRPS36	0.000	3.285
ENSG00000228436	AL139260.1	0.000	3.285
ENSG00000236200	KDM4A-AS1	0.000	3.285
ENSG00000179627	ZBTB42	0.000	3.286
ENSG00000134548	SPX	0.000	3.287
ENSG00000172115	CYCS	0.000	3.291
ENSG00000284882	AL359762.1	0.001	3.292
ENSG00000197889	MEIG1	0.001	3.294
ENSG00000276278	AC048382.6	0.004	3.301
ENSG00000123836	PFKFB2	0.000	3.309
ENSG00000272138	LINC01607	0.001	3.314
ENSG00000254109	RBPM5-AS1	0.000	3.315
ENSG00000078070	MCCC1	0.000	3.316
ENSG00000227533	SLC2A1-AS1	0.000	3.324
ENSG00000225972	MTND1P23	0.000	3.324
ENSG00000186994	KANK3	0.000	3.326
ENSG00000135617	PRADC1	0.000	3.327
ENSG00000062485	CS	0.000	3.327
ENSG00000197279	ZNF165	0.000	3.329
ENSG00000182986	ZNF320	0.001	3.329

ENSG00000269313	<i>MAGIX</i>	0.000	3.330
ENSG00000271344	<i>AC018638.6</i>	0.003	3.334
ENSG00000267060	<i>PTGES3L</i>	0.000	3.334
ENSG00000124523	<i>SIRT5</i>	0.000	3.335
ENSG00000105953	<i>OGDH</i>	0.000	3.336
ENSG00000139364	<i>TMEM132B</i>	0.002	3.338
ENSG00000232973	<i>CYP1B1-AS1</i>	0.000	3.339
ENSG00000153230	<i>OR14K1</i>	0.002	3.340
ENSG00000156467	<i>UQCRB</i>	0.000	3.342
ENSG00000115963	<i>RND3</i>	0.000	3.346
ENSG00000238198	<i>AL357055.3</i>	0.002	3.347
ENSG00000268628	<i>AL121761.1</i>	0.000	3.350
ENSG00000112294	<i>ALDH5A1</i>	0.000	3.351
ENSG00000227666	<i>CYCSP24</i>	0.000	3.351
ENSG00000280374	<i>AC019080.5</i>	0.005	3.354
ENSG00000198521	<i>ZNF43</i>	0.000	3.355
ENSG00000115129	<i>TP53I3</i>	0.000	3.358
ENSG00000078795	<i>PKD2L2</i>	0.002	3.358
ENSG00000240405	<i>SAMMSON</i>	0.000	3.359
ENSG00000247271	<i>ZBED5-AS1</i>	0.000	3.361
ENSG00000203711	<i>C6orf99</i>	0.000	3.361
ENSG00000178741	<i>COX5A</i>	0.000	3.367
ENSG00000104805	<i>NUCB1</i>	0.000	3.369
ENSG00000132854	<i>KANK4</i>	0.000	3.371
ENSG00000015285	<i>WAS</i>	0.000	3.373
ENSG00000261202	<i>Z83847.1</i>	0.007	3.375
ENSG00000231856	<i>AL162377.1</i>	0.000	3.377
ENSG00000182154	<i>MRPL41</i>	0.000	3.380
ENSG00000234705	<i>HMGA1P4</i>	0.000	3.380
ENSG00000115762	<i>PLEKHB2</i>	0.000	3.381
ENSG00000100276	<i>RASL10A</i>	0.000	3.382
ENSG00000104361	<i>NIPAL2</i>	0.000	3.384
ENSG00000197448	<i>GSTK1</i>	0.000	3.385
ENSG00000111775	<i>COX6A1</i>	0.000	3.386
ENSG00000273901	<i>AC012313.9</i>	0.000	3.394
ENSG00000226421	<i>SLC25A5P5</i>	0.000	3.395
ENSG00000248367	<i>AC008610.1</i>	0.000	3.397
ENSG00000275964	<i>AL355001.2</i>	0.000	3.400
ENSG00000273419	<i>AC004877.1</i>	0.000	3.402
ENSG00000257696	<i>AC010203.2</i>	0.000	3.403
ENSG00000160179	<i>ABCG1</i>	0.000	3.408
ENSG00000274605	<i>AL355338.1</i>	0.000	3.409
ENSG00000178075	<i>GRAMD1C</i>	0.000	3.412
ENSG00000236830	<i>CBR3-AS1</i>	0.000	3.414
ENSG00000246273	<i>SBF2-AS1</i>	0.000	3.415
ENSG00000102387	<i>TAF7L</i>	0.000	3.416
ENSG00000282057	<i>AC092807.3</i>	0.003	3.424
ENSG00000189043	<i>NDUFA4</i>	0.000	3.426
ENSG00000285641	<i>AL358472.6</i>	0.000	3.429
ENSG00000164898	<i>FMC1</i>	0.000	3.431
ENSG00000178685	<i>PARP10</i>	0.000	3.432
ENSG00000261572	<i>AC097639.1</i>	0.000	3.434
ENSG00000060971	<i>ACAA1</i>	0.000	3.434
ENSG00000211459	<i>MT-RNR1</i>	0.000	3.435
ENSG00000196743	<i>GM2A</i>	0.000	3.439
ENSG00000134590	<i>RTL8C</i>	0.000	3.440
ENSG00000174469	<i>CNTNAP2</i>	0.004	3.441
ENSG00000254251	<i>AC103770.1</i>	0.000	3.442
ENSG00000107537	<i>PHYH</i>	0.000	3.442
ENSG00000221963	<i>APOL6</i>	0.000	3.442

ENSG00000167705	<i>RILP</i>	0.000	3.445
ENSG00000227495	<i>AC004771.1</i>	0.006	3.446
ENSG00000131828	<i>PDHA1</i>	0.000	3.451
ENSG00000250722	<i>SELENOP</i>	0.000	3.452
ENSG00000260261	<i>AC124944.3</i>	0.000	3.452
ENSG00000012171	<i>SEMA3B</i>	0.000	3.455
ENSG00000225439	<i>BOLA3-AS1</i>	0.000	3.456
ENSG00000106038	<i>EVX1</i>	0.000	3.460
ENSG00000205707	<i>ETFRF1</i>	0.000	3.462
ENSG00000148935	<i>GAS2</i>	0.000	3.462
ENSG00000259345	<i>AC013652.1</i>	0.000	3.463
ENSG00000154265	<i>ABCA5</i>	0.000	3.468
ENSG00000229512	<i>AC068580.1</i>	0.001	3.469
ENSG00000169764	<i>UGP2</i>	0.000	3.472
ENSG00000279253	<i>AL121753.2</i>	0.000	3.476
ENSG00000074660	<i>SCARF1</i>	0.000	3.482
ENSG00000156709	<i>AIFM1</i>	0.000	3.483
ENSG00000187546	<i>AGMO</i>	0.002	3.484
ENSG00000088053	<i>GP6</i>	0.000	3.489
ENSG00000171970	<i>ZNF57</i>	0.000	3.489
ENSG00000214193	<i>SH3D21</i>	0.000	3.495
ENSG00000124721	<i>DNAH8</i>	0.000	3.496
ENSG00000162777	<i>DENND2D</i>	0.000	3.497
ENSG00000179277	<i>MEIS3P1</i>	0.001	3.499
ENSG00000139192	<i>TAPBPL</i>	0.000	3.501
ENSG00000273080	<i>AC009309.1</i>	0.000	3.502
ENSG00000116663	<i>FBXO6</i>	0.000	3.503
ENSG00000125148	<i>MT2A</i>	0.000	3.503
ENSG00000128564	<i>VGf</i>	0.000	3.503
ENSG00000168710	<i>AHCYL1</i>	0.000	3.507
ENSG00000273084	<i>AC092171.5</i>	0.000	3.507
ENSG00000261424	<i>ATP5PBP7</i>	0.003	3.508
ENSG00000232940	<i>HCG25</i>	0.000	3.508
ENSG00000132185	<i>FCRLA</i>	0.000	3.509
ENSG00000254373	<i>AC112191.2</i>	0.000	3.511
ENSG00000273143	<i>AL355512.1</i>	0.000	3.514
ENSG00000235214	<i>FAM83C-AS1</i>	0.003	3.517
ENSG00000170231	<i>FABP6</i>	0.000	3.518
ENSG00000230373	<i>GOLGA6L5P</i>	0.000	3.522
ENSG00000260805	<i>AC092803.2</i>	0.000	3.524
ENSG00000167283	<i>ATP5MG</i>	0.000	3.526
ENSG00000130734	<i>ATG4D</i>	0.000	3.535
ENSG00000279149	<i>AL356750.1</i>	0.007	3.536
ENSG00000267659	<i>LINC01482</i>	0.000	3.540
ENSG00000229018	<i>PMS2P7</i>	0.000	3.541
ENSG00000278978	<i>AC092611.3</i>	0.000	3.544
ENSG00000164342	<i>TLR3</i>	0.000	3.546
ENSG00000173926	<i>MARCH3</i>	0.000	3.549
ENSG00000105289	<i>TJP3</i>	0.000	3.551
ENSG00000118292	<i>C1orf54</i>	0.000	3.551
ENSG00000235663	<i>SAPCD1-AS1</i>	0.000	3.551
ENSG00000197584	<i>KCNMB2</i>	0.002	3.554
ENSG00000272217	<i>AL645940.1</i>	0.000	3.556
ENSG00000272831	<i>AC027644.3</i>	0.000	3.559
ENSG00000278095	<i>AC022509.4</i>	0.000	3.560
ENSG00000255224	<i>AC109322.1</i>	0.000	3.561
ENSG00000205593	<i>DENND6B</i>	0.000	3.564
ENSG00000120324	<i>PCDHB10</i>	0.000	3.565
ENSG00000168961	<i>LGALS9</i>	0.000	3.566
ENSG00000237899	<i>AL031289.1</i>	0.007	3.567

ENSG0000054277	<i>OPN3</i>	0.000	3.574
ENSG00000143375	<i>CGN</i>	0.000	3.575
ENSG0000010318	<i>PHF7</i>	0.000	3.577
ENSG00000232229	<i>LINC00865</i>	0.000	3.578
ENSG00000155016	<i>CYP2U1</i>	0.000	3.581
ENSG00000134575	<i>ACP2</i>	0.000	3.582
ENSG00000230613	<i>HM13-AS1</i>	0.003	3.582
ENSG00000248677	<i>LINC02102</i>	0.009	3.585
ENSG00000225676	<i>AC002378.1</i>	0.000	3.587
ENSG00000168528	<i>SERINC2</i>	0.000	3.587
ENSG00000259065	<i>AC005520.2</i>	0.000	3.589
ENSG00000105499	<i>PLA2G4C</i>	0.000	3.590
ENSG00000196118	<i>CCDC189</i>	0.000	3.594
ENSG00000260552	<i>AC023043.1</i>	0.000	3.596
ENSG00000283098	<i>AL132857.2</i>	0.000	3.599
ENSG00000163072	<i>NOSTRIN</i>	0.000	3.601
ENSG00000235527	<i>HIPK1-AS1</i>	0.000	3.603
ENSG00000005238	<i>FAM214B</i>	0.000	3.609
ENSG00000174912	<i>METTL15P1</i>	0.000	3.610
ENSG00000151320	<i>AKAP6</i>	0.000	3.616
ENSG00000265666	<i>RARA-AS1</i>	0.000	3.618
ENSG00000171817	<i>ZNF540</i>	0.000	3.622
ENSG00000227071	<i>FOCAD-AS1</i>	0.004	3.623
ENSG00000274180	<i>NATD1</i>	0.000	3.629
ENSG00000277399	<i>GPR179</i>	0.000	3.632
ENSG00000260428	<i>SCX</i>	0.000	3.633
ENSG00000254602	<i>AP000662.1</i>	0.004	3.634
ENSG00000178776	<i>C5orf46</i>	0.000	3.636
ENSG00000248027	<i>AP001351.1</i>	0.000	3.638
ENSG00000137714	<i>FDX1</i>	0.000	3.640
ENSG00000166548	<i>TK2</i>	0.000	3.642
ENSG00000106049	<i>HIBADH</i>	0.000	3.642
ENSG00000279013	<i>AC110774.1</i>	0.006	3.642
ENSG00000267219	<i>AC010504.1</i>	0.000	3.645
ENSG00000210049	<i>MT-TF</i>	0.006	3.654
ENSG00000279066	<i>HEXDC-IT1</i>	0.005	3.654
ENSG00000142530	<i>FAM71E1</i>	0.000	3.655
ENSG00000269959	<i>SPACA6P-AS</i>	0.000	3.656
ENSG00000261079	<i>AC009053.2</i>	0.004	3.657
ENSG00000101470	<i>TNNC2</i>	0.000	3.662
ENSG00000270084	<i>GAS5-AS1</i>	0.000	3.662
ENSG00000260793	<i>AC003102.1</i>	0.000	3.662
ENSG00000236152	<i>MRPS36P1</i>	0.000	3.663
ENSG00000260329	<i>AC007541.1</i>	0.000	3.663
ENSG00000241978	<i>AKAP2</i>	0.000	3.669
ENSG00000156587	<i>UBE2L6</i>	0.000	3.669
ENSG00000196071	<i>OR2L13</i>	0.000	3.671
ENSG00000228089	<i>PNKDP1</i>	0.005	3.676
ENSG00000274253	<i>AC138649.1</i>	0.001	3.684
ENSG00000188582	<i>PAQR9</i>	0.000	3.685
ENSG00000171357	<i>LURAP1</i>	0.000	3.685
ENSG00000088543	<i>C3orf18</i>	0.000	3.686
ENSG00000273473	<i>BX649601.1</i>	0.002	3.687
ENSG00000133424	<i>LARGE1</i>	0.002	3.690
ENSG00000214827	<i>MTCP1</i>	0.000	3.694
ENSG00000127249	<i>ATP13A4</i>	0.000	3.694
ENSG00000143198	<i>MGST3</i>	0.000	3.697
ENSG00000135409	<i>AMHR2</i>	0.000	3.698
ENSG00000255320	<i>AP000759.1</i>	0.000	3.698
ENSG00000224566	<i>FAM96AP2</i>	0.001	3.700

ENSG00000224051	<i>CPTP</i>	0.000	3.703
ENSG00000197748	<i>CFAP43</i>	0.000	3.703
ENSG00000264672	<i>SEPT4-AS1</i>	0.000	3.704
ENSG00000213433	<i>RPLP1P6</i>	0.000	3.710
ENSG00000165071	<i>TMEM71</i>	0.000	3.714
ENSG00000185988	<i>PLK5</i>	0.007	3.715
ENSG00000272341	<i>AL137003.2</i>	0.000	3.719
ENSG00000270021	<i>AC026691.1</i>	0.000	3.720
ENSG00000153982	<i>GDPD1</i>	0.000	3.721
ENSG00000228140	<i>AL031283.1</i>	0.001	3.722
ENSG00000279798	<i>AC018659.2</i>	0.003	3.722
ENSG00000273328	<i>AC099329.2</i>	0.000	3.724
ENSG00000223396	<i>RPS10P7</i>	0.000	3.726
ENSG00000172738	<i>TMEM217</i>	0.000	3.726
ENSG00000267073	<i>AC005256.1</i>	0.000	3.727
ENSG00000013588	<i>GPRC5A</i>	0.000	3.729
ENSG00000273221	<i>AL355816.2</i>	0.001	3.732
ENSG00000168016	<i>TRANK1</i>	0.000	3.733
ENSG00000186399	<i>GOLGA8R</i>	0.000	3.733
ENSG00000184619	<i>KRBA2</i>	0.000	3.734
ENSG00000228084	<i>AC118553.1</i>	0.000	3.738
ENSG00000233251	<i>AC007743.1</i>	0.000	3.742
ENSG00000241313	<i>WWTR1-AS1</i>	0.000	3.742
ENSG00000185187	<i>SIGIRR</i>	0.000	3.755
ENSG00000006047	<i>YBX2</i>	0.000	3.765
ENSG00000007062	<i>PROM1</i>	0.000	3.766
ENSG00000234817	<i>AL136309.2</i>	0.000	3.766
ENSG00000149761	<i>NUDT22</i>	0.000	3.775
ENSG00000180628	<i>PCGF5</i>	0.000	3.776
ENSG00000225335	<i>AC016027.1</i>	0.000	3.776
ENSG00000230530	<i>LIMD1-AS1</i>	0.000	3.776
ENSG00000169435	<i>RASSF6</i>	0.000	3.777
ENSG00000165716	<i>FAM69B</i>	0.000	3.780
ENSG00000225655	<i>BX255923.1</i>	0.000	3.789
ENSG00000111335	<i>OAS2</i>	0.000	3.789
ENSG00000125434	<i>SLC25A35</i>	0.000	3.791
ENSG00000235863	<i>B3GALT4</i>	0.000	3.794
ENSG00000263432	<i>RN7SL689P</i>	0.000	3.794
ENSG00000172794	<i>RAB37</i>	0.007	3.795
ENSG00000175773	<i>AP002986.1</i>	0.000	3.796
ENSG00000100412	<i>ACO2</i>	0.000	3.804
ENSG00000155970	<i>MICU3</i>	0.000	3.804
ENSG00000138029	<i>HADHB</i>	0.000	3.805
ENSG00000146085	<i>MUT</i>	0.000	3.806
ENSG00000259915	<i>AC017071.1</i>	0.000	3.809
ENSG00000129159	<i>KCNC1</i>	0.000	3.809
ENSG00000210082	<i>MT-RNR2</i>	0.000	3.812
ENSG00000236671	<i>PRKG1-AS1</i>	0.000	3.820
ENSG00000196951	<i>SCOC-AS1</i>	0.000	3.831
ENSG00000276644	<i>DACH1</i>	0.000	3.831
ENSG00000221821	<i>C6orf226</i>	0.000	3.832
ENSG00000183648	<i>NDUFB1</i>	0.000	3.832
ENSG00000148357	<i>HMCN2</i>	0.000	3.834
ENSG00000115525	<i>ST3GAL5</i>	0.000	3.834
ENSG00000253848	<i>AC010834.2</i>	0.001	3.837
ENSG00000174567	<i>GOLT1A</i>	0.000	3.837
ENSG00000275897	<i>AC021491.4</i>	0.008	3.838
ENSG00000105655	<i>ISYNA1</i>	0.000	3.840
ENSG00000270049	<i>AC009061.2</i>	0.000	3.841
ENSG00000134539	<i>KLRD1</i>	0.004	3.841

ENSG00000121207	<i>LRAT</i>	0.000	3.843
ENSG00000285685	<i>AC115284.3</i>	0.000	3.843
ENSG00000182583	<i>VCX</i>	0.008	3.846
ENSG00000168938	<i>PPIC</i>	0.000	3.847
ENSG00000234745	<i>HLA-B</i>	0.000	3.849
ENSG00000236137	<i>AL445231.1</i>	0.000	3.860
ENSG00000204396	<i>VWA7</i>	0.000	3.861
ENSG00000250999	<i>AC136604.3</i>	0.001	3.862
ENSG00000223547	<i>ZNF844</i>	0.000	3.863
ENSG00000204758	<i>AC008429.1</i>	0.000	3.864
ENSG00000212443	<i>SNORA53</i>	0.006	3.864
ENSG00000171291	<i>ZNF439</i>	0.001	3.866
ENSG00000139971	<i>ARMH4</i>	0.000	3.869
ENSG00000140057	<i>AK7</i>	0.000	3.869
ENSG00000243649	<i>CFB</i>	0.001	3.870
ENSG00000253477	<i>AC012213.1</i>	0.002	3.873
ENSG00000151117	<i>TMEM86A</i>	0.000	3.875
ENSG00000267077	<i>AC020663.2</i>	0.003	3.881
ENSG00000285884	<i>AL022345.4</i>	0.005	3.883
ENSG00000149743	<i>TRPT1</i>	0.000	3.885
ENSG00000177427	<i>MIEF2</i>	0.000	3.885
ENSG00000258711	<i>AL358334.2</i>	0.000	3.886
ENSG00000203872	<i>C6orf163</i>	0.000	3.889
ENSG00000167216	<i>KATNAL2</i>	0.000	3.890
ENSG00000236651	<i>DLX2-DT</i>	0.001	3.896
ENSG00000129493	<i>HEATR5A</i>	0.000	3.900
ENSG00000282034	<i>AC106886.5</i>	0.000	3.901
ENSG00000143409	<i>MINDY1</i>	0.000	3.902
ENSG00000133101	<i>CCNA1</i>	0.000	3.908
ENSG00000188747	<i>NOXA1</i>	0.000	3.909
ENSG00000121577	<i>POPDC2</i>	0.000	3.912
ENSG00000214810	<i>CYCSP55</i>	0.000	3.917
ENSG00000138642	<i>HERC6</i>	0.000	3.922
ENSG00000253123	<i>AC091182.1</i>	0.003	3.923
ENSG00000269028	<i>MTRNR2L12</i>	0.000	3.925
ENSG00000233509	<i>ZNF197-AS1</i>	0.000	3.928
ENSG00000189136	<i>UBE2Q2P1</i>	0.000	3.929
ENSG00000110876	<i>SELPLG</i>	0.000	3.930
ENSG00000236496	<i>GPS2P1</i>	0.001	3.930
ENSG00000147485	<i>PXDNL</i>	0.000	3.930
ENSG00000142235	<i>LMTK3</i>	0.000	3.942
ENSG00000215374	<i>FAM66B</i>	0.003	3.943
ENSG00000006756	<i>ARSD</i>	0.000	3.944
ENSG00000119703	<i>ZC2HC1C</i>	0.000	3.948
ENSG00000173868	<i>PHOSPHO1</i>	0.000	3.950
ENSG00000154518	<i>ATP5MC3</i>	0.000	3.952
ENSG00000166578	<i>IQCD</i>	0.000	3.953
ENSG00000222489	<i>SNORA79B</i>	0.000	3.953
ENSG00000148090	<i>AUH</i>	0.000	3.956
ENSG00000246145	<i>RRS1-AS1</i>	0.006	3.957
ENSG00000245468	<i>LINC02447</i>	0.000	3.959
ENSG00000109846	<i>CRYAB</i>	0.000	3.961
ENSG00000146038	<i>DCDC2</i>	0.000	3.966
ENSG00000223829	<i>AC004870.2</i>	0.005	3.966
ENSG00000234604	<i>AL021068.2</i>	0.005	3.972
ENSG00000259407	<i>AC021739.2</i>	0.000	3.976
ENSG00000171502	<i>COL24A1</i>	0.000	3.978
ENSG00000184831	<i>APOO</i>	0.000	3.983
ENSG00000177692	<i>DNAJC28</i>	0.000	3.985
ENSG00000215218	<i>UBE2QL1</i>	0.000	3.987

ENSG00000203663	OR2L2	0.002	3.990
ENSG00000269888	AC112491.1	0.004	3.990
ENSG00000255823	MTRNR2L8	0.000	3.992
ENSG00000139410	SDSL	0.000	3.996
ENSG00000235052	AL021154.1	0.000	4.000
ENSG00000258667	HIF1A-AS2	0.000	4.000
ENSG00000242242	NECTIN3-AS1	0.000	4.003
ENSG00000131015	ULBP2	0.000	4.004
ENSG00000146700	SSC4D	0.000	4.005
ENSG00000185340	GAS2L1	0.000	4.012
ENSG00000126217	MCF2L	0.002	4.013
ENSG00000213463	SYNJ2BP	0.000	4.021
ENSG00000107796	ACTA2	0.000	4.021
ENSG00000175170	FAM182B	0.000	4.023
ENSG00000181061	HIGD1A	0.000	4.024
ENSG00000107020	PLGRKT	0.000	4.033
ENSG00000224004	ATP5F1CP1	0.007	4.038
ENSG00000203797	DDO	0.000	4.040
ENSG00000272157	AC107373.2	0.000	4.042
ENSG00000225855	RUSC1-AS1	0.000	4.046
ENSG00000232415	ELN-AS1	0.000	4.049
ENSG00000113790	EHHADH	0.000	4.054
ENSG00000118156	ZNF541	0.001	4.055
ENSG00000125966	MMP24	0.000	4.063
ENSG00000228397	LINC01635	0.008	4.063
ENSG00000225555	AP000320.1	0.003	4.066
ENSG00000258016	HIGD1AP1	0.000	4.069
ENSG00000234492	RPL34-AS1	0.000	4.079
ENSG00000198482	ZNF808	0.000	4.080
ENSG00000226913	BSN-DT	0.000	4.088
ENSG00000266010	GATA6-AS1	0.000	4.098
ENSG00000244791	AC087667.1	0.000	4.099
ENSG00000129422	MTUS1	0.000	4.102
ENSG00000249709	ZNF564	0.000	4.105
ENSG00000117984	CTSD	0.000	4.109
ENSG00000176049	JAKMIP2	0.000	4.112
ENSG00000168685	IL7R	0.000	4.116
ENSG00000169896	ITGAM	0.001	4.117
ENSG00000064652	SNX24	0.000	4.130
ENSG00000154262	ABCA6	0.000	4.134
ENSG00000250222	AC008443.4	0.000	4.137
ENSG00000130649	CYP2E1	0.000	4.145
ENSG00000224965	LINC02586	0.001	4.147
ENSG00000205220	PSMB10	0.000	4.151
ENSG00000237436	CAMTA1-DT	0.000	4.151
ENSG00000281538	AC254562.3	0.000	4.159
ENSG00000108684	ASIC2	0.000	4.160
ENSG00000260922	AC009139.1	0.005	4.162
ENSG00000186714	CCDC73	0.000	4.162
ENSG00000185100	ADSSL1	0.000	4.164
ENSG00000240567	LINC02067	0.000	4.171
ENSG00000137628	DDX60	0.000	4.174
ENSG00000256043	CTSO	0.000	4.177
ENSG00000224418	STK24-AS1	0.003	4.181
ENSG00000285714	AL159158.1	0.001	4.182
ENSG00000054392	HHAT	0.000	4.192
ENSG00000148450	MSRB2	0.000	4.194
ENSG00000136828	RALGPS1	0.000	4.195
ENSG00000106333	PCOLCE	0.000	4.196
ENSG00000283828	AL137002.2	0.000	4.205

ENSG00000137509	<i>PRCP</i>	0.000	4.211
ENSG00000130513	<i>GDF15</i>	0.000	4.216
ENSG00000234694	<i>AL139289.2</i>	0.000	4.216
ENSG00000183208	<i>GDPGP1</i>	0.000	4.222
ENSG00000196542	<i>SPTSSB</i>	0.000	4.224
ENSG00000273492	<i>AP000229.1</i>	0.000	4.227
ENSG00000269386	<i>RAB11B-AS1</i>	0.000	4.253
ENSG00000254402	<i>LRRC24</i>	0.000	4.256
ENSG00000158859	<i>ADAMTS4</i>	0.007	4.258
ENSG00000163803	<i>PLB1</i>	0.000	4.263
ENSG00000167815	<i>PRDX2</i>	0.000	4.263
ENSG00000186951	<i>PPARA</i>	0.000	4.263
ENSG00000229869	<i>AL359878.2</i>	0.007	4.265
ENSG00000267072	<i>NAGPA-AS1</i>	0.000	4.267
ENSG00000196482	<i>ESRRG</i>	0.000	4.270
ENSG00000198270	<i>TMEM116</i>	0.000	4.281
ENSG00000163347	<i>CLDN1</i>	0.000	4.281
ENSG00000197536	<i>C5orf56</i>	0.000	4.282
ENSG00000059915	<i>PSD</i>	0.000	4.283
ENSG00000167861	<i>HID1</i>	0.000	4.284
ENSG00000250286	<i>AC021491.2</i>	0.000	4.289
ENSG00000262050	<i>AC005696.1</i>	0.000	4.291
ENSG00000144115	<i>THNSL2</i>	0.000	4.294
ENSG00000167363	<i>FN3K</i>	0.000	4.301
ENSG00000164418	<i>GRIK2</i>	0.000	4.303
ENSG00000245573	<i>BDNF-AS</i>	0.000	4.305
ENSG00000143036	<i>SLC44A3</i>	0.000	4.318
ENSG00000204044	<i>SLC12A5-AS1</i>	0.000	4.319
ENSG00000088340	<i>FER1L4</i>	0.000	4.319
ENSG00000197956	<i>S100A6</i>	0.000	4.332
ENSG00000125510	<i>OPRL1</i>	0.000	4.333
ENSG00000152582	<i>SPEF2</i>	0.000	4.334
ENSG00000261420	<i>AL022069.1</i>	0.000	4.339
ENSG00000167549	<i>CORO6</i>	0.000	4.341
ENSG00000233308	<i>OSTN-AS1</i>	0.000	4.342
ENSG00000173208	<i>ABCD2</i>	0.000	4.347
ENSG00000166349	<i>RAG1</i>	0.000	4.349
ENSG00000197857	<i>ZNF44</i>	0.000	4.349
ENSG0000014641	<i>MDH1</i>	0.000	4.355
ENSG00000166268	<i>MYRFL</i>	0.001	4.362
ENSG00000197461	<i>PDGFA</i>	0.000	4.367
ENSG00000251455	<i>AC092611.1</i>	0.000	4.372
ENSG00000171860	<i>C3AR1</i>	0.000	4.374
ENSG00000099957	<i>P2RX6</i>	0.000	4.383
ENSG00000277581	<i>AL023803.3</i>	0.003	4.384
ENSG00000231050	<i>AL109917.1</i>	0.000	4.388
ENSG00000184068	<i>SREBF2-AS1</i>	0.000	4.389
ENSG00000235070	<i>AC062015.1</i>	0.001	4.395
ENSG00000138378	<i>STAT4</i>	0.000	4.396
ENSG00000089163	<i>SIRT4</i>	0.000	4.401
ENSG00000267549	<i>AC006116.8</i>	0.000	4.405
ENSG00000139112	<i>GABARAPL1</i>	0.000	4.408
ENSG00000168062	<i>BATF2</i>	0.000	4.410
ENSG00000278828	<i>HIST1H3H</i>	0.000	4.410
ENSG00000254300	<i>LINC01111</i>	0.000	4.414
ENSG00000187013	<i>C17orf82</i>	0.000	4.419
ENSG00000117791	<i>MARC2</i>	0.000	4.423
ENSG00000166165	<i>CKB</i>	0.000	4.425
ENSG00000259118	<i>AL139022.1</i>	0.000	4.443
ENSG00000284959	<i>AC007262.2</i>	0.000	4.444

ENSG00000129048	<i>ACKR4</i>	0.002	4.445
ENSG00000135333	<i>EPHA7</i>	0.000	4.447
ENSG00000172403	<i>SYNPO2</i>	0.000	4.449
ENSG00000226944	<i>AL031847.1</i>	0.000	4.450
ENSG00000105649	<i>RAB3A</i>	0.000	4.451
ENSG00000229474	<i>PATL2</i>	0.000	4.452
ENSG00000227128	<i>LBX1-AS1</i>	0.000	4.457
ENSG00000233131	<i>AC096649.2</i>	0.000	4.466
ENSG00000222017	<i>AC011997.1</i>	0.001	4.471
ENSG00000254821	<i>AL136309.4</i>	0.002	4.477
ENSG00000260101	<i>AC008074.2</i>	0.000	4.484
ENSG00000233006	<i>MIR3936HG</i>	0.000	4.484
ENSG00000246331	<i>AC010198.1</i>	0.001	4.484
ENSG00000204706	<i>MAMDC2-AS1</i>	0.006	4.486
ENSG00000101605	<i>MYOM1</i>	0.000	4.487
ENSG00000272195	<i>AL356512.1</i>	0.000	4.487
ENSG00000163170	<i>BOLA3</i>	0.000	4.489
ENSG00000232859	<i>LYRM9</i>	0.000	4.491
ENSG0000026297	<i>RNASET2</i>	0.000	4.492
ENSG00000244468	<i>AC093001.1</i>	0.000	4.495
ENSG00000110013	<i>SIAE</i>	0.000	4.497
ENSG00000258844	<i>AL162511.1</i>	0.000	4.497
ENSG00000214216	<i>IQCJ</i>	0.000	4.499
ENSG00000121858	<i>TNFSF10</i>	0.000	4.499
ENSG00000172594	<i>SMPDL3A</i>	0.000	4.508
ENSG00000179593	<i>ALOX15B</i>	0.000	4.509
ENSG00000110011	<i>DNAJC4</i>	0.000	4.510
ENSG00000237748	<i>UQCRBP1</i>	0.000	4.521
ENSG00000283627	<i>AL137785.1</i>	0.004	4.522
ENSG00000154930	<i>ACSS1</i>	0.000	4.523
ENSG0000025708	<i>TYMP</i>	0.000	4.524
ENSG00000270638	<i>AL023806.1</i>	0.000	4.532
ENSG00000117600	<i>PLPPR4</i>	0.000	4.532
ENSG00000234353	<i>AP000346.2</i>	0.000	4.549
ENSG00000177096	<i>PHETA2</i>	0.000	4.568
ENSG00000281912	<i>LINC01144</i>	0.000	4.568
ENSG00000262223	<i>AC110285.1</i>	0.000	4.569
ENSG00000167046	<i>AL357033.1</i>	0.000	4.569
ENSG00000231133	<i>HAR1B</i>	0.000	4.571
ENSG00000100218	<i>RSPH14</i>	0.000	4.572
ENSG00000143630	<i>HCN3</i>	0.000	4.574
ENSG00000138399	<i>FASTKD1</i>	0.000	4.581
ENSG00000256193	<i>LINC00507</i>	0.000	4.588
ENSG00000162840	<i>MT2P1</i>	0.000	4.588
ENSG00000241935	<i>HOGA1</i>	0.000	4.592
ENSG00000125246	<i>CLYBL</i>	0.000	4.594
ENSG00000123119	<i>NECAB1</i>	0.000	4.623
ENSG00000237013	<i>LINC01812</i>	0.000	4.626
ENSG00000148677	<i>ANKRD1</i>	0.000	4.628
ENSG00000178695	<i>KCTD12</i>	0.000	4.630
ENSG00000160111	<i>CPAMD8</i>	0.000	4.631
ENSG00000105808	<i>RASA4</i>	0.000	4.634
ENSG00000138769	<i>CDKL2</i>	0.000	4.636
ENSG00000281358	<i>RASSF1-AS1</i>	0.000	4.648
ENSG00000204323	<i>SMIM5</i>	0.000	4.655
ENSG00000257303	<i>AC073896.2</i>	0.000	4.658
ENSG00000249306	<i>LINC01411</i>	0.000	4.660
ENSG00000225506	<i>CYP4A22-AS1</i>	0.000	4.661
ENSG00000255568	<i>BRWD1-AS2</i>	0.000	4.668
ENSG00000112981	<i>NME5</i>	0.000	4.671

ENSG00000142959	BEST4	0.001	4.672
ENSG00000244300	GATA2-AS1	0.000	4.673
ENSG00000223776	LGALS8-AS1	0.000	4.681
ENSG00000268220	AC008040.5	0.001	4.690
ENSG00000127412	TRPV5	0.000	4.692
ENSG00000125347	IRF1	0.000	4.692
ENSG00000273270	AC090114.2	0.000	4.698
ENSG00000187608	ISG15	0.000	4.701
ENSG00000088726	TMEM40	0.000	4.702
ENSG00000000971	CFH	0.000	4.702
ENSG00000166145	SPINT1	0.000	4.703
ENSG00000167971	CASKIN1	0.000	4.706
ENSG00000130066	SAT1	0.000	4.708
ENSG00000228741	SPATA13	0.000	4.718
ENSG00000206113	CFAP99	0.000	4.721
ENSG00000228594	FNDC10	0.000	4.722
ENSG00000099338	CATSPERG	0.000	4.731
ENSG00000255200	PGAM1P8	0.000	4.742
ENSG00000231324	AP000696.1	0.000	4.745
ENSG00000262772	LINC01977	0.000	4.746
ENSG00000172828	CES3	0.000	4.748
ENSG00000185418	TARSL2	0.000	4.754
ENSG00000149927	DOC2A	0.000	4.755
ENSG00000129538	RNASE1	0.000	4.756
ENSG00000125967	NECAB3	0.000	4.764
ENSG00000235652	AL356599.1	0.000	4.800
ENSG00000258386	AL352984.1	0.005	4.800
ENSG00000023445	BIRC3	0.000	4.811
ENSG00000235687	LINC00993	0.001	4.818
ENSG00000171180	OR2M4	0.000	4.819
ENSG00000272695	GAS6-DT	0.000	4.831
ENSG00000137959	IFI44L	0.000	4.851
ENSG00000183784	C9orf66	0.007	4.854
ENSG00000144648	ACKR2	0.000	4.856
ENSG00000272432	AL031432.3	0.008	4.878
ENSG00000043039	BARX2	0.000	4.886
ENSG00000245975	AC090515.2	0.000	4.892
ENSG00000168765	GSTM4	0.000	4.904
ENSG00000267498	AC007786.1	0.003	4.914
ENSG00000268129	AC026304.1	0.000	4.933
ENSG00000205838	TTC23L	0.000	4.937
ENSG00000227375	DLG1-AS1	0.000	4.939
ENSG00000277369	AC010654.1	0.000	4.945
ENSG00000115602	IL1RL1	0.000	4.950
ENSG00000272894	AC004982.2	0.000	4.954
ENSG00000276075	AC027682.6	0.000	4.958
ENSG00000177409	SAMD9L	0.000	4.960
ENSG00000091137	SLC26A4	0.000	4.963
ENSG00000126005	MMP24OS	0.000	4.964
ENSG00000100003	SEC14L2	0.000	4.972
ENSG00000271043	MTRNR2L2	0.001	4.978
ENSG00000113140	SPARC	0.000	4.984
ENSG00000154274	C4orf19	0.000	4.991
ENSG00000112561	TFEB	0.000	4.992
ENSG00000271474	AC106881.1	0.000	5.001
ENSG00000253320	AZIN1-AS1	0.000	5.009
ENSG00000185015	CA13	0.000	5.010
ENSG00000137198	GMPR	0.000	5.013
ENSG00000106302	HYAL4	0.000	5.014
ENSG00000279518	AC083843.3	0.000	5.017

ENSG00000151729	<i>SLC25A4</i>	0.000	5.017
ENSG00000279419	<i>AC004925.1</i>	0.000	5.033
ENSG00000263033	<i>AC007220.1</i>	0.000	5.042
ENSG00000266947	<i>AC022916.1</i>	0.000	5.043
ENSG00000154736	<i>ADAMTS5</i>	0.000	5.047
ENSG00000257556	<i>LINC02298</i>	0.000	5.058
ENSG00000164125	<i>FAM198B</i>	0.000	5.066
ENSG00000241361	<i>SLC25A24P1</i>	0.003	5.069
ENSG0000019991	<i>HGF</i>	0.000	5.072
ENSG00000186212	<i>SOWAHB</i>	0.002	5.076
ENSG00000270714	<i>MINOS1P2</i>	0.001	5.079
ENSG00000117054	<i>ACADM</i>	0.000	5.083
ENSG00000177993	<i>ZNRF3-AS1</i>	0.009	5.094
ENSG00000244119	<i>PDCL3P4</i>	0.000	5.098
ENSG00000165973	<i>NELL1</i>	0.001	5.099
ENSG00000203446	<i>AC004988.1</i>	0.000	5.101
ENSG00000263597	<i>MIR3936</i>	0.003	5.102
ENSG00000143382	<i>ADAMTSL4</i>	0.000	5.105
ENSG00000269293	<i>ZSCAN16-AS1</i>	0.000	5.112
ENSG00000274292	<i>AC084018.2</i>	0.000	5.121
ENSG00000280216	<i>AL022326.2</i>	0.008	5.134
ENSG00000258785	<i>LINC01580</i>	0.009	5.137
ENSG00000276855	<i>AC015922.3</i>	0.000	5.153
ENSG00000196684	<i>HSH2D</i>	0.000	5.160
ENSG00000130762	<i>ARHGEF16</i>	0.000	5.177
ENSG00000185669	<i>SNAI3</i>	0.004	5.178
ENSG00000214357	<i>NEURL1B</i>	0.001	5.180
ENSG00000279249	<i>AC007614.1</i>	0.002	5.183
ENSG00000219410	<i>AC125494.1</i>	0.000	5.184
ENSG00000161381	<i>PLXDC1</i>	0.002	5.189
ENSG00000047936	<i>ROS1</i>	0.000	5.190
ENSG00000006118	<i>TMEM132A</i>	0.000	5.191
ENSG00000273183	<i>AC093726.2</i>	0.000	5.193
ENSG00000262165	<i>AC233723.1</i>	0.000	5.199
ENSG00000267801	<i>AC087289.5</i>	0.000	5.200
ENSG00000117640	<i>MTFR1L</i>	0.000	5.200
ENSG00000271732	<i>AL137798.1</i>	0.000	5.208
ENSG00000112096	<i>SOD2</i>	0.000	5.213
ENSG00000165092	<i>ALDH1A1</i>	0.000	5.217
ENSG00000128335	<i>APOL2</i>	0.000	5.217
ENSG00000267905	<i>AC008750.3</i>	0.000	5.218
ENSG00000213937	<i>CLDN9</i>	0.000	5.228
ENSG00000180769	<i>WDFY3-AS2</i>	0.000	5.235
ENSG00000267062	<i>AC018761.2</i>	0.000	5.237
ENSG00000112183	<i>RBM24</i>	0.000	5.246
ENSG00000182179	<i>UBA7</i>	0.000	5.246
ENSG00000134193	<i>REG4</i>	0.000	5.247
ENSG00000154678	<i>PDE1C</i>	0.000	5.258
ENSG00000180425	<i>C11orf71</i>	0.000	5.261
ENSG00000146859	<i>TMEM140</i>	0.000	5.272
ENSG00000233237	<i>LINC00472</i>	0.000	5.277
ENSG00000268926	<i>AL354861.3</i>	0.007	5.284
ENSG00000204625	<i>HCG9</i>	0.007	5.291
ENSG00000272732	<i>AC004982.1</i>	0.004	5.311
ENSG00000260647	<i>AC127537.1</i>	0.008	5.311
ENSG00000272173	<i>U47924.2</i>	0.000	5.313
ENSG00000137699	<i>TRIM29</i>	0.000	5.314
ENSG00000251655	<i>PRB1</i>	0.000	5.321
ENSG00000261465	<i>AC099518.4</i>	0.003	5.325
ENSG00000245552	<i>AP000787.1</i>	0.000	5.326

ENSG00000111012	CYP27B1	0.000	5.344
ENSG00000176907	TCIM	0.001	5.344
ENSG00000137171	KLC4	0.000	5.372
ENSG00000177839	PCDHB9	0.000	5.372
ENSG00000100321	SYNGR1	0.000	5.390
ENSG00000273062	AL449106.1	0.000	5.391
ENSG00000211899	IGHM	0.000	5.395
ENSG00000234807	LINC01135	0.000	5.418
ENSG00000187391	MAGI2	0.000	5.423
ENSG00000196972	SMIM10L2B	0.000	5.428
ENSG00000107864	CPEB3	0.000	5.432
ENSG00000185880	TRIM69	0.000	5.437
ENSG00000129680	MAP7D3	0.003	5.451
ENSG00000150361	KLHL1	0.005	5.455
ENSG00000105711	SCN1B	0.000	5.458
ENSG00000251003	ZFPM2-AS1	0.000	5.462
ENSG00000253530	AC084116.3	0.005	5.469
ENSG00000205436	EXOC3L4	0.007	5.473
ENSG00000271727	AL357054.2	0.001	5.478
ENSG00000243422	RPL23AP49	0.000	5.494
ENSG00000102924	CBLN1	0.000	5.502
ENSG00000223722	AC023157.1	0.000	5.505
ENSG00000185519	FAM131C	0.000	5.506
ENSG00000230401	LINC01972	0.000	5.509
ENSG00000258884	LINC02321	0.000	5.520
ENSG00000226203	LINC01733	0.000	5.522
ENSG00000154319	FAM167A	0.000	5.549
ENSG00000085117	CD82	0.000	5.556
ENSG00000135363	LMO2	0.000	5.565
ENSG00000170369	CST2	0.000	5.565
ENSG00000172379	ARNT2	0.000	5.569
ENSG00000056558	TRAF1	0.000	5.571
ENSG00000162772	ATF3	0.000	5.577
ENSG00000184307	ZDHHC23	0.000	5.586
ENSG00000233785	AC131011.1	0.003	5.606
ENSG00000167895	TMC8	0.000	5.612
ENSG00000100985	MMP9	0.000	5.622
ENSG00000273472	AC096733.2	0.001	5.625
ENSG00000185133	INPP5J	0.000	5.627
ENSG00000228404	AP001468.1	0.005	5.630
ENSG00000162755	KLHDC9	0.000	5.638
ENSG00000227060	LINC00629	0.000	5.644
ENSG00000214264	KCTD9P4	0.002	5.647
ENSG00000197580	BCO2	0.000	5.660
ENSG00000119922	IFIT2	0.000	5.666
ENSG00000276900	AC023157.3	0.000	5.667
ENSG00000225339	AL354740.1	0.000	5.670
ENSG00000185885	IFITM1	0.000	5.674
ENSG00000253865	AC131025.1	0.000	5.676
ENSG00000254119	AC025524.2	0.000	5.676
ENSG00000224081	SLC44A3-AS1	0.000	5.676
ENSG00000186765	FSCN2	0.000	5.683
ENSG00000036530	CYP46A1	0.000	5.686
ENSG00000176845	METRNL	0.000	5.690
ENSG00000112992	NNT	0.000	5.691
ENSG00000285601	AC084262.2	0.000	5.699
ENSG00000231672	DIRC3	0.009	5.705
ENSG00000197444	OGDHL	0.000	5.721
ENSG00000242759	LINC00882	0.000	5.735
ENSG00000272986	AC009570.1	0.000	5.741

ENSG00000117595	<i>IRF6</i>	0.000	5.745
ENSG00000171503	<i>ETFDH</i>	0.000	5.751
ENSG00000261150	<i>EPPK1</i>	0.000	5.757
ENSG00000110675	<i>ELMOD1</i>	0.000	5.758
ENSG00000263105	<i>AC009171.2</i>	0.001	5.759
ENSG00000140876	<i>NUDT7</i>	0.000	5.764
ENSG00000196177	<i>ACADSB</i>	0.000	5.768
ENSG00000224281	<i>SLC25A5-AS1</i>	0.000	5.771
ENSG00000270772	<i>PDHA1P1</i>	0.000	5.774
ENSG00000101076	<i>HNF4A</i>	0.000	5.777
ENSG00000275494	<i>AC133552.5</i>	0.000	5.779
ENSG00000167964	<i>RAB26</i>	0.000	5.788
ENSG00000152315	<i>KCNK13</i>	0.000	5.799
ENSG00000266824	<i>AC129492.4</i>	0.006	5.804
ENSG00000177989	<i>ODF3B</i>	0.000	5.808
ENSG00000120833	<i>SOCS2</i>	0.000	5.813
ENSG00000267666	<i>AC004156.1</i>	0.000	5.824
ENSG00000223714	<i>LINC02601</i>	0.003	5.834
ENSG00000266304	<i>LIVAR</i>	0.000	5.851
ENSG00000049283	<i>EPN3</i>	0.000	5.854
ENSG00000100311	<i>PDGFB</i>	0.000	5.856
ENSG00000139329	<i>LUM</i>	0.000	5.862
ENSG00000166311	<i>SMPD1</i>	0.000	5.863
ENSG00000203876	<i>ADD3-AS1</i>	0.000	5.869
ENSG00000168394	<i>TAP1</i>	0.000	5.879
ENSG00000278709	<i>NKILA</i>	0.000	5.882
ENSG00000197646	<i>PDCD1LG2</i>	0.000	5.921
ENSG00000189283	<i>FHIT</i>	0.000	5.929
ENSG00000004809	<i>SLC22A16</i>	0.002	5.935
ENSG00000204642	<i>HLA-F</i>	0.000	5.938
ENSG00000273151	<i>AC073957.3</i>	0.008	5.945
ENSG00000251141	<i>MRPS30-DT</i>	0.000	5.949
ENSG00000163083	<i>INHBB</i>	0.000	5.957
ENSG00000275812	<i>AL121829.2</i>	0.000	5.959
ENSG00000048740	<i>CELF2</i>	0.000	5.961
ENSG00000144290	<i>SLC4A10</i>	0.000	5.966
ENSG00000104267	<i>CA2</i>	0.000	5.978
ENSG00000095321	<i>CRAT</i>	0.000	6.005
ENSG00000231346	<i>LINC01160</i>	0.000	6.007
ENSG00000181381	<i>DDX60L</i>	0.000	6.020
ENSG00000167136	<i>ENDOG</i>	0.000	6.024
ENSG00000215861	<i>AC245297.1</i>	0.000	6.026
ENSG00000240065	<i>PSMB9</i>	0.000	6.035
ENSG00000183486	<i>MX2</i>	0.000	6.045
ENSG00000226051	<i>ZNF503-AS1</i>	0.000	6.046
ENSG00000267475	<i>AC008736.1</i>	0.000	6.057
ENSG00000251257	<i>AC010457.1</i>	0.000	6.069
ENSG00000198520	<i>ARMH1</i>	0.000	6.082
ENSG00000166407	<i>LMO1</i>	0.000	6.093
ENSG00000244242	<i>IFITM10</i>	0.000	6.108
ENSG00000062524	<i>LTK</i>	0.000	6.109
ENSG00000260500	<i>AC010336.2</i>	0.000	6.119
ENSG00000253690	<i>AC021678.2</i>	0.000	6.126
ENSG00000198003	<i>CCDC151</i>	0.000	6.127
ENSG00000187689	<i>AMTN</i>	0.000	6.134
ENSG00000259687	<i>LINC01220</i>	0.000	6.140
ENSG00000271503	<i>CCL5</i>	0.000	6.147
ENSG00000181773	<i>GPR3</i>	0.000	6.153
ENSG00000104325	<i>DECR1</i>	0.000	6.171
ENSG00000234043	<i>NUDT9P1</i>	0.000	6.180

ENSG00000226935	<i>LINC00161</i>	0.000	6.185
ENSG00000203650	<i>LINC01285</i>	0.000	6.215
ENSG00000184678	<i>HIST2H2BE</i>	0.000	6.216
ENSG00000070540	<i>WIPI1</i>	0.000	6.216
ENSG00000070190	<i>DAPP1</i>	0.000	6.217
ENSG00000227258	<i>SMIM2-AS1</i>	0.000	6.240
ENSG00000260578	<i>AC110597.1</i>	0.000	6.256
ENSG00000254438	<i>AC022240.1</i>	0.001	6.270
ENSG00000152208	<i>GRID2</i>	0.000	6.276
ENSG00000140853	<i>NLRC5</i>	0.000	6.280
ENSG00000280623	<i>PCAT14</i>	0.000	6.284
ENSG00000232456	<i>AL355994.2</i>	0.000	6.289
ENSG00000281100	<i>AC105749.1</i>	0.000	6.302
ENSG00000179399	<i>GPC5</i>	0.000	6.307
ENSG00000196408	<i>NOXO1</i>	0.000	6.315
ENSG00000230102	<i>LINC02028</i>	0.000	6.318
ENSG00000163412	<i>EIF4E3</i>	0.000	6.333
ENSG00000175267	<i>VWA3A</i>	0.000	6.338
ENSG00000157601	<i>MX1</i>	0.000	6.361
ENSG00000089820	<i>ARHGAP4</i>	0.000	6.377
ENSG00000272941	<i>AC083862.2</i>	0.000	6.378
ENSG00000196632	<i>WNK3</i>	0.001	6.391
ENSG00000187229	<i>AC100800.1</i>	0.001	6.393
ENSG00000176945	<i>MUC20</i>	0.000	6.398
ENSG00000143217	<i>NECTIN4</i>	0.006	6.412
ENSG00000283400	<i>AL807740.1</i>	0.000	6.415
ENSG00000227110	<i>LMCD1-AS1</i>	0.000	6.420
ENSG00000165702	<i>GFI1B</i>	0.001	6.422
ENSG00000144908	<i>ALDH1L1</i>	0.000	6.438
ENSG00000177943	<i>MAMDC4</i>	0.000	6.439
ENSG00000169064	<i>ZBBX</i>	0.000	6.440
ENSG00000121769	<i>FABP3</i>	0.000	6.451
ENSG00000164037	<i>SLC9B1</i>	0.000	6.458
ENSG00000257327	<i>AC012555.1</i>	0.000	6.461
ENSG00000072954	<i>TMEM38A</i>	0.000	6.480
ENSG00000145476	<i>CYP4V2</i>	0.000	6.484
ENSG00000128510	<i>CPA4</i>	0.000	6.490
ENSG00000143158	<i>MPC2</i>	0.000	6.493
ENSG00000137460	<i>FHDC1</i>	0.000	6.505
ENSG00000109610	<i>SOD3</i>	0.000	6.505
ENSG00000272009	<i>AL121944.1</i>	0.000	6.537
ENSG00000112077	<i>RHAG</i>	0.000	6.540
ENSG00000225101	<i>OR52K3P</i>	0.004	6.556
ENSG00000184908	<i>CLCNKB</i>	0.004	6.558
ENSG00000161509	<i>GRIN2C</i>	0.001	6.559
ENSG00000233360	<i>Z83844.2</i>	0.005	6.561
ENSG00000261693	<i>AC134682.1</i>	0.000	6.574
ENSG00000132026	<i>RTBDN</i>	0.000	6.575
ENSG00000257042	<i>AC008011.2</i>	0.002	6.593
ENSG00000176919	<i>C8G</i>	0.000	6.603
ENSG00000241635	<i>UGT1A1</i>	0.000	6.606
ENSG00000187957	<i>DNER</i>	0.000	6.610
ENSG00000163694	<i>RBM47</i>	0.000	6.628
ENSG00000080493	<i>SLC4A4</i>	0.000	6.646
ENSG00000172638	<i>EFEMP2</i>	0.000	6.677
ENSG00000229848	<i>AC139149.1</i>	0.000	6.679
ENSG00000262921	<i>AC118754.2</i>	0.000	6.701
ENSG00000047457	<i>CP</i>	0.000	6.703
ENSG00000164318	<i>EGFLAM</i>	0.000	6.724
ENSG00000256139	<i>AC007637.1</i>	0.000	6.736

ENSG00000166411	<i>IDH3A</i>	0.000	6.736
ENSG00000285280	<i>AL390957.1</i>	0.000	6.740
ENSG00000231170	<i>AC002451.1</i>	0.001	6.742
ENSG00000259459	<i>LINC02568</i>	0.000	6.743
ENSG00000186162	<i>CIDECP</i>	0.000	6.762
ENSG00000279633	<i>AL137918.1</i>	0.001	6.765
ENSG00000223774	<i>AL513217.1</i>	0.000	6.809
ENSG00000268650	<i>AC005759.1</i>	0.000	6.816
ENSG00000277287	<i>AL109976.1</i>	0.000	6.827
ENSG00000105409	<i>ATP1A3</i>	0.000	6.835
ENSG00000254614	<i>AP003068.2</i>	0.000	6.879
ENSG00000159761	<i>C16orf86</i>	0.000	6.903
ENSG00000158246	<i>TENT5B</i>	0.000	6.911
ENSG00000233200	<i>AL117336.1</i>	0.000	6.956
ENSG00000248159	<i>HSPA8P11</i>	0.000	6.960
ENSG00000171219	<i>CDC42BPG</i>	0.000	6.974
ENSG00000237352	<i>LINC01358</i>	0.000	6.975
ENSG00000235244	<i>DANT2</i>	0.000	6.983
ENSG00000219891	<i>ZSCAN12P1</i>	0.000	6.988
ENSG00000119917	<i>IFIT3</i>	0.000	7.006
ENSG00000260750	<i>AC092720.1</i>	0.000	7.022
ENSG00000204052	<i>LRRC73</i>	0.000	7.089
ENSG00000204661	<i>C5orf60</i>	0.007	7.092
ENSG00000186197	<i>EDARADD</i>	0.000	7.107
ENSG00000182379	<i>NXPH4</i>	0.000	7.136
ENSG00000245748	<i>AC097382.2</i>	0.008	7.136
ENSG00000144339	<i>TMEFF2</i>	0.000	7.140
ENSG00000141854	<i>MISP3</i>	0.000	7.149
ENSG00000270276	<i>HIST2H4B</i>	0.000	7.158
ENSG00000246985	<i>SOCS2-AS1</i>	0.000	7.164
ENSG00000269814	<i>AC008403.3</i>	0.000	7.171
ENSG00000204581	<i>ACOXL-AS1</i>	0.006	7.174
ENSG00000129214	<i>SHBG</i>	0.000	7.175
ENSG00000147003	<i>CLTRN</i>	0.000	7.188
ENSG00000100342	<i>APOL1</i>	0.000	7.194
ENSG00000110628	<i>SLC22A18</i>	0.000	7.200
ENSG00000226435	<i>ANKRD18DP</i>	0.000	7.214
ENSG00000113763	<i>UNC5A</i>	0.000	7.219
ENSG00000259182	<i>AC019254.1</i>	0.000	7.235
ENSG00000273350	<i>AC004832.5</i>	0.001	7.253
ENSG00000177519	<i>RPRM</i>	0.000	7.313
ENSG00000283480	<i>AL512380.2</i>	0.006	7.335
ENSG00000231920	<i>NEBL-AS1</i>	0.001	7.337
ENSG00000105388	<i>CEACAM5</i>	0.000	7.344
ENSG00000185269	<i>NOTUM</i>	0.000	7.349
ENSG00000166432	<i>ZMAT1</i>	0.000	7.356
ENSG00000188626	<i>GOLGA8M</i>	0.006	7.367
ENSG00000141977	<i>CIB3</i>	0.006	7.373
ENSG00000066336	<i>SPI1</i>	0.000	7.384
ENSG00000167799	<i>NUDT8</i>	0.000	7.395
ENSG00000250644	<i>AC068580.4</i>	0.000	7.397
ENSG00000233246	<i>AL513327.2</i>	0.005	7.407
ENSG00000197471	<i>SPN</i>	0.000	7.421
ENSG00000271714	<i>AC010501.1</i>	0.006	7.423
ENSG00000135205	<i>CCDC146</i>	0.000	7.429
ENSG00000073737	<i>DHRS9</i>	0.000	7.454
ENSG00000250091	<i>DNAH10OS</i>	0.000	7.495
ENSG00000006016	<i>CRLF1</i>	0.000	7.497
ENSG00000130377	<i>ACSBG2</i>	0.000	7.526
ENSG00000130545	<i>CRB3</i>	0.000	7.550

ENSG00000106992	AK1	0.000	7.555
ENSG00000149599	DUSP15	0.002	7.595
ENSG00000133106	EPST11	0.000	7.620
ENSG00000234432	AC092171.3	0.000	7.654
ENSG00000078579	FGF20	0.004	7.662
ENSG00000064205	WISP2	0.000	7.684
ENSG00000096006	CRISP3	0.003	7.685
ENSG00000206140	TMEM191C	0.000	7.689
ENSG00000204291	COL15A1	0.000	7.699
ENSG00000204261	PSMB8-AS1	0.000	7.770
ENSG00000145451	GLRA3	0.000	7.782
ENSG00000118777	ABCG2	0.000	7.789
ENSG00000285159	AL627422.2	0.000	7.802
ENSG00000115461	IGFBP5	0.000	7.889
ENSG00000124256	ZBP1	0.001	7.893
ENSG00000230753	ZNF341-AS1	0.000	7.907
ENSG00000225978	HAR1A	0.000	7.920
ENSG00000235904	RBMS3-AS3	0.000	7.943
ENSG00000185745	IFIT1	0.000	7.977
ENSG00000230310	AC010422.1	0.000	7.978
ENSG00000224805	LINC00853	0.000	7.981
ENSG00000183668	PSG9	0.000	8.037
ENSG00000178462	TUBAL3	0.000	8.074
ENSG00000179583	CIITA	0.000	8.091
ENSG00000226025	LGALS17A	0.001	8.111
ENSG00000244998	AC100803.1	0.000	8.132
ENSG00000271180	AL158801.4	0.001	8.144
ENSG00000168497	CAVIN2	0.000	8.163
ENSG00000196620	UGT2B15	0.000	8.165
ENSG00000196268	ZNF493	0.000	8.186
ENSG00000145113	MUC4	0.000	8.210
ENSG00000154451	GBP5	0.000	8.222
ENSG00000272079	AC004233.3	0.000	8.239
ENSG00000262884	AC015921.1	0.000	8.239
ENSG00000263063	AC024361.2	0.002	8.251
ENSG00000187595	ZNF385C	0.000	8.325
ENSG00000134326	CMPK2	0.000	8.328
ENSG00000160801	PTH1R	0.000	8.339
ENSG00000177294	FBXO39	0.000	8.351
ENSG00000133135	RNF128	0.000	8.351
ENSG00000197587	DMBX1	0.008	8.417
ENSG00000274038	AC007014.2	0.009	8.430
ENSG00000226919	AL365184.1	0.002	8.464
ENSG00000126709	IFI6	0.000	8.481
ENSG00000268655	AC008687.4	0.000	8.487
ENSG00000224729	PCOLCE-AS1	0.000	8.510
ENSG00000223458	LMO7DN-IT1	0.002	8.511
ENSG00000113946	CLDN16	0.000	8.512
ENSG00000236947	AL139412.1	0.000	8.513
ENSG00000284491	THSD8	0.002	8.514
ENSG00000152689	RASGRP3	0.000	8.515
ENSG00000181264	TMEM136	0.000	8.518
ENSG00000261183	SPINT1-AS1	0.000	8.601
ENSG00000142623	PADI1	0.000	8.614
ENSG00000254859	AC067930.4	0.000	8.632
ENSG00000121075	TBX4	0.000	8.636
ENSG00000103034	NDRG4	0.000	8.642
ENSG00000235314	LINC00957	0.000	8.679
ENSG00000242852	ZNF709	0.000	8.682
ENSG00000224846	AL133351.1	0.000	8.688

ENSG00000158125	<i>XDH</i>	0.000	8.721
ENSG00000245870	<i>LINC00682</i>	0.007	8.727
ENSG00000266835	<i>GAPLINC</i>	0.000	8.739
ENSG00000247011	<i>AC005920.1</i>	0.000	8.749
ENSG00000075399	<i>VPS9D1</i>	0.000	8.782
ENSG00000262406	<i>MMP12</i>	0.007	8.787
ENSG00000196668	<i>LINC00173</i>	0.000	8.796
ENSG00000074276	<i>CDHR2</i>	0.000	8.849
ENSG00000237413	<i>MGC27382</i>	0.000	8.863
ENSG00000144962	<i>SPATA16</i>	0.000	8.897
ENSG00000266401	<i>AP002478.1</i>	0.000	8.980
ENSG00000232835	<i>AC107057.1</i>	0.001	9.019
ENSG00000088002	<i>SULT2B1</i>	0.001	9.029
ENSG00000253217	<i>AP001574.1</i>	0.000	9.032
ENSG00000233887	<i>AL354685.1</i>	0.008	9.035
ENSG00000139132	<i>FGD4</i>	0.000	9.038
ENSG00000236283	<i>AC019197.1</i>	0.000	9.059
ENSG00000260231	<i>KDM7A-DT</i>	0.000	9.075
ENSG00000255867	<i>DENND5B-AS1</i>	0.000	9.096
ENSG00000247131	<i>AC025263.1</i>	0.005	9.121
ENSG00000142910	<i>TINAGL1</i>	0.000	9.133
ENSG00000271913	<i>AL035530.2</i>	0.000	9.141
ENSG00000139508	<i>SLC46A3</i>	0.000	9.157
ENSG00000120053	<i>GOT1</i>	0.000	9.185
ENSG00000205809	<i>KLRC2</i>	0.000	9.203
ENSG00000102996	<i>MMP15</i>	0.000	9.238
ENSG00000154438	<i>ASZ1</i>	0.000	9.238
ENSG00000196358	<i>NTNG2</i>	0.000	9.244
ENSG00000228350	<i>LINC02585</i>	0.001	9.255
ENSG00000253557	<i>AC100849.1</i>	0.000	9.256
ENSG00000235142	<i>LINC02532</i>	0.001	9.330
ENSG00000119715	<i>ESRRB</i>	0.000	9.371
ENSG00000182885	<i>ADGRG3</i>	0.000	9.426
ENSG00000248243	<i>LINC02014</i>	0.004	9.436
ENSG00000108387	<i>38231.000</i>	0.000	9.447
ENSG00000279805	<i>Z95114.3</i>	0.004	9.497
ENSG00000078401	<i>EDN1</i>	0.000	9.510
ENSG00000178734	<i>LMO7DN</i>	0.005	9.514
ENSG00000121335	<i>PRB2</i>	0.000	9.525
ENSG00000279414	<i>CR392039.2</i>	0.005	9.562
ENSG00000272701	<i>MESTIT1</i>	0.005	9.586
ENSG00000229951	<i>FLJ31356</i>	0.000	9.718
ENSG00000255299	<i>AP003557.1</i>	0.001	9.735
ENSG00000240875	<i>LINC00886</i>	0.000	9.776
ENSG00000278558	<i>TMEM191B</i>	0.000	9.780
ENSG00000125998	<i>FAM83C</i>	0.000	9.800
ENSG00000235419	<i>AC010149.1</i>	0.000	9.814
ENSG00000109181	<i>UGT2B10</i>	0.000	9.839
ENSG00000157087	<i>ATP2B2</i>	0.001	9.857
ENSG00000184489	<i>PTP4A3</i>	0.000	9.866
ENSG00000183044	<i>ABAT</i>	0.000	9.929
ENSG00000140297	<i>GCNT3</i>	0.000	9.930
ENSG00000108381	<i>ASPA</i>	0.000	9.953
ENSG00000183087	<i>GAS6</i>	0.000	9.962
ENSG00000170579	<i>DLGAP1</i>	0.000	10.007
ENSG00000130203	<i>APOE</i>	0.000	10.228
ENSG00000276289	<i>KCNE1B</i>	0.002	10.234
ENSG00000205755	<i>CRLF2</i>	0.003	10.252
ENSG00000162645	<i>GBP2</i>	0.000	10.279
ENSG00000136274	<i>NACAD</i>	0.000	10.316

ENSG00000183569	<i>SERHL2</i>	0.000	10.430
ENSG00000141338	<i>ABCA8</i>	0.000	10.484
ENSG00000168993	<i>CPLX1</i>	0.000	10.623
ENSG00000211714	<i>TRBV7-3</i>	0.000	10.732
ENSG00000080573	<i>COL5A3</i>	0.000	10.813
ENSG00000019505	<i>SYT13</i>	0.000	10.907
ENSG00000167701	<i>GPT</i>	0.000	10.913
ENSG00000172551	<i>MUCL1</i>	0.000	11.078
ENSG00000105427	<i>CNFN</i>	0.000	11.084
ENSG00000173077	<i>DEC1</i>	0.000	11.107
ENSG00000185432	<i>METTL7A</i>	0.000	11.156
ENSG00000115267	<i>IFIH1</i>	0.000	11.215
ENSG00000145777	<i>TSLP</i>	0.000	11.236
ENSG00000170373	<i>CST1</i>	0.000	11.253
ENSG00000259910	<i>AC120498.1</i>	0.000	11.341
ENSG00000271959	<i>AC100803.3</i>	0.001	11.343
ENSG00000231993	<i>EP300-AS1</i>	0.000	11.350
ENSG00000183091	<i>NEB</i>	0.000	11.419
ENSG00000171873	<i>ADRA1D</i>	0.000	11.425
ENSG00000233765	<i>AL591479.1</i>	0.000	11.465
ENSG00000125462	<i>C1orf61</i>	0.000	11.470
ENSG00000262678	<i>AC004771.5</i>	0.009	11.491
ENSG00000099822	<i>HCN2</i>	0.000	11.564
ENSG00000230126	<i>FGF12-AS2</i>	0.001	11.693
ENSG00000060762	<i>MPC1</i>	0.000	11.733
ENSG00000155761	<i>SPAG17</i>	0.000	11.735
ENSG00000214456	<i>PLIN5</i>	0.000	11.774
ENSG00000134321	<i>RSAD2</i>	0.000	11.796
ENSG00000132530	<i>XAF1</i>	0.000	11.811
ENSG00000004848	<i>ARX</i>	0.000	11.904
ENSG00000104953	<i>TLE6</i>	0.000	11.938
ENSG00000137441	<i>FGFBP2</i>	0.000	11.962
ENSG00000284391	<i>AL139398.1</i>	0.000	11.984
ENSG00000106013	<i>ANKRD7</i>	0.007	11.993
ENSG00000204941	<i>PSG5</i>	0.010	12.001
ENSG00000251898	<i>SCARNA11</i>	0.008	12.006
ENSG00000250510	<i>GPR162</i>	0.000	12.018
ENSG00000165949	<i>IFI27</i>	0.000	12.026
ENSG00000261888	<i>AC144831.1</i>	0.000	12.036
ENSG00000279312	<i>AL136164.4</i>	0.000	12.043
ENSG00000109072	<i>VTN</i>	0.000	12.089
ENSG00000133256	<i>PDE6B</i>	0.008	12.119
ENSG00000142609	<i>CFAP74</i>	0.000	12.135
ENSG00000275223	<i>AL121906.2</i>	0.000	12.210
ENSG00000154153	<i>RETREG1</i>	0.000	12.454
ENSG00000183607	<i>GKN2</i>	0.000	12.455
ENSG00000269194	<i>AC006942.1</i>	0.001	12.466
ENSG00000160321	<i>ZNF208</i>	0.006	12.522
ENSG00000228318	<i>AP001610.1</i>	0.008	12.570
ENSG00000262768	<i>AC100791.2</i>	0.006	12.571
ENSG00000256262	<i>USP30-AS1</i>	0.000	12.604
ENSG00000225526	<i>MKRN2OS</i>	0.006	12.656
ENSG00000257624	<i>AC004024.1</i>	0.000	12.834
ENSG00000235213	<i>OR6E1P</i>	0.000	12.840
ENSG00000213657	<i>RPL31P44</i>	0.000	12.860
ENSG00000079931	<i>MOXD1</i>	0.000	12.891
ENSG00000162643	<i>WDR63</i>	0.000	12.928
ENSG00000278727	<i>AC000403.1</i>	0.000	12.987
ENSG00000182816	<i>KRTAP13-2</i>	0.005	13.090
ENSG00000166111	<i>SVOP</i>	0.005	13.162

ENSG00000259780	AC009065.1	0.000	13.344
ENSG00000198125	MB	0.000	13.431
ENSG00000248456	LINC02485	0.009	13.501
ENSG00000241829	RPL21P54	0.009	13.503
ENSG00000267302	RNFT1-DT	0.009	13.538
ENSG00000258616	LINC02303	0.000	13.554
ENSG00000229621	LINC01822	0.009	13.578
ENSG00000228039	AC253536.2	0.009	13.578
ENSG00000124467	PSG8	0.009	13.580
ENSG00000168509	HJV	0.009	13.581
ENSG00000265043	AC068418.2	0.005	13.586
ENSG00000117228	GBP1	0.000	13.610
ENSG00000184925	LCN12	0.000	13.615
ENSG00000138449	SLC40A1	0.000	13.765
ENSG00000181634	TNFSF15	0.000	13.882
ENSG00000158516	CPA2	0.000	13.888
ENSG00000244649	LINC02086	0.000	13.912
ENSG00000267385	AC011498.4	0.000	14.120
ENSG00000216588	IGSF23	0.000	14.144
ENSG00000187550	SBK2	0.000	14.156
ENSG00000188396	TCTEX1D4	0.003	14.222
ENSG00000206567	AC022007.1	0.000	14.233
ENSG00000285594	AP000902.2	0.004	14.235
ENSG00000010310	GIPR	0.000	14.249
ENSG00000105251	SHD	0.003	14.329
ENSG00000132518	GUCY2D	0.008	14.375
ENSG00000265554	AP005271.1	0.007	14.375
ENSG00000253737	AP003469.3	0.006	14.414
ENSG00000172345	STARD5	0.000	14.430
ENSG00000226193	AL049548.1	0.006	14.493
ENSG00000129675	ARHGEF6	0.000	14.527
ENSG00000271554	AL138787.2	0.007	14.535
ENSG00000172350	ABCG4	0.000	14.619
ENSG00000183773	AIFM3	0.000	14.765
ENSG00000069431	ABCC9	0.000	14.783
ENSG00000125895	TMEM74B	0.000	14.820
ENSG00000236751	LINC01186	0.000	14.851
ENSG00000269720	CCDC194	0.000	14.903
ENSG00000247033	AC099508.1	0.000	14.916
ENSG00000239944	TRBV8-2	0.000	14.936
ENSG00000116544	DLGAP3	0.000	15.026
ENSG00000078804	TP53INP2	0.000	15.061
ENSG00000226969	AL391845.1	0.000	15.122
ENSG00000180539	C9orf139	0.000	15.158
ENSG00000107187	LHX3	0.007	15.198
ENSG00000223669	AL357033.2	0.000	15.238
ENSG00000237595	AL161937.2	0.000	15.266
ENSG00000229894	GK3P	0.002	15.385
ENSG00000164742	ADCY1	0.005	15.411
ENSG00000007129	CEACAM21	0.006	15.451
ENSG00000143882	ATP6V1C2	0.000	15.559
ENSG00000275552	AC243965.2	0.000	15.645
ENSG00000277561	GOLGA8IP	0.002	15.836
ENSG00000214708	AC116407.1	0.000	15.881
ENSG00000164690	SHH	0.000	15.949
ENSG00000265752	AC010754.1	0.000	15.955
ENSG00000111186	WNT5B	0.000	16.166
ENSG00000130234	ACE2	0.005	16.195
ENSG00000130300	PLVAP	0.000	16.283
ENSG00000281920	AC007389.5	0.000	16.308

ENSG00000167080	B4GALNT2	0.004	16.322
ENSG00000174225	ARL13A	0.004	16.326
ENSG00000204929	AC007389.1	0.000	16.360
ENSG00000110079	MS4A4A	0.000	16.444
ENSG00000225964	NRIR	0.002	16.532
ENSG00000143153	ATP1B1	0.000	16.676
ENSG00000177685	CRACR2B	0.000	16.727
ENSG00000007264	MATK	0.000	16.731
ENSG00000103089	FA2H	0.000	16.778
ENSG00000103316	CRYM	0.000	17.075
ENSG00000169862	CTNND2	0.000	17.109
ENSG00000154025	SLC5A10	0.004	17.149
ENSG00000104826	LHB	0.000	17.251
ENSG00000168350	DEGS2	0.000	17.420
ENSG00000228737	AC008781.1	0.000	17.674
ENSG00000175985	PLEKHD1	0.000	17.695
ENSG00000277883	NLRP3P1	0.000	17.706
ENSG00000183346	CABCOC01	0.000	17.710
ENSG00000183837	PNMA3	0.008	17.738
ENSG00000264269	AC016866.1	0.000	17.792
ENSG00000227017	AC007036.1	0.007	17.805
ENSG00000232610	CCT6P4	0.007	17.806
ENSG00000171433	GLOD5	0.008	17.870
ENSG00000262714	AC007342.5	0.006	17.874
ENSG00000221055	MIR1302-3	0.008	17.941
ENSG00000167614	TTYH1	0.007	17.943
ENSG00000246214	AC022113.1	0.009	17.950
ENSG00000261790	AC005606.2	0.001	17.997
ENSG00000225451	AC092634.2	0.007	18.013
ENSG00000249948	GBA3	0.006	18.060
ENSG00000228997	AL136452.1	0.000	18.101
ENSG00000136514	RTP4	0.000	18.235
ENSG00000149131	SERPING1	0.000	18.279
ENSG00000257035	AC025252.2	0.000	18.320
ENSG00000224536	AC096677.1	0.000	18.354
ENSG00000206337	HCP5	0.000	18.452
ENSG00000275527	AC100835.2	0.001	18.565
ENSG00000181790	ADGRB1	0.000	18.579
ENSG00000237220	AC104777.3	0.000	18.613
ENSG00000237476	LINC01637	0.000	18.710
ENSG00000261678	SCRT1	0.001	18.728
ENSG00000227053	AC105446.1	0.002	18.818
ENSG00000188676	IDO2	0.002	18.983
ENSG00000253944	AC027117.2	0.002	19.066
ENSG00000001626	CFTR	0.001	19.122
ENSG00000165805	C12orf50	0.001	19.162
ENSG00000259702	AC024337.1	0.005	19.241
ENSG00000197888	UGT2B17	0.005	19.246
ENSG00000132274	TRIM22	0.000	19.352
ENSG00000285940	AC009899.1	0.004	19.376
ENSG00000259587	AC114546.2	0.005	19.384
ENSG00000267968	AC011523.1	0.005	19.384
ENSG00000260403	AC120498.3	0.000	19.416
ENSG00000250833	DNM1P17	0.007	19.523
ENSG00000163568	AIM2	0.000	19.607
ENSG00000154258	ABCA9	0.000	19.633
ENSG00000226709	FGF12-AS3	0.000	19.653
ENSG00000256196	AP003721.1	0.000	19.707
ENSG00000251511	AC096736.3	0.002	19.762
ENSG00000165269	AQP7	0.001	19.774

ENSG00000254927	AC027779.1	0.001	19.774
ENSG00000136928	GABBR2	0.001	19.849
ENSG00000123977	DAW1	0.000	19.856
ENSG00000253671	AC027117.1	0.000	19.995
ENSG00000227630	LINC01132	0.000	20.108
ENSG00000162654	GBP4	0.000	20.121
ENSG00000232022	FAAHP1	0.000	20.164
ENSG00000277453	AC010271.2	0.000	20.204
ENSG00000274993	AC254629.1	0.001	20.280
ENSG00000211895	IGHA1	0.000	20.454
ENSG00000120217	CD274	0.000	20.476
ENSG00000110446	SLC15A3	0.000	20.526
ENSG00000134259	NGF	0.000	20.601
ENSG00000169783	LINGO1	0.001	20.645
ENSG00000251532	AC091849.2	0.000	20.742
ENSG00000152592	DMP1	0.005	20.749
ENSG00000173641	HSPB7	0.003	20.816
ENSG00000100336	APOL4	0.003	20.889
ENSG00000213471	TTL13P	0.004	20.958
ENSG00000145103	ILDR1	0.000	20.985
ENSG00000225383	SFTA1P	0.000	21.004
ENSG00000254231	AC103760.1	0.000	21.016
ENSG00000273693	C2orf27AP1	0.003	21.028
ENSG00000169129	AFAP1L2	0.000	21.198
ENSG00000231651	DLG3-AS1	0.000	21.277
ENSG00000187715	KBTD12	0.000	21.322
ENSG00000183484	GPR132	0.000	21.517
ENSG00000258735	LINC00637	0.001	21.561
ENSG00000228903	RASA4CP	0.000	21.639
ENSG00000274560	AC010205.1	0.000	21.653
ENSG00000104827	CGB3	0.001	21.761
ENSG00000233930	KRTAP5-AS1	0.000	21.773
ENSG00000261838	AC092718.6	0.000	21.809
ENSG00000157703	SVOPL	0.000	21.897
ENSG00000177238	TRIM72	0.000	22.147
ENSG00000267149	AC011476.2	0.003	22.247
ENSG00000126218	F10	0.002	22.254
ENSG00000285698	AL049825.1	0.002	22.256
ENSG00000284669	AC092053.3	0.001	22.389
ENSG00000183742	MACC1	0.000	22.515
ENSG00000153303	FRMD1	0.000	22.522
ENSG00000258851	AL139300.2	0.000	22.673
ENSG00000257642	KCCAT198	0.000	23.015
ENSG00000254224	AP003465.1	0.000	23.205
ENSG00000182261	NLRP10	0.001	23.383
ENSG00000178403	NEUROG2	0.000	23.586
ENSG00000104112	SCG3	0.000	23.651
ENSG00000267162	SDHDP1	0.002	23.695
ENSG00000171815	PCDHB1	0.000	23.702
ENSG00000133800	LYVE1	0.001	23.732
ENSG00000173237	C11orf86	0.000	23.764
ENSG00000183347	GBP6	0.002	23.767
ENSG00000285570	AL590666.4	0.002	23.827
ENSG00000166816	LDHD	0.000	23.948
ENSG00000116983	HPCAL4	0.000	24.435
ENSG00000115112	TFCP2L1	0.000	24.978
ENSG00000101417	PXMP4	0.000	25.208
ENSG00000156006	NAT2	0.001	25.263
ENSG00000254764	TRIM53CP	0.001	25.268
ENSG00000196109	ZNF676	0.001	25.335

ENSG00000155980	<i>KIF5A</i>	0.000	25.351
ENSG00000273394	<i>AC128687.2</i>	0.000	25.663
ENSG00000108849	<i>PPY</i>	0.000	26.209
ENSG00000164181	<i>ELOVL7</i>	0.000	26.250
ENSG00000261402	<i>AL591222.1</i>	0.000	26.342
ENSG00000285771	<i>AL139095.5</i>	0.000	26.589
ENSG00000261729	<i>AL133383.1</i>	0.001	26.704
ENSG00000258285	<i>TESC-AS1</i>	0.001	26.707
ENSG00000211797	<i>TRAV17</i>	0.000	26.952
ENSG00000048540	<i>LMO3</i>	0.000	27.302
ENSG00000163032	<i>VSNL1</i>	0.000	27.440
ENSG00000185168	<i>LINC00482</i>	0.000	27.621
ENSG00000165140	<i>FBP1</i>	0.000	27.635
ENSG00000007952	<i>NOX1</i>	0.000	27.828
ENSG00000274499	<i>AC012414.7</i>	0.000	27.917
ENSG00000256870	<i>SLC5A8</i>	0.000	27.996
ENSG00000225492	<i>GBP1P1</i>	0.000	28.051
ENSG00000233975	<i>LINC02574</i>	0.000	28.141
ENSG00000243081	<i>AC092894.1</i>	0.000	28.280
ENSG00000250358	<i>LINC02200</i>	0.001	28.350
ENSG00000237972	<i>TUBG1P</i>	0.001	28.354
ENSG00000185527	<i>PDE6G</i>	0.000	28.735
ENSG00000266397	<i>AP000919.3</i>	0.000	29.082
ENSG00000215262	<i>KCNU1</i>	0.000	29.380
ENSG00000257726	<i>AC078880.2</i>	0.000	29.714
ENSG00000174950	<i>CD164L2</i>	0.000	29.734
ENSG00000278106	<i>AF254983.2</i>	0.000	29.851
ENSG00000148204	<i>CRB2</i>	0.000	30.178
ENSG00000128709	<i>HOXD9</i>	0.000	30.600
ENSG00000285586	<i>AL132875.3</i>	0.000	30.695
ENSG00000165795	<i>NDRG2</i>	0.000	30.734
ENSG00000176928	<i>GCNT4</i>	0.000	30.970
ENSG00000105642	<i>KCNN1</i>	0.000	31.130
ENSG00000137252	<i>HCRTR2</i>	0.000	31.151
ENSG00000170848	<i>PSG6</i>	0.000	31.436
ENSG00000272763	<i>AC103702.2</i>	0.000	31.647
ENSG00000228705	<i>LINC00659</i>	0.000	31.821
ENSG00000143001	<i>TMEM61</i>	0.000	32.083
ENSG00000235770	<i>LINC00607</i>	0.000	32.799
ENSG00000127561	<i>SYNGR3</i>	0.000	32.923
ENSG00000119714	<i>GPR68</i>	0.000	33.040
ENSG00000070601	<i>FRMPD1</i>	0.000	33.149
ENSG00000164089	<i>ETNPPL</i>	0.000	33.190
ENSG00000167608	<i>TMC4</i>	0.000	33.408
ENSG00000182389	<i>CACNB4</i>	0.000	33.537
ENSG00000205106	<i>DKFzp779M0652</i>	0.000	34.246
ENSG00000150244	<i>TRIM48</i>	0.000	34.426
ENSG00000251002	<i>AC244502.1</i>	0.000	35.225
ENSG00000111181	<i>SLC6A12</i>	0.000	35.425
ENSG00000152463	<i>OLAH</i>	0.000	35.489
ENSG00000272849	<i>AC084018.1</i>	0.000	35.674
ENSG00000197106	<i>SLC6A17</i>	0.000	35.677
ENSG00000253838	<i>AC007991.2</i>	0.000	35.843
ENSG00000117069	<i>ST6GALNAC5</i>	0.000	35.864
ENSG00000132965	<i>ALOX5AP</i>	0.000	36.191
ENSG00000167757	<i>KLK11</i>	0.000	36.680
ENSG00000115009	<i>CCL20</i>	0.000	37.011
ENSG00000236393	<i>AC091806.1</i>	0.000	37.186
ENSG00000243323	<i>PTPRVP</i>	0.000	37.187
ENSG00000258534	<i>AL132712.1</i>	0.000	37.315

ENSG00000163273	<i>NPPC</i>	0.000	37.385
ENSG00000085563	<i>ABCB1</i>	0.000	38.447
ENSG00000257596	<i>AC078778.1</i>	0.000	38.622
ENSG00000251218	<i>AC103764.1</i>	0.000	38.698
ENSG00000101441	<i>CST4</i>	0.000	39.709
ENSG00000248429	<i>FAM198B-AS1</i>	0.000	40.432
ENSG00000262655	<i>SPON1</i>	0.000	40.553
ENSG00000116833	<i>NR5A2</i>	0.000	40.685
ENSG00000235621	<i>LINC00494</i>	0.000	40.794
ENSG00000214510	<i>SPINK13</i>	0.000	41.035
ENSG00000255474	<i>GAU1</i>	0.000	41.702
ENSG00000251576	<i>LINC01267</i>	0.000	41.793
ENSG00000169245	<i>CXCL10</i>	0.000	41.833
ENSG00000158764	<i>ITLN2</i>	0.000	42.412
ENSG00000171195	<i>MUC7</i>	0.000	42.862
ENSG00000259527	<i>LINC00052</i>	0.000	42.874
ENSG00000221826	<i>PSG3</i>	0.000	42.938
ENSG00000147257	<i>GPC3</i>	0.000	43.138
ENSG00000169894	<i>MUC3A</i>	0.000	43.606
ENSG00000231119	<i>AL031666.1</i>	0.000	44.575
ENSG00000254271	<i>AC022390.1</i>	0.000	46.105
ENSG00000205403	<i>CFI</i>	0.000	46.158
ENSG00000142515	<i>KLK3</i>	0.000	47.666
ENSG00000275567	<i>AC008250.2</i>	0.000	48.097
ENSG00000114378	<i>HYAL1</i>	0.000	48.411
ENSG00000148795	<i>CYP17A1</i>	0.000	48.661
ENSG00000145309	<i>CABS1</i>	0.000	48.890
ENSG00000248109	<i>MARCOL</i>	0.000	49.087
ENSG00000275234	<i>AC010503.4</i>	0.000	51.198
ENSG00000131910	<i>NROB2</i>	0.000	52.315
ENSG00000229550	<i>AC012445.1</i>	0.000	53.485
ENSG00000169026	<i>SLC49A3</i>	0.000	53.774
ENSG00000002726	<i>AOC1</i>	0.000	54.289
ENSG00000019169	<i>MARCO</i>	0.000	55.895
ENSG00000188488	<i>SERPINA5</i>	0.000	57.541
ENSG00000169248	<i>CXCL11</i>	0.000	59.559
ENSG00000267811	<i>AP001160.2</i>	0.000	59.574
ENSG00000232352	<i>SEMA3B-AS1</i>	0.000	59.868
ENSG00000265542	<i>AC015845.2</i>	0.000	60.060
ENSG00000167748	<i>KLK1</i>	0.000	60.511
ENSG00000213279	<i>Z97192.2</i>	0.000	61.224
ENSG00000187026	<i>KRTAP21-2</i>	0.000	61.560
ENSG00000137491	<i>SLCO2B1</i>	0.000	62.058
ENSG00000138741	<i>TRPC3</i>	0.000	63.465
ENSG00000131203	<i>IDO1</i>	0.000	65.052
ENSG00000083782	<i>EPYC</i>	0.000	65.426
ENSG00000049249	<i>TNFRSF9</i>	0.000	66.547
ENSG00000164935	<i>DCSTAMP</i>	0.000	67.705
ENSG00000165731	<i>RET</i>	0.000	69.072
ENSG00000230657	<i>PRB4</i>	0.000	69.836
ENSG00000184032	<i>KRTAP20-2</i>	0.000	72.886
ENSG00000186474	<i>KLK12</i>	0.000	73.406
ENSG00000184524	<i>CEND1</i>	0.000	73.977
ENSG00000278214	<i>LINC02139</i>	0.000	74.705
ENSG00000087128	<i>TMPRSS11E</i>	0.000	75.851
ENSG00000197859	<i>ADAMTSL2</i>	0.000	75.875
ENSG00000124232	<i>RBPJL</i>	0.000	77.662
ENSG00000085741	<i>WNT11</i>	0.000	78.324
ENSG00000100362	<i>PVALB</i>	0.000	78.952
ENSG00000198822	<i>GRM3</i>	0.000	80.024

ENSG00000138755	CXCL9	0.000	82.936
ENSG00000105963	ADAP1	0.000	84.402
ENSG00000243137	PSG4	0.000	87.530
ENSG00000122735	DNAI1	0.000	90.258
ENSG00000169282	KCNAB1	0.000	90.459
ENSG00000109819	PPARGC1A	0.000	90.629
ENSG00000282939	TRBV7-2	0.000	91.709
ENSG00000167183	PRR15L	0.000	99.813
ENSG00000236869	ZKSCAN7-AS1	0.000	101.288
ENSG00000128438	TBC1D27P	0.000	102.443
ENSG00000175084	DES	0.000	102.737
ENSG00000134571	MYBPC3	0.000	104.796
ENSG00000205277	MUC12	0.000	111.274
ENSG00000249509	AC023886.1	0.000	124.120
ENSG00000273540	AGBL1	0.000	130.769
ENSG00000177679	SRRM3	0.000	133.017
ENSG00000008517	IL32	0.000	133.395
ENSG00000173175	ADCY5	0.000	135.238
ENSG00000264023	AC068418.1	0.000	135.661
ENSG00000174562	KLK15	0.000	139.053
ENSG00000087250	MT3	0.000	143.925
ENSG00000241104	CEACAMP10	0.000	145.201
ENSG00000223466	LINC01825	0.000	145.381
ENSG00000086205	FOLH1	0.000	173.272
ENSG00000074771	NOX3	0.000	184.856
ENSG00000143369	ECM1	0.000	191.144
ENSG00000249639	AC022092.1	0.000	196.410
ENSG00000181617	FDCSP	0.000	198.128
ENSG00000087085	ACHE	0.000	200.163
ENSG00000152595	MEPE	0.000	208.094
ENSG00000135917	SLC19A3	0.000	215.512
ENSG00000128710	HOXD10	0.000	255.752
ENSG00000186510	CLCNKA	0.000	290.900
ENSG00000152583	SPARCL1	0.000	294.470
ENSG00000256422	LINC02552	0.000	460.494
ENSG00000215246	AC116351.1	0.000	677.273
ENSG00000226306	NPY6R	0.000	705.636
ENSG00000251620	STPG2-AS1	0.000	759.501



***Contributed
publications***

ARTICLE

Open Access

Integrative analysis of transcriptomics and clinical data uncovers the tumor-suppressive activity of MITF in prostate cancer

Lorea Valcarcel-Jimenez¹, Alice Macchia¹, Natalia Martín-Martín^{1,2}, Ana Rosa Cortazar^{1,2}, Ariane Schaub-Clerigué¹, Mikel Pujana-Vaquero¹, Sonia Fernández-Ruiz¹, Isabel Lacasa-Viscasillas³, Aida Santos-Martin³, Ana Loizaga-Iriarte³, Miguel Unda-Urzaiz³, Ivana Hermanova¹, Ianire Astobiza¹, Marion Graupera⁴, Julia Starkova⁵, James Sutherland¹, Rosa Barrio¹, Ana M. Aransay¹, Arkaitz Carracedo^{1,2,6} and Verónica Torrano^{1,2}

Abstract

The dysregulation of gene expression is an enabling hallmark of cancer. Computational analysis of transcriptomics data from human cancer specimens, complemented with exhaustive clinical annotation, provides an opportunity to identify core regulators of the tumorigenic process. Here we exploit well-annotated clinical datasets of prostate cancer for the discovery of transcriptional regulators relevant to prostate cancer. Following this rationale, we identify Microphthalmia-associated transcription factor (MITF) as a prostate tumor suppressor among a subset of transcription factors. Importantly, we further interrogate transcriptomics and clinical data to refine MITF perturbation-based empirical assays and unveil Crystallin Alpha B (CRYAB) as an unprecedented direct target of the transcription factor that is, at least in part, responsible for its tumor-suppressive activity in prostate cancer. This evidence was supported by the enhanced prognostic potential of a signature based on the concomitant alteration of MITF and CRYAB in prostate cancer patients. In sum, our study provides proof-of-concept evidence of the potential of the bioinformatics screen of publicly available cancer patient databases as discovery platforms, and demonstrates that the MITF-CRYAB axis controls prostate cancer biology.

Introduction

Balanced integration of intracellular circuits operates within a normal cell to sustain physiological homeostasis. Alterations in some, if not all, of these circuits converge in changes on gene expression, which will eventually enable the acquisition and sustenance of the hallmarks of cancer cells¹. This event emphasizes the importance of

maintaining the transcriptional homeostasis in normal cells and places gene expression deregulation at the core of cancer research interests.

In the last decades, transcriptomics data derived from cancer specimens have become an important resource for the classification, stratification, and molecular driver identification in tumors. We and others have demonstrated that deregulation of gene expression is a key node for cancer pathogenesis and progression^{2–6}. Prostate cancer (PCa) research exemplifies the effort in deciphering the genomics and transcriptomics landscape of tumors, and extremely valuable data have been generated^{7–13}. In spite of the public

Correspondence: Verónica Torrano (vtorrano@cicbiogune.es)

¹CIC bioGUNE, Bizkaia Technology Park, 801* bld, 48160 Derio, Bizkaia, Spain

²CIBERONC, Madrid, Spain

Full list of author information is available at the end of the article.

These authors contributed equally: Lorea Valcarcel-Jimenez, Alice Macchia

Edited by B. Rotblat

© The Author(s) 2018



Open Access This article is licensed under a Creative Commons Attribution 4.0 International License, which permits use, sharing, adaptation, distribution and reproduction in any medium or format, as long as you give appropriate credit to the original author(s) and the source, provide a link to the Creative Commons license, and indicate if changes were made. The images or other third party material in this article are included in the article's Creative Commons license, unless indicated otherwise in a credit line to the material. If material is not included in the article's Creative Commons license and your intended use is not permitted by statutory regulation or exceeds the permitted use, you will need to obtain permission directly from the copyright holder. To view a copy of this license, visit <http://creativecommons.org/licenses/by/4.0/>.

availability of these relevant data, they are still under-exploited by the scientific community to understand PCa biology. In this regard, the computational tools and dataset selection strategies to carry out these studies are a bottleneck for the cancer research field.

By combining integrated-bioinformatics screening of clinically relevant PCa datasets with *in vivo* and *in vitro* molecular biology assays, we have recently described the metastasis suppressor activity of peroxisome proliferator-activated receptor γ (PPAR γ) coactivator alpha (PGC1 α)^{14,15}. This transcriptional coactivator is a major regulator of mitochondrial biogenesis and function, and has an inherent capacity to integrate environmental signals and cellular energetic demands. This ability empowers PGC1 α to be a driver in shaping responses to metabolic stress during different physiologic and tumorigenic processes¹⁶. As might be expected due to its fundamental role in normal and cancer scenarios, the regulation of PGC1 α expression, from the genomic to the protein level, is complex and dynamic¹⁷. At the level of mRNA expression, one of the well-defined direct regulators of PGC1 α is the Microphthalmia-associated transcription factor (MITF)¹⁸.

MITF is a basic helix-loop-helix leucine zipper (bHLHZIP) transcription factor that regulates the expression of lineage commitment programs that are essential for propagation of the melanocyte lineage¹⁹. The existence of different MITF transcript variants is the result of both alternative splicing and promoter activation that results in the cell-type-specific expression of the different MITF isoforms (A, CX, MC, C, E, H, D, B, M, J)²⁰. The melanoma-specific isoform M-MITF is the best studied isoform and, despite some controversy, its expression is generally deregulated in melanoma. Although MITF alone cannot act as a classical oncogene, it has been called a “lineage survival oncogene” for melanoma^{19,21}. Importantly, the presence or absence of the M-MITF-PGC1 α regulatory axis has stratification potential in melanoma and informs on the efficacy of BRAF inhibitor treatments^{18,22}. Although the expression of MITF has been detected in other types of tumors different from melanoma^{23,24}, its active role in the progression of these diseases, including PCa, remains unexplored.

Crystallin Alpha-B (CRYAB) is a ubiquitous small heat-shock protein that is expressed in response to a wide range of physiological and nonphysiological conditions preventing aggregations of denatured proteins. In a wide variety of tumor types CRYAB has been found to be overexpressed and associated with disease progression^{25–29} and poor prognosis^{30,31}. However, in PCa and nasopharyngeal cancers, CRYAB expression is decreased^{32,33}, pointing at possible tumor-suppressive activity of CRYAB in these cancer scenarios.

In the present study, by combining an exhaustive interrogation of seven publicly available PCa databases with refined empirical assays, we have identified MITF as a prostate tumor suppressor. In addition, we have unveiled CRYAB as a novel direct target of the transcription factor that is, at least in part, responsible for its tumor-suppressive activity in PCa. Importantly, the tumor-suppressive role for this novel MITF-CRYAB axis is supported by the enhanced prognostic potential of a signature based on the concomitant alteration of both genes in PCa patients.

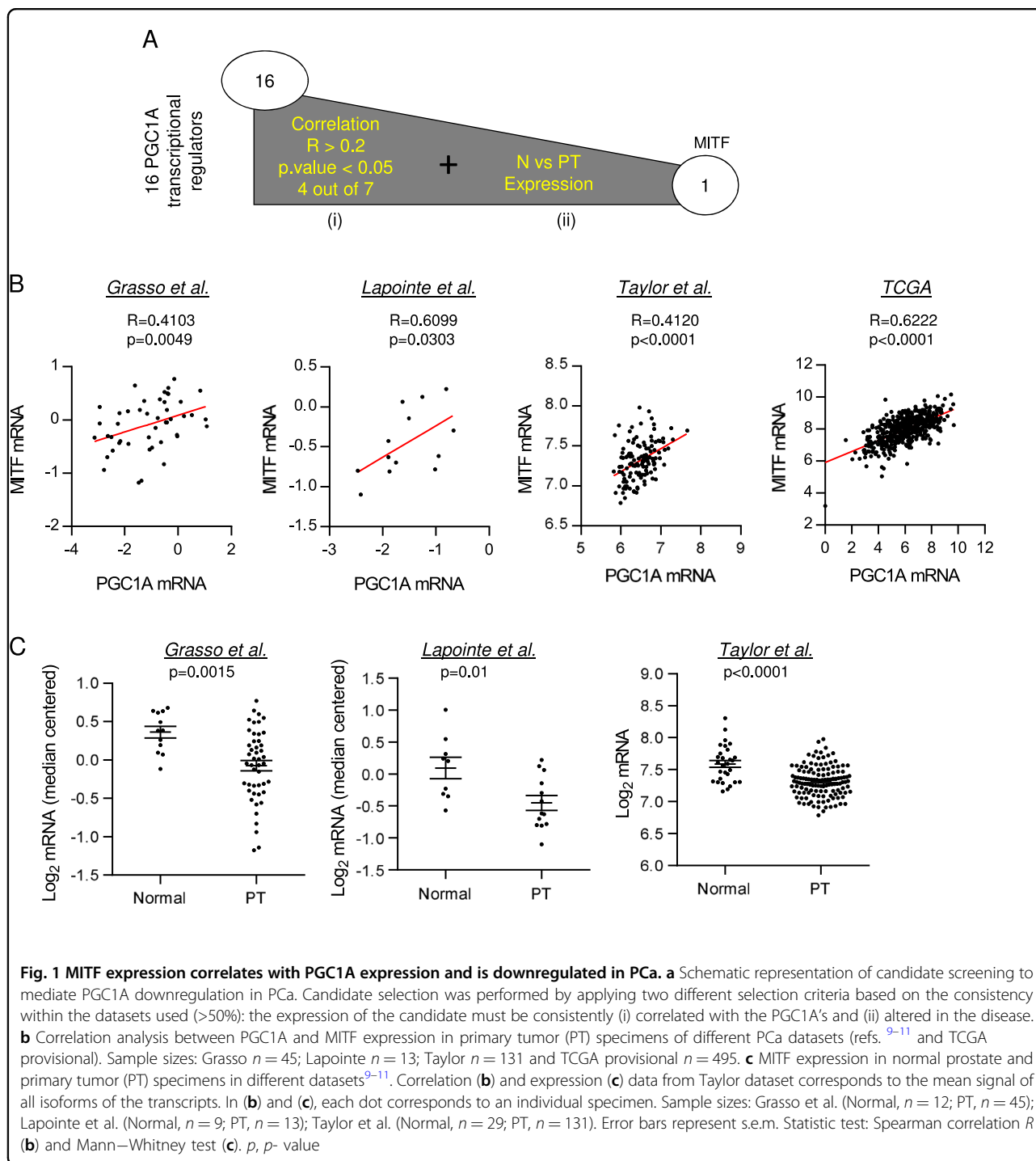
Results

Bioinformatics screening identifies MITF as a transcription factor altered in prostate cancer

We have recently demonstrated that the reduced expression of the transcriptional coactivator PGC1 α is a causal event for metastatic PCa¹⁴. We sought to identify transcriptional regulators related to the alteration in PGC1 α expression. We designed a bioinformatics strategy based on the analysis of 16 genes directly linked to the regulation of *PGC1A* gene^{17,22,34–38}, in order to identify transcription factors that could be relevant to PCa biology. For the candidate screen we applied selection criteria based on the consistency of, first, the correlation with *PGC1A* expression and second, the expression of each individual candidate in seven publicly available PCa datasets^{7,9–13} (Fig. 1a). We selected those candidates whose expression in primary tumors correlated with *PGC1A* ($R \geq 0.2$ and p value ≤ 0.05 in more than 50% of the datasets) (Supplementary Figure 1A) and was altered when compared to normal specimens. For genes exhibiting various transcript variants, the correlation analysis was initially performed using the average signal (Supplementary Figure 1A) and, when available (only Taylor dataset¹¹), the correlation was confirmed in all the individual isoforms (Supplementary Table 1). The transcription factor MITF was the sole candidate that complied with the established criteria. We observed a consistent correlation between *PGC1A* and *MITF* in four out of the seven datasets analyzed (Fig. 1b and Supplementary Figure 1A). In addition, not only the mean expression but also the expression of the individual *MITF* isoforms were reduced in primary tumor specimens when compared with the normal prostate tissue samples (Fig. 1c and Supplementary Figure 1B). Taken together, our data reveal MITF as a *PGC1A*-associated transcription factor that is consistently downregulated in PCa.

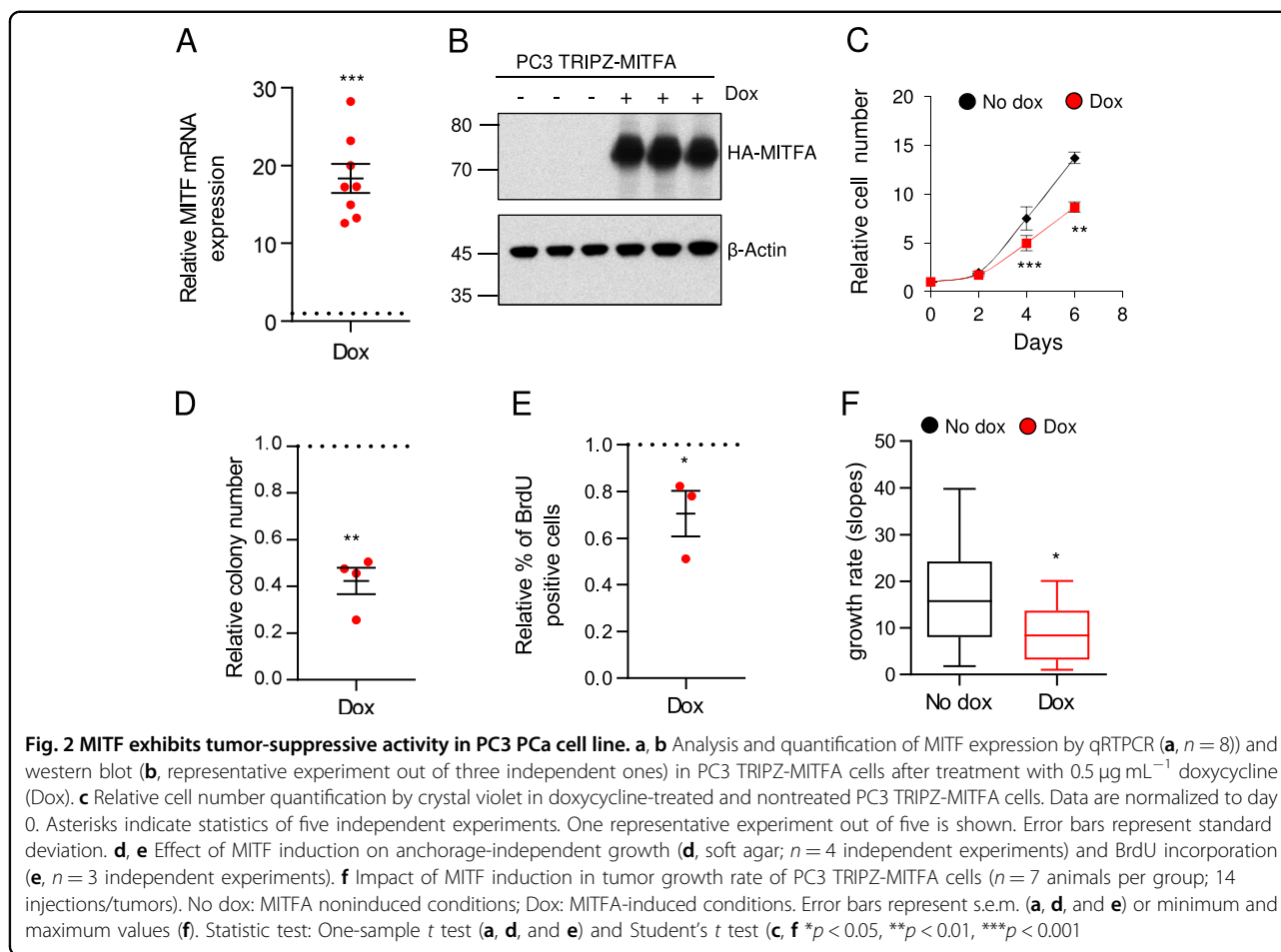
MITF exhibits tumor-suppressive activity in PCa

The expression profile of *MITF* in PCa, together with its direct correlation with *PGC1A*, was suggestive of a tumor-suppressive activity of the transcription factor. We first examined the differential expression of the distinct



mRNA isoforms of *MITF* in normal, PCa primary tumors, and PCa cell lines (Supplementary Fig. 2A–C). *MITFA* was the isoform predominantly expressed in the three scenarios analyzed, and we pursued the studies further with this isoform. Next, we aimed to analyze the biological consequences of ectopic expression of *MITFA* in PC3 PCa cells. We transduced PC3 cells with a lentiviral vector containing a doxycycline-inducible cassette for the

expression of *MITFA* resulting in the generation of the PC3 TRIPZ-*MITFA* cell line. The induction of *MITFA* expression (Fig. 2a, b) as well as the regulation of known target genes, including *PGC1A*^{14,15} (Supplementary Fig. 2D–E) was confirmed. We next evaluated the biological outcome of *MITFA* ectopic expression in PC3 cells and observed that its upregulation significantly reduced two-dimensional and anchorage-independent growth (Fig. 2c,



d), with no effect of doxycycline treatment by itself¹⁴. In line with its known function as an inhibitor of cell cycle progression³⁹, the increased expression of MITFA in PC3 cells resulted in a decrease in BrdU incorporation, a surrogate readout of proliferation (Fig. 2e).

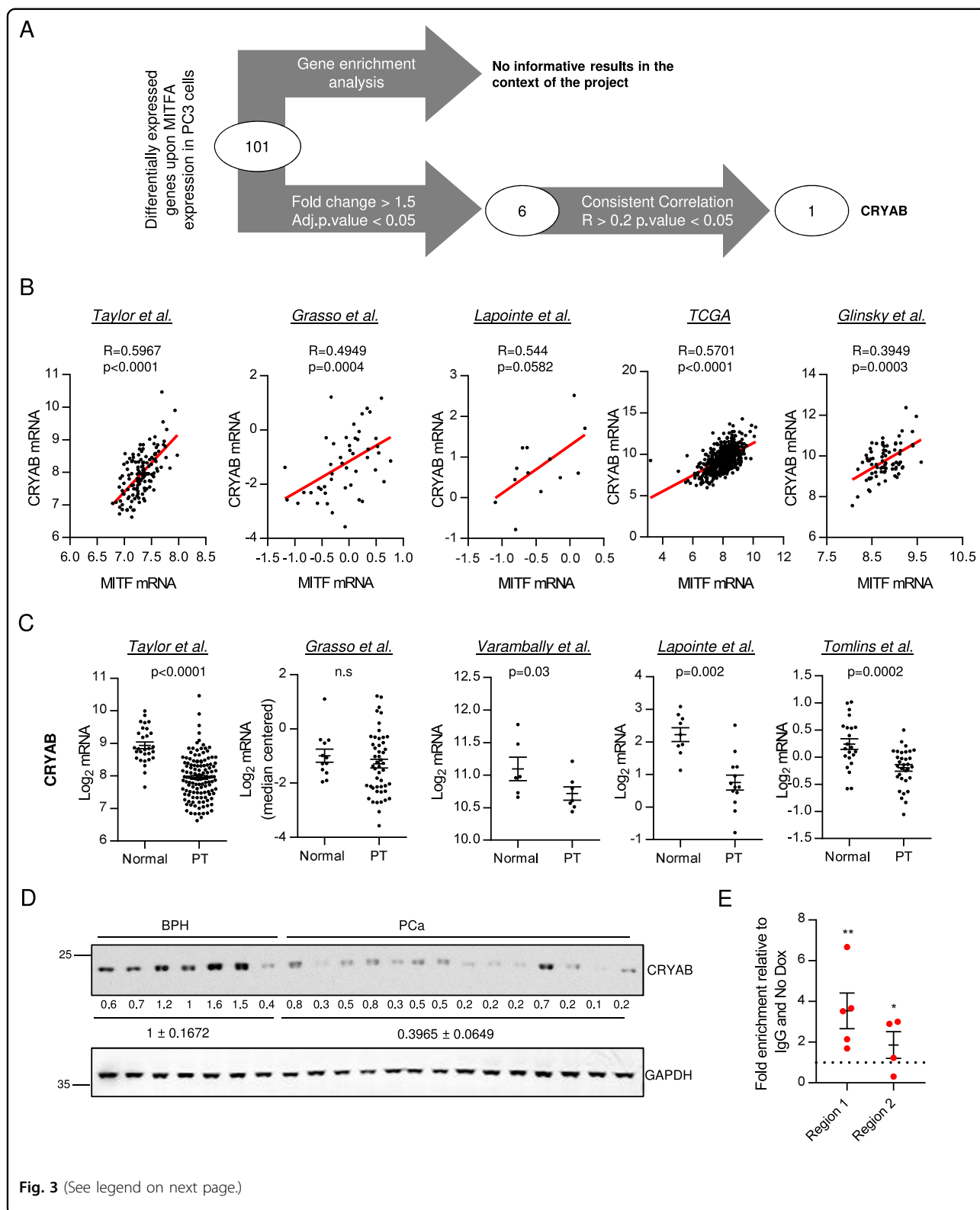
In order to ascertain whether the regulation of endogenous *PGC1A* (Supplementary Fig. 2E) was required for the antiproliferative effect of MITFA in PC3 cells, we aim at silencing *PGC1A* by using constitutive (pLKO) expression of short hairpins against it (Supplementary Fig. 2F). Transduction with the shRNA prevented the upregulation of *PGC1A* upon MITFA induction (Supplementary Fig. 2G) but the antiproliferative effect of the transcription factor remained unaffected (Supplementary Fig. 2H). These data suggested that the reduced proliferation induced by MITFA was not dependent on the regulation of endogenous *PGC1A* in PC3 cells.

Importantly, the overall reduction in cell proliferation induced by MITFA was confirmed in vivo. Using subcutaneous xenografts assays we observed that MITFA overexpression in PC3 cells (Supplementary Fig. 2I) led to a marked reduction in the tumor volume (Supplementary Fig. 2J) and growth rate (Fig. 2f), with no changes in

angiogenesis (Supplementary Fig. 2K). Altogether these results demonstrate that MITFA isoform exhibits tumor-suppressive activity in PCa.

Candidate screening of genes mediating the tumor-suppressive activity of MITF

In order to decipher the molecular mechanism driving the tumor-suppressive role of MITFA, we performed gene expression profiling of both doxycycline-treated and control PC3 TRIPZ-MITFA cells and identified 101 probes that showed statistically differential signal between both conditions (Supplementary Table 2; GEO Series accession number [GSE114345](#)). We first performed a gene enrichment analysis using the functional enrichment tool contained in CANCERTOOL⁴⁰ with those genes that displayed upregulated expression (76 genes) upon MITFA overexpression (Fig. 3a and Supplementary Table 3), as the number of downregulated genes (25) was not sufficient to obtain any gene enrichment. Next, we aimed at identifying potential MITFA effectors of relevance in human PCa. To this end, we established a threshold of 1.5-fold change over MITFA noninduced cells, which resulted in eight probes (corresponding to six annotated genes) upregulated upon



(see figure on previous page)

Fig. 3 CRYAB is the candidate to mediate its tumor-suppressive activity in PCa. **a** Workflow of the candidate screening. **b** Correlation analysis between *MITF* and *CRYAB* expression in primary tumor (PT) specimens of different PCa datasets. Sample sizes: Taylor, $n = 131$; Grasso, $n = 49$; Lapointe, $n = 13$; TCGA provisional data, $n = 495$; and Glinsky, $n = 78$. **c** *CRYAB* expression in normal prostate and primary tumor (PT) specimens in different PCa datasets^{9–13}. Sample sizes: Taylor (N, $n = 29$; PT, $n = 130$); Grasso (N, $n = 12$; PT, $n = 49$); Varambally (N, $n = 6$; PT, $n = 7$); Lapointe et al. (N, $n = 9$; PT, $n = 13$), and Tomlins (N, $n = 22$; PT, $n = 32$). Data from Taylor dataset correspond to the mean signal of all isoforms of the transcripts. In **(b)** and **(c)**, each dot corresponds to an individual specimen. **d** Western blot analysis of *CRYAB* expression in benign prostatic hyperplasia (BPH) and PCa specimens from Basurto University Hospital cohort (BPH $n = 7$ patient specimens; PCa $n = 14$ patient specimens). **e** Chromatin immunoprecipitation (ChIP) of exogenous *MITF* on *CRYAB* promoter in PC3 TRIPZ-MITFA cells after induction with $0.5 \mu\text{g mL}^{-1}$ doxycycline for 3 days ($n = 4–5$). Binding to *ANGPT4* was used as a negative control. Final data were normalized to IgG (negative-immunoprecipitation control) and to No dox condition. No dox: *MITFA* noninduced conditions; Dox: *MITFA*-induced conditions. Statistic tests: Spearman correlation (**b**); Mann–Whitney test (**c**); one-sample *t* test (**e**); Error bars represent s.e.m. * $p < 0.05$, ** $p < 0.01$

the induction of the transcription factor (Supplementary Table 2; yellow bold highlighted). We next performed correlation analysis between *MITF* and each of the six differentially expressed genes obtained from the microarray (Fig. 3a and Supplementary Figure 3A). The correlation analysis in PCa primary tumor specimens showed that a single gene, *Crystallin Alpha B* (*CRYAB*), had a consistent correlation (in more than 50% of datasets) with *MITF*, both the mean of isoforms (Fig. 3b and Supplementary Figure 3A) and the individual isoform A (Supplementary Table 4). The *MITF*–*CRYAB* correlation was confirmed using an independent cohort of PCa patients from a local hospital (Basurto cohort, Supplementary Figure 3A). Moreover, the expression of *CRYAB* either at the level of mRNA (from public datasets and Basurto cohort) and protein (from Basurto cohort) was consistently down-regulated through the progression of the disease (Fig. 3c, d and Supplementary Figure 3B–D), supporting the association of *MITF* and *CRYAB* expression in PCa.

The regulation of *CRYAB* expression by *MITFA* was further validated in vitro by western blot and quantitative real-time PCR (qRTPCR) in doxycycline-treated PC3 TRIPZ-MITFA cell lines and in vivo by qRTPCR in the xenograft samples (Supplementary Figure 3E–G). *MITF* is a transcription factor that regulates gene expression through the DNA binding to E-boxes (Myc-binding sites)¹⁹. In order to confirm the direct regulation of *CRYAB* expression by *MITFA*, we screened the promoter of the chaperon and performed chromatin immunoprecipitation assays in two Myc-binding sites (UCSC-Genome browser; Supplementary Figure 3H). As predicted, upon doxycycline treatment we detected differential binding of *MITFA* in both regions of *CRYAB* promoter (Fig. 3e).

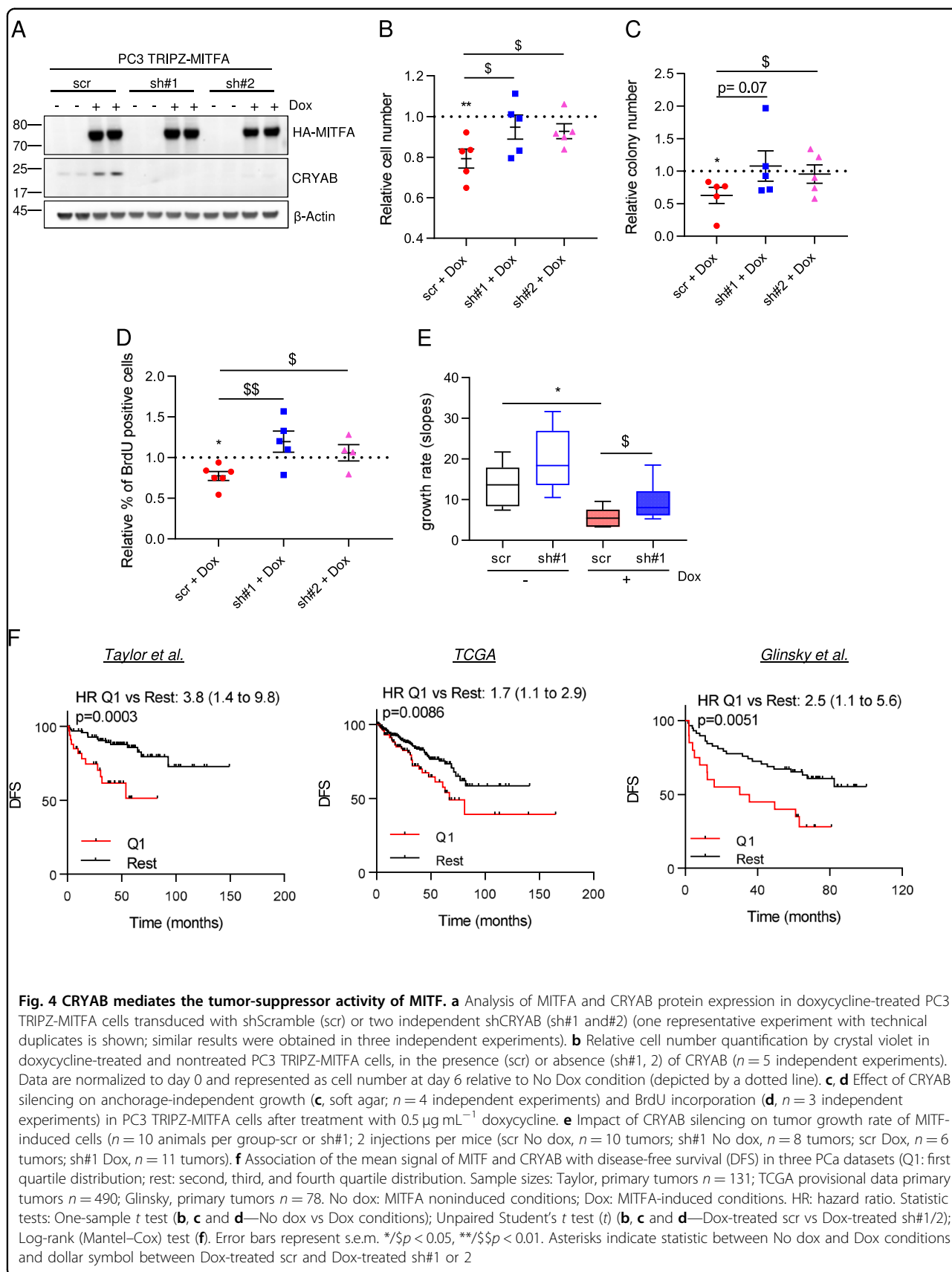
Taken together, these data presented *CRYAB* as a direct target of *MITFA* and the best candidate to mediate its tumor-suppressive activity in PCa.

CRYAB mediates the tumor-suppressive activity of MITF in PCa

We next studied the functional relevance of *CRYAB* for the tumor-suppressive activity of *MITFA* in PCa. Towards

this aim, we constitutively silenced the expression of *CRYAB* by RNAi using two independent short hairpin RNA (sh#1 and sh#2) in PC3 TRIPZ-MITFA cells. After validating that RNAi was achieved (Fig. 4a and Supplementary Figure 4A–C) the tumor-suppressive activity of *MITFA* was monitored in control and *CRYAB*-silenced conditions (PC3 TRIPZ-MITFA scr, sh#1 or sh#2 cell lines). *CRYAB* silencing blunted the antiproliferative effects of *MITFA* in vitro in two-dimensional and anchorage-independent growth when compared with scramble shRNA (Fig. 4b, c). Moreover, the reduction in BrdU induced by *MITFA* was prevented when *CRYAB* was silenced (Fig. 4d). Importantly, the requirement of *CRYAB* for the tumor-suppressive activity of *MITFA* was corroborated in vivo (Fig. 4e and Supplementary Figure 4D–F). The in vitro and in vivo data demonstrate that the induction of *CRYAB* is a major effector involved in the tumor-suppressive activity of the transcription factor *MITF* in PCa.

We next asked whether the functional association between *MITF* and *CRYAB* could be employed to identify PCa patients with high disease aggressiveness. We thus ascertained the stratification potential of the *MITF*–*CRYAB* axis in PCa by means of consistency and robustness. We download the mRNA expression raw data together with the clinical data (recurrence or not recurrence) from Taylor¹¹, Glinsky⁸, and TCGA⁷ datasets. The individual or average expression signal of *CRYAB* and *MITF* genes was calculated for each patient in each dataset. Patients were separated by quartiles according to the individual or average signal of *CRYAB* and *MITF* genes and then Kaplan–Meyer survival curves were plotted comparing patients with low expression (Quartile 1—(Q1)) of the individual genes or the gene combination (*CRYAB* and *MITF*) vs the rest of the cohort (Q2 + Q3 + Q4). Strikingly, the signature formed by the average signal of *MITF* and *CRYAB* outperformed the prognostic potential of each individual gene, strongly suggesting that the pathway described herein is strongly associated to PCa aggressiveness (Fig. 4f and Supplementary Figure 5).



Our data provide solid evidence of an unprecedented MITF-CRYAB transcriptional axis that exerts tumor-suppressive activity in PCa and could positively contribute to disease prognosis.

Discussion

Technological advances in the molecular understanding of cancer have led to a paradigmatic change in the way that we combat the disease⁴¹. We are now able to deconstruct a tumor at a molecular level using genomics, transcriptomics, proteomics, and metabolomics⁴². This, in turn, enables us to foresee, identify, and demonstrate the potential of patient stratification^{3,14,43}. Specifically, the transcriptomics characterization of tumors is an invaluable strategy to identify clinically relevant genes that play key roles in the progression of cancer, especially for those types with poorer prognosis¹⁴. Thus, the comprehensive and integrative analysis of gene expression changes and clinical parameters in cancer has become a mainstream in cancer research^{44–46}. Mining cancer-associated transcriptome datasets is an emerging approach used by top cancer research groups, but better tools are needed to increase its power and user-friendliness. In order to face this challenge, new interfaces to exploit OMICs data, such as cBioportal and CANCEERTOOL^{45,47,40}, are being designed to help scientists interrogate, integrate, and visualize large amount of information contained on multiple credible and qualified cancer datasets.

In the present study, we exploited publicly available and well-annotated (transcriptomics and clinical data) PCa databases together with experimental assays to describe a novel tumor-suppressive activity of the transcription factor MITF in PCa, which is executed, at least in part, through the direct regulation of CRYAB expression. The identification of MITF emanates from the screening of reported upstream regulators of PGC1A. It is worth noting that transcriptome-wide correlative study with the gene of interest could represent a complementary approach to predict candidate upstream regulators and downstream effectors.

The functional implication of MITF in cancer has been best defined in melanoma, in which the expression of the transcription factor is heterogeneous. Although some controversy exists regarding its oncogenic role in melanoma, MITF has been defined as a “lineage survival oncogene” with no data pointing out at a tumor-suppressive function^{19,21,39,48–51}. Even though the expression of MITF has been detected in other cancer types^{23,24,52}, no data supporting a functional role of MITF deregulation have been reported yet in a cancer scenario different from melanoma.

Here we show that MITF is downregulated in PCa when compared with normal specimens, in contrast to the elevated expression reported in hepatocellular carcinoma

and chronic myeloid leukemia^{23,52}. Moreover, the novelty of our study relies on the observation and definition of the tumor-suppressive activity of MITF in PCa. In this context, MITF upregulation was associated with a reduction in cell proliferation and DNA replication. As occurs in melanoma, the modulation of MITF expression in PCa cells induces the expression of the cell cycle inhibitor p21 but no changes in the cell cycle inhibitor p16 were observed (data not shown). Thus, our results in PCa are in line with the canonical function of MITF in cell cycle progression and proliferation in melanoma^{39,50,51}.

It is important to highlight that the tissue-specific differences in MITF expression among different cancer types suggest that in order to fully comprehend MITF's role in cancer, its expression and function has to be analyzed in the context of each particular cell and tissue type.

CRYAB is a member of the small heat-shock protein family that functions as stress-induced molecular chaperone. It inhibits the aggregation of denatured proteins, promotes cell survival, and inhibits apoptosis in the context of cancer^{53–55}. Paradoxically, CRYAB is highly expressed in some cancer types but decreased in others and in both scenarios an association with cancer progression and prognosis has been reported^{25,26,28–32,56–60}. In spite of the amount of information regarding the changes in CRYAB expression in cancer, the transcriptional regulation of this chaperone has been poorly explored⁵⁶. In this study, we described a novel direct transcriptional regulation of CRYAB by MITF. Although there is no direct nor mechanistic evidence of the MITF-CRYAB transcriptional axis in other cancer types, in melanoma both MITF and CRYAB expression are upregulated by BRAF/MEK-inhibitor treatments^{57,60}, suggesting that this regulation can go beyond both PCa scenario. Indeed, we observed that the correlation between MITF and CRYAB is also present in colorectal cancer, but not in breast nor lung cancer (data available in CANCEERTOOL⁴⁰).

In our study, the MITF-CRYAB transcriptional axis is reduced and exerts tumor-suppressive activity in PCa. This is in agreement with the reduced expression of CRYAB observed in PCa patients and its previous consideration as a protective gene against PCa³². Yet, the exact molecular mechanism underlying the tumor-suppressive activity of CRYAB remains to be elucidated.

Importantly, in the present manuscript, the extensive interrogation of PCa transcriptomes and associated clinical data has led us to propose the transcriptional axis MITF-CRYAB as a potential prognostic biomarker in PCa. The individual expression of CRYAB and MITF has been previously associated with poor prognosis in various tumor types^{26,29–31,58,59} and to therapy response in melanoma^{61–63}. However, our data showing enhanced prognostic potential of the combined signature provides a new

and exciting perspective of the functional interaction of these genes in PCa.

Our study endorses the potential of transcriptional deregulation analysis, as either a cause or a consequence of cancer, and its impact to support the discovery of novel cancer-related genes and long-term development of novel cancer treatment strategies.

Materials and methods

Cell culture and reagents

Human prostate carcinoma cell lines (PC3) were purchased from Leibniz-Institut DSMZ—Deutsche Sammlung von Mikroorganismen und Zellkulturen GmbH, who provided authentication certificate. The cell line used in this study was not found in the database of commonly misidentified cell lines maintained by ICLAC and NCBI Biosample. Cells were transduced with a modified TRIPZ (Dharmacon) doxycycline-inducible lentiviral construct in which the RFP and miR30 region was substituted by *HA-Flag-MITF*. Lentiviral shRNA constructs targeting *PGC1A* (#1-TRCN000001165 and #2-TRCN000001166) and *CRYAB* (#1-TRCN0000010822 and #2-TRCN0000010823) were purchased from Sigma and a scramble shRNA (hairpin sequence: CCGGCAACAAGATGAAGAGCACCAACTCGAGTTGGTGCTCTTCATCTTGTTG) was used as control. For *PGC1A* and *CRYAB* shRNAs, Puromycin resistance cassette was replaced by Hygromycin cassette from pLKO.1 Hygro (Addgene Ref. 24150) using *Bam*HI and *Kpn*I sites. Cell lines were routinely monitored for mycoplasma contamination and quarantined while treated if positive. Doxycycline hyclate (Dox) and Puromycin were purchased from Sigma, and Hygromycin from Invitrogen.

Xenotransplant assays

All mouse experiments were carried out following the ethical guidelines established by the Biosafety and Welfare Committee at CIC bioGUNE. The procedures employed were carried out following the recommendations from AAALAC. Xenograft experiments were performed as previously described¹⁴, injecting 10^6 cells per condition in two flanks per mouse (Nu/Nu immunodeficient males; 6–12 weeks of age). PC3 TRIPZ-HA-MITFA cells alone or under *CRYAB* silencing were injected in each flank of nude mice and 24 h post-injections mice were fed with chow or doxycycline diet (Research diets, D12100402).

Patient samples

All samples were obtained from the Basque Biobank for research (BIOEF, Basurto University Hospital) upon informed consent and with evaluation and approval from the corresponding ethics committee (CEIC code OHEUN11-12 and OHEUN14-14).

Molecular assays

Western blot was performed as previously described¹⁴. Antibodies used: HA-Tag (Cell Signalling #3724; dilution 1:10,000); MITF (Thermo Fisher Scientific MA5-14146; dilution 1:1000); β -Actin (Cell Signalling #3700; dilution 1:2000); GAPDH (clone 14C10; Cell Signalling #2218; dilution 1:1000); CRYAB (Cell Signalling #45844s; dilution 1:1000).

RNA was extracted using NucleoSpin[®] RNA isolation kit from Macherey-Nagel (ref: 740955.240C). For patients and animal tissues a Trizol-based implementation of the NucleoSpin[®] RNA isolation kit protocol was used as reported¹⁴. One microgram of total RNA was used for cDNA synthesis using Maxima[™] H Minus cDNA Synthesis Master Mix (Invitrogen M1682). Quantitative Real-Time PCR (qRT-PCR) was performed as previously described¹⁴. Universal Probe Library (Roche) primers and probes employed are detailed in Supplementary Table 5. *GAPDH* (Hs02758991_g1) housekeeping assay from Applied Biosystems was used for data normalization.

For transcriptomics analysis in PC3 TRIPZ-HA-Flag-MITFA cells, Illumina whole genome -HumanHT-12_V4.0 (DirHyb, nt) method was used as reported¹⁴. A hypergeometric test was used to detect enriched dataset categories.

Cellular assays

Cell number quantification with crystal violet was performed as referenced¹⁴.

For starvation experiments 100,000 cells per well were seeded in a six-well plate. Cells were initially plated in 10% FBS media for 24 h and then the media was changed to FBS free media and left overnight.

Soft agar assays were performed as previously described¹⁴, seeding 5000 cells per well in six-well plates.

For BrDu incorporation, cells were seeded on glass cover slips in 12-well plates and after 4 days, cells were incubated with $3 \mu\text{g mL}^{-1}$ BrDu (Sigma B5002). Cells were fixed with 4% para-formaldehyde, permeabilized with 1% Triton X-100 and incubated with a monoclonal anti-BrDu (MoBU-1) antibody (Invitrogen B35128) at a 1:100 dilution. Images were obtained with an AxioImager D1 microscope (Zeiss). At least three different areas per cover slip were quantified.

Chromatin immunoprecipitation

Chromatin Immunoprecipitation (ChIP) was performed using the SimpleChIP[®] Enzymatic Chromatin IP Kit (Cat: 9003, Cell Signalling Technology, Inc). Four million PC3 cells were grown in 150 mm dishes either with or without $0.5 \mu\text{g mL}^{-1}$ doxycycline during 3 days. Cells from three 150 mm dishes were cross-linked with 35% formaldehyde for 10 min at room temperature. Glycine was added to dishes during 5 min at room temperature. Cells were then

washed twice with ice-cold PBS, and scraped into PBS + PMSF. Pelleted cells were lysed and nuclei were harvested following the manufacturer's instructions. Nuclear lysates were digested with micrococcal nuclease for 20 min at 37 °C and then sonicated in 500 μ L aliquots on ice for 6 pulses of 20 s using a Branson sonicator. Cells were held on ice for at least 1 min between sonications. Lysates were clarified at 11,000 $\times g$ for 10 min at 4 °C, and chromatin was stored at -80 °C. HA-Tag polyclonal antibody (Cat: C29F4, Cell Signalling Technology) and IgG antibody (Cat: 2729, Cell Signalling Technology, Inc), were incubated overnight (4 °C) with rotation and protein G magnetic beads were incubated 2 h (4 °C). Washes and elution of chromatin were performed following the manufacturer's instructions. DNA quantification was carried out using a Vii7 Real-Time PCR System (Applied Biosystems) with SybrGreen reagents and primers that amplify the predicted MITFA binding region to *CRYAB* (region 1; For: ttgttctcctgtagggcttg, Rev: ttccagaccgagagagagc- region 2; For: tctggaatggtgatgctcagg, Rev: attgggtgtggacagaaagc) and *ANGPTL4* (For: gttgaccggctcaat, Rev: ggaacagctcctggcaatc) as a negative binding control.

Whole-genome gene expression characterization

Whole-genome expression characterization was conducted using Human HT12 v4 BeadChips (Illumina Inc.). In brief, cRNA synthesis was obtained with TargetAmp™ Nano-g™ Biotin-aRNA Labeling Kit for the Illumina® System, Epicentre (Cat. Num. TAN07924) and subsequent amplification, labeling and hybridization were performed according to Whole-Genome Gene Expression Direct Hybridization Illumina Inc.'s protocol. Raw data were extracted with GenomeStudio analysis software (Illumina Inc.) in the form of GenomeStudio's Final Report (sample probe profile).

Bioinformatics analysis and statistics

Database normalization

All the datasets used for the data mining analysis were downloaded from GEO and TCGA. Referenced accessions: TCGA <https://cancergenome.nih.gov/>, Grasso et al., GEO: GSE35988 (9); Lapointe et al., GEO: GSE3933 (10); Taylor et al., GEO: GSE21032 (11); Tomlins et al., GEO: GSE6099 (12); Varambally et al., GEO: GSE3325 (13); and Glinsky et al (8). GEO-downloaded data were subjected to background correction, log₂ transformation and quartile normalization. In the case of using a preprocessed dataset, this normalization was reviewed and corrected if required. TCGA data were downloaded as upper quartile normalized RSEM count, which was been log₂ transformed.

Quartile analysis in disease-free survival

Patients biopsies from primary tumors were organized into four quartiles according to the expression of the gene

of interest in three datasets. The recurrence of the disease was selected as the event of interest. Kaplan–Meier estimator was used to perform the test as it takes into account *right-censoring*, which occurs if a patient withdraws from a study.

Correlation analysis

Spearman correlation test was applied to analyze the relationship between paired genes.

Gene enrichment

The recently published tool, CANTOOL⁴⁰, harbors 11 independent enrichment databases, including the basic Gene Ontology analysis (GO, biological process (GOBP), molecular function (GOMF) and cell compartment (GOCC)), pathways and pathophysiological processes (KEGG, Biocarta, Reactome, Biocarta, Onco, DOSE, HIPC, Connectivity Map), and the upstream regulatory cue prediction tool (TFT, MIR). The prevalence of such functions within the gene list was analyzed, and statistical significance of the associations sieved according to the Benjamini–Hochberg correction (adjusted *p* value).

Statistical analysis

No statistical method was used to predetermine the sample size. The experiments were not randomized. The investigators were not blinded to allocation during experiments and outcome assessment. Unless otherwise stated, data analyzed by parametric tests are represented by the mean \pm s.e.m. of pooled experiments and median \pm interquartile range for experiments analyzed by non-parametric tests. *n* values represent the number of independent experiments performed, the number of individual mice or patient specimens. For each independent in vitro experiment, at least two technical replicates were used and a minimum number of three experiments were done to ensure adequate statistical power. For data mining analysis Student's *t* test for two component comparisons. In the in vitro experiments, normal distribution was confirmed or assumed (for *n* < 5) and Student's *t* test was applied for two component comparisons. In the statistical analyses involving fold changes, one-sample *t* test with a hypothetical value of 1 was performed. The confidence level used for all the statistical analyses was of 95% (alpha value = 0.05). Two-tail statistical analysis was applied for experimental design without predicted result, and one-tail for validation or hypothesis-driven experiments.

Gene expression array data analysis

First, raw expression data were background-corrected, log₂-transformed, and quantile-normalized using the lumi R package⁶⁴, available through the Bioconductor repository^{65,66}. Probes with a "detection *p* value" lower than 0.01 in at least one sample were considered expressed. For the

detection of differentially expressed genes, a linear model was fitted to the probe data and empirical Bayes moderated t statistics were calculated using the *limma*⁶⁷ package from Bioconductor. Adjusted p values were estimated with Benjamini–Hochberg false discovery rate method (<https://www.jstor.org/stable/2346101>)⁶⁸. Only genes with differential fold-change (FC) > 1.5 or < -1.5 and an adjusted p value < 0.05 were considered as differentially expressed. The transcriptomics data generated in this publication have been deposited in NCBI's Gene Expression Omnibus and are accessible through GEO Series accession number [GSE114345](https://www.ncbi.nlm.nih.gov/geo/query/acc.cgi?acc=GSE114345).

Acknowledgements

The work of V. Torrano is funded by Fundación Vasca de Innovación e Investigación Sanitarias, BIOEF (BIO15/CA/052), the AECC J.P. Bizkaia and the Basque Department of Health (2016111109). The work of A. Carracedo is supported by the Basque Department of Industry, Tourism and Trade (Etortek) and the Department of Education (IKERTALDE IT1106-16, also participated by A. Gomez-Muñoz), the BBVA Foundation, the MINECO (SAF2016-79381-R (FEDER/EU); Severo Ochoa Excellence Accreditation SEV-2016-0644; Excellence Networks SAF2016-81975-REDT), European Training Networks Project (H2020-MSCA-ITN-308 2016 721532), the AECC IDEAS16 (IDEAS175CARR) and the European Research Council (Starting Grant 336343, PoC 754627). CIBERONC was co-funded with FEDER funds. The work of M. Graupera is supported by the MINECO (SAF2014-59950-P). The work of A. Aransay is supported by the Basque Department of Industry, Tourism and Trade (Etortek and Elkartek Programs), the Innovation Technology Department of Bizkaia County, CIBERehd Network and Spanish MINECO the Severo Ochoa Excellence Accreditation (SEV-2016-0644). R. Barrio acknowledges Spanish MINECO (BFU2014-52282-P, Consolider BFU2014-57703-REDC), the Departments of Education and Industry of the Basque Government (PI2012/42) and the Bizkaia County. J. Starková acknowledges the Ministry of Health of Czech Republic AZV NV15-28848A. We are thankful to the Basque Biobank for Research (BIOEF) for the custody and management of human prostate specimens used in this study.

Author details

¹CIC bioGUNE, Bizkaia Technology Park, 801^a bld, 48160 Derio, Bizkaia, Spain. ²CIBERONC, Madrid, Spain. ³Department of Urology, Basurto University Hospital, 48013 Bilbao, Spain. ⁴Vascular Signalling Laboratory, Institut d'Investigació Biomèdica de Bellvitge (IDIBELL), Gran Via de l'Hospitalet 199-203, Barcelona, Spain. ⁵CLIP-Childhood Leukaemia Investigation. Dept. of Pediatric Hematology and Oncology. Second Faculty of Medicine, Charles University, Prague, Czech Republic. ⁶Biochemistry and Molecular Biology Department, University of the Basque Country (UPV/EHU), P.O. Box 64448080 Bilbao, Spain

Authors' contributions

L.V.-J. and A.M. performed the majority of in vitro and in vivo experiments, unless specified otherwise. N.M.-M. contributed to the in vivo experiments, experimental design and discussion. A.R.C. carried out the bioinformatics and biostatistical analysis. A.S.-C., M.P.-V., I.H. and I.A. contributed to the in vitro analysis and provided technical support. I.L.-V., A.S.-M., A.L.-I. and M.U.-U. provided BPH and PCa samples for gene expression analysis from Basurto University Hospital. M.G. carried out microvessel staining and quantifications. J. S. contributed as supervisor of I.H. J.S. and R.B. performed or coordinated (RB) the cloning of *MITFA* in lentiviral vectors. A.M.A. contributed to experimental design and discussion. A.C. contributed to experimental design, data analysis and discussion. V.T. supervised the project, experimental design, data generation, analysis and discussion and wrote the manuscript.

Conflict of interest

The authors declare that they have no conflict of interest.

Publisher's note

Springer Nature remains neutral with regard to jurisdictional claims in published maps and institutional affiliations.

Supplementary Information accompanies this paper at (<https://doi.org/10.1038/s41419-018-1096-6>).

Received: 10 August 2018 Revised: 19 September 2018 Accepted: 25 September 2018

Published online: 11 October 2018

References

- Hanahan, D. & Weinberg, R. A. Hallmarks of cancer: the next generation. *Cell* **144**, 646–674 (2011).
- Martin-Martin, N., Carracedo, A. & Torrano, V. Metabolism and transcription in cancer: Merging Two Classic Tales. *Front. Cell Dev. Biol.* **5**, 119 (2017).
- Martin-Martin, N. et al. Stratification and therapeutic potential of PML in metastatic breast cancer. *Nat. Commun.* **7**, 12595 (2016).
- Martin-Martin, N. et al. PPARdelta elicits ligand-independent repression of trefoil factor family to limit prostate cancer growth. *Cancer Res.* **78**, 399–409 (2018).
- Bacolod, M. D. et al. Examination of epigenetic and other molecular factors associated with mda-9/syntenin dysregulation in cancer through integrated analyses of public genomic datasets. *Adv. Cancer Res.* **127**, 49–121 (2015).
- Olvedy, M. et al. Comparative oncogenomics identifies tyrosine kinase FES as a tumor suppressor in melanoma. *J. Clin. Invest.* **127**, 2310–2325 (2017).
- Cancer Genome Atlas Research N. The molecular taxonomy of primary prostate. *Cancer Cell.* **163**, 1011–1025 (2015).
- Glinsky, G. V., Glinskii, A. B., Stephenson, A. J., Hoffman, R. M. & Gerald, W. L. Gene expression profiling predicts clinical outcome of prostate cancer. *J. Clin. Invest.* **113**, 913–923 (2004).
- Grasso, C. S. et al. The mutational landscape of lethal castration-resistant prostate cancer. *Nature* **487**, 239–243 (2012).
- Lapointe, J. et al. Genomic profiling reveals alternative genetic pathways of prostate tumorigenesis. *Cancer Res.* **67**, 8504–8510 (2007).
- Taylor, B. S. et al. Integrative genomic profiling of human prostate cancer. *Cancer Cell.* **18**, 11–22 (2010).
- Tomlins, S. A. et al. Integrative molecular concept modeling of prostate cancer progression. *Nat. Genet.* **39**, 41–51 (2007).
- Varambally, S. et al. Integrative genomic and proteomic analysis of prostate cancer reveals signatures of metastatic progression. *Cancer Cell* **8**, 393–406 (2005).
- Torrano, V. et al. The metabolic co-regulator PGC1alpha suppresses prostate cancer metastasis. *Nat. Cell Biol.* **18**, 645–656 (2016).
- Valcarcel-Jimenez, L., Torrano, V. & Carracedo, A. New insights on prostate cancer progression. *Cell Cycle* **16**, 13–14 (2017).
- Valcarcel-Jimenez, L., Gaude, E., Torrano, V., Frezza, C. & Carracedo, A. Mitochondrial metabolism: yin and yang for tumor progression. *Trends Endocrinol. Metab.* **28**, 748–757 (2017).
- Hock, M. B. & Kralli, A. Transcriptional control of mitochondrial biogenesis and function. *Annu. Rev. Physiol.* **71**, 177–203 (2009).
- Haq, R. et al. Oncogenic BRAF regulates oxidative metabolism via PGC1alpha and MITF. *Cancer Cell* **23**, 302–315 (2013).
- Wellbrock, C. & Arozarena, I. Microphthalmia-associated transcription factor in melanoma development and MAP-kinase pathway targeted therapy. *Pigment Cell. Melanoma Res.* **28**, 390–406 (2015).
- Tachibana, M. MITF: a stream flowing for pigment cells. *Pigment Cell Res.* **13**, 230–240 (2000).
- Garraway, L. A. et al. Integrative genomic analyses identify MITF as a lineage survival oncogene amplified in malignant melanoma. *Nature* **436**, 117–122 (2005).
- Vazquez, F. et al. PGC1alpha expression defines a subset of human melanoma tumors with increased mitochondrial capacity and resistance to oxidative stress. *Cancer Cell.* **23**, 287–301 (2013).
- Aggoune, D. et al. Bone marrow mesenchymal stromal cell (MSC) gene profiling in chronic myeloid leukemia (CML) patients at diagnosis and in deep molecular response induced by tyrosine kinase inhibitors (TKIs). *Leuk. Res.* **60**, 94–102 (2017).

24. Li, Y., Kong, D., Ahmad, A., Bao, B. & Sarkar, F. H. Targeting bone remodeling by isoflavone and 3,3'-diindolylmethane in the context of prostate cancer bone metastasis. *PLoS ONE* **7**, e33011 (2012).
25. Moyano, J. V. et al. AlphaB-crystallin is a novel oncoprotein that predicts poor clinical outcome in breast cancer. *J. Clin. Invest.* **116**, 261–270 (2006).
26. Voduc, K. D. et al. alphaB-crystallin expression in breast cancer is associated with brain metastasis. *NPJ Breast Cancer*, **1** (2015).
27. Shi, C., Yang, X., Bu, X., Hou, N. & Chen, P. Alpha B-crystallin promotes the invasion and metastasis of colorectal cancer via epithelial-mesenchymal transition. *Biochem. Biophys. Res. Commun.* **489**, 369–374 (2017).
28. Yilmaz, M. et al. Alpha-B-crystallin expression in human laryngeal squamous cell carcinoma tissues. *Head. Neck* **37**, 1344–1348 (2015).
29. Vollmann, J. et al. High expression of crystallin alphaB represents an independent molecular marker for unfavourable ovarian cancer patient outcome and impairs TRAIL- and cisplatin-induced apoptosis in human ovarian cancer cells. *Int. J. Cancer* **132**, 2820–2832 (2013).
30. Qin, H. et al. Elevated expression of CRYAB predicts unfavorable prognosis in non-small cell lung cancer. *Med. Oncol.* **31**, 142 (2014).
31. Shi, C. et al. Alpha B-crystallin correlates with poor survival in colorectal cancer. *Int. J. Clin. Exp. Pathol.* **7**, 6056–6063 (2014).
32. Altintas, D. M. et al. Differentially expressed androgen-regulated genes in androgen-sensitive tissues reveal potential biomarkers of early prostate cancer. *PLoS ONE* **8**, e66278 (2013).
33. Huang, Z. et al. Tumor suppressor Alpha B-crystallin (CRYAB) associates with the cadherin/catenin adherens junction and impairs NPC progression-associated properties. *Oncogene* **31**, 3709–3720 (2012).
34. Borniquel, S. et al. Inactivation of Foxo3a and subsequent downregulation of PGC-1 alpha mediate nitric oxide-induced endothelial cell migration. *Mol. Cell Biol.* **30**, 4035–4044 (2010).
35. Jin, J. et al. Transcriptional and translational regulation of C/EBPbeta-HDAC1 protein complexes controls different levels of p53, SIRT1, and PGC1alpha proteins at the early and late stages of liver cancer. *J. Biol. Chem.* **288**, 14451–14462 (2013).
36. Sancho, P. et al. MYC/PGC-1alpha balance determines the metabolic phenotype and plasticity of pancreatic cancer stem cells. *Cell Metab.* **22**, 590–605 (2015).
37. Shimizu, Y. I. et al. Fasting induced up-regulation of activating transcription factor 5 in mouse liver. *Life. Sci.* **84**, 894–902 (2009).
38. Wende, A. R. et al. Enhanced cardiac Akt/protein kinase B signaling contributes to pathological cardiac hypertrophy in part by impairing mitochondrial function via transcriptional repression of mitochondrion-targeted nuclear genes. *Mol. Cell Biol.* **35**, 831–846 (2015).
39. Carreira, S. et al. Mitf cooperates with Rb1 and activates p21Cip1 expression to regulate cell cycle progression. *Nature* **433**, 764–769 (2005).
40. Cortazar, A. R. et al. CANCERTOOL, a visualization and representation interface to exploit cancer datasets. *Cancer Res.* (2018).
41. Wang, G., Zhao, D., Spring, D. J. & DePinho, R. A. Genetics and biology of prostate cancer. *Genes Dev.* **32**, 1105–1140 (2018).
42. Karczewski, K. J. & Snyder, M. P. Integrative omics for health and disease. *Nat. Rev. Genet.* **19**, 299–310 (2018).
43. Carracedo, A. et al. A metabolic prosurvival role for PML in breast cancer. *J. Clin. Invest.* **122**, 3088–3100 (2012).
44. Cheng, P. F., Dummer, R. & Levesque, M. P. Data mining: The Cancer Genome Atlas in the era of precision cancer medicine. *Swiss Med. Wkly.* **145**, w14183 (2015).
45. Gao, J. et al. Integrative analysis of complex cancer genomics and clinical profiles using the cBioPortal. *Sci. Signal.* **6**, pl1 (2013).
46. Klonowska, K. et al. Oncogenomic portals for the visualization and analysis of genome-wide cancer data. *Oncotarget* **7**, 176–192 (2016).
47. Cerami, E. et al. The cBio cancer genomics portal: an open platform for exploring multidimensional cancer genomics data. *Cancer Discov.* **2**, 401–404 (2012).
48. Carreira, S. et al. Mitf regulation of Dia1 controls melanoma proliferation and invasiveness. *Genes Dev.* **20**, 3426–3439 (2006).
49. Vachtenheim, J. & Ondrusova, L. Microphthalmia-associated transcription factor expression levels in melanoma cells contribute to cell invasion and proliferation. *Exp. Dermatol.* **24**, 481–484 (2015).
50. Wellbrock, C. & Marais, R. Elevated expression of MITF counteracts B-RAF-stimulated melanocyte and melanoma cell proliferation. *J. Cell. Biol.* **170**, 703–708 (2005).
51. Wellbrock, C. et al. Oncogenic BRAF regulates melanoma proliferation through the lineage specific factor MITF. *PLoS ONE* **3**, e2734 (2008).
52. Thomaschewski, M. et al. Multi-color RGB marking enables clonality assessment of liver tumors in a murine xenograft model. *Oncotarget* **8**, 115582–115595 (2017).
53. Kamradt, M. C. et al. The small heat shock protein alpha B-crystallin is a novel inhibitor of TRAIL-induced apoptosis that suppresses the activation of caspase-3. *J. Biol. Chem.* **280**, 11059–11066 (2005).
54. Clark, J. I. & Muchowski, P. J. Small heat-shock proteins and their potential role in human disease. *Curr. Opin. Struct. Biol.* **10**, 52–59 (2000).
55. Goplen, D. et al. alphaB-crystallin is elevated in highly infiltrative apoptosis-resistant glioblastoma cells. *Am. J. Pathol.* **177**, 1618–1628 (2010).
56. Zhang, L. et al. Kruppel-like factor 4 promotes human osteosarcoma growth and metastasis via regulating CRYAB expression. *Oncotarget* **7**, 30990–31000 (2016).
57. Hu, R. & Aplin, A. E. alphaB-crystallin is mutant B-RAF regulated and contributes to cyclin D1 turnover in melanocytic cells. *Pigment. Cell. Melanoma Res.* **23**, 201–209 (2010).
58. Chin, D. et al. Alpha B-crystallin, a new independent marker for poor prognosis in head and neck cancer. *Laryngoscope* **115**, 1239–1242 (2005).
59. Shi, Q. M. et al. High level of alphaB-crystallin contributes to the progression of osteosarcoma. *Oncotarget* **7**, 9007–9016 (2016).
60. Smith, M. P. et al. Inhibiting drivers of non-mutational drug tolerance is a salvage strategy for targeted melanoma therapy. *Cancer Cell* **29**, 270–284 (2016).
61. Muller, J. et al. Low MITF/AXL ratio predicts early resistance to multiple targeted drugs in melanoma. *Nat. Commun.* **5**, 5712 (2014).
62. Naffouje, S., Naffouje, R., Bhagwandin, S. & Salti, G. I. Microphthalmia transcription factor in malignant melanoma predicts occult sentinel lymph node metastases and survival. *Melanoma Res.* **25**, 496–502 (2015).
63. Najem, A. et al. P53 and MITF/Bcl-2 identified as key pathways in the acquired resistance of NRAS-mutant melanoma to MEK inhibition. *Eur. J. Cancer* **83**, 154–165 (2017).
64. Du, P., Kibbe, W. A. & Lin, S. M. lumi: a pipeline for processing Illumina microarray. *Bioinformatics* **24**, 1547–1548 (2008).
65. Gentleman, R. C. et al. Bioconductor: open software development for computational biology and bioinformatics. *Genome Biol.* **5**, R80 (2004).
66. Huber, W. et al. Orchestrating high-throughput genomic analysis with Bioconductor. *Nat. Methods* **12**, 115–121 (2015).
67. Ritchie, M. E. et al. limma powers differential expression analyses for RNA-sequencing and microarray studies. *Nucleic Acids Res.* **43**, e47 (2015).
68. Benjamini, Y. & Hochberg, Y. Controlling the false discovery rate: a practical and powerful approach to multiple testing. *J. R. Stat. Soc. Ser. B (Methodol.)* **57**, 289–300 (1995).

PGC1 α Suppresses Prostate Cancer Cell Invasion through ERR α Transcriptional Control

Lorea Valcarcel-Jimenez¹, Alice Macchia¹, Eva Crosas-Molist^{2,3}, Ariane Schaub-Clerigué¹, Laura Camacho^{1,4}, Natalia Martín-Martín^{1,5}, Paolo Cicogna¹, Cristina Viera-Bardón^{1,5}, Sonia Fernández-Ruiz^{1,5}, Irene Rodríguez-Hernandez^{2,3}, Ivana Hermanova¹, Ianire Astobiza^{1,5}, Ana R. Cortazar^{1,5}, Jon Corres-Mendizabal¹, Antonio Gomez-Muñoz⁴, Victoria Sanz-Moreno^{2,3}, Verónica Torrano^{1,4,5}, and Arkaitz Carracedo^{1,4,5,6}



Abstract

The PPAR γ coactivator 1 alpha (PGC1 α) is a prostate tumor suppressor that controls the balance between anabolism and catabolism. PGC1A downregulation in prostate cancer is causally associated with the development of metastasis. Here we show that the transcriptional complex formed by PGC1 α and estrogen-related receptor 1 alpha (ERR α) controls the aggressive properties of prostate cancer cells. PGC1 α expression significantly decreased migration and invasion of various prostate cancer cell lines. This phenotype was consistent with remarkable cytoskeletal remodeling and inhibition of integrin alpha 1 and beta 4 expression, both *in vitro* and *in vivo*. CRISPR/Cas9-based deletion of ERR α suppressed PGC1 α regulation of cytoskeletal organization and invasiveness. Mechanistically,

PGC1 α expression decreased MYC levels and activity prior to inhibition of invasiveness. In addition, PGC1 α and ERR α associated at the MYC promoter, supporting the inhibitory activity PGC1 α . The inverse correlation between PGC1 α -ERR α activity and MYC levels was corroborated in multiple prostate cancer datasets. Altogether, these results support that PGC1 α -ERR α functions as a tumor-suppressive transcriptional complex through the regulation of metabolic and signaling events.

Significance: These findings describe how downregulation of the prostate tumor suppressor PGC1 drives invasiveness and migration of prostate cancer cells.

Introduction

The process of cellular transformation stems from the acquisition of genomic aberrations that altogether change the response of normal cells and enable them with hallmarks of cancer (1, 2). The mutational landscape changes within and among tumors and along time following evolutionary principles (3). In addition, nongenomic alterations harness great relevance in the process of

cancer progression. Indeed, transcriptional regulation in cancer is an emerging aspect that provides a feasible explanation to the rapid adaptation of transformed cells to hostile environments (4). Yet, the control of oncogenic and tumor-suppressive transcriptional programs remains poorly characterized.

Transcriptional coregulators encompass a family of versatile modulators of gene expression (5). These proteins harbor the capacity of controlling distinct transcriptional programs based on their partner transcription factors. In turn, transcriptional coregulators operate in a tissue- and context-specific manner, thus revealing them as major players in cell and organismal homeostasis. Among this family of genes, the PPAR γ coactivator 1 alpha (PGC1 α) controls biological responses in health and disease (6, 7). PGC1 α is a tightly regulated protein that interacts with a variety of transcription factors, including estrogen-related receptor 1 alpha (ERR α), PPARs, and nuclear factor erythroid 2-like 2 (NFE2L2, NRF2; ref. 6). As a consequence, PGC1 α coordinates metabolic and antioxidant responses, which account for its relevance in diabetes, neurodegeneration, cardiomyopathy, and cancer (7, 8).

The role of PGC1 α in cancer is largely tumor type and context-dependent. On the one hand, this transcriptional coregulator favors survival, proliferation, stem cell maintenance, and therapy resistance in pancreatic tumors, breast cancer, and melanoma cells (9–14). On the other hand, we and others have demonstrated that PGC1 α expression is reduced in renal and prostate carcinoma, as well as in metastatic melanoma, where it opposes the acquisition of aggressive features (15–17). The predominant mechanism of action of PGC1 α in cancer biology is ascribed to

¹CIC bioGUNE, Bizkaia, Spain. ²Barts Cancer Institute, Queen Mary University of London, London, United Kingdom. ³Randall Centre for Cell & Molecular Biophysics, King's College London, London, United Kingdom. ⁴Biochemistry and Molecular Biology Department, University of the Basque Country (UPV/EHU), Bilbao, Spain. ⁵CIBERONC, Madrid, Spain. ⁶Ikerbasque, Basque Foundation for Science, Bilbao, Spain.

Note: Supplementary data for this article are available at Cancer Research Online (<http://cancerres.aacrjournals.org/>).

L. Valcarcel-Jimenez and A. Macchia contributed equally to this article as first authors.

V. Torrano and A. Carracedo contributed equally to this article as last authors.

Corresponding Authors: Arkaitz Carracedo, CICbioGUNE, PARQUE TECNOLÓGICO DE BIZKAIA, Derio, Bizkaia 48160, Spain. Phone: 34-94406130; Fax: 34-94406130; E-mail: acarracedo@cicbiogune.es; and Verónica Torrano, Biochemistry and Molecular Biology Department, University of the Basque Country (UPV/EHU), Barrio Sarriena s/n, Leioa, Bizkaia 48940, Spain. Phone: 34-946015925; E-mail: vtorrano@cicbiogune.es

Cancer Res 2019;79:6153–65

doi: 10.1158/0008-5472.CAN-19-1231

©2019 American Association for Cancer Research.

the regulation of metabolism. This coregulator promotes the expression of genes that mediate mitochondrial biogenesis, oxidative metabolism, and the production of glutathione. In turn, PGC1 α enhances the oxidative utilization of nutrients and antioxidant production. However, emerging data suggest that a fraction of the activities of PGC1 α relies neither on the regulation of metabolism nor on its main partner, ERR α (16).

In prostate cancer, PGC1 α suppresses cell proliferation, anchorage-independent growth, tumor burden, and metastasis (17). This coregulator is profoundly downregulated in localized prostate cancer, with a further decrease in metastatic specimens (17). Moreover, reduced PGC1 α expression is associated to shorter time to biochemical recurrence after surgery, pointing at the relevance of this gene in the control of prostate cancer aggressiveness. Mechanistically, we previously showed that PGC1 α requires the presence of ERR α to suppress prostate cancer cell proliferation and metastatic outgrowth, which was consistent with the reduction of biosynthetic capacity of PGC1 α reexpressing cells and the elevation of nutrient catabolism (17). Moreover, a recent study revealed that the metabolic control of polyamine synthesis underlies the regulation of prostate cancer aggressiveness by this coactivator (18).

The metastatic process requires the acquisition of discreet capacities beyond cell proliferation. Specifically, the motility and invasive capacity of cancer cells are paramount for the achievement of metastasis (19). Stemming from this notion, in this study, we evaluated the contribution of PGC1 α to the acquisition of these features in prostate cancer cells. Our analysis uncovers an ERR α -dependent activity of the coactivator that suppresses the acquisition of invasive properties required for prostate cancer aggressiveness.

Materials and Methods

Reagents

Doxycycline hyclate (Sigma #D9891) was used to induce gene expression or silencing in vectors under tetracycline control. Puromycin (Sigma #P8833) and blasticidin (Invitrogen #R210-01) were used for cell selection after lentiviral transfection.

Cell culture

Human prostate carcinoma cell lines PC3 and DU145 were purchased from Leibniz-Institut DSMZ-Deutsche Sammlung von Mikroorganismen und Zellkulturen GmbH, who provided authentication certificate. Cell lines were periodically subjected to microsatellite-based identity validation. None of the cell lines used in this study were found in the database of commonly misidentified cell lines maintained by the International Cell Line Authentication Committee and NCBI Biosample. 293FT cells were used for lentiviral production. All cell lines were routinely monitored for *Mycoplasma* contamination. DU145, PC3, and 293FT cell lines were maintained in DMEM supplemented with 10% volume for volume (v/v) FBS and 1% (v/v) penicillin-streptomycin. For PGC1A expression, cells were transduced with a modified TRIPZ (Dharmacon) doxycycline-inducible lentiviral construct in which the red fluorescent protein and miR30 region was substituted by *HA-Flag-Pgc1a* (9). For *ESRRA* deletion, single-guide RNA (sgRNA) constructs targeting *ESRRA* (sgERR α #1: 5'CTCCGGCTACCACTATGGTGTGG3'; sgERR α #2: 3'AGGAACCCITTTGGACTGTCAGGG5') were designed using Crispor software (crispor.tefor.net) and cloned in a lentiviral

vector purchased from Addgene LentiCRISPR V2 (a gift from Mohan Babu, Addgene plasmid # 83480). Lentiviral vector expressing a validated shRNA against human *MYC* from the Mission shRNA Library (TRCN0000039642) was subcloned in a Plko Tet-On inducible system (Addgene plasmid # 21915; ref. 20). Cells were transfected with lentiviral vectors following standard procedures, and viral supernatant was used to infect cells. Selection was done using puromycin (2 μ g/mL) or blasticidin (for LentiCRISPR V2, 10 μ g/mL) for 3 or 5 days, respectively.

Animals

All mouse experiments were carried out following the ethical guidelines established by the Biosafety and Welfare Committee at CIC bioGUNE. The procedures employed were carried out following the recommendations from Association for Assessment and Accreditation of Laboratory Animal Care International. Xenograft experiments were performed as described previously (17), injecting 1×10^6 cells per tumor in two flanks of Hsd:ATHymic-Nude-Foxn1nu "Nude" mouse (Envigo). Once tumors reached an average of 100 mm³, animals were assigned to chow or doxycycline diet regime (Research diets, D12100402) and tumor volume was monitored with external caliper. After euthanasia, tumors were weighed, tissue was fresh frozen or paraffin embedded, and histologic evaluation of hematoxylin and eosin-stained sections was performed. Proliferation was assessed in paraffin-embedded tissue samples by using Ki67 antibody (MA5-14520, Thermo Fisher Scientific).

Cellular and molecular assays

Cell number quantification with crystal violet was performed as described in ref. 21.

Cell morphology and stress fiber content were examined by staining the cells with fluorescent phalloidin (Thermo Fisher Scientific F432; 1:400 dilution), a high-affinity F-actin probe. Images were taken with AxioImager D1 microscope at 200 \times for cell area analysis (Fiji Software) or at 400 \times for stress fiber quantification. Immunofluorescence detection and quantification of p-MLC (Ser19) were performed as described in ref. 22. Briefly, cells were fixed with 4% formaldehyde, permeabilized with 0.3% Triton, and incubated with primary antibody (p-MLC Ser19, Cell Signaling Technology #3672) overnight. Cells were then stained with secondary Alexa Fluor-488 or 647 anti-rabbit (Life Technologies), Alexa Fluor 546-phalloidin for F-actin detection (Life Technologies), and DAPI (Thermo Fisher Scientific D1306; 1:10,000 dilution).

For adhesion assays, cells were plated (40,000 cells/well) on a 12-well plate previously coated with rat tail collagen I (Corning 354236) at 50 μ g/mL (diluted in 0.02 N of acetic acid) during 1 hour. After 30 minutes, plates were washed twice with PBS, fixed with 10% formalin, and stained with crystal violet as described previously (17).

Transwell invasion assay was carried out using Matrigel-coated chambers (BD CioCoat #354480). Cells (50,000 cells/well) were resuspended in 0.1% FBS DMEM and seeded in the top part of the chamber. In the bottom part of the well, 1.4-mL solution of complete DMEM was added. Plates were maintained at 37 $^{\circ}$ C and 5% CO₂ for 48 hours. Invasion was stopped washing the well twice with PBS and using a cotton bud to remove the remaining cell of the top part of the membrane, being careful not to compromise the Matrigel. The membrane was fixed with 10% formalin (15 minutes at 4 $^{\circ}$ C) and stained with crystal violet

(Sigma C3886; 0.1% crystal violet in 20% methanol). Cells were counted under the microscope. For transwell migration, chambers with membranes of 8- μ m pores (BD Falcon 351185) were used. Cell plating as well as washing and fixation conditions were the same as in the invasion assay, but cells were fixed after 24 hours.

Spheroid cell culture and three-dimensional invasion assays were performed as described previously (23). Briefly, cells (700 cells/drop) were maintained in drops (25 μ L/drop) with DMEM and 6% methylcellulose (Sigma M0387) on the cover of a 100-mm culture plate. Drops were incubated at 37°C and 5% CO₂ for 48 hours. Once formed, spheroids were collected, resuspended in collagen I solution (Advanced BioMatrix PureCol), and added to 12-well plates. After 4 hours, complete media was then added on top of the well and day 0 pictures were taken. For invasive growth quantification, increase in area occupied by the spheroids between day 0 and day 2 was calculated using Fiji software. For three-dimensional invasion assays, cells were resuspended in an FBS-free bovine collagen I solution at 2.3 mg/mL in a 1:1 proportion to a final concentration of 15,000 cells per 100 μ L of matrix and spun down in a 96-well plate. After matrix polymerization, 10% FBS-containing media was added on top. Cells were fixed after 24 hours. The three-dimensional invasion index was calculated counting the number of cells at 50 μ m and 100 μ m divided by the number of cells at the bottom. Images for three-dimensional invasion were obtained using a Zeiss 710 confocal microscope and cell counting was analyzed using Fiji Software.

Western blot was performed as described previously (9). Briefly, cells were seeded on 6-well plates and 4 days after seeding cell lysates were prepared with RIPA buffer (50 mmol/L TrisHCl pH 7.5, 150 mmol/L NaCl, 1 mmol/L EDTA, 0.1% SDS, 1% Nonidet P40, 1% sodium deoxycholate, 1 mmol/L sodium fluoride, 1 mmol/L sodium orthovanadate, 1 mmol/L beta-glycerophosphate and protease inhibitor cocktail; Roche). The following antibodies were used: PGC1 α H300 (Santa Cruz Biotechnology #sc-13067), ERR α (Cell Signaling Technology #13826), ITG β 1 (Cell Signaling Technology #34981S), Caveolin-1 (BD Biosciences, ref: 142610059), β -actin (Cell Signaling Technology #3700S), phospho-cofilin (Cell Signaling Technology #3313), cofilin (Cell Signaling Technology #5175), GAPDH (Cell Signaling Technology #2118), c-MYC (MYC, Cell Signaling Technology #13987S), ITG β 4 (Cell Signaling Technology #14803), ITG α 3 (Santa Cruz Biotechnology #sc-374242), ITG α 6 (Cell Signaling Technology #3750S), phospho-Src (Life Technologies, ref: 44660G; p-Src Tyr419), and Src 36D10 (Cell Signaling Technology #2109). All were used at a 1:1,000 dilution, except β -actin (1:2,000). Mouse and rabbit secondary antibodies were purchased from Jackson ImmunoResearch. After standard SDS-PAGE and Western blotting techniques, proteins were visualized using the ECL system in the iBright FL1000 Imaging System.

The cytoskeleton phospho-antibody array was performed following Tebu-bio protocol (<https://www.tebu-bio.com>). Briefly, 5 \times 10⁶ induced and noninduced cells were collected and the cell pellet was frozen for further analysis by Tebu-bio services. More than 141 antibodies were present in the screening for phosphorylation rate of main cytoskeleton proteins.

RNA was extracted using NucleoSpin RNA isolation kit from Macherey-Nagel (ref: 740955.240C). For xenograft samples, a TRIzol-based implementation of the NucleoSpin RNA isolation kit protocol was used as reported (24). For all cases, 1 μ g of total RNA was used for cDNA synthesis using qScript cDNA Supermix

from Quanta (ref: 95048). Quantitative real-time PCR (qRT-PCR) was performed as described previously (9). Universal Probe Library (Roche) primers and probes employed are detailed in Supplementary Table S1. All qRT-PCR data presented were normalized using GAPDH (Hs02758991_g1 from Applied Biosystems).

Chromatin immunoprecipitation

Chromatin immunoprecipitation (ChIP) was performed using the SimpleChIP Enzymatic Chromatin IP Kit (catalog no. 9003, Cell Signaling Technology, Inc). Four million PC3 TRIPZ-Pgc1a cells per immunoprecipitation were grown in 150-mm dishes either with or without 0.5- μ g/mL doxycycline during 16 hours. Cells were cross-linked with 37% formaldehyde for 10 minutes at room temperature. Glycine was added to dishes and cells were incubated for 5 minutes at room temperature. Cells were then washed twice with ice-cold PBS and scraped into PBS + PIC. Pelleted cells were lysed and nuclei were harvested following the manufacturer's instructions. Nuclear lysates were digested with micrococcal nuclease for 20 minutes at 37°C and then sonicated in 500- μ L aliquots on ice for six pulses of 20 seconds using a Branson sonicator. Cells were held on ice for at least 20 seconds between sonications. Lysates were clarified at 11,000 \times g for 10 minutes at 4°C, and chromatin was stored at -80°C. HA-Tag polyclonal antibody (Cell Signaling Technology #3724), anti-ERR α antibody (Cell Signaling Technology #13826), and IgG antibody (Cell Signaling Technology #2729) were incubated overnight (4°C) with rotation and protein G magnetic beads were incubated for 2 hours (4°C). Washes and elution of chromatin were performed following manufacturer's instructions. DNA quantification was carried out using a Viiia7 Real-Time PCR System (Applied Biosystems) with SYBR Green reagents and primers that amplify a PGC1A binding region to MYC promoter (shown in Supplementary Table S2).

Bioinformatic analysis and statistics

Bioinformatic analysis containing patient data was performed using the web-based interface Cancertool (25).

For each available patient dataset, the values of PGC1 α -ERR α signature were calculated from the average of the expression signal of those genes that are part of the aforementioned signature (ACACB, ACSL4, ATP1B1, GSTM4, ISCU, LAMB2, NNT, PPIC, SOD2, SUCLA2). In the case of PPARGC1A/NRIP1 ratio, we calculated the average expression value of PPARGC1A, and, as values are log₂ scaled, subtracted the average expression value of NRIP1. R software (<https://cran.r-project.org/>), version 3.5.1, has been used for these calculations, together with ggplot2 package (<https://cran.r-project.org/web/packages/ggplot2>) to perform the corresponding graphs.

Individual gene expression patterns in patient dataset, as well as pairwise correlation information, can be visualized in the Cancertool interface.

The differential gene expression analysis driven by PGC1 α in PC3 cells can be obtained from GEO with reference GSE75193.

In addition, pathway and network enrichment analyses of the significantly regulated genes from GSE75193 (Supplementary Table S3) were performed using MetaCore from GeneGo Inc (<https://portal.genego.com/>).

No statistical method was used to predetermine sample size. The experiments were not randomized. The investigators were not blinded to allocation during experiments and outcome

assessment. *n* values represent the number of independent experiments performed, the number of individual mice, or patient specimens. For each independent *in vitro* experiment, normal distribution was assumed, and one-sample *t* test was applied for one-component comparisons with control and Student *t* test for two-component comparisons. For *in vivo* experiments, a nonparametric Mann–Whitney exact test was used. Two-tailed statistical analysis was applied for experimental design without predicted result, and one-tailed for validation or hypothesis-driven experiments. The confidence level used for all the statistical analyses was of 95% (alpha value = 0.05). GraphPad Prism 8 software was used for statistical calculations.

Results

To address the role of PGC1 α in the regulation of prostate cancer features beyond proliferation (17), we carried out a comprehensive evaluation of phenotypes associated to cancer aggressiveness, based on an inducible system reported previously (17). Interestingly, Pgc1 α expression elicited a remarkable reduction in the migratory capacity of PC3 and DU145 prostate cancer cells in transwell assays (Fig. 1A; Supplementary Fig. S1A). A similar effect was achieved in Matrigel-coated transwell assays as a measure of invasion (Fig. 1B; Supplementary Fig. S1B). To further characterize the regulation of invasive properties by PGC1 α , we applied two complementary assays in both cell lines. On the one hand, we performed three-dimensional invasion assays. We quantified the number of cells invading at 50 μ m and/or 100 μ m of distance from the bottom of the plate. The results showed a profound decrease in cells with invasive capacity upon Pgc1 α induction (Fig. 1C; Supplementary Fig. S1C and S1D). On the other hand, we generated spheroids using the hanging drop method to measure the invasive growth. The results corroborated that the expression of the coregulator inhibits the invasive capacity of prostate cancer cells (Fig. 1D; Supplementary Fig. S1E). Of note, this phenotype was observed at time points where proliferation was not significantly influenced by Pgc1 α or by the addition of doxycycline (Supplementary Fig. S1F–S1I; ref. 17). Overall, our results show that beyond the antiproliferative capacity of PGC1 α in prostate cancer, the transcriptional coregulator elicits a robust anti-invasive phenotype.

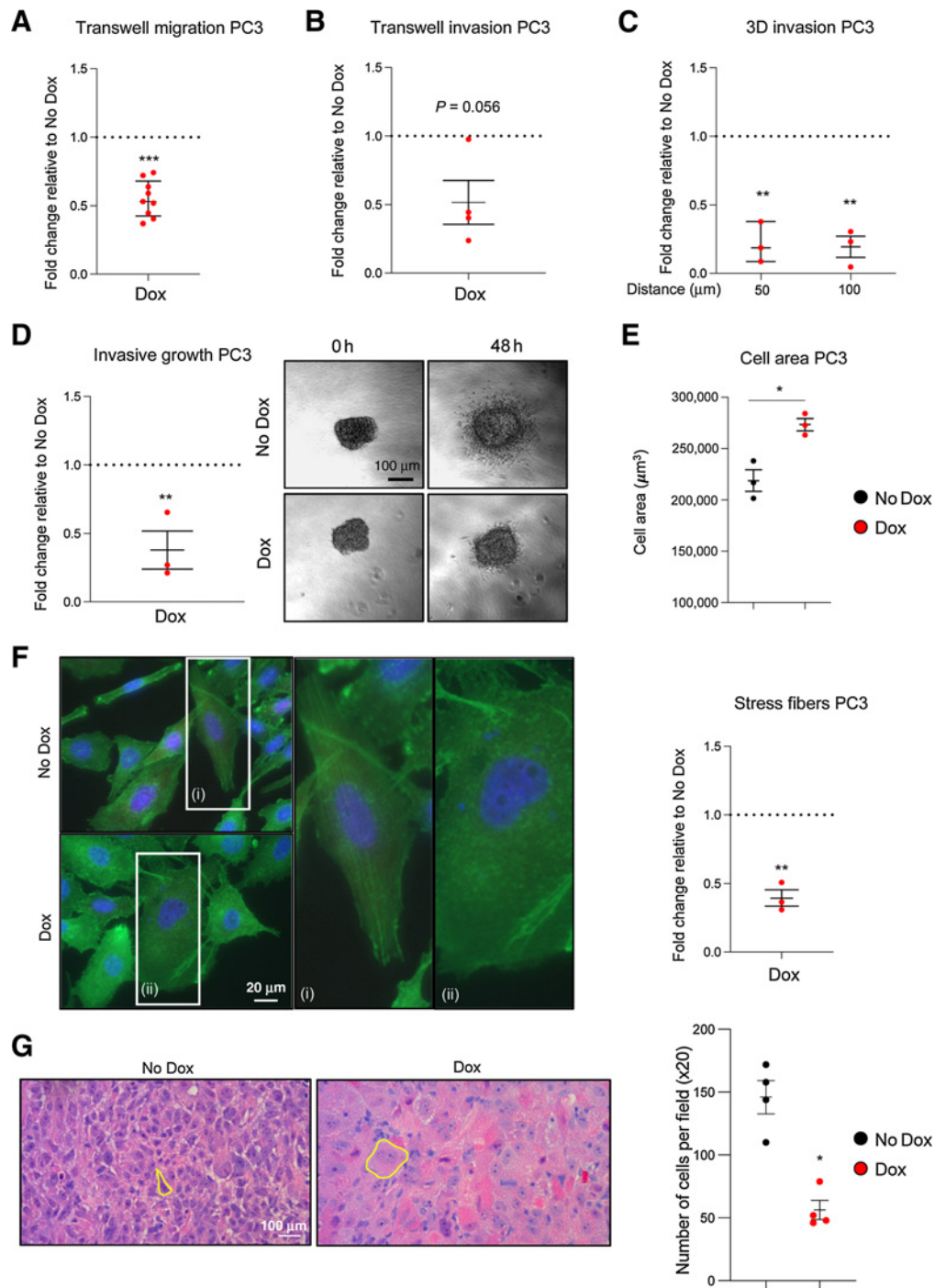
The regulation of cell migration and invasion is intertwined with cell morphology and adhesion (19). Hence, we characterized the effects of PGC1 α on these parameters. The expression of the coregulator in PC3 cells was associated with a remarkable elevation in cell area, with loss of stress fibers and with a modest increase in cell adhesion to collagen I (Fig. 1E and F; Supplementary Fig. S1J). Importantly, Pgc1 α induction in subcutaneous xenografts of PC3 cells confirmed the antitumoral activity of this gene and its impact on prostate cancer cell size *in vivo* (Fig. 1G; Supplementary Fig. S1K–S1M).

We next focused on the molecular alterations underlying the activity of PGC1 α . In a previous study, we analyzed a gene expression analysis in PC3 cells upon induction of Pgc1 α (Fig. 1; GSE75193; ref. 17). We sought to extend the analysis of this microarray by taking advantage of bioinformatic tools, such as Metacore (<https://clarivate.com/products/metacore/>) and Cancertool (25) that enable cancer researchers to perform various functional enrichment analyses. Because functional enrichment allows the integration of larger sets of data to identify underlying molecular and functional alterations, we focused our analyses on

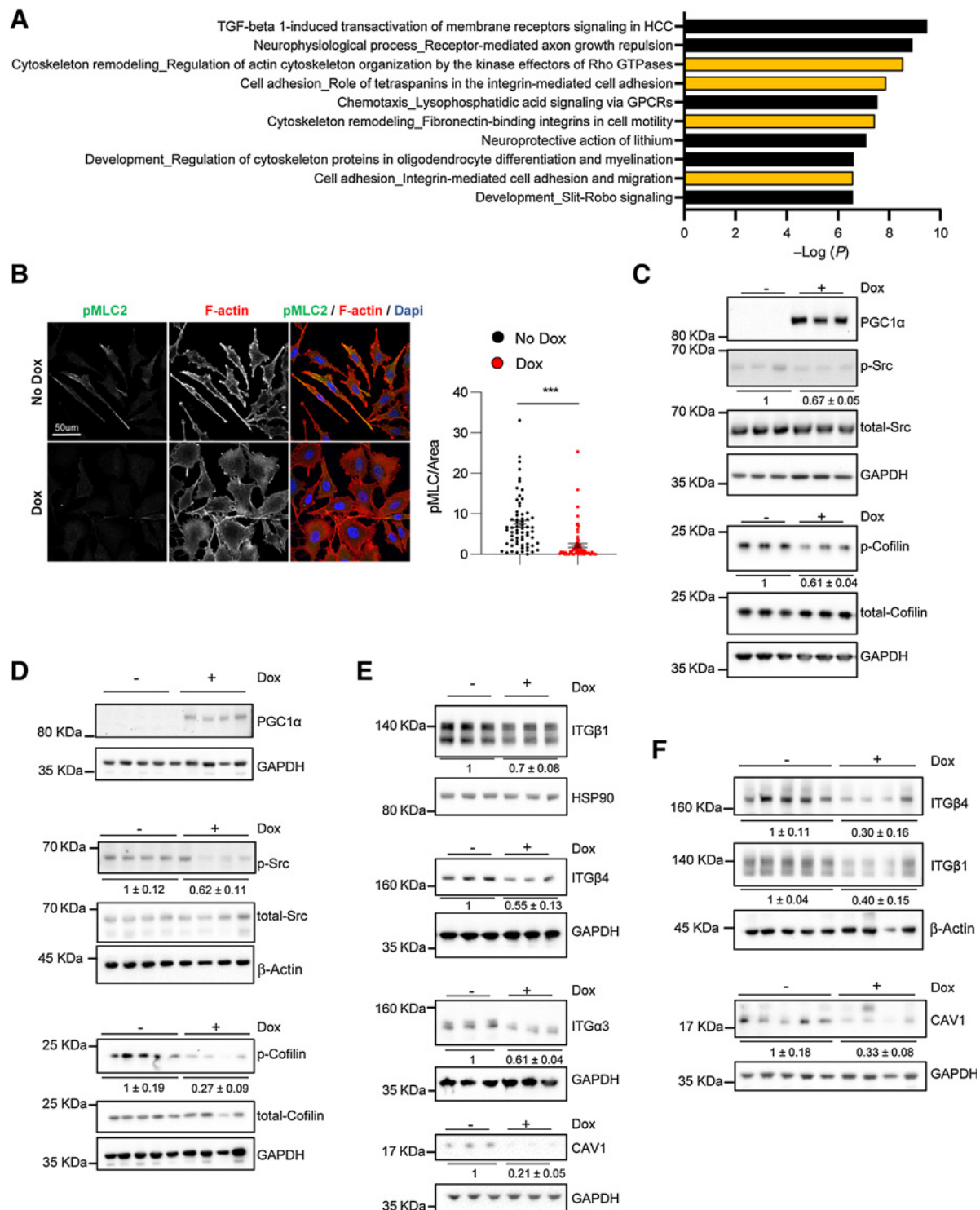
all genes whose expression was altered with a significant *P* value in the transcriptomics analysis (regardless of the *P*_{adj} value). This led to 1,347 upregulated and 990 downregulated unique gene IDs (Supplementary Table S3). Strikingly, functional enrichment of the downregulated genes revealed a significant alteration in cytoskeleton organization, migration, adhesion, and integrin and Rho signaling (Fig. 2A; Supplementary Fig. S2A; Supplementary Tables S4 and S5). Of note, we also identified other pathways with reported activities in the regulation of invasion, such as p27, FAS, and RAC, although their prevalence in the analysis and their documented association to this phenotype were minor (26–29). In line with our previous study (17), the enrichment analysis of the genes upregulated upon Pgc1 α expression confirmed a significant alteration of catabolic pathways (Supplementary Table S6). We focused our attention in the Metacore analysis of downregulated genes. The results revealed a remarkable alteration in cytoskeletal remodeling upon PGC1 α modulation in prostate cancer cells, illustrated by processes regulated by Rho kinase (ROCK). The axes containing ROCK-LIM kinase (LIMK)-Cofilin and ROCK-myosin light chain (MLC) are two key signaling pathways that regulate cytoskeletal remodeling downstream of the monomeric G protein Rho and integrin signaling (30). The immunostaining and quantification of phosphorylated myosin-light chain 2 (p-MLC2) revealed a significant reduction in this parameter in Pgc1 α -expressing PC3 cells (Fig. 2B). This result supports the notion that loss of PGC1 α in prostate cancer cells results in changes in the actin–myosin cytoskeleton that are associated with the acquisition of invasive properties. To ascertain which signaling pathways were modulated and affecting cytoskeleton organization upon Pgc1 α expression, we carried out a cytoskeleton phospho-antibody array (Supplementary Table S7). The phosphorylation of Src protein was among the most prominently reduced in the analysis (Supplementary Fig. S2B). We confirmed this result by Western blot analysis, both *in vitro* and *in vivo*, together with the reduction in cofilin phosphorylation, the final effector of actin filament polymerization downstream Src (Fig. 2C and D; Supplementary Fig. S2C and S2D).

Integrins are upstream regulators of the cytoskeleton with well-documented involvement in cancer aggressiveness (19, 31, 32). The bioinformatics analysis of PGC1 α -downregulated genes indicated an altered integrin signaling (Fig. 2A; Supplementary Fig. S2A), which would be consistent with the reduction in Src, MLC2, and cofilin phosphorylation. This, together with the fact that PGC1 α controls integrin expression in melanoma (16), prompted us to evaluate integrin expression in our experimental systems. Interestingly, the levels of various integrins and caveolin-1 (CAV1, but not CAV2) were robustly reduced at protein and mRNA levels upon Pgc1 α induction, an event that was not influenced by doxycycline treatment (Fig. 2E; Supplementary Fig. S2E–S2I). Next, we analyzed extracts from xenografts in which Pgc1 α expression was activated (Fig. 1G). The Western blot and quantitative qRT-PCR analysis corroborated the alterations elicited by the coactivator *in vivo* (Fig. 2F; Supplementary Fig. S2J and S2K). Our results suggest that PGC1 α controls a transcriptional program that results in the alteration of cytoskeleton organization with the concomitant reduction in integrin expression, an event that is consistent with the observed reduction in migratory and invasive properties of prostate cancer cells.

We then asked which effector of PGC1 α could contribute to the negative regulation of invasive properties. Inhibitors of

**Figure 1.**

PGC1 α expression impacts on invasive properties of prostate cancer *in vitro* and *in vivo*. **A** and **B**, Effect of Pgc1 α expression on transwell migration ($n = 9$ independent experiments; **A**) and on transwell invasion ($n = 4$ independent experiments; **B**) of PC3 cells. **C** and **D**, Effect of Pgc1 α expression on 3D invasion ($n = 3$ independent experiments; **C**) and invasive growth ($n = 3$ independent experiments; **D**) of PC3 cells. **D**, Right, one representative experiment of invasive growth; left, the quantification. **E** and **F**, Quantification of changes in cell area (**E**) and stress fibers (**F**) content upon Pgc1 α expression in PC3 cells *in vitro* ($n = 3$ independent experiments). **F**, Representative phalloidin staining of nonexpressing (No Dox) and Pgc1 α -expressing PC3 cells (left) and quantification (right). **G**, Quantification of changes in cell area upon Pgc1 α expression in PC3 cells *in vivo*. Left, representative hematoxylin and eosin staining of nonexpressing and Pgc1 α -expressing xenograft samples ($n = 4$ tumors each condition, No Dox and Dox). Yellow line outlines cell surface. Right, the quantification of number of cells per field. Dox, doxycycline, Pgc1 α -induced conditions; No Dox, Pgc1 α nonexpressing conditions. In **A**, **B**, **C**, **D**, and **F**, data are represented as fold change relative to No Dox condition depicted by a dotted line. Error bars, SEM. Statistic tests: one-sample *t* test with a hypothetical value of 1 (**A**, **B**, **C**, **D**, and **F**), two-tailed Student *t* test (**E**), and one-tailed Mann-Whitney U test (**G**). *, $P < 0.05$; **, $P < 0.01$; ***, $P < 0.001$.

**Figure 2.**

PGC1 α expression modulates integrin signaling of prostate cancer *in vitro* and *in vivo*. **A**, Metacore enrichment analysis of the transcriptional program downregulated by PGC1 α in PC3 cells. **B**, Effect of Pgc1 α expression on the phosphorylation of MLC protein in PC3 cells. Left, representative images of immunofluorescence staining using p-MLC antibodies. Right, quantification of p-MLC per cell area ($n = 3$ independent experiments). **C** and **D**, Representative Western blot analysis of the effect of Pgc1 α on cofilin and Src phosphorylation in PC3 cells (**C**) and xenograft samples (**D**). Representative Western blot analysis of the effect of Pgc1 α on ITG β 1, ITG β 4, ITG α 3, and CAV1 in PC3 cells ($n = 3$; independent experiments; **E**) and xenograft samples ($n = 4-5$ tumors; **F**). Dox, doxycycline, Pgc1 α -induced conditions; No Dox, Pgc1 α -nonexpressing conditions. Error bars, SEM. Western blot quantifications are presented as \pm SEM. Statistic tests: two-tailed Student t test (**B**). ***, $P < 0.001$.

differentiation are responsible for integrin repression in melanoma (16). We ruled out the potential contribution of ID2-4 to our phenotype, because their expression was not upregulated upon induction of the coactivator (Supplementary Fig. S3A). Then, we applied promoter enrichment analysis (25) to the list of Pgc1 α -repressed genes. Strikingly, the results revealed a significant enrichment in MYC within the promoters of the downregulated genes ($P = 8.5e-19$; Fig. 3A; Supplementary Tables S3 and S8). We studied the impact of PGC1 α on the expression of MYC and observed that induction of the coregulator elicited a consistent

decrease in MYC expression in prostate cancer cells in a doxycycline-independent manner (Fig. 3B; Supplementary Fig. S3B and S3C). Importantly, the effect was fully recapitulated at the transcriptional level. In addition, the analysis of previously reported targets or genes contained in the promoter analysis confirmed the reduction in MYC-dependent transcriptional program in the aforementioned conditions (Fig. 3C). We took advantage of our Pgc1 α -inducible xenograft analysis to further demonstrate that the reduction in MYC expression and function was not an artifact of *in vitro* assays (Fig. 3D and E; Supplementary Fig. S3D). These

Figure 3.

PGC1 α regulates c-Myc expression in prostate cancer. **A**, Promoter enrichment analysis of the PGC1 α transcriptional program in PC3 cells.

B, Effect of Pgc1 α expression on c-Myc protein levels in PC3 cells ($n = 3$ independent experiments).

C, Quantification of MYC gene expression and its target genes

ODC, *FASN*, *CAD1*, and *TCF4* by qRT-PCR upon Pgc1 α expression in PC3 cells ($n = 4$ independent experiments). Data are represented as fold change relative to No Dox, depicted as a dotted line.

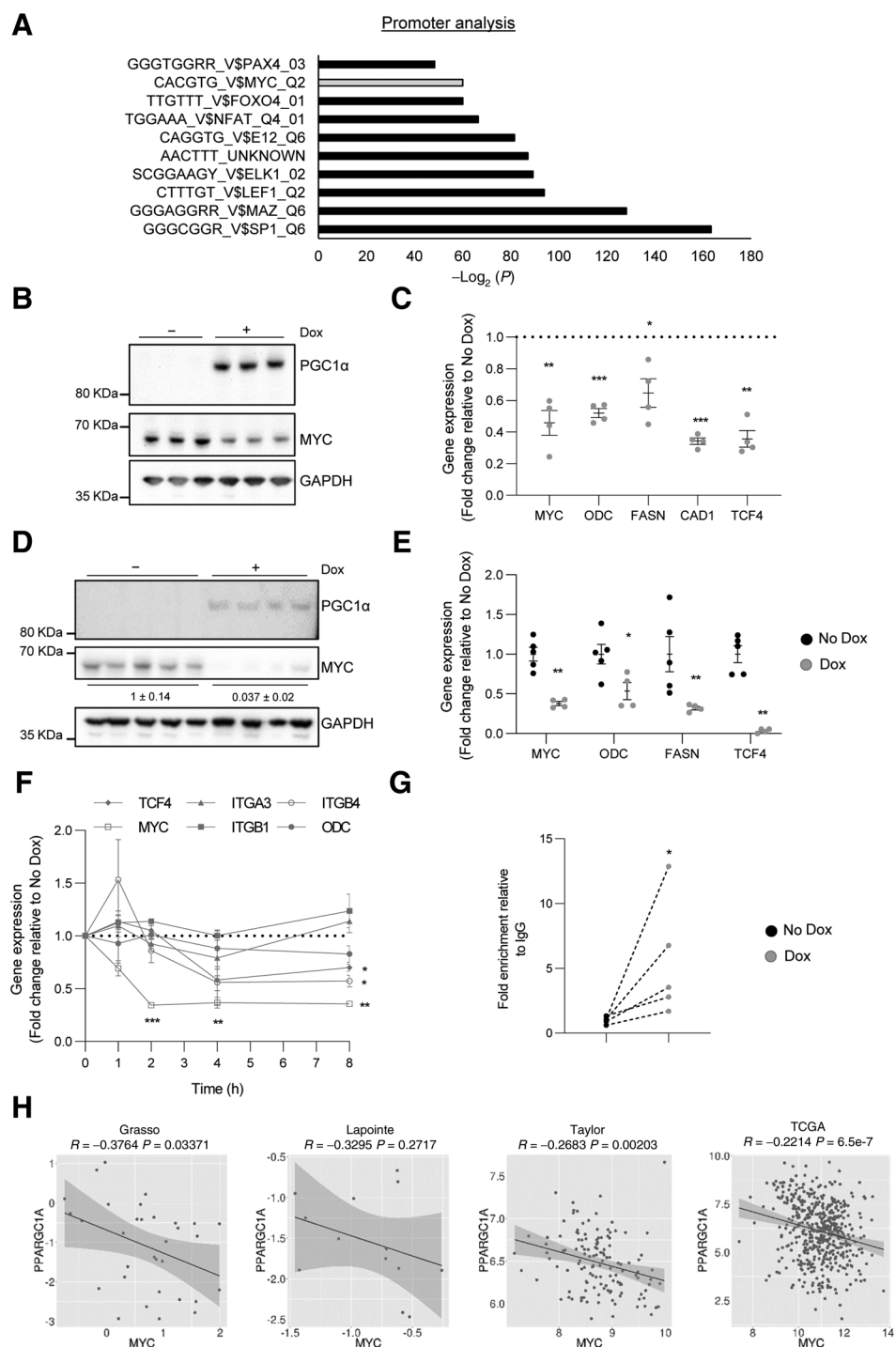
D, Effect of Pgc1 α expression on c-Myc protein levels in xenograft samples ($n = 5$ No Dox tumors; $n = 4$ Dox tumors).

E, Quantification of MYC gene expression (and its target genes) by qRT-PCR in xenograft samples cells ($n = 5$ No dox tumors; $n = 4$ Dox tumors).

F, qRT-PCR gene expression analysis of MYC, TCF4, ITGB4, ITGB1, and ITGA3 upon short acute induction of Pgc1 α expression (1, 2, 4, and 8 hours of doxycycline treatment) in PC3 cells. Data are represented as fold change relative to No Dox, depicted as a dotted line.

G, CHIP of exogenous Pgc1 α on MYC promoter in PC3 Pgc1 α cells after induction with 0.5- μ g/mL doxycycline for 16 hours ($n = 5$). Final data were normalized to IgG (negative immunoprecipitation control) and to No Dox condition.

H, Correlation analysis between PGC1A and MYC expression in primary tumor specimens of different prostate can datasets. Sample sizes: Grasso, $n = 45$; Lapointe, $n = 13$; Taylor, $n = 131$; and TCGA provisional, $n = 495$. Dox, doxycycline, Pgc1 α -induced conditions; No Dox, Pgc1 α -nonexpressing conditions. Error bars, SEM. Western blot quantifications are presented as \pm SEM. Statistic tests: one-sample *t* test with a hypothetical value of 1 (C and F), one-tailed Student *t* test (G), one-tailed Mann-Whitney U test (E), Spearman correlation *R* (H). *, $P < 0.05$; **, $P < 0.01$; ***, $P < 0.001$.



results suggest that MYC repression is upstream of the molecular and cellular alterations elicited by PGC1 α associated to prostate cancer invasion. We validated this notion by two different means. On the one hand, a time course experiment upon PGC1 α induction showed that MYC repression is prior to the reduction of its targets and integrin gene expression (Fig. 3F; Supplementary Fig. S3E–S3G). On the other hand, MYC silencing with a validated shRNA (33, 34) recapitulated the phenotype of Pgc1 α expression in cell area, p-MLC2, and invasive growth (Supplementary Fig. S3H–S3L).

The rapid repression in MYC mRNA levels prompted us to evaluate whether PGC1 α could exert a direct action on MYC promoter. To this end, we performed ChIP analysis in Pgc1 α -inducible PC3 cells with anti-HA antibody to immunoprecipitate ectopic tagged Pgc1 α . The ChIP analysis confirmed that the coregulator is bound to MYC promoter (Fig. 3G), thus suggesting that PGC1 α represses MYC expression in prostate cancer. We next sought to ascertain whether the unprecedented regulation of MYC by PGC1 α in prostate cancer could be recapitulated in human specimens. We interrogated 5 prostate cancer datasets (25, 35–37) and, in agreement with our molecular and mechanistic data, PGC1A expression was inversely correlated with MYC mRNA levels in primary tumors from the majority (four out of five) of datasets analyzed (Fig. 3H; Supplementary Fig. S3M).

Our previous studies demonstrated that the antiproliferative activity of PGC1 α in prostate cancer is dependent on its interaction with ERR α (17). To ascertain the requirement of ERR α for the anti-invasive activity of PGC1 α , we engineered Pgc1 α -inducible prostate cancer cells in which *ESRRA* was deleted using CRISPR/Cas9. ERR α expression was undetectable in PC3 cells in which *ESRRA* was deleted with two independent sgRNAs (sgERR α #1, sgERR α #2; Fig. 4A). *ESRRA* deletion abolished the induction of target genes of the transcription factor upon induction of Pgc1 α , corroborating the functionality of the genetic system (Supplementary Fig. S4A). Of note, we did not recapitulate the regulation of *ESRRA* by PGC1A observed *in vitro* (Fig. 4A) in correlative human transcriptomics analyses, suggesting that more complex ERR α -regulatory cues might operate in human disease (Supplementary Fig. S4B). In line with our previous study (17), *ESRRA* deletion hampered the growth-suppressive activity of Pgc1 α , rendering PC3 cells insensitive to the action of the coregulator (Fig. 4B). Strikingly, *ESRRA* deletion also abolished the effect of Pgc1 α on invasive properties and cell morphology at time points prior to the reduction in cell proliferation, thus demonstrating that the regulation of invasion by the coregulator is exquisitely dependent upon its interaction with ERR α (Fig. 4C and D; Supplementary Fig. S4C and S4D). The morphologic changes and growth-suppressive phenotype elicited by Pgc1 α were also absent in tumors in which *ESRRA* was deleted (Fig. 4E; Supplementary Fig. S4E–S4G). It is worth noting that despite the requirement of ERR α for the tumor-suppressive activity of PGC1 α , deletion of the nuclear receptor alone negatively influenced the establishment of tumors, suggesting that additional functions of ERR α may be required for the first stages of tumor establishment (Supplementary Fig. S4H).

We next extended our analysis of ERR α dependency to the reported molecular alterations. Our results showed that *ESRRA* deletion abrogated the reduction in protein and/or mRNA levels of MYC, MYC targets, integrins, CAV1, as well as the reduced phosphorylation of Src and cofilin (Fig. 5A and B; Supplementary Fig. S5A and S5B). Moreover, *ESRRA*-ablated tumors exhibited

unperturbed MYC, integrin, and CAV1 expression, as well as unchanged Src and cofilin phosphorylation upon Pgc1 α expression (Fig. 5C and D; Supplementary Fig. S5C). All these data are in line with the association of ERR α to MYC promoter in Pgc1 α -expressing PC3 cells (Supplementary Fig. S5D).

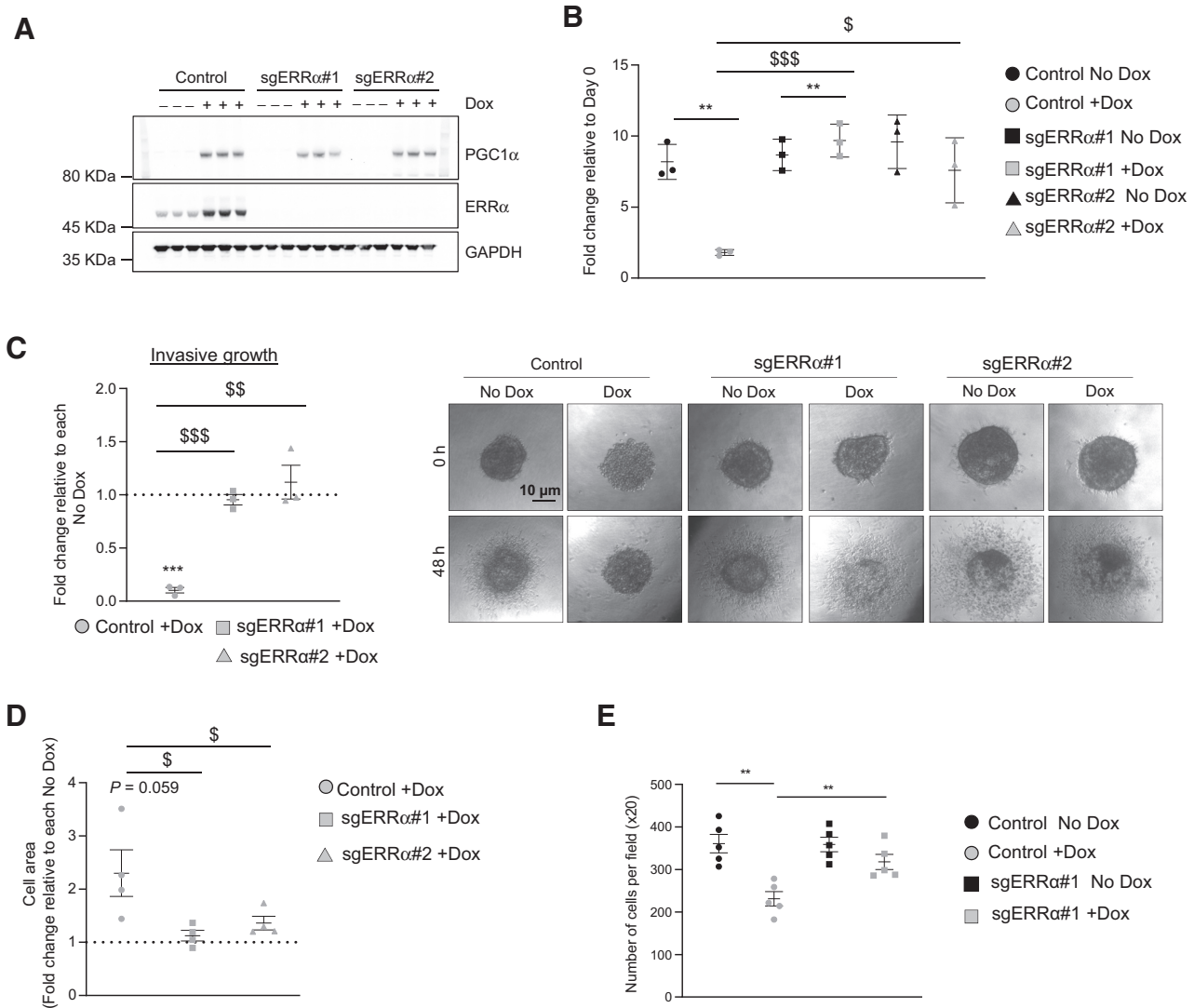
Because we have observed a robust inverse correlation between PGC1A and MYC expression in various prostate cancer datasets, we asked whether the dependency on ERR α could be recapitulated in this setting. To this end, we carried out two independent approaches in datasets of patients with prostate cancer. On the one hand, we inferred ERR α canonical activity based on the equilibrium between its main coactivators (PGC1A) and corepressors (NRIP1). We calculated the ratio of abundance of PGC1A and NRIP1 transcript (PGC1A/NRIP1), which provided an estimation of ERR α canonical activity toward its targets, as confirmed through the analysis of ACACB and LAMB2 expression (Supplementary Fig. S6A). In line with our mechanistic analysis, ERR α activity but not ERR α itself, was consistently and inversely correlated with MYC in various prostate cancer datasets (Supplementary Fig. S6B and S6C). On the other hand, we took advantage from a prognostic PGC1 α -ERR α signature that we generated previously (17). This signature was composed of 10 genes that were (i) regulated by PGC1 α *in vitro*, (ii) predicted to be ERR α targets, and (iii) correlated with PGC1A in prostate cancer datasets. In full support of our data, this PGC1 α -ERR α activity signature was inversely correlated with MYC expression in various datasets of patients with prostate cancer (Fig. 5E; Supplementary Fig. S6D).

Overall, our results provide solid evidence of the anti-invasive activity of the PGC1 α -ERR α transcriptional axis in prostate cancer.

Discussion

Metabolic deregulation is a hallmark of cancer (2) and encompasses a variety of biochemical routes, which must be coordinated to result in a phenotypic change. We postulated in the past that this strict requirement for coordination could unveil novel cancer genes. By focusing on transcriptional coregulators that control the expression of an ample set of metabolic genes, we discovered the predominant perturbation of PGC1 α in prostate cancer (7, 17). This metabolic regulator orchestrates the activation of catabolic and antioxidant pathways at the expense of anabolism (8). Interestingly, the contribution of PGC1 α to cancer biology is complex. Elegant studies have reported a role of this coregulator: (i) promoting aggressiveness of breast, pancreatic, and gastric tumors; cholangiocarcinoma; glioma; and melanoma (10–14, 38–40), and (ii) suppressing cancer aggressiveness in prostate, kidney tumors, and melanoma (9, 15–18). Moreover, the expression of this coregulator is associated with the efficacy of anticancer therapies (10, 11, 14, 15, 41, 42).

PGC1 α exhibits an activity that is dependent on the tumor type, ranging from tumor suppressor to advantageous for cancer cells (7). This coactivator is required for the activity of pancreatic cancer stem cells (13) and for the survival of breast cancer cells in circulation (12). In melanoma, the metabolic activity of PGC1 α promotes cell proliferation, whereas the nonmetabolic function opposes metastatic dissemination (10, 11, 16). This study together with reports by us and others demonstrates that PGC1 α suppresses proliferation and invasion in prostate cancer through

**Figure 4.**

ERR α deletion mediates the effect of Pgc1 α on invasive properties and morphology of prostate cancer *in vitro* and *in vivo*. **A**, Representative experiment of ERR α expression in PC3 Pgc1 α cells after treatment with 0.5- μ g/mL doxycycline (Dox; $n = 3$; independent experiments). **B**, Relative cell number quantification upon ERR α deletion (sgERR α #1 and sgERR α #2) in PC3 Pgc1 α expressing and nonexpressing cells. Data are represented as cell number at day 6 relative to day 0 ($n = 3$, independent experiments). **C**, Effect of ERR α deletion in invasive growth upon Pgc1 α expression ($n = 3$ independent experiments). One representative spheroid image of each condition is shown out of three biological replicates. **D**, Quantification of cell area by phalloidin staining after ERR α deletion alone or in combination with Pgc1 α expression ($n = 4$ independent experiments) in PC3 cells. **E**, Effect of ERR α deletion alone or in combination of Pgc1 α on the cell content and size in xenograft samples ($n = 5$ per condition). The number of cells per field is an approximate representation of cell area. Dox, doxycycline, Pgc1 α -induced conditions; No Dox, Pgc1 α nonexpressing conditions. Error bars, SEM. Dotted line, No Dox condition. Statistic tests: paired Student t test between Control –Dox and +Dox conditions (**B**), unpaired Student t test between +Dox control and sg conditions (**B**), one sample t test with a hypothetical value of 1 (**C** and **D**), and one-tailed Mann-Whitney U test (**E**). $P < 0.05$; **/\$\$, $P < 0.01$; **/\$\$\$, $P < 0.001$. Asterisks indicate statistical difference between No Dox and Dox conditions (**B**, **C**, and **E**) and dollar symbols indicate statistical difference between Control Dox and sgERR α #1/sgERR α #2 Dox (**B** and **D**).

presumably distinct molecular pathways emanating from the regulation of ERR α , consistent with its tumor- and metastasis-suppressive function (Fig. 6; refs. 17, 18). Our results mirror the anti-invasive activity of the coregulator in melanoma, whereas proliferation is regulated in opposite sense in both tumor types. This apparent discrepancy could be associated to the tissue-specific molecular cues that drive these tumors or the distinct nutrient and metabolic pathways that sustain their growth.

Cancer cell proliferation imposes tremendous pressure to meet the bioenergetics demands and to generate sufficient biomolecules to build new cells. We now possess a more comprehensive view of the metabolic deregulations that sustain or accompany cancer cell proliferation (43). However, beyond the relevance of cell proliferation in cancer, tumor cells need to acquire additional capacities that account for the clinical progression of the disease. The process of metastasis

Valcarcel-Jimenez et al.

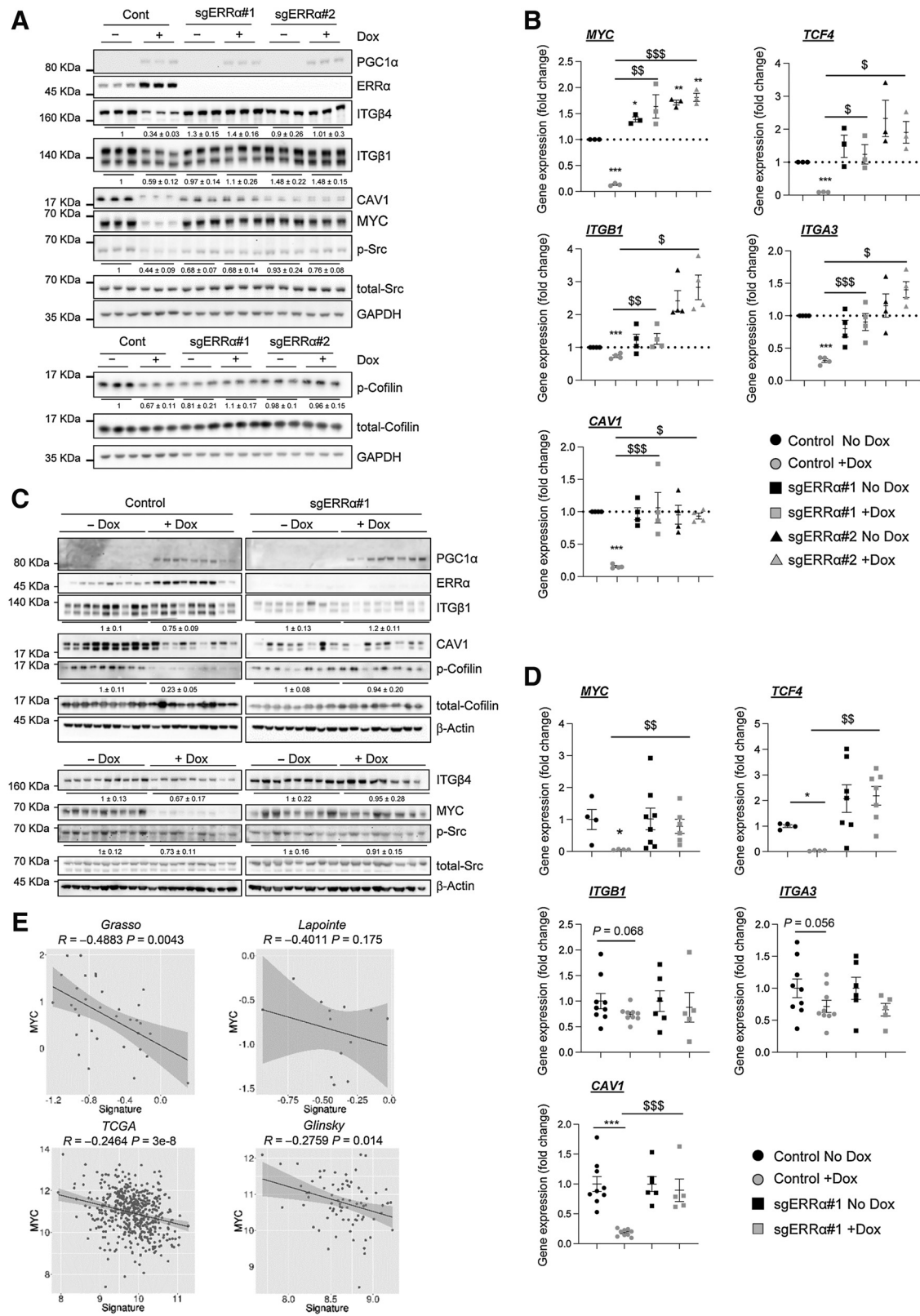
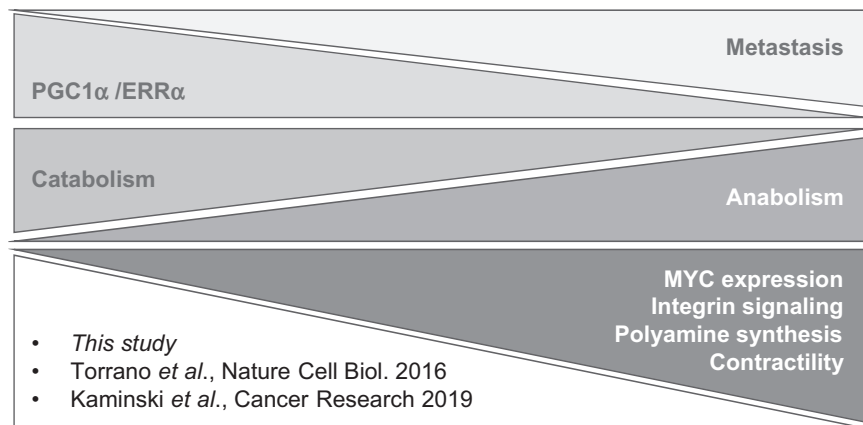


Figure 6.
Schematic summary of the main findings.
Torrano et al. (17); Kaminski et al. (18).



is the main cause of mortality in cancer and only partly depends on cell proliferation, as it requires angiogenesis, intravasation, survival in circulation, extravasation, and resuming cell growth in a distant organ (44). Our perspective around the contribution of metabolic regulators to the acquisition of these features is limited. An exciting possibility stems from the notion that factors that control metabolic programs would also regulate molecular cues associated to cancer cell dissemination.

Little is known about the activities of PGC1 α in cancer beyond proliferation. This coregulator inhibits dissemination in melanoma through the regulation of ID2-TCF4-Integrins (16). In gastric cancer, a recent report suggests that PGC1 α upregulation supports metastasis through the regulation of SNAI1 (38). Interestingly, none of these effects are ascribed to the regulation of its main transcriptional partner, ERR α . Instead, we demonstrate that the PGC1 α -ERR α transcriptional axis in prostate cancer accounts for the invasive phenotype. We demonstrate that PGC1 α /ERR α status influences signaling pathways that are important for the regulation of cytoskeletal remodeling. In turn, changes in pathways related to integrin and ROCK signaling provide a feasible explanation for the anti-invasive effects of the coregulator. Interestingly, the set of genes inhibited in PGC1 α -expressing cells that relate to cytoskeletal remodeling is enriched in MYC promoter-binding sites. These data are consistent with the notion that PGC1 α /ERR α represses MYC expression and that silencing of this transcription factor partly phenocopies the effect of PGC1 α (18).

Similar to PGC1 α , ERR α has opposing effects in different tumor types (7). Interestingly, we show that this nuclear recep-

tor is required for the tumor suppressive activity of PGC1 α , whereas its deletion delays tumor onset in immunocompromised mice independently of the induction of PGC1 α . Our results could be explained by the differential requirement of basal ERR α activity for the establishment of tumors (homing and the initial engagement of cell proliferation *in vivo*) versus the proliferation and invasion in later stages. Similar results were reported for LKB1, which is required for the bypass of anoikis and the survival of tumor cells in conditions of energetic stress, despite its tumor suppressive nature in established tumors (45, 46).

ERR α functions predominantly as a transcriptional activator and is rarely reported to repress the expression of target genes (47). However, recent studies demonstrate that a subset of the genes identified by ERR α ChIP-seq is repressed by the nuclear receptor (48). In this sense, our results demonstrating that PGC1 α /ERR α inhibits the expression of MYC broaden the spectrum of repressed genes by the protein complex. Interestingly, work by the group of Dr. Frederic Bost (French Institute of Health and Medical Research, Inserm, Paris, France) reports that PGC1 α regulates an alternative branch of metabolism (polyamine biosynthesis) through the ERR α -dependent repression of MYC-ODC1 (18), thus opening new molecular avenues connecting this coactivator to metabolic pathways that coordinate proliferation and invasion.

In summary, our study together with recent reports (18) demonstrates that PGC1 α /ERR α coordinately controls proliferative and invasive features in prostate cancer, thus providing a feasible explanation for its robust clinical association to biochemical recurrence and metastasis.

Figure 5.

ERR α mediates the effect of Pgc1 α on integrin signaling and MYC expression *in vitro* and *in vivo*. **A**, Representative Western blot of the effect of ERR α deletion alone or in combination with Pgc1 α expression on ITG β 1, ITG β 4, CAV1, and MYC protein expression as well as on cofilin and Src phosphorylation in PC3 cells ($n = 3$; independent experiments). **B**, Effect of ERR α deletion alone or in combination with Pgc1 α expression in the gene expression (qRT-PCR) of MYC, TCF4, ITGB1, ITGA3, and CAV1 ($n = 4$ independent experiments) in PC3 cells. Data are represented by fold change relative to Control No Dox condition that is depicted by a dotted line. **C**, Effect of ERR α deletion alone or in combination with Pgc1 α expression on ITG β 1, ITG β 4, CAV1, and MYC protein expression as well as on cofilin and Src phosphorylation in xenograft samples (Control No Dox, $n = 9$ tumors; Control + Dox, $n = 9$ tumors; sgERR α #1 -Dox, $n = 8$ tumors; sgERR α #2 +Dox, $n = 8$ tumors). **D**, Effect of ERR α deletion alone or in combination with Pgc1 α expression MYC, TCF4, ITGB1, ITGA3, and CAV1 gene expression analyzed by qRT-PCR in xenograft samples. (Control No Dox, $n = 4-9$ tumors; Control +Dox, $n = 4-9$ tumors; sgERR α #1 No Dox, $n = 6-8$ tumors; sgERR α #2 +Dox, $n = 5-6$ tumors). **E**, Correlation analysis between MYC and the PGC1 α -ERR α transcriptional signature in primary tumor specimens of different prostate cancer datasets. Each dot corresponds to a patient. Sample sizes: Grasso, $n = 45$; Lapointe, $n = 13$; Glinsky, $n = 78$; and TCGA provisional, $n = 495$. Dox, doxycycline, Pgc1 α -induced conditions; No dox, Pgc1 α nonexpressing conditions. Error bars, SEM. Western blot quantifications are presented as \pm SEM. Statistical tests: one sample *t* test (**B**), unpaired *t* test (**B** and **D**), and Spearman correlation *R* (**E**). */\$, $P < 0.05$; **/\$\$, $P < 0.01$; ***/\$\$\$, $P < 0.001$. Asterisks indicate statistical difference between Control No Dox and the rest of the conditions and dollar symbols indicate statistical difference between Control Dox and sgERR α #1/sgERR α #2 Dox.

Valcarcel-Jimenez et al.

Disclosure of Potential Conflicts of Interest

No potential conflicts of interest were disclosed.

Authors' Contributions**Conception and design:** L. Valcarcel-Jimenez, V. Torrano, A. Carracedo**Development of methodology:** L. Valcarcel-Jimenez, E. Crosas-Molist, V. Sanz-Moreno, V. Torrano, A. Carracedo**Acquisition of data (provided animals, acquired and managed patients, provided facilities, etc.):** L. Valcarcel-Jimenez, A. Macchia, E. Crosas-Molist, A. Schaub-Clerigué, L. Camacho, N. Martín-Martín, P. Cicogna, C. Viera-Bardón, S. Fernández-Ruiz, I. Hermanova, I. Astobiza, A.R. Cortazar, J. Corres-Mendizabal**Analysis and interpretation of data (e.g., statistical analysis, biostatistics, computational analysis):** L. Valcarcel-Jimenez, A. Macchia, N. Martín-Martín, I. Rodríguez-Hernandez, A.R. Cortazar, V. Sanz-Moreno, V. Torrano, A. Carracedo**Writing, review, and/or revision of the manuscript:** L. Valcarcel-Jimenez, I. Hermanova, V. Torrano, A. Carracedo**Administrative, technical, or material support (i.e., reporting or organizing data, constructing databases):** S. Fernández-Ruiz, I. Astobiza, A.R. Cortazar**Study supervision:** V. Torrano, A. Carracedo**Other (cosupervision of L. Camacho's work):** A. Gomez-Muñoz**Acknowledgments**

Apologies to those whose related publications were not cited because of space limitations. We are grateful to the Carracedo lab for valuable input and to Dr. James D. Sutherland for technical advice. V. Torrano is funded by Fundación Vasca de Innovación e Investigación Sanitarias, BIOEF (BIO15/CA/052), the AECC J.P. Bizkaia and the Basque Department of Health (2016111109), and the

MINECO RTI2018-097267-B-I00. The work of A. Carracedo is supported by the Basque Department of Industry, Tourism and Trade (Elkartek) and the Department of Education (IKERTALDE IT1106-16, also participated by A. Gomez-Muñoz), the BBVA Foundation, the MINECO (SAF2016-79381-R (FEDER/EU), Severo Ochoa Excellence Accreditation SEV-2016-0644-18-1, Excellence Networks SAF2016-81975-REDT), European Training Networks Project (H2020-MSCA-ITN-308 2016 721532), the AECC (IDEAS175CARR, GCTRA18006CARR), La Caixa Foundation (HR17-00094), and the European Research Council (Starting Grant 336343, PoC 754627). CIBERONC was cofunded with FEDER funds and funded by ISCIII. L. Valcarcel-Jimenez and A. Schaub-Clerigué were funded by a Basque Government predoctoral grant, A. Macchia was funded by a FPI predoctoral fellowship from MINECO (PRE2018-083607), and C. Viera-Bardón was funded by a predoctoral grant of the UPV/EHU. I. Hermanova was funded by the Juan de la Cierva program of the MINECO. V. Sanz-Moreno was supported by Cancer Research UK (CRUK) C33043/A12065 and C33043/A24478 (to V. Sanz-Moreno and E. Crosas-Molist), Royal Society RG110591 (to V. Sanz-Moreno), and Barts Charity (to V. Sanz-Moreno and E. Crosas-Molist). E. Crosas-Molist was funded by Fundación Ramón Areces. I. Rodríguez-Hernandez was funded by Fundación Alfonso Martín Escudero and Marie Skłodowska-Curie Action (H2020-MSCA-IF-2014-EF-ST).

The costs of publication of this article were defrayed in part by the payment of page charges. This article must therefore be hereby marked *advertisement* in accordance with 18 U.S.C. Section 1734 solely to indicate this fact.

Received April 17, 2019; revised August 27, 2019; accepted October 4, 2019; published first October 8, 2019.

References

- Hanahan D, Weinberg RA. The hallmarks of cancer. *Cell* 2000;100:57–70.
- Hanahan D, Weinberg RA. Hallmarks of cancer: the next generation. *Cell* 2011;144:646–74.
- Turajlic S, Sottoriva A, Graham T, Swanton C. Resolving genetic heterogeneity in cancer. *Nat Rev Genet* 2019;20:404–16.
- Martin-Martín N, Carracedo A, Torrano V. Metabolism and transcription in cancer: merging two classic tales. *Front Cell Dev Biol* 2017;5:119.
- Spiegelman BM, Heinrich R. Biological control through regulated transcriptional coactivators. *Cell* 2004;119:157–67.
- Finck BN, Kelly DP. PGC-1 coactivators: inducible regulators of energy metabolism in health and disease. *J Clin Invest* 2006;116:615–22.
- Valcarcel-Jimenez L, Gaude E, Torrano V, Frezza C, Carracedo A. Mitochondrial metabolism: Yin and Yang for tumor progression. *Trends Endocrinol Metab* 2017;28:748–57.
- Lin J, Handschin C, Spiegelman BM. Metabolic control through the PGC-1 family of transcription coactivators. *Cell Metab* 2005;1:361–70.
- Carracedo A, Weiss D, Lelijaert AK, Bhasin M, de Boer VC, Laurent G, et al. A metabolic prosurvival role for PML in breast cancer. *J Clin Invest* 2012;122:3088–100.
- Haq R, Shoaib J, Andreu-Perez P, Yokoyama S, Edelman H, Rowe GC, et al. Oncogenic BRAF regulates oxidative metabolism via PGC1alpha and MIF. *Cancer Cell* 2013;23:302–15.
- Vazquez F, Lim JH, Chim H, Bhalla K, Girmun G, Pierce K, et al. PGC1alpha expression defines a subset of human melanoma tumors with increased mitochondrial capacity and resistance to oxidative stress. *Cancer Cell* 2013;23:287–301.
- LeBleu VS, O'Connell JT, Gonzalez Herrera KN, Wikman H, Pantel K, Haigis MC, et al. PGC-1alpha mediates mitochondrial biogenesis and oxidative phosphorylation in cancer cells to promote metastasis. *Nat Cell Biol* 2014;16:992–1003.
- Sancho P, Burgos-Ramos E, Tavera A, Bou Kheir T, Jagust P, Schoenhals M, et al. MYC/PGC-1alpha balance determines the metabolic phenotype and plasticity of pancreatic cancer stem cells. *Cell Metab* 2015;22:590–605.
- Andrzejewski S, Klimcakova E, Johnson RM, Tabaries S, Annis MG, McGuirk S, et al. PGC-1alpha promotes breast cancer metastasis and confers bioenergetic flexibility against metabolic drugs. *Cell Metab* 2017;26:778–87.
- LaGory EL, Wu C, Taniguchi CM, Ding CC, Chi JT, von Eyben R, et al. Suppression of PGC-1alpha is critical for reprogramming oxidative metabolism in renal cell carcinoma. *Cell Rep* 2015;12:116–27.
- Luo C, Lim JH, Lee Y, Granter SR, Thomas A, Vazquez F, et al. A PGC1alpha-mediated transcriptional axis suppresses melanoma metastasis. *Nature* 2016;537:422–6.
- Torrano V, Valcarcel-Jimenez L, Cortazar AR, Liu X, Urosevic J, Castillo-Martin M, et al. The metabolic co-regulator PGC1alpha suppresses prostate cancer metastasis. *Nat Cell Biol* 2016;18:645–56.
- Kaminski L, Torrino S, Dufies M, Djabari Z, Haider R, Roustan FR, et al. PGC1alpha inhibits polyamine synthesis to suppress prostate cancer aggressiveness. *Cancer Res* 2019;79:3268–80.
- Pandya P, Orgaz JL, Sanz-Moreno V. Modes of invasion during tumour dissemination. *Mol Oncol* 2017;11:5–27.
- Wiederschain D, Wee S, Chen L, Loo A, Yang G, Huang A, et al. Single-vector inducible lentiviral RNAi system for oncology target validation. *Cell Cycle* 2009;8:498–504.
- Carracedo A, Ma L, Teruya-Feldstein J, Rojo F, Salmena L, Alimonti A, et al. Inhibition of mTORC1 leads to MAPK pathway activation through a PI3K-dependent feedback loop in human cancer. *J Clin Invest* 2008;118:3065–74.
- Georgouli M, Herraiz C, Crosas-Molist E, Fanshawe B, Maiques O, Perdrix A, et al. Regional activation of Myosin II in cancer cells drives tumor progression via a secretory cross-talk with the immune microenvironment. *Cell* 2019;176:757–74.
- Crosas-Molist E, Bertran E, Rodriguez-Hernandez I, Herraiz C, Cantelli G, Fabra A, et al. The NADPH oxidase NOX4 represses epithelial to amoeboid transition and efficient tumour dissemination. *Oncogene* 2017;36:3002–14.
- Ugalde-Olano A, Egia A, Fernandez-Ruiz S, Loizaga-Iriarte A, Zuniga-Garcia P, Garcia S, et al. Methodological aspects of the molecular and histological study of prostate cancer: focus on PTEN. *Methods* 2015;77–78:25–30.

25. Cortazar AR, Torrano V, Martín-Martín N, Caro-Maldonado A, Camacho L, Hermanova I, et al. CANCECTOOL: a visualization and representation interface to exploit cancer datasets. *Cancer Res* 2018;78:6320–8.
26. Jeannot P, Nowosad A, Perchey RT, Callot C, Bennana E, Katsube T, et al. p27(Kip1) promotes invadopodia turnover and invasion through the regulation of the PAK1/Cortactin pathway. *Elife* 2017;6:pii:e22207.
27. Nadeem L, Brkic J, Chen YF, Bui T, Munir S, Peng C. Cytoplasmic mislocalization of p27 and CDK2 mediates the anti-migratory and anti-proliferative effects of Nodal in human trophoblast cells. *J Cell Sci* 2013;126:445–53.
28. Steller EJ, Borel Rinkes IH, Kranenburg O. How CD95 stimulates invasion. *Cell Cycle* 2011;10:3857–62.
29. Yoon H, Kim M, Jang K, Shin M, Besser A, Xiao X, et al. p27 transcriptionally coregulates cjun to drive programs of tumor progression. *Proc Natl Acad Sci U S A* 2019;116:7005–14.
30. Pandya P, Orgaz JL, Sanz-Moreno V. Actomyosin contractility and collective migration: may the force be with you. *Curr Opin Cell Biol* 2017;48:87–96.
31. Bravo-Cordero JJ, Magalhaes MA, Eddy RJ, Hodgson L, Condeelis J. Functions of cofilin in cell locomotion and invasion. *Nat Rev Mol Cell Biol* 2013;14:405–15.
32. Hood JD, Cheresch DA. Role of integrins in cell invasion and migration. *Nat Rev Cancer* 2002;2:91–100.
33. Liu R, Zhang T, Zhu G, Xing M. Regulation of mutant TERT by BRAFV600E/MAP kinase pathway through FOS/GABP in human cancer. *Nat Commun* 2018;9:579.
34. Nakano T, Kanai Y, Amano Y, Yoshimoto T, Matsubara D, Shibano T, et al. Establishment of highly metastatic KRAS mutant lung cancer cell sublines in long-term three-dimensional low attachment cultures. *PLoS One* 2017;12:e0181342.
35. Grasso CS, Wu YM, Robinson DR, Cao X, Dhanasekaran SM, Khan AP, et al. The mutational landscape of lethal castration-resistant prostate cancer. *Nature* 2012;487:239–43.
36. Lapointe J, Li C, Higgins JP, van de Rijn M, Bair E, Montgomery K, et al. Gene expression profiling identifies clinically relevant subtypes of prostate cancer. *Proc Natl Acad Sci U S A* 2004;101:811–6.
37. Taylor BS, Schultz N, Hieronymus H, Gopalan A, Xiao Y, Carver BS, et al. Integrative genomic profiling of human prostate cancer. *Cancer Cell* 2010;18:11–22.
38. Wang P, Guo X, Zong W, Li Y, Liu G, Lv Y, et al. PGC-1 α /SNAI1 axis regulates tumor growth and metastasis by targeting miR-128b in gastric cancer. *J Cell Physiol* 2019;234:17232–41.
39. Dan L, Wang C, Ma P, Yu Q, Gu M, Dong L, et al. PGC1 α promotes cholangiocarcinoma metastasis by upregulating PDHA1 and MPC1 expression to reverse the Warburg effect. *Cell Death Dis* 2018;9:466.
40. Gelato KA, Schockel L, Klingbeil O, Ruckert T, Lesche R, Toedling J, et al. Super-enhancers define a proliferative PGC-1 α -expressing melanoma subgroup sensitive to BET inhibition. *Oncogene* 2018;37:512–21.
41. Cruz-Bermudez A, Laza-Briviesca R, Vicente-Blanco RJ, Garcia-Grande A, Coronado MJ, Laine-Menendez S, et al. Cisplatin resistance involves a metabolic reprogramming through ROS and PGC-1 α in NSCLC which can be overcome by OXPHOS inhibition. *Free Radic Biol Med* 2019;135:167–81.
42. Gentric G, Kieffer Y, Mieulet V, Goundiam O, Bonneau C, Nemati F, et al. PML-regulated mitochondrial metabolism enhances chemosensitivity in human ovarian cancers. *Cell Metab* 2019;29:156–73.
43. Zhu J, Thompson CB. Metabolic regulation of cell growth and proliferation. *Nat Rev Mol Cell Biol* 2019;20:436–50.
44. Steeg PS. Targeting metastasis. *Nat Rev Cancer* 2016;16:201–18.
45. Jeon SM, Chandel NS, Hay N. AMPK regulates NADPH homeostasis to promote tumour cell survival during energy stress. *Nature* 2012;485:661–5.
46. Carracedo A, Cantley LC, Pandolfi PP. Cancer metabolism: fatty acid oxidation in the limelight. *Nat Rev Cancer* 2013;13:227–32.
47. Stein RA, McDonnell DP. Estrogen-related receptor alpha as a therapeutic target in cancer. *Endocr Relat Cancer* 2006;13Suppl 1: S25–32.
48. Audet-Walsh E, Papadopoli DJ, Gravel SP, Yee T, Bridon G, Caron M, et al. The PGC-1 α /ERR α axis represses one-carbon metabolism and promotes sensitivity to anti-folate therapy in breast cancer. *Cell Rep* 2016;14:920–31.

Cancer Research

The Journal of Cancer Research (1916–1930) | The American Journal of Cancer (1931–1940)

PGC1 α Suppresses Prostate Cancer Cell Invasion through ERR α Transcriptional Control

Lorea Valcarcel-Jimenez, Alice Macchia, Eva Crosas-Molist, et al.

Cancer Res 2019;79:6153-6165. Published OnlineFirst October 8, 2019.

Updated version Access the most recent version of this article at:
doi:[10.1158/0008-5472.CAN-19-1231](https://doi.org/10.1158/0008-5472.CAN-19-1231)

Supplementary Material Access the most recent supplemental material at:
<http://cancerres.aacrjournals.org/content/suppl/2019/10/08/0008-5472.CAN-19-1231.DC1>

Cited articles This article cites 48 articles, 6 of which you can access for free at:
<http://cancerres.aacrjournals.org/content/79/24/6153.full#ref-list-1>

Citing articles This article has been cited by 2 HighWire-hosted articles. Access the articles at:
<http://cancerres.aacrjournals.org/content/79/24/6153.full#related-urls>

E-mail alerts [Sign up to receive free email-alerts](#) related to this article or journal.

Reprints and Subscriptions To order reprints of this article or to subscribe to the journal, contact the AACR Publications Department at pubs@aacr.org.

Permissions To request permission to re-use all or part of this article, use this link
<http://cancerres.aacrjournals.org/content/79/24/6153>.
Click on "Request Permissions" which will take you to the Copyright Clearance Center's (CCC) Rightslink site.



Targeting PML in triple negative breast cancer elicits growth suppression and senescence

Leire Arreal¹ · Marco Piva¹ · Sonia Fernández^{1,2} · Ajinkya Revandkar^{3,4} · Ariane Schaub-Clerigué¹ · Josep Villanueva^{2,5} · Amaia Zabala-Letona^{1,2} · Mikel Pujana¹ · Ianire Astobiza^{1,2} · Ana Rosa Cortazar^{1,2} · Ivana Hermanova¹ · Laura Bozal-Basterra¹ · Amaia Arruabarrena-Aristorena¹ · Jana R. Crespo¹ · Lorea Valcarcel-Jimenez¹ · Patricia Zúñiga-García¹ · Francesc Canals⁵ · Veronica Torrano^{1,2,6} · Rosa Barrio¹ · James D. Sutherland¹ · Andrea Alimonti^{3,4} · Natalia Martin-Martin^{1,2} · Arkaitz Carracedo^{1,2,6,7}

Received: 24 November 2018 / Revised: 18 July 2019 / Accepted: 23 July 2019 / Published online: 1 October 2019
© The Author(s) 2019. This article is published with open access

Abstract

Oncogene addiction postulates that the survival and growth of certain tumor cells is dependent upon the activity of one oncogene, despite their multiple genetic and epigenetic abnormalities. This phenomenon provides a foundation for molecular targeted therapy and a rationale for oncogene-based stratification. We have previously reported that the Promyelocytic Leukemia protein (PML) is upregulated in triple negative breast cancer (TNBC) and it regulates cancer-initiating cell function, thus suggesting that this protein can be therapeutically targeted in combination with PML-based stratification. However, the effects of PML perturbation on the bulk of tumor cells remained poorly understood. Here we demonstrate that TNBC cells are addicted to the expression of this nuclear protein. PML inhibition led to a remarkable growth arrest combined with features of senescence *in vitro* and *in vivo*. Mechanistically, the growth arrest and senescence were associated to a decrease in MYC and PIM1 kinase levels, with the subsequent accumulation of CDKN1B (p27), a trigger of senescence. In line with this notion, we found that PML is associated to the promoter regions of MYC and PIM1, consistent with their direct correlation in breast cancer specimens. Altogether, our results provide a feasible explanation for the functional similarities of MYC, PIM1, and PML in TNBC and encourage further study of PML targeting strategies for the treatment of this breast cancer subtype.

These authors contributed equally: Natalia Martin-Martin, Arkaitz Carracedo

Edited by M Deshmukh

Supplementary information The online version of this article (<https://doi.org/10.1038/s41418-019-0407-5>) contains supplementary material, which is available to authorized users.

✉ Arkaitz Carracedo
acarracedo@cicbiogune.es

¹ CIC bioGUNE, Derio, Spain

² CIBERONC, Derio, Spain

³ Institute of Oncology Research (IOR) and Oncology Institute of Southern Switzerland (IOSI), Bellinzona, CH 6500, Switzerland

⁴ Faculty of Biology and Medicine, University of Lausanne (UNIL), Lausanne, CH 1011, Switzerland

⁵ Vall d'Hebron Institute of Oncology (VHIO), Barcelona, Spain

⁶ Biochemistry and Molecular Biology Department, University of the Basque Country (UPV/EHU), Bilbao, Spain

⁷ IKERBASQUE, Basque Foundation for Science, Bilbao, Spain

Introduction

Breast cancer exemplifies the potential of gene expression profiling to classify the disease into molecular subtypes [1–3]. However, these classifications do not inform about the molecular mediators of tumor progression and metastasis in each subtype of breast cancer. To address this question, we and others have defined genes and pathways that are relevant to breast cancer progression, metastasis, and resistance to therapy [4–6]. The Promyelocytic Leukemia protein (PML), the essential component of the PML nuclear bodies (PML-NBs), induces apoptosis and inhibits angiogenesis and cell cycle progression in cancer, thus complying with the definition of a tumor suppressor [7, 8]. Paradoxically, PML exerts a prosurvival role conferring a selective advantage in chronic myeloid leukemia and specific solid tumors [6, 9–15]. In breast cancer, PML regulates aggressiveness and metastatic features through the control of the stem cell gene, *SOX9*, and the Hypoxia-inducible factor 1 alpha (HIF1 α) signaling [13, 15]. Moreover, the

regulation of cancer-initiating cell (CIC) and metastatic potential is restricted to PML high-expressing estrogen receptor-negative breast tumors, predominantly triple negative breast cancer (TNBC).

The concept that the perturbation of a driver cancer gene can exert an exacerbated tumor suppressive response in tumor cells is defined as “oncogene addiction” and provides a rationale for molecular targeted therapy [16]. Senescence is a stress response that involves a stable cell growth arrest as well as an adaptive process to reduce energy consumption for cell division or differentiation and therefore assure the survival and viability of the cell [17, 18]. Senescence is induced *in vitro* by different stimuli including DNA damage, oxidative stress, oncogene activation, mitochondrial dysfunction, or chemotherapy [17, 18]. Cyclin-dependent kinase inhibitor family (CDKi) is a key regulator of the senescence response, predominantly through p53-p21 and/or p16-RB axes [17, 18]. To a lesser extent, CDKN1B (p27) has been reported to participate in the activation of the senescence response, in conditions where p21 and/or p16 are not active [19, 20]. Of note, PML is required for a fully functional senescence response upon oncogene activation in tumors where it functions as a tumor suppressor. In addition, the PML-NBs coordinate the activation of p53 and the formation of the senescence-associated heterochromatin foci (SAHF) [21–23].

TNBC exhibits increased levels and activity of various oncogenes, including MYC and PIM1 [24–27]. Importantly, these genes regulate metabolic and signaling activities in this breast tumor subtype, and they represent an attractive therapeutic vulnerability [24, 26–28]. Whereas similarities exist among the reported activities of MYC, PIM1, and PML, their functional association remains obscure. In this study, we demonstrate that TNBC cells that express high PML levels are addicted to the nuclear protein, and its targeting elicits a growth suppressive response that encompasses MYC and PIM1 downregulation and the activation of p27-dependent senescence.

Results

PML silencing induces senescence and prevents tumor growth *in vivo*

The identification of PML as a novel target in aggressive breast cancer tumors [13, 15] prompted us to investigate the molecular consequences of its inhibition in an established cell culture. To this end, we generated and validated three PML-targeting doxycycline-inducible and two constitutive short hairpin RNAs (shRNAs) (Fig. 1a and Supplementary Fig. 1a) [15]. PML silencing triggered a robust morphological change in PML-high expressing cells, MDA-MB-231

(Fig. 1b and Supplementary Fig. 1b), characterized by a significant increase in size (FSC-A) and granularity (SSC-A) analyzed by FACS (Fig. 1c and Supplementary Fig. 1c). These changes in morphology were indicative of a senescence response. Indeed, the evaluation of senescence-associated β -galactosidase (SA- β -gal) activity in both inducible and constitutive systems confirmed this notion (Fig. 1d, e and Supplementary Fig. 1d, e) in MDA-MB-231 cells. Senescence is defined as an irreversible cell cycle arrest. Indeed, we could confirm the cell cycle arrest upon PML genetic inhibition, by means of BrdU analysis (Fig. 1f) and crystal violet cell number assay (Supplementary Fig. 1f, g) and that it was not due to an increase in apoptosis (Supplementary Fig. 1h). Of note, arsenic trioxide (ATO) did not elicit a senescence phenotype (Supplementary Fig. 1i). This compound exerts a biphasic effect on PML; first favors the formation of the PML NBs and then the degradation of PML. Therefore, the inability of ATO to recapitulate PML silencing could be due to its molecular mode of action.

We monitored additional features that were reported for certain types of oncogene-induced senescence [29]. On the one hand, proteomics analysis of the supernatant of these cells indicated that PML silencing resulted in a distinct secretome, without signs of a canonical SASP (senescence-associated secretory phenotype) (Supplementary Fig. 1j–l and Supplementary Table 1). On the other hand, we ascertained the formation of SAHF. We could not confirm the existence of SAHF neither at the level of chromatin condensation nor the formation of macroH2A1.1 foci (Supplementary Fig. 1m). Lamin B1 loss is a senescence-associated biomarker [30, 31]. We demonstrated that in our system PML loss induced a decrease in Lamin B1 protein levels (Supplementary Fig. 1n–o).

Of note, PML regulates oxidative stress responses [7, 32]. We ruled out that reactive oxygen species (ROS) elevation drives senescence in our system since PML loss does not induce its accumulation (Supplementary Fig. 1p).

Breast CIC capacity is reduced upon PML knockdown in TNBC cells (with high PML expression), as we demonstrated in limiting dilution assays with MDA-MB-231 cells [15]. Here, we hypothesized that the activation of senescence would result in a tumor suppressive response in established tumors, where the contribution of CIC is negligible. To test this notion, MDA-MB-231 cells were injected in the flank of immunocompromised mice, and once the tumors were established (reaching a volume of 25–130 mm³) doxycycline was administered in the food pellets to induce PML silencing. In agreement with the response observed *in vitro*, xenograft growth was curbed upon PML knockdown (Fig. 1g, h and Supplementary Fig. 1q–r) and senescence increase was confirmed by means of p-HP1 γ staining (Fig. 1i, j) [33]. Our data suggest that

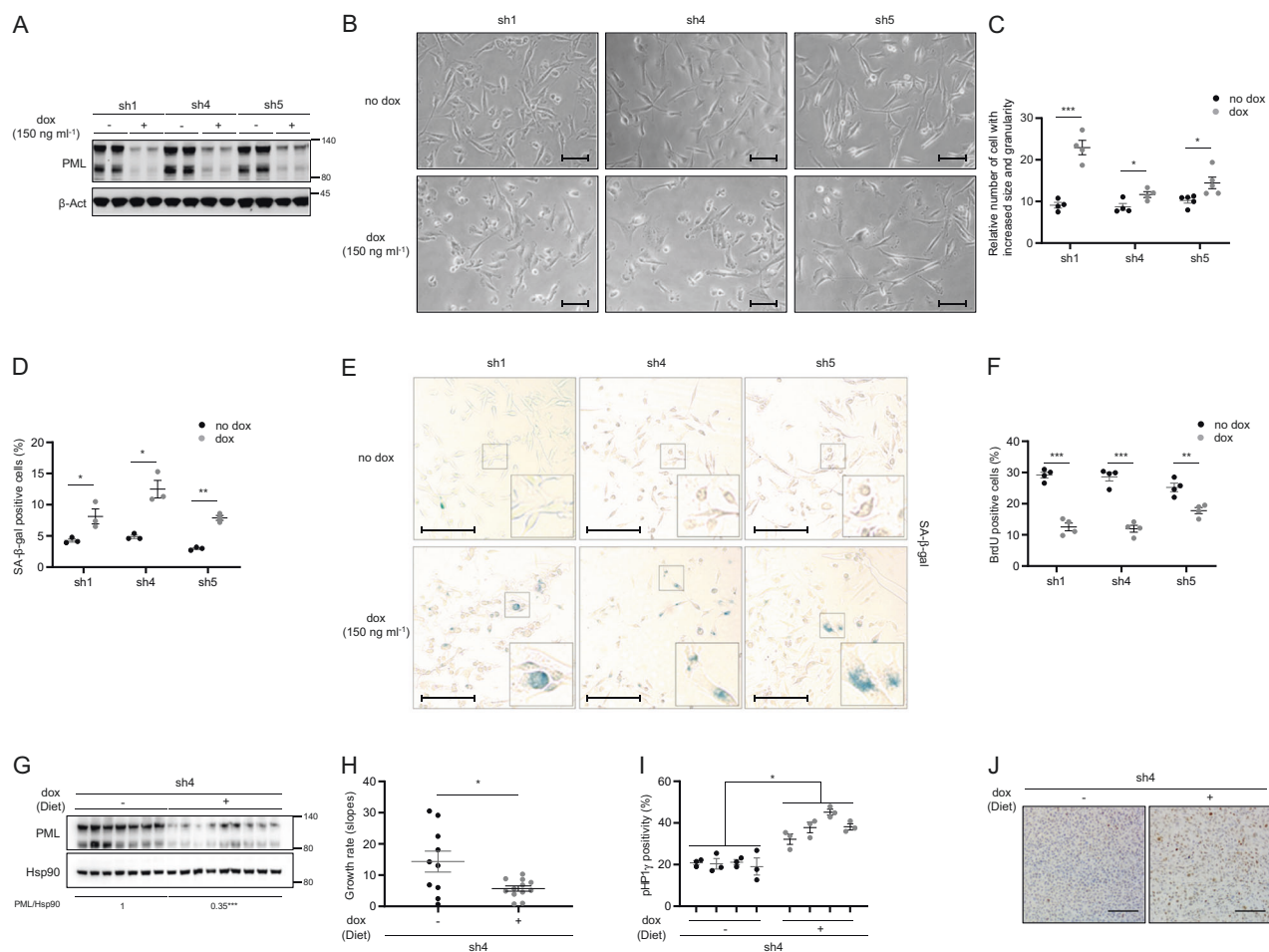


Fig. 1 PML silencing induces senescence. Effect of doxycycline-inducible (150 ng ml^{-1} ; 3 + 3 days) PML silencing (sh1, sh4, and sh5) on PML protein expression (a, representative of at least three experiments), on the morphology (b, representative images, scale bar, $50 \mu\text{m}$), on cell size and granularity (c, FACS analysis, sh1 and sh4, $n = 4$, sh5, $n = 5$), on the number of senescent cells (d; $n = 3$, representative images of SA- β -Galactosidase assay, scale bar $50 \mu\text{m}$) (e) and on the number of BrdU positive cells (f, $n = 4$) in MDA-MB-231 cells. Impact of doxycycline-inducible PML silencing (sh4) of established MDA-MB-231 xenografts on PML protein expression (g), on tumor growth rate represented as the growth rate of each tumor (h, sh4 no dox, $n = 10$; sh4 dox, $n = 12$; growth rate was inferred from the linear

regression calculated for the progressive change in tumor volume of each individual tumor during the period depicted in Supplementary Fig. 1p) and on number of senescent cells measured by p-HP1 γ staining (i, sh4 no dox, $n = 4$; sh4 dox, $n = 4$); representative images of p-HP1 γ positive cells, scale bar $100 \mu\text{m}$ (j) of the tumors. Error bars represent s.e.m. p , p -value ($*p < 0.05$, $**p < 0.01$, $***p < 0.001$). One-tailed Student's t -test was used for cell line data analysis (c, d, f) and one-tailed Mann–Whitney U -test for xenografts (h, i). sh1, sh4, and sh5: shRNA against *PML*, dox: doxycycline, SA- β -gal: senescence-associated beta-galactosidase, BrdU: bromodeoxyuridine, p-HP1 γ : phospho-heterochromatin protein-1 gamma, molecular weight markers (kDa) are shown to the right

PML silencing in a PML-high expressing TNBC cell line triggers a senescence response with a partial presence of classical markers of this process.

p27 is the driver in PML loss-induced senescence

Senescence is executed and sustained at the molecular level through the activation of growth suppressors, including p53 and the cyclin-dependent kinase (CDKs) inhibitors p21, p16, and p27 [17, 20, 29]. Since MDA-MB-231 cells harbor loss of p16 and p53 mutation [34, 35], we proposed p27 as a candidate to drive PML silencing-induced senescence in our cell system. Importantly, p27 protein levels were increased

upon both inducible (Fig. 2a and Supplementary Fig. 2a) and constitutive (Supplementary Fig. 2b) PML silencing with all the shRNA tested in MDA-MB-231 cells. Moreover, we observed that the induction of p27 protein levels occurred as soon as 2 days following PML inactivation and it was maintained up to 6 days of PML silencing (Fig. 2b, c and Supplementary Fig. 2c–f).

The function of p27 is controlled by changes in its levels along with its compartmentalization within the cell [36]. To confirm the functionality of accumulated p27 in PML-silenced cells, we quantified p27 nuclear localization by immunofluorescence. As predicted, PML silencing elicited an increase of nuclear p27 in cells with the three inducible

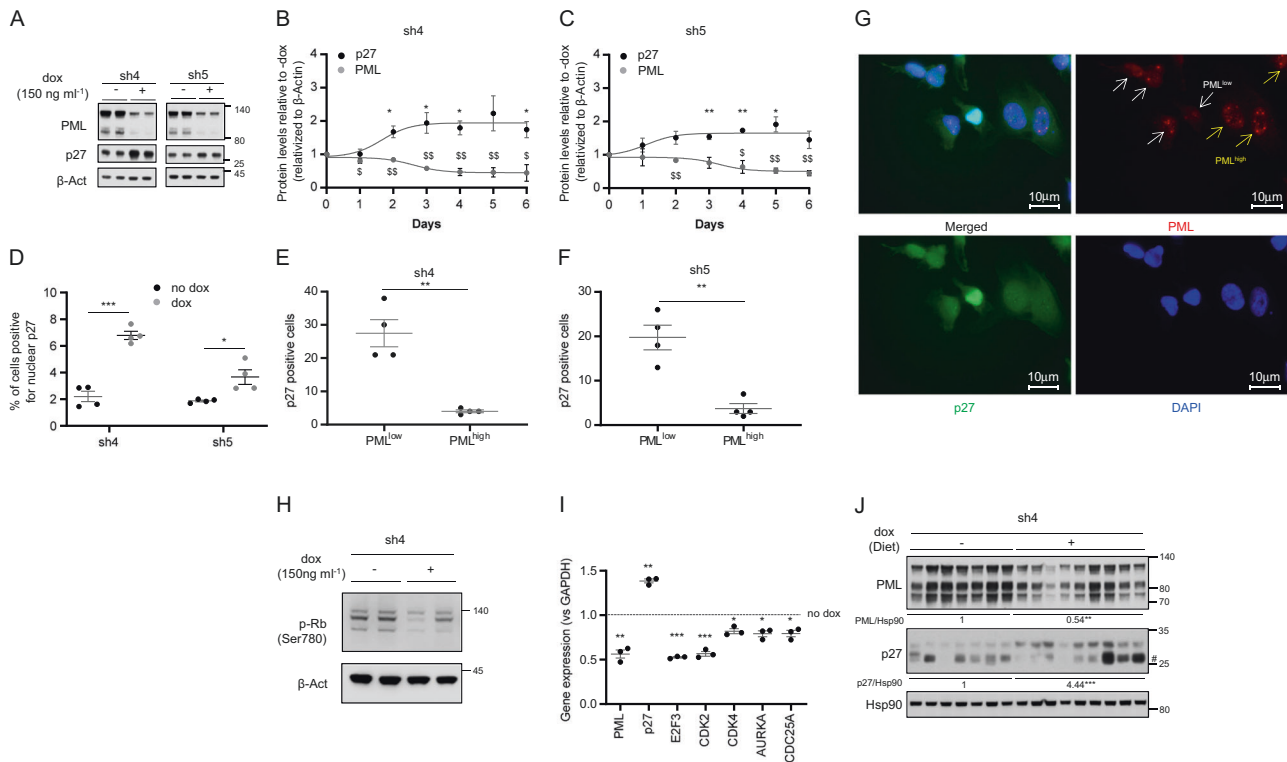


Fig. 2 p27 is induced after PML silencing. **a** Effect of doxycycline-inducible (150 ng ml^{-1} ; 3 + 3 days) PML silencing (sh4, sh5) on p27 and PML protein expression (representative of at least three experiments) on MDA-MB-231 cells. **b, c** Quantification of p27 and PML protein levels along 6 days of doxycycline-inducible PML silencing on MDA-MB-231 cells ($n = 3$) with two different shRNAs. **d** Immunofluorescence quantification of nuclear p27 positive cells upon PML inducible silencing on MDA-MB-231 cells ($n = 4$). **e–g** Immunofluorescence quantification of the correlation of p27 positive cells and PML levels in these cells (**e–f**) and representative images of p27 and PML staining (**g**) upon doxycycline-inducible PML silencing in MDA-MB-231 cells ($n = 4$). **h** Effect of doxycycline-inducible (150 ng ml^{-1} ;

3 + 3 days) PML silencing (sh4) on RB phosphorylation (Ser780) (representative of three experiments) on MDA-MB-231 cells. **i** Expression of p27-related cell cycle genes upon PML inducible silencing in MDA-MB-231 cells ($n = 3$). **j** Impact of doxycycline-inducible PML silencing (sh4) on p27 and PML protein expression on established MDA-MB-231 xenografts. Error bars represent s.e.m. p , p -value ($*/\$/p < 0.05$, $**/\$/p < 0.01$, $***/\$/p < 0.001$). One-tailed one-sample t -test (**b, c, i**) and one-tailed Student's t -test were used for cell line data analysis (**d–f**). sh4 and sh5: shRNA against *PML*, dox: doxycycline. #Unspecific band. Molecular weight markers (kDa) are shown to the right

shRNA tested (Fig. 2d and Supplementary Fig. 2g). Since the effect of shRNAs was analyzed in a pooled culture, it is plausible that there would be heterogeneity in PML levels across cells within the culture dish. We therefore evaluated whether the increase in nuclear p27 was ascribed to cells with a profound decrease in PML immunoreactivity. We established an immunofluorescence score based on previous studies [6, 15] (PML low = 0–4 dots; PML high = more than 4 dots per cell nuclei). In line with our previous results, we observed a significant inverse association between PML immunoreactivity and p27 nuclear staining (Fig. 2e–g and Supplementary Fig. 2h). Moreover, the elevated activity of p27 upon PML silencing was consistent with the increase in its mRNA levels, the blockade of Retinoblastoma protein (Rb) phosphorylation and the reduced transcription of downstream regulated cell cycle-related genes (Fig. 2h, i and Supplementary Fig. 2i). In agreement with the results observed in vitro, p27 accumulation was recapitulated upon PML knockdown in vivo (Fig. 2j).

Our results reveal that PML silencing in TNBC cells with high expression of the nuclear protein triggers a senescence response associated to p27 accumulation. To ascertain the causal contribution of p27 to the execution of the senescence response, we silenced p27 in MDA-MB-231 cells concomitantly with PML silencing, using inducible (Fig. 3a, b) or constitutive (Supplementary Fig. 3a) shRNA systems. Preventing p27 accumulation upon PML loss hampered the induction of senescence in a dose-dependent manner according to the potency of the shRNA against p27 (Fig. 3c and Supplementary Fig. 3b). Our results demonstrate that PML loss elicits a senescence response mediated by the upregulation of p27 in PML high expressing TNBC cells.

Although senescence is a major driver of growth arrest, we noticed that the amount of SA- β -Gal positivity upon PML silencing was not comparable to the extent of growth arrest detected (Fig. 1 and Supplementary Fig. 1). Taking advantage of our capacity to ablate senescence by silencing p27, we ascertained the contribution of this response to the

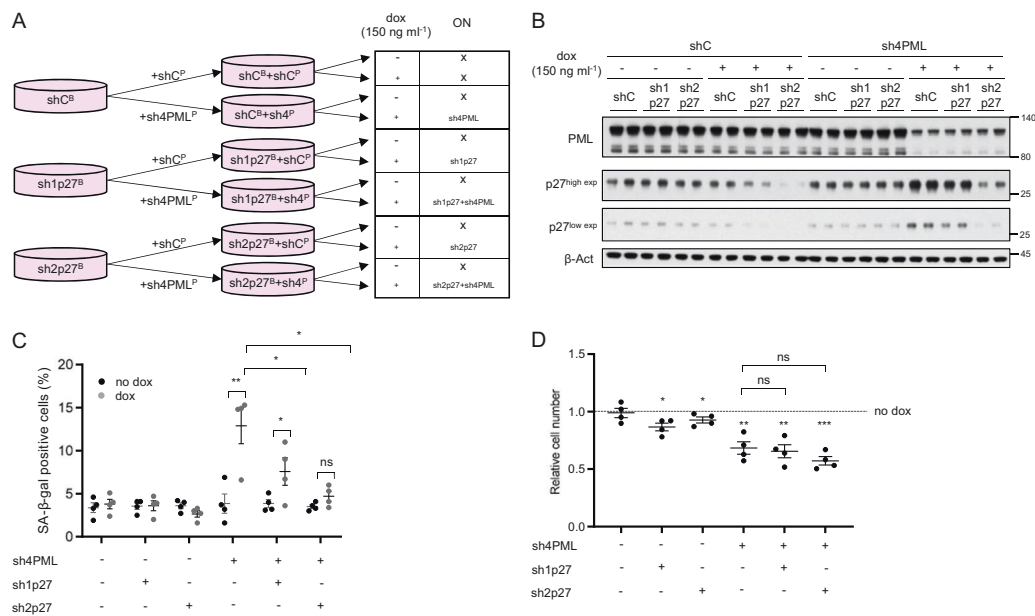


Fig. 3 p27 is the driver in PML loss-induced senescence. **a** Experimental design for inducible p27 silencing (sh1p27 and sh2p27, B: blasticidin selection) alone or in combination with inducible PML silencing (sh4, P: puromycin selection) in MDA-MB-231 cells. **b** p27 and PML protein levels upon doxycycline inducible silencing of either p27 or PML or both in MDA-MB-231 cells (representative of three experiments). **c** Effect on the number of senescent cells ($n = 4$) upon p27 and/or PML inducible silencing in MDA-MB-231 cells. **d** Effect

on the relative cell number ($n = 4$) upon p27 and/or PML inducible silencing in MDA-MB-231 cells. Error bars represent s.e.m. p , p -value ($*p < 0.05$, $**p < 0.01$, $***p < 0.001$). One-tailed Student's t -test (**c**) and one-tailed one-sample t -test (**d**) were used for cell line data analysis. shC: scramble shRNA, Dox: doxycycline, SA- β -gal: senescence-associated beta-galactosidase. Molecular weight markers (kDa) are shown to the right

cell number reduction. Importantly, the growth arrest caused by PML silencing was not recovered by blunting senescence (Fig. 3d and Supplementary Fig. 3c), thus suggesting that an additional mechanism may be involved.

MYC and PIM1 are regulated by PML in TNBC

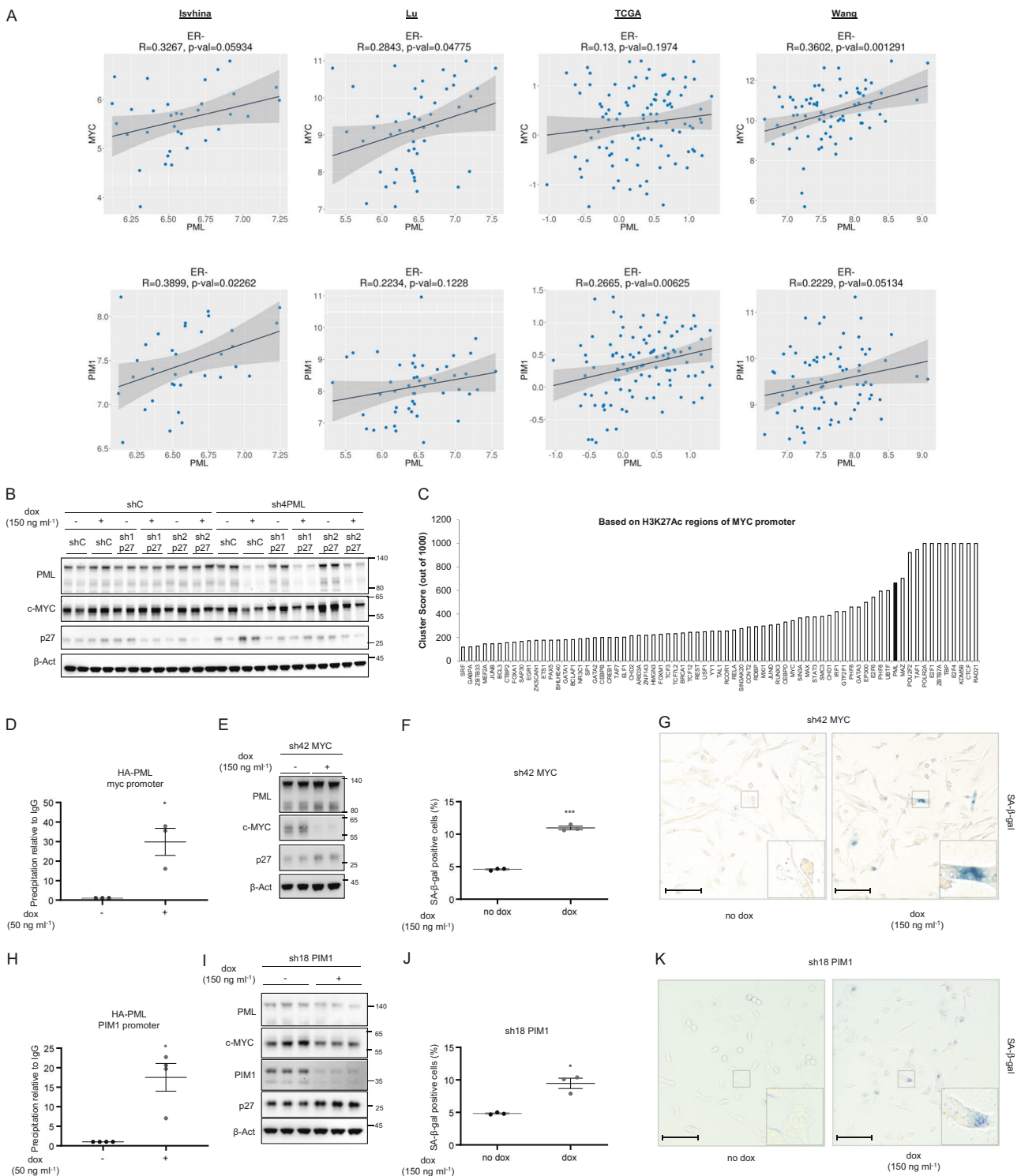
Our data demonstrate that preventing p27 accumulation is not sufficient to rescue the growth arrest caused by PML loss. We reasoned that the mechanism through which PML was regulating growth arrest, p27 accumulation and senescence might depend on a larger growth-regulatory program. Interestingly, the oncogenic axis comprised with MYC and PIM1 kinase shares many similarities with PML concerning its activity in TNBC. MYC and PIM1 are upregulated in TNBC [24, 26, 27] and inhibit p27 accumulation and function [37]. In addition, MYC regulates metabolic functions attributed to PML, including fatty acid β oxidation [6, 10, 38, 39] and its inhibition induces cellular senescence in lymphoma, osteosarcoma, and hepatocellular carcinoma [40]. With this data in mind, we first evaluated the association of PML, MYC, and PIM1 in breast cancer. We found a significant direct correlation in various breast cancer transcriptomics datasets. This association was evident in two out of four datasets for MYC-PML and four out of four for

PIM1-PML, when accounting all breast cancer subtypes (Supplementary Fig. 4a). Since the effect of these genes is restricted to tumors that lack hormone receptors, we refined the analysis by focusing on estrogen receptor (ER) negative tumors. In this scenario, the correlation was recapitulated in various datasets (Fig. 4a).

We next aimed at deconstructing the molecular regulation of PML, MYC, and PIM1. First, we monitored the impact of PML silencing on MYC abundance. As predicted, inducible PML shRNA activation resulted in a remarkable decrease in MYC protein and mRNA levels in vitro and in vivo (Supplementary Fig. 4b–h) in two PML high expressing cells, MDA-MB-231 and MDA-MB-468. Of note, in line with our senescence results (Supplementary Fig. 1i), ATO did not alter the abundance of p27 and MYC (Supplementary Fig. 4i–j).

We next asked to which extent MYC downregulation was retained in cells devoid of p27-dependent senescence response. To address this question, we checked MYC expression upon PML/p27 double silencing in MDA-MB-231 cells. The decrease in MYC expression upon PML loss was not recovered with p27 silencing (Fig. 4b), thus providing a feasible explanation for the lack of rescue in growth capacity.

We have previously shown that PML can regulate gene expression in line with its association with discreet



promoter regions [15]. Since PML silencing resulted in reduced MYC mRNA levels (Supplementary Fig. 4d, h), we interrogated MYC promoter in silico using ENCODE [41]. We found PML among the proteins with highest confidence DNA-binding score in MYC promoter region (Fig. 4c, cluster score: 527). We performed chromatin immunoprecipitation (ChIP) analysis of ectopically expressed PML and

confirmed that PML is in the vicinity of MYC promoter (Fig. 4d). To ascertain if MYC silencing recapitulated the effect of PML inhibition, we used a validated shRNA targeting this oncogene (sh42) [42, 43] and confirmed that MYC silencing resulted in increased p27 levels (Fig. 4e and Supplementary Fig. 4k), senescence (Fig. 4f, g) and growth arrest (Supplementary Fig. 4l).

◀ **Fig. 4** PML regulates MYC and PIM1 expression in TNBC. **a** Correlation analysis between PML and MYC (top panels) and between PML and PIM1 (bottom panels) mRNA levels in ER negative tumor specimens of the indicated breast cancer datasets. Sample sizes: Ivshina ($n = 34$), Lu ($n = 49$), TCGA ($n = 117$) and Wang ($n = 77$). **b** p27, MYC, and PML protein levels upon doxycycline inducible silencing of either p27 or PML or both in MDA-MB-231 cells (representative of three experiments). **c** Cluster score of DNA-binding proteins in MYC promoter region using ENCODE database. **d** MYC promoter region abundance in chromatin immunoprecipitation (ChIP) of exogenous HA-PMLIV using HA-tag antibody in MDA-MB-231 cells after induction with 50 ng ml⁻¹ doxycycline for 3 days ($n = 3$). Data were normalized to IgG (negative-binding control). **e** p27, MYC, and PML protein levels upon doxycycline inducible silencing of MYC (sh42) in MDA-MB-231 cells (representative of three experiments). Effect on the number of senescent cells ($n = 3$) (**f**) and representative images, scale bar 50 μ m, (**g**) upon MYC inducible silencing in MDA-MB-231 cells. **h** PIM1 promoter region abundance in chromatin immunoprecipitation (ChIP) of exogenous HA-PMLIV using HA-tag antibody in MDA-MB-231 cells after induction with 50 ng ml⁻¹ doxycycline for 3 days ($n = 4$). Data were normalized to IgG (negative-binding control). **i** p27, MYC, PIM1, and PML protein levels upon doxycycline inducible silencing of PIM1 (sh18) in MDA-MB-231 cells (representative of three experiments). **j–k** Effect on the number of senescent cells ($n = 3$) and representative images, scale bar 50 μ m, (**k**) upon PIM1 inducible silencing in MDA-MB-231 cells. Error bars represent s.e.m. p , p -value ($*p < 0.05$, $***p < 0.001$). One-tailed one sample t -test (**d**, **h**) and one-tailed student's t -test (**f**, **j**) were used for cell line data analysis. shC: Scramble shRNA, Dox: doxycycline, SA- β -gal: senescence-associated beta-galactosidase. Molecular weight markers (kDa) are shown to the right

In the last few years, an important body of work has demonstrated that PIM1 is an important partner of MYC function in prostate cancer and TNBC [24, 26]. Moreover, PIM1 can regulate MYC transcriptional signature and p27 [24, 26]. We monitored the impact of PML on PIM1 expression and function. PML loss resulted in a decrease in PIM1 gene expression in two PML high expressing cells, MDA-MB-231, and MDA-MB-468 (Supplementary Fig. 4m–n). Importantly, we confirmed that PML is in close proximity to PIM1 promoter by ChIP analysis (Fig. 4h, cluster score: 383 in ENCODE). We hypothesized that loss of PIM1 would further impact on MYC function and recapitulate the aforementioned PML and MYC phenotype. We silenced PIM1 using a validated shRNA (sh18) [24] and corroborated that the targeting of PIM1 led to decrease in MYC abundance, increase in p27 levels, senescence, and growth arrest in MDA-MB-231 cells (Fig. 4i–k and Supplementary Fig. 4o–q). Altogether, our results provide strong support for the role of MYC-PIM1 axis supporting PML-elicited TNBC growth and preventing the accumulation of p27 and senescence.

PML loss-elicited growth suppression in breast cancer is selective of high PML expressing TNBC

The inactivation of a single oncogene can compromise the development and survival of tumor cells despite their

genetic or epigenetic abnormalities [16]. We have previously reported that high PML levels in TNBC are required for adequate CIC function [15]. Here, the data presented support the notion that the bulk of tumor cells in a TNBC with elevated PML is “addicted” to the expression of the protein. In turn, acute depletion of the nuclear protein results in growth arrest and senescence. To ascertain whether the “addiction” was restricted to TNBC cells, we took advantage of various breast cancer cell lines belonging to distinct subtypes with differing levels of PML. A second TNBC cell line (MDA-MB-468) that presented high levels of PML protein was compared with ER+ cells [15] (Fig. 5a). Silencing of PML in MDA-MB-468 cells elicited a remarkable growth arrest, which was not detected in the ER+ cells Cama-1 and MCF7 (Fig. 5b and Supplementary Fig. 5a–c). In line with this notion, Cama-1 and MCF7 cells did not exhibit neither the reduction in MYC expression nor the induction of p27-dependent senescence, as compared with MDA-MB-468 cells (Fig. 5c, d and Supplementary Fig. 5d–g). Moreover, the morphological changes induced by the loss of PML were only present in TNBC cells (Supplementary Fig. 5h). Since PML silencing resulted in a distinct secretory phenotype (albeit not a canonical SASP), we monitored the secretome of the ER+ cell line Cama-1. In agreement with our prior data, unsupervised clustering based on the secretome was ineffective in segregating experimental conditions according to PML status. Similarly, principal component analysis and hierarchical clustering reinforced the notion that Cama-1 are refractory to PML level perturbation (Supplementary Fig. 5i–k and Supplementary Table 2).

Discussion

PML has been a paradigmatic tumor suppressor since its discovery [7, 8, 44]. A variety of molecular activities directly support its reported capacity to prevent many of the hallmarks of cancer, including the induction of apoptosis and the inhibition of proliferation or angiogenesis [7]. Molecular partners such as p53 have reinforced this notion. However, the discovery of tumoral contexts, where the presence of PML is required has broadened the picture of the roles of this nuclear protein in disease. Depletion of PML impairs the self-renewal activity in the leukemic stem cell from chronic myeloid leukemia [9, 10]. This phenotype is the consequence of both cell autonomous (the hyper-activation of mTOR complex1 and the reduction in PPAR δ -fatty acid oxidation activity [9, 10]) and non-cell autonomous activities (regulation of the mesenchymal stem cell in the leukemic niche [45]), which trigger symmetric commitment and the loss of the CIC compartment.

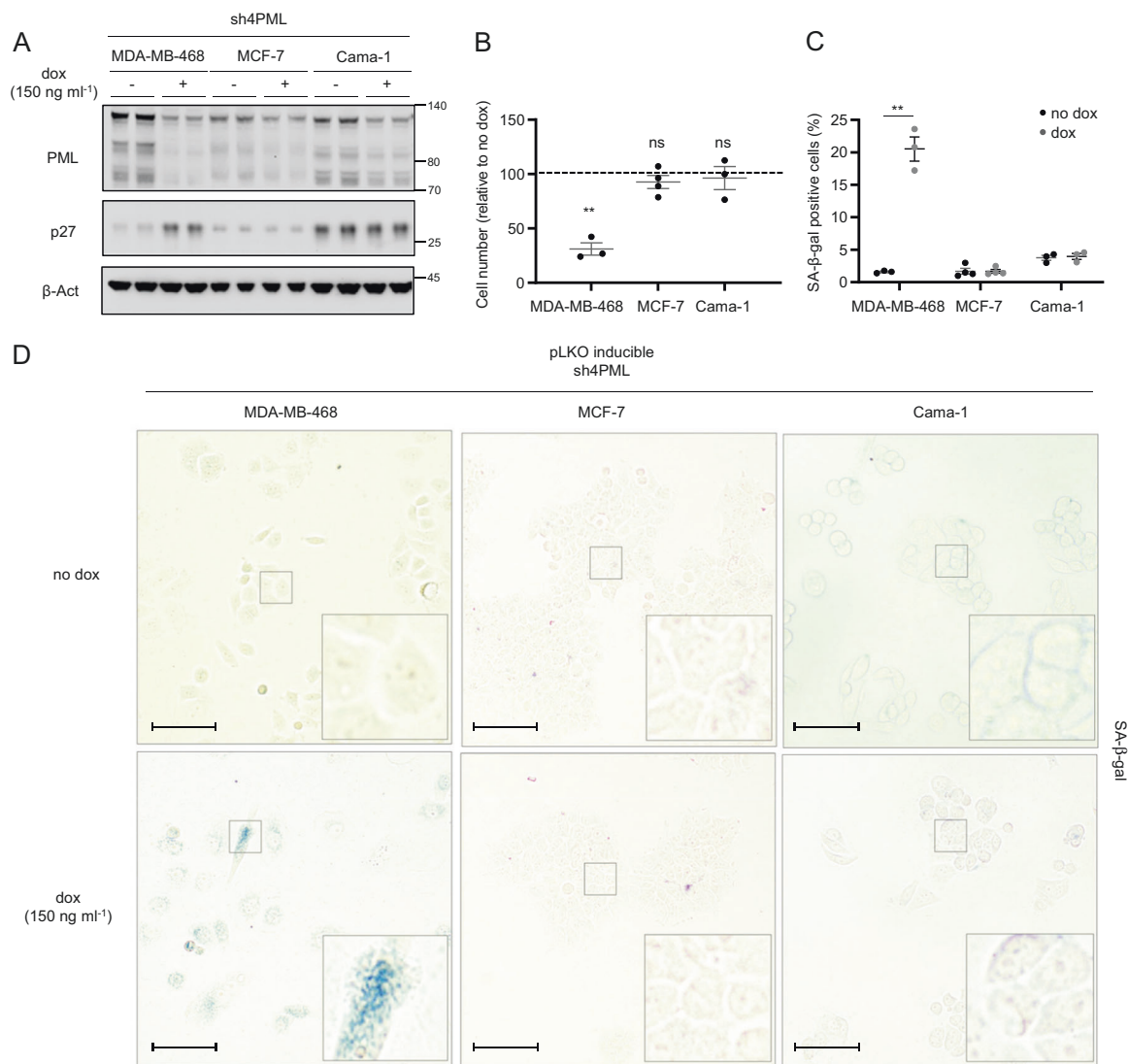


Fig. 5 The antiproliferative program elicited by PML loss is restricted to PML-high expressing TNBC cells. Effect of doxycycline-inducible (150 ng ml⁻¹; 3 + 3 days) PML silencing (sh4) on PML and p27 protein expression (**a**, representative of three experiments), on cell number (**b**, MDA-MB-468 and Cama-1, $n = 3$, MCF7, $n = 4$) and on the number of senescent cells (**c**, MDA-MB-468 and Cama-1, $n = 3$, MCF7, $n = 4$; representative images of SA-β-galactosidase positive

cells (**d**) in MDA-MB-468, MCF-7, and Cama-1 cells, scale bar 50 μm. Error bars represent s.e.m. p , p -value ($*p < 0.05$, $**p < 0.01$, $***p < 0.001$, ns: not significant). One-tailed one sample t -test (**b**) and one-tailed Student's t -test were used for cell line data analysis (**c**). Dox: doxycycline, SA-β-gal: senescence-associated beta-galactosidase. Molecular weight markers (kDa) are shown to the right

The regulation of CIC activity was recently translated to solid tumors. To date, glioma and a subset of breast cancers exhibit PML-dependent self-renewal activity [14, 15], whereas other tumors, such as ovarian cancers or some experimental models of hepatocarcinoma development, exhibit a broad tumor suppressive response upon PML inhibition [11, 12]. PML expression is selectively exacerbated in a subset of breast tumors (TNBC) [6, 13, 15]. Yet, we lack basic understanding around the impact of PML on the function of this cell subtype. In this study, we demonstrate that PML depletion in the bulk of TNBC cells in culture and in vivo triggers a tumor suppressive response

consisting on growth arrest and the activation of senescence.

PML has been previously related to the regulation of the senescence response [21]. However, the majority of studies associate PML expression to the execution of this growth suppressive response upon the activation of oncogenes or replicative stress [11]. Experimentally, ectopic PML expression triggers senescence, and, conversely, PML deletion bypasses the senescence response elicited by the oncogenic form of RAS, thus enabling transformation [46–48]. Mechanistically, PML supports p53 activity and participates in the formation of SAHF [21]. In turn, PML loss

bypasses the senescence response. Paradoxically, our results indicate that, in cancer cells with high dependence on PML expression, its inhibition also triggers a senescence response that lacks canonical SASP and SAHF. This phenomenon might have been overlooked in prior studies due to the lack of data at the time on the role of PML favoring cancer cell function in specific tumor subsets. Of note, the activation of senescence in non-transformed fibroblasts upon PML depletion adds complexity to already extensive portfolio of PML activities [49].

Oncogene addiction [16] is perceived as an attractive opportunity in the era of targeted therapies. Our results are consistent with PML addiction in TNBC cells, even if this protein cannot be formally considered an oncogene. The data produced by us and others [6, 13, 15] argue in favor of a molecular make up in this subtype of breast cancer that requires the presence of PML in high doses, as opposed to estrogen receptor-positive tumor cells. In this regard, the control of MYC and PIM1 expression by PML provides a feasible explanation for the accumulation of p27 and the induction of senescence when PML is silenced. To which extent the relationship between PML, MYC, and PIM1 is operative in other tumor types becomes now an exciting question to address. Since PML lacks a dedicated domain to recognize and bind discreet DNA sequences, the existence of yet unidentified PML-interacting transcription factors that enable this regulatory mode warrants further research.

The results obtained in this study represent a conceptual leap in how we perceive the role of PML in TNBC, and suggest that targeting this nuclear protein can be beneficial at multiple levels, including impairing the CIC function [15], blunting hypoxia signaling [13], and triggering a senescence response. The quantification of the relative relevance of each PML effector pathway in the overall activity of PML could open new opportunities to apply the biology of PML-regulated TNBC function for breast cancer treatment.

Materials and methods

Cell culture

MDA-MB-231, MDA-MB-468, MCF-7, and Cama-1 cell lines were obtained from the American Type Culture Collection (ATCC, Manassas, VA, USA) or from Leibniz-Institut—Deutsche Sammlung von Mikroorganismen und Zellkulturen GmbH (DMSZ) who provided an authentication certificate. None of the cell lines used in this study was found in the database of commonly misidentified cell lines maintained by ICLAC and NCBI Biosample. Cell lines were routinely monitored for mycoplasma contamination and quarantined while treated if positive. MDA-MB-231

and MCF-7 cells were maintained in DMEM media, MDA-MB-468 were maintained in RPMI media, and Cama-1 were maintained in DMEM-F12 media, all supplemented with 10% (v/v) foetal bovine serum and 1% (v/v) penicillin-streptomycin.

Generation of stable cell lines

293FT cells were used for lentiviral production. Lentiviral vectors expressing shRNAs against human *PML* and *p27* from the Mission® shRNA Library were purchased from Sigma-Aldrich. Cells were transfected with lentiviral vectors following standard procedures, and viral supernatant was used to infect cells. Selection was done using puromycin (2 µg ml⁻¹; P8833, Sigma) for 48 h or blasticidin (10 µg ml⁻¹; Cat. 15205, Sigma) for 5 days. As a control, a lentivirus with scrambled shRNA (shC) was used. Short hairpins sequence: shC: CCGCAACAAGATGAAGAG CACCAACTCGAGTTGGTGTCTTTCATCTTGTGTTT TT; sh1PML (TRCN000003865): CCGCAATAACAAC GACAGCCCAGAACTCGAGTTCTGGGCTGTCGTTGT ATTGTTTTT; sh4PML (TRCN 000003867): CCGGG CCAGTGTACGCCTTCTCCATCTCGAGATGGAGAAG GCGTACACTGGCTTTTTT; sh5PML (TRCN 000003868): CCGGGTGTACCGGCAGATTGTGGATCTCGAGATCC-ACAATCTGCCGGTACACTTTTT; sh1p27 (TRCN 0000039928): CCGGGTAGGATAAGTGAAATGGATA CTCGAGTATCCATTTCACTTATCCTACTTTTTG; sh2p27 (TRCN 0000039930): CCGGGCGCAAGTGGAA TTTTCGATTTCTCGAGAAATCGAAATTCACCTGCGC TTTTTG. sh42MYC (TRCN0000039642): CCGGCCTGA GACAGATCAGCAACAACACTCGAGTTGTTGCTGATCT GTCTCAGGTTTTT. sh18PIM1 (TRCN0000010118): CCGGACATCCTTATCGACCTCAATCCTCGAGGATT GAGGTGATAAGGATGTTTTTT.

Sub-cloning of shC, sh1PML, sh4PML, sh5PML, and sh42myc into pLKO-Tet-On-Puromycin vector was done introducing *AgeI* and *EcoRI* in the 5' end of top and bottom shRNA oligos respectively (following the strategy provided by Dr. Dmitri Wiederschain [50], Addgene plasmid: 21915). Sub-cloning of shC, sh1p27, sh2p27, and sh18PIM1 into pLKO-Tet-On-Blasticidin was done following the same procedure. Puromycin resistance cassette was replaced by Blasticidin cassette following Gibson assembly strategy.

Reagents

Doxycycline (Cat. D9891, Sigma) was used at 150 ng ml⁻¹ to induce the expression of shRNA from pLKO-Tet-On vectors. Doxycycline-mediated inducible shRNA expression was performed by treating cell cultures for 72 h with the antibiotic (150 ng ml⁻¹) and then seeding for cellular or

molecular assays in the presence of doxycycline for three more days (unless otherwise specified). ATO (Cat. A1010, Sigma-Aldrich) was prepared at a concentration of 100 mM in NaOH 1 N and subsequently diluted to 0.1 mM in PBS for a working solution. ATO was used at 150 nM for 6 days as indicated in figure legends.

Cell growth analysis and size measurement by FACS

Cell number quantification was done with crystal violet as reported [5]. For FACS analysis MDA-MB-231 cells were trypsinized and resuspended in PBS to be analysed based on their size (FSC) and granularity (SSC) using a BD FACS-Canto™ II (BD Biosciences) flow cytometer upon PML doxycycline-inducible silencing. Data represented in Fig. 1c correspond to the sum of Q1 + Q2 + Q3 populations selected as in Supplementary Fig. 1c. Data were analysed using the FlowJo software; cell populations were selected for each shRNA (no dox condition) and differences quantified for increasing size and granularity.

Senescence associated- β -galactosidase detection

To quantify the number of senescent cells, constitutive or inducible PML/MYC/PIM1/p27 silencing cells was performed as described previously and cells were seeded in 24-well plates in duplicate. An overnight incubation with the senescence detection kit (QIA117, Calbiochem) was performed and SA- β -Gal activity was revealed and quantified (three areas per well, more than 200 cells per condition). The number of senescent cells in each area was relativized to the number of total cells counted per area. Cells were seeded in plates or glass cover slips to acquire images with EVOS® cell imaging station ($\times 20$ magnification objective).

Western blotting, immunofluorescence and BrdU

Western blot analysis was carried out as previously described [5]. Briefly, cells were seeded on six-well plates. Cell lysates were prepared with RIPA buffer (50 mM TrisHCl pH 7.5, 150 mM NaCl, 1 mM EDTA, 0.1% SDS, 1% Nonidet P40, 1% sodium deoxycholate, 1 mM Sodium Fluoride, 1 mM sodium orthovanadate, 1 mM beta-glycerophosphate and protease inhibitor cocktail; Roche). The following antibodies were used for Western blotting: rabbit polyclonal anti-PML, 1:1000 dilution (Cat: A301-167A, Bethyl laboratories), mouse monoclonal anti-p27[Kip1], 1:1000 dilution (Cat: 610242, BD Biosciences), mouse monoclonal anti-beta-ACTIN, 1:2000 dilution (Cat: 3700, Cell Signaling), rabbit polyclonal Hsp90, 1:2000 dilution (Cat: 4874, Cell Signaling), rabbit polyclonal c-Myc, 1:1000 dilution (Cat: 13987, Cell Signaling), rabbit

polyclonal PIM1, 1:1000 dilution (ab75776, Abcam), rabbit polyclonal Lamin B1 (ab133741, Abcam), rabbit monoclonal anti-cleaved PARP (Asp214), 1:1000 dilution (Cat: 5625, Cell Signaling), rabbit polyclonal anti-cleaved caspase 3 (Asp175), 1:1000 dilution (Cat: 9661, Cell Signaling), mouse monoclonal anti- α -Tubulin (66031-1-Ig, Proteintech), 1:2500 dilution, rabbit monoclonal anti-phospho-Rb (Ser780) 1:1000 dilution (Cat: 9307, Cell Signaling). After standard SDS-PAGE and Western blotting techniques, proteins were visualized using the ECL on iBright™ CL1000 Imaging System (Cat: A32749, Invitrogen). Densitometry-based quantification was performed using ImageJ software. Uncropped scans are provided in Supplementary Fig. 6.

For immunofluorescence, cells were seeded on glass cover slips in 24-well plates, cells were fixed with 4% para-formaldehyde (15 min), PBS (three times wash), 1% Triton X-100 (5 min), PBS (three times wash), 10% goat serum (1 h) and anti-PML antibody 1:100 dilution (catalog A301-167A; Bethyl laboratories), anti-p27[Kip1] antibody 1:100 dilution (Cat: 610242, BD Biosciences) and anti-macroH2A1.1 antibody 1:100 (Cat: 12455, Cell Signaling) were added ON (4 °C) in goat serum. Cover slips were washed with PBS three times and incubated with secondary antibodies (anti-rabbit Alexa488, anti-rabbit Alexa594, anti-mouse Alexa488, and anti-mouse Alexa594; Invitrogen-Molecular Probes) for 1 h (room temperature). Cover slips were washed with PBS three times, and DAPI added to stain nuclei (10 min), followed by mounting with ProLong™ Gold Antifade Mountant (Cat: P36930, Invitrogen). Immunofluorescence images were obtained with AxioImager D1 microscope (Zeiss) or with a confocal microscopy (Leica SP8) with $\times 63$ objectives. At least three different areas per cover slip were quantified.

For BrdU analysis cells were seeded as for immunofluorescence. Prior to fixing, cells were incubated in the presence of BrdU (3 $\mu\text{g ml}^{-1}$). Cells were fixed with 4% para-formaldehyde (15 min), PBS (three times wash) and DNA exposed with 2 M HCl (5 min), PBS (3 times wash) and 0.1 M sodium borate. After that, PBS (three times wash), 1% Triton X-100 (5 min), PBS (three times wash), 10% goat serum (1 h), and monoclonal anti-BrdU (MoBU-1) antibody 1:100 dilution (Cat: B35128, Invitrogen) was added ON (4 °C) in goat serum. Cover slips were washed three times with PBS and incubated with secondary antibodies (anti-mouse Alexa594; Invitrogen-Molecular Probes) for 1 h (room temperature). Cover slips were washed three times with PBS and DAPI added to stain nuclei (10 min), followed by mounting with ProLong™ Gold Antifade Mountant (Cat: P36930, Invitrogen). Images were obtained with an AxioImager D1 microscope (Zeiss). At least three different areas per cover slip were quantified.

Quantitative real-time PCR

Cells were seeded as for western blot. Total RNA was extracted from cells using NucleoSpin RNA isolation kit from Macherey-Nagel (ref: 740955.250). Complementary DNA was produced from 1 µg of RNA using Maxima™ H Minus cDNA Synthesis Master Mix (Cat# M1682, Invitrogen). Taqman probes were obtained from Applied Biosystems. Amplifications were run in a Viia7 or QS6 Real-Time PCR Systems (Applied Biosystems) using the following probes: PML (Hs00971694_m1, cat: 4331182). For p27 (CDKN1B), MYC, PIM1, CDK2, CDK4, E2F3, AURKA, and CDC25A amplification, Universal Probe Library (Roche) primers and probes were employed (p27, For: ccctagagggcaagtacgagt, Rev: agtagaactcgggcaagctg, probe: 39; MYC, For: gctgcttagacgctggattt, Rev: taacttgaggggcactcg, probe: 66; PIM1, For: atcaggggccaggttttc, Rev: gggccaagcaccatctaat, probe: 13; CDK2, For: aaagcagaacaagttagc, Rev: gtactgggcacaccctcagt, probe 77; CDK4, For: gtgcagtcggtgtacctg, Rev: aggcagagatcctgtgt, probe 25; E2F3, For: ggttctggaaatgcccttac, Rev: gatgaccgctttctcctagc, probe 40; AURKA, For: gca-gatttgggtgtcagt, Rev: tccgacctcaatcattca, probe 79; CDC25A, For: cgtcatgagaactcaaacctga, Rev: tctgtctctcaactgacc, probe 67). All quantitative PCR with reverse transcription data presented were normalized using GAPDH (Hs02758991_g1, cat: 4331182) from Applied Biosystems as housekeeping.

Mice

Xenograft experiments were carried out following the ethical guidelines established by the Biosafety and Welfare Committee at CIC bioGUNE. The procedures employed were carried out following the recommendations from AAALAC. Xenograft experiments were performed as previously described [5], injecting 3×10^6 cells per tumor, two injections per mouse, one per flank. All mice (female Hsd: Athymic Nude-Foxn1 nu/nu) were inoculated at 8–12 weeks of age. Nineteen days post injection, once tumors were established ($25\text{--}130\text{ mm}^3$), mice were fed with chow or doxycycline diet (Research diets, D12100402) until the experimental endpoint.

p-HP1γ immunohistochemistry

After sacrifice, formalin-fixed paraffin embedded xenograft tissues were stained for p-HP1γ. Tissues were deparaffinized using the standard procedure and unmasking/antigen retrieval was performed using pH 6.0 solution for 20 min at 98 °C in water bath. Tissue sections were stained for p-HP1γ using primary antibody Phospho-HP1γ (Ser83) (Cat. No: 2600, Cell Signaling technologies, 1:200) and

secondary antibody Biotinylated antibody Anti-Rabbit (BP-9100, Vector Laboratories, 1:200). This was followed by Vectastain ABC solution incubation (PK-6100, Vector laboratories, 1:150) and DAB staining (SK-4105, Vector laboratories) as per the manufacturer's protocol. Stained slides were scanned using Leica Aperio AT2 slide scanner. The criteria for senescent staining used for quantification was a very prominent nuclear staining in which the nucleus was bigger in size and its staining was darker brown than the other cells.

ChIP

ChIP was performed using the SimpleChIP® Enzymatic Chromatin IP Kit (Cat #9003, Cell Signaling Technology, Inc) as reported [15]. DNA quantification was carried out using a Viia7 Real-Time PCR System (Applied Biosystems) with SybrGreen reagents and primers that amplify the predicted PML binding region to MYC promoter (chr8:128748295–128748695) as follows: left primer: CCGGCTAGGGTGAAGAG, right primer: GCTGCTA TGGGCAAAGTTTC and PIM1 promoter (chr6: 37137097–37137612) as follows: left primer: ACTCCCTC CGTGACTCATGT, right primer: ACGAGGGTGG TCTTTCTGTG.

Secretome analysis

Secretomes were prepared as previously described [51]. MDA-MB-231 sh4 PML tet on and Cama-1 sh4 PML tet on cells were pre-induced with doxycycline (150 ng ml^{-1}) for 3 days. Three 150 cm^2 plates were seeded per condition: 4×10^6 cells per plate of non-induced cells and 5×10^6 cells per plate of doxycycline induced cells. After two days, cell supernatants were removed and cells were washed five times: the first two washes were performed with PBS and the last three were made with serum-depleted DMEM. Cells were left to grow for 24 h in serum-depleted DMEM. Doxycycline was maintained (150 ng ml^{-1}). Two biological replicates, each with three technical replicates were processed.

After 24 h supernatant was collected and one dish per condition was trypsinized and counted to check cell number and PML expression. The supernatant was first spun at 1000 rpm for 5 min followed by filtration through $0.2\text{ }\mu\text{m}$ filtering bottles. After this, it was concentrated using 10 kDa Amicons; first, 15 mL Amicons (Ref. UCF901024, Merck) were used, followed by 0.5 mL Amicons (Ref. UCF501069, Merck) to get final volumes close to $80\text{ }\mu\text{L}$. The concentrated secretome was frozen at $-20\text{ }^\circ\text{C}$ until proteomics analysis. Protein concentration was determined with a Pierce BCA protein assay kit (Thermo Scientific). All samples were digested with trypsin in-solution prior to

analysis by liquid chromatography–mass spectrometry (LC–MS). Tryptic digests were analysed by shotgun proteomics using an LTQ Velos-Orbitrap mass spectrometer (Thermo Fisher Scientific, Bremen, Germany). The RAW files of each MS run were processed using Proteome Discoverer (Thermo Fisher Scientific), and MS/MS spectra were searched against the human database of Swiss-Prot using the MASCOT (Matrix Science, London, U.K) algorithm. The results files generated from MASCOT (.DAT files) were then loaded into Scaffold (Proteome Software, Portland, OR), resulting in a nonredundant list of identified proteins per sample achieving a protein false discovery rate (FDR) under 1.0%, as estimated by a search against a decoy database.

Secretome statistical analysis

Relative spectral counting-based protein quantification analysis was performed on the different samples analyzed using Scaffold. Files containing all spectral counts for each sample and its replicates were generated and then exported to R software for normalization and statistical analysis [52]. All statistical computations were done using the open-source statistical package R. The data were assembled in a matrix of spectral counts, where the different conditions are represented by the columns and the identified proteins are represented by the rows. An unsupervised exploratory data analysis by means of principal components analysis and hierarchical clustering of the samples on the SpC matrix was first performed. Then, the GLM model based on the Poisson distribution was used as a significance test [52]. Finally the Benjamini and Hochberg multitest correction was used to adjust the *p*-values with control on the FDR.

Full information regarding the proteins detected in the secretome analysis can be found in Supplementary Tables 1 and 2.

ROS analysis

MDA-MB-231 cells with inducible shRNA against PML (sh4) were pre-induced with doxycycline (150 ng ml⁻¹) for 3 days. Then, cells were seeded in a six-well plate in triplicate (1.5 × 10⁵ cells/well) maintaining the doxycycline concentration. Two additional wells with non-induced cells were used for positive and negative ROS controls respectively.

After 72 h, 10 μM of 2', 7'-Dichlorofluorescein diacetate (DCF-DA) (Sigma-Aldrich Ref: 35845) reactive was added to each well and cells were incubated for 30 min. In the last 5 min of the incubation time, 1 M hydrogen peroxide (H₂O₂) was added to the positive control well.

Subsequently, cells were washed with PBS and raised from plates employing 500 μL of trypanLE reactive (Gibco™

ref: 12563–011). After that, cells were washed twice with abundant PBS to eliminate the excess of DCF-DA reactive and pellets were re-suspended in 500 μL PBS for FACS analysis. Samples were analyzed in FACS CANTO II for green fluorescence.

Datasets

Database normalization

All the datasets used for the data mining analysis were downloaded from GEO and TCGA, and subjected to background correction, log₂ transformation, and quartile normalization. In the case of using a pre-processed dataset, this normalization was reviewed and corrected if required.

Correlation analysis

Pearson correlation test was applied to analyse the relationship between paired genes. From this analysis, Pearson coefficient (R) indicates the existing linear correlation (dependence) between two variables *X* and *Y*, giving a value between +1 and -1 (both included), where 1 is total positive correlation, 0 is no correlation, and -1 is total negative correlation. The *p*-value indicates the significance of this R coefficient.

Statistical analysis

No statistical method was used to predetermine sample size. The experiments were not randomized. The investigators were not blinded to allocation during experiments and outcome assessment. Data analysed by parametric tests are represented by the mean ± s.e.m. of pooled experiments unless otherwise stated. *n* values represent the number of independent experiments performed or the number of individual mice. For each in vitro independent experiment, technical replicates were used and a minimum number of three experiments were performed to ensure adequate statistical power. In the in vitro experiments, normal distribution was assumed and one sample *t*-test was applied for one component comparisons with control and Student's *t*-test for two component comparisons. For in vivo experiments, a non-parametric Mann–Whitney *U*-test was used. Two-tailed statistical analysis was applied for experimental design without predicted result, and one-tail for validation or hypothesis-driven experiments. The confidence level used for all the statistical analyses was of 0.95 (alpha value = 0.05).

Acknowledgements Apologies to those whose related publications were not cited due to space limitations. LA, AS, MPu, AA-A, and LV-J were supported by the Basque Government of education. IH was

supported by the Program “Juan de la Cierva” from MINECO. FC acknowledges the Proteomics Unit at VHIO is a member ProteoRed, PRB3 (Grant IPT17/0019—ISCIII-SGEFI/ERDF. RB acknowledges projects BFU2017–84653-P, Consolider BFU2014–57703-REDC, and SAF2017–90900-REDT (MINECO/FEDER, EU). The work of VT is founded by Fundación Vasca de Innovación e Investigación Sanitarias, BIOEF (BIO15/CA/052), the AECC J.P. Bizkaia, the Basque Department of Health (2016111109) and the MINECO (RTI2018–097267-B-I00 (MCIU/AEI/FEDER, UE)). AA was supported by ERC consolidator (683136) and Swiss Cancer League (KFS4267–08–2017) grant, Dr. Josef Steiner Foundation, Swiss Card-Onco-Grant of Alfred and Annemarie von Sick grant, Helmut Horten Foundation, SNSF (310030_176045) and PCUK (RIA15-ST2–018). NM-M was supported by the Spanish Association Against Cancer (AECC), AECC JP Vizcaya and CIBERONC. The work of A. Carracedo is supported by the Basque Department of Industry, Tourism and Trade (Elkartek) and the department of education (IKERTALDE IT1106–16), the BBVA foundation, the MINECO (SAF2016–79381-R (FEDER/EU); Severo Ochoa Excellence Accreditation SEV-2016–0644; Excellence Networks SAF2016–81975-REDT), European Training Networks Project (H2020-MSCA-ITN-308 2016 721532), the AECC (IDEAS175CARR, GCTRA18006CARR), La Caixa Foundation (HR17–00094), FERO foundation, the AstraZeneca Oncology prize and the European Research Council (Starting Grant 336343, PoC 754627). CIBERONC was co-funded with FEDER funds and funded by ISCIII.

Authors contributions LA, NM-M, and MP performed the majority of the in vitro and in vivo experiments, unless specified otherwise. SF-R, JRC, AA-A, LV-J, PZ-G, and IH contributed to specific in vitro analyses. MPu and AZ-L performed ROS analyses. AS and VT coordinated or performed secretome preparation. AR performed the histochemical staining and quantification of p-HP1 γ staining. IA contributed to the sub-cloning of shC, sh1p27, and sh2p27 into pLKO-Tet-On- Blastocidin. ARC performed the bioinformatic and biostatistical analysis. JV and FC performed or coordinated the secretome analysis. LB-B provided support with imaging analyses. RB and JDS provided technical advice. AA supervised the histochemical staining and quantification of p-HP1 γ staining. AC and NM-M directed the project, contributed to data analysis and wrote the manuscript.

Compliance with ethical standards

Conflict of interest The authors declare that they have no conflict of interest.

Publisher’s note Springer Nature remains neutral with regard to jurisdictional claims in published maps and institutional affiliations.

Open Access This article is licensed under a Creative Commons Attribution 4.0 International License, which permits use, sharing, adaptation, distribution and reproduction in any medium or format, as long as you give appropriate credit to the original author(s) and the source, provide a link to the Creative Commons license, and indicate if changes were made. The images or other third party material in this article are included in the article’s Creative Commons license, unless indicated otherwise in a credit line to the material. If material is not included in the article’s Creative Commons license and your intended use is not permitted by statutory regulation or exceeds the permitted use, you will need to obtain permission directly from the copyright holder. To view a copy of this license, visit <http://creativecommons.org/licenses/by/4.0/>.

References

- Sorlie T, Perou CM, Tibshirani R, Aas T, Geisler S, Johnsen H, et al. Gene expression patterns of breast carcinomas distinguish tumor subclasses with clinical implications. *Proc Natl Acad Sci USA*. 2001;98:10869–74.
- van de Vijver MJ, He YD, van’t Veer LJ, Dai H, Hart AA, Voskuil DW, et al. A gene-expression signature as a predictor of survival in breast cancer. *N Engl J Med*. 2002;347:1999–2009.
- Curtis C, Shah SP, Chin SF, Turashvili G, Rueda OM, Dunning MJ, et al. The genomic and transcriptomic architecture of 2000 breast tumours reveals novel subgroups. *Nature*. 2012;486:346–52.
- Bos PD, Zhang XH, Nadal C, Shu W, Gomis RR, Nguyen DX, et al. Genes that mediate breast cancer metastasis to the brain. *Nature*. 2009;459:1005–9.
- Carracedo A, Ma L, Teruya-Feldstein J, Rojo F, Salmena L, Alimonti A, et al. Inhibition of mTORC1 leads to MAPK pathway activation through a PI3K-dependent feedback loop in human cancer. *J Clin Invest*. 2008;118:3065–74.
- Carracedo A, Weiss D, Leliaert AK, Bhasin M, de Boer VC, Laurent G, et al. A metabolic prosurvival role for PML in breast cancer. *J Clin Invest*. 2012;122:3088–100.
- Tessier S, Martin-Martin N, de The H, Carracedo A, Lallemand-Breitenbach V. Promyelocytic leukemia protein, a protein at the crossroad of oxidative stress and metabolism. *Antioxid Redox Signal*. 2017;26:432–44.
- Bernardi R, Pandolfi PP. Structure, dynamics and functions of promyelocytic leukaemia nuclear bodies. *Nat Rev Mol Cell Biol*. 2007;8:1006–16.
- Ito K, Bernardi R, Morotti A, Matsuoka S, Saglio G, Ikeda Y, et al. PML targeting eradicates quiescent leukaemia-initiating cells. *Nature*. 2008;453:1072–8.
- Ito K, Carracedo A, Weiss D, Arai F, Ala U, Avigan DE, et al. A PML–PPAR- δ pathway for fatty acid oxidation regulates hematopoietic stem cell maintenance. *Nat Med*. 2012;18:1350–8.
- Chung YL, Wu ML. Dual oncogenic and tumor suppressor roles of the promyelocytic leukemia gene in hepatocarcinogenesis associated with hepatitis B virus surface antigen. *Oncotarget*. 2016;7:28393–407.
- Liu SB, Shen ZF, Guo YJ, Cao LX, Xu Y. PML silencing inhibits cell proliferation and induces DNA damage in cultured ovarian cancer cells. *Biomed Rep*. 2017;7:29–35.
- Ponente M, Campanini L, Cuttano R, Piunti A, Delledonne GA, Coltella N, et al. PML promotes metastasis of triple-negative breast cancer through transcriptional regulation of HIF1A target genes. *JCI Insight*. 2017;2:e87380.
- Zhou W, Cheng L, Shi Y, Ke SQ, Huang Z, Fang X, et al. Arsenic trioxide disrupts glioma stem cells via promoting PML degradation to inhibit tumor growth. *Oncotarget*. 2015;6:37300–15.
- Martin-Martin N, Piva M, Urosecvic J, Aldaz P, Sutherland JD, Fernandez-Ruiz S, et al. Stratification and therapeutic potential of PML in metastatic breast cancer. *Nat Commun*. 2016;7:12595.
- Weinstein IB, Joe A. Oncogene addiction. *Cancer Res*. 2008;68:3077–80. discussion 3080.
- Childs BG, Durik M, Baker DJ, van Deursen JM. Cellular senescence in aging and age-related disease: from mechanisms to therapy. *Nat Med*. 2015;21:1424–35.
- Nardella C, Clohessy JG, Alimonti A, Pandolfi PP. Pro-senescence therapy for cancer treatment. *Nat Rev Cancer*. 2011;11:503–11.
- Lin HK, Chen Z, Wang G, Nardella C, Lee SW, Chan CH, et al. Skp2 targeting suppresses tumorigenesis by Arf-p53-independent cellular senescence. *Nature*. 2010;464:374–9.

20. Majumder PK, Grisanzio C, O'Connell F, Barry M, Brito JM, Xu Q, et al. A prostatic intraepithelial neoplasia-dependent p27 Kip1 checkpoint induces senescence and inhibits cell proliferation and cancer progression. *Cancer Cell*. 2008;14:146–55.
21. Ivanschitz L, De The H, Le Bras MPML. SUMOylation, and Senescence. *Front Oncol*. 2013;3:171.
22. Zhang R, Poustovoitov MV, Ye X, Santos HA, Chen W, Daganzo SM, et al. Formation of MacroH2A-containing senescence-associated heterochromatin foci and senescence driven by ASF1a and HIRA. *Dev Cell*. 2005;8:19–30.
23. Lo Re O, Vinciguerra M. Histone MacroH2A1: a chromatin point of intersection between fasting, senescence and cellular regeneration. *Genes (Basel)*. 2017;8.
24. Braso-Maristany F, Filosto S, Catchpole S, Marlow R, Quist J, Francesch-Domenech E, et al. PIM1 kinase regulates cell death, tumor growth and chemotherapy response in triple-negative breast cancer. *Nat Med*. 2016;22:1303–13.
25. Cancer Genome Atlas N. Comprehensive molecular portraits of human breast tumours. *Nature*. 2012;490:61–70.
26. Horiuchi D, Camarda R, Zhou AY, Yau C, Momcilovic O, Balakrishnan S, et al. PIM1 kinase inhibition as a targeted therapy against triple-negative breast tumors with elevated MYC expression. *Nat Med*. 2016;22:1321–9.
27. Horiuchi D, Kusdra L, Huskey NE, Chandriani S, Lenburg ME, Gonzalez-Angulo AM, et al. MYC pathway activation in triple-negative breast cancer is synthetic lethal with CDK inhibition. *J Exp Med*. 2012;209:679–96.
28. Zhao W, Qiu R, Li P, Yang J. PIM1: a promising target in patients with triple-negative breast cancer. *Med Oncol*. 2017;34:142.
29. Hernandez-Segura A, Nehme J, Demaria M. Hallmarks of cellular senescence. *Trends Cell Biol*. 2018;28:436–53.
30. Dreesen O, Chojnowski A, Ong PF, Zhao TY, Common JE, Lunny D, et al. Lamin B1 fluctuations have differential effects on cellular proliferation and senescence. *J Cell Biol*. 2013;200:605–17.
31. Freund A, Laberge RM, Demaria M, Campisi J. Lamin B1 loss is a senescence-associated biomarker. *Mol Biol Cell*. 2012;23:2066–75.
32. Niwa-Kawakita M, Ferhi O, Soilhi H, Bras le M, Lallemand-Breitenbach V, Huges de H. PML is a ROS sensor activating p53 upon oxidative stress. *J Exp Med*. 2017;214:3197–206.
33. Di Mitri D, Toso A, Chen JJ, Sarti M, Pinton S, Jost TR, et al. Tumour-infiltrating Gr-1+ myeloid cells antagonize senescence in cancer. *Nature*. 2014;515:134–7.
34. Bazarov AV, Van Sluis M, Hines WC, Bassett E, Beliveau A, Campeau E, et al. p16(INK4a)-mediated suppression of telomerase in normal and malignant human breast cells. *Aging Cell*. 2010;9:736–46.
35. Bykov VJ, Issaeva N, Shilov A, Hultcrantz M, Pugacheva E, Chumakov P, et al. Restoration of the tumor suppressor function to mutant p53 by a low-molecular-weight compound. *Nat Med*. 2002;8:282–8.
36. Rodier G, Montagnoli A, Di Marcotullio L, Coulombe P, Draetta GF, Pagano M, et al. p27 cytoplasmic localization is regulated by phosphorylation on Ser10 and is not a prerequisite for its proteolysis. *EMBO J*. 2001;20:6672–82.
37. Morishita D, Katayama R, Sekimizu K, Tsuruo T, Fujita N. Pim kinases promote cell cycle progression by phosphorylating and down-regulating p27Kip1 at the transcriptional and post-transcriptional levels. *Cancer Res*. 2008;68:5076–85.
38. Carracedo A, Cantley LC, Pandolfi PP. Cancer metabolism: fatty acid oxidation in the limelight. *Nat Rev Cancer*. 2013;13:227–32.
39. Camarda R, Zhou AY, Kohnz RA, Balakrishnan S, Mahieu C, Anderton B, et al. Inhibition of fatty acid oxidation as a therapy for MYC-overexpressing triple-negative breast cancer. *Nat Med*. 2016;22:427–32.
40. Wu CH, van Riggelen J, Yetil A, Fan AC, Bachireddy P, Felsner DW. Cellular senescence is an important mechanism of tumor regression upon c-Myc inactivation. *Proc Natl Acad Sci USA*. 2007;104:13028–33.
41. Consortium EP. The ENCODE (ENCyclopedia Of DNA Elements) Project. *Science*. 2004;306:636–40.
42. Liu R, Zhang T, Zhu G, Xing M. Regulation of mutant TERT by BRAF V600E/MAP kinase pathway through FOS/GABP in human cancer. *Nat Commun*. 2018;9:579.
43. Nakano T, Kanai Y, Amano Y, Yoshimoto T, Matsubara D, Shibano T, et al. Establishment of highly metastatic KRAS mutant lung cancer cell sublines in long-term three-dimensional low attachment cultures. *PLoS One*. 2017;12:e0181342.
44. Martin-Martin N, Sutherland JD, Carracedo A. PML: not all about tumor suppression. *Front Oncol*. 2013;3:200.
45. Guarnerio J, Mendez LM, Asada N, Menon AV, Fung J, Berry K, et al. A non-cell-autonomous role for Pml in the maintenance of leukemia from the niche. *Nat Commun*. 2018;9:66.
46. Bischof O, Kirsh O, Pearson M, Itahana K, Pelicci PG, Dejean A. Deconstructing PML-induced premature senescence. *EMBO J*. 2002;21:3358–69.
47. Ferbeyre G, de Stanchina E, Querido E, Baptiste N, Prives C, Lowe SW. PML is induced by oncogenic ras and promotes premature senescence. *Genes Dev*. 2000;14:2015–27.
48. Pearson M, Carbone R, Sebastiani C, Cioco M, Fagioli M, Saito S, et al. PML regulates p53 acetylation and premature senescence induced by oncogenic Ras. *Nature*. 2000;406:207–10.
49. Marchesini M, Matocci R, Tasselli L, Cambiaghi V, Orleth A, Furia L, et al. PML is required for telomere stability in non-neoplastic human cells. *Oncogene*. 2016;35:1811–21.
50. Wiederschain D, Wee S, Chen L, Loo A, Yang G, Huang A, et al. Single-vector inducible lentiviral RNAi system for oncology target validation. *Cell Cycle*. 2009;8:498–504.
51. Gregori J, Villarreal L, Sanchez A, Baselga J, Villanueva J. An effect size filter improves the reproducibility in spectral counting-based comparative proteomics. *J Proteom*. 2013;95:55–65.
52. Villarreal L, Mendez O, Salvans C, Gregori J, Baselga J, Villanueva J. Unconventional secretion is a major contributor of cancer cell line secretomes. *Mol Cell Proteom*. 2013;12:1046–60.

